Researching
Net Offshore Bar Migration
at
Wanganui, New Zealand

COASTAL SYSTEMS LIMITED

MASSEY UNIVERSITY

Researching
Net Offshore Bar Migration
at Wanganui New Zealand

Roger D. Shand, PhD

Front cover Camera equipment used to record time-exposure imagery during the 1990s. Included are neutral density filter, filter mount and housing, lens hood, light proof bag, SLR 35mm film camera, release cord and support tripods. The camera was located 42 m above MSL and 130 m landward of the foredune toe. Several output examples are included within the text.

Published by Coastal Systems Ltd

www.coastalsystems.co.nz

Printed by Hanton and Anderson Ltd, 2025

Whanganui, New Zealand

ISBN 978-0-473-75207-1

PREFACE

During the 1990s, coastal researchers were experimenting with image-based methods of data acquisition which relied on breaking waves to infer surf zone morphology and processes. This was particularly helpful on wider surf zones, typically multi-barred coasts subject to higher energy and shorter wave period; on these coasts more conventional direct measurement-based approaches where logistically challenging and expensive so such environments had lagging in scientific attention.

Research site on the southwest of the New Zealand North Island was one such coast. From a cliff-top camera site at Wanganui, several kms of coast could be photographed or videoed when waves (breaking on all bars), tide (low to mid), and weather condition (day time and anything other than storms) permitted.

Massey University had a state-of-the-art Image Analysis Unit so processing the raw imagery to obtain a birds-eye perspective of the morphology and corresponding hydrodynamic data was enabled.

The availability of high resolution temporal and quasi-3D morphology (elevation being at a relative scale), resulted in the identification and quantification of a systematic (net) seaward bar migration pattern (NOM), as well as discovering several other new surf zone behaviours.

This story is summarised in the text below, with further explanation in the appended publications for those readers interested in the detail.

ACKNOWLEDGEMENTS

Perhaps I should begin by thanking fate – luck that my parents happened to chose coastal environments in which to live. Beach, dune, estuaries, cliffs and the streams that flowed down and into them dominated my early life.

Later, surfing increased the physical contact. I became intimate with the energy, the sediment and settings, and realised that there were so many different types of coast.

Next I met Dr Mike Shepherd, my lecturer in coastal geomorphology at Massey University. He introduced another aspects of this world such as how it changed over different time-scales and how to unlock its secrets by measurement and analysis. Mike was totally likeable and a wonderful research supervisor. He tolerated my frequent wanderings down rabbit holes – knowing that I would return to the path with a greater breadth of knowledge.

By contrast, my second supervisor Dr Bob Kirk (University of Canterbury), kept a close eye on the objectives. Bob had a great depth of knowledge in contemporary coastal dynamics and an intellect to suit. I remain greatly in debt to my supervisors; sadly both have now passed away.

Another key assistor was Dr Don Bailey, image processer extraordinaire at Massey. Don relished the chance to apply his pixel-pushing skills to my abundant imagery of the coastal environment, and several early papers were published on such endeavours. A fun time.

And a late comer to the team was Tom, now Dr Tom Shand, the Coastal Engineering Technical Manager at Tonkin and Taylor. He also grew up on the coast and in the surf, and was likely more familiar with research techniques than his lecturers. Tom keeps me sharp following the challenging projects they do, keeps me up-to-date in ever changing coastal science and engineering, and is full of what-to-do next suggestions.

CONTENTS

1 Introduction 11

2 Photo and Video Data Acquisition 12

3 Cross-shore Bar Migration 13

4 Morphological Variation 15

4.1 Bar Splitting 15

4.2 Bar Switching 16

4.3 Morphological Configurations 17

4.4 Shoreline Erosion 19

5 Balancing Sediment Transport 20

6 Follow-up 21

7 Conclusions 22

APPENDICES of PUBLICATIONS 23

1. 1990. *The subaqueous morphology at the entrance to a jetty controlled river mouth on a moderate to high energy littoral drift dominated coast: Wanganui, New Zealand 1981-1987.*

2. 2000. *Offshore migration of coastal sand-bars at Wanganui New Zealand.* PhD.

3. 1993. *Determining large-scale sand-bar evolution.*

4. 1994. *Determining wave run-up using automated video analysis.*

5. 1995. *Videographic acquisition of surf zone data: a summary of present techniques and future possibilities*

6. 1996. *Determining large-scale sand-bar behaviour*

7. 1997. *Data fusion issues in analysing coastal morphodynamic systems.*

8. 1999. *An inter-site comparison of net offshore bar migration characteristics and environmental conditions*.

9. 1999. *A review of net offshore bar migration with photographic illustrations from Wanganui, New Zealand*.

10. 2000. *Hatherton Award*.

11. 2001. *Longshore realignment of nearshore parallel sand-bars at Wanganui, New Zealand.*

12. 2002. *Temporal variation in morphological configuration within a multi-bar surf zone at Wanganui, New Zealand.*

13. 2003. *Relationships between episodes of bar switching, cross-shore bar migration and outer bar degeneration at Wanganui, New Zealand.*

14. 2003. *A conceptual beach-state model for the inner bar of a storm-dominate, low to moderate tidal range coast at Wanganui, New Zealand.*

15. 2003. *Associations between net offshore bar migration and backshore erosion.*

16. 2004. *Beach cut in relation to net offshore migration.*

17. 2004. *Rip-associated bathing hazards on beaches characterised by net offshore bar migration*.

18. 2005. *Sediment budget implications associated with bar splitting within a net offshore migrating (NOM) bar system.*

19. 2007 *Bar splitting: system attributes and sediment budget implications for a net offshore migrating bar system.*

20. 2012 *Automated detection of breaking wave height using an optical technique.*

RESEARCH SUMMARY

1 INTRODUCTION

During the 1990s I was somewhat obsessed with developing methods of capturing coastal morphology and discovering the behavioural secrets of a site near Wanganui on the southwest coast of the New Zealand's North Island (Figure 1).

The motivation for investigating such sand bar behaviour came from a 1990 study of local rivermouth morphology using bathymetric charts routinely collected by the local harbour authority. In one instance, the rivermouth bar, which extended along the adjacent coast, migrated seaward then flattened out and disappeared (Publication 1). This fascinating, and not previously reported behaviour was very much in mind when the opportunity subsequently arose to select a PhD topic. The scene was set.

Figure 1 *The lower photo shows the 6 km long field site with the jetty controlled Wanganui Rivermouth in the foreground. The asterisk locates the camera site and the dashed white line marks the pre-jetty coastline.*

The Wanganui coast is wide, has multiple sand bars and is dominated by relatively high wave and wind energy (its stormy), this made standard methods of morphological and process data acquisition (such as bathymetric sounding, vertical aerial photography and in-situ metering) impractical at the desired spatial and temporal sampling scales. New approaches were necessary and photography and videography from an elevated position coupled with image processing, a relatively new field at the time, provided the means when coupled with traditional data collection.

The secrets were gradually uncovered, conceptually modelled and sediment dynamics hypothesised. This monograph summarises the journey and then reproduces the published literature as chronologically numbered appendices for those readers interested in the detail. The PhD thesis which contains much of the early research, has not been included due to size, but it is downloadable from the Massey University Library, or from the Coastal Systems Ltd web site (www.coastalsystems.co.nz).– The Abstract is included as Publication 2.

2 PHOTO AND VIDEO DATA ACQUISITION

The concept of collecting time-lapse photos using several minute exposure times (referred to as "time-exposure" images) came from Dr Rob Holman[1] of Oregon State University.

The subsequent computer transformation to produce a vertical (birds eye) perspective, as well as generating "time-stacks[2]" for analysing bar-crest behaviour and abstracting hydrodynamic data were developed under the guidance of Dr Don Bailey[1] who operated the Image Analysis Unit at Massey University.

An example of such photography and image processing for defining morphology and behaviour is shown in Figure 2, and relevant published papers are attached as Publications 3, 4, 5, 6, and 7. In such photos/images the higher intensity areas represent shallows while lower intensity represents deeper areas – the third dimension (elevation) is thus relative.

A sequence (panorama) of 8 such photos so transformed and merged together produced an intensity map covering six kilometres of coast by 500 m across-shore. Developing such methods and collecting/processing these maps acquired over 6 years formed the basis of the morphological identification and behaviour research findings contained herewithin. Interestingly, despite more recent technological advances, this remains the most practical and cost-effective way of collecting morphological information at these scales.

---

1. *Rob Holman would later set up the ARGUS camera and image processing network at several global sites, and Don Bailey would later modify the Wanganui algorithms for use with cameras established around the New Zealand coast by NIWA.*

2. *Time-stacks are generated by taking intensity slices along the same cross-shore transect for a sequence of rectified time-exposure images and stacking them next to each other. An example is given in Figure 2 (inset). The dots locate intensity maxima which have been joined to represent the bar migration track through time.*

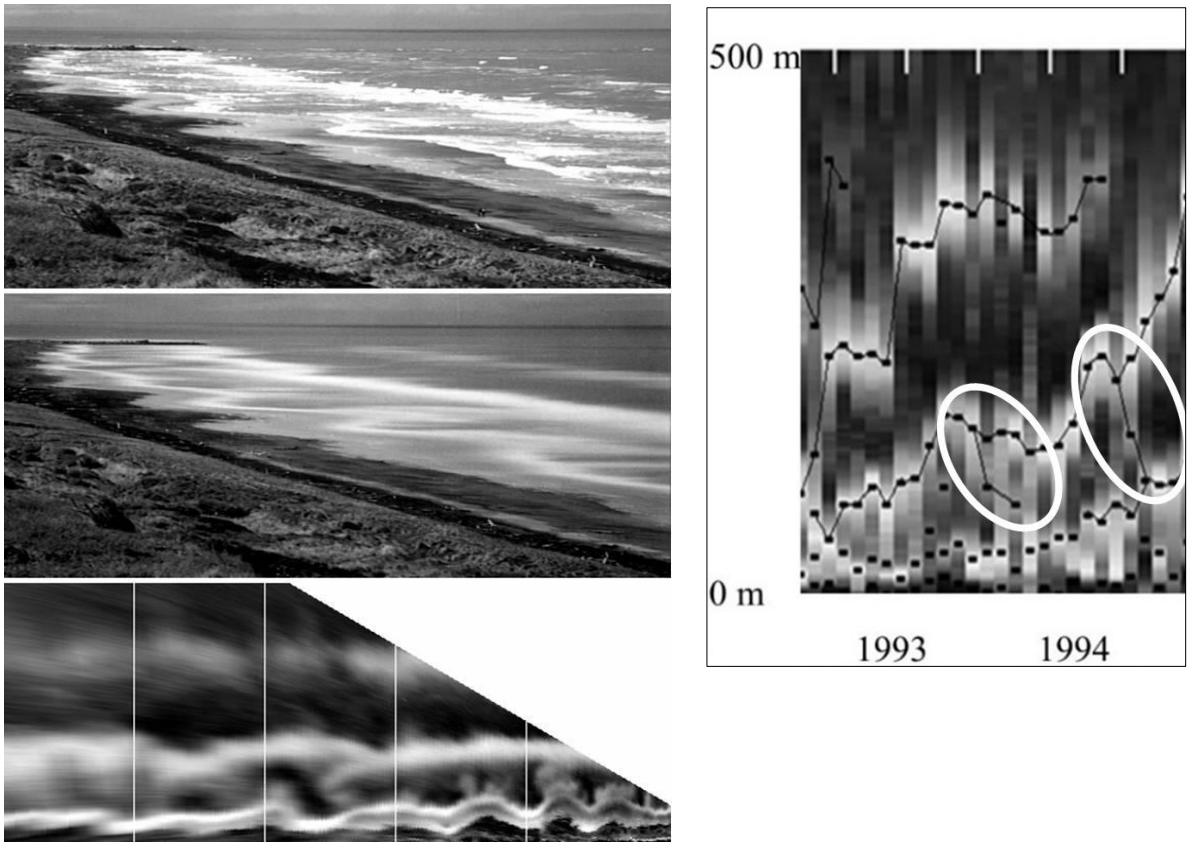

Figure 2 *Imagery from the Wanganui field site (rivermouth moles some 3200 m distant. The central ("time-exposure") image is the output from an SLR film camera fitted with a #96 neutral density filter and exposed for 5 minutes. The upper photo is the corresponding instantaneous (1/125th second) photo, and the lower image is the time-exposure image transformed (rectified) to give a birds-eye (vertical/metric) perspective. Inset is a 2 year "time-stack" image for a cross-shore transect located mid-way alongshore. The ellipses locate "bar splitting", a behaviour described in Section 4.1.*

3 CROSS-SHORE BAR MIGRATION

The dominant behaviour in the Wanganui data clearly consists of sandbars forming on the lower inter-tidal beach, systematically migrating seaward and then disappearing in the outer surf zone several years later - a 3-stage process referred to as net offshore bar migration or NOM. Examples of NOM time-series are shown in Figure 3.

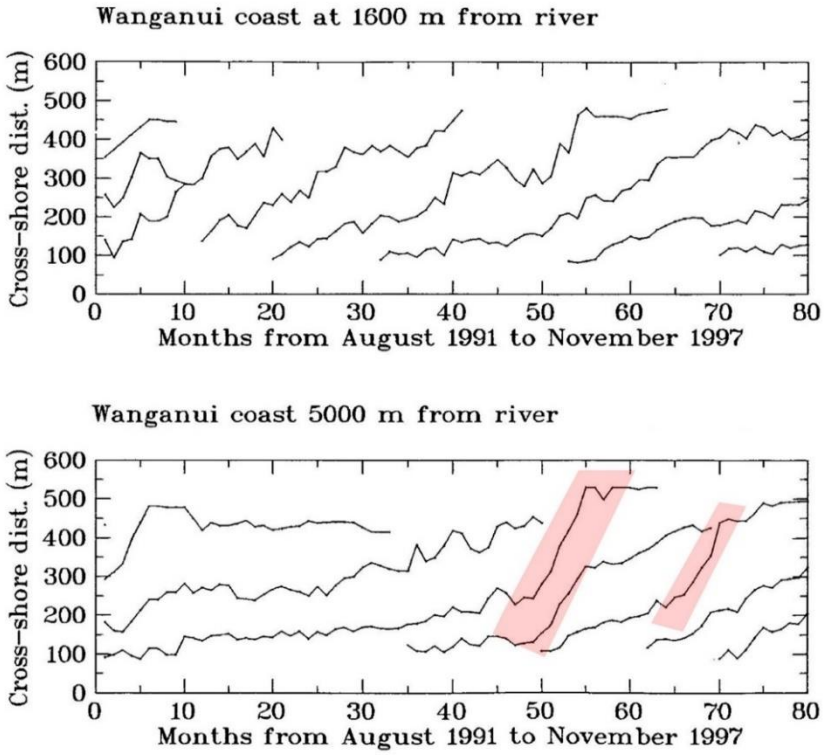

Figure 3 *Bar-crest time-series for two cross-shore transects on the Wanganui Coast with data derived from rectified time-exposure images and time-stacks. Distance datum is the foredune-toe. In the lower graph, the highlighted seaward "jumps" in bar location result from "bar switching", a behaviour described in Section 4.2.*

At the same time NOM and its behavioural characteristics were being investigated at Wanganui, the process had been discovered independently by specialist research organisations on the Dutch and North Carolina coasts. In the former case seabed measurement was by annual sounding along transects spaced 1 km apart, and in the latter, a sled-based instrument as winched along a single transect at fortnightly intervals (Publication 8). NOM behaviour varied in the different environments and enabled comparative analyses which found average NOM width could vary between 195 and 930 m, and corresponding NOM duration between 1.2 to 11.3 years. NOM duration was found to best represent the system and correlated with various sediment and energy parameters thus enabling an underlying drive-mechanism to be proposed. In particular, that the systematic seaward shift in bar location results from offshore directed current and sediment transport under storms conditions exceeding the onshore directed current experienced during intervening fairweather periods. In 1999 these results were published in the Journal of Coastal Research (see Appendix Publication 9) and were particularly well-received by the editors and also by the New Zealand Royal Society, the latter conferring the Hatherton Award 2000 (Publication 10).

4 MORPHOLOGICAL VARIATION

As illustrated in Figure 3, significant variation can occur in the offshore migration track for individual sand bars. Such variation was subsequently investigated by resampling and investigating the image data set, and this led to the identification of the following new morphological processes and relationships.

4.1 Bar Splitting

Bar splitting occurs where a section of sand bar splits in the longshore direction with the landward portion migrating onshore often to merge with the adjacent bar or with the intertidal beach, a process that could take several weeks to complete (see Publications 18 and 19). An example of bar splitting is shown in Figure 4. Bar splitting happens on the landward section (horn) of crescentic bars, especially where that section is overly long and/or voluminous. Bar splitting causes a bifurcation in the bar-crest time-series – two of which are marked on the insert time-stack in Figure 2.

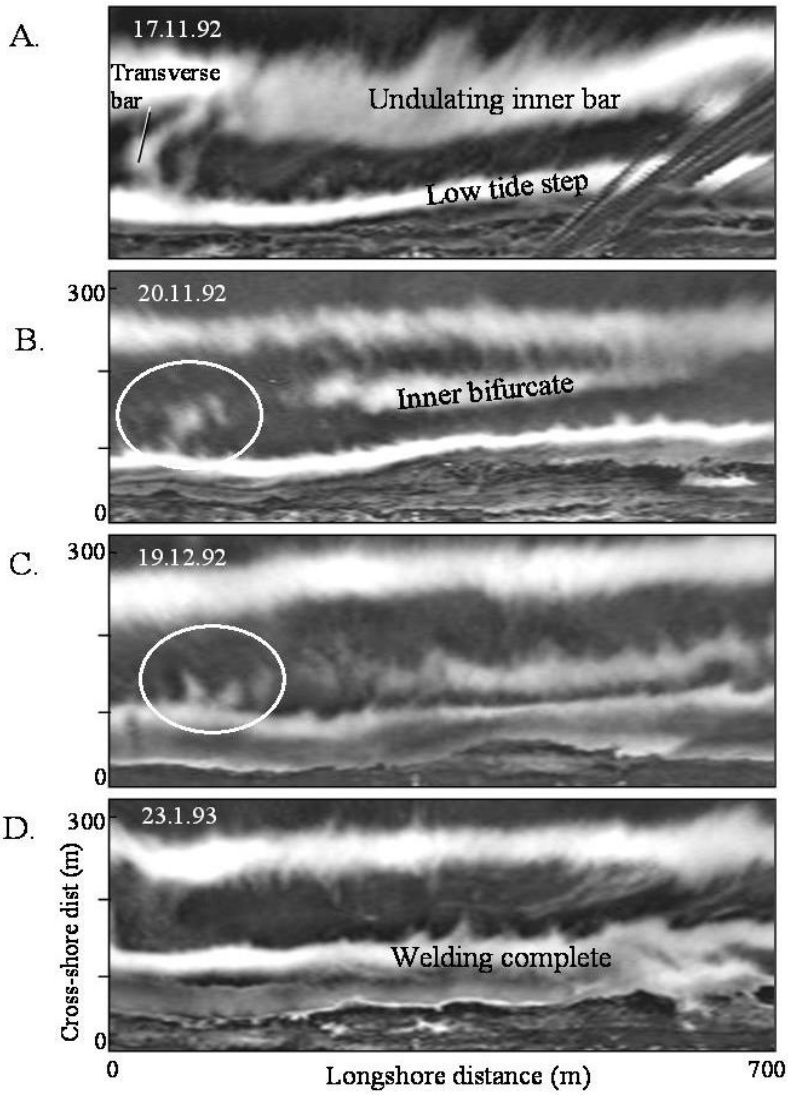

Figure 4. *An example of bar splitting at Wanganui using a sequence of rectified time-exposure images. The form of the bar prior to splitting is depicted in A, with B illustrating the subsequently bifurcated morphology. The inner bifurcate has progressed landward in C, and has welded to the inter-tidal beach in D. The ellipses in B and C depict the transverse bar marked in A, merging with the inner bifurcate and thus welding to the beach. This transverse bar occurrence and behaviour was a common observation and appears to be and integral part of the bar splitting process.*

4.2 Bar switching

Bar switching occurs where a shore-parallel bar separates such that one side realigns with a more landward bar and the other with a more seaward bar, a process that could take several months to complete. An example of bar-switching is shown in Figure 5. In this case switching progresses from the outer surf zone to the intertidal beach and is referred to as a "shoreward propagating switch episode". Alternatively, a less common behaviour is where an episode began in the central surf zone and the switch location remains approximately stationary, this being referred to as a "stationary switch episode". The occurrence and type of switching appeared to be controlled by variation in alongshore sediment volume within the outer surf zone. The time-stack switch signature is typically a very rapid change in bar location such as demonstrated by the highlighted bar tracks in Figure 3. For further explanation of bar switching see Appendix Publications 11 and 13.

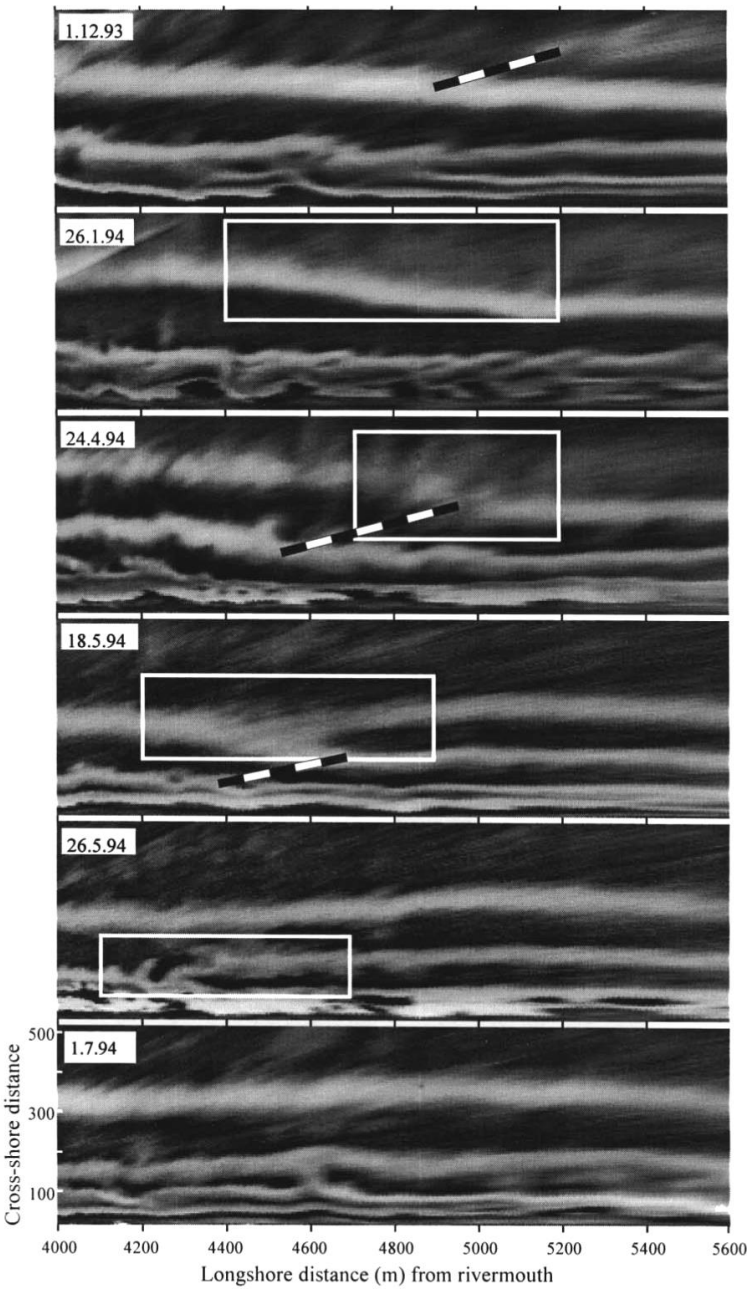

Figure 5 *An example of shoreward propagating bar switching at Wanganui using rectified time-exposure imagery. The bold dashed lines show where switching is about to happen and the rectangles define the transition zones within which switching is occurring.*

4.3 Morphological configurations

Morphologcal configurations were found to systematically change as a bar progresses seaward during a NOM cycle (Publications 12, 17). An example of classification-based configurations using rectified images is shown in Figure 6, with a typical configuration sequence depicted in Figure 7. Of note is how the size/length of rip channels increase (Publication 14) as the (inner) bar extends seaward during NOM– suggesting this mechanism is effective in transferring sediment seaward.

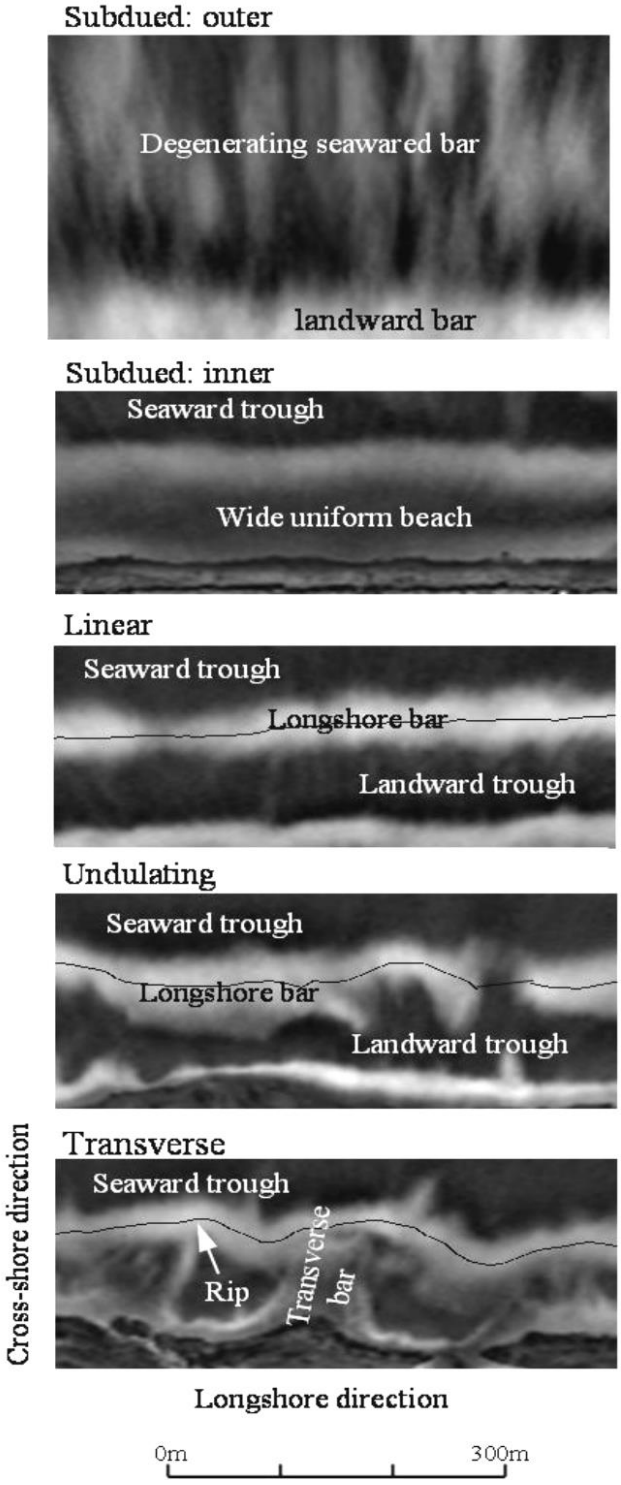

Figure 6 *Rectified time-exposure imagery illustrating the differing morphological configurations found in the study area.*

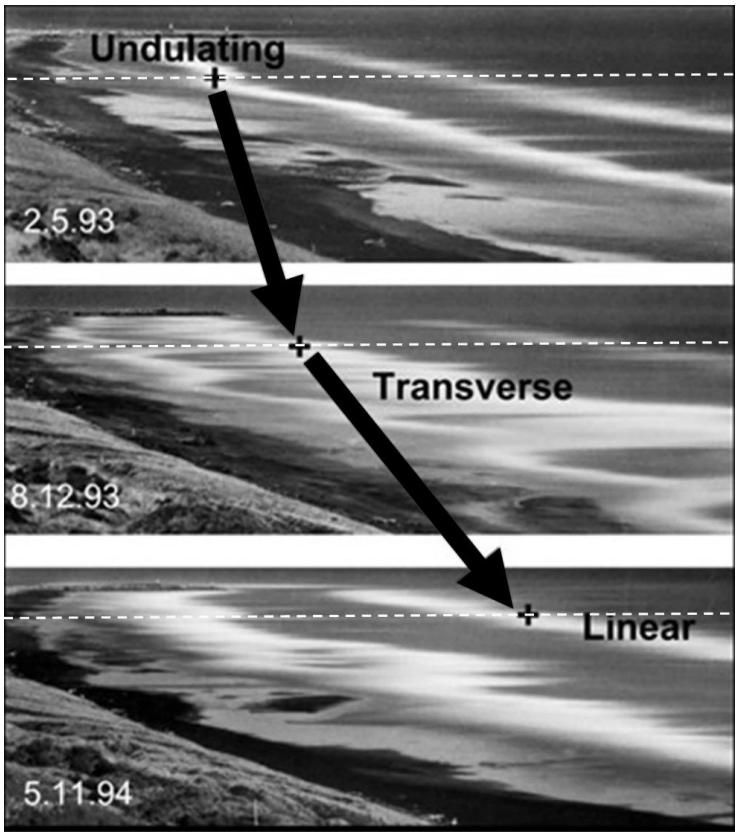

Figure 7 *Typical morphological configurations which accompany a NOM cycle. Here NOM is occurring along the dashed-line transect on these non-rectified time-exposure images. It is accompanied by.*

For completion, inner bar transitions from one configuration (State) to another were detected, and their relationship with wave/longshore current, tide and antecedent morphology, modelled (see Figure 8); this is described in detail in Publication 14.

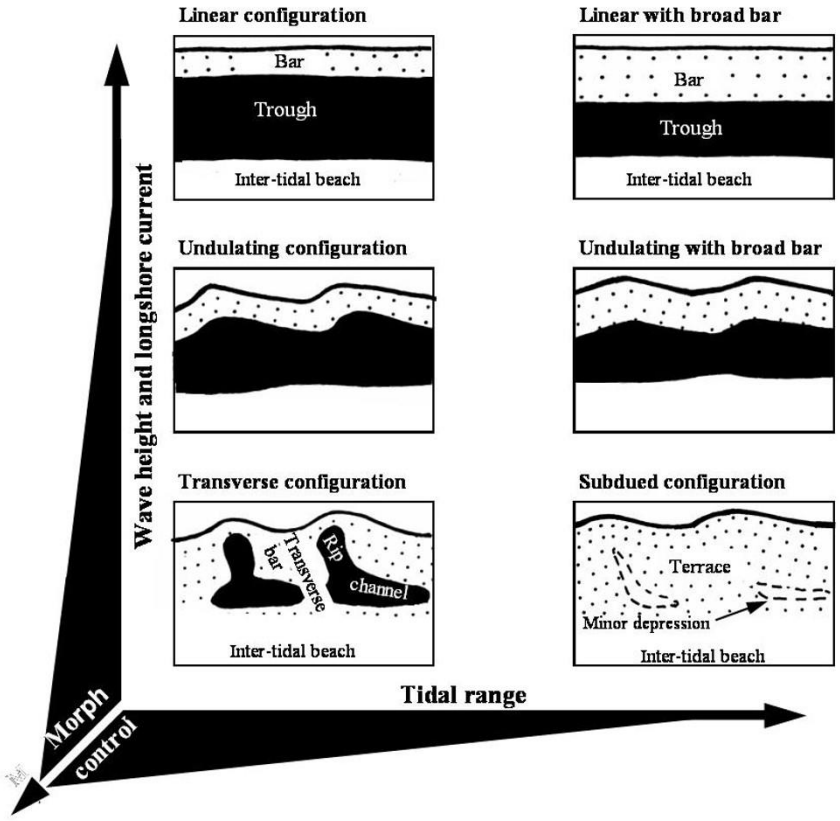

Figure 8 *Schematic representation of inner bar configurations and transitions, and their relationship to wave height and longshore current, tide range (neap/spring) and relative importance of morphological control.*

4.4 Shoreline erosion

Different types of shoreline erosion were found to correspond with the NOM cycle and modelled in Figure 9, which includes both morphological configurations and wave forcing. The most extensive type, lateral erosion, occurred when the seawardmost bar was in a subdued state and only a single bar occurred within the surf zone, thus enabling greater wave energy to reach the shoreline. Lateral erosion of the foredune toe could extend alongshore for hundreds of metres and the escarpment exceed 3 meters when driven by storm waves coupled with a higher (spring) tide range. Rip-embayment erosion occurred under a transverse configuration and well -developed seaward bar morphologies - ranging between 50 and 100 m alongshore and 1 to 2 m high escarpment. Overwash channel erosion was a miner feature typically limited to about 0.5 m and it occurred when seaward bars were well- developed. For further explanation see Appendix Publications 15 and 16

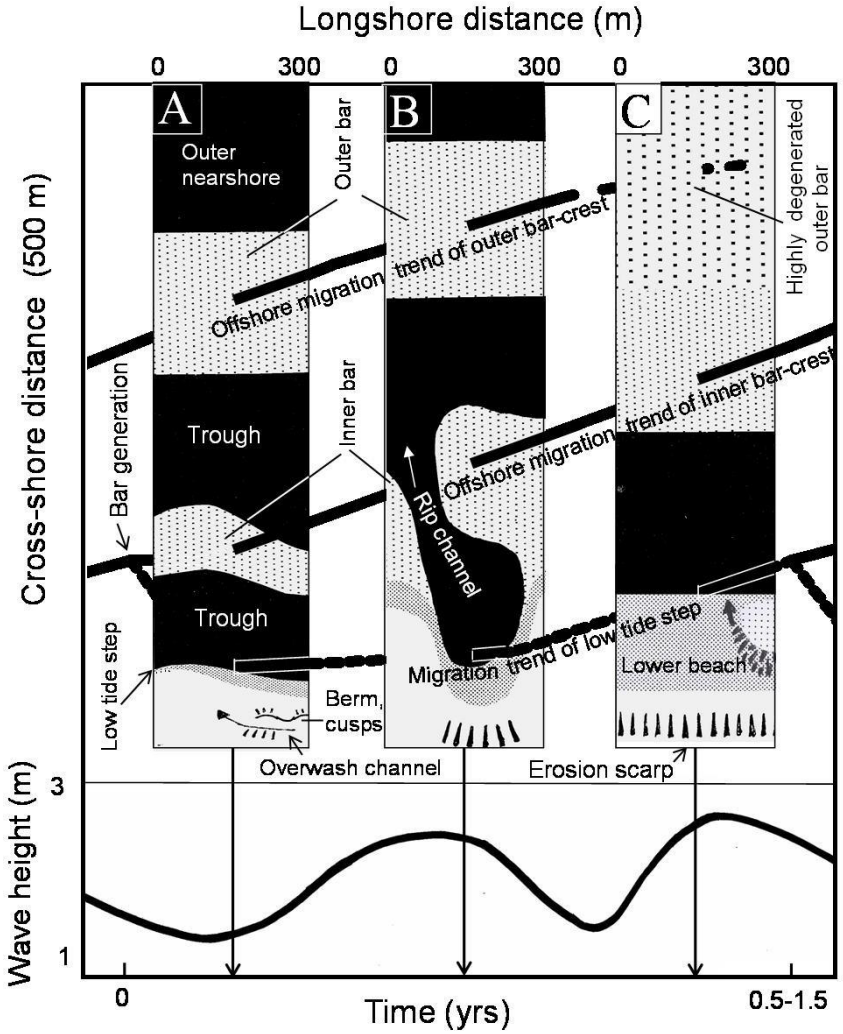

Figure 9 *Conceptual model illustrating the relationships between types of beach cut and NOM for the Wanganui study site data. Variation in morphological configuration and wave height are included. Panel A depicts overwash channel and berm-front erosion, Panel B depicts rip-embayment erosion and Panel C depicts laterally extensive erosion.*

5 BALLANCING SEDIMENT TRANSPORT

While the sediment supply was found to be important in terms of controlling the nature and timing of episodes of seaward bar migration, of particular interest was the lack of relationship between the existence of NOM and longer-term shoreline behaviour (erosional, stable or accretional). Given that net sediment transport is directed seaward or landward under storm or fairweather conditions respectively, NOM coasts may be expected to be erosional over the longer-term. This led to a focus on landward-directed sediment transport mechanisms and resulted in the hypothesed conceptual model shown in Figure 10. The model is further explained and detailed in Publications 18 and 19.

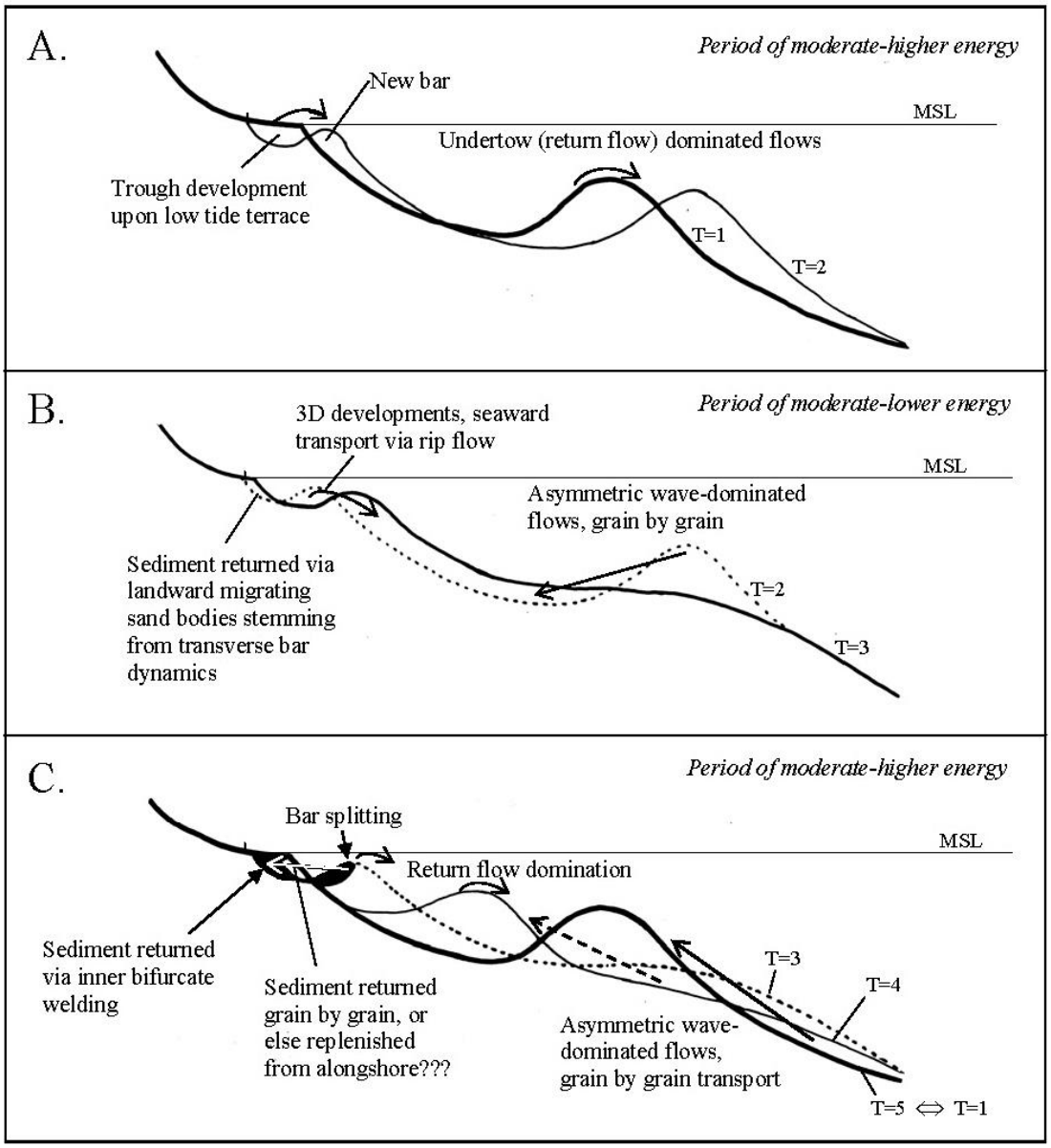

Figure 10 *Conceptual model of bar migration/sediment transport mechanisms for the NOM system at Wanganui to enable, over time, a balanced shoreline sediment supply. At time T=1, the profile contains a single sub-tidal sand-bar; this profile being replicated by T5 after a cycle of NOM. Hypothesised sediment transport mechanisms are marked.*

6 FOLLOW-UP

The need to refine and test the NOM-associated sediment transport models led to a renewal of image-based data collection at the site in 2009 and this continued for several years. Some progress was made in data abstraction; for example, a method was developed to accurately define breaking wave height at any location within the surf zone (Figure 11, Publication 20) – the potential of which was earlier raised in our research (see Publication 5).

But while the morphological imagery helped better define the onset and the progression of key behaviours, more pressing projects meant that we were unable to develop a method to quantify that all important third (elevation) dimension. This endeavour has also eluded other researchers who have resorted to methods such as drone or helicopter GPS-based "dip-sticking", or towing sonar devices within the surf zone using very shallow draft vessels – all accurate, but too limited in temporal and spatial sampling, and restricted by wave and weather conditions.

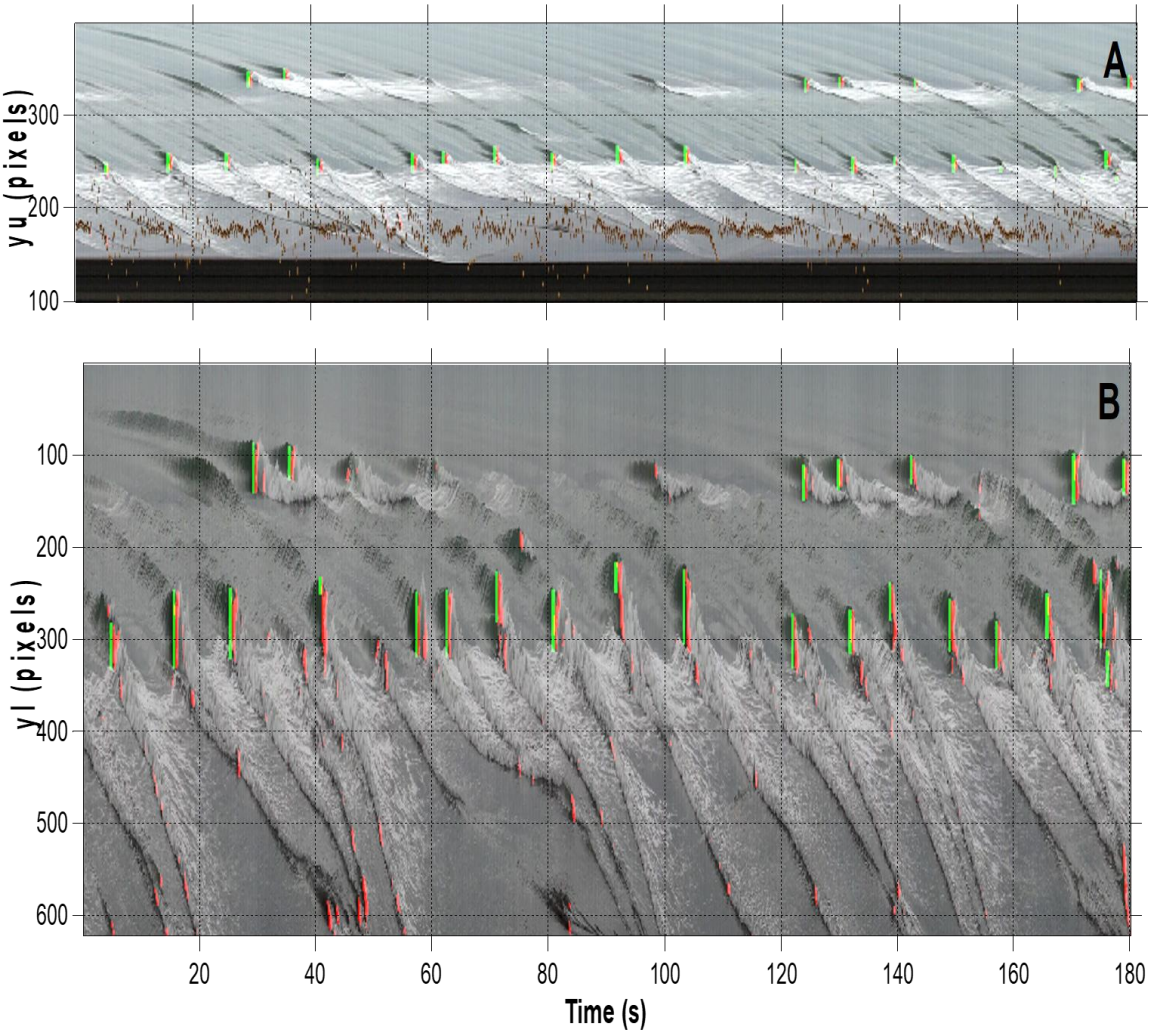

Figure 11. *Image processing used to define breaking wave height. In these examples, sampled from the Wanganui Site in 2010, the time-stacks have been subject to edge detection (red) used to extract break-point distance from the upper camera (A) and the vertical extent of the breaking edge defined by green strips used to extract wave height from the lower camera (B) .*

7 CONCLUSIONS

The advent of image-based approaches to define both surf zone morphology and behaviour in the 1990s, and also to obtain simultaneous hydrodynamic data (waves and currents), led to an investigative surge as this hostile environment became open to research.

For researching the morphology and behaviour of high energy surf zones the results were substantive, and several practical applications followed. For example, predication of bar location could assist port managers in planning rivermouth dredging programmes, and configuration predictability, in particular rips, could assist surf lifesaver resource allocations. The discerning surfer could also benefit from rip prediction as well as recognising bar switch and bifurcation occurrence as all these behaviours can generate morphologies angled to the approaching wave fronts, i.e. with suitable “peel angles” for surfing waves.

But, as typically occurs with new technologies, the implementation/research potential was quickly explored and exhausted. This has left hypotheses regarding some fundamental aspects of NOM to be addressed by future scientists and practitioners - questions which, to some extent, must await new methodological innovation from another generation of researchers.

APPENDICES (PUBLICATIONS)

1

Shand, R.D., 1990. **(ABSTRACT ONLY)** The subaqueous morphology at the entrance to a jetty controlled river mouth on a moderate to high energy littoral drift dominated coast: Wanganui, New Zealand 1981-1987. Research project: Post-graduate Diploma in Science, Massey University, New Zealand, 102p.

CHAPTER I

INTRODUCTION

The Wanganui River (Figure 1) is the third longest river in New Zealand. Its navigable entrance ensured rapid human settlement of the Wanganui region. The bathymetry of the rivermouth area, however, was particularly variable and as this presented a hazard to shipping, and a constraint on development, control structures in the form of entrance jetties were established between 1880 and 1938 (Figure 2).

When completed these works greatly increased the morphological stability and depth at the river entrance but bar and channel variability still occurred. In 1925 monthly soundings were initiated and these have continued at varying regularity and density up to the present day.

This study investigates the entrance morphology over the period from 1981 to mid 1987 which is the longest period continuously free from the influence of dredging during the last decade. Analysis of the record over a period of such length was considered necessary given the natural variability which was known to occur within the system.

2

Shand, R.D., 2000. **(ABSTRACT ONLY)** Offshore migration of coastal sand-bars at Wanganui New Zealand. PhD thesis, Massey University, New Zealand, Miscellaneous Publication Series 2000/8, 295 p.

ABSTRACT

Net offshore bar migration (NOM) refers to the systematic seaward migration of coastal sand-bars across the surf zone. These bars form near the shore-line and disappear in the outer surf zone. NOM behaviour is repetitive and has been described as cyclic. Over the past decade NOM has been recognised on the North Carolina coast, the Dutch coast and by the author on the west coast of the New Zealand North Island. The aim of this project is to elaborate on the behaviour and causative processes of NOM.

The New Zealand data used in this study comprise a 6.3 year bar-crest record from an approximately six kilometre long field site at Wanganui. These data were collected using aerial and terrestrial photography and supplemented with ground surveys. Image processing techniques were developed for photographic data abstraction and analysis. Published data from the other 'global' NOM sites were analysed and compared after data compatibility procedures had been developed and applied. The NOM cycles were quantified using parameters for NOM width (cross-shore migration distance), duration and rate, together with return period.

The global NOM sites are characterised by multiple sand-bars, the predominance of sea waves and a narrow band of storm strength wind and wave conditions. The longer-term (average cyclic) parameter values for the global data-set were as follows: NOM width ranged between 195 and 930 m; duration ranged between 1.2 and 13 years; NOM rate ranged between 35 and 196 m/yr, and NOM return period varied between 1.2 and 14.4 years. NOM characteristics for the global sites were found to be correlated with cross-shore slope, coastal orientation and extreme wave height.

The Wanganui bar-crest data were also analysed for shorter-term (within-cycle) bar behaviour. Cross-shore bar migrations had a bimodal frequency distribution. The group of larger migrations, termed 'episodic seaward jumps', significantly influenced the characteristics of individual NOM cycles. Episodic seaward jumps appear to be preceded by the degeneration of the adjacent seaward bar. Longshore non-synchronous variation in NOM characteristics were found to be mainly related to 'bar switching' (longshore bar realignment).

Based on the above results, a conceptual morphodynamic model for NOM was formulated. The model incorporates three main components: a drive mechanism; a morphodynamic modification mechanism; and a timing mechanism.

Net offshore bar migration is a significant mode of morphological behaviour within the surf zone. Its influence upon other aspects of coastal geomorphology such as shoreline change, and its relationship with existing 'beach-state' based models, require further investigation.

3

Bailey, D.G., and Shand, R.D., 1993. Determining large-scale sand-bar evolution. Proceedings of the 1st New Zealand Conference on Image and Vision Computing, pp. 109-116.

Determining Large Scale Sandbar Evolution

Donald G. Bailey and Roger D. Shand

Image Analysis Unit, and Geography Department
Massey University, Palmerston North
Ph: +64 6 350 4063, Fax: +64 6 354 0207
E-mail: D.G.Bailey@massey.ac.nz

Abstract

To study the morphology of coastal sandbars and their change with time, it is necessary to obtain a sequence of bathymetric maps over the period of interest. Traditional techniques such as vertical aerial photography or echosounding over a grid are expensive and subject to environmental constraints, especially in higher energy situations. Photographic methods assume that the position and intensity of waves breaking on bars are strongly related to the position and depth of the bars. An alternative approach is to use image processing to transform a panorama of photographs taken from adjacent elevated ground.

The individual photographs are normalised with respect to lighting variations, and rectified to map coordinates using the horizon and two ground control points. However, the coordinates of interest are longshore and offshore distances. A smooth curve is therefore fitted through the shore baseline, and the image warped to make this line straight. The sandbar crest positions within in this image are detected, and then tracked with time to investigate how the bars evolve.

1. Background

A significant and increasing proportion of the worlds population and wealth is concentrated in the sand-dominated coastal zone [1]. This region, however, is highly variable and unstable with erosion exceeding deposition globally [2,3]. The predicted greenhouse associated sea-level rise is likely to exacerbate this situation [4,5]. There is clearly a practical need to maximise our understanding of the Earth's coastal systems.

The coastal zone can be subdivided into a number of interrelated subzones or subsystems, each characterised by distinctive processes and morphologies (see figure 1). Contemporary geomorphological field studies have tended to concentrate on the inner nearshore and backshore zones of low to moderate energy coasts [6], because of their relative ease of access.

To facilitate comprehensive nearshore investigations, in particular those on moderate to high energy coasts, methods of acquiring morphological data at a variety of scales, both spatial (10^1 to 10^{3+} metres longshore) and temporal (10^0 to 10^3days), are required.

2. Existing methods of bathymetric sampling

A variety of techniques have been used for bathymetric sampling and a summary is given in table 1. Ideally accurate 3-dimensional data is required for morphodynamic modelling. However, cost, longshore coverage limitations, and logistical problems prohibit the

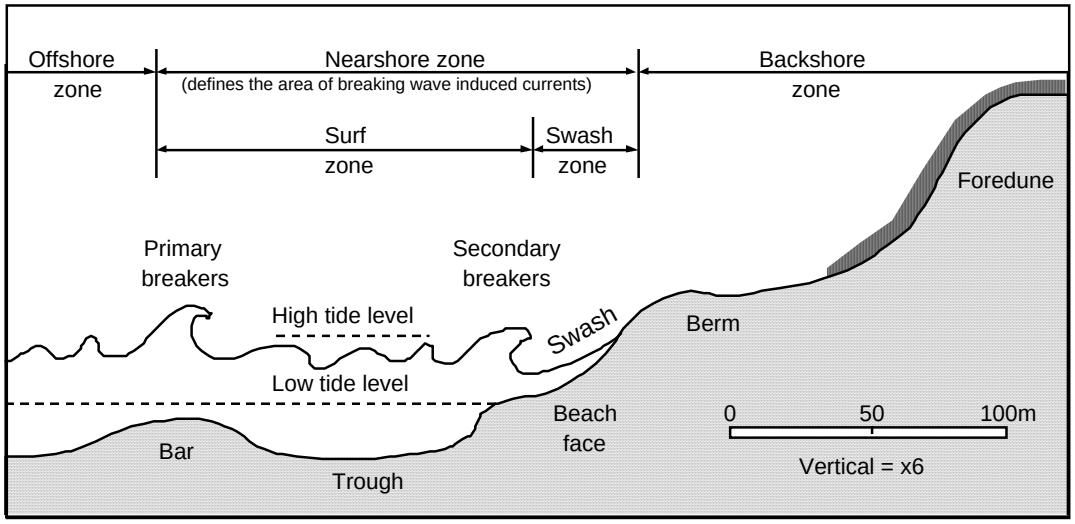

Figure 1: Profile depiction of typical (marine driven) coastal morphodynamic zones.

widespread use of the most definitive methods (A and B) especially in higher energy environments.

Imaging techniques (C and D) increase longshore coverage and utilise increased energy levels in the form of the breaking wave pattern and intensity to signal form and relative depth [7]. Atmospheric restrictions (cloudless conditions) and high costs restrict the aerial (including satellite) option.

A recent development has been elevated terrestrial imaging (C) incorporating rectification of the oblique pictures to map coordinates (vertical projection), and long-exposure techniques to improve morphological feature definition. This cheap and flexible method has great potential especially for the higher energy sand-dominated environments which also tend to be backed by elevated ground [8] suitable for camera sites.

Technique	Description	Environment for regular sampling	Coverage per day	Cost per day	Accuracy 3-D
A. Bottom moving instruments	Longshore transits. Offshore distances by EDM or cable. Depths by EDM or pressure transducer	Low/mod energy	Low	High	High
B. Surface moving instruments	Longshore transits. Offshore distances by sextant or EDM. Depths by echosounder	Low/mod energy	Low	High	High
C. Elevated terrestrial imaging	Oblique photo/video. Time exposure option. Location by grid overlay or rectification. Depth inferred from wave intensity	Mod/high energy	High	Low	Location high, depth mod
D. Aerial imaging	Vertical photographs. Location by reference points or rectification. Depth by waves or visible forms	Low/mod/ high energy	High	High	Location high, depth mod

Table 1: Nearshore morphological sampling: main methods and characteristics.

2.1 The rectified long exposure method

The initial work in developing this approach can be credited to Rob Holman and Tom Lippmann at Oregon State University. They utilised a 40 m tower and the extensive

resources of the US Army Corps of Engineers CERC Field Research Facility on the Outer Banks of North Carolina to refine and ground truth-test the technique (see [7] and [9]).

Their work, however, was based on the use of a single longshore image covering a rectified length of up to 660 m. Their images were taken at the same time each day regardless of atmospheric, sea or tide conditions, all of which greatly affect image quality and bathymetric representativeness.

It is necessary to explore the limits and possibilities of the method with respect to the morphological scale objectives described above. This paper covers our image processing work while the other aspects, that is the influences of equipment and environmental variations, are reported elsewhere [10].

3. Objectives

A panorama of eight photographs was taken from a single site 100 m behind and 43 m above the spring high tide mark. The four central shots were taken using a 55 mm focal length lens to give good coverage of the area without sacrificing detail. To obtain satisfactory resolution for the four end shots, a 135 mm focal length lens was used. Each photograph was taken using a three minute time exposure to average the effects of individual waves. The following image processing steps were carried out to maximise the resolution potential and to facilitate statistical analysis:

- Compensate for variations in image density.
- Enhance images such that 3-dimensional detail and longshore coverage is maximised.
- Correct for perspective distortion, including automatically calculating the horizon location and camera tilt.
- Straighten the coastline while minimising shore-normal distortion.
- Detect shore-parallel intensity maximums corresponding to the bars.

4. Image preprocessing

A 512 x 512 image is captured of each photograph, with a 2:3 aspect ratio. While capturing the photographs, it is ensured that the top and bottom edges of the photographs are visible in the image since these are required for determining the camera tilt. It is also ensured that the left and right edges of the photographs are out of the field of view, otherwise artefacts may be introduced when mosaicing the photographs.

Since the panorama spans about 160° there is a considerable variation in lighting from one photograph to another because of differing sun angles. In addition to this, there may be sun glare from the sea or clouds and vignetting caused by the lens and neutral density filters. These effects are all exacerbated by reciprocity failure caused by the long exposures required. The first step is to normalise the contrast range of each image as much as possible. This contrast normalisation is performed using the following steps:

1. The image is filtered by selecting the minimum pixel value within a 21 x 21 pixel box. This effectively shrinks the lighter regions of the bars preventing them from being removed by the process. At this stage we are interested in finding the background level.
2. This image is then filtered using the average pixel value within a 55 x 55 pixel box to obtain an estimate of the local average density. Variations in this image correspond to density variations in the original image.
3. The average is subtracted from the original image to remove the density variations. An offset of 128 is added to allow negative differences to be represented conveniently.

Figure 2: A typical image after normalising variations in lighting and enhancing the contrast.

4. Finally, the contrast of the image is enhanced using a linear stretch to expand the range of pixel values from 116 to 208 to fill the available range (0 to 255).

The resulting contrast normalised image is shown in figure 2.

5. Rectification

Each photograph has perspective distortion resulting from the viewing geometry. This distortion must be removed before the individual photographs can be mosaiced to give the full panorama. Finally, since the coast is curved, the image needs to be warped further to put the information into a form that is convenient to use.

5.1 Correction of perspective distortion

The first step in this process is to correct for the perspective distortion present in each of the images. At this stage, a convenient coordinate system is based on map coordinates. We have actually used rotated map coordinates since the stretch of coast under study runs SE to NW, resulting in unnecessarily large images to contain the detail of interest.

If we assume that the earth is flat (a reasonable assumption since the ranges of interest are within 3.5 km from the camera location) the perspective correction equation may be represented by

$$X = \frac{a_0 x + a_1 y + a_2}{a_6 x + a_7 y + a_8}, \quad Y = \frac{a_3 x + a_4 y + a_5}{a_6 x + a_7 y + a_8} \qquad (1)$$

where (x,y) are the pixel coordinates in the image before rectification, and (X,Y) are the corresponding rectified coordinates. Note that this equation will only correctly transform one 2-D plane to a second 2-D plane. The input plane is the film plane of the camera, and the output plane corresponds to sea level. The 9 unknowns in equation (1) are solved by knowing the camera position, the positions of two surveyed ground control points (GCPs) within each image, the sea level, and the horizon. The common denominator of the perspective transformation represents the perspective vanishing line in the photographs.

$$a_6 x + a_7 y + a_8 = 0 \qquad (2)$$

If the earth were truly flat, this line would correspond to the horizon. However, because of the curvature of the earth, the apparent horizon will be below the true "flat earth" horizon (figure 3). It can be shown that the angle between the true and apparent horizon is

$$\theta \approx \sqrt{\frac{2h}{R}} \tag{3}$$

where h is the height of the camera above sea level, and R is the radius of the earth. Although this angle is small ($\theta = 0.21°$ for h =43 m), the error is significant, giving a 4 pixel shift in the horizon for photographs taken using a 55 mm lens and a 9.5 pixel shift with a 135 mm lens.

From the positions of the ground control points in the image, the position of the apparent horizon is estimated. A linear edge detection operation is applied within that region to detect the maximum intensity gradient (corresponding to the horizon). A least squares fit is applied to the detected points to give the line of the horizon. This is then corrected for θ to give a_6, a_7 and a_8. Note that equation (2) is normalised so that

$$a_6^2 + a_7^2 = 1 \tag{4}$$

The program draws the detected horizon on the input image and asks the user if it has been detected correctly. If not, the user defines the correct horizon by entering two points. This step is necessary because the position of the horizon may not be detected accurately if the weather is hazy or if the sea has rough and calm patches on it.

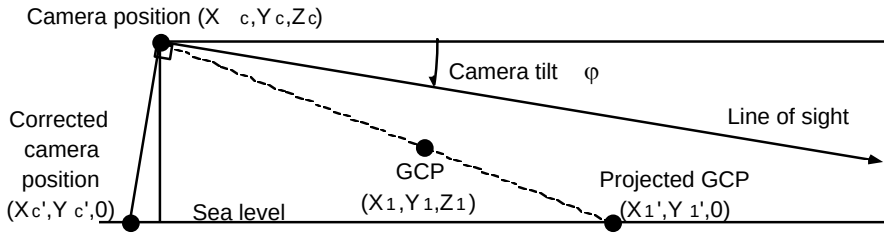

Figure 4: Correcting for camera tilt and projecting ground control points to sea level.

The next step is to reference the camera and ground control points to sea level (the reference plane for our perspective corrected image). The GCPs are projected to sea level as shown in figure 4. This projection may be represented as in equation (5).

$$X_1' = \frac{Z_1 X_c - Z_c X_1}{Z_1 - Z_c}, \quad Y_1' = \frac{Z_1 Y_c - Z_c Y_1}{Z_1 - Z_c} \tag{5}$$

Lines perpendicular to the horizon on the input image all fall on planes which pass through the camera. Therefore these lines all converge at the camera point in the rectified image. If the camera is tilted below the true horizon, the point of intersection of the horizon perpendiculars will move behind the camera as shown in figure 4. It is assumed that the pixel mid way between the top and bottom edge of the photograph is along the line of sight of the camera (that is normal to the film plane). The tilt is calculated knowing the angle of the line

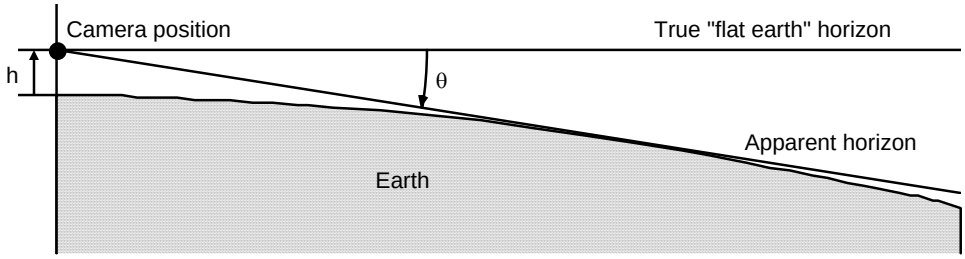

Figure 3: Error between true horizon and apparent horizon.

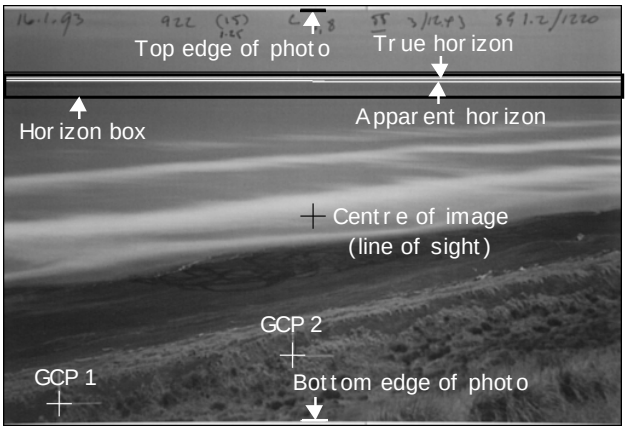

Figure 5: The input image with key features labelled.

of sight below the true horizon. The camera position may be referenced to sea level as

$$X_c^{'} = X_c - Z_c \tan\varphi \sin\gamma, \quad Y_c^{'} = Y_c - Z_c \tan\varphi \cos\gamma \tag{6}$$

where γ is the direction of the line of sight. In practise, the direction of the line of sight is calculated by solving equation (1) assuming no tilt (using (X_c,Y_c)). The centre pixel of the image (256,256) is then transformed to give the direction of the line of sight. This is used to correct the camera position for tilt and equation (1) is solved again. Figure 5 shows the input image with the key features labelled.

Lines perpendicular to the horizon intersect at the corrected camera position after transformation. These lines may be parameterised by

$$x = a_6 t + b_0, \quad y = a_7 t + b_1 \tag{7}$$

where b_0 and b_1 are arbitrary constants. Substituting these into equation (1) gives

$$\begin{aligned} X_c^{'} &= \underset{t\to\infty}{Limit} \frac{a_0(a_6 t + b_0) + a_1(a_7 t + b_1) + a_2}{a_6(a_6 t + b_0) + a_7(a_7 t + b_1) + a_8} \\ &= \frac{a_0 a_6 + a_1 a_7}{a_6^{\,2} + a_7^{\,2}} \quad = a_0 a_6 + a_1 a_7 \end{aligned} \tag{8}$$

Each GCP gives a further independent equation in a_0, a_1 and a_2, as in equation (9).

$$\begin{aligned} X_1^{'} &= \frac{a_0 x_1 + a_1 y_1 + a_2}{a_6 x_1 + a_7 y_1 + a_8} \\ &= \frac{a_0 x_1 + a_1 y_1 + a_2}{H_1} \end{aligned} \tag{9}$$

where H_1 is a constant (all its terms are known). Equation (8) and equation (9) for each GCP give three simultaneous equations that are solved to give

$$\begin{aligned} a_0 &= \frac{X_c^{'}(y_1 - y_2) - a_7(H_1 X_1^{'} - H_2 X_2^{'})}{a_6(y_1 - y_2) - a_7(x_1 - x_2)} \\ a_1 &= \frac{a_6(H_1 X_1^{'} - H_2 X_2^{'}) - X_c^{'}(x_1 - x_2)}{a_6(y_1 - y_2) - a_7(x_1 - x_2)} \\ a_2 &= X_1^{'} H_1 - a_0 x_1 - a_1 y_1 \end{aligned} \tag{10}$$

Similar equations may be obtained for a_3, a_4 and a_5. Equation (1) is then used to transform each pixel in the input image, giving figure 6. The transformed image is sampled with 2 m resolution.

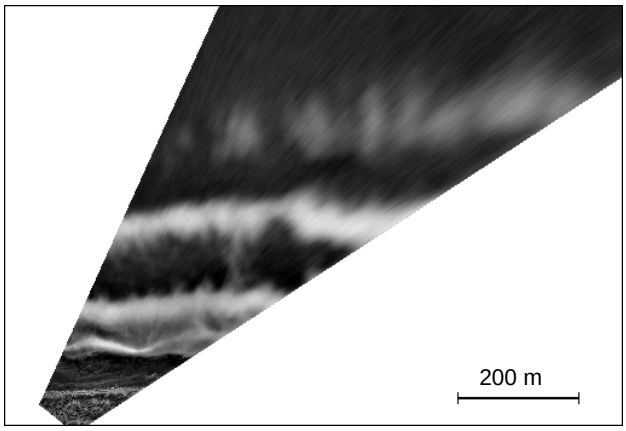

Figure 6: The perspective corrected image.

5.2 Mosaicing

After correcting for perspective distortions in each of the eight input photographs, the images are combined into a single view of the coast. The views provided by the individual photographs overlap slightly. To reduce the possibility of artefacts from the joins, in the region of overlap between adjacent views, the images are merged using a linear spline as shown in figure 7. The resulting mosaic is shown in figure 8.

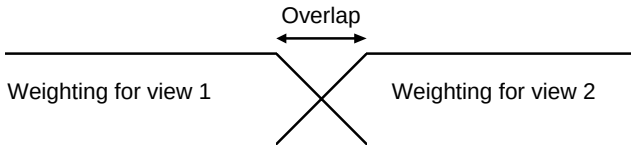

Figure 7: Linear spline applied to the overlap between images.

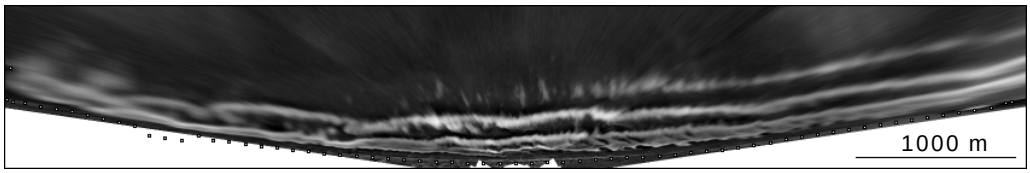

Figure 8: Mosaic of eight perspective corrected images.

5.3 Straightening of coastline

In determining the positions of the bars, a more useful coordinate system is longshore and offshore coordinates. To facilitate conversion to these coordinates, a separate series of ground control points was surveyed along the toe of the foredune at 100m intervals. These points define the baseline for offshore distance measurements. A smooth curve is fitted to these points using a piecewise parabolic fit. A least squares parabolic fit is made over 1000 m sections, with 500 m overlap between the sections. The overlapping regions are combined using a linear spline.

The image is then incrementally rotated (or unrolled) to make the baseline straight. At each point along the baseline, the shore normal is calculated and the image resampled along the shore normal. The resulting image is shown in figure 9. Having the offshore and longshore variations separated enables the offshore scale to be amplified to highlight the sandbar morphology.

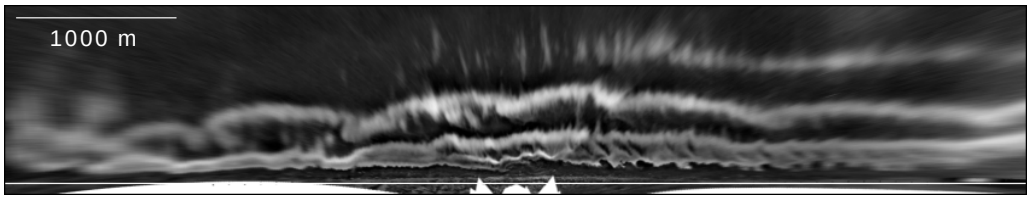

Figure 9: Image after straightening the coastline (offshore distance scale x2).

6. Detection of sandbars

The next step is to detect the positions of the sandbars. The positions of the bar crests can be inferred from the position of maximum intensity along the bar. Although not completely accurate (since the position of maximum intensity depends on both the tide and wave energy) this measure provides the best estimate from the information available. The bar crests are detected using the following steps:

1. The image is filtered by selecting the maximum pixel within a 1 x 21 pixel box. This is then subtracted from the image before filtering. The difference will be 0 only in the positions of local maxima, where local is defined by the 1 x 21 box. By thresholding the difference to select only the 0 pixels, the positions of all the local maxima are detected in the image.
2. Many of the local maxima detected correspond to noise, so the image is ANDed with the original to obtain the maximum values. This is then thresholded at an intensity of 80 to select only the significant maxima, corresponding to the bar crests.
3. Finally the detected crests are thinned to a single pixel thickness. The resulting image is shown in figure 10 overlaid on the original.

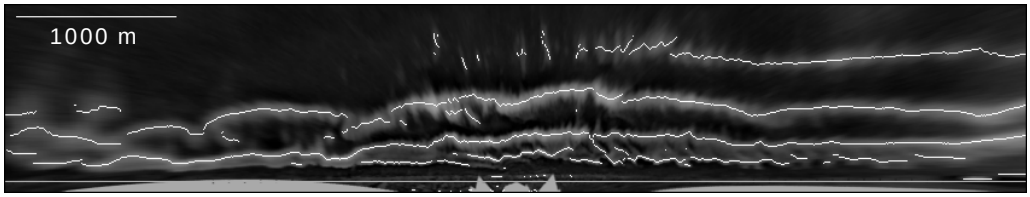

Figure 10: Detected sandbars (offshore distance scale x2).

Quantitative measurements may be made of the bar positions by measuring the offshore distances of the bars from the baseline. By examining a series of images taken at regular intervals, the morphodynamics of the coastal system may be investigated.

7. Summary

An inexpensive method of obtaining data for studying the time evolution of sandbars on moderate to high energy coasts is to use elevated terrestrial imaging. A panoramic series of eight oblique photographs are normalised with respect to lighting variations and rectified to map coordinates. The resulting mosaiced image is warped again, straightening the coastline, to give the more useful longshore and offshore coordinates. The positions of the bar crests are detected by the locating intensity maxima, and then tracked with time to study how the bars behave.

8. Acknowledgments

We acknowledge financial support for the project from the Massey University Graduate Research Fund and Geography Department. We also acknowledge field assistance in surveying the ground control points from the Wanganui District Council. We are grateful to

Dr Rob Holman of Oregon State University for useful suggestions and the loan of neutral density filters.

References

1 **R.W.G. Carter.** Man's Response to Sea-Level Change. In R.J.N. Devoy, editor, *Sea Surface Studies: A Global View*, 464-497, Croom Helm, London, 1987.

2 **R.W.G. Carter.** *Coastal Environments.* Academic Press, London, 1988.

3 **E.C.F. Bird.** *Coastline Changes: A Global View.* John Wiley & Sons, London, 1985.

4 **J. Orford.** Coastal Processes: The Coastal Response to Sea-Level Variation. In R.J.N. Devoy, editor, *Sea Surface Studies: A Global View*, 415-451. Croom Helm, London,, 1987.

5 **H.A. Viles.** The Greenhouse Effect, Sea-Level Rise and Coastal Geomorphology. *Progress in Physical Geography*, 13:452-461, 1989.

6 **G. Masselink and A.D. Short.** The Effect of Tide Range on Beach Morphodynamics and Morphology: A Conceptual Beach Model. *Journal of Coastal Research*, in press.

7 **T.C. Lippmann and R.A. Holman.** Quantification of Sand Bar Morphology: A Video Technique Based on Wave Dissipation. *Journal of Geophysical Research*, 94(C1): 995-1011, 1989.

8 **J.L. Davies.** Geographical Variation in Coastal Development. In K.M. Clayton, editor, *Geomorphology Texts 4.* Longman, London, 1980.

9 **R.A. Holman and T.C. Lippmann.** Remote Sensing of Nearshore Bar Systems: Making Morphology Visible. In N.C. Kraus, editor, *Coastal Sediments '87. ASCE*, 929-944, 1987.

10 **R. Shand and D.G. Bailey.** *Environmental and Equipment Limitations of Elevated Terrestrial Imaging* . in preparation.

11 **R.C. Gonzalez and P. Wintz.** *Digital Image Processing.* Addison Wesley, Reading Massachusetts, 1987.

Bailey, D.G., and Shand, R.D., 1994. Determining wave run-up using automated video analysis. Proceedings of the 2nd New Zealand Conference on Image and Vision Computing, pp. 2.11.1 - 2.11.8.

Bailey, D.G., and Shand, R.D., 1994. Determining wave run-up using automated video analysis. Proceedings of the Second New Zealand Conference on Image and Vision Computing, pp. 2.11.1 - 2.11.8.

Determining Wave Run-Up Using Automated Video Analysis

Donald G. Bailey and Roger D. Shand

Image Analysis Unit, and Geography Department
Massey University, Palmerston North
E-mail: D.G.Bailey@massey.ac.nz

Abstract

Wave run-up characteristics are important to a variety of coastal workers. Traditional methods of collecting the data encounter instrumentation difficulties, operator subjectivity, and high labour input and cost. By video taping the wave motion and then applying image processing techniques, these problems are overcome thereby enabling the collection of large spatial and temporal data sets.

The video record is replayed into an image analysis system which captures the intensity variation along one (or more) shore-normal transects. The resulting time-stack visually depicts the run-up motion as a function of time. An algorithm has been developed that is capable of automatically tracking the foamy water (swash) edge under most conditions.

Tracking errors may result from cloud or rain induced low contrast, foam accumulations associated with high energy conditions, or camera vibration caused by high winds. By observing the tracking characteristics in these situations and then simulating such "errors" on "ideal" output, it is found that their effect on the frequency spectrum, which is a typical end use of run-up data, is superficial in most cases.

1.0 Introduction

Determining the nature of wave run-up on a beach-face is important to coastal works: planners in defining hazard zoning and set-back criterion, engineers in designing shoreline protection and other structures, and scientists in their efforts to understand past sea levels, landscape evolution, contemporary nearshore morphodynamics with particular emphasis on low frequency water level motions, and a variety of other coastal phenomenon.

The term run-up is commonly used to describe the height or elevation to which a wave runs up the beach-face with the thin sheet of (usually broken or foamy) water being described as swash on the way up and backwash on the return [1]. Duncan [2] identified the lower limit of this swash/backwash cycle being where the sand is momentarily exposed. To convert the slope-based excursions described above into vertical and/or horizontal components the beach profile must undergo some form of survey, for example see [3-5].

In this paper the terms run-up and swash will be used interchangeably to refer to the continuous oscillations of water across the beach-face. The terms swash-front or swash- edge will refer to the actual boundary between sand and water. No consideration will be made of the vertical or horizontal components.

Previous methods of run-up sampling will be summarised and the associated limitations and difficulties outlined. The development of a video-based swash-front detection procedure using

image processing is then described. This procedure overcomes many of the problems of previous methods and facilitates collection of the spatially and temporally extensive sets of run-up time series data which investigations often require. The final section evaluates the effectiveness of the new technique. As run-up measurements reflect a variety of fluid motions with differing amplitudes, periods and directions, spectral analysis is often applied to such hydrodynamic data. This, therefore, forms the basis of the evaluation criterion regarding tracking variation (error).

2.0 Previous Methods of Run-up Sampling

While run-up spectra can be derived from nearshore current records using shallow water wave theory [6], it is logistically simpler to directly measure run-up at the beach-face where a variety of sampling techniques have been used.

The use of dual resistance wires established across the beach face was described by Guza and Thornton [7] and appraised by Holman and Guza [8]. The technique was objective and the analog sensor's output easily digitized. However, it was sensitive to wire height and gain which resulted in a variance of 25%. There was also a phase error especially at higher frequencies. Field deployment was critical, and prone to fouling especially during high energy events.

Time-lapse photography using movie cameras and manual digitization by detecting the swash-front on individual frames taken one second apart has been a common procedure, for example see [9-12]. This method was found by Holman and Guza [8] to be low cost, easy to deploy even during high energy conditions, had the potential for digitizing a number of longshore ranges, and let the user "see" the phenomenon. The tedious and subjective nature of manual swash-front tracking was the major drawback with times of 30 minutes to digitise a 2048 point time series being reported. Visibility constraints, for example fog or lack of daylight was also a limitation. Using different operators, they found a standard deviation of up to 10% and that spectral coherences were losing significance for frequencies above 0.05 Hz.

Differences between measuring techniques can only be treated in terms of an intercalibration factor [8]. Their comparison using the same run-up field found systematic differences between these direct and remote sensing approaches. The film technique had a slightly higher mean (set-up) but much greater swash excursion variance - the difference being 83% This was attributable to the wires being higher than the swash thickness at its excursion extremes.

More recently, video recordings have been used and two digitization procedures developed. Quasi real time processing using an image processing package to search individual transects at regular time intervals has been used by Holman et al [13].

Alternatively, construction of an image by capturing intensity values along a profile of interest at regular time intervals and stacking them has enabled clear identification of the swash-front through the sampling period. Aagaard and Holm [3] developed this time-stack method. They then manually digitized the swash-edge. The digitization of a 2048 point (34 minute) series took approx 30 minutes and the estimated replicate standard deviation was 5%. The reduced error relative to the earlier frame by frame manual digitizing method has been attributed to the greater ability to estimate indistinct edges using the time-stack.

Holland and Holman [14] have further automated the time-stack procedure by applying standard image processing algorithms to detect the swash-edge. Manual refinements were still required as their method could not cope in situations with low contrast between the swash and beach. Such conditions, however, are characteristic of cloud and rain and as this often accompanies higher energy events it is important that the associated run-up data can be determined.

3.0 Field Measurement

Run-up sampling for this exercise was carried out using a Panasonic MS1 video camera set up on a 45 m high cliff overlooking an oceanic coast of moderate to high wind and wave energy on

the southwest coast of New Zealand's North Island. The site was 100 metres behind the foredune toe and the camera was directed seaward. The same camera orientation angles were achieved for all samples by using ground control points. These were also used for locating run-up transects. Figure 1 shows the camera view with three shore-normal transects having been selected. Multi-transect measurements are useful in determining wave type by examining the longshore phase relationship [12].

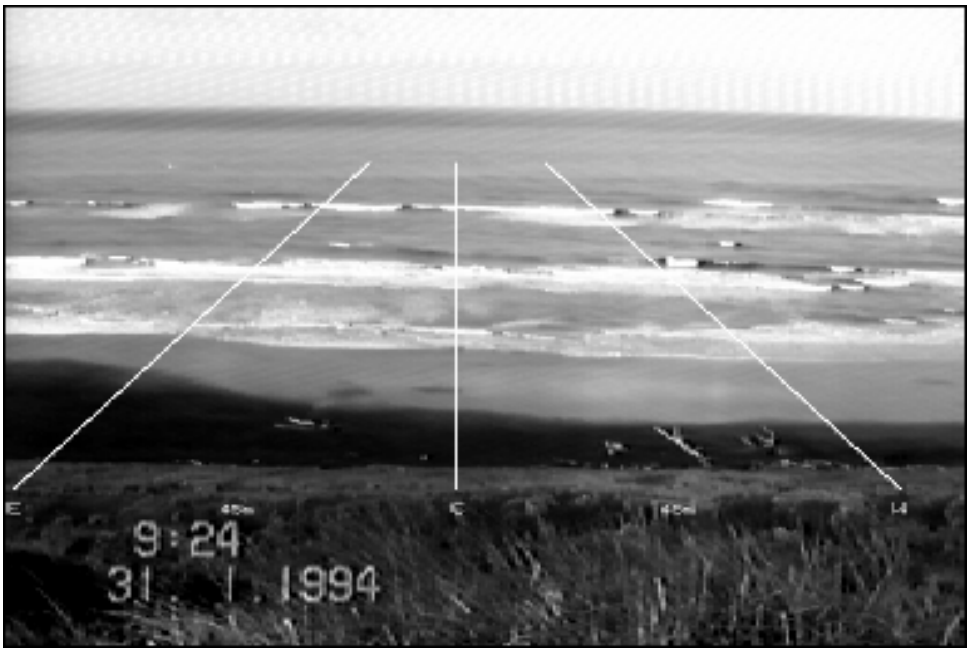

Figure 1: A video still of the field site with three shore-normal transects marked.

4.0 Image Processing Procedure

For this application, it is required that the process of extracting the swash-edge from the videotape be automated as much as practical to reduce the effects of operator subjectivity and the time associated with manual digitisation. The steps required to accomplish this will be described in turn.

4.1 Transect selection

The purpose of this step is to select the transects along which data is to be taken from the videotape. Run-up studies often require multiple shore-normal transects and replicability over time. To facilitate this, a permanent marker post has been established directly seaward of the camera and behind the foredune. When the swash is videotaped, this marker is positioned in the centre of the field of view horizontally, defining the position of the central transect. For this exercise, two additional transects 45 m on either side of the central transect are also used. In principle, these could be calculated knowing the position of the central transect and the focal length of the lens. In practise, they were determined by measuring along the beach before the study started. The transect lines are defined by the points on the beach at one end, and where the central line intersects with the horizon at the other end. (Actually the intersection point is slightly above the apparent horizon because of the curvature of the earth [15]). If the same focal length lens is used in obtaining all of the videotaped samples, the positions of the side transects may be precalculated.

On the image processing system, a single image frame is captured from the video player. This is of the form of figure 1 (without the profile lines). The user locates and indicates the position of the permanent marker using the mouse. This determines the position of the central transect both

horizontally and vertically within the image, and therefore the positions of the two side transects which are at precalculated offsets from the centre.

Since the sample length varies from 10 minutes to several hours, this needs to be specified at this stage. Because of computer memory limitations, the maximum length that may be captured at any one time is limited to 68 minutes. However, this does not pose a problem as longer samples may be captured in sections (with 2 to 4 minutes overlap) and spliced together after processing. Samples of up to 180 minutes (one full videotape) have been captured in this manner.

4.2 Time series digitisation

The next step is to capture the data from the videotape and form a time-stack. To do this, the videotape is rewound to the start of the sample, and played into the image processing system. Every quarter of a second, a single frame is captured and a 3 pixel wide strip along each of the three transect lines is loaded from the frame buffer memory into the computer. The data in each strip is then averaged horizontally to reduce noise, and the result inserted into a single column in the time-stack image. By inserting the results of successive frames captured into successive columns of the time-stack, a picture of what happens along each transect as a function of time is built up. Figure 2 shows a 6 minute segment of the time-stack for the central profile in figure 1.

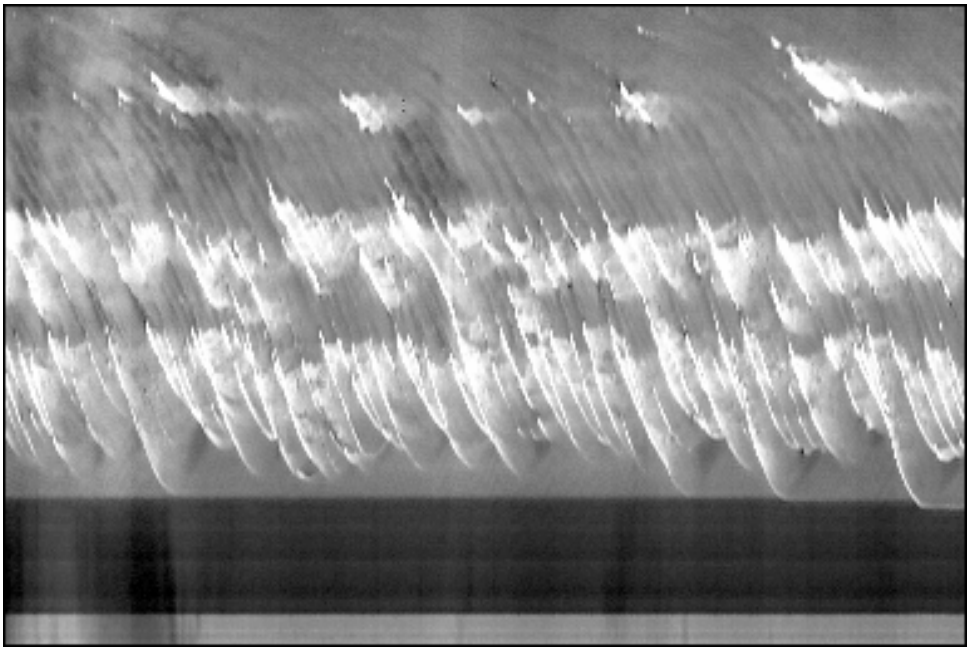

Figure 2: A 6 minute section of the time stack from the centre profile.

Although this paper is primarily concerned with measuring run-up, there are several features within figure 2 of interest. The four or five white patches along the top of the image are waves breaking on the outer bar. The periodic nature indicates the presence of low frequency (approximately 0.013 Hz) sea level changes which may be associated with wind wave grouping [16]. The band of white across the image just above half way corresponds to waves breaking on the inner bar. Further down the image is the trough (the area where almost no waves are breaking) and then the secondary breakers and swash zone. The dark area below that corresponds to the unsaturated beach surface. The average intensity of the waves breaking gives an approximate indication of the water depth along the profile [17]. Individual waves may be identified by the diagonal lines moving from upper left to lower right. As the horizontal axis corresponds to time, if the image was corrected for perspective distortion, the slope of these lines would give a measure of the wave speed.

4.3 Selection of the swash region

Each time-stack contains an enormous volume of data. For example, a 60 minute sample generates three time-stacks, each containing about 3.6 Mbytes. In wave run-up studies, only the swash zone is of immediate interest. Cropping out the unnecessary parts from the time-stack reduces the image size by about a factor of 3, speeding subsequent processing. It was also found that without cropping, the detected swash front occasionally went out to the first sand bar when there was swash activity and low contrast.

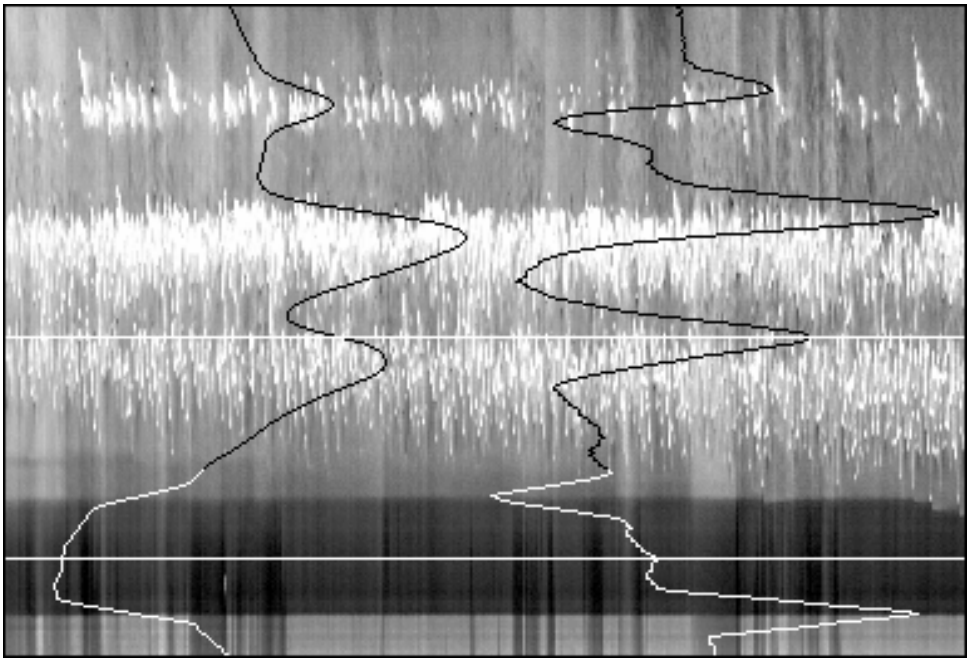

Figure 3: Compressed time stack (52 minutes) with plots of the average intensity (left) and intensity gradient (right). The region of interest crop lines are shown.

On the landward side of the swash zone, the image may be cropped anywhere on the unsaturated sand, ensuring that enough image is kept for the swash from the largest waves not to be clipped. On the seaward side, the boundary between the secondary breakers and the trough allows for maximum swash excursion when tracking while preventing errors from jumping out to the bar when there is no visible swash activity.

A procedure was developed for this step to assist the user to select appropriate cropping positions, and to remove much of the subjectivity involved. The first step is to calculate the average of the intensities of each row in the image. This average is plotted in the left half of figure 3. This is then differentiated to give the average intensity gradient (shown in the right half of figure 3). The complete time stack is compressed onto a single screen, and the intensity gradient plotted. The user is asked to select with a mouse points on the sand landward of the saturation line and on the trough seaward of the swash zone. The program then adjusts the selected points to the local maxima of the intensity gradient, and draws the limits of the swash zone, as shown in figure 3, for confirmation. The section corresponding to figure 2 is shown cropped in figure 4A.

The variation of intensity and contrast in figure 3 is caused by passing clouds.

4.4 Swash front tracking

This step takes the cropped image and detects the boundary between the sand and water. The swash is clearly defined by the heavy white lines moving downwards towards the right. The backwash is less distinct, often showing as "shadows" to the right of the swash peaks. While it would be desirable to track the backwash, this is often not possible because of its much lower

and variable contrast. A more convenient approach is to track to the swash peak and then allow jumps back to the next wave. Our testing showed that the exact nature of the return track had an insignificant effect on the spectral output at the low frequencies (below 0.1 Hz). The processing sequence is as follows:

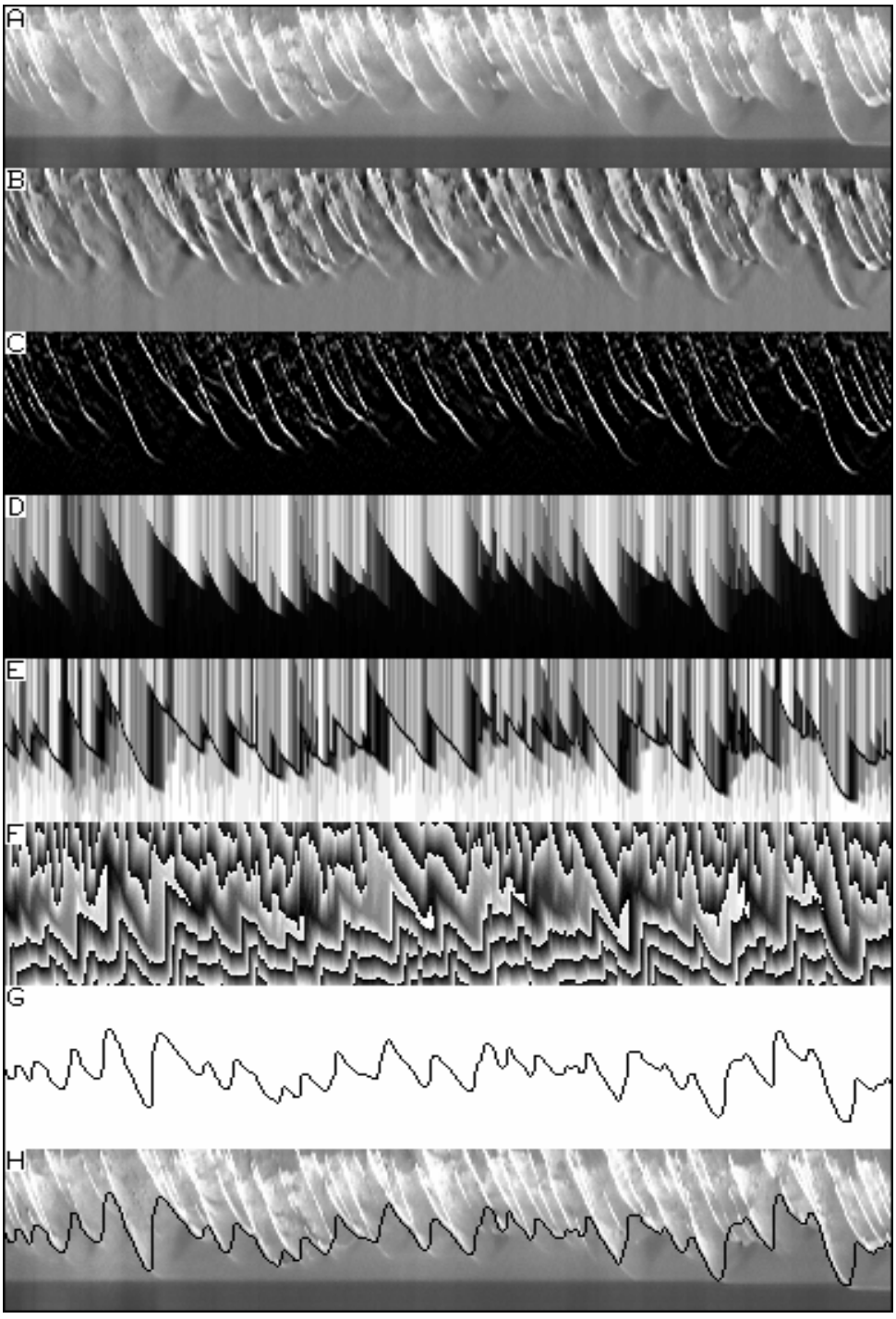

Figure 4: Swash tracking sequence: A) cropped image; B) background removed; C) vertical edges; D) smeared upwards; E) tracking penalty function; F) path cost; G) least cost path, representing tracked swash; H) path overlaid on original

1) Subtract out a horizontal average. One significant boundary in figure 4A is the line between the saturated and unsaturated sand. This boundary changes position slowly, except when the swash crosses it, as it does on the right hand edge of the figure. Other horizontal features that don't move, or only move slowly with time are debris on the beach, or, more importantly, accumulations of foam under high wind conditions. With a strong onshore wind, the foam associated with the swash comes in with the swash, but as the water recedes the foam tends to sit at the swash maximum before slowly dissipating. By averaging using a 1 x 55 pixel window (corresponds to about 14 seconds) and subtracting this average from the image, such slowly varying features are eliminated. The resultant image is then contrast stretched, giving figure 4B.

2) Detect vertical edges. The swash edges may then be detected using a linear difference filter with the result shown in figure 4C. This step has been made effective by the removal of horizontal features in step 1. The backwash, having little or no contrast, is not detected unless it is accompanied by foam. As the swash reaches its maximum landward incursion, there is a often a reduction in contrast and the strength of the detected edge is correspondingly reduced. This is caused in part by the removal of the horizontal average in the previous step. Variations in contrast caused by passing clouds also tend to affect this area the most, and therefore require compensation in later steps.

3) Smear the edges upwards. By definition, anything behind the swash is in the water. Therefore, to assist the algorithm in tracking the swash edge past gaps within the edge, and making jumps from the swash maximum to the next swash, the detected edges are smeared seawards. This may be accomplished by processing the image from the bottom row upwards. If a pixel is less than the pixel below it, the value from below is copied up. The effect of this is to fill in behind the swash edge as shown in figure 4D. Gaps within the detected swash edge appear as darker vertical bands within the image. The smearing process also provides convenient links between the different waves.

4) Normalise the local contrast. Variations in contrast, formed either by a series of weak waves or by passing clouds (one small region is apparent toward the left hand end of figure 4D), are normalised at this stage. The top row of the image contains the maximum value in each column (as a result smearing operation). This is averaged horizontally using a 1 x 35 pixel window (corresponding to about 9 seconds) to obtain the trends in contrast rather than isolated variations. The image is then divided by this average to enhance the contrast where it is lower. This step enables the swash edge to be successfully tracked in all but the worst conditions. Keeping the average short allows for the compensation of even sudden changes in contrast caused by scattered cloud.

5) Define the edge region. The steps till now effectively place a boundary on the seaward extend of the swash line. Pixels with a value greater than 128 are very likely to be on the seaward side of the line, and those with values less than 128 are likely to be on the landward side. The edge region is therefore those pixels with values close to 128. However, simple thresholding is not appropriate in this instance because the contrast at the swash peak drops off gradually giving a wide indistinct region. The approach taken was to blur the image slightly (by averaging with a 3x3 window) to ensure that all edges contained pixels of intermediate values, and then calculate the absolute difference with 128. This (figure 4E) defines the edge regions, where the lower pixel values are candidate edge pixels.

6) Find the least cost path through the edge region. One approach to extract the "best" edge from figure 4E is to treat it as an optimisation problem with the pixel values in the image as a penalty function. The cost of a path from the left hand edge to the right hand edge can be defined as the sum of the values of the pixels making up that path. The path which has the smallest sum is therefore the best path, and defines the swash edge. This path is shown in figure 4G, and overlaid on the original image in figure 4H. This approach has the benefit that it is able to skip over small gaps in the defined swash boundary.

4.5 Editing

A manual editor has been included with the programme. It operates by clicking the mouse at a series of points along the desired path where serious mistracking has occurred. The selected points are simply joined with straight lines. However, it is desirable to avoid editing if possible because it is time consuming, and also introduces user subjectivity. Fortunately, our investigations found that it was rarely necessary to use it.

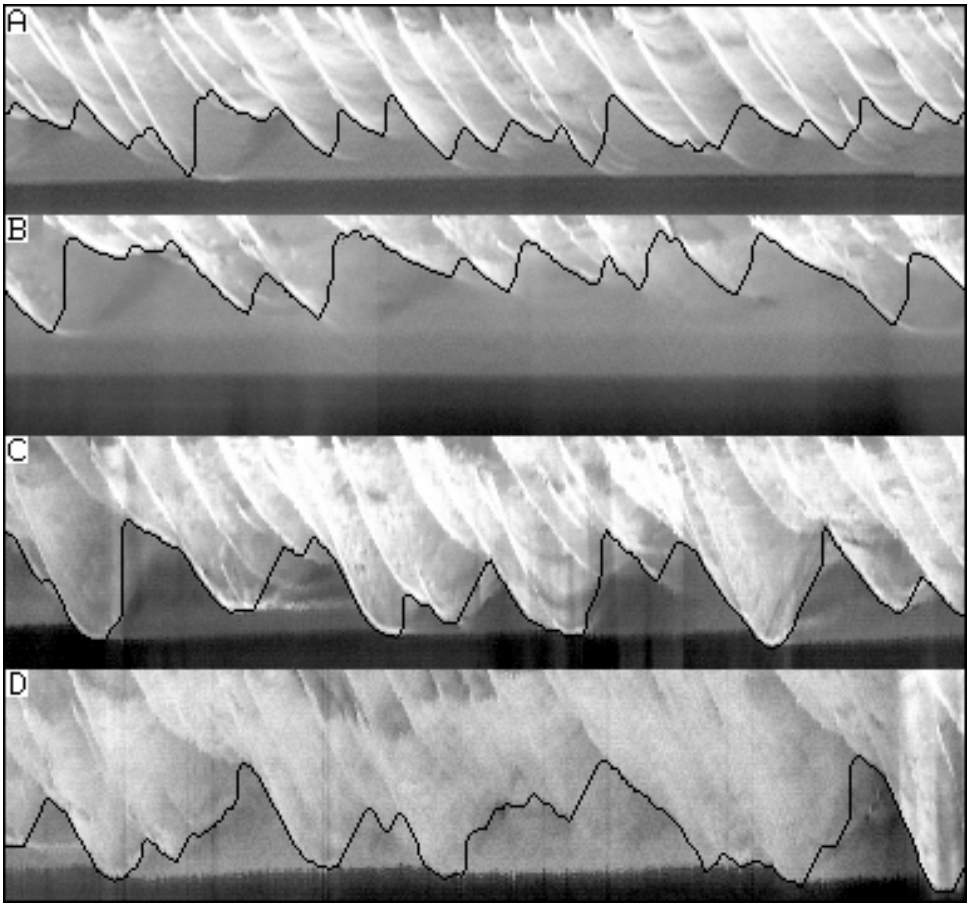

Figure 5: Tracking under different conditions: A) ideal conditions; B) low contrast; C) foam accumulation; D) very low contrast, during a rain squall.

5.0 Technique Evaluation

Since the true run-up on a natural beach is not known [8] we cannot evaluate the technique in this way. Images captured under "ideal" conditions, however, showed that the tracking algorithm yielded output consistent with that which would be manually selected.

Repeatability was generally a major weakness with the earlier techniques involving manual digitization. Repeated application of our algorithm to the same time-stack gave only slight differences between corresponding data points depending on where the cropping limits were selected. The intensity-gradient based method of determining these limits as described in section 4.3 however, achieves absolute objectivity and consistency.

The time series digitisation stage takes the same time as the sample record, however, data along three transects are acquired simultaneously. The tracking algorithm requires approximately 5 minutes to process an 8200 (35 minute) point series for each transect, compared with 30 minutes reported for the manual digitisation methods.

While the swash-edge detection algorithm was generally successful in countering serious and obvious mistracking when images suffered from a variety of contrast deviations (cloud or rain) and also from foam accumulation (high wind or wave action), they still resulted in tracking characteristics which varied from the "ideal". As editing is time consuming, it was important to determine how extensive these deviations could be before affecting the results of a spectral analysis; the typical means of analysis for such hydrodynamic data.

By observing examples of mistracking we were able to identify their characteristic signatures. Foam accumulation gave higher contrast at the swash maxima, drawing the track out past the maximum excursion before returning to the following swash front (figure 5C). Low contrast resulted in early track return to the following swash front, effectively reducing the amplitude variation (figure 5B). In very low contrast conditions, the swash was not always reliably detected. The saturation line increased in contrast as the contrast of the swash diminished (figure 5D). In extreme cases the detected swash edge tracked along the saturation line, joining successive swash maximums. This latter situation is equivalent to missing sections of the time series data.

The characteristics of early return (low contrast) and late return (residual foam) situations were simulated upon a sample with ideal conditions by manually editing the images (figure 6). The results were then subjected to spectral analysis to investigate the effects of the deviations. Visually, the important features were similar and the spectral coherence was significant for the low frequencies, up to about 0.08 Hz. In most studies, it is this low frequency region that is of interest and no editing would be required. However, if higher frequencies are required then the detected path may need to be edited manually.

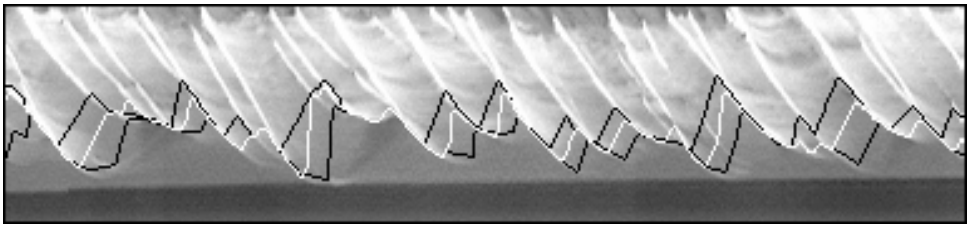

Figure 6: Automatically detected path under ideal conditions (white) and simulated early and late returns (black).

The near horizontal (very low contrast) tracking situation was simulated by setting different length segments along both the time series mean and also along the saturation line. A loss of up to 20% of the sample data in this way had little effect on the frequency spectrum in the region calculated (up to 0.3 Hz), although those which had the swash path set along the saturation line introduced a very low frequency artefact at 0.004 Hz. This indicates that the tracked path for any sections that follow the saturation line should be edited to follow along the time series mean.

6.0 Conclusion

The main drawbacks associated with previous methods used to measure run-up consisted of the logistics of establishing and maintaining swash-zone sensors. Video techniques are affected by low light and weather conditions. Manual digitisation techniques can be used to overcome these, but are both subjective and time consuming.

In this paper, we have used the time-stack method together with image analysis to extend the usefulness of video techniques. Camera operation is still limited to daylight hours, however, atmospheric limitations such as cloud, rain, and wind have largely been overcome. While extreme storm events prohibit outside operation, housing the camera would overcome this difficulty. The only restrictions are very low contrast such as a lack of daylight or sustained heavy rain. Our results to date indicate that this technique will provide an effective yet logistically simple and inexpensive method of collecting extensive run-up information.

References:

1. **Carter R.W.C.** Coastal Environments: an Introduction to the Physical, Ecological and Cultural Systems of Coastlines. Academic Press, p 611 (1988).

2. **Duncan J.R. Jr.** The Effects of Water Table and Tide Cycle on Swash-Backwash Sediment Distribution and Beach Profile Development. *Marine Geology*, **2**:186-197 (1964)

3. **Aagaard T. and Holm J.** Digitization of Wave Run-Up Using Video Records. *Journal of Coastal Research*, **5**(3): 547-551 (1989)

4. **Holman R.A., Lippmann T.C., O'Neill P.V., and Hathaway K.** Video Estimation of Subaerial Beach Profiles. *Marine Geology*, **97**:225-231 (1991)

5. **Holman R.A., and Sallenger A.H.** Setup and Swash on a Natural Beach. *Journal of Geophysical Research*, **90**(C1): 945-953 (1985)

6. **Sallenger A.H., and Holman R.A.** Infragravity Waves Over a Natural Barred Profile. *Journal of Geophysical Research*, **92**(C9): 9531-9540 (1987)

7. **Guza R.T. and Thornton E.B.** Swash Oscillations on a Natural Beach. *Journal of Geophysical Research*, **87**(C1): 483-491 (1982)

8. **Holman R.A., and Guza R.T.** Measuring Run-up on a Natural Beach. *Coastal Engineering*, **8**:129-140 (1984)

9. **Wright P.** A Cine-Camera Technique for Process Measurement on a Ridge and Runnel Beach. *Sedimentology*, **23**:705-712 (1976)

10. **Carlson C.T.** Field Studies of Run-Up on Dissipative Beaches. *Proceedings of the 19th International Conference on Coastal Engineering, ASCE*. 708-723 (1984)

11. **Holman R.A. and Bowen A.J.** Longshore Structure of Infragravity Wave Motions. *Proceedings of the 16th International Conference on Coastal Engineering, ASCE*. 6446-6452 (1984)

12. **Holman R.A. and Sallenger A.H.** Longshore Variability of Wave Run-Up On Natural Beaches. *Proceedings of the 16th International Conference on Coastal Engineering, ASCE*. 1896-1921 (1984)

13. **Holman R.A., Howd P., Oltman-Shay J., and Komar P.** Observations of the Swash Expression of Far Infragravity Wave Motions. *Proceedings of the 22nd International Conference on Coastal Engineering, ASCE*, 1242-1253 (1990)

14. **Holland K.T. and Holman R.A.** The Statistical Distribution of Swash Maxima on Natural Beaches. *Journal of Geophysical Research*, **98**(C6):10,271-10,278 (1993)

15. **Bailey D.G. and Shand R.D.** Determining Large Scale Sandbar Evolution. *Proceedings of the First NZ Conference on Image and Vision Computing*, 109-116 (1993)

16. **Huntley D.A. and Kim C.S.** Is Surf Beat Forced Or Free? *Proceedings of the 19th International Conference on Coastal Engineering, ASCE*, 871-885 (1984)

17. **Lippmann T.C. and Holman R.A.** Quantification of Sand Bar Morphology: A Video Technique Based on Wave Dissipation, *Journal of Geophysical Research* **94**:995 - 1011 (1989)

Shand, R.D., and Bailey, D.G., 1995. Videographic acquisition of surf zone data: a summ of present techniques and future possibilities. School of Global Studies, Massey University, New Zealand, Miscellaneous Publication Series 95/4, 38p.

Videographic acquisition of surf zone data:

a summary of present techniques and future possibilities

R. D. Shand and D. G. Bailey

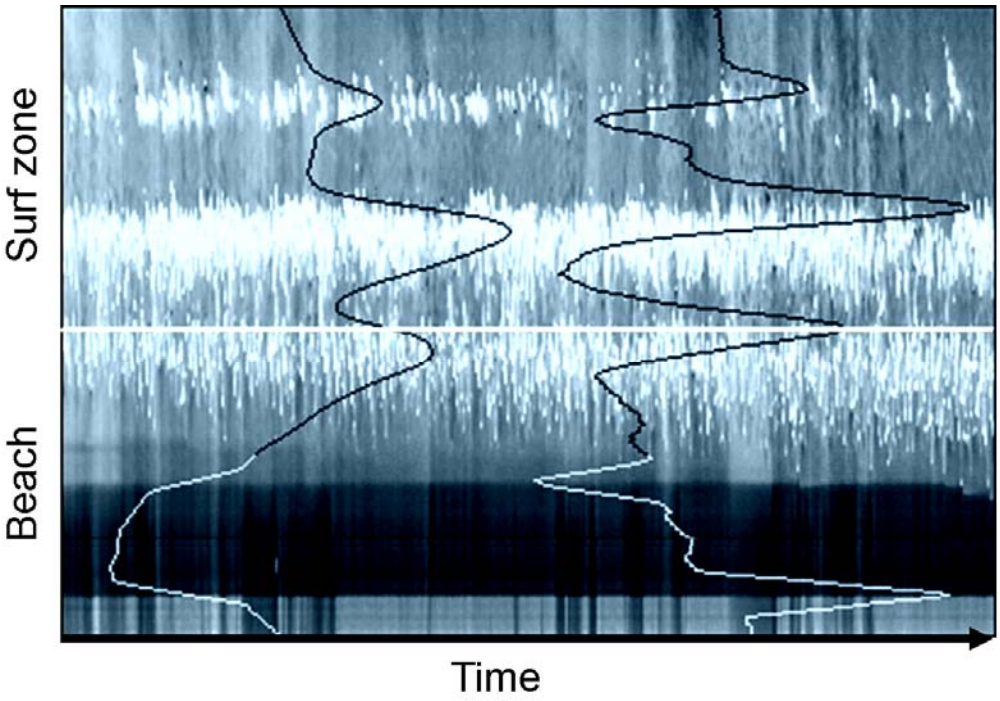

School of Global Studies

MISCELLANEOUS PUBLICATION SERIES 95/4

1995

MASSEY
UNIVERSITY

Reference: Shand, R.D., and Bailey, D.G., 1995. Videographic acquisition of surf zone data: a summary of present techniques and future possibilities. School of Global Studies, Massey University, New Zealand, Miscellaneous Publication Series 95/4, 38p.

© 1995 The Authors

Cover image

Fifty two minute long video time-stack image covering beach (lower-mid) and surf zone (mid-upper) and sampled across a single shore-normal transect with the camera located ~44 m above MSL and facing seaward. This image appears in the paper as Figure 4B and its construction and characteristics are discussed in Sections 4 and 6.

ABSTRACT

There is an increasing demand for quantitative information about the dynamic coastal zone at 'intermediate' temporal and spatial scales. Methods of morphological and hydrodynamic sampling are described and subjected to a comparative analysis with the most generally acceptable method being elevated terrestrial electronic sensing using video cameras coupled with subsequent digital image processing (i.e. videography). 'Time-stacking', an image processing procedure common to many of the data abstraction algorithms is described with reference to existing and potential uses of videography for acquiring and interpreting geo/hydro-physical data. Additional advantages of the image-based approach, including retrodictive data acquisition and flow visualization, are also documented.

1.0 INTRODUCTION

With increasing pressure being placed on the world's oceanic coastal resources, together with emphasis on 'sustainability' (Carter, 1987; de Viend, 1993; Ward, 1993), and the threat of greenhouse induced sea-level rise (Viles, 1989), the acquisition of both shorter and longer-term quantitative geophysical data is becoming increasingly important to coastal planners, engineers and scientists.

The coastal environment, however, presents logistical difficulties which make it one of the potentially most difficult, dangerous, and expensive locations to collect data. There are many morphological and process variables which can be measured, so the question of which parameters or indicators to monitor becomes significant. Resource-management researchers stress the necessity to clearly define monitoring objectives, as the purpose of the monitoring will influence both the parameters measured and the nature of the sampling programme, and these in turn, govern the effectiveness and cost of the monitoring (Ward 1993). Objectives, however, change with time, so there is a need to develop monitoring systems that are capable of detecting the widest range of data types.

The active coastal zone can be divided into a number of subzones (Figure 1) each characterised by distinctive morphological and hydrodynamic characteristics (e.g. see Wright and Short, 1984). While energy levels and associated sediment transport are greatest within the surf zone, the hostility of this environment has tended to impede data collection and this has resulted in the inshore region, probably the most significant to human activity, being relatively poorly understood. This paper addresses data acquisition across the surf zone.

There exists a hierarchy of process-response scales operating within the surf zone. At the micro-scale (minutes-hours), bed dynamics are influenced by the passage of a single wave (e.g. Marra, 1992). At the meso-scale (days to weeks), individual meteorologically driven events (storms-fairweather episodes) alter beach and bar form (e.g. Goldsmith et al., 1982;

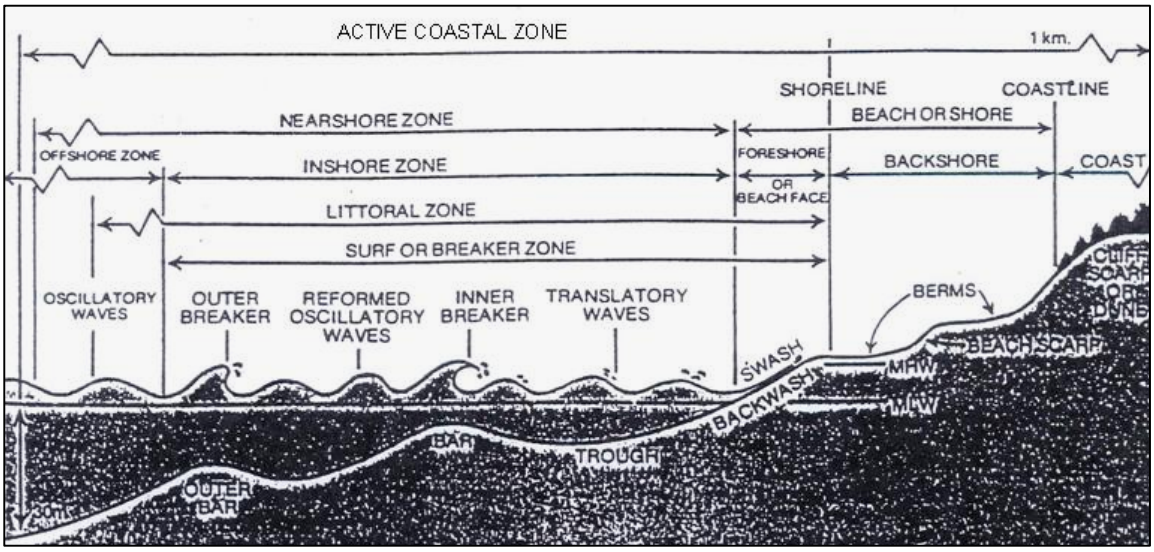

Figure 1
A typical coastal profile depicting the various zones of active sediment transport and common terminology.

Sallenger et al., 1985; and Aagaard, 1991). At the macro-scale (months to yrs), larger-scale atmospheric/oceanic processes influencing coastal morphology (e.g. McLean and Thom, 1975; Aubrey, 1979). At even larger (mega) time scales (10^2 to 10^7 years) process-response interactions associated with secular climatic change can dramatically change coastal environments at regional and global scales (e.g. Gibb, 1979; Roy and Thom, 1981; Sallenger, 1988; Peltier, 1987). Factors other that climatic forcing also influence coastal change, for example natural and man induced variation in sediment supply (e.g. Komar, 1983; McFagen, 1985; Shepherd, 1987; Carter, 1988; Eliot and Clarke, 1989).

Morphological data at the meso-scale has important application for scientific, engineering, planning, and recreational interests, so it is the scale that this study focuses on. The spatial dimension of interest is 10^1 to 10^4 m, and temporal resolution at c. 5 to 30 days. The associated process (hydrodynamic) data, however, must be sampled at much shorter temporal scales (10^0 to 10^1 sec) over intervals up to 10^2 sec and then synthesized (Balsillie and Carter, 1984; De Viend, 1993; Goda, 1983). Spatial variability occurs vertically, cross-shore, and often also alongshore.

In the past, field methods for morphological sampling have required instruments to physically traverse the surf zone. For short-term morphodynamic studies, instruments are fixed within the surf zone itself; however, for longer-term data they may be located in the less energetic region further offshore with wave theory being used to equate deepwater and breakpoint parameters (see CERC, 1984). Water contact, and spatially discrete sampling of these approaches have precluded comprehensive monitoring, especially on moderate to higher energy coasts. These methods are generally time-consuming, expensive, and reliant

on specialist technical staff both for data collection and for the subsequent processing-reduction phase (Hemsley et al., 1991).

A need therefore exists for surf zone data acquisition systems that meet the following criteria:

- wide-ranging in terms of type of acquired data;
- flexible in terms of operating environment and in particular can operate in moderate to high energy conditions;
- able to meet meso-scale spatially continuous sampling requirements;
- able to meet the corresponding temporal scale sampling requirements;
- capable of achieving meso-scale accuracy in terms of morphological and hydrodynamic elevation plus the other hydrodynamic 'core' parameters;
- user-friendly in terms of operator skill level with respect to establishment, operation, and information abstraction, and
- relatively low cost for establishment, operating, data reduction and capital depreciation.

The present study will not consider the various manual-visual observation methods which have often been used to collect surf zone morphological and hydrological data. While such approaches have definite logistical and cost advantages they contain varying degrees of subjectivity and are limited in terms of spatial and temporal scales, and accuracy. Given such limitations, together with the general requirement of surfzone-nearshore process-response studies for continuous data, the visually based methods find greatest use in providing long-term data where cost or accessibility constraints apply. A description of these techniques, their characteristics, and major monitoring programmes using them can be found in: Chappell and Eliot, 1979; Short, 1979; Patterson, 1985; Smith and Wagner, 1991; Hamsley et. al,. 1991; Schneider and Weggel, 1980; Patterson and Blair, 1983; Balsillie and Carter, 1984; Plant and Griggs, 1992; and Smith and Wagner, 1991.

Data acquisition typically occurs in two stages: data (field) collection, and data abstraction which may include visual interpretation or manual/automated digitization methods. However, when collection involves remotely sensed images the abstraction phase can be subdivided into a capture stage a subsequent processing stage where specific data sets are obtained and analysis may be included (Austin et al 1994).

Remote sensing is used here to imply a separation between observer or recorder and the object of measurement. Remote sensing field techniques from elevated terrestrial sites is a relatively new and promising option. In this situation ‘elevated’ refers to the instrument platforms being well above the sea surface. The evolution of such an approach has an interesting history. Briefly, remote sensing using aerial photography and image rectification by analogue or perspective grid processing has been successfully used to collect moderate to long term coastal morphological data since the 1930's (e.g. Eardley, 1941; Slama, 1980). While remotely sensed surf zone process data has been satisfactorily acquired from elevated

platforms, it has mainly been limited to scientific experiments where photographic and radar sensing have been used (e.g. Crowson et al., 1988; Bailey and Shand, 1994; Goda, 1983). More recently, technological developments have enabled the use of video sensing and digital image processing to acquire both morphological and hydrodynamic surf zone data. This approach is referred to as **videography** (Placio-Prieto and Lopez-Blanco, J., 1994).

The present paper begins (Section 2) by describing and evaluating existing methods of morpho/hydro geophysical data collection and reduction for the purpose of assessing the relative significance of the videographic approach. As videographic methodology is relatively unknown, a general description of image sensing and processing characteristics is given in Section 3. Section 4 describes 'time-stacking', a newly developed and significant image processing technique being incorporated in many videographic data abstraction algorithms. The visualization permitted by time-stack imagery suggests a variety of potential methods for deriving surf zone data and these are described in Sections 5 and Section 6 for morphological and hydrodynamic videographic data acquisition respectively. Finally, the discussion section (7) focuses on relative and additional advantages of the video/image processing approach for surf zone data acquisition and research in general.

2. DATA ACQUISITION TECHNIQUES

Instrument-based morphological data acquisition methods and their salient features are listed in Table 1 and hydrodynamic methods are summarised in Table 2. The listed methods are not exhaustive, but they do cover the main alternatives. The field-techniques appear in the left-hand column where they have been classified with respect to instrument location, the nature of the platform, and the sensor type. Across the top of the tables are listed the characteristics associated with the study criteria identified in Section 1. Due to the diverse nature of the methods only a categorical assessment using 'first order' grouping has been attempted. At the meso-scale, a wide range of data types are required and this further complicates assessment and inter-method comparison, and necessitates the assignment of some conditions, particularly regarding costs. These assumptions are detailed in the extensive notes accompanying the tables.

Evaluation has simply been based on three classes: high, moderate and low. As an approximation "high" (or in some cases "low") grading relate to short-term or micro-scale investigations, and "moderate" grades relate to meso-scale work. If a method has a particular characteristic evaluation satisfying the micro-scale criterion, it will, therefore, probably also meet meso-scale requirements. A description of the groupings associated with each characteristic together with the acceptance grade are provided in the table notes. In cases where the criteria are satisfied, the ratings given in the tables have been underlined.

Morphological techniques

The five foreshore techniques considered in Table 1 (coded $) are generally more successful than the inshore methods as is evidenced by the greater numbers of acceptance criteria satisfied. No particular characteristic was consistently weak and, in contrast with most inshore methods, skill and cost levels were acceptable. These results reflect the relative ease of access to and within the survey environment and the ability of sensors to have direct contact with the measurement surface.

The other 16 techniques in Table 1 relate to the hostile and logistically more difficult inshore zone. While in general they met less acceptance criteria than the foreshore methods, there are distinct patterns both within and between the methods. The underlined evaluation ratings tend to group with respect to "Instrument Location", indicating that particular types of instrument measure (successfully) similar things. There is a strong division between the water/ground-contact and the aerial/space-based methods in terms of depth delineation (elevation resolution) versus data output, sampling environment, and spatial coverage. However, all require high skill level and have greater cost. By contrast, the elevated terrestrial methods also have the positive evaluation characteristics while avoiding the high skill/cost requirements. The ease of 'access' of the sensor platform to the survey area, together with the need for less sophisticated and expensive equipment accounts for this situation.

There are some problems with the elevated terrestrial techniques. The results in Table 1 show that both the photographic and videographic approaches struggle with elevation. These techniques, together with certain aerial and space-based methods, use wave breaking patterns to infer depth variation, thereby providing a measure of relative elevation. Variation in the location of wave breakpoints characterize natural wave-fields and these modulations reduce the accuracy of the foam-intensity/morphology relationship. The terrestrial methods, however, enable the use of time-averaging which result in a statistically stable sample with detailed depth graduation based upon intensity change (Lippmann and Holman, 1989). The information loss is thus minimised and there is a future possibility of metrication being achieved. This approach is considered further in Sections 3 and 4.

A further limitation of the elevated terrestrial methods is the requirement of a raised platform. While there is a tendency for moderate to higher energy coasts to be associated with regions of greater relief (Davies, 1980), in many instances it will be necessary to use an artificial means of elevation. If existing buildings are not available, then a tower 20 to 40 meters high (depending on site and the nature of the investigation) would need to be erected such as has occurred at the CERC Field Research Station in North Carolina (see Holman and Lippmann, 1987). The expense of providing such a platform was not taken into account when calculating the costs in Table 1.

Table 1

Surf zone morphological data acquisition: instrument-based methods and characteristics

FIELD METHOD (location of platform & sensor @1)	Output Data @2	Sampling Environment @3	Spatial Scale @4	Temp Scale @5	Elevation Resolution @6	Skill Level @7	Total Cost @8	References @9
Acceptance Criteria #1	3D or Plan	mod/high	mod/high	mod/high	mod/high	low/mod	low/mod	
Ground Contact								
Level: Eye $	Profile	low/mod	low	mod/high	high	mod	low	24
Theodolite: Laser $	3D	low/mod	low/high	mod/high	vhigh	mod/high	mod	
Photo$	3D	low	low/high	mod	high	mod/high	mod	25
Skids: Laser	Profile	low/high	low	high	mod/high	mod/high	high @8*	18
Pressure	Profile	low	low	mod	mod	high	high	22
Tracked Gyroscope	Profile	low/mod	low	mod	high	mod/high	high	11, 30
Wheeled Laser	Profile	mod	low	mod	high	mod/high	high	14
Sea Surface								
Vessel: Depth Sonar	Profile	low	low	low	mod	high	high	26, 28
Vessel: Sidescan Sonar#	Profile#	low	low	low	mod	high	high	33, 28, 29
Terrestrial (elevated)								
Elevated: Photo $	Profile	mod	low	high	high	mod	low	21
Elevated: Photo	Plan	mod/high##	mod/high	mod/high	low	mod	low	3, 10
Elevated: Electr:video$	Profile	low/mod	low/mod	high	high/mod	mod	low	20
Elevated: Electr:video	Plan	mod/high##	mod/high	mod/high	low	mod	low	4, 19
Aerial								
Balloon: Photo$	Plan	low##	mod	low	low	mod/high	mod	27
Aircraft: Photo (vertical)	3D	low/mod*#	high	low	mod	vhigh	high	5,9,31
Aircraft: Photo (vertical)	Plan	mod/high*##	high	low/mod	low	vhigh	high	1,6,7,8
Aircraft: Photo (oblique)	Plan	mod/high##	high	mod	low	mod/high	high	8
Aircraft: Electr:radar	Plan	low*	high	low	low	vhigh	high	2
Aircraft: Electr:lazer	3D	low/mod	high	mod	mod/high	vhigh	high	2,32
Space								
Satellite: Electr: MSS	Plan	mod/high*##	vhigh	low/mod	low	vhigh	vhigh	2
Satellite: Electr:radar	Plan	low	vhigh	low	low	vhigh	vhigh	2, 33

Notes for Table 1

Assessment Grading: Low, Mod(erate), High. Where greater detail is required: a slash (/) e.g. mod/high is used to Indicate that value could lie in either group. V(ery) is used to indicate value at extreme end of overall range. Details of the grades are given in the the following notes.

1# Acceptance Criteria: These evaluation grades meet the study (acceptance) criteria.
As a first order approximation "high" (or in some cases "low") gradings relate to short-term or micro-scale investigations, and "moderate" grades relate to meso-scale work. If a method has a characteristic evaluation satisfying the micro-scale criterion, it will, therefore, probably also meet lower scale requirements.
In the Table the underlined grades meet the acceptance criteria for this study.
Note that for Data Output entries the actual measurement has been recorded in the table to assist cognition.
Assessment and study criterion acceptance (underlining), however, have still been based on the low/medium/high System detailed below.

@1 Platform: For sensor or target; documented if notable
Side-scan sonar#: Option using the submerged 'fish' to house the sensors is impractical for the surf zone so only surface traveling sensors are considered here.
Sensor: For elevation detection, position fixing is by predetermined transits, GPS, or photogrammetry.
Photo = chemically sensitive emulsion (visible spectrum)
Electr. = electronic detection (type described)
$ = Subaerial/foreshore features are detected. All the other methods survey the inshore region.

@2 Acquired data: Primary nature of data collection: profile (shore-normal distance and elevation measured. No data on longshore dimension), plan (location data with relative elevation data), 3D (position and elevation measurements are recorded).
* side-scan or multi-beam sonar is effected by depth limitations in the inner nearshore/surf zone which results in the typical 60 degree scan covering only approximately 2 metres of sea-bed! and this makes continuous spatial coverage infeasible as traverse lines are usually spaced, for practical reasons, at least 20 metres apart.
High = 3D, Medium = Plan, Low = Profile.
Study criterion: Moderate/High but for clarrity the actual data types are listed in the table under Data Output.

@3 Sampling Enviromnent: Relates to instrument design atmospheric and oceanographic energy levels
* Requires no cloud cover if platform at high altitude.
# Requires high water clarity (visible sea-bed)
Requires wave breaking (inferred depth) and lower tidal stage.
High: Hb > 2m, Wind speed >45Kh^-1. Moderate: Hb = 1 to 2m, wind = 25 to 45Kh^-1, Low: Hb < 1m, wind <25Kh^-1.
Study Criterion: Moderate/High

@4 Spatial scale: longshore swath only as all methods satisfy sampling criteria in the cross-shore direction.

High > 100m, Moderate = 10 to 100m, Low <10m.
Study Criterion: Moderate/High

@5 Temporal scale refers to the sampling rate (in days) likely for required monitoring environment, i.e. mod/high energy.
High < 5 days, Moderate 5 to 20 days, Low > 20 days.
Study Criterion: Moderate/Hig

@6 Elevation resolution refers to vertical measurement accuracy. Different grading is used for the foreshore and the inshore zones reflecting different processes, measurement methods and data usage.
Foreshore: High < .05m, Moderate = .05m to .15m, Low > .15m
Inshore: High < .1m, Moderate = .1 to .5m, Low > .5m
Study Criterion for both the Foreshore and Inshore: Moderate/High

@7 Skill: refers to the overall level of user training and experience required for equipment establishment, operation/maintanence, data reduction etc.
High = extensive professional training/experiemce, Moderate = technical training/experience required,
Low = little training/experience required.
Study Criterion: Low/Moderate

@8 Total Cost: refers to cost per survey of equipment and labour for establishment, operating, maintenance, reduction, capital cost depreciation etc.
Assumptions: Number of surveys; 50 to 100 over 2 to 5 years at 14 to 30 day intervals.
For non-imaging (profiling) methods minimum of 10 profile to be measured.
Profile lengths: foreshore 200m, nearshore 1000m
@8* Only two fixed shore-normal transits possible for this technique.
Low < $500, Moderate = $500 to $1000, High = > $1000.
Study Criterion: Low/Moderate.

@9 References: literature cited is either technique-focused, or for a major project utilising the technique.
1: Horikawa (1978), 2: Lillesand and Kiefer (1987), 3: Bailey and Shand (1993), 4: Lippmann and Holman (1989), 5: Okamoto (1982), 6: Chandler et al (1989), 7: Wolf (1974), 8: Salma (1980), 9: Karara (1980), 10: Holman and Lippmann (1987), 11: Seymour et al (1978), 12: Fox and Davis (1978), 13: Emery (1961), 14: Birkemeier (1984), 18: Sallenger et al (1983), 19 Lippmann and Holman (1993), 20: Holman et al., (1991), 21: Hoad (1991), 22: Seymour and Bothman (1984), 24: Wilson (1977), 25: Collins and Madge (1981), 26: Admiralty (1938), 27: Preu et al (1989), 28: Ingham (1975), 29: Black and Healy (1983), 30: Aubrey and Seymour (1989), 31: Colwell (1960), 32: Penny et al (1986), 33: Lewis (1994).

Hydrodynamic techniques

The hydrodynamic techniques in Table 2 also exhibit, albeit to a lesser extent, the underlined evaluation ratings' tendency to group with respect to "Instrument Location". There is a division between the water-contact and the aerial/space-based methods, in this case in terms of the temporal sampling/accuracy versus sampling environment/spatial coverage. However, once again the division is less well defined than with the morphological techniques. High skill/cost levels again dominate these extreme groups. As with the morphological methods, the centrally located terrestrial options tend to incorporate the advantages of the other groups while avoiding the skill/cost disadvantage.

The water-contact options appear to be more successful in achieving the necessary range of data output. However, closer inspection shows that this is the result of instrument combination. The only individual methods presently capable of satisfying acceptance criteria were the dual balloon or dual helicopter techniques. The elevated terrestrial video option fails to meet acceptance criteria only with respect to short wave elevation (wave height) and this limitation is potentially solvable (addressed later in Section 6). We therefore think that this approach has potential to be a successful stand-alone technique for some applications. However, its inability to sense the water column itself, in particular subsurface currents, i.e. orbital velocities and mean flows, which are a fundamental requirement for scientific applications such as micro-scale process-response studies. It should be noted that some researchers argue that to numerically model meso-scale morphodynamics it it necessary to integrate micro-scale behaviour (Sherman and Bauer, 1993) hence making it mandatory to be able to acquire data at this level. But others question this approach, due to the inherent nonlinearities within natural systems (de Vriend, 1991; Terwindt et al., 1991).

Table 2

Surf zone hydrodynamic data acquisition: instrument-based methods and characteristics

FIELD METHOD (location platform & sensor @1)	Measured Output(s) Data @2	Sampling Environment @3	Spatial Scale @4	Temp Scale @5	Accuracy @6	Skill Level @7	Total Cost @8	References @9
Acceptance Criteria #1	mod/high	mod/high	mod/high	mod/high	mod/high	mod/low	mod/low	
Sea-Bed/Water Column								
Beach-face:Restistance	L(RF)	low/high	low/high#	low/high	high	high	low/mod	18,19
Bed: Pressure (PS)	S(EPF),L(EF)	Low/mod	low	low/high	high	high	high	1,3
Bed: Cluster PS array	S(EDPF),L(EF)	low/mod	low	low/high	high	high	high	1
Bed: Acoustic #	S(EPF),L(EF)	Low	low	low/high	high	high	high	1
Coln: Ducted Impellor	CC	Low	low	low/high	high	high	high	1
Coln: Electromagnetic(EM)	CC	low/mod	low	low/high	high	high	high	1,21
Coln: Doppler Accoustic	CC	low/mod	low	low/high	high	high	high	1
Coln: Puv meter; PS plus EM	S(EPF),L(EF),CC	low	low	low/high	high	high	high	1
Bed/coln: Mobile sled mast PS and EM	S(EDPF)L(EF),CC	low/mod	low/high#	low/high	high	high	high	20
Surface								
Buoy Accelerometer#	S(EDPF)	low	low	low/high	high	high	high	1,3
Bed fixed & Surface piercing:								
Staff: Stepped electrodes	S(EPF),L(EF)	low	low	low/high	mod/high	high	high	1,3
Staff: resistance wires	S(EPF),L(EF)	low	low	low/high	high	high	high	1,3
Cluster: staff array	S(EDPF),L(EF)	low	low	low/high	mod/high	high	high	1
Spatial arrays: staff and/or PS, EM	S(EDPF),L(EF),CC	low/mod	low/high	low/high	mod/high	high	high	19
Terrestrial								
Surface: Microsiesmograph.	S(ET)	Low/high	low??	low/mod	mod	mod	low/mod	7 *
Surface: Electr: radar	S(DP)	Low/high	low/high	low/mod	high	mod	low/mod	4,8,9
Elevated: Photo Emulsion	L(RF) CS	low/high	low/high	low/mod	mod	mod	low/mod	13,14,22
Elevated: Electr: video	S(DPF)L(RF)CS	low/high	low/high	low/high	mod/high	mod	low/mod	6,15,16,17
Aerial								
Balloon:(2) Photo Emulsion	S(EDT)L(RF)CS	low	low/high	low/mod	mod	mod/high	mod/high	10,12
Helecop:(2) Photo Emulsion	S(EDT)L(RF)CS	low/mod	low/high	low/mod	mod	high	high	11
Aircraft: Photo Emulsion	S(ED)	low/high*	low/high	low/mod	mod	high	high	3
Aircraft: Electr: radar#	S(EDL)	low/high	high	low	mod/high	high	high	9,5
Space								
Satellite: Electr: radar#	S(EDL)	low/high	high	low	mod/high	high	high	2,5,9
Satellite: Electr. MSS	CS	low/high*	high	low	low	high	high	23

Notes for Table 2

Assessment Grading:
Low, Mod(erate), High. Where greater detail is required: a slash (/) eg mod/high, is used to indicate value could lie in either group. V(ery) is used to indicate value at extreme end of overall range.
Details of the grades are given in the the following notes.

1# Acceptance Criteria: These evaluation grades meet the study (acceptance) criteria.
As a first order approximation "high" (or in some cases "low") gradings relate to short-term or micro-scale investigations, and "moderate" grades relate to meso-scale work. If a method has a characteristic evaluation satisfying the micro-scale criterion, it will, therefore, probably also meet lower scale requirements.
In the Table the underlined grades meet the acceptance criteria for this study.
Note that for Data Output entries the actual measurement has been recorded in the table to assist cognition. Assessment and study criterion acceptance (underlining), however, have still been based on the low/medium/high system detailed below.

@1 Sensor detail: Electr: = electronic detection of electromagnetic radiation followed by spectral range of sensor e.g.
radar = microwave.
Radar#: land contamination is likely to influence nearshore hydradynamic data collected by space-based radar sensing.
Accoustic#: Foam from breaking waves contaminates signal therefore not suited to surfzone unless very low energy
Buoy#: Direction can only be derrived if fitted with pitch, roll and heave detectors.

@2 Output Data
Short Wave (S): Elevation (SE), Direction (SD), Phase Speed (SP), Frequency if continuous record (SF), Period if discrete record (ST), Lengths (if determined independent of period and phase speed) (SL).
Long Wave (L): Elevation for inshore zone (LE), Frequency for inshore zone (LF), Runnup (horizontal) using swash(LR), Runup Frequency (LRF).
Current Velocity (C): Surface (CS), Water Column (CC).

Grading catagories: the medium catagory (meso-scale) has been set so as to enable the application of general sediment transport formulae.
High = S(*), C(*), and either LE and LF or else LR and LRF. Medium = SE, SF, either SD or CS or CC, and either LF or LRF. Low = any other combination.
Study Criterion: moderate/high but for clarity the actual parameters are listed in the Table under Data Output.

@3 Environment: Relates to instrument design atmospheric and oceanographic energy levels.
A low grading can imply instrument can cope with high energy if sited seaward of the surf zone.
* Requires no cloud cover if platform at high altitude.
High: Hb > 2m, Wind speed >45Kh^-1. Moderate: Hb = 1 to 2m, wind = 25 to 45Kh^-1, Low: Hb < 1m, wind <25Kh^-1.
Study criterion: moderate/high

@4 Spatial scale: refers to a longshore swath only as all methods (except those tagged #) satisfy sampling criteria in the cross-shore direction.
refers to cross-shore spatial scale as this differs from longshore sample spacing.
High > 100m, Moderate = 10 to 100m, Low < 10m.
Study criterion: moderate/high

@5 Temporal Scale: refers to the nature (discrete/continuous) and rate of sampling.
High = continuous sampling @ < 10^5 seconds, ie approximatey 24 hours (spectral components obtainable).
Medium = discrete sampling @ < 10^5 seconds (parameters obtained).
Low = discrete sampling @ > 10^5 seconds (parameters obtained)
Study criterion: moderate/high

@6 Accuracy; includes measurement limitations plus system errors

	SE(m)	SD(degr)	SP(ms-1)	SF(Hz)	ST(sec)	SL(m)	LE(m)	LF(Hz)	LR(m)	LRF(Hz)	CS(ms-1)	CC(ms-1)
High	.1	10	.1	.001	.1	1	.1	.001	.1	.001	.1	.05
Medium	.25	20	1	.015	1	5	.1	.001	1	.001	.25	.1
Low	>	>	>	>	>	>	>	>	>	>	>	>

If not all data output parameters for a particular method fit a single grade (high/med/low) then the group tendency, which was always evident, was assigned.
Study criterion; moderate/high

@7 Skill Level; refers to the overall level of user training and experience required for equipment establishment, operation/maintanence, data reduction etc.
High = extensive professional training/experiemce, Moderate = technical training/experience required, Low = little training/experience required.
Study Criterion: low/moderate

@8 Total Cost; refers to cost per month for equipment and labour to cover establishment/recovery, operating, maintenance, downloading and reduction, depreciation etc.
Assumptions: Data collection period of 2 to 5 years,
Minimum of one set of readings per day,
For instruments capable of measuing at a single site 3 units are required to achieve spatial coverage.
Low < $1000, Medium = $1000 to $2000, High > $2000.
Study Criterion: low/moderate

@9 Reference literature is either specifically techique focused or is a major project utilising the technique.
1: Hemsley et al (1991), 2: Shum et al (1993), 3: Goda (1983), 4: Stewart and Teague (1980), 5: Lillesand and Kiefer (1987), 6: Lippman and Holman (1991), 7: Fox and Davis (1978), 8:Mattie and Harris (1978), 9:Shemer (1993), 10: Sasaki et al. (1976), 11: Horikawa and Sasaki(1972), 12: Katoh (1981), 13: Holman and Bowen (1984), 14: Carlson (1984), 15: Holland and Holman (1993), 16: Bailey and Shand (1994), 17: Holland et al (1991), 18 Thornton and Guza 1982 19: Guza and Thornton 1989 NSTS, 20: Sallenger et al 1983, 21: Aubrey 1989 NSTS, 22: Tang and Dalrymple 1989 NSTS, 23; Nayak and Sahai 1985.

The acceptance criteria achievement results for the different morphological and hydro-dynamic measurement techniques are summarized in Table 3. These results demonstrate better all around performance by the elevated terrestrial-based methods.

Table 3

Relative performance of measurement methods.

METHOD	MORPHOLOGICAL			HYDRODYNAMIC		
(location based)	n	Mean	Range	n	Mean	Range
Ground Contact	6	2.2	2 to 3	2	2.0	2 to 2
Water column	1	1.0	1 to 1	3	2.0	2 to 2
Sea surface	1	1.0	1 to 1	3	2.0	2 to 2
Terrestrial	4	4.5	4 to 5	4	4.25	3 to 7
Aerial	5	1.9	1 to 3	4	2.25	1 to 5
Outer Space	2	2.0	2 to 2	1	4.0	4 to 4

3. IMAGE SENSING and PROCESSING

Remotely Sensed Images

Remote sensing implies the observation and measurement of an object without contacting that object, thereby including force fields, acoustic wave distributions, or electromagnetic radiation. The previous section identified methods using sensors elevated above the sea surface as being most likely to meet the study objectives for both morphological and hydrodynamic data acquisition. Such sensors usually detect electromagnetic radiation. This energy has interacted with the atmosphere and earth surface features thereby containing signals from which information can be extracted (Curran 190). The energy source may be externally generated by for example the sun (passive systems), or self generated such as with radar (active systems) (Wolf, 1974).

With remote sensing, the term 'image' is used generically for any pictorial representation of data (Lillisand and Kiefer, 1987). In the case of elevated sensing, the image data has usually been detected either electronically or photographically using solid state or chemical emulsion to 'sense' electromagnetic radiation (Lillisand and Kiefer, 1987). Whereas photographic sensors detect both the signal and its record (by the emulsion), detected video signal (like that of other electronic sensors), is recorded separately, either onto a magnetic tape as occurs with a video, or to computer disc (Lillisand and Kiefer, 1987). These recorded signals are the image data, hence produce images upon display, either a photograph or on a VDU.

Video and photographic comparison

Elevated terrestrial data collection equipment includes both video and photographic cameras. This was to be expected as their sensors sample a similar portion of the electromagnetic spectrum and produce similar images both of which may be subjected to digital image processing. However, there are several important differences between photographic and videographic methods which should be recognised.

Video sensors have a broader spectral range, narrower spectral band imaging ability, improved calibration, can electronically transmit data, the system is interactive, cheaper to operate, can have audio input and provides a moving record of an event (Everitt, 1988; Lillisand and Kiefer, 1987; Meisner and Lindstrom, 1985). By cantrast, the photographic image, however, has greater spatial resolution and is more suited to hard copy end use (Lillisand and Kiefer, 1987).

Image information abstraction

Obtaining information from images was initially limited to visual image interpretation methods which utilized the ability of the human mind to qualitatively evaluate spatial pattern within a scene (Lillisand and Kiefer, 1987). However, in addition to the high labour/skill requirement, limitations in detecting tonal differences, or simultaneously analysing multiple spectral images, encouraged the development of quantitative methods (Lillisand and Kiefer, 1987).

Optical filtering techniques to enhance first photographic and later radar images began in the 1950's (Marion, 1991). Later, with the advent of third generation digital computers, image digitisation (based on intensity variation) and subsequent processing became possible (Marion, 1991). With developments in (remotely sensed) object capture and digital image processing hardware and software these methods have now found application in most disciplines (Marion, 1991).

With image processing, the image data may represent an object which is itself an image such as a map, or alternatively has only an immaterial existence such as a mathematical concept, (Marion, 1991). Image processing consists of procedures involving: object illumination; image capture, i.e. sensor imaging and digitisation; and algorithm development and implementation, i.e. the actual image processing (Bailey, 1985). Image processing is often defined or described by the types of applications it is used for (Gonalez and Wintz, 1977, Marion, 1991) and the main applications are:

1) “Image coding” where image processing is used to reduce the volume of data in an image for storage or transmission by coding, compression, and image approximation techniques.

2) “Computer assisted vision” where pictorial information is improved in preparation for human interpretation. These techniques include:

- mathematical transformations for image rectification associated with lens distortion, perspective distortion, or to achieve a particular map projection,
- image enhancement which involves processes such as noise reduction, nonlinearity compensation, contrast adjustment, and edge sharpening,
- image restoration recovers information from a degraded image such as a blurred photograph, and
- Image reconstruction which restructures information into a more convenient form for display or further processing, and

3) “Image (or scene) analysis” to extract information contained in the various objects of an image for uses such as automated machine control of an activity (machine vision), or pattern recognition using mathematical morphology. The basic techniques are attribute or invariant property extraction, and segmentation. However, such algorithms may incorporate techniques already described for computer assisted vision as preprocessing steps.

Image processing enables the potentially huge amounts of spatial and temporal data contained in surf zone image sets to be rapidly utilised. Recent coastal studies incorporating such techniques include: dune morphology (Jungerius and Schoonderbeek, 1992); step/bar crest detection (Lippmann and Holman, 1990; Lippmann et al., 1993); beach-face effluent zone detection (Shoshany and Degani, 1992); and swash-front detection (Holman et al., 1990, Holland and Holman, 1993; Bailey and Shand, 1994).

4. TIME-STACK IMAGERY

An image processing technique recently used in several surf zone data abstraction algorithms, is 'time-stacking'. The resulting image provides an alternative way of viewing time-dependent data for interpretation and analysis purposes. It appears Aagaard and Holm (1989) were the first to use time-stack images in coastal investigations and their application is described later in Section 6.

The time-stack process is based on the construction of a new image comprising a particular section of image (intensity data) from an overlaid sequence of images (photos, video frames) being stacked along another (time) axis. If the entire (registered) photo, video or map series is utilized, the then the resulting image may be described as a **three-dimensional (3D) time-stack.** However, image-based 3D site-stacks are not at present used due to computing/memory limitations. Alternatively, if a slice of each input image is used for the input image set, (say sampled along a transect on each photo), then the result may be described as a **2D time-stack**. Finally, if a single point (or group of adjacent points) are sampled from each image and stacked, then the result may be referred to as a 1D time-stack.

The nature of the time-stack is also a function of the type of input image. For our purposes the following types are used:

- 'instantaneous images' where the exposure time is < ~1 sec such as individual video frames, cine film or photographs.

- 'time-averaged images' where numerous instantaneous images have their corresponding intensity values averaged. Such images are referred to as 'time-exposure' images where a number of video or cine frames are used, or 'time-lapse or long exposure' images in the case of still photography where averaging is achieved by the use of extended shutter times and compensating neutral density filters,

With respect to surf zone data, time-stacks created using instantaneous images depict the sea surface as influenced by the passage of individual incident waves, so the output image essentially contains hydrodynamic information and may thus also be referred to as a **hydrodynamic time-stack**.

In practice, a hydrodynamic time-stack is formed by playing the video record of interest through a VCR connected to a PC fitted with a frame grabber card. This captures the assigned intensity values from a point, line, or plane (the entire image), into the frame buffer memory and this digital output image is then transferred to computer storage. By repeating the process on each sequential video frame at a predetermined sampling rate, the time-stack is constructed.

To demonstrate this, along with a variety of other videographic techniques considered in this document, a surf zone video record from a site on the moderate to high energy, sand dominated New Zealand west coast will be used. Figure 2 shows a sample video frame from the seaward orientated camera located on cliff top 44 m above MSL. The image processing system we use consists of a 66MHz DX2, 16MB ram, frame grabber card, 14" SVGA monitor, 17" image display consol, and operates VIPS6 (vision image processing system) originally developed by Bailey and Hodgson (1988).

An example of a 1D instantaneous or hydrodynamic time-stack, for the location marked A in Figure 2, is shown in Figure 3. This image represents the sea-surface change as it is affected by gravity waves in the region of the inner bar break point over a 60 second interval.

Examples of 2D-hydrodynamic time-stacks from the central shore-normal transect in Figure 2 are shown in Figure 4A and Figure 4B. These two images illustrate individual wave histories using different record lengths and sampling rates. The higher time resolution in Figure 4A enables visualisation of wave transformation from shoaling to runup to bachrush. In Figure 4B, longer-term breakpoint and run-up variations are demonstrated. Further interpretation of these hydrodynamic time-stacks is included within Section 6.

As wave breaking is a function of water depth, the foam pattern shown on an instantaneous image is indicative of the underlying morphology. In any sample involving gravity waves, however, a height distribution occurs resulting in some cross-shore variation in the breakpoint location. The foam pattern will also vary intensity-wise from instant to instant depending on the location of shoreward propagating broken waves. If the instant images are intensity averaged over say 5 to 10 minutes, then all information concerning individual waves is lost; but by filtering out the intensity variations associated with individual waves, the resulting intensity pattern provides a stable signal of seabed (relative) topography, thus defining surf zone morphology with higher intensity areas inferring wave breaking and thus shallower than areas without wave breaking (deeper). Figure 5A depicts a time-averaged image, referred to as a time lapse or **time-exposure image**, derived from 5 minutes of record of the scene in Figure 2. Note that two adjacent time-lapse photos, taken with a Kodak Wratten 4.60 Neutral Density filter, have been joined to create the Figure 5A raw image. Also note that the intensity profile for the central transect in 5A is identical to that shown by the curve on the left side of Figure 4B

To be more useful for data abstraction these time-averaged images are next ‘rectified’ to remove perspective distortion (thereby creating a ‘birds eye’ view), and then ‘georeferenced’ to ground co-ordinates allow direct comparison with other media. This is described in Bailey and Shand (1993). The transformation of Figure 5A is depicted in Figure 5B. The three white lines shown in Figures 5 illustrate the level of perspective correction carried out the rectification algorithm. To further facilitate subsequent analysis, a 'coastline straightening' transformation (Bailey and Shand, 1993) was written to providing a rectilinear planimetric view.

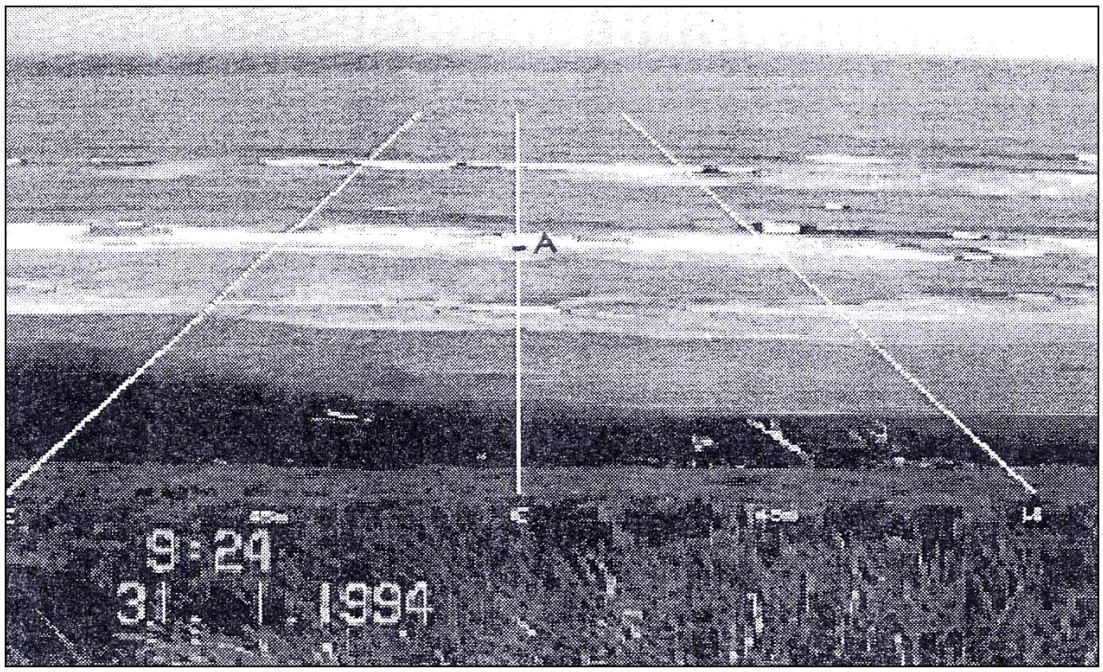

Figure 2
A video frame image of a surf zone from the moderate to high energy sand dominated New Zealand west coast. The camera has been orientated seaward and three shore-normal transcects marked.

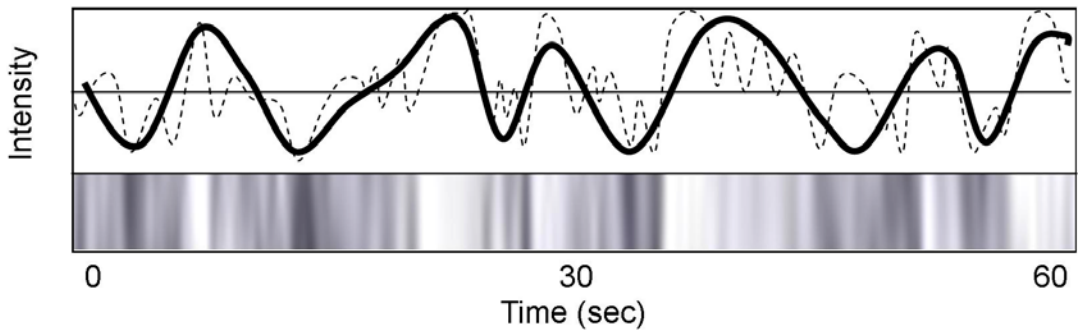

Figure 3
A 1D hydrodynamic time-stack image depicting the sea surface at point A in Figure 2, i.e. this time-stack comprises sequential intensity values from a single point. Note that along the base of the image the intensity values have been expanded in width for illustrative clarity. Depicted above this time-stack is a graph of the intensity values with the thick line having been smoothed to define six wave motions.

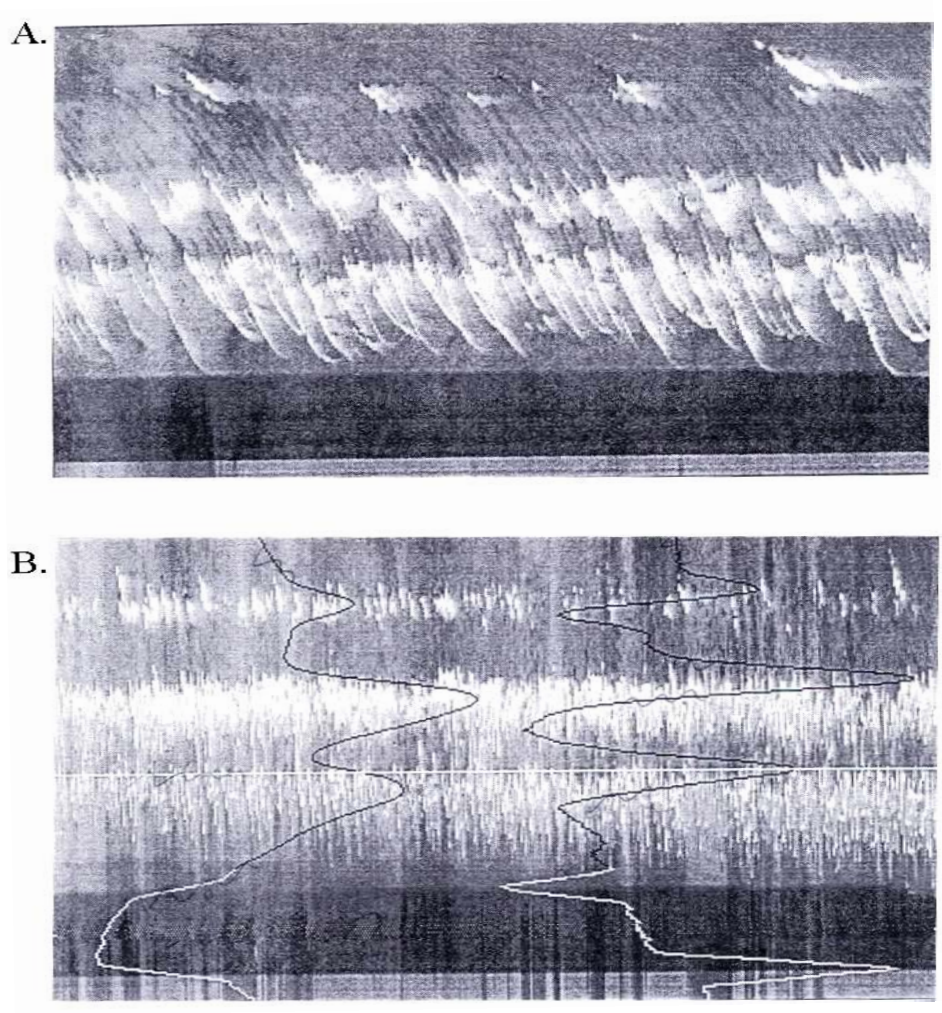

Figure 4
Both figures depict 2D-hydrodynamic time-stacks images from the central transect of Figure 2. Figure 4A was sampled every 0.25 seconds over 6 minutes while Figure 4B was sampled every 2 seconds over 52 minutes. Note that the vertical curve on left of B denotes time-averaged intensity which in fact infers the underlying morphology (see text). The curve on right depicts the derivatives used to help locate change in intensity.

The time-stack image constructed using time-averaged input images is referred to as a **morphological time-stack**. . Figures 6A and B show examples of such time-stacks using time averaged, rectified input images. In these cases the slicing has been carried out shore-normally so the vertical axis represents offshore distance. Interpretation and data obtainable from time-averaged images and morphological time-stacks will be considered further in Section 5.

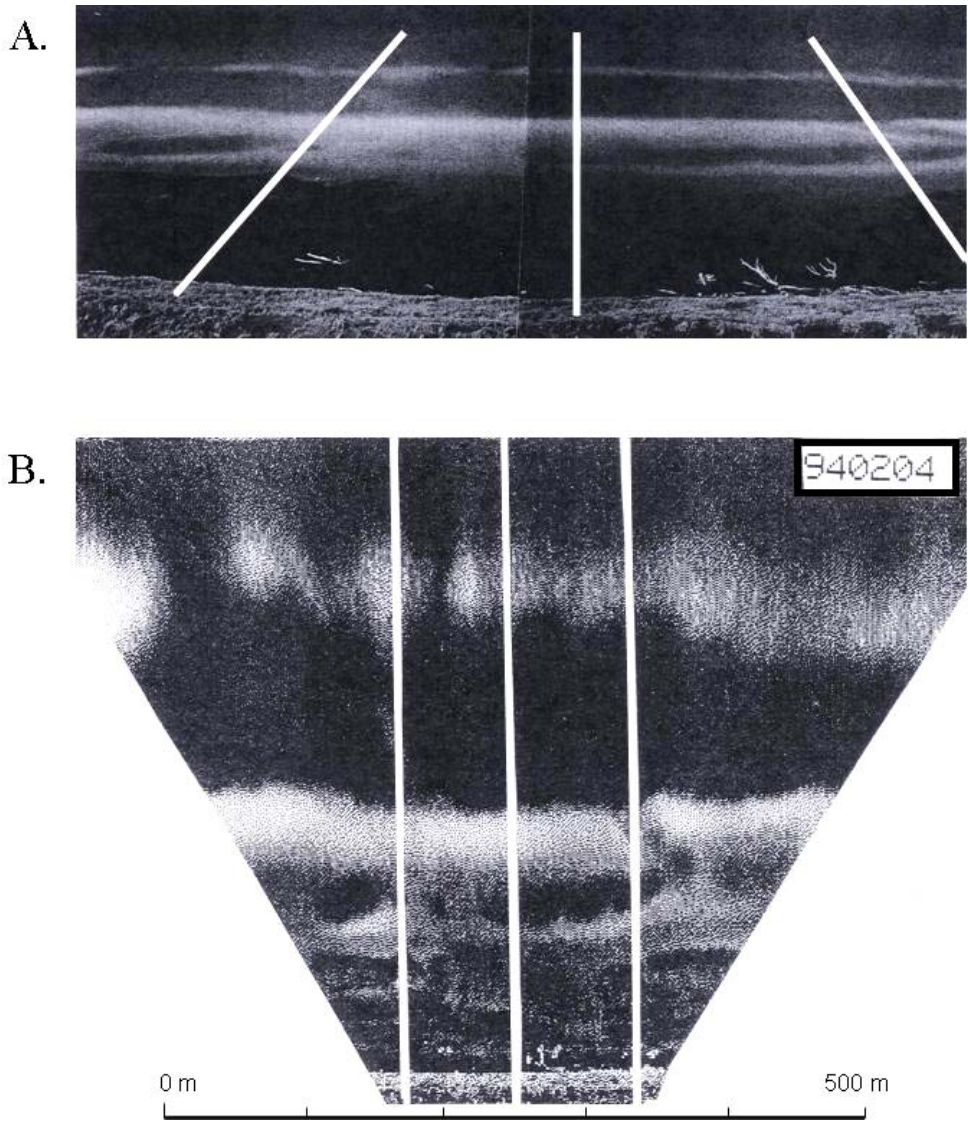

Figure 5
The upper figure (A) depicts a time-exposure image created by time-averaging intensity values from a set of video frames (or by taking a filtered time-lapse photograph). The resulting image infers the underlying morphology across the area of interest. Figure B displays the corresponding perspective-corrected or 'rectified' image from which spatial measurements can be made directly. The white 3 lines illustrate the extent parallel lines (Fig B) are perspective distorted in an oblique image (Fig A). Also note that the intensity variation along the central transect in Fig A, is identical to that shown by the time-averaged curve in the hydrodynamic time-stack in Figure 4B.

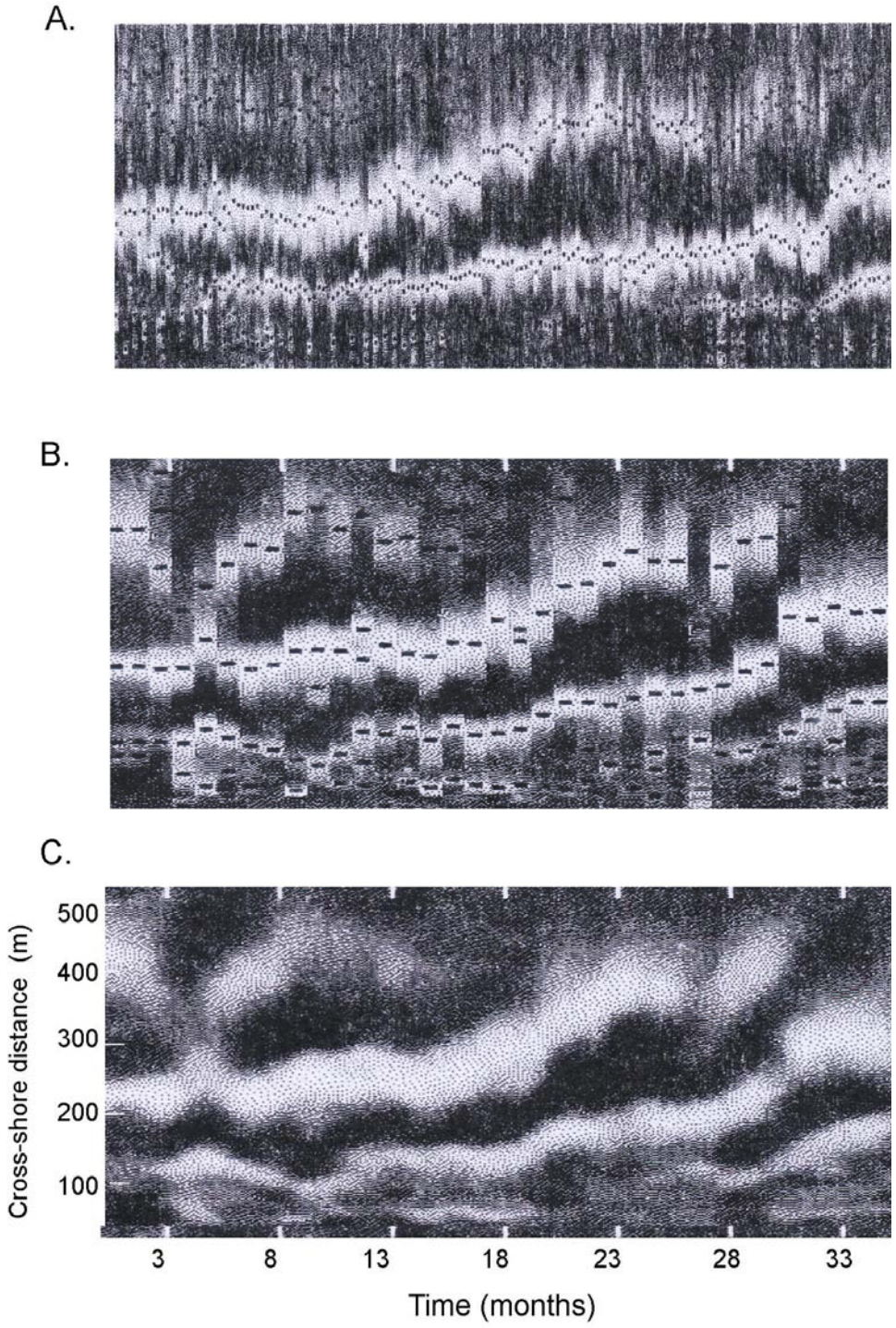

Figure 6
These examples of 2D-morphological time-stacks show beach and bar change through time along transect C in Figures 2. The input sequence for Figure 6A is sampled at 3 to 5 days over a 36 month period. The black rectangles define bar crests based on the location of intensity maxima determined by fitting a parabola to each intensity profile. Figure 6B used the same record but sampled at monthly intervals. In Figure C, the data for B has been interpolated and intensity-normalized.

5 MORPHOLOGICAL DATA FROM VIDEO RECORDS

Beach morphology

Beach (foreshore) profile data have recently been obtained by Holman et al. (1991) using terrestrial video records from a single camera site and subsequent image processing. While their field images were captured at low tide from an elevated location, some form of physically marking the transect surface was required prior to recording. Vertical resolution was controlled by pixel size to 0.1 m. More labour-intensive methods have been used such as recording a set of permanent calibrated poles and manually reducing the beach surface intersection (Hoad, 1991) using photographic images; the technique applies equally well to video frame images.

As described in Section 4, planimetric (2D) data of foreshore morphology can be derived from a single elevated video frame or photographic image taken at low tide and subjected to filtering and oblique photogrammetric rectification. To incorporate elevation to derive 3D data, photogrammetric analysis of a stereo pair is required (Slama, 1980). Although variations are possible such as the single image system developed by Collins and Madge (1981) for obtaining discrete 3D coordinates for a set of vertically graduated targets using manual photogrammetry.

Inshore Morphology

The main morphological use of video records has been to provide information seaward of the low-tide step (Lippmann and Holman, 1989; Lippmann and Holman, 1990; Lippmann, et al., 1993). As with aerial photographic images, determining surf zone morphology has been based on the preferential breaking of incident waves in shallower water and as described in Section 4 with the intensity profile mimicking bar - trough bathymmetry (N.B the average intensity curve in Figure 4B which is equivalent to the intensity variation along the central transect on Figure 5A.

Ground truthing at the CERC Field Research Centre at Duck, North Carolina by Lippmann and Holman (1989) verified that such digitised intensity curves were similar in form to their associated surveyed morphological profiles. We may thus refer to these analogues, i.e. the intensity image and associated digitised curve as **morphological intensity images**. While geometric transformation to a horizontal plane was described earlier, the intensity profile cannot be directly calibrated with elevation or position as the intensity at each point (or pixel co-ordinates) on the transect is influenced by, i.e. is a function of, several variables. These variables will either horizontally translate the intensity values, which in this case alter cross-shore distance, i.e. the length scale or location (L) of features such as bar crests or troughs, and/or alter the intensity contrast which changes the profile amplitude scale or relief (R). These problematic variables can be grouped as equipment limitations, photogrammetric

parameters, environmental controls, and sampling variations. Of particular significance are breaking wave height, and sea level, in particular tidal change.

While some of the limiting factors can be minimized by, for example, successive samplings at the same sea-level and similar wave height, it is important to understand the nature and magnitude of these intensity controls as they determine the final image resolution. With these constraints in mind, the image-based technique can successfully detect morphological features at various spatial and temporal scales unobtainable using conventional methods in moderate to high energy environments. The data abstracted from 'morphological intensity images' is usually limited to bar crest and trough location because of the relative nature of the elevation dimension. As noted in Section 4, feature-detection algorithms have been written by the authors to automatically detect these locations (e.g. bar crests) on the intensity profiles and these are depicted by the black rectangles in Figure 5A and B.

Further detail on morphological intensity image techniques including photographic and video recording, error analysis, image rectification, and image analysis, can be found in Lippmann and Holman (1989), Lippmann and Holman (1993), Bailey and Shand (1993) and Bailey and Shand (1994).

Morphological behaviour

Morphological change can be visualised using morphological time-stacks. As noted Section 4, the 1D time-stack displays relative bed elevation change at a point within the scene view. The 2D stack displays the relative elevation over time along a line (usually a shore-normal transect for surf zone studies), and the 3D stack (future display option)) depicting plan-view relative elevation. The latter case is equivalent to the area-time prism developed by Davis and Fox (1972) for visualisiing erosion and deposition change in the surf zone.

The following points of geomorphological interest are evident in the time-stacks displayed in Figure 6:

- Primary sand bars **form** on the lower beach (base of image);
- The bars **systematically migrate** seaward (toward the top);
- The bars appear to **dissipate** in the outer surf zone a couple of years later, and
- The bars may **bifurcate** during their offshore migration with the inner segment migrating landward and either dissipating within the trough, or else welding onto the adjacent bar or beach-face, a process taking up to 3 months.

These different features are significant in terms of assessing and developing morphodynamic models for the littoral environment. For example, these data challenge the generally accepted behaviour of inshore sand-bars as being features in dynamic equilibrium (O'Hare and Huntley, 1994). While experimental work (e.g. Bowen and Inman, 1971) and numerical modeling (e.g. Davidson-Arnott, 1981; Dally and Dean, 1984) have demonstrated such

stability can occur under certain conditions, field verification has been generally lacking, possibly due to the difficulty in acquiring comprehensive data. The extensive CERC foreshore/nearshore profile archive collected by the CERC Field Research Facility at Duck North Carolina provides the exception. Three net offshore bar migrations can be identified in 11 years (1981 to 1992) of fortnightly profile data (Birkemeier, 1984; Lee and Birkemeier, 1993; Lippmann et al., 1993). Some of these authors speculated this behaviour may have been associated with migrating oblique bars such as noted by Short (1975), Verhagen (1989) and Kroon (1991); however, such bars have been attributed to high tidal currents (Van de Meene and Van Rijn, 1994) which neither either on the Duck coast nor at the New Zealand study site. Terrestrial-based videographic data may now help resolve the matter of how widespread systematic seaward migration is on the worlds open coasts.

Data in the nearshore literature provides evidence for a number of apparent bifurcations of inshore sand bars, although this behaviour was not recognised by any of the authors (e.g. Greenwood and Davidson-Arnott, 1975; Owens, 1977; Holman and Sallenger, 1986; Holman and Lippmann, 1987; Bauer and Greenwood, 1991; Kroon, 1991; Van de Meene and Van Rijn, 1994). To explain such phenomena it is necessary define the process and closely sampled time-exposure images offer a feasible way of achieving this. Animating the rectified images and producing/analysing morphological time-stacks are also promising.

Shorelines

Video imagery and its analysis can clearly show the location and behaviour of the boundary between the dry upper beach face and the saturated lower beach. In the 6 min time-stack (Figure 7A) the boundary is controlled by wave runup, while in the 6 hr time-stack (Figure 7B) the influence of the high tide is evident. The wet/dry boundary on historical aerial photographs has been used as a shoreline proxy in coastal change studies (Morton, 1991; Thieler and Danforth, 1994). However, even the simple video imagery presented here show such an approach must be used with caution. Nonetheless, such imagery offers future potential for defining more stable shoreline indicators.

6. HYDRODYNAMIC DATA FROM VIDEO RECORDS

Foreshore techniques

Video records have recently been used to obtain overwash velocities by Holland et al. (1991) using methodology similar to that described below for deriving wave phase speed. Others such as Marra (1992) have obtained swash/backwash velocities and depths via manual frame by frame digitization procedures.

Photographic of cine movie film, and more recently video records, have been used in a number of studies investigating wave run-up by collecting slope excursion data (Wright,

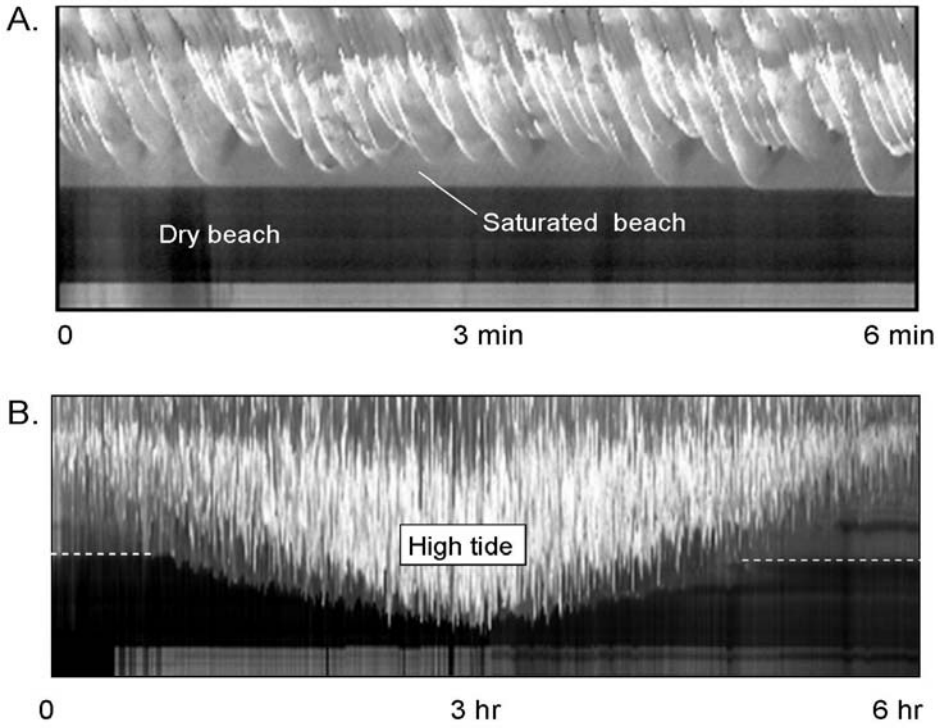

Figure 7
Two-dimensional hydrodynamic time-stacks from the field site illustrating wet and dry beach-face partition sometimes used in shore-line change studies. In Figure A the boundary is controlled by wave run-up. By contrast, the longer sampling period in B (6 hours c.f. 6 minutes) illustrates the tidal influence.

1976; Carlson, 1984; Holman and Bowen, 1984; Holman and Sallenger, 1984; Holman and Sallenger, 1985; Holman and Sallenger 1987; Aagaard, 1990; Holman et al., 1990; Holland and Holman, 1993). The history of the development of such techniques can be found in Bailey and Shand (1994) by way of introducing an automated swash-front detection algorithm which uses an instantaneous video sequence of images to make a 2D-hydrological time-stack covering the swash zone. Their programme detects and tracks the swash-front under all but the lowest light and contrast conditions and a manual override is available is these situations. Applying this algorithm to the time-stack in Figure 4A yields the track shown in Figure 8.

Inshore Methods

Video (or photographic) records have been used to a lesser extent in the acquisition of surf zone hydrodynamic data. Huntley and Bowen, 1975; Hotta and Mizuguchi, 1980; Carlson, 1984; Crowson et al., 1988, obtained water level and breaking wave data at discrete locations across the surf zone using cine film and graduated pole arrays Lippmann and Holman (1991) have measured wave phase speed and direction using video records and 1D-hydrodynamic time-stacks, such as shown in Figure 3. In this case, input image sequences from video tape

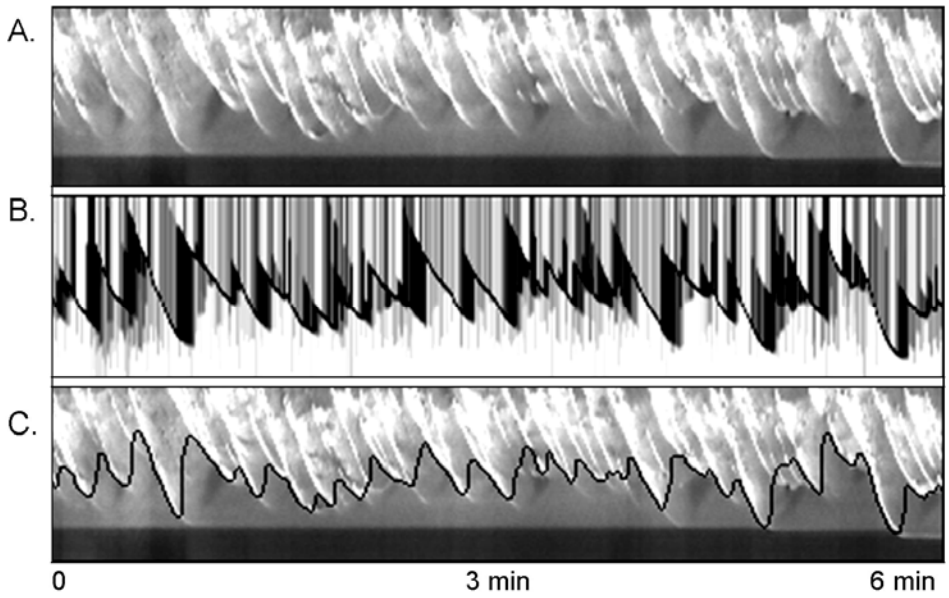

Figure 8
A raw 2D-hydrodynamic time-stack (A) depicting waves running up and down beach face. Swash-front detection using the automated tracking algorithm (Bailey and Shand, 2004) is, in part, (graphically) illustrated in B, with final result overlaid in C.

are obtained for known locations within the surf zone. By comparing the time- stack images with corresponding pressure transducer records they demonstrated that the images were analogous to surface elevation changes corresponding to broken gravity waves. Velocity components of the primary wave train were then determined by two methods: firstly using celerity and peak wave number spectra, and secondly using sensor separation and time lag between individual breakers using both the cross- covariance function and phase spectrum. Results showed “close agreement” between different methods and also with wave theory.

It should be possible to derive other standard wave properties including wave height at the break-point(s), wave period(s), wave length, and wave speed by utilizing 2D-hydrodynamic time-stack. These parameter signatures are illustrated in Figure 9 which depicts a series of incident waves being transformed as they cross the surf zone. Such features can be metricated for individual waves using image geometry, and image processing can also define breakpoint modulation. Determining wave parameters by repeating the process to gain a statistically representative sample, however, would be time consuming and impractical on anything other than an experimental basis**.** At present the authors are developing algorithms which will automate the extraction procedure thereby providing a viable means of collecting such hydrodynamic data. In addition, we anticipate the isolation of a continuous water level records for sites across the surf zone suitable for Fourier Analysis.

The ability to determine H_b using the 2D-hydrodynamic time-stack would provide a means of testing various linear and nonlinear wave shoaling theories. Accurate calibration can also be carried out for wave height visual observations and instrument-assisted techniques such as the pole horizon method (Patterson, 1985; Patterson and Blair, 1983).

The surf zone video record would not directly enable the detection of sea-surface oscillations in the infragravity and far infragravity bands as they have no direct breakpoint intensity expression. However, such frequencies are discernable from either the run-up record as already described or, perhaps from the tide/gravity-wave height combination where preferential groups of incident waves break as illustrated by the sporadic wave breaking on the outer bar on the hydrodynamic time-stack in Figure 3. These breaking wind waves define infragravity motions as they lie in the depression between trapped, free, and interacting longwave peaks (Symonds et al., 1982; Huntley and Kim, 1984; Lippmann, 1993; List, 1992; O'Hare and Huntley, 1994).

The visual wave history presented in the 2D-hydrodynamic time-stack also provides a means to study other aspects of breaking wave dynamics including Galvanian (1968) wave types, nonlinear interactions associated with multi-wave trains, shoaling, and bar/beach-face breaking associations. For example, the formation and behaviour of secondary waves or solitons (Davidson-Arnott and Randall, 1984; Galvin, 1968; Huntley and Bowen, 1975), can be seen in Figure 4a and Figure 9.

Studying sea-surface dynamics associated with river inflow, rip-channel activity, or other surfzone/nearshore circulation, could also be facilitated by the use of elevated video records and image processing to track natural or artificially created (dye injection) colour boundaries. It is also possible that automated foam tracking algorithms could be written, thereby providing spatially extensive and temporally continuous surface current data.

Although not part of the present work, video images have recently been used in morpho-hydrodynamic wave flume experiments. In a comprehensive investigation of vortices associated with wave breaking Zhang (1994) was able to track their development and morphological impact using video records. Video cameras were also used to record a continuous image of surf zone wave transformation, swash, and run-up during the meticulously monitored SUPERTANK experiments at Oregon State University (Kraus et al., 1992). Time-stack techniques could be applied to such data. Wave-tank data may also be able to verify video-derived parameter values.

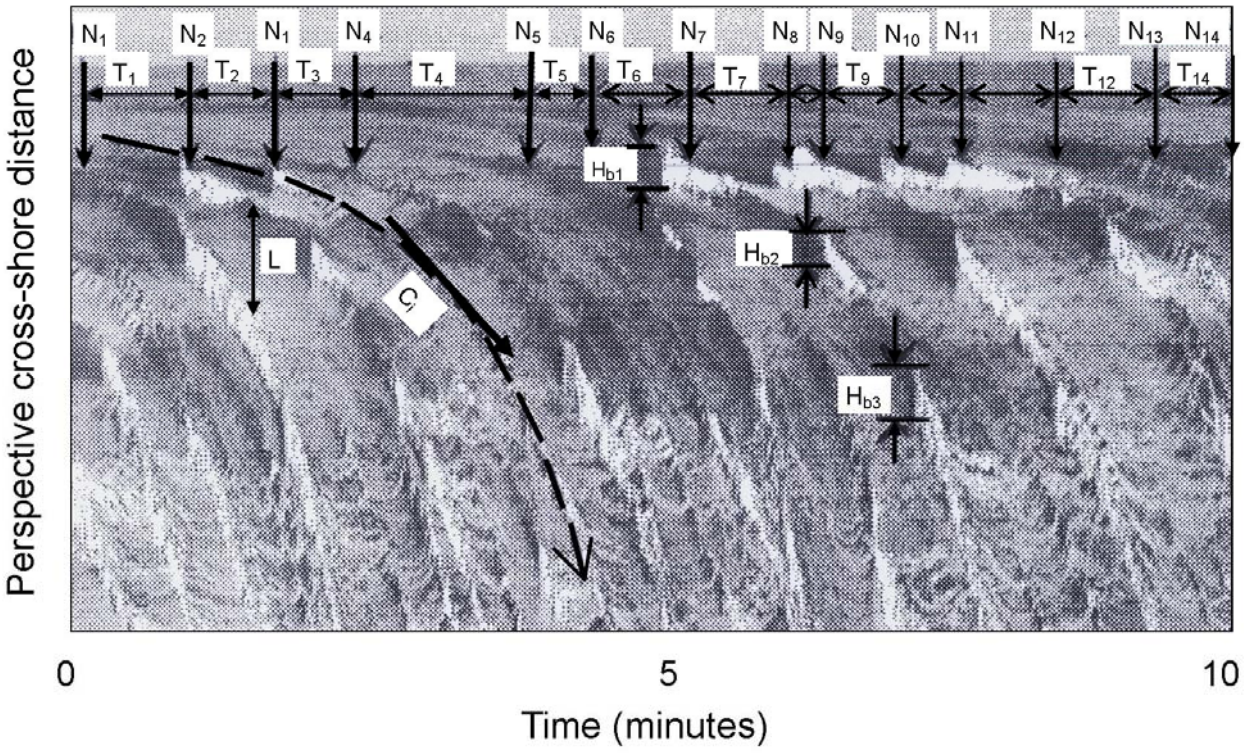

Figure 9
In this 10 min long 2D-hydrodynamic time-stack, a sequence of waves numbered ($_{N1-14}$) have been defined along an outer bar, plus two more further landward. Incident wave periods [T_{1-14}], are also marked along with examples of the breaking wave height signal at different cross-shore break-points ($H_b n$). Examples of instantaneous wave speed Ci at time t within the surf zone (where Ci = dDi/dt and Di is cross-shore distance to the wave at time t), and wave length (L) just landward of the outer ber are also marked.

7. DISCUSSION

The morphological and hydrodynamic data acquisition method comparisons (Tables 1 and 2) demonstrated the advantage of elevated terrestrial video sensing and image processing in meeting our monitoring criteria. The only significant morphological area of videographic limitation was an inability to deliver absolute bathymetric elevation data. The requirements for visible light and wave breaking during the data collection phase are not generally constraints at the sampling time-space scales under consideration. Other present hydrodynamic shortfalls such as automated acquisition of incident wave heights and current measurement, should be videographically derivable using the time-stack approach.

Sampling Advantages

Video sampling and other elevated image-based methods of field data collection, allow for a variety of sampling advantages which further increase its ability to meet our data acquisition objectives. The non-contact aspect of such data collection is particularly important for coastal monitoring where dangerous or difficult conditions, or access limitations hamper or prevent data collection at the required scales (Kidson and Manton, 1973; Lillisand and Kiefer, 1987). An image-based approach permits sampling at the required temporal scale rather that at a resolution constrained by the nature of the morphology under investigation (Lane et al 1993), and thus avoids the practical spatial/temporal scale mismatches which often occur with geomorphological field work.

As the image is an unbiased data source which records an infinite number of data points, potentially usable information is contained at each visible point (Chandler and Moore, 1989). This characteristic facilitates retrodictive data acquisition if alternative aspects, or even different phenomena, require investigation at a later date. For example, the identification of bar bifurcations during the net offshore bar migration process (Figure 6) was an unexpected result, and now the image data will enable subsequent in depth study of this phenomena.

Image Processing and Visualisation

We have shown how video records facilitate subsequent digital image processing and the construction of time-stack images. This hydro/morpho image, together with other artificial and raw images, offers a variety of computer-assisted vision opportunities both for data abstraction and system comprehension.

Computer-assisted vision is now a major user of image processing as the speed, memory and storage capacity of present generation of computers, together with the recent ability to collect comprehensive data, enable algorithms to now transform large data sets into the universal language of pictures (Kaufman, 1994). This is referred to as

scientific visualisation which, often with the aid of interactive graphics, provides for provoking insights into the make up of the associated phenonemon (Kaufman, 1994).

The two primary subfields of scientific visualization are volume (static form), and flow (time varying) visualization (Kaufman, 1994). The latter, also referred to as dynamic scene or image sequence processing (Aggarwal, 1986), consists of visualizing features and tracking their evolution, thereby providing information on the nature, behaviour, and causal associations of areas of scientific interest (Samtaney et al., 1994). The application potential for coastal science is vast.

While flow visualization is ultimately concerned with 3D feature extraction, tracking, and modeling algorithms, i.e. quantitative analysis (Balder, 1983, Samtaney et al., 1994), as we have already demonstrated, visualising an object history with a time-stack can be of primary importance in identifying fundamental forms and processes. Simply viewing animated processed data using video technology, i.e. scientific video animation (Globus and Raible, 1994) is also a highly effective form of flow visualisation as is demonstrated by, for example, Cole and McGregor (1994) regarding sea surface temperature change, or phenomenon initialization with atmospheric circulation (Wood, 1992). Our initial video animation indicate such flow visualization will prove very useful for investigating the initial states, formative processes and evolutionary behaviour of surf zone features described earlier when considering morphogical time-stack examples.

Cognitive Psychology

To appreciate why we can gain information and insights when viewing images it is necessary to consider the work of cognitive psychologists. Gestalt psychologists have found that elements of an image look different when viewed in a wider context. Symmetry or continuity can be perceived when embedded in more general pattern (Haber and Henshenson, 1980). These psychologists have also found that we are able to detect unification when objects are placed near to each other (Haber and Henshenson, 1980). We would also expect this to occur temporally with animation.

Visualisation has been found to assist in the isolation of invariants and regions of interest and this enables the extensive data sets obtainable by remote sensing to be constrained thereby becoming more manageable for analysis and modeling (Samtaney, 1994). This is of particular relevance to surf zone scientists for whom the search for primary indices and associated data rendering has been fundamental in their attempts to model the multivariate, data rich coastal environment (de Vriend, 1993).

8. CONCLUSIONS

Videographic techniques have been shown to generally out perform other methods of surf zone geophysical data acquisition at medium spatial/temporal scales. Indeed, we consider this approach has the potential to almost be a successful stand-alone technique, i.e. is capable of providing all types of coastal data. This success is largely associated with the image-based nature of the system which facilitates sampling and post-processing including such as time-stack construction. More flexible sampling regimes can be achieved and visual inspection of both raw and processed images provide for new insights into the nature of the phenomenon under study. This can subsequently identify relevant data for rendering and analysis and also suggest the makeup of image processing algorithms to abstract these data.

ACKNOWLEDGMENTS

We wish to thank Dr Mike Shepherd (Massey University), Professor Bob Kirk (Canterbury University) and Drs Terry Hume and Andrew Lang (NIWA) for their comments on the manuscript**.**

REFERENCES

Aagaard, T., 1990. Infragravity waves and nearshore bars in protected, storm-dominated coastal environments. Marine Geology, 94, 181-203.

Aagaard, T., and Holm, J., 1989. Digitisation of wave run-up using video records. Journal of Coastal Research, 5(3), 547- 551.

Augaard, T.; Nielsen, N., and Nielsen. J., 1994. Cross-shore structure of infragravity standing wave motion and morphological adjustment: An example from Northern Zealand, Denmark. Journal of Coastal Research, 10(3), 716-731

Admiralty. 1938. Manual of Hydrographic Surveying. Hydrographic Dept, Admiralty London.

Aggarwal, J.K., 1986. Motion and time-varying imagery. In Badler, N.I., and Tsotsos, J.K. (eds.), Motion: Representation and Perception. Elsevier Science Publishing Co., pp163-170.

Aubrey, D.G., 1979. Seasonal patterns of onshore-offshore sediment movement. Journal of Geophysical Research, 84, 6347-6354.

Aubrey, D.G., 1989. Measurement errors for electromagnetic current meters. In: R.J. Seymour (ed.), Nearshore Sediment Transport Study.

Aubrey, D. G., and Seymour, R.J., 1989. Methods for position control and beach face profiling. Marine Geology 49: 257-78.

Austin, J.; Blakemore, K.; Cooper, J.; Davies, P.; Dean, M.; Fairbairn, R.; Gower, R., and Pitty, A., 1994. Geographical Abstracts: Physical Geography.

Bailey, D.G., 1985. Hardware and software developments for applied digital image processing. PhD thesis, University of Canterbury, New Zealand.

Bailey, D.G., and Hodgson, R.M., 1988. VIPS - a digital image processing algorithm development environment. Image and Vision Computing, 6, 176-184.

Bailey, D.G., and Shand, R.D., 1993. Determining large-scale sand bar evolution. Proceedings of the First New Zealand _Conference on Image and Vision Computing, pp. 109-116.

Bailey, D.G., and Shand, R.D., 1994. Determining wave run-up using automated video analysis. Proceedings of the Second _New Zealand Conference on Image and Vision Computing,ÿpp. 2.11.1 - 2.11.8.

Balsillie,J.H., and Carter, R.W.G., 1984. The visual estimation of shore-breaking wave heights. Coastal Engineering, 8, 367-385.

Bauer, B.O., and Greenwood, B., 1990. Modification of a linear bar-trough system by a standing edge wave. Marine Geology, 92, 177-204.

Bauer, B.O., and Greenwood, B., 1991. Dynamics of beach-dune systems. Progress in Physical Geography

Birkemeier, W.A., 1984. Time scales of nearshore profile change. Proceedings of the 19th International Conference on coastal Engineering, ASCE, pp. 1507-1521.

Black, K., and Healy, T., 1993. Side-scan sonar survey: Marsden Point. A report prepared for the Northland Harbour Board, New Zealand, 68p.

Bowen, A.J., and Inman, D.L., 1971. Edge waves and crescentic bars. Journal of Geophysical Research, 76, 8662-8671.

Carlson, C.T., 1984. Field studies of run-up on dissipative beaches. Proceedings of the 19th International Conference on Coastal Engineering, ASEC. pp708-723.

Carter, R.W.C., 1988. Coastal Environments: an Introduction to the Physical, Ecological and Cultural Systems of Coastlines. Academic Press, New York, pp. 617.

CERC, 1984. Shore Protection Manual, Vol. 1. US Coastal Engineering Research Centre.

Chandler, J.H., Moore, R., 1989. Analytical photogrammetry: a method for monitoring slope instability. Quarterly Journal of Engineering Geology, London, 22, 97–110.

Chandler, J.H.; Cooper, M.A.R., and Robson, S., 1989. Analytical aspects of small format surveys using oblique aerial photographs. Journal of Photographic Science, 37, 235-240.

Chappell, J., and Eliot, I.G., 1979. Surf-beach dynamics in time and space - an Australian case study, and elements of a predictive model. Marine Geology, 32, 231-250.

Cole, R., and McGregor, J., 1994. Cook Strait circulation dynamics observed using geostationary meteorological satellite (GMS). Proceedings of the 2nd New Zealand Conference on Image and Vision Computing.

Collins, B.J., and Madge, B., 1981. Photo-radiation: a new method for monitoring beach movement. Chartered Land Surveyor/Chartered Minerals Surveyor, 3, 4-11.

Colwell, R.N., 1960. Procurement of aerial photography. In Colwell, R.N. (ed.), Manual of Photo Interpretation. American Society of Photogrammetry, Falls Church, Virginia, p19-.

Crowson, R.A.; Birkemeier, H.M.; Klein, H.M., and Miller, H.C., 1988. SUPERDUCK nearshore process experiment: Summary of studies. CERC Field Research Facility, Tech Rep. CERC-88-12, 81p.

Curran, P.J., 1990. Electromagnetic radiation at the Earths surface. IEEE Transaction on Geoscience and Remote Sensing.

Dally, W.R., and Dean, R.G., 1984. Suspended sediment transport and beach profile evolution. Journal of Waterway, Port, Coastal and Ocean Engineering, 110-1, 15-33.

Davidson-Arnott, R.G.D., 1981. Computer simulation of nearshore bar formation. Earth Science Processes and Landforms 6, 23-34.

Davidson-Arnott. R.G.D. and Randall. D.C., 1984. Spatial and temporal variations in spectra of storm waves across a barred nearshore. Marine Geology, 60, 15-30.

Davidson-Arnott. R.G.D. and McDonald. R.A., 1989. Nearshore water motion and mean flows in a multiple parallel bar systems. Marine Geology, 86, 321-228

Davies, J.L., 1980. Geographical variation in coastal development. In: Clayton, K.M., (ed.), Geomorphology Texts 4. Longman, London. 212 p.

Davis, R.A., and Fox, W.T., 1972. Coastal processes and nearshore sand bars. Journal of Sedimentary Petrology, 42(2), 401-412.

Davis, R.A., and Fox, W.T., 1972. Four-dimensional model for beach change and inner nearshore sedimentation. Journal of Geology 80, 484-493.

De Vriend, H.J., 1991. Mathematical modelling and large- scale coastal behaviour, Part 1: Physical Processes. Journal of Hydraulic Research 29(6) 727-740.

De Vriend, H.J.; Capobianco, M.; Chesher, T.; de Swart, H.E.; Latteux., and Stive, M.J.F., 1991. Approaches to long-term modelling of coastal morphology: a review. Coastal Engineering, 21, 225-269.

Dolan, R., B. Hayden, P. May, and S. May., 1980. The reliability of shoreline change measurements from aerial photographs. Shore and Beach, 48:22-29.

Duncan, J. R., 1964. The effects of water table and tide cycle on swash-backwash sediment movement and beach profile development, Journal of Geology, 2, 186-197.

Eardley, A.J., 1941. Aerial photographs: their use and interpretation. Harper and Brothers, New York, 201 p.

Emery, K.O., 1961, A simple method of measuring beach profiles: Limnology and Oceanography, 6, 90-93.

Everitt, J.H., 1988. Introduction to videography: historical overview, relation to remote sensing, advantages and disadvantages. Proceedings of Videography: First Workshop, Indianna State University, 19-20 May 1988 American Society for Photogrammetry and Remote Sensing.

Fox, W.T., and Davis, R.A., 1978. Seasonal variation in beach erosion and sedimentation on the Oregon coast. Geological Society of America Bulletin, 89, 1541-1549.

Galvan, C.J., 1968. Breaker type classification on three laboratory beaches. Journal of Geophysical Research, 73(12), 3251- .

Gibb, J.G., 1979: Late Quaternary Shoreline Movements in New Zealand. Unpublished Ph.D. Thesis, Victoria University of Wellington, New Zealand.

Gibson, J.J., (1979). The Ecological Approach to Visual Perception. Boston: Houghton Mifflin.

Globus, A., and Raible, E., 1994. Fourteen ways to say nothing with scientific visualization. Computer, 86-88.

Goda, Y., 1983. Wave measurements and utilisation of wave data. Proceedings of the Sixth Australian Conference on Coastal and Ocean Engineering, Gold Coast, Australia, pp. 1- 9.

Gonzalez, R.C, and Wintz. P., 1987. Digital Image Processing. Addison-Wesley, Sydney.

Greenwood, B., and Davidson-Arnott, G.D., 1975. Marine bars and nearshore sedimentary processes, Kouchibouguac Bay, New Brunswick. In: Hails, J., and Carr, A., (eds.), Nearshore Sediment

Dynamics and Sedimentation. John Wiley and Sons, New York, pp.123-150.

Guza, R.T., and Thornton, E.B., 1989. Nearshore sediment transport. In: Seymour, R.J. (ed) Models for Surf Zone Dynamics. Plenum Press, New York, pp. 337-370.

Haber, R.N., and Hershenson, M., 1980. The Psychology of Visual Perception (second edition). Holt, Rinehart and Winston, London.

Hemsley, J.M., McGehee, D.D. and Kucharski, W.M., 1991. Nearshore oceanographic measurements: hints on how to make them. Journal of Coastal Research, 7 (2), 301-315.

Hoad, J.P., 1991. Monitoirng the response of the inter-tidal beach profile to tidal and wave forcing. Proceedings of Coastal Sediments ’91, 385-712.

Holland, T.K.; Holman, R.A., and Sallenger, A.H. Jnr., 1991. Estimation of overwash bore velocities using video techniques. Proceedings Coastal Sediments ’91, ASCE, pp. 489-497.

Holland, K.T., and Holman, R.A., 1993. The statistical distribution of swash maxima on natural beaches. Journal of Geophysical Research, 98(C6), 10,271-10,278.

Holman, R.A., 1986. Extreme value statistics for wave run-up on a natural beach. *Coastal Engineering*, 9: 527-544.

Holman, R.A., and Bowen, A.J., 1984. Longshore structure of infragravity wave motions. Proceedings of the 16th International Conference on Coastal Engineering, ASEC. pp 6446-6452.

Holman, R.A, Lippmann, T.C, O'Neill, P.V, and Hathaway, K., 1991, Video Estimation of Subaerial Beach Profiles. Marine Geology, 97, 225-231.

Holman, R.A., and Lippmann, T.C., 1987. Remote sensing of nearshore bar systems - making morphology visible. Proceeding of Coastal Sediments'87, ASCE, pp. 927-944.

Holman, R.A., and Sallenger, A.H., 1984. Longshore variability of wave run-up on natural beaches. Proceedings of the 16th International Conference on Coastal Engineering, ASEC. pp. 1896-1921.

Holman, R.A., and Sallenger, A. H., 1985. Setup and Swash on a Natural Beach. Journal of Geophysical Research, 90(C1), 945-953

Holman, R.A., and Sallenger, A.H., 1986. High energy nearshore processes. EoS Trans., AGU 67, 1369-1371.

Horikawa, K., and Sasaki, T., 1972. Field observations of nearshore current system. Proceedings of the 13th Conference on Coastal Engineering, pp. 635-652.

Hotta, S., and Mizuguchi, M., 1980. A field study of waves in the surf zone. Coastal Engineering Japan, JSCE, 23, 79-89.

Huntley, D.A., and Bowen, A.J., 1975. Comparison of the Hydrodynamics of steep and shallow beaches. In: Hails, R.J., and Carr, A.P., (eds.), Nearshore Sediment Dynamics and Sedimentation. Wiley-Interscience, New York.

Huntley, D.A., and Kim, C.S., 1984. Is surf beat forced or free? Proceedings of 19th International Conference on Coastal Engineering, 19, 871-885.

Komar, P. D., 1983. Handbook of Coastal Processes and Erosion, CRC Press.

Kroon, A., 1991. Three-dimensional morphological changes of a nearshore bar system along the Dutch coast near Egmond aan Zee. Proceedings of the Skagen Symposium, Journal of Coastal Research Special Issue, 9, 430-451.

Ingham, A.E., 1975. Sea Surveying. John Wiley and Sons London. 235 p.

Jungerius, P.D., and Schoonderbeek, D., 1992. The use of Leica Quantimet 970 for scanning blowout development in sequential airphotos of the 'dunes de slack"', N.W. France. Catena Supplement 23, 59-73.

Katoh. K., 1981. Analysis of edgewaves by means of empirical eigenfunction. Report of the Port and Harbour Research Institute. 20(3), 3- .

Kaufman, A.E., 1994. Visualisation. Computer, 27(7), 18-19.

Kidson, C., and Manton, M.M.M., 1973. Assessment of coastal change with the aid of photogrammetric and computer-aided techniques. Estuarine and Coastal Marine Science, 1, 271-283.

Kraus, C.J.; McKee-Smith, J., and Sollitt, C.K., 1992. Supertank laboratory data collection project. Proceedings of the 23rd international Conference on Coastal Engineering, ASCE. P2191-2204.

Lane, S.N.: Richards, K.S., and Chandler, J.H., 1993. Developments in photogrammetry; the geomorphological potential. Progress in Physical Geography, 17(3), 306-328.

Lewis, K., 1994. New maps of the seabed. NIWA, New Zealand, Water and Atmosphere 2, 8-11.

Lillisand, T.M., and Kiefer, R.W., 1987. Remote sensing and image interpretation. John Wiley and Sons.

Lee, G., and Birkemeier, W.A., 1993. Beach and nearshore data: 1985-1991 CERC Field Research Facility. Technical Report CERC-93-3, 13p.

Lippmann, T.C., 1992. Edge wave response to a modulating incident wave field. PhD thesis, Oregon State University, 213 p.

Lippmann, T.C., and Holmam, R.A., 1989. Quantification of sand-bar morphology: a video technique based on wave dissipation. Journal of Geophysical Research, 94, 995- 1011.

Lippmann, T.C.; Holmam, R.A., and Hathaway, K.K., 1993. Episodic, nonstationary behaviour of a double bar system at Duck, North Carolina, U.S.A., 1986-1991. Journal of Coastal Research, Special Issue, 15, 49-75.

McFagen, B.G., 1985. Late Holocene stratigraphy of coastal deposits between Auckland and Dunedin, New Zealand. Journal of the Royal Society of New Zealand, 15, 27-65.

McLean, R.F., and Thom, B.G., 1975. Beach changes at Moruya, 1972-1974. Proceedings of the 2nd Australian Conference on Coastal and Ocean Engineering, Institute of Engineers, Australia, 75(2), 177-184.

Marion, A., 1991. An Introduction to Image Processing. Chapman and Hall.

Marra, J. J., 1992. Swash zone dynamics in a rythmic black sand beach system, Unpublished PhD., University of Canterbury, New Zealand, 235p.

Mattie, M.G., and Harris, D.L., 1978. The use of imaging radar in studying ocean waves. Proceedings of the 16th Conference on Coastal Engineering, pp. 174-189.

Meisner, D.E., and Lindstrom, O.M., 1985. Design and operation of a color-infrared aerial video system. Photogrammetric Engineering and Remote Sensing, 51, 555-560.

Morton, R.A. 1991. Accurate shoreline mapping: past, present, and future. American Society of Civil Engineers, Coastal Sediments, 1, 997-1010.

Nayak, S., and Sahai, B., 1985. Coastal morphology: a case study in the Gulf of Khambhat (Cambay). International Journal of Remote Sensing, 6(3 & 4), 559-568.

O'Hare, T.J., and Huntley, D.A., 1994. Bar formation due to wave groups and associated long waves. Marine Geology, 116, 313-325.

Okamoto, A., 1982. Wave influence in two-media photogrammetry. Photogrammetric Engineering and Remote Sensing, 48(9), 1487-1499.

Osborne, P.D., and Greenwood, B., 1992. Frequency dependent cross-shore suspended sediment transport: 2. A barred shoreface. Marine Geology 106, 25-51

Owens, E.H., 1977. Temporal variations in beach and nearshore dynamics. Journal of Sedimentary Petrology, 47(1), 168- 190.

Patterson, D.C., 1985. Low cost visual determination of surf zone parameters. Unpublished MSc Thesis, University of Queensland, Australia, 144p.

Patterson, D.C., and Blair, R.J., 1983. Visually determined wave parameters. Proceedings of the 6th Australian Conference on Coastal and Ocean Engineering, Gold Coast, Australia, pp. 151-155.

Peltier, W.R., 1987. Mechanisms of relative sea-level change and the geophysical responses to ice-water loading. In: Devoy, R.J.N., (ed.), Sea Surface Studies. London, Croom and Helm, pp 57-91.

Penny, M.F.; Abbot, R.H.; Phiilips, D.M.; Billard, B.; Rees, D.; Faulkner, D.W.; Cartwright, D.G.; Woodcock, B.; Perry, D.G.; Wilsen, P.J.; Adams, T.R., and Richards, J., 1986. Airborne laser hydrography in Australia. Appl Opt., 25(13), 2046-2058.

Placio-Prieto, J.L., and Lopez-Blanco, J., 1994. Using video imagery for gully erosion evaluation. Zeitschrift fur Geomorphologie, 38(1), 33-43.

Plant, N.G., and Griggs, G.B., 1992. Comparison of visual observations of wave height and period to measurements made by an offshore slope array. Journal of Coastal Research, 8, 957-965.

Preu, Chr.; Sterr, H., and Zumach, W.-D., 1989. Monitoring of the coastal environments by means of a remote controlled balloon-borne camera (LAP-technique). Proceedings of the 6th Symposium on Coastal & Ocean Management (Coastal Zone ‘89), pp. 4847-4861.

Roy, P.S., and Thom, B.G., 1981. Late Quaternary marine deposition in New South Wales and southern Queensland - an evolutionary model. Journal of the Geological Society of Australia, 29, 471-489.

Salinger, M.J., 1988. New Zealand climate: past and present. In: Climate Change: The New Zealand Response, Ministry of the Environment, pp 17-24.

Sallenger, A.H.; Howard, P.C.; Fletcher, C.H., and Howd, P.A., 1983. A system for measuring bottom profile, waves, and currents in the high-energy nearshore environment. Marine Geology, 51, 63-76.

Sallenger, A.H; Holman, R.A, and Birkemeier, W.A., 1985. Storm-induced response of a nearshore-bar system. Marine Geology, 64, 237-257.

Sallenger, A.H, and Holman, R.A., 1987. Infragravity waves over a natural barred profile. Journal of Geophysical Research, 92(C9): 9531-9540.

Salma, C. C., 1980. Manual of Photogrammetry, 4th edition. American Society of Photogrammetry, Falls Church, Virginia.

Samtaney, R.; Silver, D.; Zabusky, N., and Cao, J., 1994. Visualizing features and tracking their evolution. Computer, 27(7), 20-27.

Sasaki, T.; Horikawa, K., and Hotta, S., 1976. Nearshore current on a gently sloping beach. Proceedings of the 15th Conference on Coastal Engineering, pp. 626-644.

Schneider, J.R., and Weggel, M., 1980. Visually observed data at Pt Mugu, California. Proceedings of the 17th Coastal Engineering Conference, ASCE, pp. 381-93.

Seymour, R.J., and Bothman, D.P., 1984. A hydrostatic profiler for nearshore surveying. Coastal Engineering, 8: 1-14.

Shepherd, M.J., 1987. Coasts: the edge of the land. In: Saunders. D., (ed.), Manawatu and its neighbours. Miscellaneous Publication. Geography Department, Massey University, New Zealand.

Shemer, L., 1993. Interferometric SAR imagery of a monochromatic ocean wave in the presence of the real aperture radar modulation. International Journal of Remote Sensing, 14(6), 3005-3019.

Sherman, D. J., and Bauer, B.O., 1993. Coastal geomorphology through the looking glass, Geomorphology, 7, 225-49.

Short, A. D., 1975. Offshore bars along the Alaskan Arctic coast. Journal of Geology, 83, 209-221.

Short, A. D., 1979. Three-dimensional beach-stage model. Journal of Geology, 87, 553-571.

Shoshany, M., and Degani, A., 1992. Shoreline detection by digital image processing of aerial photography. Journal of Coastal Research, 8(1), 29-34.

Shum, C.K.,; Tapley, B.D., and Ries, J.C., 1993. Satellite altimetry: application and accuracy assessment. Advances in Space Research, 13(11), 315-324.

Slama, C.C., 1980. The manual of photogrammetry, 4th edition. American Society of Photogram-metry, 1049p.

Smith, E.J., and Wagner, E., 1991. Littoral environment observation programme. Journal of coastal Research, 7, 595- 605.

Stewart, R.H., and Teague, C.C., 1980. Dekameter radar observations of ocean wave growth and decay. Journal of Oceanography, 10, 128-143.

Sunamura, T., and Horikawa, K., 1978. Visible-region photographic remote sensing of nearshore waters. Proceedings of the 16th International Conference on Coastal Engineering, pp. 1439-1453.

Tang, E.C.-S. and Dalrymple, R.A., 1989. Nearshore circulation: rip currents and waves over an irregular bathymetry. Journal of Fluid Mechanics, 201, 299-322.

Terwindt, J.H.J., and Wijnberg, K.M., 1991. Thoughts on large scale coastal behaviour. Proceedings of Coastal Sediments'91, ASCE, pp. 1476-1487.

Thieler, E.R., and Danforth, W.W., 1994. Historical shoreline mapping: (1) Improving techniques and reducing positioning errors. Journal of Coastal Research, 10(3), 549-563.

Thornton, E.B., and Guza, R.T., 1982. Transformation of wave height distribution. Journal of Geophysical Research, 88 (C10), 5925-5938.

Van de Meene, J.W.H., and Van Rijn, L.C., 1994. Tide and storm-driven sediment transport on the inner shelf along the Dutch coast. Proceedings of Coastal Dynamics '94, ASCE, New York, pp 822-836.

Verhagen. H.J. 1989. Sand waves along the Ditch Coast. Coastal Engineering, 13, 129-147.

Viles, H.A., 1989, The greenhouse effect, sea-level rise and coastal geomorphology. Progress in Physical Geography, 13 (3), 452-461.

Ward, J.C., 1993. Indicators of the state of the coastal environment and management practices. Information Paper No. 48. Report No. 2595/1. Lincon University, New Zealand.

Wolf, P.R., 1974. Elements of Photogrammetry (with air photo interpretation and remote sensing). McGraw-Hill, New York.

Wood. E., 1992. Sharper Images. New Zealand Science Monthly, 3(2), 8-12.

Wright, P., 1976. A cine-camera technique for process measurements on a ridge and runnel beach. Sedimentology, 23, 705-712.

Wright, L.D., and Short, A.D., 1984. Morphodynamic variability of surf zones and beaches: a synthesis. Marine Geology, 56, 93-118.

Zhang, D.P., 1994. Wave flume experiments on the formation of longshore bars produced by breaking waves. University of Tsukuba: Institute of Geoscience, Science Report A-15, pp. 47-105.

6

Bailey, D.G., and Shand, R.D., 1996. Determining large-scale sand-bar behaviour. Proceedings of the IEEE International Conference on Image Processing, Lausanne, Switzerland, (2), 637-640.

Proceedings of the IEEE International Conference on Image Processing, 16-19 September 1996, Lausanne Switzerland, pp. 637-640

DETERMINING LARGE SCALE SANDBAR BEHAVIOUR

Donald G. Bailey and Roger D. Shand

Image Analysis Unit and Geography Department
Massey University, Palmerston North, New Zealand
E-mail: D.G.Bailey@massey.ac.nz

ABSTRACT

To study the morphology of coastal sandbars and their change with time, it is necessary to obtain a sequence of maps over the period of interest. Traditional techniques such as vertical aerial photography or echo-sounding over a grid are expensive and subject to environmental constraints, especially in higher energy situations.

Image processing is used to rectify elevated terrestrial images where morphological features are inferred from breaking wave patterns. As the coordinates of interest are longshore and offshore distances, the image is then warped to make the coastline straight. The sandbar crest positions within this image are detected. An error analysis shows that useful quantitative data may be obtained. The temporal evolution of the bars can be identified from time stack images.

1. INTRODUCTION

A significant and increasing proportion of the worlds population and wealth is concentrated in the sand-dominated coastal zone [1]. This region, however, is highly variable and unstable with erosion exceeding deposition globally [2,3]. The predicted greenhouse associated sea-level rise is likely to exacerbate this situation [4,5]. There is clearly a practical need to maximise our understanding coastal systems.

Contemporary geomorphological field studies have tended to concentrate on the inner nearshore and backshore zones of low to moderate energy coasts [6], because of their relative ease of access.

To facilitate comprehensive nearshore investigations, in particular those on moderate to high energy coasts, methods of acquiring morphological data at a variety of scales, both spatial (10^1 to 10^{3+} metres longshore) and temporal (10^0 to 10^{3+} days), are required.

A variety of techniques have been used in the past for bathymetric sampling. Cost, longshore coverage limitations, and logistical problems prohibit the widespread use of bottom or surface moving instruments, especially in higher energy environments. Aerial imaging techniques increase longshore coverage but atmospheric restrictions (cloudless conditions) and high costs restrict the aerial (including satellite) option.

With the increasing power of personal computers, the use of image processing techniques now enables inexpensive morphological data to be obtained from elevated terrestrial surfzone images [7,8].

It is necessary to explore the limits and possibilities of the method with respect to the morphological scale objectives described above. This paper covers our image processing work and presents some of our preliminary results based on field data from Wanganui, New Zealand.

2. PREPROCESSING

A panorama of eight photographs was taken from a single site 150 m behind and 43 m above mean sea-level. The four central shots were taken using a 55 mm focal length lens to give good coverage of the area without sacrificing detail. To obtain satisfactory resolution for the four end shots, a 135 mm focal length lens was used. Each photograph was taken using a three minute time exposure to average the effects of individual waves.

A 512 x 512 image is captured of each photograph, with a 2:3 aspect ratio. While capturing the photographs, it is ensured that the top and bottom edges of the photographs are visible in the image since these are required for determining the camera tilt. It is also ensured that the left and right edges of the photographs are out of the field of view, otherwise artefacts may be introduced when mosaicing the photographs.

Since the panorama spans about 160° there is a considerable variation in lighting from one photograph to another because of differing sun angles. In addition to this, there may be sun glare from the sea or clouds and vignetting caused by the lens and neutral density filters. The first step is to normalise the contrast range of each image as much as possible.

1. The image is filtered by selecting the minimum pixel value within a 21 x 21 box. This effectively shrinks the lighter regions of the bars preventing them from being removed with the background.
2. This image is then filtered using the average within a 55 x 55 box to obtain an estimate of the local density. Variations in this image correspond to density variations in the original image.
3. The average is subtracted from the original image to remove the density variations. Differences in the range -12 to 80 are mapped to fill the available range (0 to 255) to enhance the contrast.

Figure 1 shows a typical contrast normalised image.

3. RECTIFICATION

Each photograph has perspective distortion resulting from the viewing geometry. This distortion must be removed before the individual photographs can be mosaiced to give the full panorama.

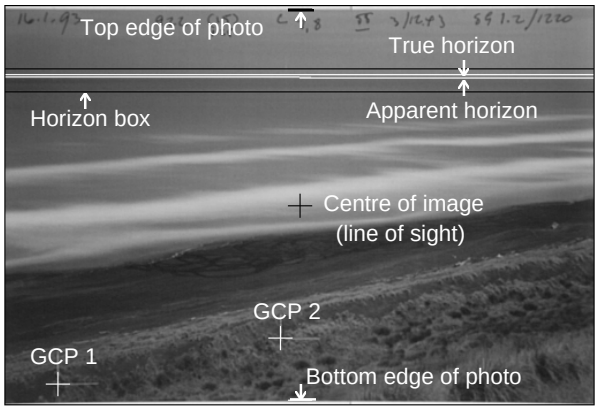

Figure 1: A typical contrast enhanced input image with key features labelled.

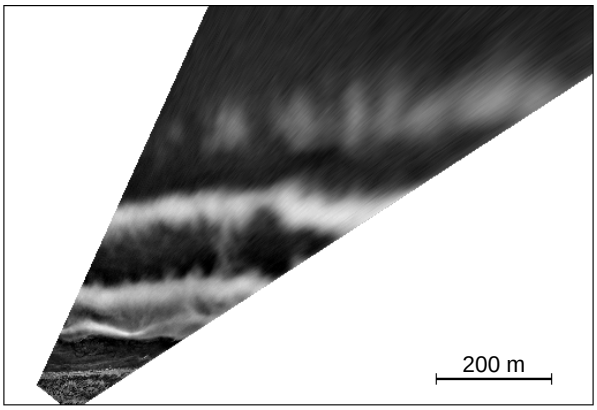

Figure 2: The perspective corrected image.

3.1 Correction of perspective distortion

At this stage, a convenient coordinate system is based on map coordinates. We have actually used rotated map coordinates since the stretch of coast under study runs SE to NW. If it is assumed that the earth is flat (a reasonable assumption since the ranges of interest are within 3.5 km from the camera location) the perspective correction equation may be represented by

$$X = \frac{a_0 x + a_1 y + a_2}{a_6 x + a_7 y + a_8}, \quad Y = \frac{a_3 x + a_4 y + a_5}{a_6 x + a_7 y + a_8} \qquad (1)$$

where (x,y) are the pixel coordinates in the image before rectification, and (X,Y) are the corresponding rectified coordinates. The 9 unknowns in equation (1) are solved from the camera position, the positions of two surveyed ground control points (GCPs) within each image, the sea level, and the horizon.

The common denominator of the perspective transformation represents the perspective vanishing line in the photographs:

$$a_6 x + a_7 y + a_8 = 0 \qquad (2)$$

If the earth was truly flat, this line would correspond to the horizon. However, because of the curvature of the earth, the visible horizon will be below the true "flat earth" horizon. Although the angle between them is small ($\theta = 0.21°$ for camera height of 43 m), this error is significant, giving a 4 pixel shift in the horizon for photographs taken using a 55 mm lens and a 9.5 pixel shift with a 135 mm lens.

From the positions of the ground control points in the image, the position of the apparent horizon is estimated. A linear edge detection operation is to detect the maximum intensity gradient within that region. A least squares fit is applied to the detected points to give the horizon. The program draws the detected horizon on the input image and asks the user if it has been detected correctly. If not, the user defines the correct horizon by entering two points. This step is necessary because the position of the horizon may not be detected accurately if the weather is hazy or if the sea has rough and calm patches on it.

The horizon is then corrected for θ to give a_6, a_7 and a_8. Note that equation (2) is normalised so that

$$a_6^{\,2} + a_7^{\,2} = 1 \qquad (3)$$

The next step is to reference the camera and ground control points to sea level. The GCPs are projected to sea level to remove their height, giving coordinates (X_1',Y_1') and (X_2',Y_2').

Lines perpendicular to the horizon on the input image all fall on planes which pass through the camera. Therefore these lines all converge at the camera point in the rectified image. If the camera is tilted so that the line of sight is below the true horizon, the point of intersection of the horizon perpendiculars will move behind the camera. Determining the seal-level referenced camera position requires knowing the line of sight.

It is assumed that the pixel mid way between the top and bottom edge of the photograph is along the line of sight of the camera. The tilt, φ, is calculated from the focal length and position of the horizon in the image. The direction of the line of sight is calculated by solving equation (1) assuming no tilt (using actual camera coordinates (X_c,Y_c)). The centre pixel of the image is then transformed to give the direction of the line of sight, γ. This is used to correct the camera position for' tilt (equation 4) and equation (1) is solved again.

$$X_c^{'} = X_c - Z_c \tan\varphi \sin\gamma, \quad Y_c^{'} = Y_c - Z_c \tan\varphi \cos\gamma \qquad (4)$$

Lines perpendicular to the horizon intersect at the corrected camera position after transformation. These lines may be parameterised by

$$x = a_6 t + b_0, \quad y = a_7 t + b_1 \qquad (5)$$

where b_0 and b_1 are arbitrary constants. Substituting these into equation (1) gives

$$\begin{aligned} X_c^{'} &= \underset{t\to\infty}{Limit} \frac{a_0(a_6 t + b_0) + a_1(a_7 t + b_1) + a_2}{a_6(a_6 t + b_0) + a_7(a_7 t + b_1) + a_8} \\ &= \frac{a_0 a_6 + a_1 a_7}{a_6^{\,2} + a_7^{\,2}} = a_0 a_6 + a_1 a_7 \end{aligned} \qquad (6)$$

Each GCP gives a further independent equation in a_0, a_1 and a_2, as in equation (7)

$$X_1^{'} = \frac{a_0 x_1 + a_1 y_1 + a_2}{a_6 x_1 + a_7 y_1 + a_8} = \frac{a_0 x_1 + a_1 y_1 + a_2}{H_1} \qquad (7)$$

where H_1 is a constant (all its terms are known). Equation (6) and equation (7) for each GCP give three simultaneous equations that are solved to give

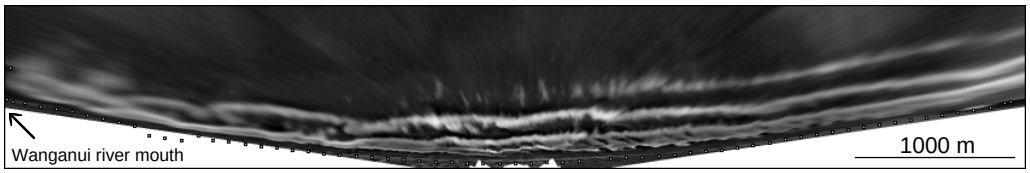

Figure 3: Mosaic of 8 perspective corrected images.

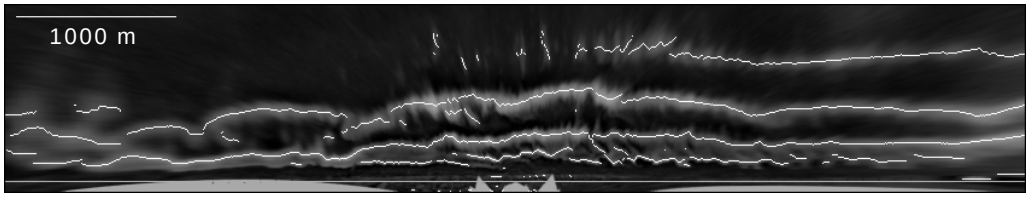

Figure 4: Detected sandbars and waterline (offshore distance scale x2)

$$a_0 = \frac{X_c'(y_1 - y_2) - a_7(H_1X_1' - H_2X_2')}{a_6(y_1 - y_2) - a_7(x_1 - x_2)}$$
$$a_1 = \frac{a_6(H_1X_1' - H_2X_2') - X_c'(x_1 - x_2)}{a_6(y_1 - y_2) - a_7(x_1 - x_2)} \quad (8)$$
$$a_2 = X_1'H_1 - a_0x_1 - a_1y_1$$

Similar equations may be obtained for a_3, a_4 and a_5. Equation (1) is then used to transform each pixel in the input image, giving figure 2. The transformed image is sampled with 2 metre resolution.

3.2 Mosaicing

After correcting for perspective distortions in each of the eight input photographs, the images are combined into a single view of the coast. The views provided by the individual photographs overlap slightly. To reduce the possibility of artefacts from the joins, the images are merged using a linear transition in the region of overlap between adjacent views. The resulting mosaic is shown in figure 3.

3.3 Straightening of coastline

In determining the positions of the bars, a more useful coordinate system is longshore and offshore coordinates. To facilitate conversion to these coordinates, a separate series of ground control points was surveyed along the toe of the foredune at 100m intervals. These points define the baseline for offshore distance measurements. A least squares parabolic fit is made over 1000 m sections, with 500 m overlap between the sections. The overlapping regions are combined using a linear spline giving a smooth piecewise cubic fit.

The image is then incrementally rotated (or unrolled) to make the baseline straight. At each point along the baseline, the shore normal is calculated and the image resampled along the shore normal. Having the offshore and longshore variations separated enables the offshore scale to be amplified to highlight the sandbar morphology.

4. DETECTION OF SANDBARS

The positions of the bar crests can be inferred from the position of maximum intensity along the bar. Although not completely accurate (since the position of maximum intensity depends on environmental factors such as tide, wind and wave height) this measure provides the best estimate from the information available. The following steps are used to detect the bar crests:

1. The image is filtered to detect the local maximum pixels using a 1 x 21 pixel box. The maxima are coded with their pixel values.
2. Many of the local maxima detected correspond to noise, so the image is thresholded at a pixel value of 80 to select only the significant maxima, corresponding to the bar crests.
3. Finally the detected crests are thinned to a single pixel thickness. The resulting image is shown in figure 4 overlaid on the original.

Quantitative measurements may be made of the bar positions by measuring the offshore distances of the intensity maxima from the baseline.

5. RESULTS

The elevated terrestrial imaging approach described here provides good accuracy (±10m) in the offshore direction, but deteriorates rapidly in the longshore direction with distance from the camera. There are three main sources of longshore error which all vary approximately linearly with distance: resolution of captured images (±40m at 3km); photogrammetric errors (±60m at 3km) and blur caused by the height of the waves (±75m at 3km). As these sources are independent, the corresponding variances have been added to give a longshore error of ±2m directly out from the camera up to ±100m at a distance of 3km. The effect of deteriorating resolution with range can be seen in figures 3 and 4.

In addition to these, the intensity maxima shift as a function of environmental variables (tide, wind and wave height). This shift can be reduced by longshore averaging during image processing. The shift in maxima ranged from ±15m when averaging over 200 m up to ±35m for narrow offshore transits. The averaging process effectively trades longshore morphological detail for offshore accuracy. Field work by Lippmann and Holman at Duck indicates that the actual bar crest is likely to be in this range [7].

An ongoing data gathering program has been established consisting of four years of nearshore activity captured at monthly intervals. The temporal resolution of this data allows seasonal variations to be determined. In addition, a weekly data set over a two year period allows the effects of individual weather patterns to be determined.

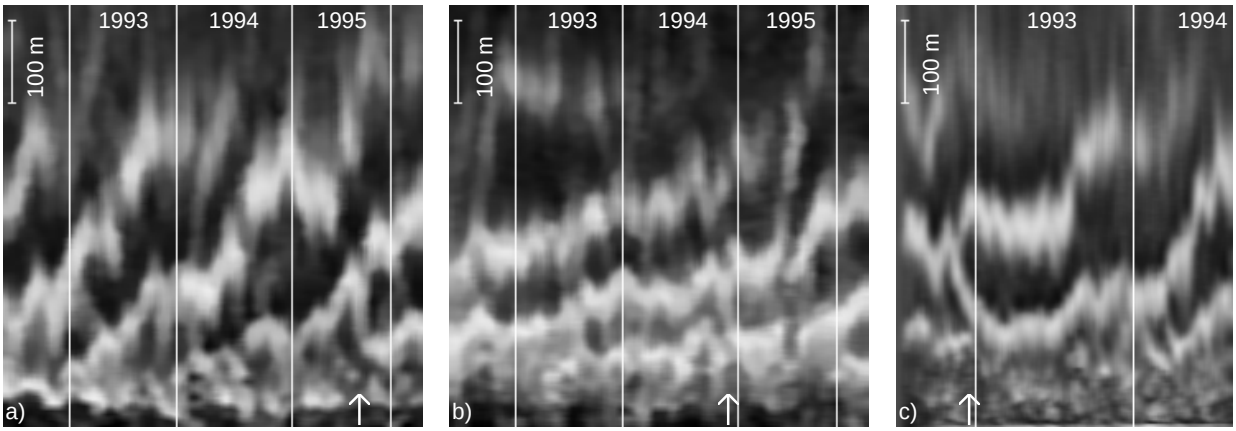

Figure 5: Time-stacks showing bar movements and bifurcation. a) Four year monthly series at 1500 m from river mouth b) Four year monthly series at 6000 m from river mouth; c) Two year weekly series at 3500 m from river mouth.

The morphodynamic evolution of the sandbars is investigated by examining the positions of the bars detected in a series of images taken at regular intervals. This three dimensional data set (offshore, longshore, and time coordinates) may be viewed as a series of time-stack images with offshore and time axes. Each time-stack shows bar behaviour at a particular longshore location as a function of time. Figure 5 shows three time-stacks at different locations and temporal sampling resolution.

A number of new morphological phenomena have been identified. The bars can be observed to have an underlying offshore migration trend with weak seasonal cycles superimposed on this. Such behaviour is easily recognised on the time-stack images in figure 5. It can be clearly seen that the bars closer to the river mouth (for example figure 5a) have a stronger seasonal cycle, with offshore movement occurring predominantly in the winter months when the energy within the system is higher. Comparing time-stacks for different longshore locations (figures 5a and 5b) also shows that the average offshore migration rates are faster nearer the river mouth.

A second characteristic involves bars splitting or bifurcating longshore. Examples appear in each time-stack in figure 5 as marked by the arrows. In each case, the inner portion moved landward to merge with the beach or adjacent bar. This could be an important sediment return mechanism. Similar bifurcations can be seen in figure 4 where they occur at approximately 1000 m intervals.

6. SUMMARY

An inexpensive method of obtaining data for studying the time evolution of sandbars on moderate to high energy coasts is to use elevated terrestrial imaging. A panoramic series of eight oblique photographs are normalised with respect to lighting variations and rectified to longshore and offshore coordinates. The positions of the bar crests are detected by the locating intensity maxima. An error analysis for this study site shows that quantitatively useful data may be obtained. Time-stack images may be used to show how the bars evolve over several seasons.

7. ACKNOWLEDGMENTS

We acknowledge financial support for the project from the Massey University Graduate Research Fund, the Massey University Research Fund, and the Geography Department. We also acknowledge field assistance in surveying the ground control points from the Wanganui District Council.

REFERENCES

[1] **R.W.G. Carter.** Man's Response to Sea-Level Change. In R.J.N. Devoy, editor, *Sea Surface Studies: A Global View*, 464-497, Croom Helm, London, 1987.

[2] **R.W.G. Carter.** *Coastal Environments.* Academic Press, London, 1988.

[3] **E.C.F. Bird.** *Coastline Changes: A Global View*. John Wiley & Sons, London, 1985.

[4] **J. Orford.** Coastal Processes: The Coastal Response to Sea-Level Variation. In R.J.N. Devoy, editor, *Sea Surface Studies: A Global View*, 415-451. Croom Helm, London, 1987.

[5] **H.A. Viles.** The Greenhouse Effect, Sea-Level Rise and Coastal Geomorphology. *Progress in Physical Geography*, 13:452-461, 1989.

[6] **G. Masselink and A.D. Short.** The Effect of Tide Range on Beach Morphodynamics and Morphology: A Conceptual Beach Model. *Journal of Coastal Research*, 9:785-800, 1993.

[7] **T.C. Lippmann and R.A. Holman.** Quantification of Sand Bar Morphology: A Video Technique Based on Wave Dissipation. *Journal of Geophysical Research*, 94(C1): 995-1011, 1989.

[8] **D.G. Bailey and R.D. Shand.** Determining Large Scale Sandbar Evolution, *Proceedings of the First New Zealand Conference on Image and Vision Computing*, 109-116, 1993.

7

Bailey, D.G., and Shand, R.D., 1997. Data fusion issues in analysing coastal morpho-dynamic systems. Proceedings of the 1st joint Australian and New Zealand Conference on Digital Image and Vision Computing: Techniques and Applications, New Zealand, pp. 107-112.

Proceedings of the first joint Australia and New Zealand Conference on Digital Image Processing and Vision Computing: Techniques and Applications, DICTA'97, IVCNZ'97, Auckland, December 1997, pp 107-112

Data Fusion Issues in Analysing Coastal Morphodynamic Systems

D. G. Bailey and R. D. Shand
Physics Department and Geography Department
Massey University, Palmerston North, New Zealand
E-mail: D.G.Bailey@massey.ac.nz, R.D.Shand@clear.net.nz

Abstract

This paper describes a range of coastal data acquisition techniques and discusses some of the associated data fusion issues. To better understand the form and process dynamics at the interface between land and ocean, there is a need for comprehensive data. Traditional water contact methods of acquiring morphological data such as echo-sounding are discussed, and some of the more recent remote techniques incorporating photographic and video imaging are described. The inherent differences in the calibration requirements for data acquired by these methods are considered based on field results from Wanganui, New Zealand. Reconciling such differences may be important, and this can enable data sets to be extended both spatially and temporally. Comparison of contemporaneous data is carried out to identify systematic errors and develop corresponding compensation corrections.

Keywords: data fusion, sandbars, time-exposure, echo-sounding, time-stacks

1. Introduction

There is a growing need to understand coastal systems and how they change with time. Of particular interest is the 'active zone', that area of the coast subjected to wave influenced sediment transport [1]. This zone is highly dynamic and unstable with erosion exceeding deposition globally [2]. A variety of topographical data acquisition techniques have been developed for the coastal active zone [3,4]. The method selected is determined by the physical environment, the resolution and accuracy required, and the available equipment, skill and manpower.

There is often a need to combine data sets obtained under different environmental conditions or by different acquisition methods. Such data fusion may be required to increase the record length, to extend the spatial coverage, to enable intersite comparison where different data acquisition methods were used, or to increase the quality of the data by identifying and correcting systematic errors. Each technique has its own interpretation and error limitations which must be identified and accounted for when data sets are combined for use in morphodynamic (interactions between form and process) analysis.

This paper describes a range of data acquisition techniques and some of the data fusion issues that we have encountered at Wanganui, on the south west coast of the North Island, New Zealand. The site includes the Wanganui river mouth and 5 km of adjacent coast to the west as shown in figure 1. The active zone is approximately 400 m wide.

Figure 1: An aerial photograph of the field site with the Wanganui river breakwaters in the foreground, and the cliffs used as the camera platform in the upper right.

2. Data Acquisition Methods

2.1 Echo soundings

The river mouth is echo-sounded monthly by the Port Company for navigational purposes (figure 2(a)). Sounding requires low sea and wind conditions. A bathymetric chart covering 200 m by 600 m is produced from the survey output at 20 m resolution (figure 2(b)). Errors are ±0.3 m elevation and ±5 to 10 m position. An image is produced from each chart by digitising traced contour maps with contours drawn at 0.5 m intervals (figure 2(c)).

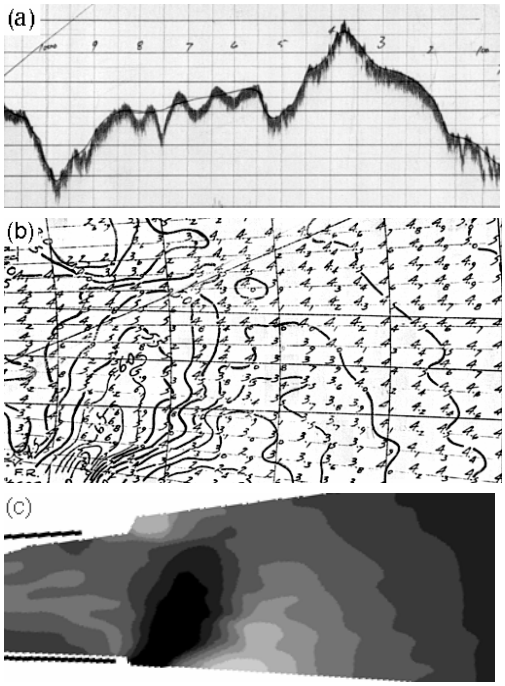

Figure 2: Echo sounding data. (a) A trace of the echo along the central profile. (b) Several profiles combined to make a bathymetric chart. (c) The depth contours are digitised and converted to give a depth map image.

On the coast, cross-shore transits at 200, 1600, and 5000 m to the west of the river mouth were surveyed at three monthly intervals by echo-sounding and levelling using a theodolite. Echo-sounding was carried out seaward of the low tide mark between July 1991 and October 1993. Errors are ±0.3 m elevation and ±5 to 10 m position. The intertidal beach was levelled between December 1989 and May 1994. Errors are ±0.025 m elevation and ±2.5 m position. The sonar and levelling data were merged. The location of the bar crests were determined using the common method of fitting a power curve to the profile and determining the locations of maximum residuals [5] as shown in figure 3. The active zone can be identified from the profile envelope, and standard deviations about the mean profile.

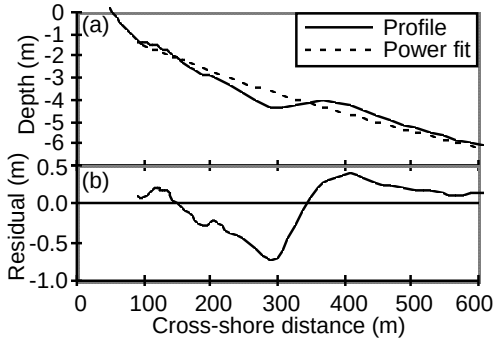

Figure 3: (a) A sounding profile with power curve fitted. (b) Residuals with maxima indicating bar crests.

2.2 Aerial photography

The river mouth and coast were surveyed by vertical aerial photography on 8 occasions between August 1991 and July 1993. Such aerial photography required clear skies and waves large enough to break on all sandbars (greater than 2 m). The photographs (one of which is shown in figure 4) were digitised, rectified using a series of surveyed ground control points, and mosaiced to produce a composite image of the study site (as in figure 10(a)). Position errors on the sea surface are ±12 m. As wave breaking is depth dependent, the location of a bar crest is inferred on the images from the positions of local maximum intensity. Elevation is therefore only known in a relative sense. Environmental variables such as wave height and sea level at the time of sampling influence the inferred crest location.

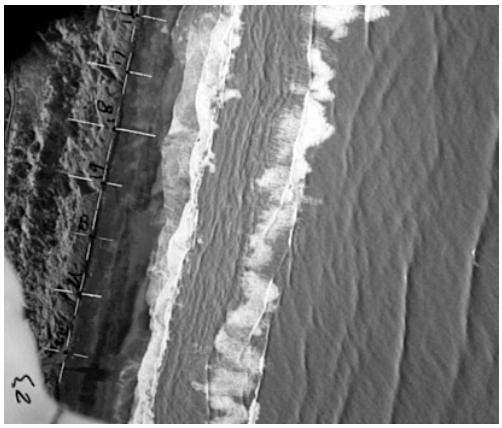

Figure 4: One of a sequence of vertical aerial photographs. Crosses locate ground control points at 100 m intervals.

2.3 Time-exposure photography

Photographic techniques using long exposure times have been developed to reduce the effects of wave height modulation [6]. At the study sight, multiple wave trains are often present (for example, see figure 1), and ocean wave heights often have a Rayleigh distribution. The breakpoint therefore varies, and this introduces a random error when locating bar crests using intensity maxima from instantaneous photographs (compare figures 5(a) and 5(b)). The study site was surveyed by oblique terrestrial time-exposure (4 minutes) photography at monthly intervals between June 1992 and June 1996. The photographs were digitised, rectified, and mosaiced to produce composite images as shown in figure 5(c) [7,8]. The environmental errors that apply to aerial images also apply to the time exposure images. For the study site, the offshore error is approximately ±10 m. The longshore error deteriorates rapidly with distance from the camera. There are three main sources of longshore error which all vary approximately linearly with distance: pixel resolution of captured images (±40 m at 3 km); photogrammetric errors (±60 m at 3 km); and an offset caused by the height of the waves (±75 m at 3 km). As these error sources are independent, the corresponding variances may be added to give a longshore error of ±2 m directly out from the camera up to ±100 m at a distance of 3 km.

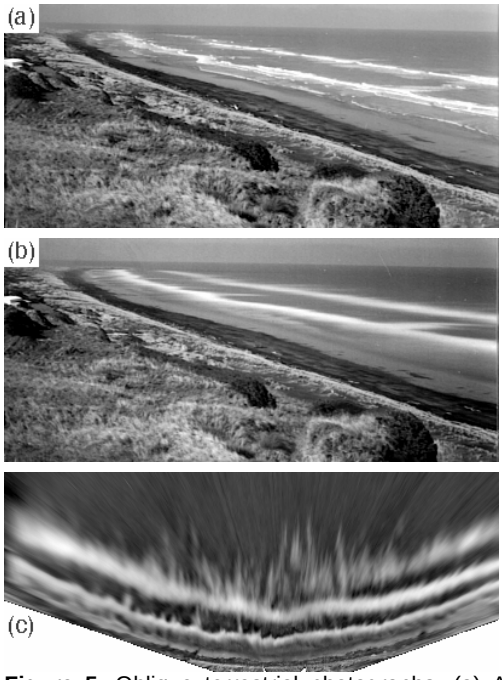

Figure 5: Oblique terrestrial photographs. (a) An instantaneous photograph showing individual waves. (b) A 4 minute time exposure. (c) A mosaic of 8 photographs spanning 5 km (offshore scale x2).

2.4 Video techniques

Oblique terrestrial videos were captured of waves breaking on the bars opposite the camera (figure 6(a)) to obtain intensity inferred morphological data and also hydrodynamic data over a small area. The intensity data on the 3200 m transit was captured from the video images at 0.25 second intervals to form a time-stack or image of what happened on that transit as a function of time [9]. Such video time-stacks (for example figure 6(b)) clearly show the wave height modulation effects. A time-stack taken over the tidal cycle shows the movement of the inferred crest location as the sea level changes. Low frequency wave motions can be detected using intensity patterns on the bars and beach face. Alternatively, time averaging video frames gives a time exposure image equivalent to the photographic long exposure.

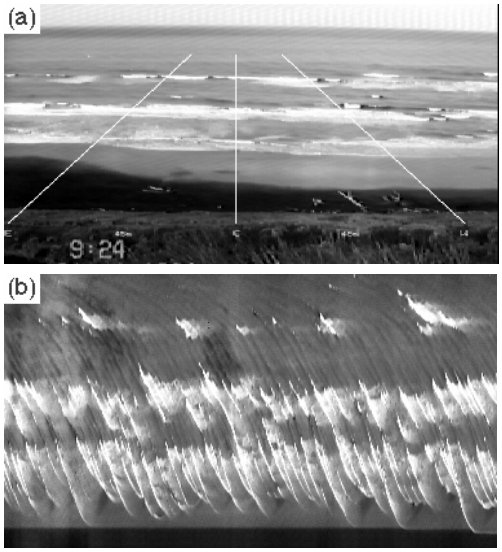

Figure 6: (a) A single video frame showing three shore normal transits. (b) A 6 minute time-stack taken from the central transit.

Data Fusion Issues:

Terrestrial time-exposure photography or video are the preferred data acquisition methods because they allow large areas to be surveyed, are easily automated, relatively cheap to operate and function under a wide range of environmental conditions. The disadvantage is that there is no quantitative information on depth, and the detected bar locations need to be adjusted for environmental conditions.

Environmental factors influencing wave breaking include: incident wave height, low frequency (>20 s) wave heights, tide level, wind or pressure storm surges, and morphological configuration. Figure 7 shows rectified time exposure images sampled 24 hours apart. Wind, barometric pressure, tide level, and wave period remained approximately constant. Changes in incident wave height (2.2 to 1.2 m), wave setup, low frequency surges, and differences in the morphological configuration are responsible for the movement of intensity maxima as indicated in figure 7(c). While significant spatial variation occurs (compare (i) and (ii)) this can be reduced by longshore averaging (as in (iii)).

The tide shift translates the intensity pattern cross-shore in response to changing depth (figure 8). Some of the fluctuation in the detected intensity maxima locations (figure 8(b)) can be attributed to low frequency sea level oscillations. Spectral and time series analyses at Wanganui have consistently shown that such oscillations range in period from 30 seconds to over 60 minutes. However, most of the energy occurs at periods less than 15 minutes, so time averaging over this interval significantly reduces this source of random error.

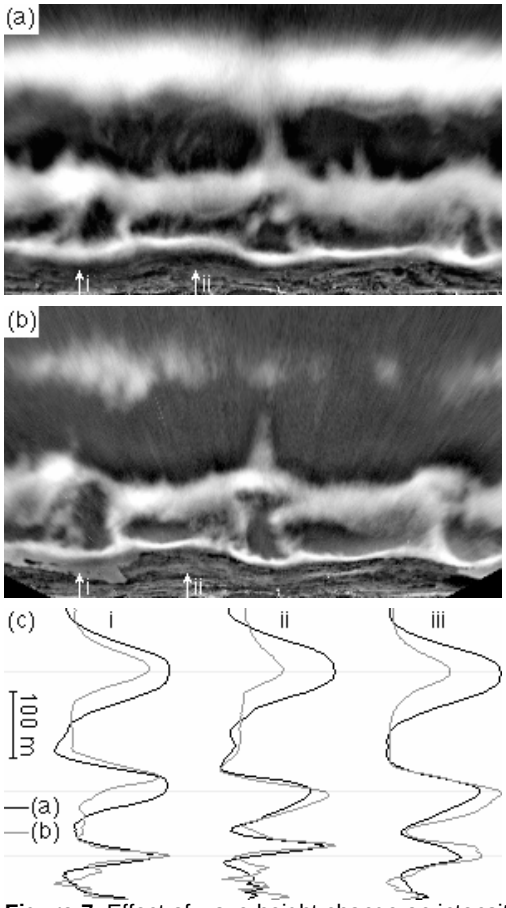

Figure 7: Effect of wave height change on intensity distribution (offshore scale x2). (a) 2.2 m. (b) 1.2 m. (c) i) & ii) Intensity profiles of indicated positions (averaged over 150 m), iii) Intensity profile averaged over 1500 m.

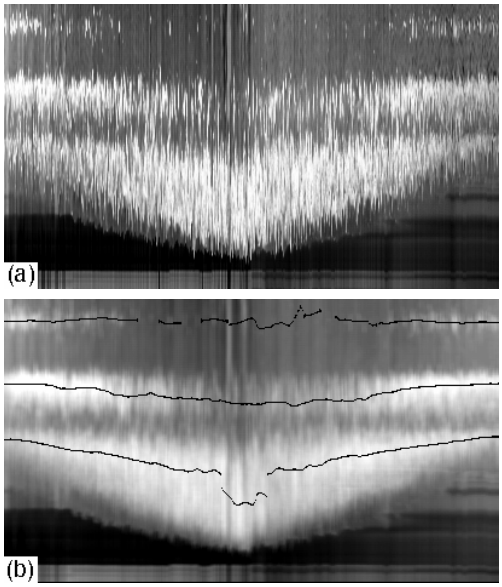

Figure 8: Effect of sea level (tide) on intensity maxima positions. (a) A compressed time stack taken over 6 hours including high tide. (b) The same time stack with a 4 minute running average. Superimposed are the detected intensity maxima.

The incident wave height also offsets the intensity maximum away from the camera as illustrated in figure 9.

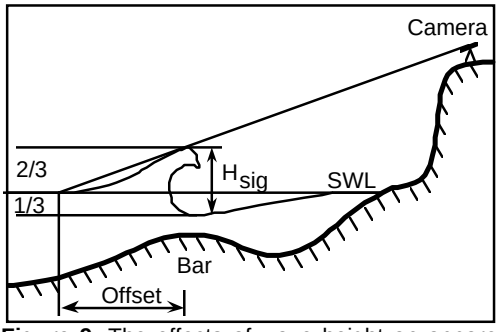

Figure 9: The effects of wave height on apparent breaker position.

The different types of data obtained from different sources allows systematic errors to be identified, and an empirical correction applied. For example, the photogrammetric errors associated with the vertical aerial images are uniformly distributed, while those associated with the oblique time-exposure images vary significantly with distance from the camera. Any differences between images captured using the two methods at the same time can be attributed to the rectification model used with the oblique time-exposure images. Figures

10(a) and (b) show corresponding aerial and terrestrial long exposure images. An error surface figure 10(c) was fitted to the location differences between corresponding intensity maxima in several such pairs. This allows such systematic errors to be removed from time exposure data.

Comparing oblique time-exposure intensity profiles with echo-soundings enables correspondence between the inferred bar-crest and the actual bar-crest to be determined. By comparing time-averaged bar-crest locations with time-averaged ground profiles, contamination by environmental variables is eliminated. Figure 11 shows the differences between these crests as a function of depth for the measured transits. The relationship shows that landward intensity maxima are displaced offshore, while seaward intensity maxima are displaced onshore. This result is consistent with the depth control over wave breaking.

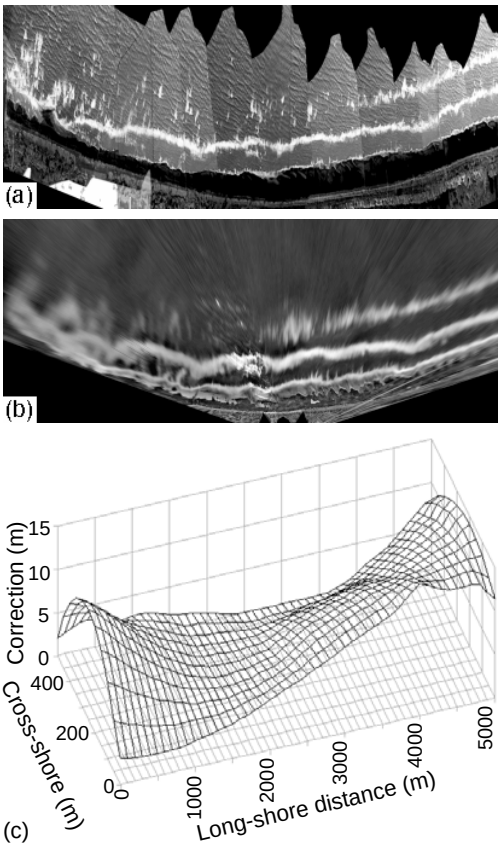

Figure 10: Sea surface intensity accuracy. (a) An example of an vertical aerial mosaic (offshore scale x2). (b) The corresponding terrestrial long exposure mosaic (offshore scale x2). (c) The error surface found empirically by comparing several such sets of data.

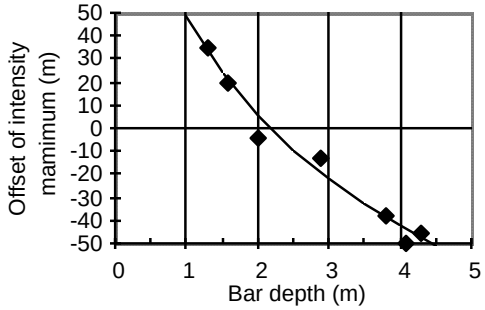

Figure 11: Image to ground survey crest location offsets as a function of depth, taken from transits at 200, 1600 and 5000 m.

What happens at the river mouth is of primary interest for navigation. The oblique time exposure method does not adequately image the river mouth as it is too far away from the camera site, it is partially obscured by the mole, and the water is too deep for the waves to break reliably. Extending the data set spatially to include the river mouth involves combining the available bathymetric data with the image data. In spite of the fact that these data sets contain different types of information, the relationship between the sandbars adjacent to the river mouth and the deeper bars within the river mouth is readily apparent in figure 12(a). While the bathymetric data locates the bar crest by minimum depth rather than by the power residual method, and the systematic correction of figuew 10(c) has not been applied, the landward offset of the coastal image

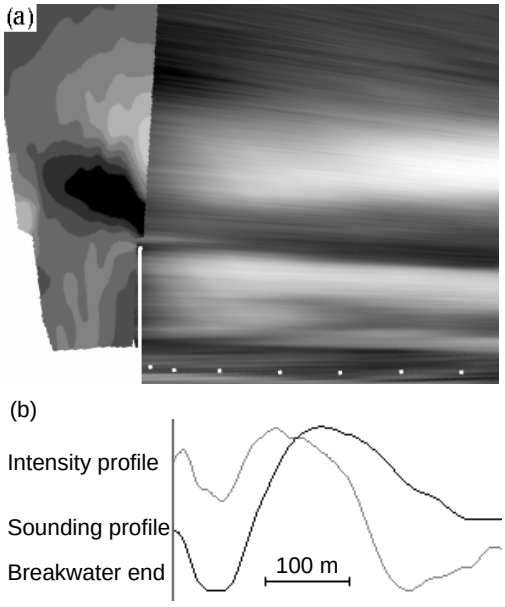

Figure 12: River mouth data fusion. (a) The sounding depth image overlaid on the rectified long exposure image. (b) Comparison of adjacent sounding and intensity profiles beyond then end of the breakwater.

intensity maximum figure 12(b) is in agreement with that predicted from figure 11(b).

When investigating coastal morphodynamics, it is important to determine the movement of the bar locations with time. One convenient method of analysing this data is to view the data at a particular transit as a function of time, using a timestack. However, the contrast of the input images varies (figure 13(a)) depending on reflection (the sun angle, and whether or not it is cloudy), wave height (smaller waves do not break as strongly, and produce less foam), and different lens speeds (the different lenses for near and far photographs produce images with different contrasts). To overcome this, the individual images are normalised (figure 13(b)) prior to constructing the timestack by shaping their histograms to the average histogram over the whole sequence. A typical normalised and filtered time-stack is shown in figure 13(c), illustrating the net offshore migration of the sandbars with time.

4. Summary

The availability of data and images from several different sources can be used to improve the overall quality and quantity of the data. The different sources are subject to different systematic errors and environmental influences. Comparing data from different sources can enable systematic and environmental errors to be identified and removed. The spatial or temporal coverage may be extended by utilising all the data available, although special consideration needs to be taken when combining data from disparate sources to ensure that the data is compatible.

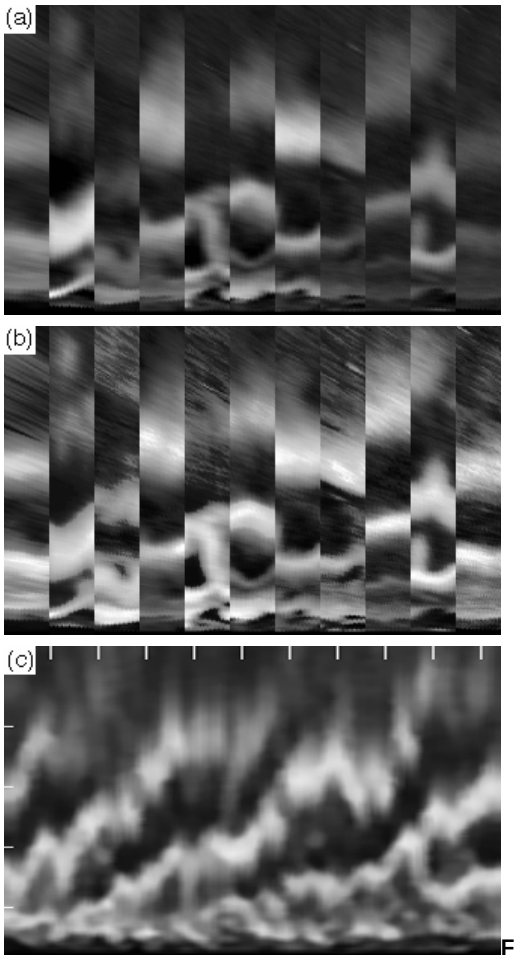

Figure 13: Image normalisation for time stack construction. (a) Slices from a series of images showing variations in brightness and contrast. (b) The same slices after intensity normalisation. (c) The resultant time stack from monthly data over 4 years.

References

[1] R.J. Hallermeier, "Sand Transport Limits in Coastal Structure Design", Proceedings Coastal Structures '83, 703-716, 1983.
[2] E.C.F. Bird, Coastline Changes: A Global View, John Wiley & Sons, London, 1985.
[3] R.A. Holman & A.H. Sallenger, "High energy nearshore processes", EOS Trans. AGU 67, 1369-1371, 1986.
[4] K. Horikawa, Nearshore Dynamics and Coastal Processes, University of Tokyo Press, 1988.
[5] A.J. Bowen & R.A. Holman, "Bars, bumps, and holes: models for the generation of complex beach topography", Journal of Geophysical Research, 84, 457-468, 1982.
[6] T.C. Lippman & R.A. Holman, "Quantification of Sand Bar Morphology: A Video Technique Based on Wave Dissipation", Journal of Geophysical Research, 94, 995-1011, 1989.
[7] D.G. Bailey & R.D. Shand, "Determining Large Scale Sandbar Evolution", Proceedings 1st NZ Conference on Image and Vision Computing, 109-116, 1993.
[8] D.G. Bailey & R.D. Shand, "Determining Large Scale Sandbar Behaviour", Proceedings IEEE International Conference on Image Processing, 2, 637-640 , 1996.
[9] D.G. Bailey & R.D. Shand, "Determining Wave Run-up using Automated Video Analysis", Proceedings 2nd NZ Conference on Image and Vision Computing, 2.11.1-2.11.10, 1994.

Shand, R.D., and Bailey, D.G., 1999. A review of net offshore bar migration with photographic illustrations from Wanganui, New Zealand, Journal of Coastal Research, 15(2), 365-378.

Journal of Coastal Research	15	2	365–378	Royal Palm Beach, Florida	Spring 1999

A Review of Net Offshore Bar Migration with Photographic Illustrations from Wanganui, New Zealand

Roger D. Shand† and Donald G. Bailey‡

†Geography Department
Massey University
Palmerston North,
New Zealand

‡Physics Department
Massey University
Palmerston North,
New Zealand

ABSTRACT

SHAND, R.D. and BAILEY, D.G., 1999. A Review of Net Offshore Bar Migration with Photographic Illustrations from Wanganui, New Zealand. *Journal of Coastal Research,* 15(2), 365–378. Royal Palm Beach (Florida), ISSN 0749-0208.

Field studies, processes, and mechanisms associated with net offshore bar migration are reviewed. Net offshore bar migration (NOM) has been reported at multi-bar locations on the Dutch coast and at North Carolina on the eastern USA seaboard. NOM has also been documented by the present authors as occurring on the New Zealand west coast. Dutch researchers have developed a three stage 'life-cycle' morphological model based on data from sites in The Netherlands. These stages consist of bar generation near the shore-line (stage 1), systematic offshore migration of the bar across the surfzone (stage 2), and bar disappearance in the outer surfzone (stage 3). Non-linear morphological configurations have also been associated with net offshore bar migration. NOM phenomena are illustrated using sequential time-exposure imagery obtained from a field site at Wanganui, New Zealand. Consistency between the results from the different locations indicates that net offshore bar migration may be a phenomenon common to many multi-bar coasts.

This review suggests that while the overall net offshore bar migration operates at a temporal scale of years and at a spatial scale of 100s to 1000s of metres, the system is influenced by components operating at a range of scales. Episodes of offshore bar migration are driven by storm events. The timing and nature of offshore bar migrations are influenced by antecedent morphology. Finally, the overall NOM characteristics are related to the large-scale physical boundary conditions such as cross-shore slope and coastal orientation.

ADDITIONAL INDEX WORDS: *Multi-bar coast, image processing, morphodynamics, geomorphological scales.*

INTRODUCTION

Sand-bars are ridges on the sea-bed which are usually aligned parallel to the shoreline. These dominant morphological features are found on most sandy coasts. The number of bars can vary between sites. Morphological characteristics of sand bars are related to wave conditions, tidal range, sediment characteristics and topographical gradients (see *e.g.* MASSELINK and SHORT, 1993).

Conceptual models have been developed to account for the morphology and behaviour of coastal sand-bars. The earliest and simplest model involves two states or morphological configurations. Beach morphology oscillates between a dissipative profile with a seaward bar and a reflective barless profile with a landward berm terrace. The former state is associated with higher energy conditions and the latter with fair-weather conditions. The model was developed for single-bar oceanic coasts which display strong seasonality and is referred to as the storm/swell, summer/winter, or bar/berm profile model (see *e.g.* KOMAR, 1976; HARDISTY, 1990). This model is two-dimensional (2D), in that it can be depicted by a single shore-normal profile.

97145 Received 10 August 1997 and accepted in revision 29 April 1998.

Conceptual models incorporating three-dimensional (3D) states were subsequently developed for coasts which experienced rhythmic topography, *e.g.* see DAVIS and FOX (1972), SONU (1973), DAVIS and FOX (1975), FOX and DAVIS (1976), OWENS (1977), CHAPPELL and ELIOT (1979), SHORT (1979), WRIGHT et al. (1979), and SASAKI (1983). A bench-mark in this work was Wright and Short's (1984) morphodynamic model which is often referred to as the 'Australian' model. This model consists of a sequence of six beach-states with end members similar to the morphologies of the bar/berm model. Four 'intermediate' configurations with three-dimensional topography complete the sequence. Distinctive 'process-signatures' are associated with each state. The Australian model primarily applies to sections of coast with a single bar, or to the innermost bar where multiple bars exist. Three-dimensional beach-state investigations of different coasts frequently identify variants of the Australian model, *e.g.* NUMMEDAL *et al.* (1984), SHAW (1985), MARRA (1991), and SHORT (1992). SONNENFELD (1987) speculated that there is a single global nearshore bar sequence and each surfzone displays incomplete portions of the sequence in accord with its own combination of wave and tide conditions.

The 3D beach-state approach has been applied to multi-bar coasts by researchers such as HOM-MA and SONU (1962), GOLDSMITH *et al.* (1982), AAGAARD (1990), SHORT (1992),

and SHORT and AAGAARD (1993). While such modeling has identified certain configurations and sequences the task has been thwarted by the greater morphological complexity and spatial extent of multi-bar surfzones. The data-bases have usually consisted of aerial photographs or relatively small areas of bathymetric map. In either case temporal limitations have occurred because of low sampling rates or the short time-spans of research projects. However, in a few instances temporally extensive data have been collected and new morphological phenomena have been identified. Of particular interest is a repeating (cyclic) offshore migration trend underlying sand-bar behaviour (*e.g.* see BIRKEMEIER, 1984; DE VROEG, 1988; RUESSINK and KROON, 1994; WIJNBERG, 1995; BAILEY and SHAND, 1996).

Net offshore bar migration (NOM) has been observed at sites on the Terschelling and Holland coasts (The Netherlands), the North Carolina coast (USA) and on the southwest coast of New Zealand's North Island (see Figure 1). The published data sets demonstrating NOM at these sites are shown in Figures 2.

Researchers from the Netherlands (*e.g.* RUESSINK and KROON, 1994; WIJNBERG, 1995) have proposed a general three-stage conceptual model to describe the NOM cycle. Authors describing data sets from Wanganui on the New Zealand west coast (SHAND, 1990; BAILEY and SHAND, 1996) and from Duck on the USA east coast (BIRKEMEIER, 1984; LIPPMANN *et al.*, 1993) have alluded to such a model. Reports of multi-bar sites on the Oregon coast (CHESSER, 1993) and along the Nile Delta (KHAFAGY *et al.*, 1992), suggest that the model may also apply at those locations. In this paper the conceptual NOM model will be referred to as the 'Dutch' model. The three stages of the Dutch model are: bar generation near the shore-line; bar maturity and systematic seaward migration across the inner nearshore; and finally bar dissipation (flattening out) and disappearance in the outer nearshore. Smaller scale detail and possible mechanisms underlying the NOM behaviour have been identified from those data sets which have higher sampling rates (BIRKEMEIER, 1984; LIPPMANN *et al.*, 1993; KROON 1994).

While the Dutch model describes shore-normal change, three-dimensional morphological configurations also appear to be important in the NOM cycle. For example: KROON (1994) and RUESSINK and KROON (1994) have discussed the influence of longshore migrating bars; WIJNBERG (1995) has described alignment changes in longshore bars; and KROON (1994) and BAILEY and SHAND (1996) have described double bar development in the mid surfzone.

This paper reviews the literature on net offshore bar migration within the framework of the three-stage Dutch model, i.e. bar-generation, systematic seaward migration, and bar disappearance. Three-dimensional morphologies associated with NOM are then reviewed. Sequences of photographic images from Wanganui (New Zealand) are used to illustrate the different NOM phenomena. Comments are made about additional aspects of NOM evident within the imagery. Detail is also provided about the imaging techniques and image interpretation. The paper begins by considering the different methods used to acquire data at the various NOM sites together with the steps taken to reconcile inherent measurement differences—thereby enabling meaningful comparisons to be made.

THE REVIEW

Methods

A range of measurement systems have been used for obtaining bar-crest data at the different NOM field sites. Field surveys for the Dutch data began in 1964 and have continued at yearly intervals using vertical aerial photogrammetry and echo-sounding (see RUESSINK and KROON, 1994; WIJBERG, 1995). Data collection at Duck, North Carolina, began in 1981 and has continued at approximately fortnightly intervals using ground-contact instruments (see GUAN-HONG LEE and BIRKEMEIER, 1993). Wanganui Rivermouth (New Zealand) data collection began in 1925 and has continued at two to four weekly intervals (see GIBB *et al.*, 1962; BURGESS, 1971; SHAND, 1990; SHAND, 1995). Data collection for the Wanganui coast began in 1991 at two to four weekly intervals using levelling, echo-sounding, vertical aerial photogrammetry and elevated oblique terrestrial photogrammetry (see PATTERSON, 1991; BAILEY and SHAND, 1993; BAILEY and SHAND, 1996; BAILEY and SHAND, 1997).

The oblique terrestrial imagery from Wanganui (see Figures 2I and 2J) utilised photographic long-exposure (time-exposure) field sampling, analytical rectification, and further image processing to obtain the morphological data sets. Photographs were obtained using a neutral density filter and exposure times of approximately four minutes. The resulting time-averaged photographic image gave a statistically stable sample of the breaking wave pattern. As wave breaking is depth dependent the intensity variation provides an analogue of surfzone morphology (see HOLMAN and LIPPMANN, 1987; LIPPMANN and HOLMAN, 1989; LIPPMANN and HOLMAN, 1990). Oblique images were digitised and rectified using an algorithm which incorporates ground control points, the horizon, sea-level, and the camera geometry to solve the transformation parameters (see LIPPMANN and HOLMAN, 1989; BAILEY and SHAND, 1993; BAILEY and SHAND, 1996). BAILEY and SHAND used a mosaicing routine to splice an eight frame panorama of photographic images. By locating the camera on a cliff top approximately 40 metres above MSL, and using different focal length lenses, they were able to produce output images (morphological maps) of up to six kilometres of coast. Figures 5 and 6 show sections of these maps. Ground truthing by LIPPMANN and HOLMAN (1989) showed that intensity maxima approximated bar crest locations and the shoreline. To facilitate temporal analysis of bar crests within a sequence of images a time-series image termed a 'time-stack' was constructed using cross-shore segments from a particular longshore location. Such image processing is discussed in AAGAARD and HOLM (1989), BAILEY and SHAND (1994), HOLLAND and HOLMAN (1993), BAILEY and SHAND (1996) and the technique was used in creating the time-stacks in Figures 2, 5 and 6. The time-stacks in Figure 2 have also been smoothed horizontally, i.e. in time, to emphasise the bar-crest migration trends.

In all NOM studies the bar crests were detected using curve fitting techniques and the crest location was based on

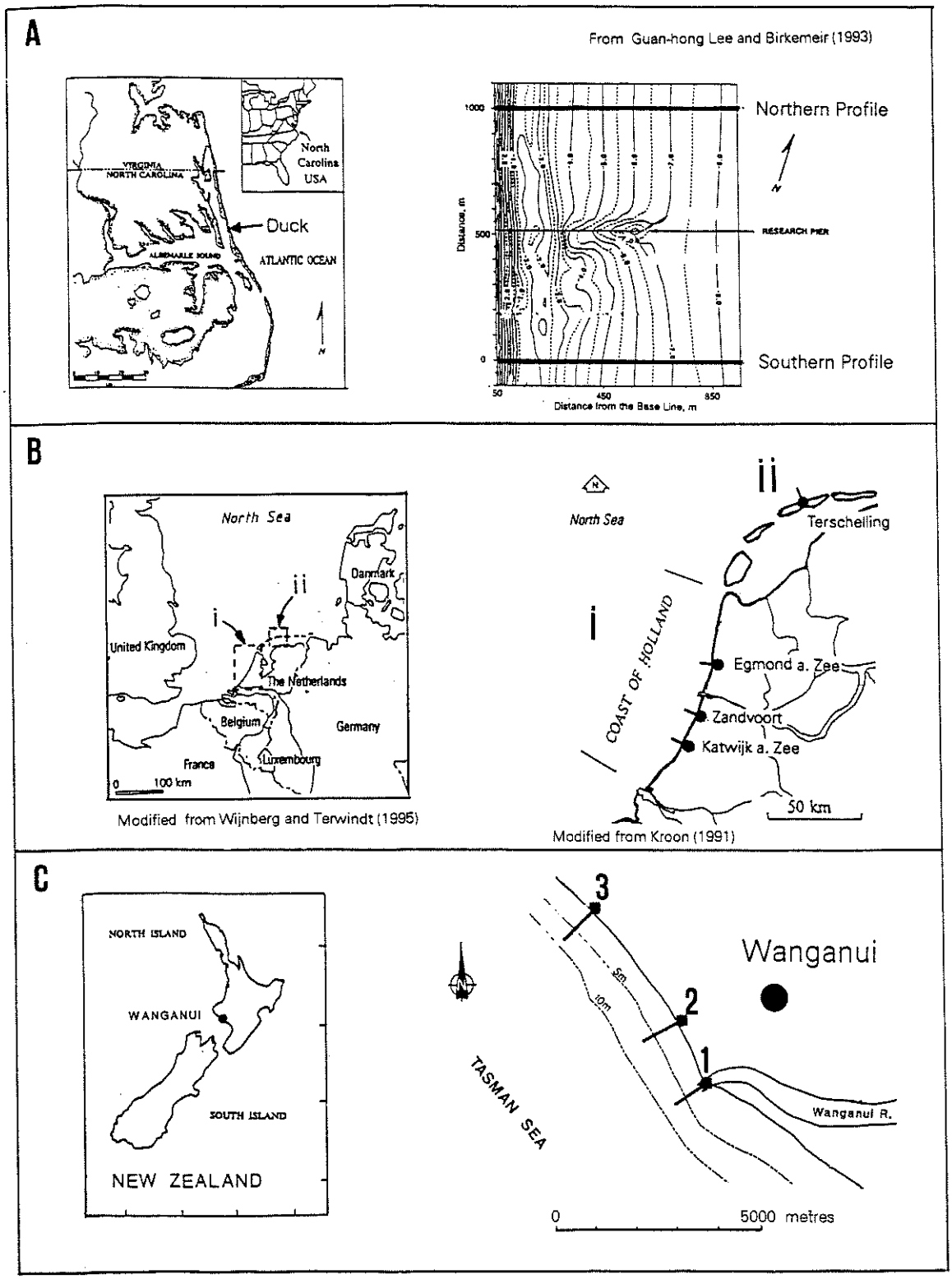

Figure 1. Location maps for the net offshore bar migration sites in North Carolina (A), The Netherlands (B) and New Zealand (C). The cross-shore survey transects are shown by bold lines.

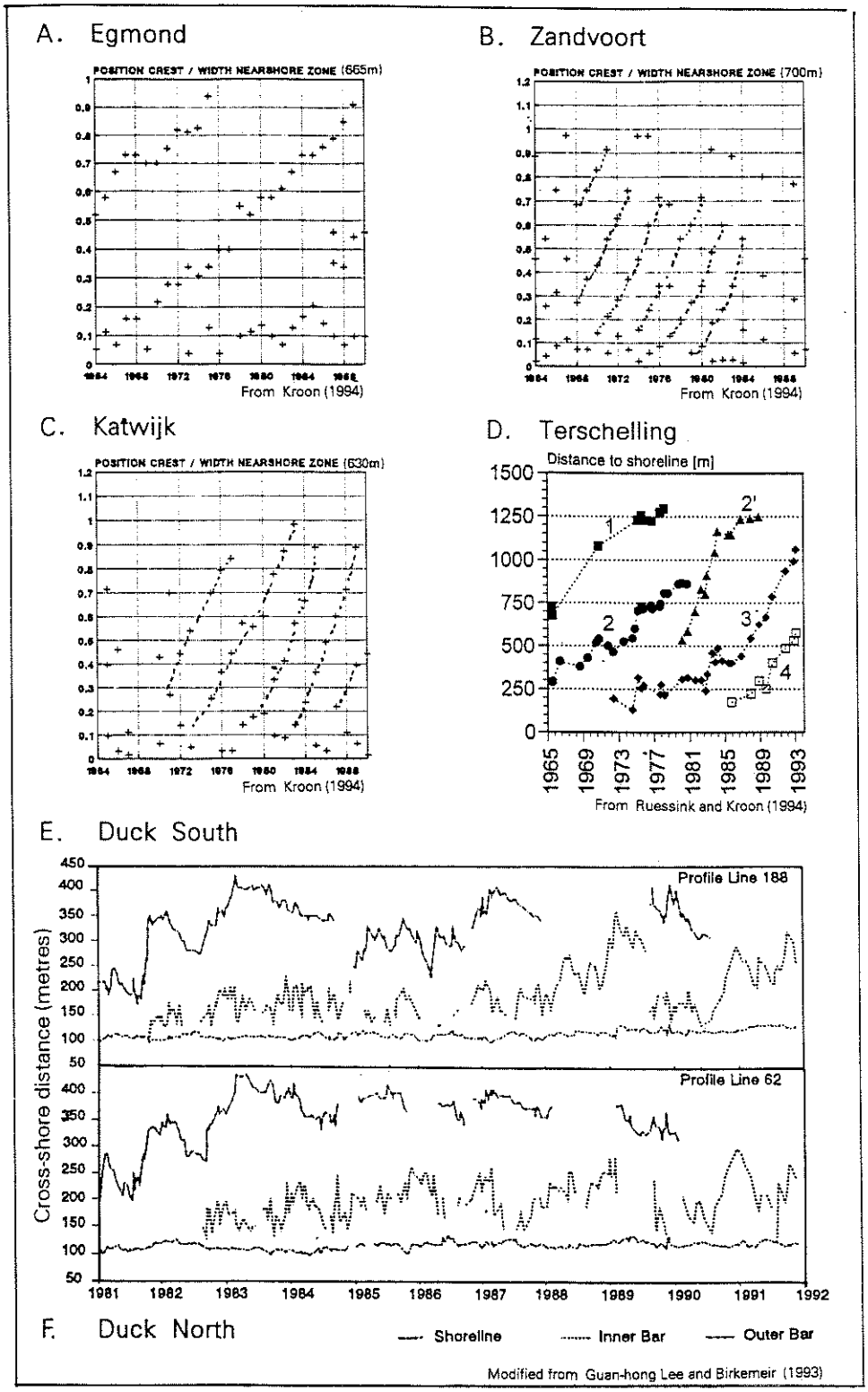

Figure 2. Published bar-crest time-series showing net offshore bar migration at sites in The Netherlands (A to D), North Carolina (E and F), and New Zealand (G to J).

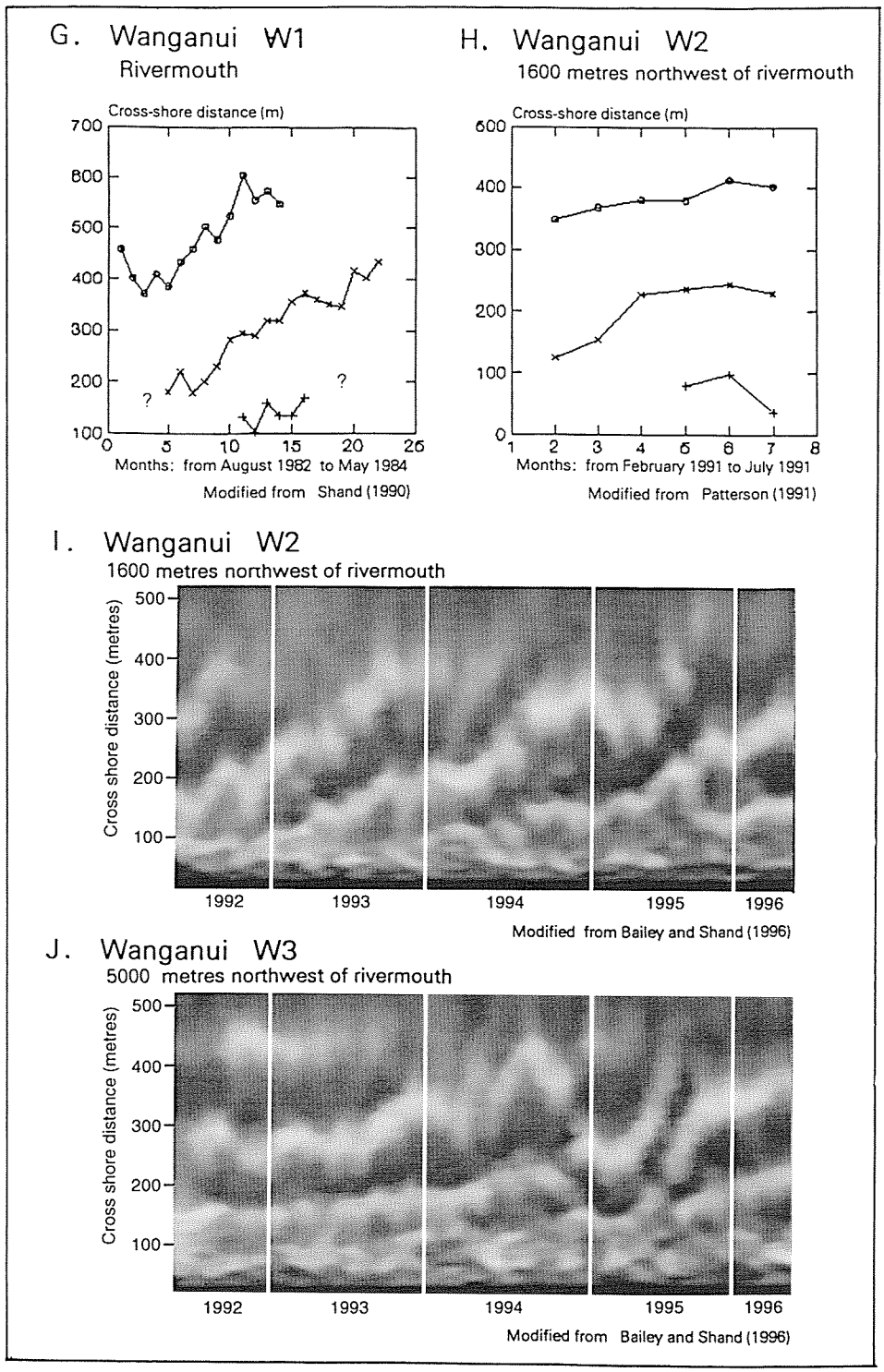

Figure 2. Continued.

cross-shore distance from a benchmark landward of the beach. Crest detection for the ground profile data, i.e. data obtained by survey instruments that detect the sea-bed, was based on the maximum positive residual from a smooth fitted curve as advocated by HOLMAN and BOWEN (1982). Crest detection for the intensity profile data, i.e. data obtained by detecting intensity variation associated with broken wave foam, was based on locating the point on a fitted parabola with zero slope. Crest locations obtained by the two methods are similar but not identical. This is to be expected as intensity values are depth controlled whereas the ground profile crest locations are shape controlled. A correction must be applied if such data sets are to be quantitatively compared. BAILEY and SHAND (1997) have developed an empirical relationship which shows the image value to be 50 m seaward of the corresponding ground value at a depth of 1 metre below MSL, 50 m landward at 4.5 m below MSL, and approximately coincident at the two metre depth.

Errors associated with the different field methods and data reduction and processing proceedures have been discussed by; HORIKAWA (1988), SHAND (1990), GAUN-HONG LEE and BIRKEMIER (1993), SHAND (1995), WIJNBERG (1995), BAILEY and SHAND (1996), BAILEY and SHAND (1997). For temporal data the cross-shore accuracy for bar-crest detection varied between ± 1 m for foreshore leveling to ± 10 m for nearshore echo-sounding and photogrammetry. Locational resolution varied between 5 m on the foreshore and 25 m in the outer surfzone.

Historical Background

Reports of the systematic offshore migration of coastal sand bars have occurred since the 1970s. EDELMAN (1974) (cited in WIJNBERG 1995) described the phenomenon in data from the Holland section of the Netherlands coast (see Figure 1B). Net offshore bar migration was next identified by BIRKEMEIER (1984) at Duck on the North Carolina coast. Further field evidence and descriptions of NOM were subsequently presented in: DE VROEG (1988), KROON (1991), KROON and HOESKSTRA (1993), KROON (1994), WIJNBERG (1995) on the Holland coast; HOEKSTRA *et al.* (1994), and RUESSINK and KROON (1994) on the Terschelling coast; LARSEN and KRAUS (1992), and LIPPMANN *et al.* (1993) at Duck on the North Carolina coast; and PATTERSON (1991), and BAILEY and SHAND (1996) at Wanganui on the south west coast of New Zealand's North Island. NOM was also described at the Wanganui Rivermouth by SHAND (1990). The bar-crest location histories used by these researchers in identifying and describing NOM have been reproduced in Figure 2. RUESSINK (1992) (cited in HOEKSTRA *et al.*, 1994) appears to have been the first writer to report on a NOM system consisting of three distinct stages.

Bar Formation

Reports on NOM have consistently observed bars to form 'near' the shoreline and thereby initiate the cycle of offshore migration (BIRKEMEIER, 1984; LIPPMANN *et al.*, 1993; RUESSINK and KROON, 1994; WIJNBERG, 1995). Field evidence not associated with NOM investigations also supports bar formation about the lower foreshore/inner nearshore (*e.g.* SHORT, 1975; FOX and DAVIS, 1976; SALLENGER and HOWD, 1989). A landward origin has been found to occur in both wave tank experiments (*e.g.* SUNAMURA, 1989; ZHANG, 1993) and in numerical modeling (*e.g.* DALLY and DEAN, 1984; HEDEGAARD *et al.*, 1991) where formation occurred in response to depth controlled break-point processes. Such bars subsequently migrated well offshore if higher energy conditions (wave height and steepness) were maintained. Bar generation seaward of the foreshore has been observed by the authors to occur only when existing bars 'bifurcate'. This process will be described and illustrated in a later section.

Specific morphological configurations appear to accompany bar formation. LIPPMANN *et al.* (1993) described incipient bar formation upon a low tide terrace. Many authors also described offshore movement of adjacent seaward bars either prior to or contemporaneous with the formation of new bars (*e.g.* BIRKEMEIER, 1984; LIPPMANN *et al.*, 1993; KROON, 1994). These spatial relationships suggest that standing waves are important in the generation mechanism. Sediment transport mechanisms associated with standing infragravity waves and break-point processes (mentioned earlier) form the bases of the main theoretical explanations of bar generation (see HOLMAN and SALLENGER, 1993).

An example of bar generation on the lower foreshore at Wanganui is shown in Figure 3. The pre-generation foreshore morphology (Figure 3A) was relatively two-dimensional and characterised by a low-tide terrace configuration. This is consistent with the observation of LIPPMANN *et al.* (1993) noted earlier. Figure 3B was taken four days later and shows a well defined longshore bar developed at the seaward margin of the terrace. A longshore trough had formed in the mid-terrace region. The relatively small differences in environmental conditions experienced during pre- and post-generation sampling (Table 1) are not considered sufficient to distort the morphology depicted by the intensity patterns. The inter-survey process data, shown in Table 1, shows that this bar was generated under conditions of high wind, high and steep waves, and strong longshore currents. Bar generation therefore appears to occur under storm conditions coupled with strong longshore currents. This observation is consistent with the environmental conditions which accompanied two documented instances of bar formation/development on the lower foreshore at Duck (see SALLENGER *et al.* 1985; HOWD and BIRKEMEIER, 1987).

The length of time that new bars may reside near the formation zone is variable. RUESSINK and KROON (1994) observed that new bars at Terschelling remained near the formation zone for 'some time' before trending seaward. The higher temporal resolution data sets from Duck (Figures 2E and 2F) also show new bars to have variable periods of residence within the inner surfzone. However, at times the landward bar can be seen to disappear from the record. LARSEN and KRAUS (1992) note that bar disappearance at Duck can be the result of a bar welding to the shore; presumably to form a low tide terrace. Bar-crests may also disappear from a time-series record when rhythmic features migrate longshore. Such 3D configurations often occur closer to the shore; this will be described in the following section. A new bar may

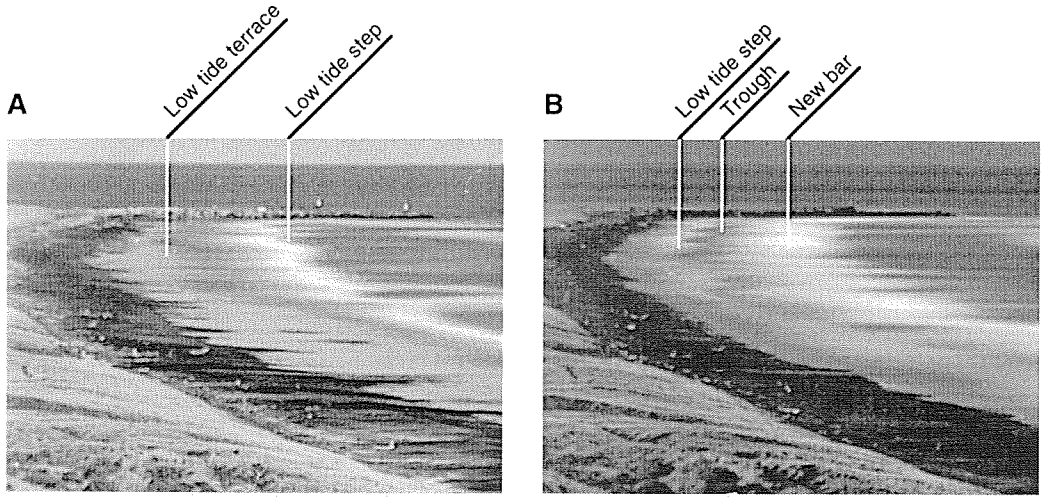

Figure 3. An example of pre-bar generation beach morphology (A) and post-generation morphology (B) on the lower foreshore at Wanganui, New Zealand, using non-rectified time-exposure photographs. Approximately 2500 metres of coast is depicted with the 200 metre long rivermouth jetty evident in the top of the image. The corresponding process variable data are provided in Table 1.

also disappear from the record following higher energy events as under such conditions the size and location of the bar offers little resistance to erosion (see ORME and ORME, 1988; KROON, 1994). However, a number of positive feedback mechanisms are likely to occur following bar generation which encourage further growth (see HOLMAN and SALLENGER, 1993). This suggests that a bar's survival and continued development is assured once it reaches a certain size. While the Wanganui bar-crest time-series in Figures 2I and 2J also show variable residence time near the generation zone, a slow offshore migration trend appears to underlie this behaviour. Discontinuities also appear to occur within the Wanganui record; however these are somewhat obscured by the horizontal smoothing.

Systematic Offshore Bar Migration

The second stage of the Dutch model is characterised by behavioural regularity. KROON (1994) described regularity in bar number and bar spacing. KROON (1994), RUESSINK and KROON (1994), and WIJNBERG (1995) described inter-bar coupling in which the seaward bar movement leads or coincides with landward bar change. This behaviour was also described at Duck by BIRKEMEIER (1984), and LIPPMANN *et al.* (1993). KROON (1994) also found that the bars at Egmond tended to temporarily reside at certain cross-shore locations. Such preferred locations are also evident at other sites by the undulations on time-averaged profile bundles (see LARSEN and KRAUS 1992; KROON, 1994; RUESSINK and KROON, 1994). Furthermore, regular NOM behaviour at the Holland sites occurs despite annual storm variation (WIJNBERG, 1995). These consistencies were considered by RUESSINK and KROON 1994, and WIGNBERG 1995 to indicate strong positive morphological feedback within the NOM system.

Large-scale boundary conditions appear to influence the underlying NOM behaviour. While longshore variation in the average rates of NOM occur along the Holland coast (see Table 2) there is no significant longshore variability in the mean annual wave climate (KROON and HOEKSTRA, 1993). However, correlation between NOM characteristics and the internal boundary conditions of nearshore slope and coastal orientation are evident (KROON and HOEKSTRA, 1993; KROON, 1994; WIJNBERG, 1995). The possible influences of ebb tide deltas and engineering structures on NOM behaviour were discussed in WIJNBERG (1995).

Analysis of higher resolution data generally supported the Dutch model and also enabled identification of a number of superimposed (smaller-scale) bar-crest movements. Seasonality, i.e. net seaward bar migration during winter months and net landward movement during summer, was identified in the Duck bar-crest data by BIRKEMEIER (1984) and LIPPMANN *et al.* (1993). Greater variability in bar-crest locations closer to the shore was observed by the Duck researchers who ascribed this to increased 3D development. This behaviour was also observed in three monthly data from Egmond by KROON (1994), and it is discussed by HOEKSTRA *et al.* (1994) on the Terschelling coast and WIJNBERG (1995) along the Holland coast. BIRKEMEIER (1984) and LIPPMANN *et al.* (1993) found that the bars at Duck often experienced episodic seaward jumps. This behaviour was also observed by KROON (1994) in the three monthly data set from Egmond. KROON found differences in timing of the episodic jumps occurred between profiles separated by only 500 metres. Such out of phase behaviour is further evidence that antecedent morphology influences net offshore bar migration. From the Duck data, BIRKEMEIER (1984) found that bar positions were relatively stable between the episodic jumps, with fluctuations reflecting storm-recovery cycles. Both BIRKEMEIER (1984) and LIPPMANN *et al.* (1993) found that while high energy events always accompanied offshore episodic movements, at other times such high energy input may have little effect on

Table 1. *Process variables associated with the bar formation morphology at Wanganui shown in Figure 3. Climatic values are included to indicate relative significance of the conditions experienced during the inter-sampling period.*

Date	Sampling Times (Photograph)	Wave Height (Metres)[1]	Period (Seconds)	Wind Direction (Degrees)[2]	Wind Speed (m/s)[3]	Longshore Currents (m/s)[4]	Pressure (hPa)[3]
930324	AM	1.41	11.7	38	5.15	+27	1018.3
	PM (15.15 hr)			297	2.92		1017.7
930325	AM	1.21	7.6	7	4.80	+73	1017.6
	PM			295	6.43		1017.2
930326	AM	1.21	6.8	335	5.15	+60	1017.2
	PM	1.94		293	13.90		1015.3
930327	AM	1.94	8.4	285	12.60	+70	1014.1
	PM			298	13.60		1012.5
930328	AM (09.30 hr)	1.27	7.0	295	8.90	+47	1012.4
	PM			193	4.44		1014.4
Climatic comparison values	Mean:	1.30	10.3		5.27		1015.7
	Other:	Upper 10% = 1.90		Predominant = 290	Upper 5% = 12.9	Upper 5% = 60	Range = 5.9

[1] Wave height (deepwater, significant) was estimated using the "line of sight method" described in Patterson and Blair (1983), and Patterson (1985). Wave climate parameters were based on daily observations between 28.7.89 and 25.5.97.
[2] Angle of coast = 147/327 degrees.
[3] Wind velocity and atmospheric pressure (at MSL) data were measured at Wanganui Airport by the National Institute of Water and Atmospheric Research. The airport is 5 km from the study site.
[4] Longshore currents were determined by timing floats in the swash zone at mid tide. Positive valued longshore currents are directed from northwest to southeast.

Table 2. *Approximate average values for parameters defining net offshore bar migration.*

Location[1]		Duration (y)	Rate (m/y)	Return Period (y)
Egmond	Dutch coast	15–20	30	15
Zandvoort		10	60–70	3–4
Katwijk		6–8	60	4–5
Tershelling		20	50	7.5
Duck south	North Carolina	4.6	67	3.2
Duck north		4.3	70	6.8
Wanganui 1	New Zealand	2.5	200	1.2
Wanganui 2		3.0	146	1.4
Wanganui 3		4.8	109	1.4

[1] Location details are shown in Figure 1.

the bar behaviour. The sensitivity of bar behaviour to the initial morphology, together with the apparent form/process feedback mechanisms, lead LIPPMANN *et al.* (1993) to suggest that the NOM bar system had the characteristics of a 'non-linear dynamical system' (see HUGGETT, 1990; MIDDLETON, 1990).

Bar Degeneration

When a bar migrates into the outer surfzone it begins to flatten out. An example of such outer bar degeneration at Wanganui is shown in Figure 4. Bar degeneration in The Netherlands data occurred at critical offshore distances and depths after which the crest depth increased, the shape flattened, and the crest tended to move further offshore (RUESSINK and KROON, 1993; KROON, 1994; WIJNBERG, 1995). However, at Duck outer bar disappearance consisted of shoreward crest migration during periods of amplitude reduction (BIRKEMEIER, 1984; LARSEN and KRAUS, 1992; LIPPMANN *et al.*, 1993). At Wanganui, the data presented in Figures 2I, 2J,

Figure 4. A typical outer-bar degeneration sequence at Wanganui, New Zealand. These echo-sounded profiles are located 1600 metres northwest of the Wanganui Rivermouth (Transect 2 in Figure 1C). Modified from Patterson (1991).

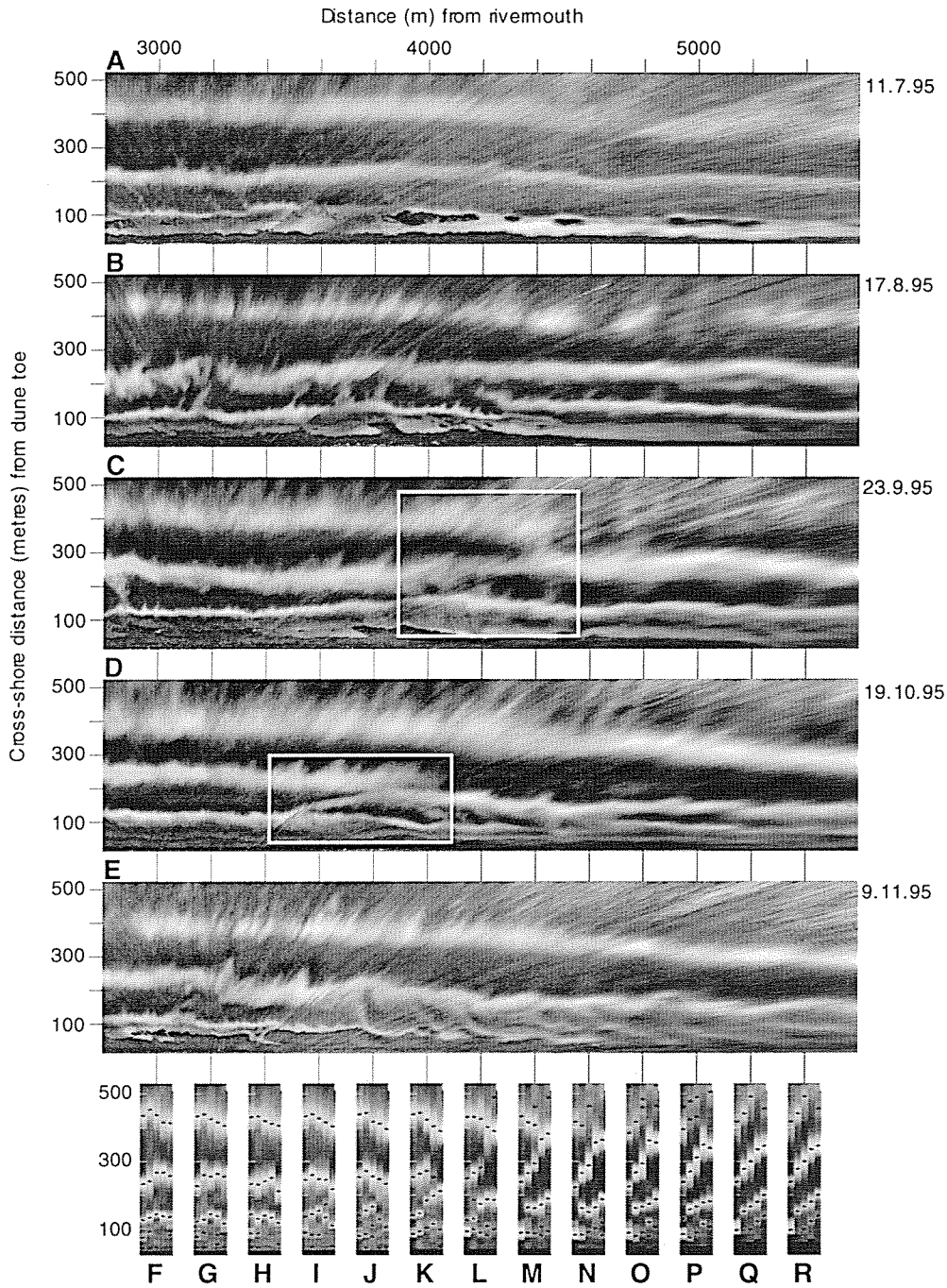

Figure 5 An example of bar switching at Wanganui, New Zealand, using a sequence of rectified time-exposure photographs with the coastline straightened (A - E). Bar switching occurs within the transition zones defined by the rectangles in C and D. The landward bars to the right of the transition zones are realigning with the seaward bars to the left. Time-stack images showing bar-crest behaviour at the marked cross-shore transits are shown in F to R. The black dots in the time-stacks mark the location of relative intensity maxima which represent morphological features such as bar-crests and the low tide step.

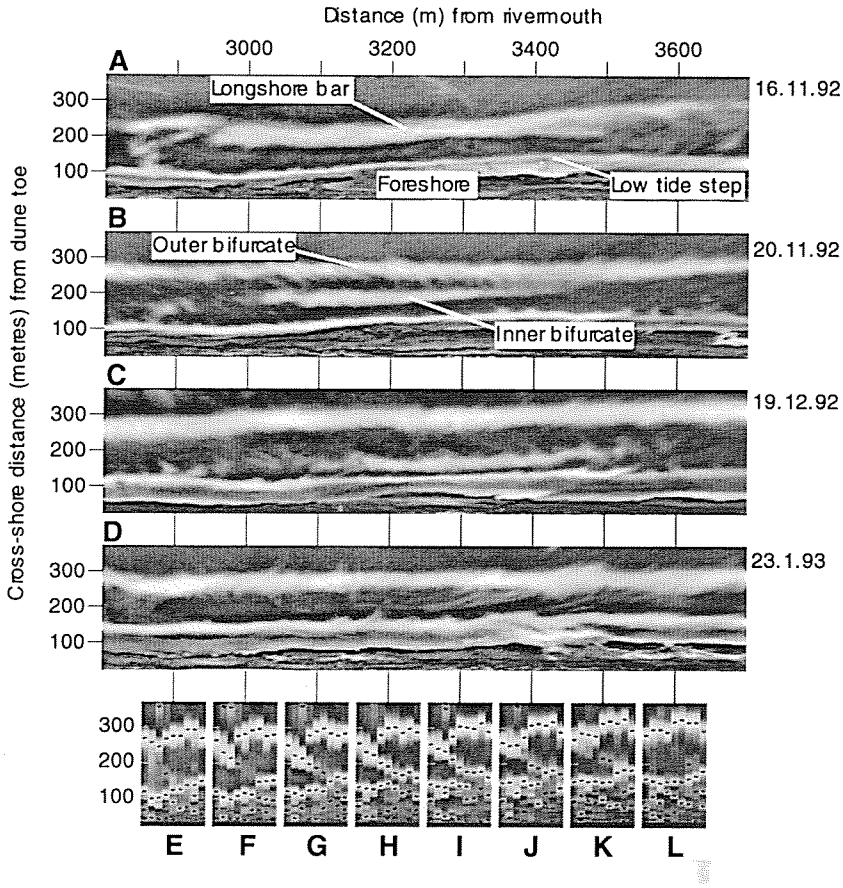

Figure 6. An example of bar bifurcation at Wanganui, New Zealand, using rectified time-exposure photographs (A–D). The bifurcation has occurred in B and the inner bifurcate is merging with the lower foreshore in D. Time-stack images showing bar-crest behaviour at the marked cross-shore transects are shown in E to L. Nine samples were used to construct each time-stack with slices from A,B,C,D appearing in the time-stacks as samples 3,4,6,9 respectively. The black dots in the time-stacks mark the location of relative intensity maxima.

and 4 show both landward and seaward migrations occur in the outer surfzone. While the field evidence shows landward migration can accompany degeneration, bars do not appear to undergo significant return movement. Analysis of the higher depth/temporal resolution data from Duck suggests that while bar degeneration is a one way process, outer bar regeneration does occur at times (LARSEN and KRAUS, 1992).

Processes associated with asymmetric waves appear to accompany degeneration of the outer bar. At Duck, BIRKEMEIER (1984), and LARSEN and KRAUS (1992) observed that both lowering of bar height and reduction in bar volume were associated with extended periods of non-breaking wave conditions. LARSEN and KRAUS (1992) also noted that steady onshore sediment transport appeared to occur across the bar during the disappearance phase. WIJNBERG (1995) used sediment budget evidence from the Holland coast to argue that some sediment from the outer bar moved further landward than the adjacent trough during the degeneration stage. In some cases the final disappearance of a bar has been observed to accompany a major storm event (LIPPMANN *et al.*, 1993; KROON, 1994). However, LARSEN and KRAUS 1992 also noted that at Duck outer-bar rejuvenation occurred under higher energy (fall and winter) conditions. Recently WIJNBERG (1995) has hypothesised that bar maintenance occurs under intense breaking of waves while bar degeneration occurs with highly asymmetric waves. Once degradation begins positive feedback mechanisms then prevent significant bar redevelopment or shoreward migration as increasingly severe storm waves are required to maintain the bar and increasing wave size is required to produce effective wave asymmetry. Field measurements by HOEKSTRA and HOUWMAN (1994), together with results from an applied theoretical analysis by WIJNBERG (1995), provided further support for this hypothesis.

The characteristics of the outer bar appear to control landward bar behaviour in a multi-bar system. Observations from the Holland sites (KROON, 1994; WIJNBERG, 1995), the Terschelling site (RUESSINK and KROON, 1994), and at Duck (LIPPMANN *et al.*, 1993) indicated that systematic offshore migration of landward bars only occurred when outer bars were poorly developed, i.e. when the trough depth to bar-crest depth ratio is low. Furthermore, a well developed seaward

bar was observed to prevented offshore migration. KROON (1994), and RUESSINK and KROON (1994) speculated that the depth/location of the seaward bar controls the cross-shore wave height distribution and the cross-shore structure of standing infragravity waves. Whether landward bars are fixed or free to move offshore may therefore be governed by break-point or standing wave-based sediment transport mechanisms (see KIRBY *et al.*, 1981; THORNTON and GUZA, 1983).

Defining Net Offshore Bar Migration

A variety of parameters and terminology has been used to define and describe overall NOM by different researchers (DE VROEG, 1988; KROON and HOEKSTRA, 1993; KROON, 1994; RUESSINK and KROON, 1993; WIJNBERG, 1995). The time a bar exists for has been referred to as the duration or the life-span. The frequency with which a bar recurs at any location in the surfzone has been called the return period or the passage interval. The average rate of offshore migration is also used as a NOM parameter.

Parameter values for the nine NOM sites in Figure 1 are provided in Table 2. The values for the Holland sites are those reported in KROON and HOEKSTRA (1993). Values for the other sites were approximated from the published data sets shown in Figure 2. The intensity data from Wanganui (Figure 2 I and J) were transformed to ground-profile distances by using the empirical calibration referred to earlier in the Methods section. Wide inter-site variation is evident for all parameters with average duration ranging between 2.5 and 20 years, average rate ranging between 30 and 200 m per year, and average return period ranging between 1.2 and 15 years. As noted earlier, the Dutch researchers (KROON and HOEKSTRA, 1993; KROON, 1994; WIJNBERG, 1995) considered that large-scale boundary conditions are associated with the variation in overall NOM behaviour evident in the Holland data.

Oblique Bar Orientations

Net offshore bar migration has been associated with three-dimensional bar behaviours. The most obvious 3D influence is where obliquely oriented sand bars with a shore attachment migrate alongshore. Such morphologies have been reported on different coasts and occur at a variety of scales (*e.g.* BRUUN, 1955; SHORT, 1976; HUNTER *et al.*, 1979; SHORT, 1979; STEWART and DAVIDSON-ARNOTT, 1988; KROON, 1991; TROWBRIDGE, 1995; ANITA, 1996). In some of these cases, however, the proximal (landward) end of the bar lags behind the distal (seaward) end in the longshore translation so a net onshore bar migration occurs at each cross-shore location. KROON (1991), LIPPMANN *et al.* (1993), and KROON (1994) have suggested that the NOM phenomenon may simply be a consequence of the longshore migration of oblique bars where the proximal end leads. However, WIJNBERG (1995, p.166) used the results of a sediment budget/profile volume analysis of data from the Holland coast to argue that such "cyclic bar dynamics are essentially a cross-shore sediment redistribution process within the nearshore zone."

Bar Switching

Bar switching is also a 3D morphological behaviour which influences net offshore bar migration. In this situation, bar alignments alter, following the development of a discontinuity in which landward bars on one side of the discontinuity join with the seaward bars on the other. The term 'bar-switching' is used by the authors to describe this phenomenon. WIJNBERG and WOLF (1994), and WIJNBERG (1995) referred to this behaviour as 'longshore out-of-phase development' and the area in which the switch occurred as a transition zone. These researchers found on the Holland coast that the transition zones had a longshore length scale of one to three kilometres, and that they could migrate alongshore. WIJNBERG and WOLF (1994), and WIJNBERG (1995) used the term 'out-of-phase' to describe bar switching phenomena because they observed that bars to each side of a transition zone were longshore 'incoherent' and 'out-of- phase' with respect to their offshore migration cycles. WIJNBERG and WOLF (1994), and WIJNBERG (1995) further observed that the development of large-scale rhythmic topography appeared to be a prerequisite for the onset of switching and that out-of-phase bar morphologies were most persistent where NOM rates were low. Other examples of apparent bar switching are shown in RUESSINK and KROON (1994) at Tershelling, in LIPPMANN *et al.* (1993) at Duck and in CARTER (1986) on the Magilligan coast of Northern Ireland.

An example of bar switching at Wanganui is illustrated by the images in Figure 5. Figures 5A to 5E show a four month sequence of rectified images with the coastline straightened. Each image represents the morphology over a 2800 m (longshore) by 500 m (cross-shore) area. The pre-switch morphology has a shore-parallel bar configuration (Figure 5A). In Figure 5B the outer bar has lowered to the right of *c.* 4200 m. Bar switching is occurring within the transition zones defined by the rectangles in Figures 5C and 5D. Translation of the transition zone suggests that bar switching begins in the outer surf zone and progresses landward. Some longshore migration towards the rivermouth, *i.e.* to the left, is evident. The post-switch morphology (Figure 5E) has regained the shore-parallel configuration. During the switch the time-stacks (Figures 5F to 5R) demonstrate how bar behaviour is differs on either side of the transition zone. The bars to the left of the transition zone (Figures 5F to 5H) either remain approximately stationary or trend landward. The present authors refer to this situation as a 'negative' switch. In contrast, the bars to the right of the transition zone move rapidly seaward (Figures 5N to 5R) and this is referred to as a 'positive' switch. The time-stacks within the transition show variable and complex bar behaviour which is often characterised by discontinuities.

Bar Bifurcations

Bar bifurcation is another 3D morphological behaviour which influences net offshore bar migration. In this situation a section of bar splits longitudinally. The seaward bifurcate 'jumps' seaward while the inner bifurcate moves into the landward trough. The inner bifurcate then either disappears or migrates further shoreward to merge with the adjacent

bar/low tide step which results in the seaward movement of that feature. Such bar behaviour was recently described by BAILEY and SHAND (1996). KROON (1991), KROON (1994), and WIJNBERG (1995) have described the occurrence of 'double bars' on the Holland coast which are probably the result of bar bifurcations. KROON (1994) found double bar development at Egmond appeared to be necessary to reinitiate seaward bar migration after a period of inactivity. Other field examples of possible bar bifurcations are shown in GREENWOOD and DAVIDSON-ARNOTT (1975), OWENS (1977), HOLMAN and SALLENGER (1986), HOLMAN and LIPPMANN (1987), and BAUER and GREENWOOD (1990). GREENWOOD and DAVIDSON-ARNOTT (1975) referred to the inner bifurcate as a 'tail', while HOLMAN and LIPPMANN (1987) used the term 'winged bar' for this feature. In all the documented examples the apparent bifurcations occur where bars broaden, e.g. at the horn area of a crescentic bar.

An example of bar bifurcation at Wanganui is illustrated by the image sequence in Figure 6 which was sampled over a nine week period. The rectified and straightened images (Figures 6A to 6D) show the morphology over a 900 m (longshore) by 375 m (cross-shore) section of coast. The pre-bifurcation morphology (Figure 6A) shows a broad inner bar. As noted earlier, this appears to be a pre-requisite for the onset of bar bifurcation. The bifurcation is shown in Figure 6B and within two months the inner bifurcate merged with the lower foreshore (Figure 6D). The accompanying time-stacks show the outer bifurcate and low tide step trending seaward during the bifurcation process (Figures 6G to 6K) while the morphology on either side of the bifurcation zone maintains a shore-parallel configuration (Figures 6E, 6F, and 6L). These patterns contrast with the time-stack histories associated with bar-switching. Furthermore, these examples of a bar switch and a bar bifurcation suggest that the spatial and temporal scales of switching are at least double that associated with bar bifurcation. However, as with bar switching, the onset of bar bifurcation appears to require the prior development of three-dimensional morphological configurations. Both bifurcation and switching result in the surfzone morphology returning to a more two-dimensional configuration.

Edge waves may be an important control in the bifurcation mechanism. KROON (1991) speculated that the development of double bars resulted from a changing cross-shore structure of a low mode edge wave in the infragravity range. BAUER and GREENWOOD (1990) observed bar bifurcation to occur at a multi-bar field site in the presence of a standing infragravity edge wave. Laboratory experiments have shown a bifurcation to develop on a crescentic bar which was evolving in response to a standing edge wave field (BOWEN and INMAN, 1971). A change in the type of edge wave may also be important. For example, on multi-bar coasts AAGAARD (1991) found progressive infragravity waves to be associated with large storms while standing infragravity waves were associated with moderate energy situations. With the onset of high energy conditions the structure and associated drift velocities of progressive edge waves (see BOWEN, 1980; CARTER *et al.*, 1993) would be expected to be associated with trough development on landward extending shoal zones thereby generating a bifurcation. The extensive 300 metre long shore-parallel split defining the bifurcation in Figure 6B is consistent with the suggested progressive edge wave influence in bar bifurcation morphodynamics.

CONCLUSION

Similar bar behavioural characteristics appear to occur at all sites where NOM has been observed. The three stage Dutch conceptual model seems to apply to the data from Wanganui—New Zealand, and Duck—North Carolina. Furthermore, 3D configurations and behaviour such as bar switching and bar bifurcations, are also evident at all NOM sites. Such inter-site consistency supports WIJNBERG's (1995, p. 164/5) contention that the sequential process of the NOM cycle may be a common generation mechanism for multiple bar systems.

This review suggests that while the overall net offshore bar migration operates at a temporal scale of years and at a spatial scale of 100s to 1000s of metres the system is influenced by components operating at a range scales. Episodes of offshore bar migration are driven by storm events, *i.e.* smaller-scale. The timing and nature of offshore bar migrations are influenced by small to moderate-scale antecedent morphology. Finally, the overall NOM characteristics are related to large-scale physical boundary conditions such as cross-shore slope and coastal orientation.

Inter-site variation in NOM parameter values provides a means to further investigate large-scale NOM morphodynamics. A detailed inter-site comparison of NOM characteristics, physical boundary conditions, and process variables has recently been completed by the authors and will be reported in a following paper (Shand and Bailey submitted).

ACKNOWLEDGMENTS

This study was supported by grants from the Massey University Graduate Research Fund, the Massey University Research Fund, and the Massey University Vice Chancellors Research Fund. The authors wish to thank: Katerine Wijnberg, Aart Kroon, and Gerben Ruessink for their permission to reproduce illustrations, and Drs. Gerben Ruessink, Mike Shepherd, Bob Kirk, and Phil Osborne for their useful comments on the manuscript. Special thanks also go to staff at the Wanganui Port Company, the Wanganui District Council; the Wanganui Surf Life-saving Club; and members of the principal author's family, for assistance with field surveys which were often conducted under physically demanding conditions.

LITERATURE CITED

AAGAARD, T., 1990. Infragravity waves and nearshore bars in protected, storm-dominated coastal environments. *Marine Geology*, 94, 181–203.

AAGAARD, T. and HOLM, J., 1989. Digitisation of wave run-up using video records. *Journal of Coastal Research*, 5(3), 547–551.

ANITA, E.E., 1996. Shoreface-connected ridges in German and U.S. Mid-Atlantic Bights: similarities and contrasts. *Journal of Coastal research*, 12(1), 141–146.

BAILEY, D.G. and SHAND, R.D., 1993. Determining large-scale sand bar evolution. *Proceedings of the First New Zealand Conference on Image and Vision Computing*, pp. 109–116.

BAILEY, D.G. and SHAND, R.D., 1994. Determining wave run-up using automated video analysis. *Proceedings of the Second New Zealand Conference on Image and Vision Computing,* pp. 2.11.1–2.11.8.

BAILEY, D.G. and SHAND, R.D., 1996. Determining large-scale sand bar behaviour. *Proceedings of the IEEE International Conference on Image Processing,* Lausanne, Switzerland, (2), 637–640.

BAILEY, D.G. and SHAND, R.D., 1997. Data fusion issues in analysing coastal morphodynamic systems. *Proceedings of the First Joint Australian and New Zealand Conference on Digital Image and Vision Computing: Techniques and Applications* (Auckland, New Zealand), pp. 107–112.

BAUER, B.O. and GREENWOOD, B., 1990. Modification of a linear bar-trough system by a standing edge wave. *Marine Geology,* 92, 177–204.

BIRKEMEIER, W.A., 1984. Time scales of nearshore profile change. *Proceedings of the 19th International Conference on Coastal Engineering* (ASCE), pp. 1507–1521.

BOWEN, A.J., 1980. Simple models of nearshore sedimentation; beach profiles and longshore bars. *In:* McCann, S.B. (ed.), *The Coastline of Canada.* Geological Survey Canada Paper 80-10, pp. 1–11.

BOWEN, A.J. and INMAN, D.L., 1971. Edge waves and crescentic bars. *Journal of Geophysical Reseach,* 76, 8662–8671.

BRUUN, P., 1955. Migrating sand waves or sand humps, with special reference to inverstigations carried out on the Danish North Sea Coast. *Proceedings of the 5th International Conference on coastal Engineering* (ASCE), pp. 269–295.

BURGESS, J.S., 1971. Coastline Change at Wanganui, New Zealand. Unpublished PhD. thesis, University of Canterbury, New Zealand. 99p.

CARTER, T.G.; LIU, P.L.F., and MEI, C.C, 1973. Mass transport by waves and offshore sand bedforms. Proceedings of the American Society of Civil Engineers, *Journal of the Waterways, Horbors and Coastal Engineeing Division,* 99, 165–184.

CHAPPELL, J., and ELIOT, I.G., 1979. Surf-beach dynamics in time and space—an Australian case study, and elements of a predictive model. *Marine Geology,* 32, 231–250.

CHESSER, S.A., 1993. Seasonal erosion/accretion cycles in a littoral cell. *In:* List, J.H., (ed.), *Large-Scale Coastal Behaviour '93.* US Geological Survey Open-File Rept., 93-381:33–36.

DALLY, W.R. and DEAN, R.G., 1984. Suspended sediment transport and beach profile evolution. *Journal of Waterway, Port, Coastal and Ocean Engineering,* 110-1, 15–33.

DAVIS, R.A. and FOX, W.T., 1972. Coastal processes and nearshore sand bars. *Journal of Sedimentary Petrology,* 42(2), 401–412.

DAVIS, R.A. and FOX, W.T., 1975. Process-response patterns in beach and nearshore sedimentation: 1. Mustang Island, Texas. *Journal of Sedimentary Petrology,* 45(4), 852–865.

DE VROEG, J.H.; SMIT, E.S.P., and BAKKER, W.T., 1988. Coastal Genesis. *Proceedings of the 21st International Conference on coastal Engineering* (ASCE), pp. 2825–2839.

EDELMAN, T., 1974. *Bijdrage tot de historische geografie van de Nederlandse kuststrook.* Rijkswaterstaat/directie waterhuishouding en waterbeweging. Den Haag, The Netherlands, 84p.

FOX, W.T. and DAVIS, R.A., 1976. Weather Patterns and Coastal Processes. *In:* Davis, R.A. and Ethington, R.C., (eds.), *Society of Economic Paleontologists and Mineralogists,* Special Publication 24, 1–23.

GIBB, Sir Alexander and Partners. 1962: *Tongariro River Power Development, Wanganui Harbour.* Report to the New Zealand Ministry of Works, 39p.

GOLDSMITH, V.; BOWMAN, D., and KILEY, K., 1982. Sequential stage development of crescentic bars: Hahoterim beach, southeastern Mediterranean. *Journal of Sedimentary Petrology,* 52, 233–249.

GREENWOOD, B. and DAVIDSON-ARNOTT, R., 1979. Sedimentation and equilibrium in wave formed bars: a review and case study. *Canadian Journal of Earth Science,* 16, 312–332.

GUAN-HONG, L. and BIRKEMEIER, W.A., 1993. *Beach and Nearshore Data: 1985–1991 CERC Field Research Facility.* Technical Report CERC-93-3, 13p.

HARDISTY, J., 1990. *Beaches: Form and Process.* London: Unwin Hyman, 319p.

HEDEGAARD, I.D.; DEIJAARD, J., and FREDSOE, J., 1991. Onshore/offshore sediment transport and morphological modeling of coastal profiles. *Proceedings of Coastal Sediments'91* (ASCE), pp. 643–657.

HOEKSTRA, P. and HOUWMAN, K.T., 1994. Hydrodynamic processes on the lower shoreface of the Dutch coast. *Proceedings of Coastal Dynamics '94* (ASCE), pp. 852–871.

HOEKSTRA, P.; HOUWMAN, K.T.; KROON, A.; VAN VESSEM, P., and RUESSINK, B.G., 1994. The Nourtec experiment of Terschelling: Process-orientated monitoring of a shoreface nourishment (1993–1996). *Proceedings of Coastal Dynamics '94* (ASCE), pp. 402–416.

HOLLAND, K.T. and HOLMAN, R.A., 1993. The statistical distribution of swash maxima on natural beaches. *Journal of Geophysical Research,* 98(C6), 10,271–10,278.

HOLMAN, R.A. and BOWEN, A.J., 1982. Bars, bumps, and holes: models for the generation of complex beach topography. *Journal of Geophysical Research,* 84, 457–468.

HOLMAN, R.A. and LIPPMANN, T.C., 1987. Remote sensing of nearshore bar systems—making morphology visible. *Proceeding of Coastal Sediments'87* (ASCE), pp. 927–944.

HOLMAN, R.A. and SALLENGER, A.H., 1986. High energy nearshore processes. *Eos,* 67(49), 1369–1371.

HOLMAN, R.A. and SALLENGER, A.H., 1993. Sand bar generation: a discussion of the Duck experiment series. *Journal of Coastal Research,* Special Issue, 15, 75–92.

HOM-MA, M. and SONU, C., 1962. Rythmic patterns of longshore bars related to sediment characteristics. *Proceedings of the 8th International Conference on Coastal Engineering* (ASCE), pp. 248–278.

HOWD, P.A. and BIRKEMEIER, W.A., 1987. Storm-induced morphology changes during Duck85. *Proceeding of Coastal Sediments'87* (ASCE), pp. 927–944.

HUGGETT, R.J., 1990. *Catastrophism: Systems of Earth History.* London: Edward Arnold, 233p.

HUNTER, R.E.; CLIFTON, H.E., and PHILLIPS, R.L., 1979. Depositional processes, sedimentary structures, and predicted vertical sequences in barred nearshore systems, Southern Oregon coast. *Journal of Sedimentary Petrology,* 49(3), 711–726.

KHAFAGY, A.A.; NAFFAA, M.G.; FANOS, A.M., and DEAN, R.G., 1992. Nearshore coastal changes along the Nile Delta shores. *Proceedings of the 23rd International Conference on coastal Engineering* (ASCE), pp. 3260–3272.

KIRBY, J.T.; DALRYMPLE, R.A., and LIU, P.L.F., 1981. Modification of edge waves by barred-beach topography. *Coastal Engineering,* 5, 35–49.

KOMAR, P.D., 1976. *Beach Processes and Sedimentation,* Englewood Cliffs, New Jersey: Prentice-Hall, 429p.

KROON, A., 1991. Three-dimensional morphological changes of a nearshore bar system along the Dutch coast near Egmond aan Zee. *Proceedings of the Skagen Symposium, Journal of Coastal Research,* Special Issue, 9, 430–451.

KROON, A., 1994. Sediment Transport and Morphodynamics of the Beach and Nearshore Zone Near Egmond, The Netherlands. PhD thesis, Utrecgt University, The Netherlands, 275p.

KROON, A., and HOESKSTRA, P., 1993. Nearshore bars and large-scale coastal behaviour. *In:* List, J.H., (ed.), *Large-Scale Coastal Behaviour '93.* US Geol Surv. Open-File Rep., 93-381: 92–95.

LARSEN, M. and KRAUS, N.C., 1992. *Analysis of cross-shore movement of natural longshore bars and material placed to create longshore bars.* Technical Report CERC DRP-29-5, 115p.

LIPPMANN, T.C. and HOLMAN, R.A., 1989. Quantification of sand-bar morphology: a video technique based on wave dissipation. *Journal of Geophysical Research,* 94, 995–1011.

LIPPMANN, T.C. and HOLMAN, R.A., 1990. The spatial and temporal variability of sand-bar morphology. *Journal of Geophysical Research,* 95, 11,575–11,590.

LIPPMANN, T.C.; HOLMAN, R.A., and HATHAWAY, K.K., 1993. Episodic, nonstationary behaviour of a double bar system at Duck, North Carolina, U.S.A., 1986–1991. *Journal of Coastal Research,* Special Issue, 15, 49–75.

MARRA, J.J., 1992. Swash Zone Dynamics in a Rhythmic Black Sand

Beach System, Unpublished PhD., University of Canterbury, 235p.

MASSELINK, G. and SHORT, A.D., 1993. The effect of tide range on beach morphodynamics and morphology: a conceptual beach model. *Journal of Coastal Research,* 9(3), 785–800.

MIDDLETON, G.V., 1990. Non-linear dynamics and chaos: potential applications in the earth sciences. *Geoscience Canada,* 17, 3–11.

NUMMEDAL, D.; SONNENFELD, D.L., and TAYLOR, K., 1984. Sediment transport and morphology at the surf zone of Presque Isle, Lake Erie, Pennsylvania. *Marine Geology,* 60, 99–122.

ORME, A.R. and ORME, A.J., 1988. Ridge and runnel enigma. *The Geographical Review,* 78, 169–184.

OWENS, E.H., 1977. Temporal variations in beach and nearshore dynamics. *Journal of Sedimentary Petrology,* 47(1), 168–190.

PATTERSON, D.C., 1985. Low Cost Visual Determination of Surfzone Parameters. Unpublished MSc Thesis, University of Queensland, Australia, 143p.

PATTERSON, D.C. 1991: *Wanganui Port Development: Coastal Engineering Considerations.* A report (unpublished) for Ocean Terminals and the Wanganui District Council, 48p.

PATTERSON, D.C. and BLAIR, R.J., 1983. Visually determined wave parameters. *Proceedings of the Sixth Australian Conference on Coastal and Ocean Engineering* (Gold Coast, Australia), pp. 151–155.

RUESSINK, B.G., 1992. *The nearshore morphology of Terschelling (1965–1991).* Institute for Marine an Atmospheric Research Utrecht, IMAU report R92-11, 30p.

RUESSINK, B.G. and KROON, A., 1994. The behaviour of a multiple bar system in the nearshore zone of Terschelling, the Netherlands: 1965–1993. *Marine Geology,* 121, 187–197.

SALLENGER, A.H; HOLMAN, R.A., and BIRKEMEIER, W.A., 1985. Storm-induced response of a nearshore-bar system. *Marine Geology,* 64, 237–257.

SALLENGER, A.H. and HOWD, P.A., 1989. Nearshore bars and the break-point hypothesis. *Coastal Engineering,* 12, 301–313.

SASAKI, T., 1983. *Three dimensional topographic changes on the foreshore zone of sandy beaches.* University of Tsukuba: Institute of Geoscience, Science Report A-4, pp. 69–95.

SHAND, R.D., 1990. *The subaqueous morphology at the entrance to a jetty controlled river mouth on a moderate to high energy littoral drift dominated coast: Wanganui New Zealand 1981–1987.* Post Graduate Diploma in Science—Research Project, Massey University, New Zealand. 102p.

SHAND, R.D., 1995. *Hydrographic Automation Options for the Port of Wanganui Rivermouth Survey.* A Report to the Manager and Board of Directors, Ocean Terminals, Wanganui, 14p.

SHAND, R.D. and BAILEY, D.B., (submitted). Net offshore bar migration: an inter-site comparison. Submitted to the *Journal of Coastal Research,* November 1997.

SHAW, J., 1985. Beach Morphodynamics of an Atlantic Coast Embayment: Runkerry Strand, County Antrim. *Irish Geography,* 18, 51–58.

SHORT, A.D., 1975. Offshore bars along the Alaskan Arctic coast. *Journal of Geology,* 83, 209–221.

SHORT, A.D., 1979. Three Dimensional Beach-Stage Model. *Journal of Geology,* 87, 553–571.

SHORT, A.D., 1992. Beach systems of the central Netherlands coast: processes, morphology, and structural impacts in a storm driven multi-bar system. *Marine Geology,* 107, 103–127.

SHORT, A.D. and AAGAARD, T., 1993. Single and multi-bar beach change models. *Journal of Coastal Research,* Special Issue, 15, 141–157.

SONNENFELD, D.L. and NUMMEDAL, D., 1987. Morphodynamics and sediment dispersal of a tideless surf zone. *Proceedings of Coastal Sediments'87* (ASCE), pp. 1938–1949.

SONU, C.J., 1973. Three-dimensional beach changes. *Journal of Geology,* 81, 42–64.

STEWART, C.J. and DAVIDSON-ARNOTT, R.G.D., 1988. Morphology, formation and migration of longshore sandwaves; Long Point, Lake Erie, Canada. *Marine Geology,* 81, 63–71.

SUNAMURA, T., 1989. Sandy beach geomorphology elucidated by laboratory modeling. *In:* Lakhan, V.C., and Trenhaile, A.S., (eds.), *Applications in Coastal Modeling: Amsterdam:* Elsevier Oceanography Series 40, pp. 159–202.

THORNTON, E.B. and GUZA, R.T., 1983. Transformation of wave height distribution. *Journal of Geophysical Research,* 88, 5925–5938.

TROWBRIDGE, J.H., 1995. A mechanism for the formation and maintenance of shore-oblique sand ridges on storm-dominated shelves. *Journal of Geophysical Research,* 100-C8, 16071–16086.

WIJNBERG, K.M., 1995. Morphologic Behaviour of a Barred Coast Over a Period of Decades. PhD thesis, Utrecgt University, The Netherlands, 245p.

WIJNBERG, K.M. and TERWINDT, J.H.G., 1995. Extracting decadal morphological behaviour from high-resolution, longterm bathymetric surveys along the Holland coast using eigenfunction analysis. *Marine Geology,* 126, 301–330.

WIJNBERG, K.M. and WOLF, F.C.J., 1994. Three-dimensional behaviour of a multiple bar system. *Proceedings of Coastal Dynamics '94* (ASCE), pp. 59–73.

WRIGHT, L.D.; CHAPPELL, J.; THOM, G.B; BRADSHAW, M.P., and COWELL, P., 1979. Morphodynamics of reflective and dissipative beaches and inshore systems: Southeastern Australia. *Marine Geology,* 32, 105–140.

WRIGHT, L.D. and SHORT, A.D., 1984. Morphodynamic variability of surf zones and beaches: a synthesis. *Marine Geology,* 56, 93–118.

ZHANG, D.P., 1994. *Wave Flume Experiments on the Formation of Longshore Bars Produced by Breaking Waves.* University of Tsukuba: Institute of Geoscience, Science Report A-15, pp. 47–105.

Shand, R.D., Bailey, D.G. Shepherd, M.J., 1999. An inter-site comparison of net offshore bar migration characteristics and environmental conditions. Journal of Coastal Research, 15 (3), 750-765.

Journal of Coastal Research	15	3	750–765	Royal Palm Beach, Florida	Summer 1999

An Inter-Site Comparison of Net Offshore Bar Migration Characteristics and Environmental Conditions

Roger D. Shand†, Donald G. Bailey‡, and Mike J. Shepherd†

†Geography Dept.
Massey University
North Palmerston, New Zealand

‡Physics Dept.
Massey University
Palmerston North, New Zealand

ABSTRACT

SHAND, R.D.; BAILEY, D.G., and SHEPHERD, M.J., 1999. An Inter-Site Comparison of Net Offshore Bar Migration Characteristics and Environmental Conditions. *Journal of Coastal Research,* 15(3), 750–765. Royal Palm Beach (Florida), ISSN 0749-0208.

In this paper we quantitatively identify behavioural characteristics of net offshore bar migration (NOM) and present the results of an inter-site comparison. The net offshore migration of sandbars on multi-bar coasts has been reported at sites on the Dutch coast, the eastern USA seaboard, and the New Zealand west coast. The NOM phenomenon is repetitive, with the life-cycle of each bar consisting of three stages: bar generation near the shore-line (stage 1), systematic offshore migration of the bar across the surf zone (stage 2), and finally bar disappearance in the outer surf zone (stage 3). The NOM sites are on multi-bar coasts with relatively short period waves and a narrow range of storm strength wind and wave conditions. They encompass a wide range of geometrical dimensions, physical boundary conditions and wind and wave approach angles relative to the shoreline. Parameters measuring migration width, duration, return period and rate of NOM are used to identify bar migrational characteristics for each stage. There is wide variation in the parameter values, both between the zones representing the NOM stages at each site, and between corresponding zones at different sites. NOM duration for stage 2 is identified as the system index parameter. An inter-site correlation analysis between NOM duration and key environmental parameters shows NOM activity to increase, *i.e.* NOM duration decreases, with increasing nearshore slope and decreasing wave height. NOM duration also decreases when the predominant wind direction tends towards a maximum of 40 to 45 degrees from the coastline. It is suggested that bar size and longshore currents influence NOM and possible mechanisms are discussed.

ADDITIONAL INDEX WORDS: *Multi-bar coast, surf zone, geomorphological scale, coastal orientation, nearshore slope, bar volume, longshore current.*

INTRODUCTION

Conceptual beach-change models have generally been based upon the morphological configurations and sequences which develop in response to varying inputs of wave energy. The most comprehensive of these models are three-dimensional, that is the models incorporate longshore variation in cross-shore (two-dimensional) profiles. Such three-dimensional modelling has focused on the most landward bar and on coasts with low tidal ranges, e.g. DAVIS and FOX (1972), SONU (1973), DAVIS and FOX (1975), FOX and DAVIS (1976), OWENS (1977), CHAPPELL and ELIOT (1979), SHORT (1979), WRIGHT *et al.* (1979), SASAKI (1983), NUMMEDAL *et al.* (1984), WRIGHT and SHORT (1984), SHAW (1985), SUNAMURA (1988), and LIPPMANN and HOLMAN (1990). Some beach-change modelling has been carried out on coasts with higher tidal ranges, *e.g.* KING (1972), JAGO and HARDISTY (1984), and MASSELINK and SHORT (1993). While research into morphological models for the whole surf zone on multi-bar coasts has been less common, useful contributions have been made by authors such as HOM-MA and SONU (1962), GOLDSMITH *et al.* (1982), BOWMAN and GOLDSMITH (1983), AAGAARD (1990), SHORT (1992), and SHORT and AAGAARD (1993).

Progress in developing conceptual beach-change models for multi-bar coasts has been thwarted by difficulties in collecting comprehensive morphological and process data. The difficulties involved in surf zone data collection were described by HOLMAN and SALLENGER (1986) Data-bases for the typically extensive surf zones of multi-bar coasts usually consist of either aerial photographs or relatively small areas of bathymetric map. In each case temporal limitations have occurred either because of low sampling rates or short project time-spans. Nevertheless, researchers have identified certain morphological configurations and sequences. In the few instances where temporally extensive data have been collected new morphological phenomena have been identified; of particular interest is a repeating (cyclic) offshore migration trend underlying sand-bar behaviour, *e.g.* BIRKEMEIER (1984), DE VROEG (1988), WIJNBERG (1995).

Researchers from the Netherlands (*e.g.* RUESSINK and KROON, 1994; WIJNBERG 1995) have proposed a general three-stage conceptual model to describe the net offshore bar migration (NOM) cycle. The three stages of this 'Dutch model' are: bar generation near the shore-line; bar maturity and sys-

97153 received 27 November 1997; accepted in revision 15 October 1998

tematic seaward migration across the inner nearshore; and finally bar dissipation (flattening out) and disappearance in the outer nearshore. Authors describing data sets from Wanganui on the New Zealand west coast (*e.g.* BAILEY and SHAND, 1996) and from Duck on the USA east coast (*e.g.* LIPPMANN *et al.*, 1993) have alluded to such a model. The sites where NOM has been reported are shown in Figure 1. Two examples of bar-crest time-series demonstrating NOM behaviour are given in Figures 2A and 2B. The full set of published bar-crest time-series from the sites in Figure 1 have been reproduced in SHAND and BAILEY (1999). Research at multi-bar sites on the Oregon coast (*e.g.* CHESSER, 1993) and along the Nile Delta (*e.g.* KHAFAGY *et al.*, 1992), suggests such a phenomenon may also occur at those locations. Smaller-scale detail and possible mechanisms underlying NOM behaviour have been identified from data sets which have higher sampling rates (*e.g.* LIPPMANN *et al.*, 1993).

While the Dutch model describes shore-normal change, three-dimensional morphological configurations also appear to influence the NOM cycle. KROON (1994) and RUESSINK and KROON (1994) have discussed the influence of longshore migrating bars. WIJNBERG (1995) and SHAND and BAILEY (1999) described longshore bar alignment switching. KROON (1994), BAILEY and SHAND (1996), and BAILEY and SHAND (1999) described bifurcation and double bar developments in the mid surf zone.

In a recent NOM review SHAND and BAILEY (in press) concluded that whilst the NOM cycle operates at a temporal scale of years and at a spatial scale of 100s to 1000s of metres the system is influenced by components operating at a range of scales. Episodes of offshore bar migration are driven by storm events, *i.e.* smaller-scale. The timing and nature of seaward bar crest migrations are influenced by small to moderate-scale antecedent morphology. The overall NOM characteristics are related to the large-scale physical boundary conditions such as cross-shore slope and coastal orientation.

The NOM review (SHAND and BAILEY, 1999) also found that while similar bar behavioural characteristics appeared to occur at all NOM sites, significant inter-site variation in NOM behaviour was also evident. These findings suggest that the three-stage Dutch model applies to other multi-bar coasts which experience NOM and that an inter-site quantitative analysis may provide further conceptual information on the morphodynamics of NOM systems. The purpose of this paper is firstly to study the larger scale NOM system by undertaking a quantitative assessment of the average cyclic morphological characteristics at each site using the published NOM data, and secondly to carry out an inter-site comparison between these NOM characteristics and the corresponding physical boundary and process conditions. The paper begins with a description of the environmental conditions at each site and the methods used to obtain comparable data.

STUDY SITES

The study sites are described in terms of a range of environmental parameters. These parameters are used in the inter-site analysis and their selection was based on likely associations with NOM characteristics suggested in previous reports. Because of the variation in data available from the different sites a number of specific definitions and assumptions were made to provide comparable statistics.

Cross-shore morphological zones were defined as follows. The foreshore/nearshore boundary is the location on the average (ground survey) profile, about spring low tide elevation, where there is a distinct change in slope. Data limitations required that the landward boundary of the foreshore be located at the mean sea level/average profile intersect. The nearshore/shoreface boundary is typically defined as the cross-shore location corresponding to the seaward limit of significant surf related effects on the seabed, i.e. the 'closeout depth' (HALLERMEIER, 1978; HALLERMEIER, 1981; BIRKEMEIER, 1985). The elevation variability within the profile bundles was found to converge where the standard deviation about the mean profile was approximately 0.2 metres. An illustration of these cross- shore boundaries for Wanganui (site) 2 is shown in Figure 3. Foreshore and nearshore limits for the Wanganui Rivermouth site (Wanganui 1) are based on values from the closest available profile bundle which was for a site located 200 metres to the northwest.

The physical parameters for inter-site comparison are shown in Table 1. These parameters consist of: the average slope ($\tan\beta$) of the mean sea-bed profile between the described boundaries; the nearshore width and the depth from MSL to the mean profile at the nearshore/shoreface boundary; the time-averaged number of bar-crests across each profile; and the median grain size (D50) from locations approximating the MHWL and the mid-nearshore. Representative sediment size values for these two locations are derived by spatial averaging in order to minimise size variation associated with the bar/trough morphology at the time of sampling.

Process characteristics are described using the parameters listed in Table 2. Wave data is based on deep water records. It is assumed that all wave recorders were established at depths sufficient to exclude the effects of sea-bed interactions, *i.e.* refraction/diffraction, friction and shoaling. The average condition is described using the mean daily significant wave height and the severe condition is parametised by the 1% wave height exceedence value. The mean daily significant wave period is used. For sites in The Netherlands, wind data from the centrally located Texel light-ship was used. The use of the Texel data is considered acceptable as WESTLAKE (1995, p35) reported that "It has been established that there exists a strong correlation between wind velocities measured at Ijmuiden (on the mid-Holland coast) and Terschelling. . ." Only storm-strength winds (taken as the upper 10% of wind speeds) are considered in this study as episodes of seaward migration appear to occur under high energy conditions (BIRKEMEIER, 1984; KROON, 1994; LIPPMANN *et al.*, 1993). The wind direction parameter (for the predominant storm winds) is measured relative to the coastline.

Physical boundary parameter values are presented in Table 1, and values for the process-variables are given in Table 2. While all nine sites are characterised by multiple bars and sea-wave environments, inter-site variability occurs for all parameters. Average bar numbers range between 1.4 at North Duck and 3.2 at Zandvoort. Nearshore widths range between 313 metres at South Duck and 1250 metres at Ter-

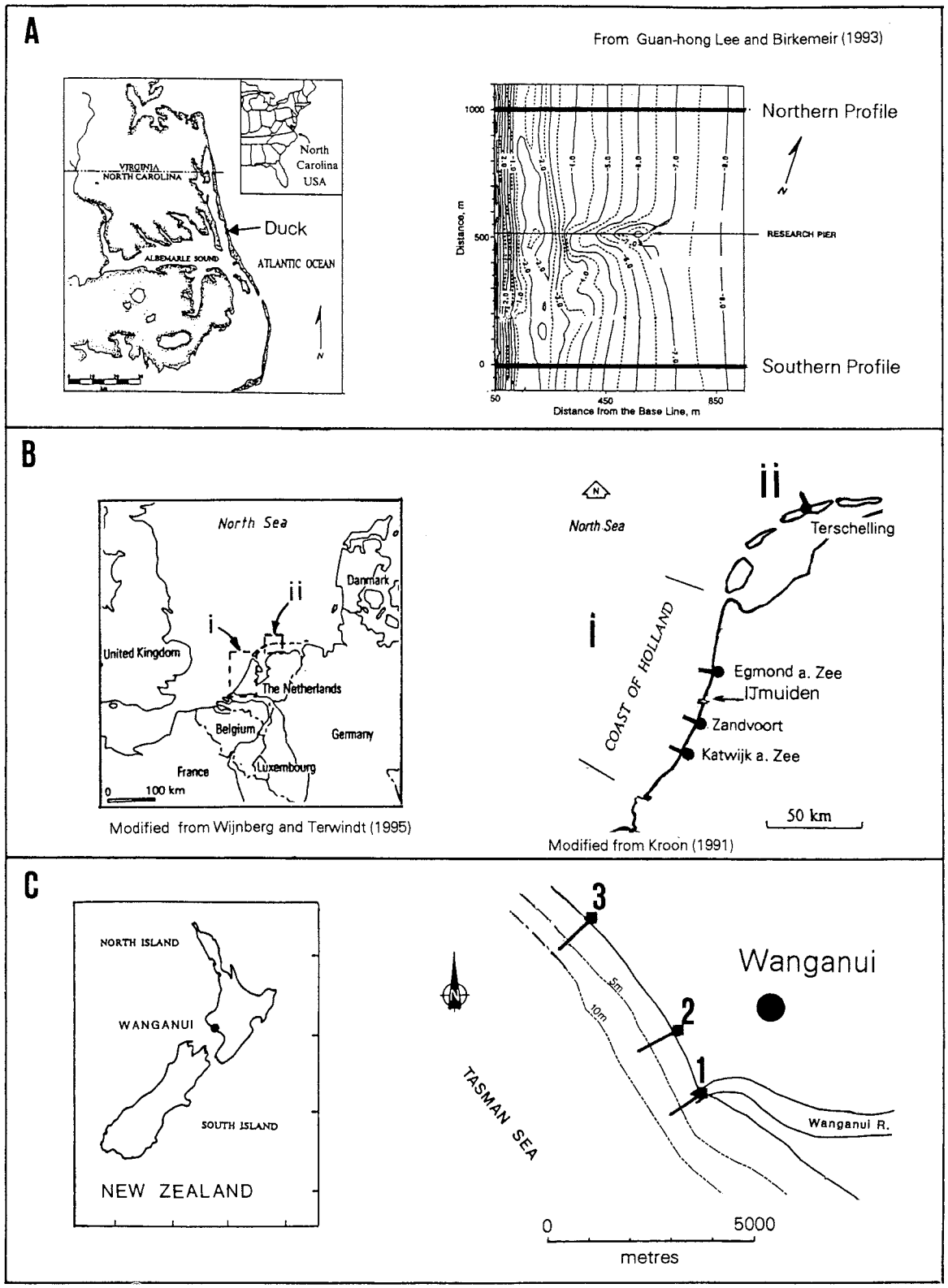

Figure 1. Location maps for the net offshore bar migration sites in North Carolina (Figure 1A), The Netherlands (Figure 1B) and New Zealand (Figure 1C). Survey transits are shown by the bold cross-shore lines.

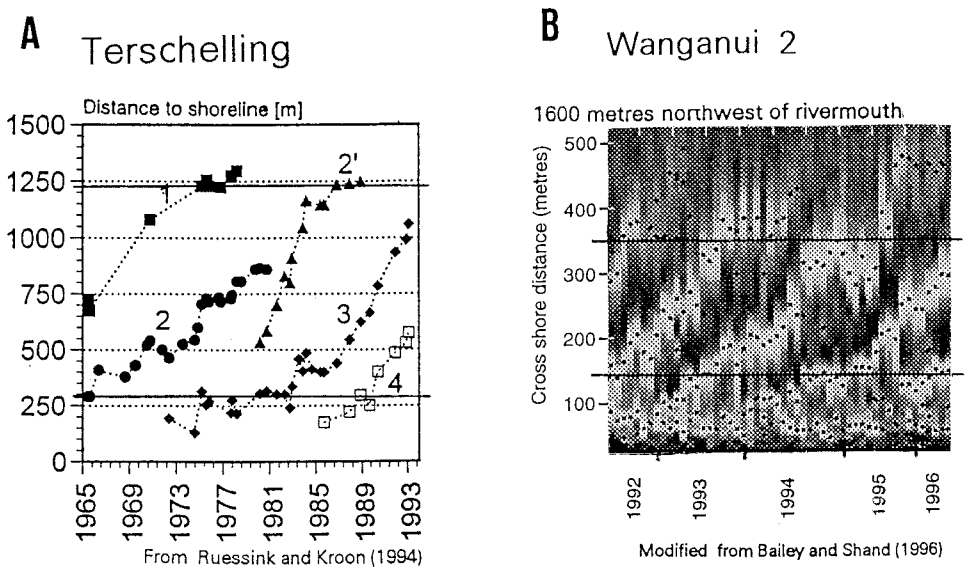

Figure 2. Examples of the net offshore migration of bar-crests for data acquired using different techniques. Figure 2A is from Terschelling in The Netherlands and uses echo-sounded data, Figure 2B is from site 2 on the Wanganui coast of New Zealand and uses rectified oblique photographic time-exposure images. The black dots in the 'time-stack' (Figure 2B) mark the location of relative intensity maxima which are used to locate the bar-crests. The underlying seaward trend in bar-crest movement is evident in both examples. The two bold horizontal lines in each figure divide the cross-shore into zones (see text) which represent the three NOM stages.

schelling, while nearshore depths at the seaward limit range from 4.7 metres (South Duck) up to 8.0 metres (Terschelling). Nearshore slopes vary between .0041 (Terschelling) and .0098 (North Duck) and the steeper foreshore slopes range from .015 (Terschelling) up to .06 (North Duck). Nearshore sediment size (median) ranges between .16 mm (Wanganui 1, Zandvoort) and .21 mm (Egmond) while the foreshore sediments range from .21 mm (Zandvoort) up to .47 mm (Duck). Wave heights (upper 1%) varied between 3.05 metres at Duck and 4.3 metres at Terschelling, while wave periods ranged from 6 seconds for The Netherland sites to 7.8 seconds at Wanganui. Wind speeds (upper 10%) ranged between 12.3 m/s (Duck) and 14.8 m/s (Wanganui). In contrast to these relatively narrow ranges of severe wave height and storm wind speed, storm wind directions were highly variable and ranged from 17 degrees (to the coastline) at Terschelling to 82 degrees at Egmond. The energy values indicate that all sites are located in, or near to, the storm dominated environments identified by DAVIES (1980).

A variety of anthropogenic, geomorphological and geological conditions occur at the different study sites which may influence NOM characteristics; however, these typically larger-scale factors have not been included within the NOM/environmental parameter analysis. Both the Dutch and North Carolina regions may still be affected by submergence associated with glacio-isostasy, hydro-isostasy and possibly geoidal deformation (PELTIER, 1987). Tectonic deformation at Wanganui has resulted in seaward tilt across the coast (PILLANS, 1990). Both Terschelling and the Wanganui sites are situated on, or near, active ebb tide deltas (BURGESS, 1971; RUESSINK, 1998). At Wanganui, Duck and on the mid Holland coast, jetties have been constructed (BURGESS, 1971; MILLER *et al.*, 1983; WIGNBERG, 1995), and beach nourishment has occurred along the Holland coast (WIGNBERG, 1995). At the regional scale coastal stability studies indicate shoreline and/or shoreface erosion exists at all sites; however, at the local scale cross-shore and longshore variations in erosion and accretion often occur (DOLAN and HAYDEN, 1983; FENSTER and DOLAN, 1994; JOHNSTON, 1985; WIJNBERG, 1995).

DATA ACQUISITION METHODS

Details of the data collection systems used in this comparative study are summarised in Table 3. Field surveys for the Dutch data began in 1964 and have continued at yearly intervals using vertical aerial photogrammetry and echo-sounding (RUESSINK and KROON, 1994; WIJNBERG, 1995). Data collection at Duck began in 1981 and has continued at approximately fortnightly intervals using ground contact instruments (GUAN-HONG LEE and BIRKEMEIER, 1993). Wanganui Rivermouth data was collected at monthly intervals between August 1982 and May 1984 using echo-sounding (SHAND, 1990). Data collection on the Wanganui coast began in 1991 at two to four weekly intervals using levelling, echo-sounding, vertical aerial and oblique terrestrial photogrammetry (PATTERSON, 1991; BAILEY and SHAND, 1993; BAILEY and SHAND, 1996; BAILEY and SHAND, 1997). The nearshore photogrammetry at Wanganui (sites 2 and 3) used the breaking wave pattern at mean low water level to signal the seabed morphology. The associated data acquisition methods

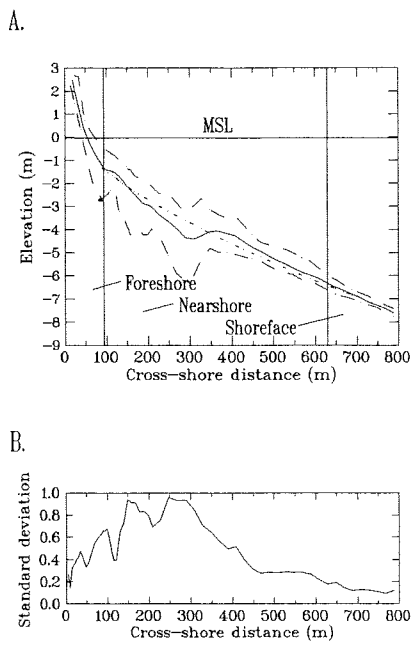

Figure 3. Ground (sea-bed) profile results for Wanganui site 2 (1600 metres from the rivermouth). The continuous curve in Figure 3A shows the mean (time-averaged) seabed elevation, the long dashed lines define the profile envelop and the short dashed line shows a power curve ($Elev = -.102Dist^{.658} + 0.612$) fitted to the mean nearshore profile. The power curve is used to detect time-averaged protuberances which represent modal bar-crest locations (see text). The foreshore and nearshore boundaries defined in the text are illustrated in Figure 3A. Cross-shore elevation variability is shown by the envelop limits in Figure 3A and alternatively by the standard deviations in Figure 3B.

have been described in LIPPMANN and HOLMAN (1989) and BAILEY and SHAND (1996).

In all NOM studies the bar-crests were detected using curve fitting techniques and the crest location was based on cross-shore distance from a benchmark situated landward of the beach-face. Bar-crest detection for the ground profile data, *i.e.* data obtained by survey instruments that sense the sea-bed such as echo-sounders, was based on the maximum positive residual from a smooth fitted curve as advocated by HOLMAN and BOWEN (1982). An example of a bar-crest time-series for echo-sounded data is shown in Figure 2A. Bar-crest detection for the intensity profile data, *i.e.* data obtained by detecting intensity variation associated with foam from broken waves, was based on locating the point on a fitted parabola with zero slope. Crest locations obtained by the two methods are similar (LIPPMANN and HOLMAN, 1989), but, as discussed below, not identical (see Figure 4). This is to be expected as intensity values are depth controlled whereas the ground profile crest locations are shape controlled. An example of a bar-crest time-series (time-stack) for intensity data is shown in Figure 2B.

To compare the NOM behaviour at the different study sites the Wanganui sea-surface intensity-based data was converted to equivalent ground (sea-bed) profile distances. This conversion, discussed in BAILEY and SHAND (1997), utilised intensity and ground survey data collected over the same time period at three cross-shore transits. Each set of data was time-averaged to minimise environmental errors and non-synchronised sampling errors. Protuberances representing modal bar positions on the averaged profiles were located using the bar-crest detection methods described earlier. Figure 3 shows an example of a power curve fitted to the Wanganui 2 mean profile. Figure 4 shows the protuberance detection curves for the intensity and ground survey data for data from the Wanganui 2 transit. The corresponding image and ground survey protuberance locations were differenced and related to depth. The best-fit correction function was:

$$C = -451D^{.133} + 500 \qquad \text{for } D > 1, D < 5$$

where: C = correction (m), and D = depth (m)) of ground profile protuberance below MSL. For protuberances located in shallow water landward corrections to intensity data are required, while for protuberances located in deeper water seaward corrections are required.

Errors associated with data suitable for time-series analysis are also summarised in Table 3. Elevation accuracy varies from ± 0.025 metres for levelling to ± 0.35 metres for echo-sounding. However, for oblique terrestrial photogram-

Table 1. *Morphological and sediment characteristics at the NOM sites.*

Site	Width (m) Nearshore	Depth (m) Nearshore Below MSL	Slope (tanβ) Nearshore	Slope (tanβ) Foreshore	Bar Number	Sediment Foreshore D50 (mm)	Sediment Nearshore D50 (mm)
Egmond	670	6.8	.0079	.020	2.2	0.32	0.21
Zandwoort	705	5.0	.0054		3.2	0.21	0.16
Katwijk	510	4.8	.0064		2.4	0.27	0.17
Terschelling	1250	8.0	.0041	.015	2.5	0.21	0.17
Duck South	313	4.7	.0096	.052	1.5	0.47	0.18
Duck North	460	6.0	.0098	.060	1.4	0.47	0.19
Wanganui 1	405	5.4	.0089	.031	2.2	0.40	0.16
Wanganui 2	536	6.3	.0092	.034	2.5	0.41	0.18
Wanganui 3	662	6.5	.0083	.029	2.7	0.23	0.20
Minimum	313	4.7	.0041	.015	1.4	0.21	0.16
Maximum	1250	8.0	.0098	.060	3.2	0.47	0.21

Sources: Burgess (1971), Larson and Kraus (1992), Short (1992), Stauble (1992), Gaun-hong Lee and Birkemeier (1993), Kroon (1994), Ruessink and Kroon (1994), Westlake (1995), plus Wanganui data collected and analysed by the authors.

Table 2. *Energy characteristics at the net offshore bar migration sites.*

Site	Wave Recorder Depth (m)	Mean Wave Height (m)	Severe Wave Height (m)	Wave Period (seconds)	Spring Time Range (m)	Storm Wind Speed (m/s)	Wind/coast Angle (degrees)
Egmond	21	1.35	4.10	6.00	1.78	13.4	82
Zandwoort	21	1.35	4.10	6.00	1.84	13.4	67
Katwijk	21	1.35	4.10	6.00	1.86	13.4	58
Terschelling	15 & 26	1.35	4.30	6.00	2.50	13.4	17
Duck South	18	1.10	3.05	6.40	1.20	12.3	40
Duck North	18	1.10	3.05	6.40	1.20	12.3	40
Wanganui 1	30	1.20	3.20	7.80	2.36	14.8	43
Wanganui 2	30	1.20	3.20	7.80	2.36	14.8	37
Wanganui 3	30	1.20	3.20	7.80	2.36	14.8	20
Minimum	18	1.10	3.05	6.00	1.20	12.3	17
Maximum	30	1.35	4.30	7.80	2.50	14.8	82

Sources: Wieringa and Rijkoort (1985), Macky et al. (1988), Ministry of Transport (1989), Patterson (1991), Larson and Kraus (1992), Patterson (1992), Short (1992), Gaun-hong Lee and Birkemeier (1993), Hoekstra et al. (1994), Kroon (1994), Ruessink and Kroon (1994), Westlake (1995), Wijnberg (1995), also: Birkemeier (1997 pers. com.) for tidal information from Duck; Wanganui raw wind data were obtained from the National Institute of Water and Atmospheric Research (NZ).

metry the intensity variation only represents relative depth change. Cross-shore accuracy varies from c. ±1 metre for foreshore levelling to c. ±10 metres for nearshore echo-sounding and nearshore photogrammetry (as used at Wanganui 2 and 3, see Figure 1). In the photogrammetric situation the error increases with increased distance cross-shore; from ± 8.4m at 200m offshore to ± 12.9m at 500m offshore. It should also be noted that with aerial and terrestrial nearshore photogrammetry, accuracy relates to the position of sea-surface intensity maxima rather than to the location of morphological features on the seabed. If adjustments are made for environmentally associated errors when reducing echo- sounded data or when rectifying photographs then the errors decrease by approximately 40% and 55% respectively. As noted earlier, differences also occur between image-based data and ground survey data and these must be reconciled if a comparative analysis is made.

METHODS OF ANALYSIS

In order to quantitatively define inter-site bar migrational characteristics associated with each NOM stage, it was necessary to develop a method capable of dividing the foreshore/nearshore into three zones representing the three NOM stages. While a preferred method would have been to determine the actual stage boundaries by studying behavioural characteristics of each bar sequence as depicted on ground profiles, this was not possible as complete ground profile data were not available for all sites. A method was therefore required that could utilise both the bar-crest time-series and the time-averaged profile data which were available for all sites.

The method adopted here is based upon the indication in precious reports on NOM that preferential locations of bar residence may be associated with bar generation and bar degeneration (see KROON, 1994; RUESSINK and KROON, 1994; and WIJNBERG, 1995). Such a location of preferential residence would be expected to leave a stationarity signature in the form of an upwardly directed protuberance on the time-averaged profile. The protuberances would then identify 'equivalent' locations at each site which may separate out the three cross-shore NOM stages. To test this hypothesis the bar-crest locations for Wanganui 2, the Wanganui site with the longest record, were analysed.

Locations associated with bar generation, degeneration and the positions of maximum upward protuberance on the time-averaged profile for Wanganui 2 are shown in Figure 5. It is

Table 3. *Details of data collection systems at the different sites.*

Site	Record Years	Field Methods		Sampling Rate (/y)	Elevation Accuracy (m)	Cross-shore Accuracy (m)
Egmond	1964–90	nearshore:	echo-sounder	1	±0.25	±10
Zandvoort	1964–90	foreshore:	aerial photo	1	±0.10	±2.0
Katwijk	1964–90		theodolite	1	±0.01	±1.0
Terschelling	1965–93	nearshore:	echosounder	1	±0.20	±10
Duck north	1981–92	nearshore:	theodolite	24	±0.03	±1.5
Duck south	1981–92	foreshore:	theodolite	24	±0.03	±1.5
Wanganui 1	1981–84	nearshore:	echosounder	12	±0.25	±10
Wanganui 2/3	1991–96	nearshore:	aerial/terrestrial photography	12	relative	±11
	1991–93	nearshore:	echosounder	4	±0.30	±10
	1990–94	foreshore:	theodolite	4	±0.025	±2.5

Sources: Horikawa (1988), Shand (1990), Gaun-hong Lee and Birkemeier (1993), Shand (1995), Wijnberg (1995), Bailey and Shand (1996).

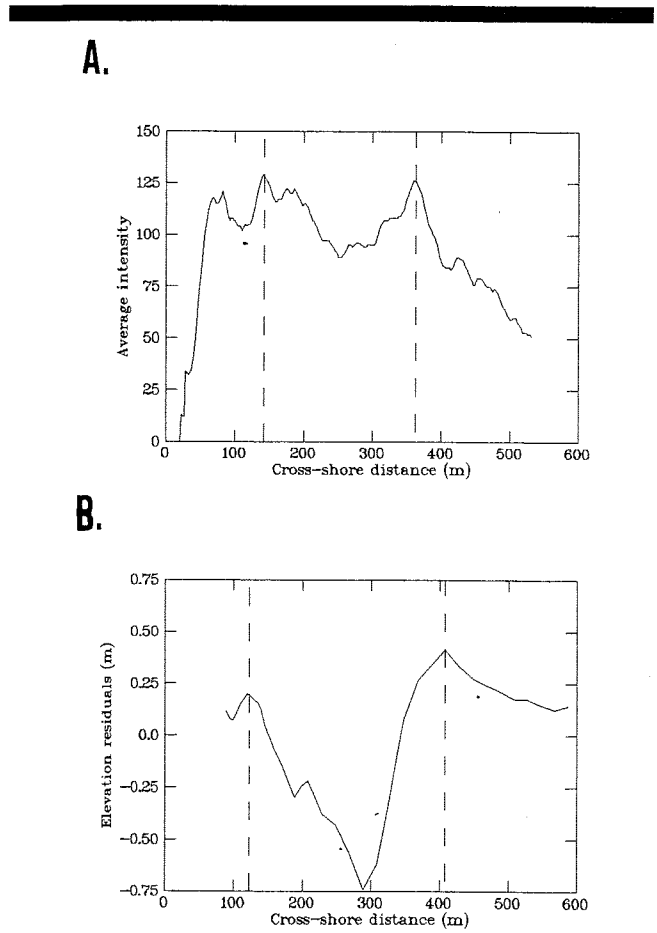

Figure 4. The difference between protuberance locations from time-averaged intensity data and time-averaged ground survey data sampled over the same period at Wanganui site 2 (the ground survey data are plotted in Figures 3A). Figure 4A shows the time-averaged intensity profile for monthly data sampled between 8.91 and 11.93. Figure 4B shows the residuals from the power curve fitted to time-averaged ground survey profiles. Vertical lines locate the corresponding maxima. The intensity maxima based on wave breaking displaces the protuberances, i.e. the modal bar-crest locations, seaward in the inner nearshore and landward further offshore.

evident on Figure 5A that the vertical lines representing protuberance maxima do, for this site at least, separate the cross-shore into three zones which isolate the generating and degenerating bars from those undergoing systematic offshore migration. Note that the location of the protuberance maxima used to construct Figure 5A are slightly different to those indicated by the maxima on Figure 4; 119m c.f. 122m and 395m c.f. 408m. Figure 5B illustrates bar degeneration sequences in terms of elevation difference between the trough and adjacent seaward crest. In these examples it is evident that following the onset of bar degeneration a bar resides within a relatively narrow band of cross-shore distance (between c. 380 to 410 metres). The bar location histogram in Figure 5B illustrates how a frequency maximum accompanies, and thus signals, the onset of bar degeneration. Unfortunately, data were not available to determine how the inner maximum on time-averaged profiles relates to bar generation sequences.

The parameters used to define net offshore migrational behaviour in this paper are illustrated in Figure 6. A variety of parameters and terminology has been used by various authors to define and describe the NOM (DE VROEG, 1988; KROON and HOEKSTRA, 1993; KROON, 1994; RUESSINK and KROON, 1994; WIJNBERG, 1995). Three parameters are required to define a site's characteristic NOM cycle: the average cross-shore distance over which the bars migrate; the average duration of the bar migrations; and the average return period, that is the average time between migration cycles. These parameters will be used in the following inter-site comparative analysis. The average rate of offshore migration is also used. While rate is not an independent measure of NOM, the normalisation of migration distance with respect to time is useful when comparing sites and it has been widely used the other writers when describing sand-bar dynamics.

To determine the NOM parameter values for all three zones the identification of a landward boundary for zone 1, and a seaward boundary for zone 3 was required. Unfortunately the data needed to identify individual bar generation locations was only available for Wanganui site 2. In this case the foreshore/nearshore boundary was found to be landward of all bar generation locations and subsequent locations (see Figure 5A). This boundary was therefore used as the landward limit for zone 1 in the inter-site analysis. At each site, the seaward limit for zone 3 was taken as the average of the seaward excursion maxima for the bars. Figure 5B shows that while most of the bar degeneration at Wanganui occurred within a relatively narrow band of cross-shore distance, substantial seaward migration of the subdued bar could still occur prior to complete disappearance of the bar. This contrasts with some NOM sites such as at Duck where a landward trend appears to occur in bar migration during degeneration. Because of this directional variability during the degeneration stage, the average rate of NOM in zone 3 was determined by the slope of a linear regression line fitted to all bar location points following the onset of degeneration, *i.e.* once the bar had crossed the zone 2/3 boundary.

RESULTS

This section will describe the NOM parameters' values, identify an index parameter to represent the morphological system, and determine the associations between environmental variables and the index parameter for each site.

A wide variation in NOM parameter values are evident between the different field sites (see Figure 7). The Netherland sites tend to have NOMs with greater average migration widths, longer average durations, and lower average migration rates than the Wanganui and Duck sites. Terschelling is notable for its extensive width of zone 2, and narrowness of zone 3. Terschelling and Egmond have particularly long durations and return periods. Egmond has a very low NOM rate. The return periods for the Wanganui sites are notably lower than at the other sites.

The NOM parameter results in Figure 7 also show that a similar pattern of inter-zonal behaviour occurs at each site.

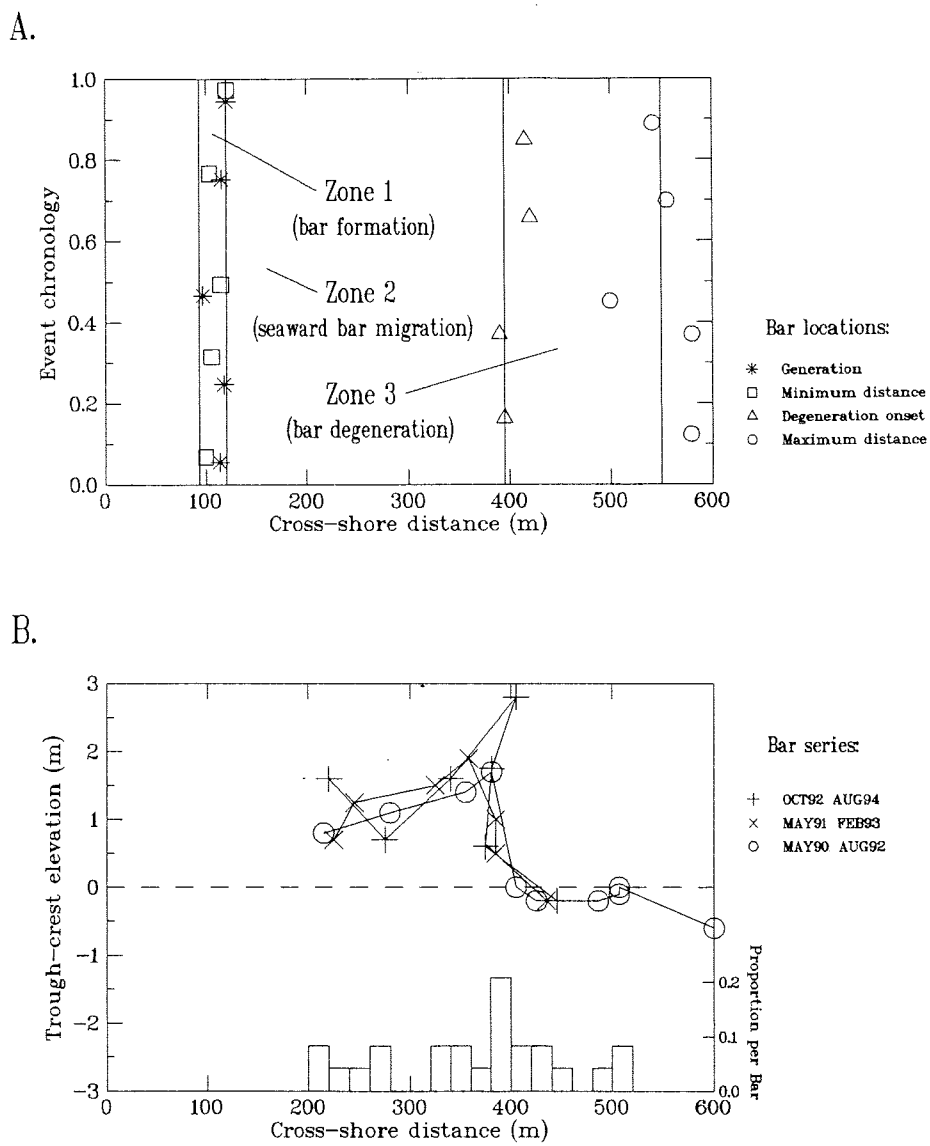

Figure 5. Figure 5A shows bar-crest generation and degeneration locations relative to the NOM zonal boundaries (see text) at Wanganui site 2. Bar-crest data in Figure 5A was taken from a data set sampled at monthly intervals between June 1990 to May 1996. While data was mainly collected using imaging techniques, all image-based data has been converted to equivalent ground profile distances (see text). The vertical lines marking the zone boundaries appear to separate bar-crest locations on the basis of NOM stage characteristics. Figure 5B shows bar-crest degeneration sequences and the corresponding frequency distribution for Wanganui site 2. The bar-crest time-series in Figure 5B were sampled at three monthly intervals between January 1990 and August 1994 using ground profiling techniques. Shape flattening of the bar (i.e. progressive degeneration) is defined by the elevation difference between the crest residual from a fitted power curve and the adjacent (landward) trough residual. Most degeneration occurs within a relatively narrow cross-shore zone and this results in the frequency maximum between 380 to 400m. Note that the degeneration time-series can still have seaward migration trends.

Inter-zonal return periods are approximately constant at each site. However, significant inter-zonal variation occurs for duration, width and rate; higher values occur in zone 2 than in zones 1 and 3. While parameter values in zones 1 and 3 are similar, zone 3 values show greater variation than those in zone 1. Such zonal separation is further illustrated by the bivariate confidence ellipses in Figure 8.

Correlation analysis identified duration as the parameter most strongly associated with the other NOM parameters (see Figure 9). Duration was therefore selected as the index parameter to represent NOM behaviour in the analysis with environmental parameters. Only the zone 2 data were used for the inter-site analysis because zone 2 is the most spatially and temporally extensive zone and systematic offshore migration is the dominant type of bar behaviour.

A linear correlation analysis between (zone 2) duration and the physical boundary variables identified associations with a level of significance of 10% *i.e.* $p < .1$) in all cases except

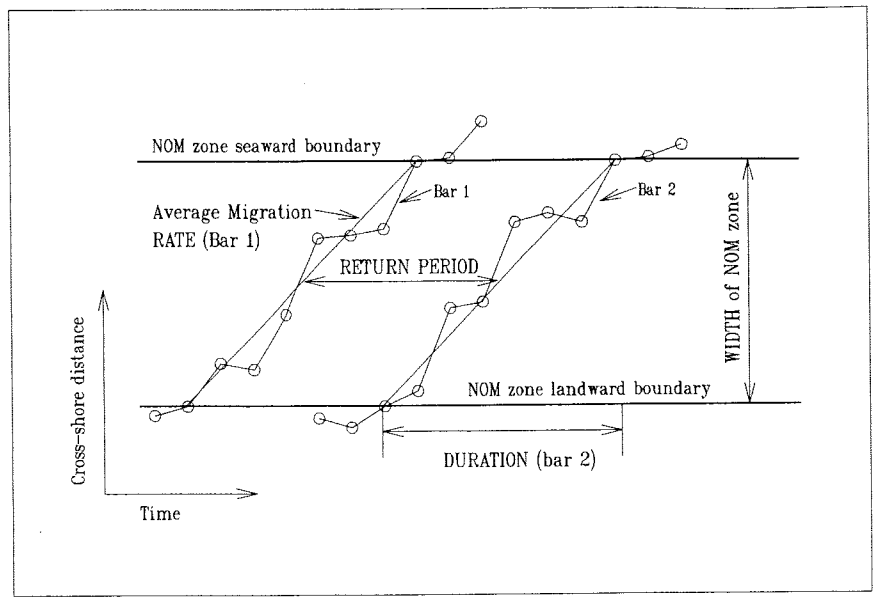

Figure 6. Diagrammatic representation of the parameters used to define net offshore bar migration.

bar number and nearshore sediment size (see Table 4A). Curvilinear regression models incorporating power functions appear to better fit the sediment/duration and slope/duration data (see Figure 10). Such nonlinear relationships may be appropriate given the typically nonlinear relationships between sediment size and cross-shore slope (see KOMAR, 1976a; HARDISTY, 1990; STAUBLE, 1993; HOEKSTRA *et al.*, 1994). Of particular interest is the apparent outlier status of Egmond which will be discussed later. The nearshore sediment size only began to show a visually identifiable association with duration when both the Egmond data and the Wanganui Rivermouth (W1) data were excluded (Figure 10C). Data from the latter site may have been contaminated by finer flood-borne river sediment prior to sampling.

The duration/process variable results should be interpreted with caution. Nonequivalency errors in the wave data, short record lengths, difficulties reconciling various statistics used in the different publications, and the relatively small inter-site ranges for many parameters may have resulted in errors that could affect the correlation strength.

The only process variables to show significant associations ($p < .1$) with duration are the mean and severe wave heights. However, the correlation coefficients in Table 4B are based on 9 independent samples while the wave data comes from only four recorders (see Table 2). To account for this lack of independence in the wave height data the NOM durations were averaged to provide only one value per wave height sample and the correlation analysis was then repeated. While the resulting associations with duration were weaker the severe wave height relationship remained significant.

No linear association is evident between duration and the wind parameters in Table 4B, however, a strong nonlinear relationship appears to exist with wind direction as is shown in Figure 11A. The wind direction variable was based on the angle between the shore-line and predominant (storm) wind approach and therefore incorporates the boundary condition of coastal orientation. Figure 11A shows that duration decreases from a high value at high angle (*i.e.* predominating wind tending shore-normal) to reach a minimum at approximately 45 degrees. Duration values increase again as the angle decreases toward zero (*i.e.* predominant wind tending shore-parallel). Repetition of the regression using a quadratic function improved the correlation coefficient from $r = .133$ (Table 4B) to $r = .846$. Residuals from the fitted parabolic curve shown in Figure 11A suggest that the actual relationship is asymmetrical with lower durations being maintained from c. 45 degrees toward c. 20 degrees before rapidly increasing.

DISCUSSION

The similar inter-zonal pattern in NOM parameter values evident at each site indicates that each NOM stage is subjected to different morphodynamics as would be expected by the Dutch model.

The wide inter-site variability in NOM parameter values, however, indicates that the actual morphodynamics are site specific. The high variability in bar behaviour for the degeneration zone is of particular significance in this regard. As the seaward zone is the first to interact with incoming wave energy its morphology is likely to be particularly responsive to the different environmental conditions characterising each study site. Recently RUESSINK (1998) has also speculated on the possibility of site specific NOM morphodynamics. Ruessink developed a conceptual model of NOM at Terschelling based on net suspended sediment transport paths; however, its applicability to other coastal sites with different process conditions and NOM characteristics appeared to be doubtful.

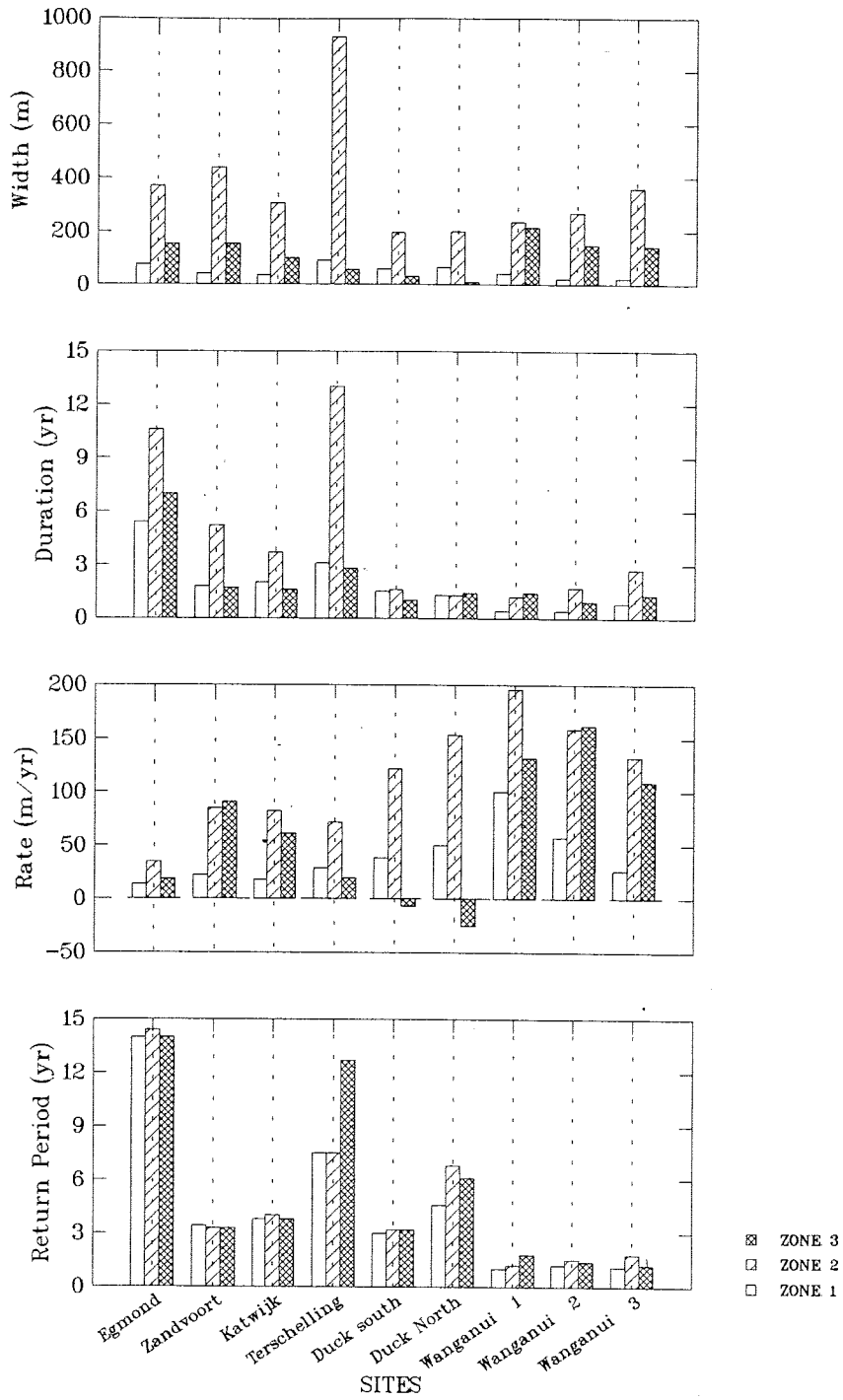

Figure 7. Graphs showing bar migration parameter values for the three zones at each site. With the exception of return period there is significant variation between the inter-zonal values at each site. Inter-site variation is also significant with The Netherlands sites tending to differ from the duck and Wanganui sites.

The different migrational trends that occur in zone 3, *i.e.* the degeneration zone, at the various sites (Figure 7) are consistent with the degeneration behaviours described by other researchers and summarised by SHAND and BAILEY (1999). This consistency further supports the zonation method of NOM stage separation developed for use in this study.

The Holland data subset (Egmond, Zandvoort and Katwijk) suggests oppositely directed NOM/slope relationships to

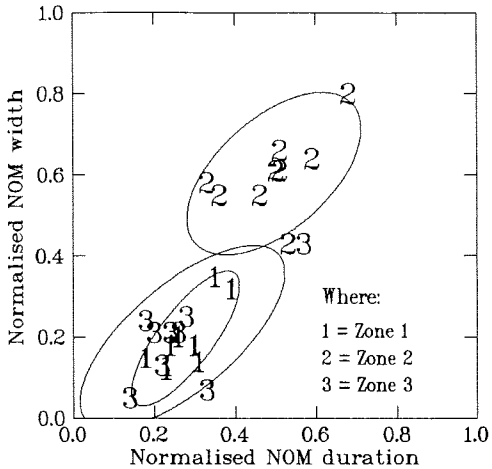

Figure 8. NOM width and NOM duration at each site plotted with gaussian bivariate confidence ellipses (99%). The values have been normalised by the total width and duration. The ellipses show that different NOM bar behaviour occurs in each zone. Zone 2 has higher magnitudes while zone 3 values have greater variability than zone 1 values.

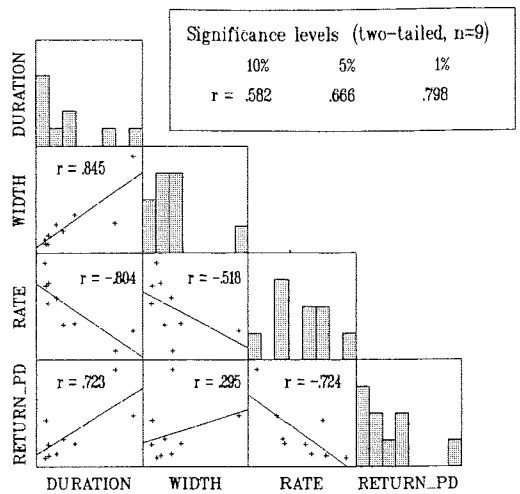

Figure 9. Correlation plots for NOM parameters showing fitted linear regression models, Pearson correlation coefficients and critical values for different levels of significance (two tailed for n = 9) are also shown.

those for the full data set (see Figure 10). KROON (1994) suggested possible NOM control mechanisms based on the negative NOM rate/slope relationship. However, the outlying status of the duration/slope data-point for Egmond appears to be the cause of this anomaly. WIJNBERG (1995) had noted that Egmond did not demonstrate the typical gradient/surf zone width/bar-number relationships observed on other coasts (KOMAR, 1976a) and which are also evident within the correlation matrix of Table 4A. In a study of large scale coastal behaviour along the Holland coast, WIJNBERG (1995) identified five differently behaving regions with Egmond and Zandvoort/Katwijk belonging to adjacent 'coastal cells'. While that investigation was unable to determine the controlling factors it was evident that the 2.5 kilometre long harbour moles at Ijmuiden (see Figure 1B) partitioned the cells and enhanced the differences in the adjacent bar systems.

Table 4. *Pearson correlation matrixes for NOM duration (zone 2) with morphological and sediment variables (Table 4A), and process variables (Table 4B).*

A.

	Duration (zone 2)	Sediment Foreshore	Sediment Nearshore	Slope Foreshore	Slope Nearshore	Depth Nearshore	Width Nearshore	Bar Number
Duration (zone 2)	1.000							
Sediment foreshore	−0.599	1.000						
Sediment nearshore	0.149	0.127	1.000					
Slope foreshore	0.653	0.680	0.000	1.000				
Slope nearshore	−0.739	0.862	0.397	0.620	1.000			
Depth nearshore	0.693	−0.325	0.385	−0.472	−0.322	1.000		
Width nearshore	0.854	−0.728	−0.049	−0.593	−0.823	0.789	1.000	
Bar number	0.302	−0.837	−0.295	−0.541	−0.658	0.134	0.487	1.000

B.

	Duration (zone 2)	Mean Wave Height	Severe Wave Height	Wave Period	Storm Wind Speed	Storm Wind Approach	Spring Tide Range
Duration (zone 2)	1.000						
Mean wave height	0.740	1.000					
Severe wave height	0.825	0.960	1.000				
Wave period	−0.576	−0.487	−0.691	1.000			
Storm wind speed	−0.129	0.154	−0.105	0.788	1.000		
Storm wind approach	0.133	0.423	0.395	−0.463	−0.226	1.000	
Spring tide range	0.287	0.424	0.248	0.496	0.860	−0.383	1.000

Critical values (two tailed) for 9 observations:	p = .1	.05	.01
	r = .582	.666	.798

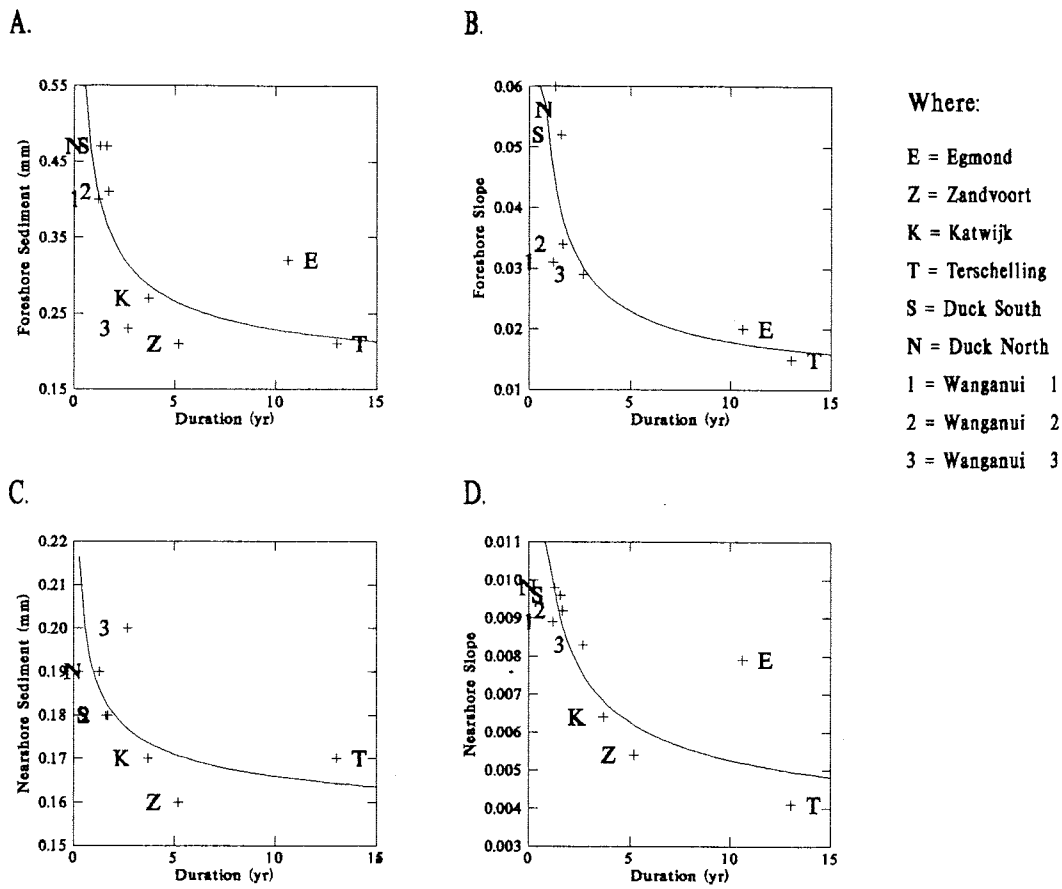

Figure 10. Plots showing nonlinear associations for NOM duration with sediment and slope. Power curves are fitted to the full data set in Figures 10A, B and D but Egmond and Wanganui site 1 are excluded in Figure 10C. These curves indicate that an underlying negative nonlinear association exists. The outling nature of the Egmond data is illustrated.

The results suggest that cross-shore slope has a strong influence upon bar migrational behaviour during NOM stage 2. Nearshore slope probably has greater causal association with NOM than foreshore slope given its closer proximity to NOM activity.

A possible explanation for the nearshore slope/NOM duration association is suggested by the cross-shore width, depth, and wave height relationships. By definition, cross-shore slope equals the depth to width ratio, *i.e.* tanβ. The correlation coefficients in Table 4A suggest that at the NOM sites the nearshore widths have greater influence over nearshore slope than does the depth at the seaward nearshore boundary; so lower slopes should correspond to wider and somewhat deeper nearshores. In a study of multi-barred coasts in the Great Lakes and Gulf of St Lawrence, DAVIDSON-ARNOTT (1988) found cross-shore width and outer bar depth were positively correlated with wave height (using fetch as an analogue). A similar result occurs for the global NOM sites in this study; the nearshore width/severe wave height correlation coefficient = .692. Davidson-Arnott explained this association by the increasing breaking depth achieved by the highest waves. Davidson-Arnott also found wave height to be related to bar height, although no causal mechanism was identified. From studies involving the analysis of bar size on multi-bar coasts (see LARSEN and KRAUS, 1992; and RUESSINK and KROON, 1994) it is evident that bar height is proportional to bar volume. As higher waves are also associated with longer NOM duration it can be hypothesised that differences in NOM activity may result from the different time taken for bars of different size to translate offshore under storm conditions. This is because larger bars take longer than smaller bars to migrate across the surf zone owing to the higher volumes of sediment to be transported. The relationship between seaward bar movement and storm events is well documented and supported by sediment transport theory (OSBORNE and GREENWOOD, 1992; ROELVINK and STIVE, 1989). This mechanism invôlves the suspension of sediment by broken waves and subsequent transport under seaward directed mean flows (*e.g.* GREENWOOD *et al.*, 1991; LARSEN and KRAUS, 1989).

To test this hypothesis that bar volume controls NOM duration, the sizes of bars at the study sites were compared with the corresponding NOM duration parameters. Bar volumes were based on the area enclosed by the positive residuals

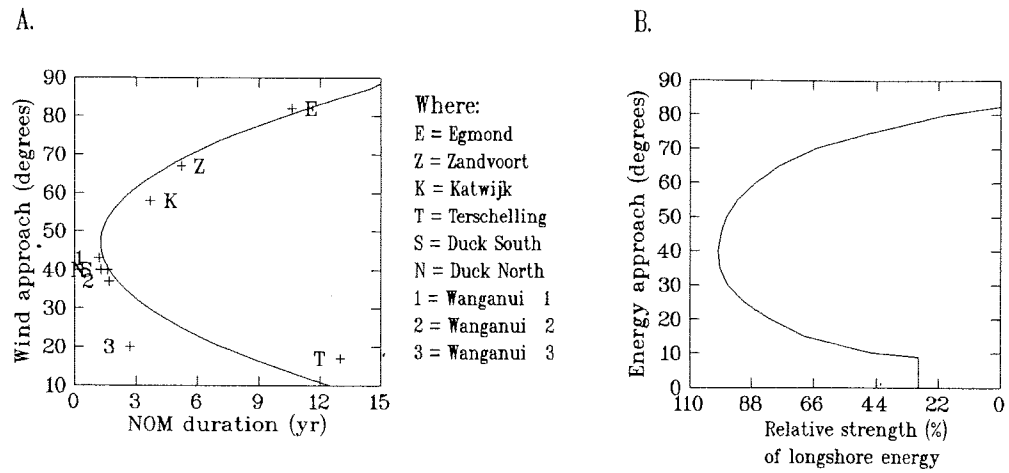

Figure 11. Nonlinear relationships between the angle of wind approach relative to the shoreline with NOM duration (Figure 11A), and the angle of wind/wave approach with the relative strength of the longshore energy component (Figure 11B). Low angle asymmetry in the duration/wind approach data (Figure 11A) is demonstrated by the deviations from the fitted parabola. The combined influence of both wind and wave energy have been incorporated in Figure 11B by adapting the method used by Whitford and Thornton (1993) to the average environmental conditions at the NOM sites. The 'relative strength of the longshore energy' in Figure 11B refers to the ratio of each angle's longshore energy value to the maximum value. The similarity between Figures 11A and 11B suggests that longshore currents may be significant in NOM morphodynamics.

(used to locate the bar crest) and the average profile curve, per metre longshore. Where possible, the volumes were derived for bars just prior to the onset of degeneration. This condition was imposed as bar size tends to increase across the nearshore until degeneration begins (LARSEN and KRAUS, 1992; KROON, 1994; RUESSINK and KROON, 1994). However, neither equivalent nor complete bar volume data was acquired for all study sites so the results shown in Table 5 are only approximate. Nevertheless, they do support the proposition that the sites with highest durations have larger bars and those with the lowest durations have the smallest bars.

Nearshore slope may also have some influence NOM activity by gravitationally induced downslope transport. However, while such effects have been included as part of the bed-load and suspended load contributions in energetics-based cross-shore sediment transport models (BOWEN, 1980; BAILARD, 1981), subsequent studies (STIVE, 1986; THORNTON *et al.*, 1996; and GALLAGHER *et al.*, 1998) suggest that the gravity driven transport is of relatively minor importance. The influence of coastal orientation on NOM may be via longshore currents. Strong local winds with an oblique orientation to the shoreline generate longshore currents via the longshore component of surface wind stress (*e.g.* NUMMEDAL and FINLEY, 1978; HUBERTZ, 1986; WHITFORD and THORNTON, 1993) in combination with changes in the radiation stress from obliquely approaching broken waves (*e.g.* LONGUET-HIGGENS, 1972; KOMAR, 1976b; SHERMAN, 1988). A distinct similarity is evident between the theoretical curve for longshore current/energy approach angle (Figure 11B) and for the NOM duration/wind approach angle relationship identified in this study (Figure 11A). Influence of longshore currents on NOM activity may involve a number of mechanisms such as edge waves, flow continuity, or morphological configuration.

HOWD *et al.* (1991) and HOWD *et al.* (1992) have shown theoretically that progressive edge waves moving in the same direction as a strong longshore current assist seaward bar migration. Progressive edge waves commonly occur in the presence of strong longshore currents and high incident wave energy (OLTMAN-SHAY *et al.*, 1989; HOWD *et al.*, 1991; and HOWD *et al.*, 1992).

Seaward bar migration may result when troughs and topographic constrictions are subjected to increases in longshore flow. Field and modelling evidence from the Terschelling nourishment programme gives some support to this mechanism. HOEKSTRA *et al.* (1996) found that troughs re-established across the nourishment zone in response to increased longshore flow. However, additional evidence of greater flow concentration on the seaward side of the trough would be required to account for offshore bar migration. Bar switching and the associated seaward migration (see SHAND and BAILEY, 1999) may be forced when constricted channels are affected by high longshore flows. Bar switching has been observed to occur at Wanganui during conditions of higher wind/wave energy with oblique approach.

Strong persistent longshore currents are associated with

Table 5. *Average NOM durations and bar volumes for the study sites.*

Site	NOM Duration (y) For Zone 2	Average Bar Volume (m^3)
Duck	1.2–1.3	60–100
Wanganui sites 2 and 3	1.5–2.5	70–120
Zandvoort and Katwijk	3.7–5.2	125–180
Egmond	10.6	180–250
Terschelling	13.0	450–700

Sources: Kroon (1994), Larsen and Kraus (1993), Ruessink and Kroon (1994), Wijnberg (1995), Wanganui ground profile data.

shore-parallel topography (SHORT, 1975; FOX and DAVIS, 1976) and this type of morphology may promote seaward bar migration. Such two-dimensional (2D) morphological configurations would be expected to increase the longshore uniformity of return flows, while the cellular hydrodynamics associated with 3D morphology (SONU, 1972; KOMAR, 1976a) would produce an irregular pattern of seaward flow. Two-dimensional morphology may therefore be capable of forcing more laterally continuous offshore bar migration.

CONCLUSION

The coastal environments of the NOM study sites are characterised by multiple bars, a wide range of physical boundary characteristics, short period waves, a narrow range of storm strength wind and wave conditions, and widely varying approach directions of the predominant wind relative to the shoreline. The environmental similarities may be conducive to NOM.

Both inter-site similarities and differences were observed in NOM parameter values. The consistent inter-site pattern of parameter values within each NOM zone suggest that each zone is characterised by distinctive bar migrational behaviour as would be expected by the three stage NOM model. However, the wide inter-site variability which occurs in NOM parameter values suggests that the actual morphodynamics are sensitive to differences in the environmental conditions occurring at each site.

NOM duration was identified as the parameter most discriminative of NOM morphological behaviour and was used as the system index parameter for inter-site comparison. The analysis found both lower cross-shore slopes and higher wave energy were associated with longer NOM durations. As bar volumes are greater at sites characterised by these type of conditions it appears that the different levels of NOM activity may result from the different lengths of time required for bars of different sizes to migrate seaward across the nearshore. NOM duration was found to be nonlinearly correlated with the angle that the predominant storm-strength wind approached the shoreline. This indicated that longshore current strength influenced NOM behaviour and possible mechanisms were suggested which incorporate edge-waves, flow continuity, and morphological configuration.

ACKNOWLEDGMENTS

This study was supported by the Massey University Graduate Research Fund, the Massey University Research Fund, and a Vice Chancellors Special Grant. The authors wish to thank Drs Gerben Ruessink, Bob Kirk and Phil Osborne for their useful comments on the manuscript. We also thank Gerben Ruessink for permission to reproduce illustrations, and Bill Birkemeier for providing wind and tidal data from the CERC Field Research Center at Duck. Special thanks also go to staff at the Wanganui Port Company, the Wanganui District Council, the Wanganui Surf Life-saving Club and members of the principal author's family, for assistance with field surveys which at times had to be carried out under the most demanding conditions.

LITERATURE CITED

AAGAARD, T., 1990. Infragravity waves and nearshore bars in protected, storm-dominated coastal environments. *Marine Geology,* 94, 181–203.

BAILARD, J.A., 1981. An energetics total load sediment transport model for a plane sloping beach. *Journal of Geophysical Research,* 86, 10938–10954.

BAILEY, D.G. and SHAND, R.D., 1993. Determining large-scale sand bar evolution. *Proceedings of the First New Zealand Conference on Image and Vision Computing,* pp. 109–116.

BAILEY, D.G. and SHAND, R.D., 1996. Determining large-scale sand bar behaviour. *Proceedings of the IEEE International Conference on Image Processing,* (Lausanne, Switzerland), 2, pp. 637–640.

BAILEY, D.G. and SHAND, R.D., 1997. Data fusion issues in analysing coastal morphodynamic systems. *Proceedings of the combined conferences on Digital Image Computing Techniques and Applications, and Image and Vision Computing New Zealand.* pp. 107–112.

BIRKEMEIER, W.A., 1984. Time scales of nearshore profile change. *Proceedings of the 19th International Conference on Coastal Engineering,* (ASCE), pp. 1507–1521.

BIRKEMEIER, W.A., 1985. Field data on the seaward limit of profile change. *Journal of Waterway, Port, and Coastal Engineering,* 111(3), 598–602.

BOWEN, A.J., 1980. Simple models of nearshore sedimentation; beach profiles and longshore bars. In: S.B. McCann (ed.), *The Coastline of Canada,* Geological Survey Canada Paper 80-10, pp. 1–11.

BOWEN, D. and GOLDSMITH, V., 1983. Bar Morphology of dissipative beaches: an emperical model. *Marine Geology,* 51, 15–33.

BURGESS, J.S., 1971. Coastline Change at Wanganui, New Zealand, Unpublished. PhD. Thesis, University of Canterbury, New Zealand. 99 p.

CHAPPELL, J. and ELIOT, I.G., 1979. Surf-beach dynamics in time and space - an Austrailian case study, and elements of a predictive model. *Marine Geology,* 32, 231–250.

CHESSER, S.A., 1993. Seasonal erosion/accretion cycles in a littoral cell. In: List, J.H., (ed.), *Large-Scale Coastal Behaviour '93.* US Geological Survey Open-File Report, 93-381:33–36.

DAVIDSON-ARNOTT, R.G.D., 1988. Controls on bar formation and forms of barred nearshore profiles. *The Geographical Review,* 78, 185–193.

DAVIES, J.L., 1980. Geographical variation in coastal development. In: Clayton, K.M., (ed.), *Geomorphology Texts 4.* London, Longman, 212 p.

DAVIS, R.A. and FOX, W.T., 1972. Coastal processes and nearshore sand bars. *Journal of Sedimentary Petrology,* 42(2), 401–412.

DAVIS, R.A. and FOX, W.T., 1975. Process-response patterns in beach and nearshore sedimentation: 1. Mustang Island, Texas. *Journal of Sedimentary Petrology,* 45(4), 852–865.

DOLAN, R. and HADEN, B., 1983. Patterns and prediction of shoreline change. In: Komar, P., (ed.), *Handbook of Coastal Processes and Erosion.* CRC Press, pp. 123–149.

FENSTER, M. and DOLAN, R., 1994. Large-scale reversals in shoreline trends along the U.S mid-Atlantic coast. *Geology,* 22, 543–546.

FOX, W.T. and DAVIS, R.A., 1976. Weather Patterns and Coastal Processes. In: Davis, R.A. and Ethington, R.C., (eds.), *Society of Economic Paleontologists and Minerologists,* Special Publication 24, pp. 1–23.

GALLAGHER, E.L.; ELGAR, S. and GUZA, R.T., 1998. Observations of sand bar evolution on a natural beach. *Journal of Geophysical Research,* 103, 3203–3215.

GOLDSMITH, V.; BOWMAN, D. and KILEY, K., 1982. Sequential stage development of cresentic bars: Hahoterim beach, Southeastern Mediterranean. *Journal of Sedimentary Petrology,* 52, 233–249.

GREENWOOD, B.; OSBORNE, P.D. and BOWEN, A.J., 1991. Measurement of suspended sediment transport: prototype shorefaces. *Proceedings of Coastal Sediments '91,* (ASCE), pp. 284–299.

GUAN-HONG, L. and BIRKEMEIER, W.A., 1993. *Beach and Nearshore Data: 1985-1991 CERC Field Research Facility.* Technical Report CERC-93-3, 13 p.

HALLERMEIER, R.J., 1978. Uses for a calculated limit depth to beach erosion. *Proceedings of the 16th Conference on Coastal Engineering,* (ASCE), pp. 1493–1512.

HALLERMEIER, R.J., 1981. A profile zonation for seasonal sand beaches from wave climate. *Coastal Engineering,* 4, 253–277.

HARDISTY, J., 1990. *Beaches: Form and Process.* London, Unwin Hyman, 319 p.

HOLMAN, R.A. and BOWEN, A.J., 1982. Bars, bumps, and holes: models for the generation of complex beach topography. *Journal of Geophysical Research,* 84, 457–468.

HOM-MA, M. and SONU, C., 1962. Rythmic patterns of longshore bars related to sediment characteristics. *Proceedings of the 8th International Conference on Coastal Engineering,* (ASCE), pp. 248–278.

HOEKSTRA, P.; HOUWMAN, K.T.; KROON, A.; VAN VESSEM, P. and RUESSINK, B.G., 1994. The Nourtec experiment of Terschelling: Process-orietated monitoring of a shoreface nourishment (1993–1996). *Proceedings of Coastal Dynamics '94,* (ASCE), pp. 402–416.

HOEKSTRA, P.; HOUWMAN, K.T.; KROON, A.; RUESSINK, B.G.; ROELVINK, J.A. and SPANHOFF, R., 1996. Morphological development of the Terschelling shoreface nourishment in response to hydrodynamic and sediment transport processes. *Proceedings of the 25th International Conference on Coastal Engineering,* (ASCE), pp. 2897–2910.

HOLMAN, R.A., 1983. Edge waves and the configuration of the shoreline. In: Komar, P.D., (ed.), *Handbook of Coastal Processes and Erosion.* CRC Press, pp. 21–33.

HOLMAN, R.A. and SALLENGER, A.H., 1986. High energy nearshore processes. *EoS,* 67, 1369–1371.

HOWD, P.A; BOWEN, A.J.; HOLMAN, R.A. and OLTMAN-SHAY, J., 1991. Infragravity waves, longshore currents and linear sand bar formation. *Proceedings of Coastal Sediments '91,* (ASCE), pp. 72–84.

HOWD, P.A; BOWEN, A.J. and HOLMAN, R.A., 1992. Edge waves in the presence of strong longshore currents. *Journal of Geophysical Research,* 97-C7, 11357–11371.

HUBERTZ, J.M., 1986. Observations of local wind effects on longshore currents. *Coastal Engineering,* 10, 275–288.

HUNTLEY, D.A., 1980. Edge waves in a cresentic bar system. In: McCann, S.B., (ed.), The Coastline of Canada. Geological Survey Canada Paper 80-10, pp. 111–121.

JAGO, C. and HARDISTY, J., 1984. Sedimentology and morphodynamics of a macrotidal beach, Pendine Sands, SW Wales. *Marine Geology,* 60, 123–154.

JOHNSTON, R.M.S., 1985. Coastal change and hazard delineation on the Rangitikei-Wanganui coast. *Proceedings of the 8th Australasian/conference on Coastal and Ocean Engineering,* (Christchurch New Zealand), pp. 411–420.

KING, C.H.M., 1972: *Beaches and Coasts.* London, Butler & Tanner Ltd., 570 p.

KOMAR, P.D., 1976a. *Beach Processes and Sedimentation.* Englewood Cliffs New Jersey, Prentice-Hall, 429 p.

KOMAR, P.D., 1976b. Evaluation of wave-generated longshore current velocities and sand transport rates on beaches. In: Davis, R.A. and Ethington, R.C., (eds.), *Beach and Nearshore Sedimentation.* Society of Economic Paleontologists and Minerologists, Special Publication 24, pp. 48–53.

KHAFAGY, A.A.; NAFFAA, M.G.; FANOS, A.M. and DEAN, R.G., 1992. Nearshore coastal changes along the Nile Delta shores. *Proceedings of the 23rd International Conference on Coastal Engineering,* (ASCE), pp. 3260–3272.

KROON, A., 1994. Sediment transport and morphodynamics of the beach and nearshore zone near Egmond, the Netherlands. PhD thesis, Utrecht University, the Netherlands, 275 p.

LARSEN, M. and KRAUS, N.C., 1989. *SBEACH: Numerical Model for Simulating Storm-Induced Beach Change. Report 1. Emperical Foundation and Model Development.* Technical Report CERC-89-9, 267 p.

LARSEN, M. and KRAUS, N.C., 1992. *Analysis of Cross-Shore Movement of Natural Longshore Bars and Material Placed to Create longshore Bars.* Technical Report CERC DRP-29-5, 115 p.

LIPPMANN, T.C. and HOLMAN, R.A., 1989. Quantification of sand-bar morphology: a video technique based on wave dissipation. *Journal of Geophysical Research,* 94, 995–1011.

LIPPMANN, T.C. and HOLMAN, R.A., 1990. The spatial and temporal variability of sand-bar morphology. *Journal of Geophysical Research,* 95, 11575–11590.

LIPPMANN, T.C.; HOLMAN R.A. and HATHAWAY, K.K., 1993. Episodic, nonstationary behaviour of a double bar system at Duck, North Carolina, U.S.A., 1986-1991. *Journal of Coastal Research,* Special Issue, 15, 49–75.

LONGUET-HIGGINS, M.S., 1971. Recent progress in the study of longshore currents. In; Meyer, R.E. (ed.), *Waves on Beaches and Resulting Sediment Transport.* New York, Academic Press, pp. 203–248.

MACKY, G.H.; CUMMING, R.J. and VALENTINE, E.M., 1988. *Measurements of Ocean Wave Climate at Wanganui and Himitangi Beach.* Department of Scientific and Industrial Research. Hydrology Centre, Christchurch, New Zealand, 14 p.

MASSELINK, G. and SHORT, A.D., 1993. The effect of tide range on beach morphodynamics and morphology: a conceptual beach model. *Journal of Coastal Research,* 9(3), 785–800.

MILLER, H.C.; BIRKEMEIER, W.A. and DEWALL, A.E., 1983. Effects of CERC research pier on nearshore processes. In: *Proceedings of the International Conference on Coastal Structures '83* (New York), pp. 765–782.

NUMMEDAL, D. and FINLEY, R., 1978. Wind-generated longshore currents. *Proceedings of the 16th International Conference of Coastal Engineering,* (ASCE), pp. 1428–1438.

NUMMEDAL, D.; SONNENFELD, D.L. and TAYLOR, K., 1984. Sediment transport and morphology at the surfzone of Presque Isle, Lake Erie, Pennsylvania. *Marine Geology,* 60, 99–122.

OLTMAN-SHAY, J.; HOWD, P.A. and BIRKEMEIER, W.A., 1989. Shear instabilities of the mean longshore current; 2. field observations. *Journal of Geophysical Research,* 94, 18031–18042.

OSBORNE, P.D. and GREENWOOD, B., 1992. Frequency dependent cross-shore suspended sediment transport. 2. A barred shoreface. *Marine Geology,* 106, 25–51.

OWENS, E.H., 1977. Temporal variations in beach and nearshore dynamics. *Journal of Sedimentary Petrology,* 47(1), 168–190.

PATTERSON, D.C. 1991: *Wanganui Port Development: Coastal Engineering Considerations.* A report (unpublished) for Ocean Terminals and the Wanganui District Council, 48p.

PELTIER, W.R., 1987. Mechanisms of relative sea-level change and the geophysical responses to ice-water loading. In: Devoy, R.J.N., (ed.), *Sea Surface Studies.* London, Croom Helm, pp. 57–91.

PILLANS, B.J., 1990. *Late Quaternary marine terraces South Taranaki—Wanganui.* New Zealand Geological Survey Miscellaneous Series Map 18, Department of Scientific and Industrial Research, New Zealand, 46 p.

ROELVINK, J.A. and STIVE, M.J.F., 1989. Bar generating cross-shore flow mechanisms on a beach. *Journal of Geophysical Research,* 94-C4, 4785–4800.

RUESSINK, B.G., 1998. Infragravity waves in a dissipative multiple bar system. PhD thesis, Utrecht University, The Netherlands, 245 p.

RUESSINK, B.G. and KROON, A., 1994. The behaviour of a multiple bar system in the nearshore zone of Terschelling, The Netherlands: 1965–1993. *Marine Geology,* 121, 187–197.

SHAND, R.D., 1990. The subaqueous morphology at the entrance to a jetty controlled river mouth on a moderate to high energy littoral drift dominated coast: Wanganui New Zealand 1981-1987. Post Graduate Diploma in Science—Research Project, Massey University, New Zealand, 102 p.

SHAND, R.D. and BAILEY, D.G., 1999. A Review of Net Offshore Bar Migration with Photographic Illustrations from Wanganui, New Zealand. *Journal of Coastal Research,* 15(2), 365–378.

SASAKI, T., 1983. *Three Dimensional Topographic Changes on the Foreshore Zone of Sandy Beaches.* University of Tsukuba: Institute of Geoscience, Science Report A-4, pp. 69–95.

SHAW, J., 1985. Beach morphodynamics of an atlantic coast embayment: Runkerry Strand, County Antrim. *Irish Geography,* 18, 51–58.

SHERMAN, D.J., 1988. Emperical evaluation of longshore-current models. *Geographical Review,* 78, 158–168.

SHORT, A.D., 1975. Offshore bars along the Alaskan Arctic coast. *Journal of Geology,* 83, 209–221.

SHORT, A.D., 1979. Three dimensional beach-stage model. *Journal of Geology,* 87, 553–571.

SHORT, A.D., 1992. Beach systems of the central Netherlands coast: processes, morphology, and structural impacts in a storm driven multi-bar system. *Marine Geology,* 107, 103–127.

SHORT, A.D. and AAGAARD, T., 1993. Single and multi-bar beach change models. *Journal of Coastal Research,* Special Issue, 15, 141–157.

SONU, C.J., 1972. Field observation of nearshore circulation and meandering currents. *Journal of Geophysical Research,* 77(18), 3232–3247.

SONU, C.J., 1973. Three-dimensional beach changes. *Journal of Geology,* 81, 42–64.

STAUBLE, D.K., 1992. *Long-term Profile and Sediment Morphodynamics: Field Research Facility Case History.* Technical Report CERC-92-7, 69 p.

STIVE, M.J.F., 1986. A model for cross-shore sediment transport. *Proceedings of the 20th International Conference on Coastal Engineering,* (ASCE), pp. 1550–1564.

SUNAMURA, T., 1988. Beach morphologies and their change. In: Horikawa, K., (ed.), *Nearshore Dynamics and Coastal Processes.* University of Tokyo Press, pp. 133–166.

THORNTON, E.B.; HUMISTOM, R.T. AND BIRKEMEIER, W., 1996. Bar/trough generation on a natural beach. *Journal of Geophysical Research,* 101, 12097–12110.

WESTLAKE, S.J. 1995. Behaviour of a shoreface nourishment, Terschelling, The Netherlands. Masters thesis International Institute for Infrastructural, Hydraulic and Environmental Engineering, Delft, the Netherlands, report HH249, 95 p.

WHITFORD, D.J. and THORNTON, E.B., 1993. Comparison of wind and wave forcing of longshore currents. *Continental Shelf Research,* 13(11), 1205–1218.

WIJNBERG, K.M., 1995. Morphologic behaviour of a barred coast over a period of decades. PhD thesis, Utrecht University, The Netherlands, 245 p.

WRIGHT, L.D.; CHAPPELL, J.; THOM, G.B,; BRADSHAW, M.P. and COWELL, P., 1979. Morphodynamics of reflective and dissipative beaches and inshore systems: Southeastern Australia. *Marine Geology,* 32, 105–140.

WRIGHT, L.D. and SHORT, A.D., 1984. Morphodynamic variability of surf zones and beaches: a synthesis. *Marine Geology,* 56, 93–118.

10

Hatherton Award 2000. The Royal Society of New Zealand

`

HATHERTON AWARD
2000

Roger Duncan Shand

For his contribution in the paper
"An Intersite Comparison of Net Offshore Bar Migration Characteristics and Environmental Conditions".

The Hatherton Award is for the best scientific paper by a student registered for the degree of Doctor of Philosophy at a New Zealand University in Physical Sciences, Earth Sciences or Mathematical and Information Sciences.

The Royal Society of New Zealand

11

Shand, R.D., Bailey, D.G. Shepherd, M.J., 2001. Alongshore realignment of nearshore parallel sand-bars at Wanganui, New Zealand. Marine Geology 179 147-161

ELSEVIER

Marine Geology 179 (2001) 147–161

MARINE GEOLOGY
INTERNATIONAL JOURNAL OF MARINE GEOLOGY, GEOCHEMISTRY AND GEOPHYSICS

www.elsevier.com/locate/margeo

Longshore realignment of shore-parallel sand-bars at Wanganui, New Zealand

Roger D. Shand[a,*], Donald G. Bailey[b], Mike J. Shepherd[a]

[a]*Department of Geography, School of Global Studies, Massey University, Private Bag 11-222 Palmerston North, New Zealand*
[b]*Institute of Information Sciences and Technology, Massey University, Palmerston North, New Zealand*

Received 24 November 2000; accepted 25 July 2001

Abstract

The disconnection and realignment of shore-parallel nearshore sand-bars in the longshore direction is a recently identified morphological behaviour which is referred to as bar switching. This phenomenon has been observed in data from multi-bar coasts in The Netherlands, in North Carolina on the east coast of the USA, and on the west coast of the New Zealand North Island.

This paper identifies the characteristics of bar switching along a 6 km stretch of coast at Wanganui, New Zealand. Analysis of a 6.3 yr record of image-based morphological data identified nine periods or episodes of bar switching. Switching occurred within transition zones which had longshore lengths between 500 and 1000 m. Episodes occurred throughout the study period at intervals ranging from 0 to 64 weeks (mean = 25 weeks). Episode duration ranged from 8 to 27 weeks (mean = 14 weeks). Episodes tended to occur sequentially at centres located 2000–3000 and 4400–5200 m from the nearby Wanganui River mouth which marks the southeastern boundary of the study area. Two types of switching episodes were identified. Shoreward propagating episodes originate in the outer surf zone and the location of switching then moves landward. By contrast, stationary episodes begin and remain within the mid-surf zone. Episodes of bar switching are characterised by strong longshore currents, peak significant wave height values that are usually greater than the 1% exceedence level (3.2 m), and significant wave heights above the 5% exceedence level (2.6 m) for at least 4.5% of the switching period. While high-energy conditions are necessary for bar switching to occur, such energy levels do not always result in this type of morphological behaviour. Antecedent morphology and other hydrodynamic factors may also play important roles in the morphodynamics of bar switching. © 2001 Elsevier Science B.V. All rights reserved.

Keywords: Sand-bar; Multi-bar; Surf zone; Nearshore; Morphodynamics; Bar switching

1. Introduction

Nearshore sand-bars are found on many of the world's sand-dominated coasts and are significant features for the following reasons. The volume of sand contained within the bars may be important in terms of the nearshore sediment budget. Bars provide a natural barrier to shoreline erosion by dissipating incident wave energy during storm conditions. Sand-bars may be very dynamic, particularly during higher energy conditions and they affect most surf zone processes. Recently, a new type of sand-bar behaviour has been identified on some multi-barred coasts. This involves shore-parallel bars becoming discontinuous and the landward bars on one side of the discontinuity realigning and joining the seaward bars on the other side (Shand and Bailey, 1999). This non-linear

* Corresponding author. Tel.: +64-6-344-4214.
E-mail address: r.d.shand@clear.net.nz (R.D. Shand).

0025-3227/01/$ - see front matter © 2001 Elsevier Science B.V. All rights reserved.
PII: S0025-3227(01)00223-7

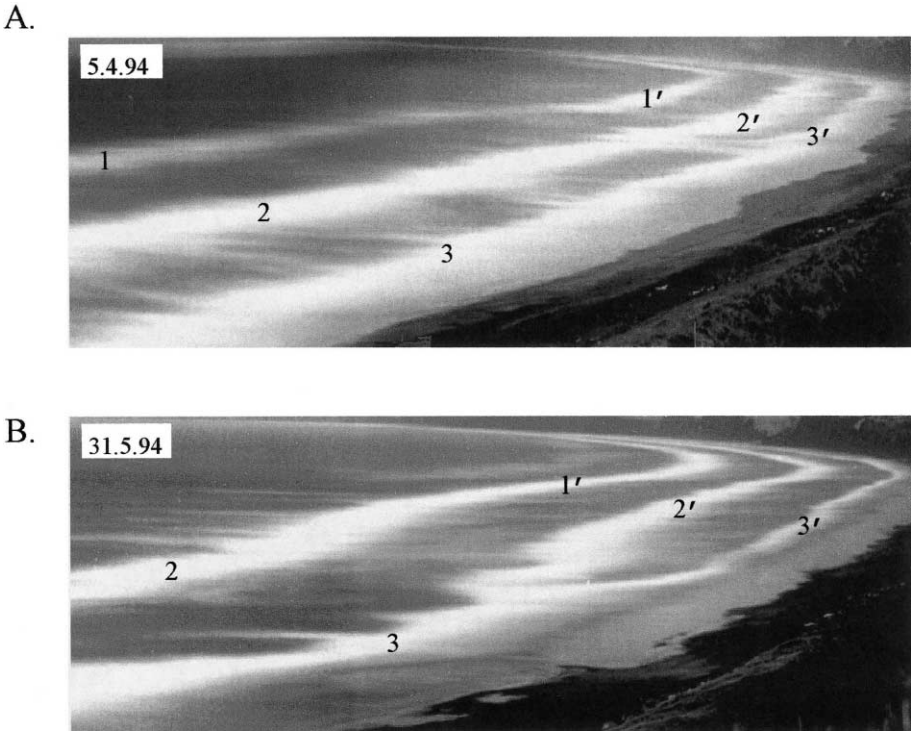

Fig. 1. An example of bar switching within the Wanganui study area. These time-exposure images were obtained using techniques described in Section 3. The high intensity bands signal bar-crests. In the foreground these bars have been marked 1–3 and in the distance as $1'$–$3'$. In (B), bar 2 near the observer has realigned with bar $1'$, and bar 3 is realigning with bar $2'$.

behaviour is henceforth referred to as bar switching. As noted below, bar switching has recently been recognised on other multi-bar coasts for which long-term data-sets are available. Bar switching may therefore be a common type of morphological behaviour, and will need to be well understood if comprehensive surf zone modelling is to be achieved in the future.

An illustration of bar switching is given in Fig. 1. The high intensity bands parallel to the coastline result from breaking waves; these areas broadly define topographic highs such as sand-bars. This technique is discussed later in Section 3. In this example, the switching involves the bar marked 2 in the foreground realigning with bar $1'$ in the distance, and bar 3 in the foreground is about to realign with bar $2'$. This episode of switching is illustrated later in greater detail.

Wijnberg and Wolf (1994) first described such bar behaviour along the Holland coast. Using empirical eigenfunction analysis of bathymetic data, they found that the underlying cycles of net offshore bar migration[1] which characterise meso-scale bar behaviour along that coast, became out-of-phase in the longshore direction. The region linking two such parts of the bar system was referred to as the transition area. These authors provided data showing the bars in each part making alternating attachments across the transition area. Bar switching, as defined above, therefore occurred within this transition area or transition zone.

Examples of bar switching at two locations on the west coast of the New Zealand North Island have recently been published by Donohoe (1998) and

[1] Net offshore bar migration refers to the systematic offshore migration of sand-bars on multi-bar coasts; see Shand and Bailey (1999) for a review. Briefly, a bar is formed (generated) near the shoreline and then migrates seaward across the surf zone to finally flatten out (degenerate) in the outer surf zone. This process takes several years to complete.

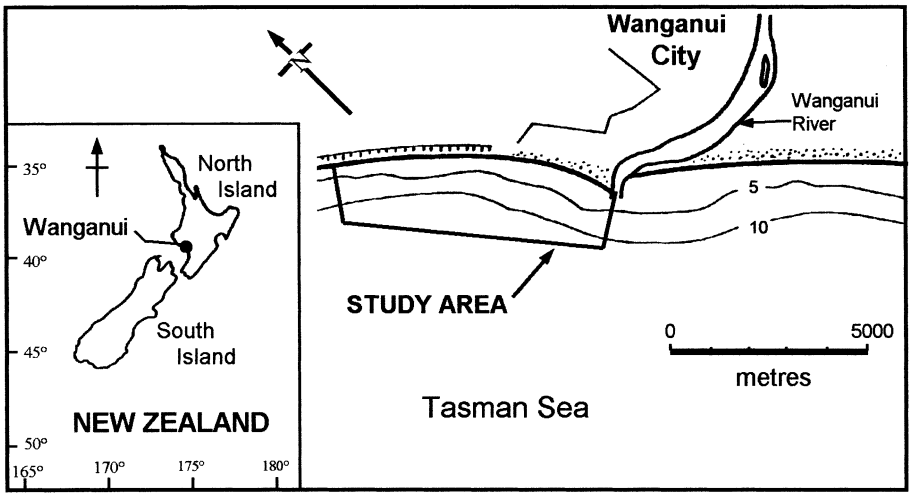

Fig. 2. Location map of the study area. Depth contours are in metres below chart datum where chart datum is 1.8 m below MSL.

Shand and Bailey (1999). These authors used video and photographically based imaging techniques, respectively, to derive their morphological data. Near Auckland, Donohoe (1998) identified a bar realignment at Muriwai Beach. Further south at Wanganui, Shand and Bailey (1999) described a set of interrelated switchings and analysed the associated cross-shore bar migration to show how the bar behaviour differed on each side of the transition zone.

Other published examples of apparent bar switching are shown in Ruessink and Kroon (1994) at Terschelling Island in the Netherlands, Lippmann et al. (1993) and Plant et al. (1999) at Duck in North Carolina, and Carter (1986) on the Magilligan coast of Northern Ireland.

Existing conceptual surf zone models such as two-dimensional storm/fairweather or bar/berm models (Komar, 1976), or more comprehensive three-dimensional beach-state or morphodynamic models (Wright and Short, 1984; Short and Aagaard, 1993), do not accommodate bar switching. For some coasts these models will need to be modified to incorporate this newly identified type of bar behaviour. The purpose of the present paper is to identify the spatial and temporal characteristics of bar switching on the Wanganui coast. Incident energy conditions associated with the switching are also described because high energy is likely to be an important driving force for bar switching given the well established positive relationship between energy and sediment transport on barred coasts (Larsen and Kraus, 1992; Ruessink, 1998).

2. The study site

The study site covers 6 km of coast to the northwest of the Wanganui River mouth (Fig. 2). This coast is tectonically active with uplift rates of approximately 0.25 mm/yr at the shoreline and subsidence occurring further offshore (Pillans, 1983). The Wanganui River is 305 km long and has a catchment area of 7120 km^2 (Tonkin and Taylor, 1978). River mouth jetties were constructed between 1884 and 1940 (Gibb, 1962), and the shoreline response has been to prograde by approximately 700 m near the entrance and 100 m at the northwestern end of the study area (Smith and Ovenden, 1998). Observations made over the past decade indicate that the shoreline has prograded a further 10 m during that period. The accretion is superimposed upon a regional erosion trend of 0.2–0.6 m/yr (Johnston, 1985). The bathymetry depicted in Fig. 2 shows the ebb-tide delta of the Wanganui River extending across the eastern part of the study area.

The time-averaged nearshore width ranges from 425 m near the river mouth to 625 m in the northwest part of the study area (Shand, 2000). The nearshore

region is defined by the intersect of the mean profile and spring low tide level, and, to seaward, where vertical change in the profile bundle becomes approximately constant. The average cross-shore slope flattens with increasing distance from the river and has values ranging from 0.0094 near the entrance to 0.0082 in the northwest (Shand, 2000). The nearshore is characterised by fine sand with the mean size of samples ranging from 2 to 3 phi (Shand, 2000).

Two to three sand-bars occur in the cross-shore direction closer to the rivermouth, while two to four bars occur in the northwest of the study area. Bar behaviour is characterised by net offshore migration with the average time interval between bar formation and bar disappearance, i.e. the life cycle of a bar, being 3.5 yr (Shand and Bailey, 1999; Shand, 2000).

Daily wave height data during the 3439 day study period (see Section 3) were collected using the 'stake and horizon' method described by Patterson and Blair (1983) and Horikawa (1988). While these data may deviate from instrument-based measurement, they do provide an accurate record of relative wave height (Patterson, 1985). A limitation of our data-set will be its tendency to underestimate peak values for higher energy events as only one or two measurements were made on most days. Nonetheless, these data should enable any qualitative pattern between wave energy and switching to be identified relatively easily, as storm events capable of moving the large amounts of sediment required for bar switching, normally have a duration exceeding one day. The resulting mean significant wave height was 1.4 m, and the 5% exceedence value was 2.6 m. These values compare closely with the deepwater wave climate statistics of 1.3 and 2.5 m, respectively. The wave period was measured by counting the number of waves breaking over a 2 min interval; the resulting mean wave period was 10.3 s. Spectral analysis of deep water sea-level data (265 days) carried out by Patterson (1992), showed that both sea and swell populations usually co-exist, with approximately 75% of the wave energy occurring at sea wave frequencies. Directional wave studies found 35% of waves had a shore-normal approach, 43% approached from the west and 22% from the east (McLean and Burgess, 1969).

The mean spring and neap tide ranges at the study site are 2.4 and 0.8 m, respectively (Ministry of Transport, 1989).

Long-term wind data from Wanganui Airport (5 km to the east) reveals a mean speed of 5.3 m/s and a 5% exceedence value of 12.4 m/s. Correlation analysis of process data (158 days) collected by the authors during 1994, indicated that wind speed was strongly associated with wave height ($p \ll 0.01$, where p is the probability of an association having arisen by chance alone). The dominant wind approach direction for the airport data was 290° which makes an angle of ~30° with the shoreline. Sixty percent of the long-term wind data had a northwesterly component, 25% a southeasterly component, and during the remaining 15% calm conditions prevailed.

Inner surf zone longshore current data collected during the 158 day process study, had a median value of 0.26 m/s and a maximum value of 0.83 m/s. In this study, measurements were made at a single location some 1500 m northwest of the river mouth and these data were obtained by timing floats released into the inner surf zone. Longshore currrent was positively associated with wave height, wave direction, and the longshore wind component, with $p \ll 0.01$ in each case. Tidal currents account for ~23% of the total longshore flow (Bell, 1990, 1991). Littoral drift reflects the longshore energy regime with NW to SE estimates ranging from 300,000 to 600,000 m^3/yr and SE to NW estimates ranging from 60,000 to 280,000 m^3/yr (Shand, 2000).

The mean annual flow of the Wanganui River is 224 m^3/s, the mean annual flood flow is 2221 m^3/y, and the annual bedload yield (gravel plus sand) is approximately 114 ktons (Tonkin and Taylor, 1978). However, the southeast-trending process conditions described above, together with minerological evidence (Fleming, 1953), indicate that most of the rivers' sediment load is deposited south of the study area.

3. Methods

The morphological data used in this study were derived from a 6.3 yr record of photographs taken between August 1991 and November 1997. Field sampling was carried out at approximately fortnightly intervals with closer sampling (1–5 days) at times of rapid morphological change. These sampling rates enabled morphological change to be confidently tracked within a sequence of images.

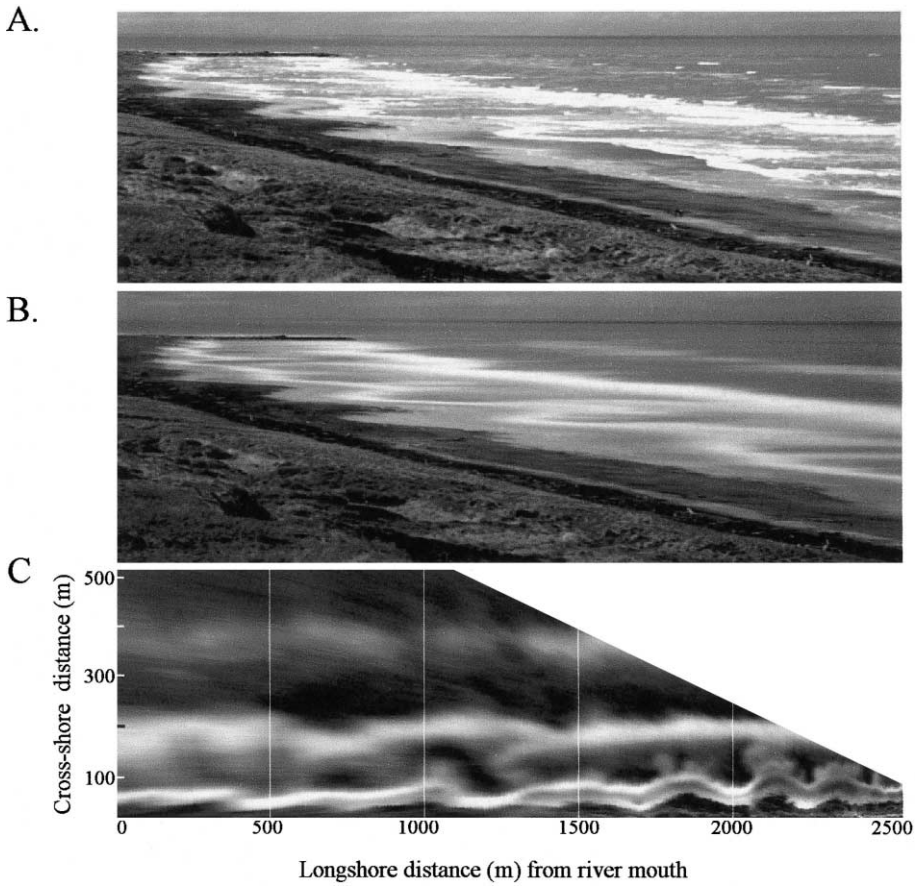

Fig. 3. Examples of an instantaneous (1/125th s) photograph (A) and corresponding time-exposure photograph (B) showing the southeastern section of the study area. The river mouth jetties are evident in the distance. (B) has been rectified and straightened to make the image in (C).

The camera was located on a cliff-top mid-way along the study area. This site is ~3200 m from the river mouth, ~130 m landward of the foredune toe and ~42 m above mean sea-level. A panorama of eight photographs was required to give full coverage of the study area. The four central photographs within the panorama were taken with a 55 mm focal length lens, whilst the end shots were taken with a 135 mm telephoto lens.

Each photograph was exposed for 4 min to minimise tidal change during a panoramic sampling and to provide a relatively stable representation of the breaking wave pattern. Such images are referred to as time-exposures. These images provide an analogue for surf zone morphology because elevated topography such as sand-bars are characterised by locations of higher intensity resulting from wave breaking which is depth-dependent. Examples of an instantaneous (1/250th s) photograph and the corresponding time-exposure photograph of the eastern end of the study area are shown in Fig. 3A and B, respectively. Time-exposure photographic images are equivalent to the video-based time-exposure images produced by the Argus system which is described in Holman (1995).

Field sampling was carried out during lower tide levels and higher wave conditions to maximise the likelihood of waves breaking on all bar-crests. Furthermore, by limiting sampling (photography) to these conditions, the influence of different wave heights and tide levels on break-point location were minimised; this is described in detail by Shand (2000).

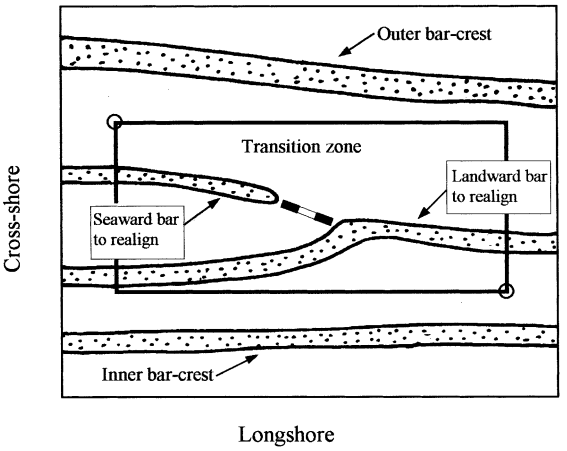

Fig. 4. A schematic illustration of the method used in this study to locate transition zone boundaries. The dashed line shows where realignment is about to occur, and the transition zone within which this realignment occurs is defined by the rectangle. Points represented by the circles at the upper left and lower right corners, delineate the rectangle. The means by which these two points are located is described in the text.

The landwardmost intensity maxima usually relates to wave breaking over a step feature observed to occur where the landwardmost trough joins the foreshore; we refer to this as the low tide step. Sand-bars have been defined by positive residuals from a smooth curve fitted to the cross-shore profile (e.g. Holman and Bowen 1982; Larsen and Kraus, 1992; Kroon, 1994). Under this definition the low tide step is a sand-bar and it will be considered as such for this study.

Digital image processing was used to rectify each photograph to ground co-ordinates and then to merge this output with adjacent images. This combined output image was subsequently transformed to straighten the coastline, thereby facilitating viewing and analysis. These procedures have been described by Bailey and Shand (1993, 1996). Fig. 3C shows the rectified and straightened output image corresponding to the time-exposure photograph in Fig. 3B. The cross-shore resolution of bar-crest data from output images is estimated at ± 20 m, while the longshore resolution varies between ± 1 m opposite the camera to approximately ± 100 m at the ends of the study area (Shand, 2000).

Data used for analysis in the present study were selected from the data-base of rectified images after taking the following considerations into account. During an episode, several months could pass with little change to the morphological configuration; this situation is illustrated later in the paper. To minimise the analysis of repetitious configurations, samples at monthly intervals were selected. However, as significant configuration change could occur within several days, smaller intervals were used for such periods.

The method used in this study to identify transition zone boundaries is illustrated in Fig. 4. The two circles denote points which define the rectangle marking the transition zone boundaries. The seaward cross-shore limit was defined by the mid point between the seawardmost bar-crest (intensity maximum) undergoing switching and the adjacent offshore bar (intensity maximum). The landward transition zone boundary was the mid point between the landward-most bar undergoing switching and the adjacent inner bar. The low tide step was used as the most landward bar in the switching process. The longshore boundaries of the transition zone were where bar morphology appeared to have been unaffected by the realignment process. Identification of the boundaries was assisted by zooming onto the relevant section of rectified image, applying colour enhancement, and overlaying a $50\,\text{m} \times 50\,\text{m}$ grid. The accuracy of visually locating the cross-shore and longshore transition zone boundaries is estimated at ± 10 and ± 50 m, respectively.

The data resolution limitations and the errors in locating the transition zone boundaries, are not sufficient to affect significantly the results and conclusions described later in this study.

Bar switching was deemed to have begun when the usually distinct intensity minimum resenting a longshore trough between adjacent bars, was not evident. The switching was considered to have finished when a distinct trough was apparent between bars involved in the realignment.

The high energy events, i.e. storms, which are expected to occur at times of bar switching, may be characterised by parameters representing wave intensity, duration and frequency. When the wave field has been sampled at hourly intervals, parameters such as those described in Kroon (1994) and Lee et al. (1998) may be used. However, in the present study only one or two daily samples were available, so alternative parameters were used. The first was the maximum

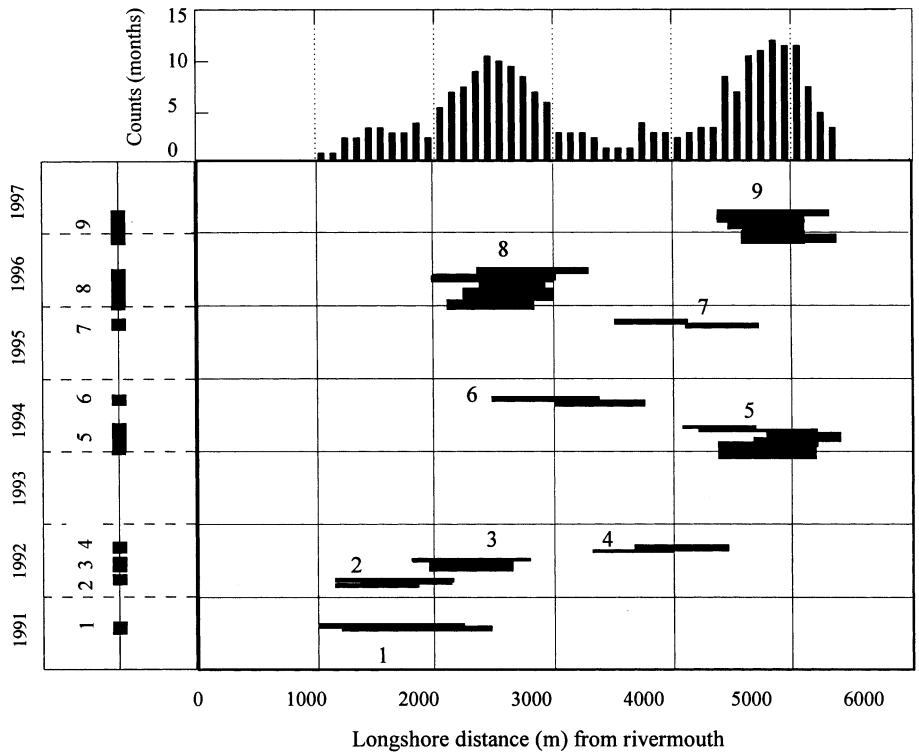

Fig. 5. Longshore distribution of 33 transition zones defining nine chronologically numbered episodes of bar switching at the Wanganui study site between 1991 and 1997. The time-line for the episodes is shown on the left of the figure, and a histogram of the number of months transition zones occurred at each longshore location is depicted along the top of the figure.

(peak) wave height for each period of bar switching (or non-bar switching). The second was a cumulative time-based high energy parameter consisting of the number of days that wave height was greater than the 5% exceedence level (2.6 m) during an interval of bar switching (or non-bar switching) normalised by the total number of days within the interval. The 5% level was used as all episodes experienced wave heights above that value.

4. Results

4.1. Temporal characteristics

Nine separate periods of bar switching were identified within the study area. A period of bar switching consisted of a set of interrelated bar realignments and is referred to as an episode of bar switching. The nine episodes have been plotted and chronologically numbered on the time-line in Fig. 5. Duration for the episodes of bar switching ranged from 8 to 27 weeks with a mean of 14 weeks. Episodes occurred throughout the study with a mean spacing of 25 weeks. However, the episodes occurred somewhat irregularly, with the spacing ranging between zero and 64 weeks.

4.2. Spatial characteristics

4.2.1. Longshore

The longshore location of the set of transition zones associated with each episode of bar switching is plotted against time in Fig. 5. Longshore length dimensions of these transition zones ranged from 500 to 1000 m with a mean of 760 m. Longshore movement in transition zone location during episodes of switching is evident in Fig. 5. Sixty percent of the net displacements were from the northwest to the southeast. The maximum movement of the centre of

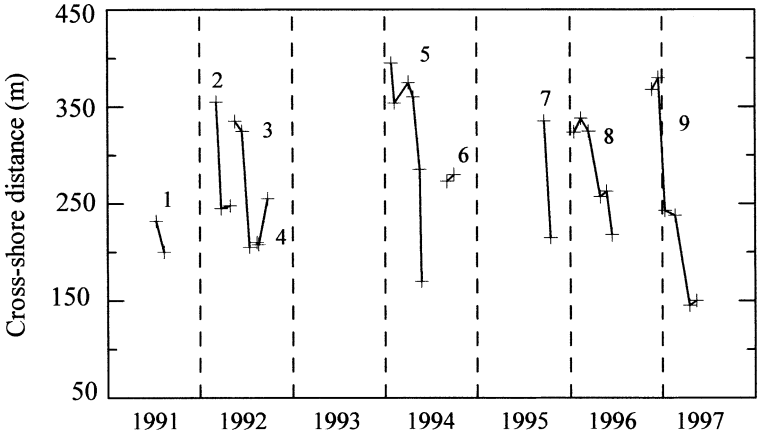

Fig. 6. Time-series depicting cross-shore locations of centre of mass of transition zones associated with each episode of bar switching. The episodes have been chronologically numbered.

mass of the transition zones between the beginning and end of each episode was 625 m, the minimum movement was 25 m and the mean was 315 m. The rates of change in location of the transition zones ranged between 1 and 305 m/month with a mean of 115 m/month.

A histogram of the number of months that transition zones occurred at different longshore locations is shown at the top of Fig. 5. The centre of mass of each transition zone was used for this analysis. The result shows a bimodal distribution with frequency peaks between 2000 and 3000 m alongshore (from the river mouth) and between 4400 and 5200 m alongshore. Switching occurred approximately 12% of the time at these locations. At least one episode of switching occurred at each location between 1000 and 5400 m; however, switching was absent at each end of the study area.

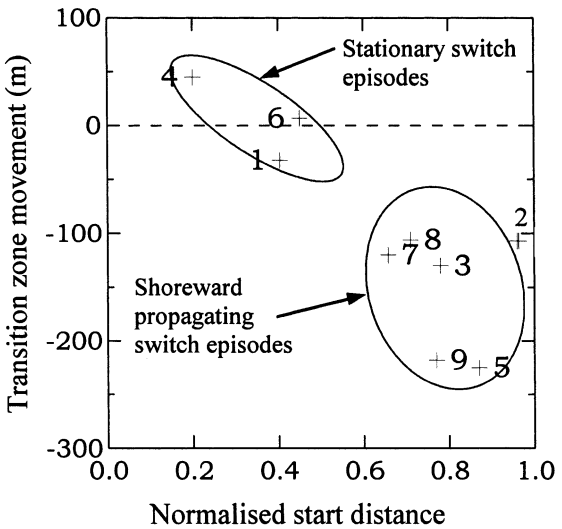

Fig. 7. Bivariate plot for cross-shore start distance and cross-shore transition zone movement for each of the nine episodes of bar switching. Start distances have been normalised with respect to surf zone width. Positive transition zone movements are directed seaward. The partitioning is based on 95% confidence ellipses.

The results in Fig. 5 also show that the longshore location of the nine episodes of bar switching tended to alternate between the two frequency distribution centres. This longshore alternation was disrupted during the period 1992 through 1993 when no switching occurred. This time interval was characterised by lower wave energy levels and will be considered further in Section 4.3 which examines process conditions experienced during the study period.

4.2.2. Cross-shore

The cross-shore location of transition zones associated with each episode of bar switching are depicted in Fig. 6. These results show that most episodes of bar switching (episodes 2, 3, 5, 7, 8 and 9) began in the seaward portion of the outer surf zone, and the transition zone location subsequently shifted shoreward. The remaining episodes (1, 4 and 6) began closer to shore and their subsequent transition zones remained in approximately the same place. These results are more clearly depicted in Fig. 7. The start

locations have been normalised with respect to the distance between the landward and seaward proturberances on the time-averaged profile, as most of the nearshore sand-bars occurred within this region (Shand, 2000). These distances increase with increasing distance from the rivermouth in a similar manner to the change in nearshore width described earlier. The two groups of switching episodes are henceforth referred to as shoreward propagating episodes and stationary episodes.

Examples of morphological configuration sequences which clearly depict landward propagating and stationary episodes of bar switching are shown by the images in Fig. 8A (episode 5) and B (episode 6), respectively. The shoreward propagating episode consists of three separate bar realignments, while the stationary episode consists of a single realignment.

It is further noted that switching episode 1 may not be a stationary type for the following reasons. The first available data showing longshore morphological variation were a set of echo-sounding profiles sampled in July 1991. It is possible that the episode began prior to this. If this was the case, then the landward movement of the observed transition zones suggest that this episode may have originated further seaward. Episode 1 may therefore be a shoreward propagating type, rather than a stationary type, and it will be reclassified as such for this study.

Re-analysis of the earlier bar switching characteristics in light of these two types of realignment, show that the two stationary switch episodes (4 and 6) had lower durations (8 weeks) than the shoreward propagating episodes, which ranged up to 27 weeks.

4.3. Process characteristics

The maximum wave height that occurred between each set of morphological surveys is depicted in Fig. 9A, and the maximum (peak) wave height which occurred during (and between) each episode of bar switching is depicted in Fig. 9B. Seven of the nine episodes experienced a peak wave height value greater than the 1% exceedence level (3.2 m). The remaining two episodes experienced peak values greater than the 5% exceedence level; these episodes (4 and 6) were of the stationary type. By comparison, only 4 of the 10 non-switching intervals experienced peak values greater than the 1% level. For the six remaining periods of non-switching, three experienced a peak wave height greater than the 5% level, two had a peak value less than the 5% level and in one case there was no interval between episodes. It is noteworthy that the highest peak value (3.7 m) occurred during a period of non-switching.

The cumulative time-based high energy parameter values for switching and non-switching intervals are depicted in Fig. 9C. These results show that for all periods of bar switching, wave heights exceeded the 5% level (2.6 m) for at least 4.5% of each time interval. By comparison, only 5 of the 10 periods of non-switching exceeded this cumulative value. However, as with peak wave height, the greatest value for this parameter (0.115) was experienced during a period of non-switching.

5. Discussion

Comparison of the Wanganui bar switching results with those derived from the Holland data presented in Wijnberg and Wolf (1994) and Wijnberg (1995), show that episode durations at Wanganui were shorter (0.15–0.51 yr cf. up to 5 yr), the average longshore length of transition zones were shorter (750 m cf. 2500 m), and the longshore migration rates of transition zones were higher (maximum 306 m/month cf. 92 m/month). These differences may relate to the larger sediment volume contained in bars along the Holland coast, which may in turn be a consequence of higher overall levels of wave energy (see Shand et al., 1999). Empirical eigenfunction weighting diagrams presented in Wijnberg and Wolf (1994) and Wijnberg (1995), suggest that bar switching along the Holland coast tends to occur at preferential locations as is the case at Wanganui (Fig. 5).

The energy parameter results described in Section 4.3, identified possible conditions under which bar switching did (and did not) occur. In particular, bar switching coincided with very high peak wave height values, together with the relatively frequent occurrence of high values throughout the episode. While lower peak and cumulative values often occurred during non-switch intervals, particularly high levels also occurred during such periods. These relationships suggest that while high energy levels are necessary for the occurrence of

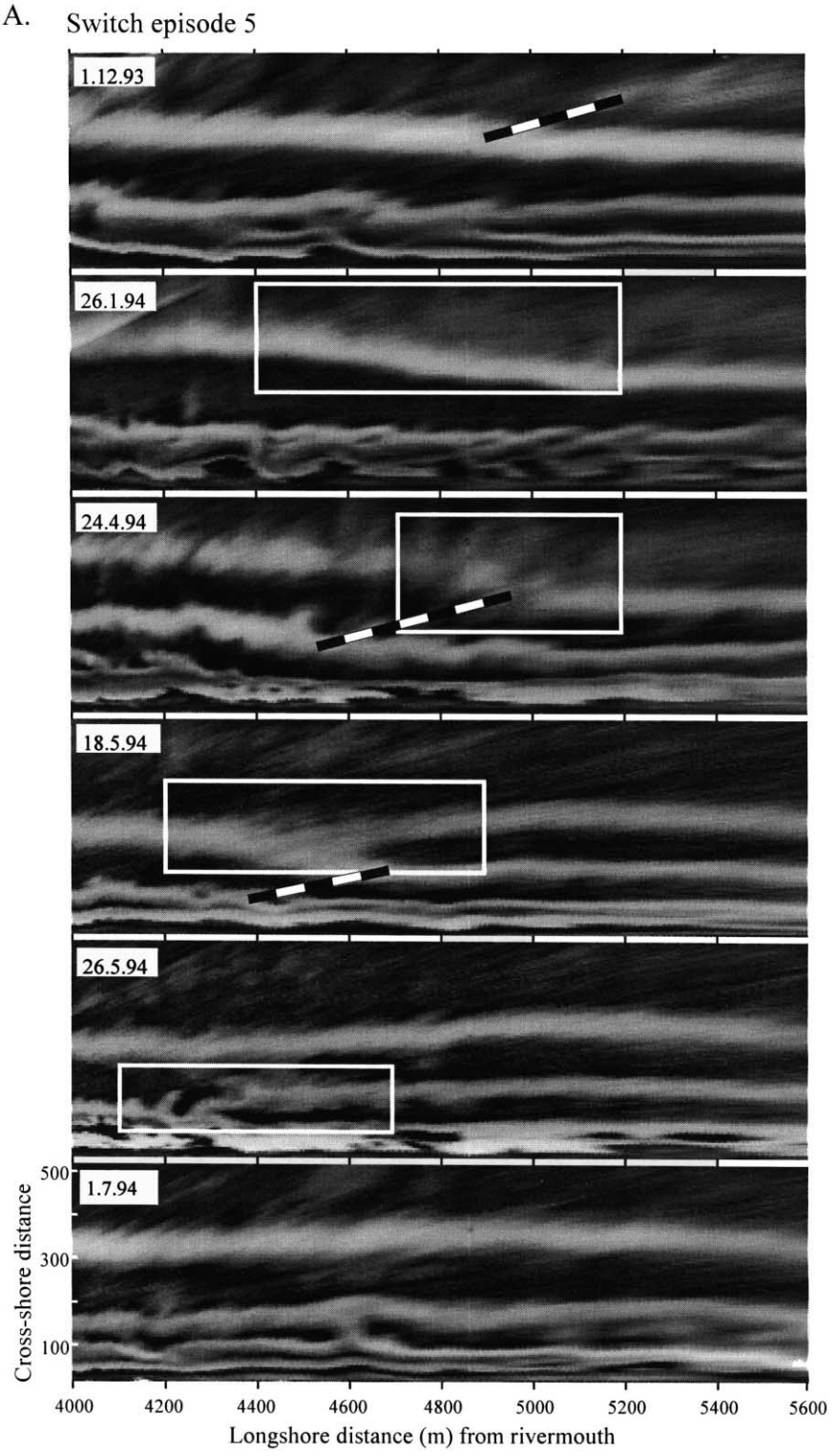
A.
Switch episode 5
1.12.93
26.1.94
24.4.94
18.5.94
26.5.94
1.7.94
Cross-shore distance
500
300
100
4000
4200
4400
4600
4800
5000
5200
5400
5600
Longshore distance (m) from rivermouth

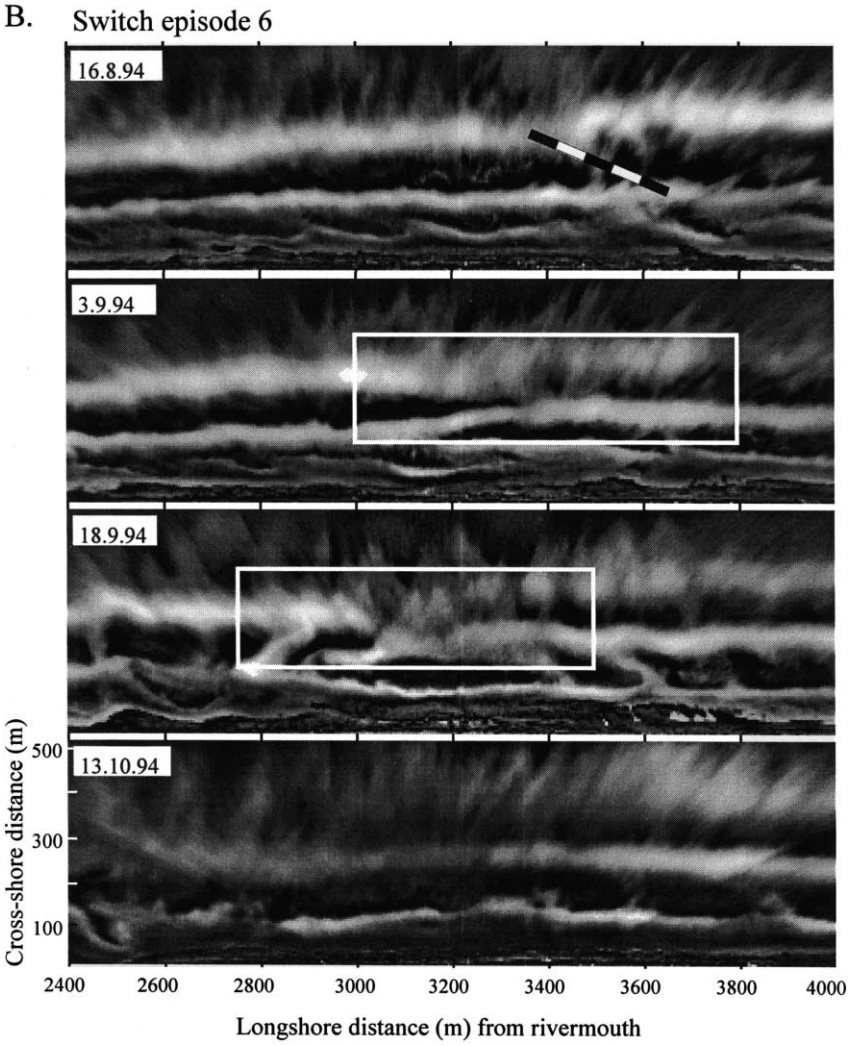

Fig. 8. Configuration sequences depicting an example of a shoreward propagating switch episode (A) and a stationary switch episode (B). The bold dashed lines show where bar switching is about to happen and the rectangles define the transition zones within which bar switching is occurring.

bar switching, high energy levels alone do not necessarily result in switching. Bar switching therefore appears to be forced by high energy acting in combination with factors such as other types of hydrodynamic conditions or antecedent morphology. Other types of hydrodynamic influences are considered later in this section, and support for morphological control has recently been provided by Shand (2000) who showed that longshore variation in the depth and shape of the seawardmost bar in the vicinity of the transition zone, precedes bar switching.

The highly significant positive correlation between wave height and longshore currents described earlier in Section 2, indicate that strong longshore currents occur during bar switching. In addition, the importance of longshore current for switching morphodynamics is suggested by the similarity between net longshore movement of transition zones (60% toward the southeast and 40% toward the

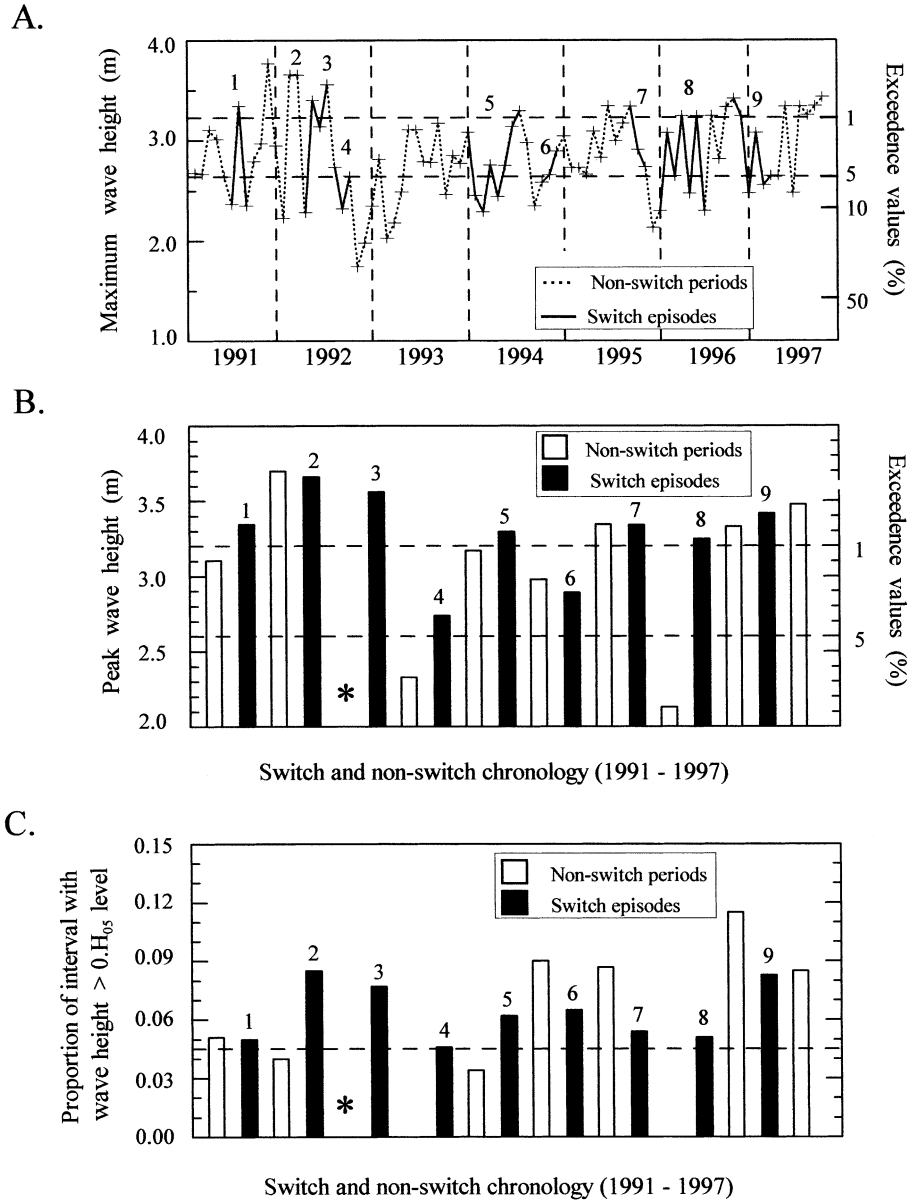

Fig. 9. Maximum significant wave height between each morphological inter-survey period is depicted in A, with the solid lines relating to chronologically numbered episodes of bar switching. Peak wave height for each switching episode, and for the interval between switching episodes, is shown in B. The proportion of each episode of switching, and each period of non-switching, for which wave height was greater than the 5% exceedence level, i.e. $H_{0.05} > 2.6$ m, is depicted in C. The asterisks denote instances where there was no time between successive episodes of switching.

northwest) and the directional wind and wave statistics described in Section 2.

The absence of bar switching between 5400 m and the northwestern boundary of the study site, raises the question of whether bar switching is a local rather than a regional phenomenon. However, morphological configurations consistent with bar switching are evident on aerial photographs taken of

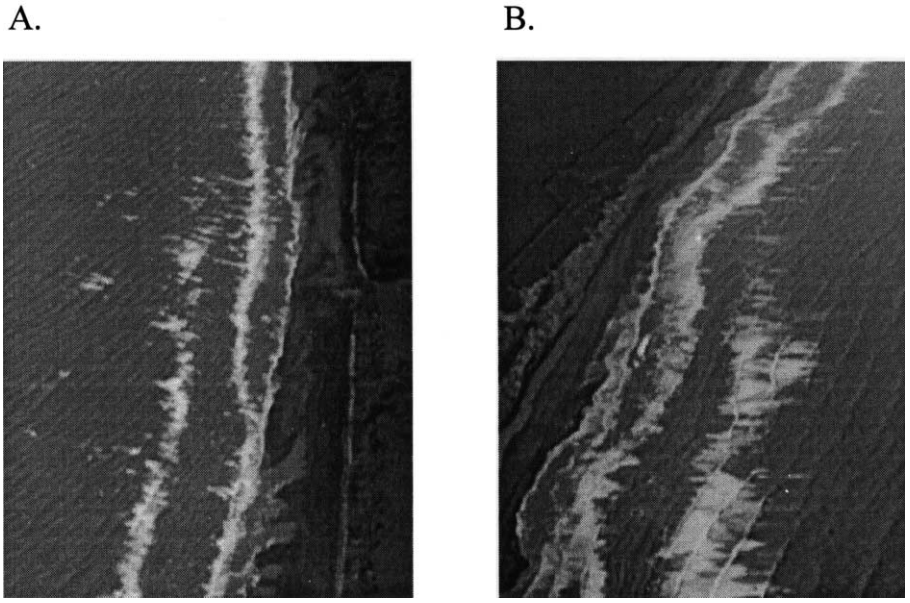

Fig. 10. Examples of morphological configurations from outside the Wanganui study area which are consistent with bar switching. (A) is located approximately 11.5 kms northwest of the Wanganui River mouth, while (B) is approximately 25 km southeast of the river.

the Wanganui coast beyond the study area. Examples of two such configurations located ~11.5 km northwest and ~25 km southeast of the river mouth are depicted in Fig. 10A and B. It is noted that the northwestern location is a multiple of 2300 m from the river mouth, and this spacing is very similar to that associated with the two preferred locations of bar switching within the study site (2500 and 2400 m, as depicted in Fig. 5).

The apparent existence of bar switching along the Wanganui coast beyond the study area, together with the regularity in the longshore location of switching both at Wanganui and along the coast of Holland, suggest that a regional hydrodynamic control may be important in morphodynamics associated with this phenomenon. Such mechanisms may involve the influence of low frequency standing edge waves, or instabilities in the wave/current field, both of which have been theoretically shown to be capable of generating regularly spaced three-dimensional nearshore morphologies (e.g. see Hino, 1974; Holman and Bowen, 1982; Holman, 1983; Damgaard Christensen et al., 1994). Alternatively, the observed longshore preference in the location of bar switching may result from morphodynamics linked to the changes in cross-shore slope or bar number, which occur along the ebb delta and adjacent coasts.

While the transition zone analysis identified two apparent populations of bar switching (stationary and shoreward propagating), this is not unequivocal. If an initial seaward switching was undetected because of under-sampling or low image resolution, then the seaward transition zone would also remain undetected, thereby resulting in the spurious identification of stationary switching. Alternatively, the single and multiple bar realignments associated with the examples of stationary and shoreward propagating episodes, respectively (Fig. 8), suggest that the two types of episode may be the product of the same realignment process, with the difference being a function of differing numbers of bars. Nevertheless, the differing levels of three-dimensionality apparent within the antecedent morphologies of Fig. 8A and B, suggests that an underlying difference in morphodynamics may occur between the two types of bar switching. For example, the greater level of 3D morphology associated with the antecedent configuration of stationary switching, may constrain longshore flows, thereby locally enhancing nearshore currents and increasing sediment transport potential. This

process could explain the observed occurrence of lower peak energy levels with stationary switching.

6. Conclusions

This paper has identified the characteristics of nine episodes of bar switching at Wanganui by analysing the transition zones within which bar realignment occurred. Episodes of bar switching happened throughout the study period at an average spacing of 25 weeks. The duration of the episodes ranged from 8 to 27 weeks (mean = 14 weeks). Episodes tended to occur sequentially at centres located 2000–3000 and 4400–5200 m from the river mouth.

The transition zone analysis identified two types of switching episodes. Shoreward propagating episodes originate in the outer surf zone and switching then moves landward. Stationary episodes begin and remain within the mid-surf zone. However, further research is required to determine whether these are fundamentally different types of morphological behaviour.

Episodes of bar switching were characterised by the following process conditions: strong longshore current; peak significant wave height usually exceeding the 1% level (3.2 m); and, significant wave height exceeding the 5% level (2.6 m) for at least 4.5% of the switching period. While these results suggest that very high energy levels are a necessary condition for the occurrence of bar switching, high-energy conditions also prevailed during some of the periods when bar switching did not occur. High energy conditions alone are therefore not sufficient to cause bar switching, and this phenomenon may also be controlled by other hydrodynamic factors and antecedent morphology.

Acknowledgements

This study was supported by the Massey University Graduate Research Fund, The Massey University Research Fund, and a Vice Chancellors Special Grant. The authors wish to thank Professor Rob Holman (Coastal Imaging Laboratory, Oregon State University) for supplying lens filters and initial advise on the acquisition of time-exposure images. We also wish to thank Professor Bob Kirk (University of Canterbury, New Zealand), Dr Karin Bryan (National Institute of Water and Atmosphere Research Ltd. (NIWA), Hamilton, New Zealand), Dr Gerben Ruessink (Delft Hydraulics, the Netherlands), and Professor Andy Short (Coastal Studies Unit, University of Sydney) for their useful comments on the manuscript.

References

Bailey, D.G., Shand, R.D., 1993. Determining large-scale sand bar evolution. Proceedings of the First New Zealand Conference on Image and Vision Computing, pp. 109–116.

Bailey, D.G., Shand, R.D., 1996. Determining large-scale sand bar behaviour. Proceedings of the IEEE International Conference on Image Processing, Lausanne, Switzerland, 2, pp. 637–640.

Bell, R., 1990. Oceanography of Wanganui Coastal Waters. Final Report of the Wanganui District Council on the Recommended Scheme for Wastewater Treatment and Disposal for the City of Wanganui. Water Quality Centre, DSIR, New Zealand, 33pp.

Bell, R., 1991. Oceanography of Wanganui Coastal Waters. Environmental Impact Assessment Report for the Wanganui Wastewater Working Party. Water Quality Centre, DSIR, New Zealand. 33p.

Carter, R.W.G., 1986. The morphodynamics of beach-ridge formation: Magilligan, Northern Island. Mar. Geol. 73 (2), 191–214.

Damgaard Christensen, E., Deigaard, J., Fredsoe, J., 1994. Sea bed stability on a long straight coast. Proceedings of the 24th International Conference on Coastal Engineering, pp. 1865–1879.

Donohoe, B.F.P., 1998. Spatial and temporal bar morphodynamics of Muriwai Beach, MSc thesis, Auckland University, New Zealand, 104pp.

Fleming, C.A., 1953. Geology of the Wanganui subdivision. Geol. Surv. Bull. n.s. 52 Department of Scientific and Industrial Research, New Zealand, 362pp.

Gibb, A., 1962. Tongariro River Power Development, Wanganui Harbour. Report to the New Zealand Ministry of Works. A report prepared for the Ministry of Works, by Sir Alexander Gibb and Partners, London, 39pp.

Hino, M., 1974. Theory of formation of rip-current and cuspidal coast. Proceedings of the 14th International Conference on Coastal Engineering, pp. 909–919.

Holman, R.A., 1983. Edge waves and the configuration of the shore-line. In: Komar, P. (Ed.), Handbook of Coastal Processes and Erosion. CRC Press, Boca Raton, pp. 21–33.

Holman, R.A., 1995. The Argus Program. Coastal Imaging Laboratory, Oregon State University, 6pp.

Holman, R.A., Bowen, A.J., 1982. Bars, bumps, and holes: models for the generation of complex beach topography. J. Geophys. Res. 84, 457–468.

Horikawa, K., 1988. Nearshore Dynamics and Coastal Processes. University of Tokyo Press, Tokyo, Japan, 522pp.

Johnston, R.M.S., 1985. Coastal change and hazard delineation on the Rangitikei–Wanganui coast. Proceedings of the Eighth

Australasian Conference on Coastal and Ocean Engineering, pp. 411–420.

Komar, P.D., 1976. Beach Processes and Sedimentation. Prentice-Hall, Englewood Cliffs, NJ, 429pp.

Kroon, A., 1994. Sediment transport and morphodynamics of the beach and nearshore zone near Egmond, the Netherlands. PhD thesis, Utrecht University, The Netherlands, 275pp.

Larsen, M., Kraus, N.C., 1992. Analysis of cross-shore movement of natural longshore bars and material placed to create longshore bars. Technical Report CERC DRP-29-5, 115pp.

Lee, G-h., Nicholls, R.J., Birkemeier, W.A., 1998. Storm-driven variability of the beach-nearshore profile at Duck, North Carolina, USA, 1981–1991. Mar. Geol. 148, 163–177.

Lippmann, T.C., Holman, R.A., Hathaway, K.K., 1993. Episodic, non-stationary behaviour of a double bar system at Duck, North Carolina, USA. J. Coastal Res., Special Issue 15, 49–75.

McLean, R.F., Burgess, J.S., 1969. Investigations of the entrance to Wanganui Harbour. Collected Interim Reports to the Engineer Wanganui Harbour Board. University of Canterbury, Geography Department, 105pp.

Ministry of Transport, 1989. New Zealand Nautical Almanac 1989–1990. Marine Transport Division, Ministry of Transport, New Zealand, 176pp.

Patterson, D.C., 1985. Low cost visual determination of surf zone parameters. Unpublished MSc thesis, University of Queensland, Australia, 143pp.

Patterson, D.C., 1992. Wanganui Port development feasibility studies: coastal engineering aspects. A report for Ocean Terminals and the Wanganui District Council, New Zealand, 51pp.

Patterson, D.C., Blair, R.J., 1983. Visually determined wave parameters. Proceedings of the Sixth Australian Conference on Coastal and Ocean Engineering, Gold Coast, Australia, pp. 151–155.

Pillans, B.J., 1983. Quaternary marine terrace chronology and deformation, South Taranaki, New Zealand. Geology 11, 292–297.

Plant, N.G., Holman, R.A., Freilich, M.H., Birkemeier, W.A., 1999. A simple model for inter-annual sand bar behaviour. J. Geophys. Res. 104 (C7), 15,755–15,776.

Ruessink, B.G., 1998. Infragravity waves in a dissipative multiple bar system. PhD thesis, Utrecht University, the Netherlands, 245pp.

Ruessink, B.G., Kroon, A., 1994. The behaviour of a multiple bar system in the nearshore zone of Terschelling, the Netherlands: 1965–1993. Mar. Geol. 121, 187–197.

Shand, R.D., 2000. Offshore migration of coastal sand-bars at Wanganui New Zealand. PhD thesis, Massey University, New Zealand. School of Global Studies, Miscellaneous Publication Series, 00/8 295pp.

Shand, R.D., Bailey, D.G., 1999. A review of net offshore bar migration with photographic illustrations from Wanganui, New Zealand. J. Coastal Res. 15 (2), 365–378.

Shand, R.D., Bailey, D.G., Shepherd, M.J., 1999. An inter-site comparison of net offshore bar migration characteristics and environmental conditions. J. Coastal Res. 15 (3), 750–765.

Short, A.D., 1993. Single and multi-bar beach change models. J. Coastal Res., Special Issue 15, 141–157.

Smith, R.K., Ovenden, R., 1998. Wanganui District Council Coastline Stability Investigation Between Kai Iwi and Harakeke. Report: WNG80202. National Institute of Water and Atmospheric Research Ltd, New Zealand, 32pp.

Tonkin, Taylor, 1978. Water Resources of the Wanganui River. A report prepared by Tonkin and Taylor, Consulting Engineers, for the Rangitikei–Wanganui Catchment Board, New Zealand, 167pp.

Wijnberg, K.M., 1995. Morphologic behaviour of a barred coast over a period of decades. PhD thesis, Utrecht University, the Netherlands, 245pp.

Wijnberg, K.M., Wolf, F.C.J., 1994. Three-dimensional behaviour of a multiple bar system. Proceedings of Coastal Dynamics'94. ASCE, New York, p. 59–73.

Wright, L.D., Short, A.D., 1984. Morphodynamic variability of surf zones and beaches: a synthesis. Mar. Geol. 56, 93–118.

`

Shand, R.D., 2002. Temporal variation in morphological configuration within a multi-bar surf zone at Wanganui, New Zealand. School of People, Environment and Planning, Massey University, New Zealand, Occasional Paper 2002/4, 41p.

Temporal variation in morphological configuration within a multi-bar surf zone at Wanganui, New Zealand

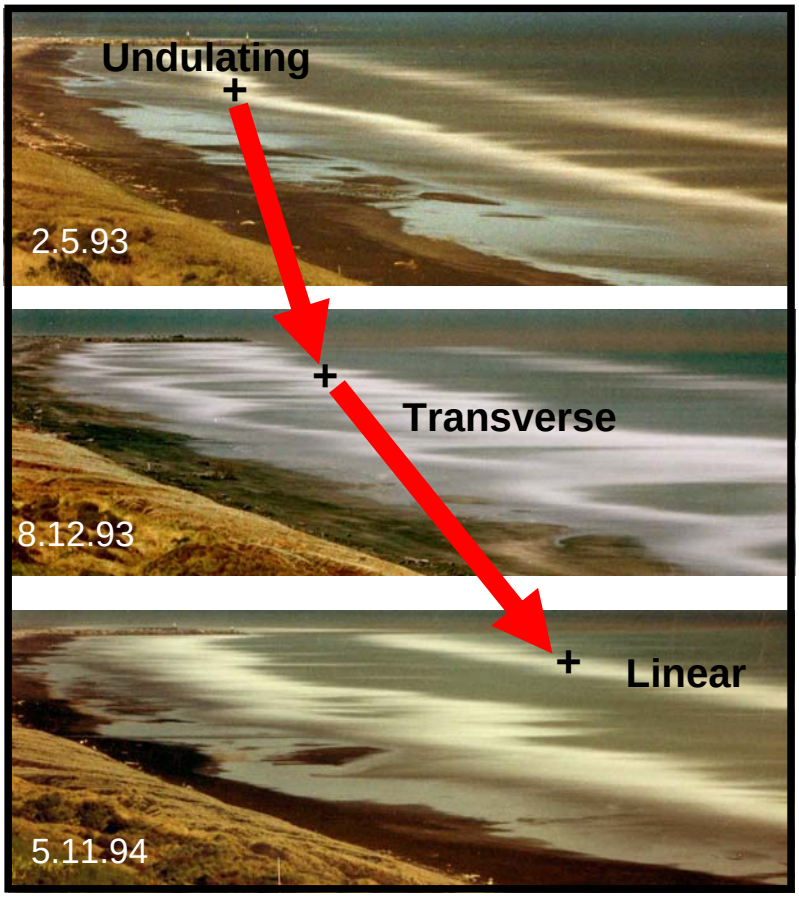

Roger D Shand
Geography Programme
Massey University
Palmerston North
New Zealand

School of People Environment and Planning
Occasional Paper 2002/4

Temporal variation in morphological configuration within a multi-bar surf zone at Wanganui, New Zealand

Roger D. Shand

Geography Programme
Massey University
Palmerston North
New Zealand

School of People Environment and Planning
Occasional Paper 2002/4

Cover Series of three time-lapse photographs in which the regions of higher intensity are caused by wave breaking; such areas represent elevated morphology such as sand bars. The red arrows illustrate the process of net offshore bar migration; a longer-term morphological behaviour which has recently been shown to characterise many multi-bar coasts. The terms *undulating, transverse* and *linear* refer to different (plan-view) morphological configurations which the bar undergoes during its offshore migration.

Abstract

This paper investigates morphological configuration (plan-view) change within the triple bar system at Wanganui on the southwestern coast of the New Zealand North Island. In particular, morphological variation associated with the inter-annual cycle of net offshore bar migration (NOM) is identified, and shorter-term configuration change (days to months) is also analysed and compared with the predominantly wave-driven conceptual beach-state model for multi-bar coasts developed by Short and Aagaard (1993). Configurations were derived by applying a mutually exclusive classification scheme to a 2 year, image-based, data-set.

A longer-term systematic change in configuration was found to occur as bars migrated seaward under the process of NOM. In particular, subdued bar configurations tended to predominate in both the landwardmost and seawardmost locations, while transverse, undulating and linear configurations predominate in turn with increasing distance offshore.

In the shorter-term, there was some general support for the model of Short and Aagaard, such as configurations becoming increasingly linear with increased distance seaward. However, analysis of the inner, mid and outer bars provided varying levels of agreement. The outermost bar, with its typically subdued configurations associated with NOM related bar degeneration, behaved in a manner which was mainly inconsistent with the model. While configurations and morphological behaviour of the middle bar system were largely in agreement with the Short and Aagaard model, modification is required to account for the frequently observed non-rhythmic morphologies. Inner bar configurations and behavioural characteristics were less consistent with the model, with results indicating that both longshore currents and tidal change associated with the neap tide/spring tide cycle, influence the morphodynamic system. The significance of tidal change comes despite the relative tide range at Wanganui being below the generally accepted threshold for tidal influence.

***Key words*: surf zone, beach-state models, offshore bars, net offshore bar migration**

1. Introduction

Sand-bars are found on many of the worlds sandy coasts and have both scientific and social importance. For example, the outer bar(s) cause large storm waves to break offshore, thereby influencing landward surf zone processes, and also reducing wave energy that may otherwise be available for shoreline erosion.

Bar morphologies vary in cross-shore geometry, bar number and morphological configuration (plan-view shape) depending on the environmental settings, i.e. the site-specific energy regime, sediment characteristics and physical boundary conditions (e.g. Carter, 1988; Hardisty, 1990; Komar, 1998). Of particular relevance to the present study are morphological configurations which occur on those coasts exposed to both swell and sea waves, and also characterised by lower tidal range and multiple sand-bars (in the cross-shore direction).

In a review of existing morphodynamic studies on multi-bar coasts, coupled with analysis of additional material from the southeastern coast of Australia, Short and Aagaard (1993) found that the morphological configurations were dynamic and ranged from linear bars (in the longshore direction), to crescentic forms (where longshore bars had a quasi-regular wave-like or undulating plan shape), and morphologies in which adjacent bars (in the cross-shore direction) tended to merge and produce transverse morphologies. In addition to the above terminology describing morphological configurations, a linear configuration may also be referred to as two-dimensional (2D) morphology as it can be defined by a single cross-shore profile. By contrast, non-linear morphologies may be referred to as three-dimensional (3D) as >1 cross-shore profile is required to define their configuration. Individual 3D morphological shapes may be referred to as 3D structure.

Short and Aagaard (1993) produced a multi-bar conceptual model for beaches with a lower tidal range. The model identified the morphological configurations likely to occur at different cross-shore locations, and it also incorporated sequential configuration changes. The authors refer to configurations as beach-states. The Short and Aagaard (1993) model has the following configuration-based characteristics:

- Non-linear configurations decrease, and linear configurations increase, with greater distance seaward;
- Configuration change in landward bars is more rapid than configuration change in seaward bars;
- The inner bar wavelength of non-linear structures is approximately half that of adjacent seaward structures, and nonlinear structures are predominately rhythmic with a mainly shore-normal orientation of axes;
- Under conditions of higher incident wave energy a sand-bar moves seaward and bar configuration becomes increasingly linear, while under conditions of lower incident wave energy a sand-bar moves landward and bar configuration becomes increasingly non-linear;
- Antecedent morphology influences system morphodynamics associated with inner bar change.

The model states that inner bar behaviour is analogous to the single-bar system as described in Wright and Short (1984). It is also noted that the Wright and Short (1984) and Short and Aagaard (1993) models relate aspects of beach morphology to edge waves at infragravity frequencies. This aspect of their models, however, is not considered in this paper.

There are limitations with the configurations changes in the Short and Aagaard (1993) model. For example, most of the field data consisted of annually sampled aerial photographs, so configuration sequences were inferred. Furthermore, the Short and Aagaard (1993) model does not take into account inter-annual cycles of net offshore bar migration which have been observed on some multi-barred coasts.

Net offshore bar migration (NOM) refers to the systematic seaward migration of coastal sand-bars across the surf zone (see Shand and Bailey, 1999, for review). Bars form near the shoreline and disappear several years later in the outer surf zone. Since the mid 1980s, NOM has been recognised on the North Carolina coast (e.g. Birkemeier, 1984; Lippmann et al., 1993), the Dutch coasts (e.g. de Vroeg et al., 1988, Kroon and Hoekstra, 1993; Ruessink and Kroon, 1994); at Wanganui, New Zealand (Shand, 1990; Shand and Bailey, 1999), and recently at Hasaki, Japan (Kuriyama and Lee, 2000). NOM has also been described as the offshore progression

cycle by Wijnberg (1996) and as inter-annual cyclic bar behaviour by Ruessink and Terwindt (2000).

While some morphological configuration studies have been carried out on coasts which experience NOM, e.g. Lippmann et al. (1993) at Duck North Carolina, Short (1992) along the coast of Holland, and Van Enckevort and Ruessink (2001) at Noordwijk on the coast of Holland, these works did not focus on associations between morphological configuration and the inter-annual NOM cycle. However, results from theses studies, together with those from other multi-barred coasts summarized in Short and Aagaard (1993), suggest that as a sand-bar progresses through its cycle of NOM and moves further offshore, the bar configuration will systematically change from a highly non-linear state within the inner surf zone, i.e. in the vicinity of the bar generation area, to a linear configuration in the outer surf zone, i.e. in the vicinity of the bar degeneration area.

The aim of the present study is to investigate temporal variation in morphological (plan-view) configuration by analysing a previously unused 2 yr image-based data-set collected from the multi-barred coast at Wanganui. The following nomclature will be adopted. Longer-term refers to morphological change associated with the inter-annual NOM cycle, while shorter-term refers to morphological change occurring at daily, weekly and monthly time-scales. The paper will test the following hypotheses:

- In the longer-term, a sand-bar undergoes a systematic change from a strongly three-dimensional to a two-dimensional configuration as it progressively crosses the surf zone under the process of NOM; and
- In the shorter-term, bar configuration behaves in the manner described by the Short and Aagaard (1993) beach-state model, hereafter referred to simply as the Short and Aagaard model.

The paper begins by describing the environmental conditions at the field site. This is followed by a description of the data acquisition and processing techniques used to obtain morphological data, configuration data, and wave height data. The results are then described and discussed.

2. Field Site

The 500 m long field site is ~3 km from the Wanganui Rivermouth on the southwestern coast of the North Island of New Zealand (Fig 1). While the shoreline is migrating seaward at ~1.5 m/yr in response to rivermouth jetty construction in the late 19th/early 20th century (Smith and Ovenden, 1998), this accretion is superimposed upon a regional erosion rate of approximately 0.3 m/yr (Johnston, 1985). The nearshore is characterised by fine sand (2 to 3 phi), and has a cross-shore slope of ~0.0085 and width of ~550 m. Three sand-bars are usually present; these bars undergo net offshore migration, with the mean life-cycle of a bar being ~3 yr (Shand et al., 1999). A foredune and cliff lie to the rear of the beach. The camera used for photographing the surf zone was located on top of the 42 m high cliff which lies 100 m behind the dune toe and 3200 m alongshore from the Wanganui Rivermouth.

The process conditions are summarized as follows. The mean neap tide range is 0.8 m and the mean spring tide range is 2.4 m. The mean deepwater significant wave height is 1.3 m and the 5% excedence value is 2.5 m (Macky et al., 1988). The mean wave period is 10.1 s (range 3.5 s to19 s) with sea wave conditions occurring for 75% of the time and swell waves for the remaining 25% (Patterson, 1992). Five years of daily wave observations, which encompassed the study period, show 42% of waves approach from the west, 24% from the south and 34% are shore-normal. Analysis of official wind data collected at nearby Wanganui Airport, show prevailing winds approach the coast at ~35 deg from the shoreline. The 5% excedence value for the wind speed is 12.4 m/s. The longshore wind component in the southeast direction occurs ~60% of the time, while the northwesterly directed wind component occurs for ~25% of the time.

3. Methods

This section describes how image-based morphological data and wave height data were obtained. The following subsections cover:

- the description of field collection and processing techniques used to derive rectified image data;

- the method used to determine the cross-shore location of bar-crests;
- the technique developed to identify morphological configurations;
- the collection of wave height data and the selection of a representative parameter.

3.1. Image data

A panorama of 4 photographs was needed to cover the 500 m long study area. Each photo was exposed for 4 mins to minimise tidal change experienced during sampling and to ensure a relatively stable representation of the breaking wave pattern. Such images are referred to as time-exposures and are equivalent to images produced by time- averaging video frames (Lippmann and Holman, 1989). These images provide an analogue for surf zone morphology because elevated topography such as sand-bars are characterised by locations of higher intensity due to waves breaking preferentially in shallower water (Lippmann and Holman, 1989). An example of a time-exposure panorama which encompasses the study site, is shown in the upper portion of Fig 2.

Field sampling was carried out during lower tide levels and higher wave conditions to maximise the likelihood of waves breaking on all bars. Furthermore, by limiting sampling (photography) to these conditions, the influences of wave height modulation and tide level on break-point location was minimised.

Digital image processing was used to rectify each photograph to ground co-ordinates and to merge this output with adjacent images from the panorama. To facilitate subsequent viewing and analysis, the coastline was then straightened using a further transformation. These image processing techniques have been described in detail by Bailey and Shand (1993, 1996). An example of the final output image is shown in the lower portion of Fig 2.

The 500 m length of coast used in the present study is marked in Fig 2. This length was selected as it was the maximum which provided equal coverage for all bars .Furthermore, it was considered likely to contain the morphological configurations likely to occur at the study site. A further 200 m segment of image was retained to each side (in the longshore direction) of this 500 m length to facilitate configuration identification near the margins of the study area. The remaining image,

beyond these interpretation segments, was cropped. In a further effort to minimise file size, the image seaward of 500m was also cropped. This latter cropping did not affect results as all bars located beyond 500 m were in a state of degeneration and had the same configuration type.

Morphological data used in this study was derived from a 2 yr set of time-exposure photographs collected between September 1992 and August 1994. Field sampling was carried out at ~4 day intervals (standard deviation = 2 days), and this resulted in 175 photographic samples. Such a sampling regime may not detect some of the linear morphology associated with higher energy conditions, because other studies, such as Lippmann and Holman (1990), found linear configurations could have residence times of shorter duration than the average sampling interval used in this study. However, more frequent sampling was carried out during times of higher energy in an effort to minimise this potential limitation.

While no bars completed a full cycle of NOM during the 2 yr sampling period, in combination, the set of bar-crest time-series cross the entire zone of systematic offshore migration (see Fig 3A). These data show that an inner, middle and outer bar occurred throughout the study period. Much of the analysis in this study is based on this tripartite arrangement. To illustrate how the higher resolution two year data fits within the associated cycles of NOM, a longer-term monthly bar-crest location data-set is depicted in Fig 3B.

3.2. Cross-shore bar location

Intensity maxima only approximate a bar-crest location as environmental conditions such as sea-level and incident wave height, together with bar-crest depth and bar form, influence break-point location (Plant and Holman, 1998). The different approaches used to quantify and eliminate or minimise these factors, have recently been reviewed in Shand (in press). The combined error increases with increased distance from the camera with maximum errors (using the 95 % confidence interval) at the margins of the study area being 15 m in the cross-shore direction and 12 m in the longshore direction (Shand, 2000).

The cross-shore distance used to define the location of a bar-crest is identified by fitting a parabola to the cross-shore intensity profile, and then determining the distance corresponding to the parabola maximum. This procedure works satisfactorily for well defined bar-crests; however, the following problems occur toward both the landward and seaward extremes of the surf zone. During advanced bar degeneration, wave breaking can result in a patchy intensity pattern (Shand, in press). Within the inner surf zone, bar-crests may be nearly (or completely) exposed during sampling and this can result in minimum intensity values corresponding to the crest. In addition, light reflection off water within the landward trough can result in maximum intensity values, rather than the expected minimum values. All bar-crest and trough locations were therefore identified after first inspecting the original photographs.

To identify a single cross-shore distance to represent a 500 m longshore length of bar-crest, the intensities were first averaged in the longshore direction and then the parabola fitting routine was applied. This procedure was used to derive the data points plotted in Fig 3.

To identify a continuous longshore bar-crest line, referred to as a barline, the parabola fitting routine was repeated for adjacent cross-shore segments which were 10 m wide in the longshore direction.

After eliminating samples where morphology could not be confidently identified, there were 30 outer bar samples, 129 middle bar samples, and 160 inner bar samples. The lower sample number with increasing distance offshore is the result of waves breaking less often further offshore due to increasing water depth.

3.3. Determining morphological configuration

Because 3D surf zone morphology has such a wide variety of forms, representative configurations are often used in its analysis. Identification of such configurations has typically been made by observing a series of samples and abstracting (by observation) a sequence of configurations, e.g. Davis and Fox, (1972), Goldsmith et al. (1982), Sasaki (1983), Sonnenfeld and Nummedal (1987), Aagaard (1991), Bogle et al. (1999). More objective approaches involve the application of classification procedures based either on observed morphological assemblages, e.g. Wright and

Short (1984), Short and Aagaard (1993), or on shape-based criteria, e.g. Chappell and Elliot (1979), Lippmann and Holman (1990). A combination of these two approaches has also been used, e.g. van Enckevort and Ruessink (2001). While user subjectivity enters both types of classification technique, it is minimised by specifying a range of qualifiers (see below). In addition, the shape-based classification approach results in classes which are mutually exclusive, whereas the morphological assemblage-based approach may be unable to assign some configurations to a single class.

More recently, the alternative techniques incorporating an increased level of quantification, have been used to analyse 3D configurations. Ruessink et al. (2000) analysed barlines using complex eigenfunctions, and van Enckevort and Wijnberg (1999) analysed the deviations between the barline and a fitted linear model. While both approaches provide useful information, they are limited by a requirement for longshore uniformity in the length scales of 3D structures. Furthermore, they are unable to process some complex 3D morphologies which may occur within the inner surf (e.g. Goldsmith et al., 1982, Bogle et al., 2000), or the intensity patterns which signal bar degeneration. Because most non-linear 3D structures at Wanganui have complex plan-forms, and as the present study is to include bars across the entire surf zone, a mutually exclusive classification scheme based on the Lippmann and Holman (1990) approach was developed.

The following three criteria, and associated binary decisions shown within brackets, were used to categorise different intensity patterns (morphological configurations):

- cross-shore bar profile relief (pronounced c.f. subdued);

- longshore variability (linear c.f. non-linear) of a barline;

- longshore variability (continuous c.f. discontinuous) of a trough, where a trough is represented by a discernable region of low intensity values located landward of a bar. Shand (in press) has shown that such an intensity pattern is consistent with bathymetrically defined longshore (bar and) trough topography.

The following qualifiers were used to ensure consistency in allocating samples to configuration classes:

- A pronounced (c.f. subdued) bar profile was defined as having a landward trough;

- Linear (c.f. non-linear) configurations were defined to occur where barline amplitudes, i.e. cross-shore deviations from a linear model fitted to the structure's barline, were less than 5 m. This threshold appeared to visually separate linear from non-linear configurations.

- Discontinuous (c.f. continuous) troughs were defined to occur when an area of high intensity values filled, or substantially filled, the trough; such an area signaling significant sediment accumulation.

This classification scheme resulted in 5 configuration types (A – E), as depicted in Fig 4. However, upon application, type C was found to be difficult to distinguish from type E, so they were combined. It is noted that Lippmann and Holman (1990) did not include a class with type C characteristics. Four classes were therefore used to represent morphologies contained within the image data-set. These morphological classes are identified using the following descriptors: subdued, linear, undulating and transverse. Examples of these configuration types are shown in Fig 5.

It is noted that two distinct high intensity patterns met the subdued class characteristics. These patterns were located in the outer and inner surf zones, so they were referred to as outer subdued and inner subdued respectively. Inner subdued configurations had the appearance of either an area containing very low amplitude undulatory features or a wide low tide terrace, extending seaward from the beachface.

The Lippmann and Holman (1990) classification scheme also included scaling criteria which separated smaller (10^{1} m) morphological features, referred to by the authors as incident-scaled, from larger ($10^{2\text{-}3}$ m) features, referred to as infragravity-scaled. These scalings appear to separate foreshore features from nearshore features. In the present study, only those sand-bars which subsequently underwent NOM were

studied; in all cased such bars formed when crest distances were greater than 10^2 m from the dune-toe, so cross-shore scaling-based criteria were not required.

The 4 configuration classes used for the present study are broadly similar to the morphological configurations used in the two key morphological classification studies, i.e. Wright and Short (1984), and Lippmann and Holman (1990), and this is depicted in Fig 6. The main difference lies with their inclusion of regularity characteristics for non-linear structures. This level of detail was not included within the classification scheme in the present study, because 89% of 3D structures at Wanganui were irregular (defined later). However, statistics describing the geometry of 3D structures is included within the results section.

Because different types of configuration could occur contemporaneously at different locations along the 500 m long study site, the modal class for each sample, i.e. the class with the greatest longshore length, was used for analysis. A further requirement for assigning the modal class incorporated classification errors which could occur under the range of wave and tidal conditions experienced during sampling. Errors of up to 100 m were observed in the (longshore) length assigned to a particular class, so modal class status was only assigned when the length was at least 100 m greater than that of any other configuration class present within a sample. Following these procedures, 26 outer bar samples, 111 middle bar samples and 125 inner bar samples were available for subsequent analysis.

3.4. Wave data

Wave height data used to test whether morphological configurations at Wanganui change as predicted by the Short and Aagaard model, consisted of daily observations made using the 'staff and horizon' method described in Patterson and Blair (1983) and Horikawa (1988). This technique measures wave height at the break-point and has been shown to provide an accurate record of relative wave height (Patterson, 1985). The Wanganui data used in the present study were part of a 3439 day record which had a mean value of 1.4 metres and the 5% excedence value of 2.6 m; these values are close to the deepwater significant wave height statistics reported earlier (1.3 m and 2.5 m respectively).

The selection of a wave-based parameter was made after considering the following studies which analysed morphological change within the surf zone. Lippmann et al. (1993) tested a range of wave parameters and found they all "behaved in a similar manner when correlated with morphology" (p11,583). Thereafter, Lippmann used the daily maximum significant wave height. Sunamura and Takeda (1993) analysed profile data collected at fortnightly intervals and used the inter-survey maximum significant wave height value because "topographic change is most sensitive to larger waves during the interval between surveys" (p138). In contrast, Larsen and Kraus (1992) used the mean inter-survey significant wave height when analysing fortnightly profile data; however, wave heights were only included in their analysis "where significant changes had occurred between profile surveys" (p60). It is further noted that the present study is not concerned with identifying threshold wave height values associated with morphological change, rather, it is concerned with the identification of relative wave heights associated with such morphological change. Based on the above results and arguments, the inter-survey maximum (daily) wave height was selected as the wave-based parameter for use in this study.

4. Results

This section begins by describing bar-crest location and morphological configuration data. The characteristics of 3D structures are then described and this is followed by configuration sequences for the 5 bars which occurred during the study period. Finally, associations between morphology and corresponding wave height data are identified.

4.1. Description of data

Time-series depicting the cross-shore migration and modal configuration classes associated with each bar are shown in Fig 7. The bars have been chronologically numbered from the oldest (bar 1) to the youngest (bar 5). The time-series in Fig 7A, show that, with the exception of bar 1 which was in the final stage of degeneration, an underlying offshore migration trend characterised bar behaviour during the study period. Linear regression analysis show the NOM process explained 53%, 83.2%, 72.9% and 88.6% of the cross-shore migration associated with bars 2, 3, 4 and 5 respectively. Shorter-term bar migration accounts for the remaining variance.

The underlying process of NOM resulted in the cross-shore status of bars, i.e. inner, middle or outer, changing as they systematically migrated across the surf zone. The development of two new bars (4 and 5) can be seen in Fig 7A to correspond with the disappearance of previously existing outer bars (1 and 2 respectively). This type of bar behaviour is a typical characteristics of NOM systems (e.g. Lippmann et al., 1993, Ruessink and Kroon, 1994; Wijnberg, 1996; Shand and Bailey, 1999). The occurrence of a new bar was taken to be from the time a pronounced form was first observed.

Histograms showing the cross-shore distribution for each type of morphological configuration are depicted in Fig 8. The subdued configurations are bimodal, with this configuration type only occurring for inner and outer bars. The results show (inner) subdued configurations tended to be closest to shore, with transverse, undulating, linear and (outer) subdued configurations each being located further seaward.

The frequency (percentage) of each type of configuration for inner, middle and outer bars are depicted in Fig 9. These data show that the inner bar experienced all 4 types of configuration with transverse occurring most frequently (55%), followed by undulating (17%), subdued (15%) and linear (13%) . Middle bars were predominantly characterised by undulating (47 %) and linear configurations (51%). Two occurrences (2%) of transverse configuration were observed for middle bars, these were both associated with the process of bar splitting (Shand and Bailey, 1999). The outer bar configuration was dominated by subdued morphology (73%) with linear configurations accounting for the remaining 27% of observations

The residence time, i.e. the persistence, of each type of configuration for the inner, middle and outer bars are depicted in Fig 10. The inner bar results indicate that transverse configurations were the most persistent (mean = 12.6 days) followed by subdued (mean = 9.25 days), linear (mean = 5.7 days) and undulating (mean = 5.2 days). These transverse and undulating values are similar to those reported for the inner bar at Duck, North Carolina (Lippmann and Holman, 1990). However, the linear value is 2-3 times higher than the Duck value and, as noted earlier, may reflect under-sampling at Wanganui.

As with the inner bar results for Wanganui, the middle bar had similar persistence means for undulating configurations (12.5 days) and linear configurations (13.6 days), but magnitudes were 2-3 times lower. The mean for middle bar transverse configurations (3.0 days), was substantially lower than the inner bar value.

Outer bar residence times for linear configurations (mean = 62 days) were several times longer than the corresponding landward bar value, and subdued configurations (mean = 100 days) were the most persistent of all. While low sample size (linear = 2, subdued = 5) may bias outer bar results, the individual values in each sample were all higher than the means for the corresponding landward classes; this offers qualitative support for the validity of the outer bar results.

With the exception of transverse configurations, the results in Fig10 show residence times lengthened, and hence the configurations became increasingly stable, with increasing seaward distance. Finally it is noted that there was, in general, a large amount of within-class variability in residence times, this being indicated by the high standard deviation values compared with the mean values. This characteristic was also evident in the results from Duck (Lippmann and Holman, 1990).

4.2. Geometry of 3D structures

The wavelength, regularity and orientation of 3D structures are summarised in Table 1. These values were obtained from images sampled at monthly intervals as these data had greater longshore coverage and this enabled 3D structures with wavelengths extending beyond the study area to be included in the analysis. Each structure was identified from the associated barline. Average wavelength was determined for inner, middle and outer bars. The results in Table 1A, show the wavelength of 3D structures within the inner bar system (mean = 147 m, range = 40 to 450 m) to be approximately half those of the more seaward (middle) bar system (mean 279.7 m, range 70 to 750 m). The outer bar rarely contained 3D structures and the 3 occurrences were all in the range of 200 to 270 m.

Regularity (rhythmicity) was defined to occur when a barline had similar values for all wavelengths and for all amplitudes. Visual comparison suggested that

wavelengths appeared regular when variations were no greater than +/- 10% of the mean value, while amplitudes appeared to be similar when variations were no greater than +/-25% of the mean value. These values were therefore used to discriminate between regular and non-regular structures. The results in Table 1B, show that 3D structures were predominantly irregular, with values of 86.4% for the inner bar and 92% for the middle bar.

Orientation of 3D structures was based on the direction of the axes of rip channels or larger-scaled 3D features. Where several structures occurred along the same barline, the modal orientation was adopted. The following 4 groups were used: axis oblique toward the northwest; axis shore-normal; axis oblique toward the southeast; and no modal orientation. The results in Table 1C, show the orientation of 3D structures to be a function of cross-shore distance with the majority (68.8%) of inner bar axes being offset to the southeast, while the majority (76.5%) of middle bar axes were shore-normal.

4.3. Configuration sequences

The sequence of configurations associated with each bar, as depicted in Fig 7B-F, are now described.

- Bar 1 was only evident during the initial 3 months of the study period; during that time the morphological configuration was subdued.

- Bar 2 existed for all but the final 3 months of the study. For the initial 8 months, the configuration was predominantly linear (91%). The bar configuration then changed to subdued as the bar degenerated. This process appeared to have been completed 3 months before the end of the study period as there was no intensity signal during that time.

- Bar 3 existed throughout the study, being the inner bar for the first three months, the middle bar for the following 18 months and the outer bar for the final 2-3 months. The predominant configuration during the initial month was transverse with the configuration then fluctuating between undulating and linear as the bar migrated across the mid surf zone. During the final months of

the study the configuration was subdued.

- Bar 4 formed within the inner surf zone at approximately the same time that bar 1 disappeared from the outer surf zone. It then spent the following 18 months as the inner bar; during this time the predominant configuration was transverse (60%), with both undulating and subdued configurations occurring in 17% of the observations, and linear occurring for the remaining 6%.

- Bar 5 only existed for the final three months of the study, its formation coinciding with the disappearance of bar 2. During that time, all 4 types of bar configuration occurred with transverse predominating (65%), then linear (21%) and both undulating and subdued configurations in 7% of observations.

4.4. Wave height associations

When investigating the relationship between bar migration and wave height, the following procedure was followed. Each barline was represented by a single cross-shore distance; this was achieved by longshore intensity averaging as described earlier. Such averaging removes the component of cross-shore bar migration associated with the longshore translation of 3D structures, a process induced by longshore currents and observed to occur at Wanganui. Ruessink et al. (2000) have shown that such longshore translation can dominate the cross-shore bar migration signal at shorter-time scales. To minimise the effect of survey inaccuracies and to increase the likelihood of identifying statistically significant relationships between morphological behaviour and wave height, only those samples for which cross-shore migration was equal to, or greater than, 10 m (in either the landward or seaward direction) were considered. Furthermore, data were only used where the sampling interval was lower than, or equal to, 10 days. No outer bar data met these sub-sampling requirements.

Graphs depicting cross-shore bar migration versus maximum inter-survey wave height for inner bar and middle bar locations, are shown in Figs 11A and B respectively. Linear models have been fitted to each set of data points. The correlation coefficient (r) which quantifies the level of association between 2 variables, together with the probability (p) of such an association having arisen by chance alone, are marked on each graph. Furthermore, the F-ratio and associated probability, which

relates to whether the slope of a linear regression line approaches zero, are also shown. The inner bar results (Fig 11A) show no significant association between wave height and cross-shore bar migration with $r = 0.189$ and $p >> 0.1$. However, a highly significant association did occur for the middle bar (Fig 11B) with $r = 0.700$ and $p << 0.001$. These results show that in the case of the inner bar, 3.8% of the cross-shore variation was explained by changes in wave height, while 49% of the variation was explained for the middle bar.

To identify possible associations between morphological configuration change and wave height, the maximum inter-survey wave height corresponding to each configuration change to a particular class, were obtained. The means and standard deviations for such wave heights associated with inner bar class changes and middle bar class changes are shown in Figs 12A and B respectively. Two-sample t-tests were used to determine if the differences in the wave heights corresponding to these different configuration changes, were significant. Table 2 lists the t-values with bold and thin underlining used to denote significant differences at the 5% ($p = 0.05$) and 10% ($p = 0.1$) levels respectively. It is noted that the t-test assumption requiring samples be normally distributed, was met in all cases as the skewness coefficient values were non-significant (ratio of skewness to the standard error of skewness <2): this being a sufficient condition for normalicy in small samples according to Wilkenson (1998).

The inner bar results (Fig 12A) show similar mean wave heights corresponding to class changes to transverse (1.94 m) and subdued (2.01 m) configurations, but relatively higher mean values for class changes to increasingly linear configurations: 2.42 m for undulating and 2.61 m for linear. The t-test results (Table 2) show that the probability (p) of different wave heights associated with morphological change to transverse and to subdued classes was insignificant. However, the t-test results do show a significant wave height difference firstly between change to the transverse and change to undulating configurations, and secondly between change to transverse and change to linear configurations. The difference between undulating and linear configurations was not statistically significant ($p = 0.339$); however, this may reflect small sample size ($N = 5$ for linear) rather than lack of relationship.

As with the inner bar, the middle bar results (Fig 12B) also show the mean wave height associated with change to undulating configurations (2.16 m) was less than the mean heights associated with changes to linear configurations (2.36 m). While the t-test probability ($p = 0.220$) showed an increased likelihood of a wave height difference compared with the inner bar data, the result was still not statistically significant.

Finally, the possibility of antecedent morphology within the inner bar system influencing configuration change (within the inner bar system) was tested by comparing the inter-survey maximum wave heights associated with periods when configuration change occurred (Fig 12A), with the wave heights corresponding to periods when no change occurred (Fig 13). Only transverse configurations showed a statistically significant difference ($t = -2.271$, $p= 0.036$) which indicate such configurations could endure wave heights which were associated with class change to undulating or linear configurations. Strongly non-linear configurations at Wanganui therefore do appear to influence inner bar morphodynamics.

5. Discussion

The frequency results in Figs 8 and 9 suggest that bars at the study site undergo a systematic change in configuration as they migrate seaward under the process of NOM. However, to confirm such a change, the trend must be observed in the configuration time-series for each bar. Data depicted in Figs 7B-F, show that each bar systematically changed its configuration such that (inner bar) subdued changed to transverse, transverse to undulating, undulating to linear and linear to (outer bar) subdued with increasing distance from the shore.

It is noted that the configuration time-series (Figs 7B-F) show initial pronounced morphologies of newly generated bars (bars 4 and 5) were either of undulating or linear configuration rather than transverse which dominated the more shoreward inner bar locations (Fig 9). Neither undulating nor linear configurations developed from widening and deepening of smaller-scaled runnels which were observed to occur on the lower foreshore in ~20% of samples. It is also noted that the formation of bar 4

followed the landward progression of an inner bifurcate associated with double bar development on bar 3 (this process is depicted in Shand and Bailey (1999) Fig 6). In contrast, bar 5 developed upon a previously subdued foreshore morphology.

Comparison between the shorter-term results for Wanganui and the characteristics of the Short and Aagaard model (as itemised in the introductory section), are summarised in Table 3. Excluding the outermost surf zone, an increase in linear (non-linear) configurations with increasing (decreasing) distance seaward, does occur at Wanganui (Fig 9). The predominance of subdued configurations in the outer surf zone differed from the model. This may reflect the inability of aerial photos (the typical data-source for the multi-bar studies) to detect advanced bar degeneration, and/or the Short and Aagaard data-base did not include many beaches that are subject to the NOM process.

Determination of whether or not configuration change is more rapid when bars are located closer to the shore was difficult using the Wanganui data for the following reason. A configuration change was defined to occur when a change in modal class occurred. The interval between two relevant samples therefore controls the rate at which configuration class change can be detected. However, class residence times (Fig 10) provide a measure of relative configuration stability and this indicates the relative ease with which class change occurs at different cross-shore locations. The results in Fig 10, therefore suggest that configurations change more slowly with increasing seaward distance, in accord with the Short and Aagaard model.

The Wanganui results were consistent with the Short and Aagaard model characteristic that the wavelength of 3D structures in the landward position is approximately half that of the adjacent seaward bar (Table 1A). However, coupling between inner and middle bar configurations was only observed in 21% of samples. Furthermore, the additional requirement that configurations be predominantly rhythmic (regular wavelength and amplitude) was only met in 13.6% of inner bar samples and 7.1% of middle bar samples (Table 1B). This highly irregular nature of the 3D structures at Wanganui, together with the predominance of obliquely orientated axes within the inner bar system (Table 1C), suggest that longshore

currents play a more important morphodynamic role here than at the sites upon which the Short and Aagaard model was based.

While cross-shore bar migration for the inner bar (Fig 11A) showed no statistically significant association with wave height, highly significant results consistent with the Short and Aagaard model, did occur for the middle bar (Fig 11B). In the latter case wave height was able to explain 48.6% (i.e. $r^2 = 0.486$) of the variation in bar migration, and the F-ratio ($p < 0.005$) and positive correlation coefficient ($r = +0.697$) show that offshore migration occurred under higher wave conditions and onshore migration under lower wave conditions. These results are qualitatively similar to those observed at other multi-bar sites; for example, van Enckevort (2001) found that direct wave forcing was of subordinate importance for an inner bar compared with a more seaward bar in a 3.4 yr study at Noordwijk on the coast of Holland. These results support the claim that the seaward bar(s) act as a filter of incident wave energy, a possibility raised by several other workers in relation to multi-bar systems (e.g. Lippmann et al., 1993; Ruessink and Kroon, 1994; Ruessink and Terwindt, 2000). It may be an oversimplification to describe inner bar behaviour as analogous to single bar systems, as is done in the Short and Aagaard model.

Different wave conditions did broadly relate to changes in morphological configurations (Fig 12) in a manner consistent with the Short and Aagaard model, in that the occurrence of increasingly (decreasingly) linear configurations were associated with increasing (decreasing) wave height. However, inner bar change to subdued configurations occurred under the same (relatively low) wave conditions that accompanied changes to transverse configurations. This situation will now be considered further.

The occurrence of both transverse and subdued configurations under lower wave conditions, suggest that tidal influence may significantly affect shorter-term morphodynamic processes at Wanganui. The ability of tidal change, i.e. changing water depth, to influence sediment transport processes and seabed morphology is well recognised in both the theoretical (e.g. Davidson-Arnott 1981; Dally and Dean, 1984; Hedegaard et al., 1991) and empirical (e.g. King, 1972; Carter, 1988; Short, 1991) literature. Briefly, tides cause the wave break-point, together with the swash, surf and

shoal zones, to translate back and forth across the profile thereby controlling the nature and duration of sediment transport processes at different cross-shore locations. Lower tidal range enables distinct bar features to evolve, whilst larger tidal range retards bar development and more uniform and subdued morphologies occur. Existing beach-state models such as Wright and Short (1984), and Short and Aagaard (1993), assume micro-tidal conditions with upper limits of 2 m (Wright and Short, 1984) or 3 m (Short, 1991). However, beach morphology is not simply dependent upon tidal range, but rather is the product of the interaction between tide and wave conditions (Davis and Hayes, 1984). This has led to the use of the ratio of (spring) tide range to (modal breaking) wave height, termed the relative tide range (RTR), as a more appropriate tide-based parameter. In a simulation study into the effects of tide on beach morphodynamics, Masselink (1993) found that when RTR <2, the effect of tide could be excluded and the beach-state models of Wright and Short (1984) and Short and Aagaard (1993) applied. When the RTR was >2, shoaling wave processes became increasingly dominant and more subdued morphologies occurred. In a field-based study, Masselink and Short (1993) found that, in general, when RTR < 3 beaches may be classified using these beach-state models.

At Wanganui the spring tide range is 2.4 m and the RTR is 1.85 m, so the lower tide range models should apply. However, the subdued inner bar configurations identified in the present study, suggests that variation in tidal range, i.e. the change between neap and spring tides, may be morphodynamically important. The hypothesis that subdued configurations for the inner bar occur under higher tidal range, while prounced configurations (transverse, undulating and linear) occur under lower tidal range, was tested using Wanganui data.

The tidal range corresponding to each of the maximum inter-survey wave heights used in the wave height/modal configuration analysis (Fig 12A), were obtained and the mean and standard deviation values for each configuration determined (see Fig 14). Tide data were derived from predicted tide heights prepared by the Hydrographic Branch of the Royal NZ Navy; for Wanganui these predictions have an RMS error of 0.13 m. A random error of this magnitude would not affect the results as the analysis was based on the mean tidal values. The results depicted in Fig 14 show similar tide ranges occurred during changes to all three of the pronounced types

of configuration, with t-values having $p>0.376$. However, there was a significant difference between subdued and pronounced configurations with t-values having $p< 0.034$. These results therefore support the tidal range/configuration change hypothesis.

The results in Figs 12A and 14 suggest that while transverse and subdued configurations can form under similar (relatively low) wave conditions, they form under contrasting tidal range conditions. Transverse configurations required relatively low (c. neap) values while subdued configurations required relatively high (c. spring) values. While breaking wave-associated processes may be the dominant forcing agent when the RTR < 2 (Masselink, 1993), or <3 (Masselink and Short, 1993), the Wanganui results suggest that tidal influence can still play an important morphodynamic role.

6. Conclusion

A configuration (plan-view) analysis was carried out on a 2 year image-based data-set of the triple bar system at Wanganui. The following configuration preferences occurred: inner bar configurations fluctuated between transverse, undulating, linear and subdued; middle bar configurations fluctuated between undulating and linear; and outer bar configurations were either linear or subdued. A longer-term systematic change in configuration was found to occur as bars migrated seaward under the process NOM. In particular, subdued bar configurations tended to dominate the landwardmost and seawardmost locations, while transverse, undulating and linear configurations predominate in turn with increasing distance offshore.

In the shorter-term, there was some general support for the predominantly wave-driven model of Short and Aagaard, such as configurations becoming increasingly linear with increased distance seaward. However, analysis of the inner, mid and outer bars provided varying levels of agreement. The outermost bar, with its predominantly subdued configurations associated with NOM related bar degeneration, behaved in a manner which was mainly inconsistent with the model. While configurations and morphological behaviour of the middle bar system were largely in agreement with the Short and Aagaard model, modification is required to account for the frequently

observed non-rhythmic morphologies. Inner bar configurations and behavioural characteristics were less consistent with the existing model, with results indicating that both longshore currents and tidal change associated with the neap tide/spring tide cycle, influence the morphodynamic system. The significance of tidal change comes despite the relative tide range at Wanganui being below the generally accepted threshold for tidal influence. Development of an inner bar beach-state model for coastal environments such as that found at Wanganui, is the subject of a further paper (Shand et al., in prep).

Acknowledgements

This study was supported by the Massey University Research Fund, a Vice-Chancellors Special Grant and Research Fellowship (contract MAUX0104) from the New Zealand Foundation for Science and Technology. The author thanks Drs Mike Shepherd (Massey University), Patrick Hesp (Louisiana State University), and Gerben Ruessink (Utrecht University) for their useful comments on the manuscript.

References

Aagaard, T., 1991. Multiple-bar morphodynamics and its relation to low-frequency edge waves. *Journal of Coastal Research* 7(3), 801-813.

Bailey, D.G., and Shand, R.D., 1993. Determining large-scale sand bar evolution. *Proceedings of the First New Zealand Conference on Image and Vision Computing*, pp. 109-116.

Bailey, D.G., and Shand, R.D., 1996. Determining large-scale sand bar behaviour. *Proceedings of the IEEE International Conference on Image Processing*, Lausanne, Switzerland, (2), 637-640.

Birkemeier, W.A., 1984. Time scales of nearshore profile change. *Proceedings of the 19th International Conference on coastal Engineering*, ASCE, pp. 1507-1521.

Bogle, J.A.; Bryan, K.R.; Black, K.P.; Hume, T.M., and Healy, T.R., 1999. Observations of geomorphic parameters using video images. *Proceedings of the 14th Australasian Coastal and Ocean Engineering Conference and the 7th Australasian Port and Harbour Conference*, Perth, Australia, pp. 70-75.

Bogle, J.A.; Bryan, K.R; Black, K.P.; Hume, T.M., and Healy, T.R., 2000. Video observations of rip formation and evolution. *Journal of Coastal Research, Special Issue 34*, 117-127.

Chappell, J., and Eliot, I.G., 1979. Surf-beach dynamics in time and space - an Australian case study, and elements of a predictive model. *Marine Geology*, 32, 231-250.

Carter, R.W.C., 1988. *Coastal Environments: An Introduction to the Physical, Ecological and Cultural Systems of Coastlines*. Academic Press, London, 611p.

Dally, W.R., and Dean, R.G., 1984. Suspended sediment transport and beach profile evolution. *Journal of Waterway, Port, Coastal and Ocean Engineering*, 110(1), 15-33.

Davidson-Arnott,R.G.D., 1981. Computer simulation of nearshore bar formation. *Earth Science Processes and Landforms* 6, 23-34.

Davis, R.A., and Fox, W.T., 1972. Four-dimensional model for beach change and inner nearshore sedimentation. *Journal of Geology*, 80, 484-493.

Davis, R.A., and Hayes, M.O., 1984. What is a wave-dominated coast? *Marine Geology*, 60, 313-329.

De Vroeg, J.H.; Smit, E.S.P., and Bakker,W.T., 1988. Coastal Genesis. *Proceedings of the 21st International Conference on coastal Engineering*, ASCE, pp. 2825-2839.

Goldsmith, V.; Bowman,D., and Kiley, K., 1982. Sequential stage development of crescentic bars: Hahoterim beach, southeastern Mediterranean. *Journal of Sedimentary Petrology*, 52, 233-249.

Hardisty, J., 1990. *Beaches: Form and Process*. Unwin Hyman, London, 319p.

Hedegaard, I.D.; Deijaard, J., and Fredsoe, J., 1991. Onshore/offshore sediment transport and morphological modeling of coastal profiles. *Proceedings of Coastal Sediments'91,* ASCE, pp. 643 -657.

Johnston, R.M.S., 1985. Coastal change and hazard delineation on the Rangitikei-Wanganui coast. *Proceedings of the 8th Australasian Conference on Coastal and Ocean Engineering*, pp. 411- 420.

King, C.H.M., 1972. *Beaches and Coasts*. Butler & Tanner Ltd., 570p.

Komar, P. D., 1998. *Beach Processes and Sedimentation*, New Jersy,Prentice-Hall, Inc.

Kroon, A., and Hoeskstra, P., 1993. Nearshore bars and large-scale coastal behaviour. In: List, J.H., (ed.), *Large- Scale Coastal Behaviour '93*. U.S. Geological Survey, Open- File Report 93-381, pp. 92-95.

Kuriyama, Y., and Lee J.H., 2001. Medium-term beach profile change on a bar-trough region at Hasaki, Japan, investigated with complex principal component analysis. *Proceedings of Coastal Dynamics'01,* ASCE, pp. 959-968.

Larsen, M., and Kraus, N.C., 1992. *Analysis of cross-shore movement of natural longshore bars and material placed to create longshore bars.* Technical Report CERC DRP-29-5, 115p.

Lippmann, T.C., and Holmam, R.A., 1989. Quantification of sand-bar morphology: a video technique based on wave dissipation. *Journal of Geophysical Research*, 94, 995-1011.

Lippmann, T.C., and Holmam, R.A., 1990. The spatial and temporal variability of sand-bar morphology. *Journal of Geophysical Research*, 95, 11,575-11,590.

Lippmann, T.C. Holman, R.A. and Hathaway, K.K., 1993: Episodic, non-stationary behaviour of a double bar system at Duck, North Carolina, U.S.A., 1986-1991, *Journal of Coastal Research, Special Issue 15*, 49-75.

Macky, G.H.; Cumming. R, J., and Valentine, E. M., 1988. *Measurements of ocean wave climate at Wanganui and Himitangi Beach.* Hydrology Centre, Departmemt of Scientific and Industrial Research, Christchurch New Zealand.

Masselink, G., 1993. Simulating the effects if tides on beach morphodynamics. *Journal of Coastal Research, Special Issue 15*, 180-197.

Patterson, D.C., and Blair, R.J., 1983. Visually determined wave parameters. *Proceedings of the Sixth Australian Conference on Coastal and Ocean Engineering*, Gold Coast, Australia, pp. 151-155.

Patterson, D.C., 1992. *Wanganui Port development feasibility studies: coastal engineering aspects.* A report for Ocean Terminals and the Wanganui District Council, New Zealand, 51p.

Plant, N.G., and Holman, R.A., 1998. Extracting morphologic information from field data. *Proceedings of the 26th International Conference on Coastal Engineering*, ASCE, pp. 2773-2784.

Ruessink, B.G. and Kroon, A., 1994: The behaviour of a multiple bar system in the nearshore zone of Terschelling, the Netherlands: 1965-1993, *Marine Geology*, 121, 187-197.

Ruessink, B.G., and Terwindt, J.H.J., 2000. The behaviour of nearshore bars on a time scale of years: a conceptual model. *Marine Geology*, 163, 289-302.

Ruessink, B.G., van Enckevort, I.M.J.; Kingston, K.S., and Davidson, M. A., 2000. Analysis of observed two- and three-dimensional nearshore bar behaviour. *Marine Geology*, 169, 161-183

Sasaki, T., 1983. *Three-dimensional topographic changes on the foreshore zone of sandy beaches.* University of Tsukuba: Institute of Geoscience, Science Report A-4, pp. 69-95.

Shand, R.D., 1990. *The subaqueous morphology at the entrance to a jetty controlled river mouth on a moderate to high energy littoral drift dominated coast: Wanganui New Zealand 1981-1987.* Research project: post graduate diploma in science, Massey University, New Zealand, 102p.

Shand, R.D., 2000. *Offshore migration of coastal sand-bars at Wanganui New Zealand.* PhD thesis, Massey University, New Zealand. School of Global Studies, Miscellaneous Publication Series, 00/8, 295p.

Shand, R. D., (in press). Relationships between bar bar switching, cross-shore bar migration and outer bar degeneration at Wanganui, New Zealand. *Journal of Coastal Research ???*

Shand, R.D. and Bailey, D.G., 1999: A review of net offshore bar migration with photographic illustrations from Wanganui, New Zealand, *Journal of Coastal Research,* 15(2), 365-378.

Shand, R.D.; Bailey, D.G., and Shepherd, M.J., 1999. An inter-site comparison of net offshore bar migration characteristics and environmental conditions. *Journal of Coastal Research*, 15(4) 173-202.

Shand, R.D.; Bailey, D.G.; Hesp, P., and Shepherd, M.J., (in preparation). A conceptual beach-state model for the inner bar of a storm-dominated, low to moderate tidal range coast at Wanganui, New Zealand. *Proceeding of Coastal Sediments'0*3, May 2003.

Short, A.D., 1991. Macro-meso tidal beach morphodynamics - an overview. *Journal of Coastal Research,* 7(2), 417-436.

Short, A.D., 1992. Beach systems of the central Netherlands coast: processes, morphology, and structural impacts in a storm driven multi-bar system. *Marine Geology*, 107, 103-127.

Short, A.D. and Aagaard, T., 1993: Single and multi-bar beach change models, *Journal of Coastal Research, Special Issue 15,* 141-157.

Smith, R.K. and Ovenden, R., 1998. *Wanganui District Council Coastline Stability Investigation Between Kai Iwi and Harakeke.* Report: WNG80202. National Institute of Water and Atmospheric Research Ltd, New Zealand, 32p.

Sonnenfeld, D.L., and Nummedal, D., 1987. Morphodynamics and sediment dispersal of a tideless surf zone. *Proceedings of Coastal Sediments '87,* ASCE, pp. 1938-1949.

Sunamura, T., and Takeda, I., 1993. Bar movement and shoreline change: predictive relations. *Journal of Coastal Research, Special Issue 15*, 125-140.

Van Enckevort, I.M.J and Wijnberg, K.M., 1999 Intra-annual changes in bar plan shape in a triple bar system. *Proceeding Coastal Sediments'99,* ASCE, pp.1094-1108.

van Enckevort, I.M.J., 2001. *Daily to yearly nearshore bar behaviour.* PhD thesis, Utrecht University, The Netherlands, 174p.

Van Enckevort, I.M.J., and Ruessink, B.G., 2001. Effect of hydrodynamics and bathymetry on video estimates of near shore sandbar position. *Journal of Geophysical Research,* 106: 16969-16980.

Wijnberg, K.M., 1996. On the systematic offshore decay of breaker bars. *Proceedings of the 25th International Conference on Coastal Engineering,* ASCE, pp. 3600-3613.

Wilkenson, L., 1998. Systat 8: Statistics. Chicago, SPSS Inc., 1017p.

Wright, L.D., and Short, A.D., 1984. Morphodynamic variability of surf zones and beaches: a synthesis. *Marine Geology*, 56, 93-118.

Table 1 Statistics describing different characteristics of 3D structures observed at Wanganui. Wavelength (A) refers to the longshore length of a 3D structure, regularity or rhymicity (B) requires similar wavelengths and similar amplitudes of multiple 3D structures which occur along the same barline, and (C) orientation refers to the direction of the axis of a 3D structure.

A. Wavelength (m)

	Inner bar	Middle bar	Outer bar
Sample size	83	46	3
Minimum	40	70	200
Maximum	450	750	270
Mean	147.2	279.7	230.0
Standard dev	90.9	177.7	36.1

B. Regularity

	Inner bar	Middle bar	Outer bar
Sample size	22	14	1
Regular	3	1	0
Irregular	19	13	1

C. Orientation

	Inner bar	Middle bar	Outer bar
Sample size	24	23	2
Offset to NW	3	1	0
Shore-normal	2	13	0
Offset to SE	11	3	1
Indeterminant	8	6	1

Table 2 T-values comparing wave heights corresponding with changes to different configuration classes, i.e. for data depicted in Fig 12. The boldly underlined values identify a significant difference at the 5% level ($p<0.05$), while the thinly underlined values identify a significant difference at the 10% level ($p<0.1$).

	Inner Transverse	Inner Undulating	Inner Linear	Inner Subdued	Mid Undulating	Mid Linear
Inner Tranverse	+					
Inner Undulating	2.587	+				
Inner Linear	3.391	0.878	+			
Inner Subdued	0.343	1.840	2.570	+		
Mid Undulating	-1.438	1.487	2.389	-0.769	+	
Mid Linear	-2.112	0.192	1.602	-1.666	-1.256	+

Table 3 Summary table comparing the characteristics of the Short and Aagaard (1993) model with Wanganui morphology and wave data.

Characteristic from the Short and Agaard model	Outer bar	Middle bar	Inner bar
Increasing (decreasing) linearity with increasing (decreasing) cross-shore distance	Does not apply[1]	Yes	Yes
Configuration change slows with increased cross-shore distance	Yes	Yes	Yes
Wavelength of bar is approximately half that of adjacent seaward bar	Does not apply[2]		Yes[3]
Rhythmicity (regularity) predominates	Does not apply[2]	No	No
Axis orientation of 3D structures is predominantly shore-normal	Does not apply[2]	Yes	No[4]
Wave height positively related to cross-shore bar migration	Insufficient data	Yes	No
Wave height related to configuration change	Insufficient data	Yes	Yes/No[5]
Anteceedent morphology influences inner bar change	Does not apply	Does not apply	Yes

1 Subdued configurations predominate
2 Non-linear configurations rarely observed
3 Inter-bar coupling rarely observed
4 Indicates longshore currents are important
5 Spring tide/neap tide cycle also mportant

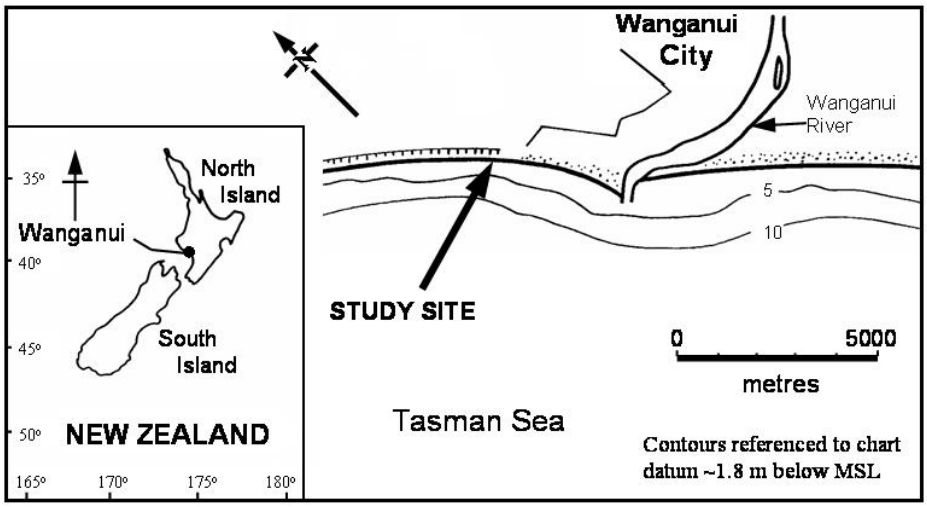

Figure 1 Location map of the Wanganui study site.

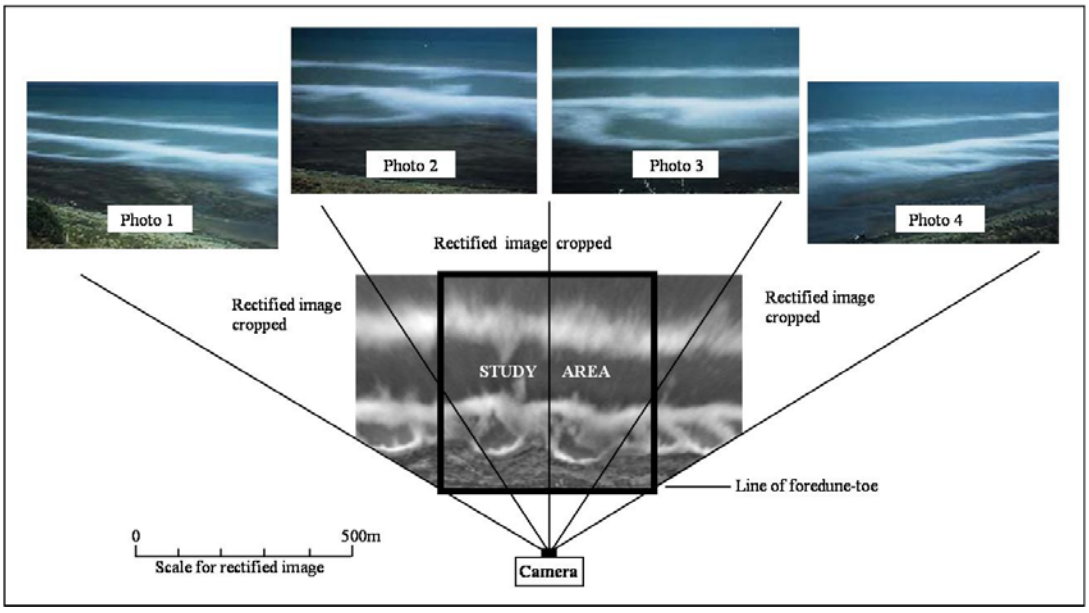

Figure 2
An example of a panorama of 4 time-exposure photographs (above), and the corresponding rectified and merged images (below). Such an output image provides an analogue of surf zone morphology, with high intensity areas representing elevated features such as sand-bars, and the intermediate areas of low intensity representing rip channels and longshore troughs. Two hundred metre wide segments of rectified image have been retained at the longshore margins of the 500 m long study site to assist in the interpretation of 3D configurations.

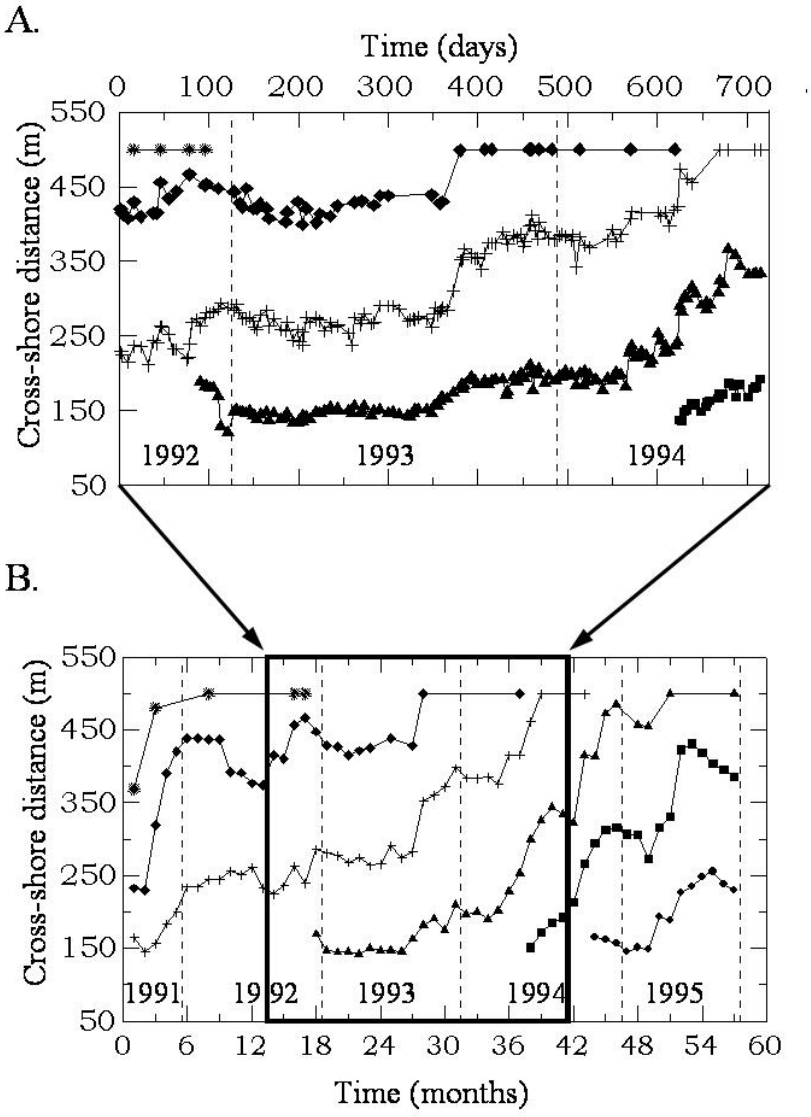

Figure 3
Bar-crest location time-series for the data-set used in this study (A), together with a temporally extended time-series (B) which was sampled at monthly intervals. This latter series is included to illustrate how the shorter data-set (A) fits within the longer-term pattern of NOM.

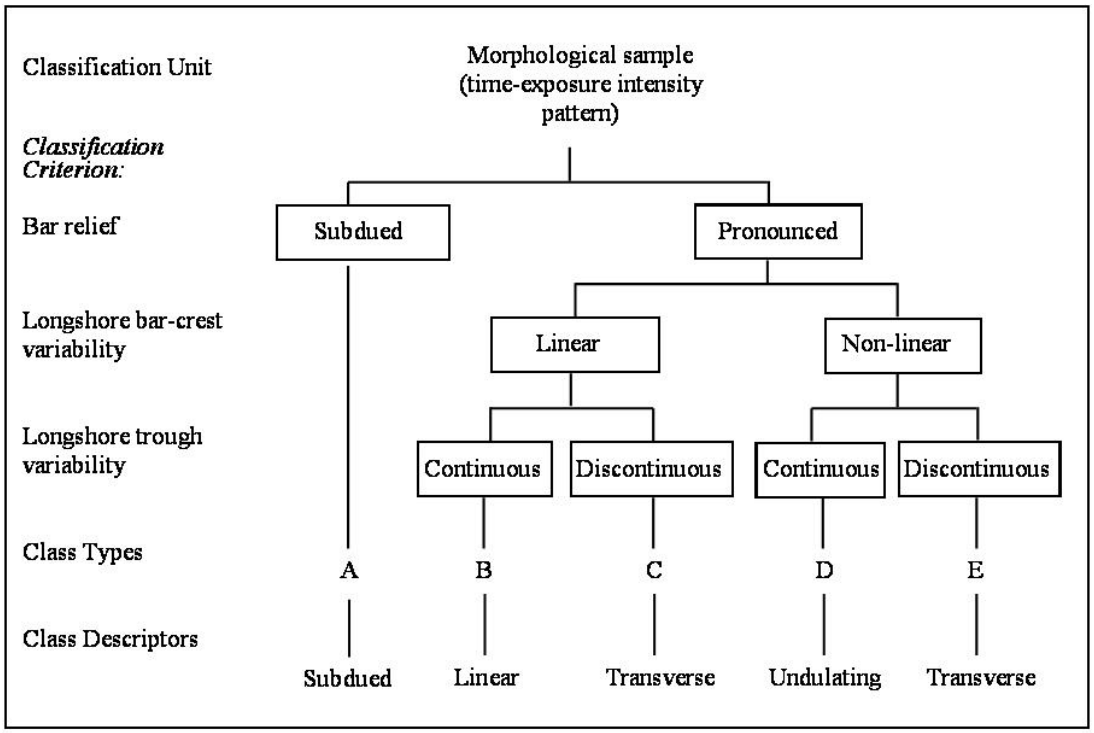

Figure 4
Classification scheme of morphological configurations used in this study. Terms are described in the text. Type C and E were subsequently combined leaving 4 classes, examples of which are shown in Fig 5.

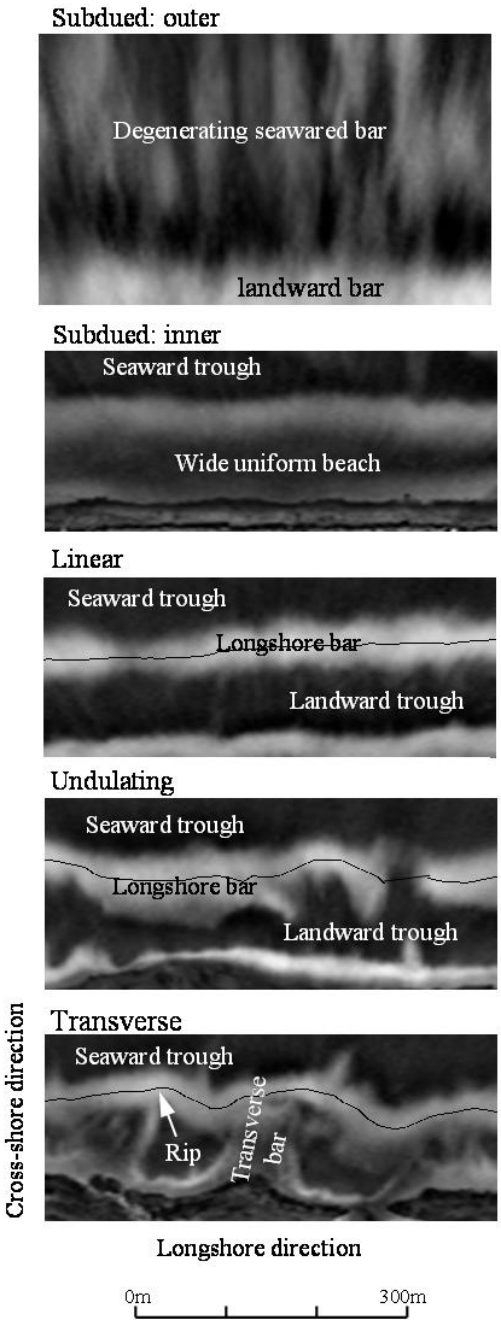

Figure 5
Examples of morphologies corresponding to the configuration classes derived in Fig 4. The continuous black lines (referred to as barlines in the text) denote bar-crests for the pronounced types of configuration, i.e. transverse, undulating and linear.

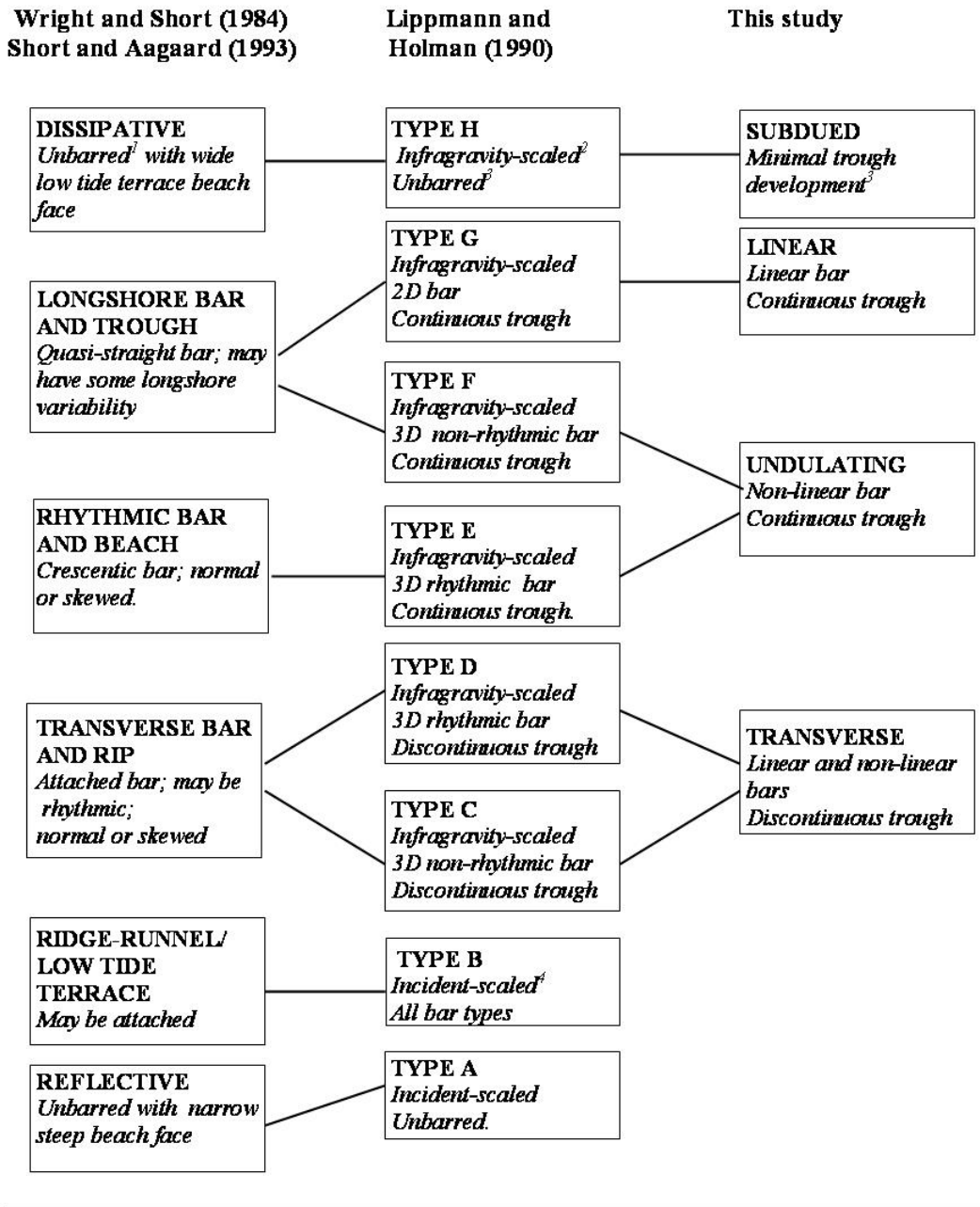

Figure 6
Comparison between configurations used in other (key) studies, with the classes derived in Fig 4 for use in the present study.

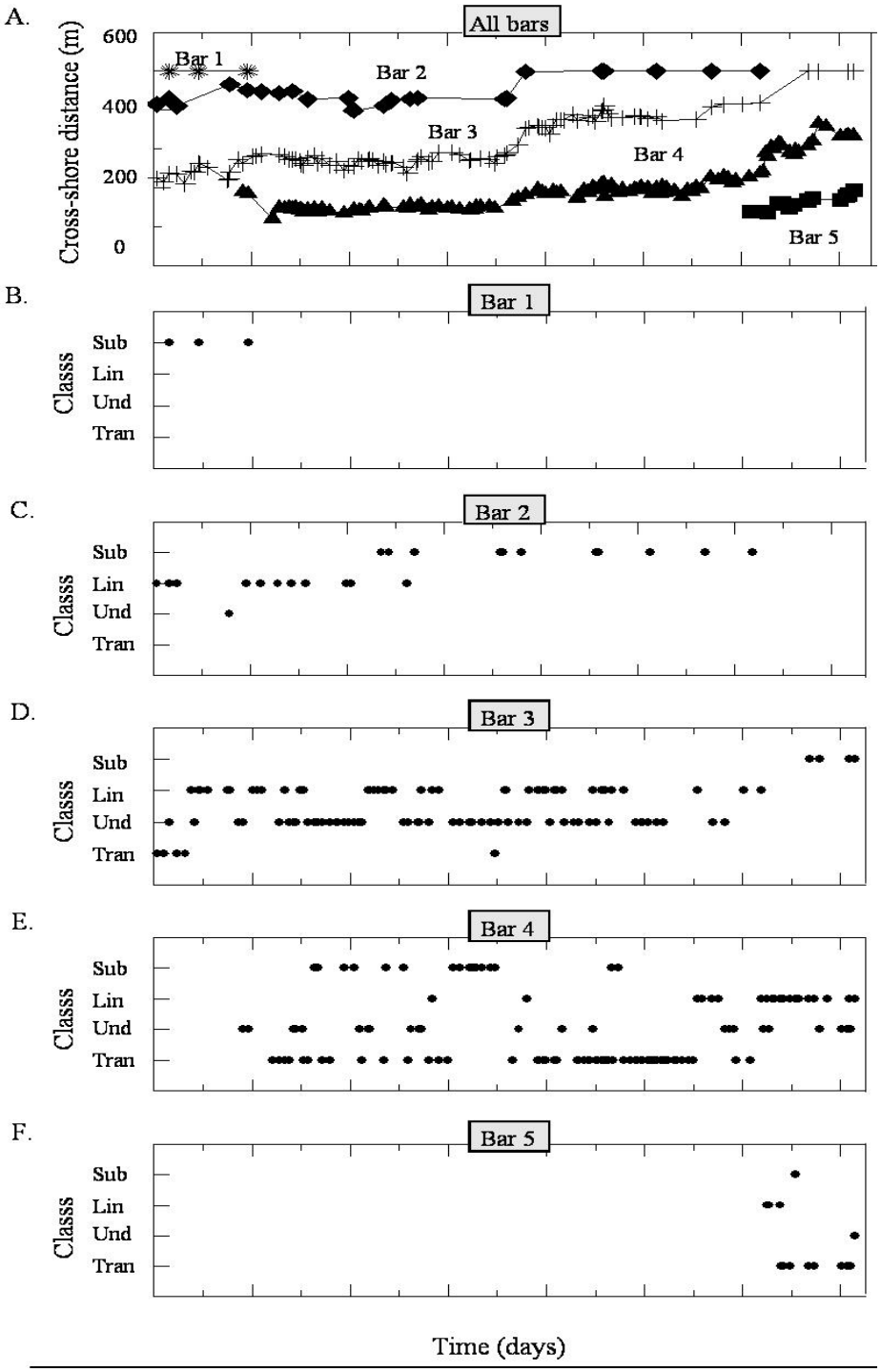

Figure 7
Bar-crest time-series of cross-shore locations (from dune-toe) for the 5 bars observed during the study period (A). The corresponding morphological configurations, in terms of the modal class for each sample, are shown in B (bar 1) to F (bar 5).

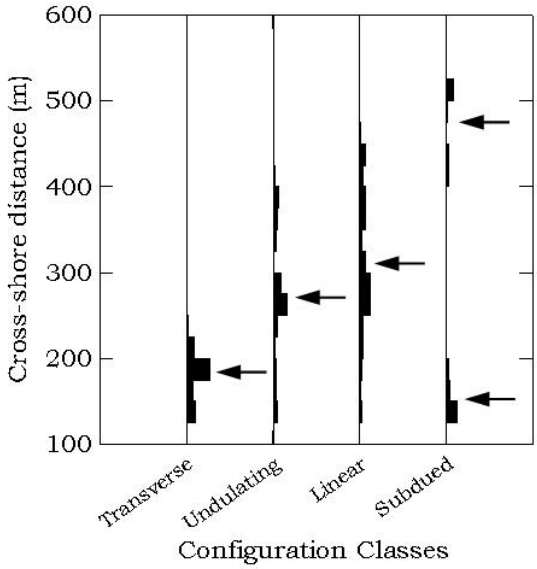

Figure 8
Histograms depicting the cross-shore distribution for each type of configuration class. Arrows locate the mean cross-shore distance for each class with the exception of the bimodally distributed subdued configurations, in this case means for both populations are marked.

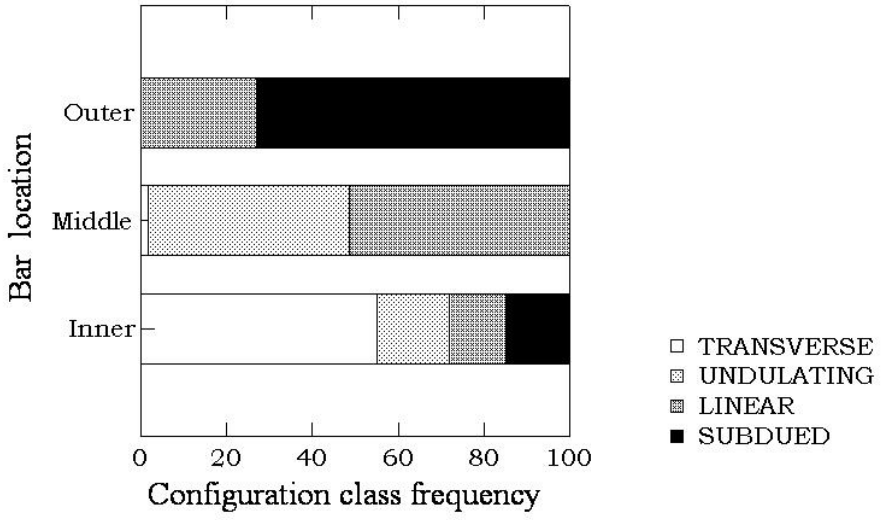

Figure 9
Configuration class frequencies (percentages) for inner, middle and outer bars.

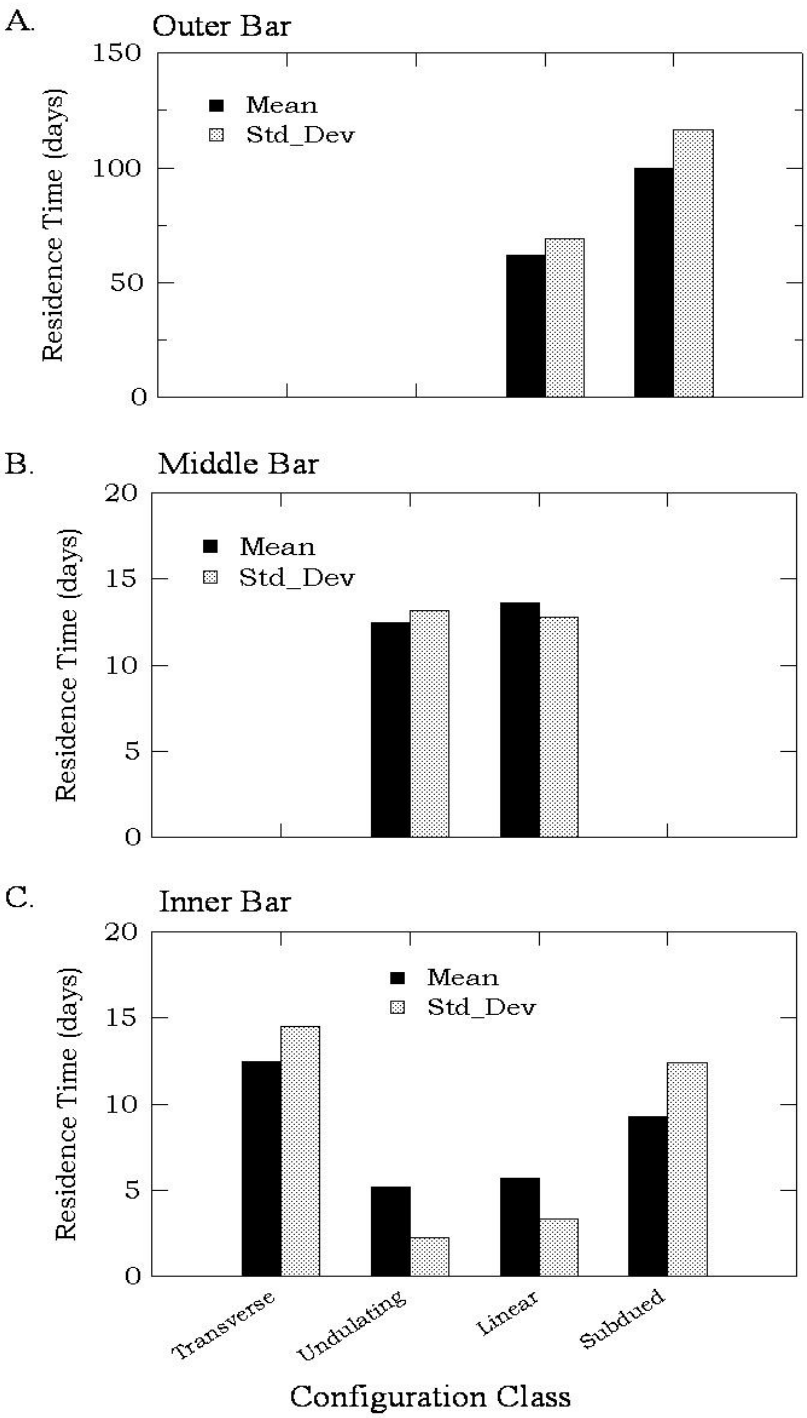

Figure 10
Mean and standard deviations of configuration class residence times for outer (A), middle (B) and inner (C) bars.

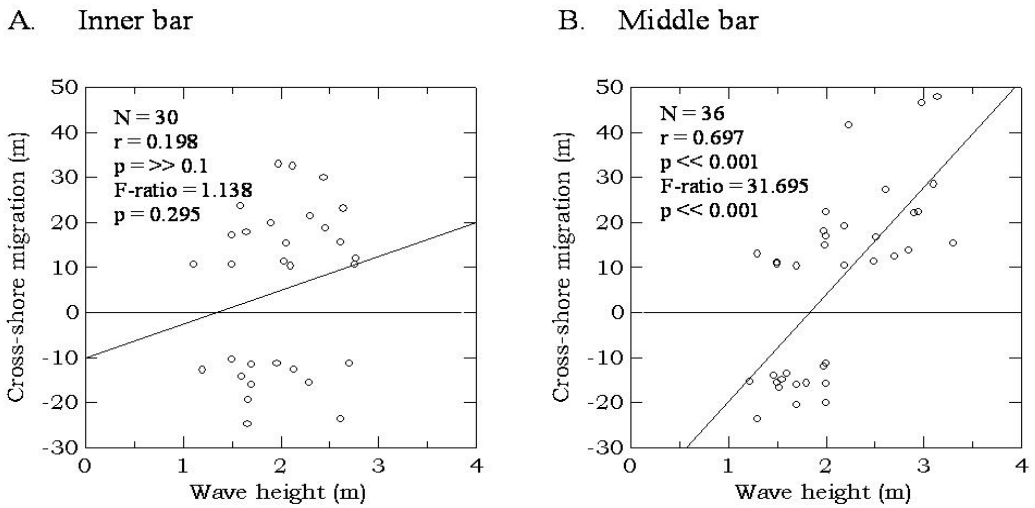

Figure 11
Plots of cross-shore bar migration versus maximum inter-survey wave height for inner (A) and middle (B) bars. Positive cross-shore bar migrations refer to seaward directed movements, while negative values refer to landward bar movements. A linear model has been fitted to each set of data-points and analysis statistics (described in the text) are also shown.

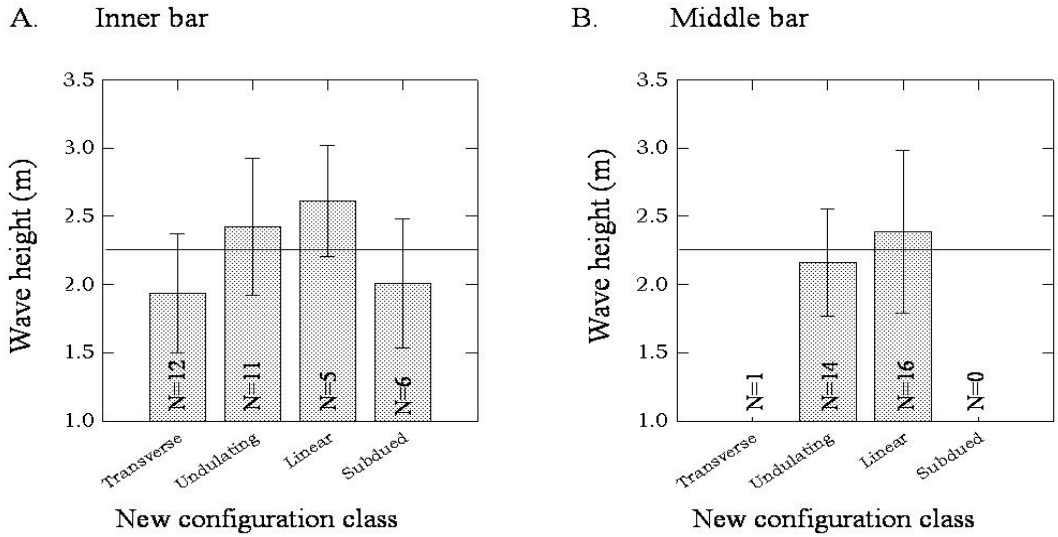

Figure 12
Mean wave height associated with changes to each configuration class for inner and middle bars. Vertical error bars represent one standard deviation about the mean. The number of changes (N) to each configuration class are also shown. The method of determining wave height values is detailed in the text.

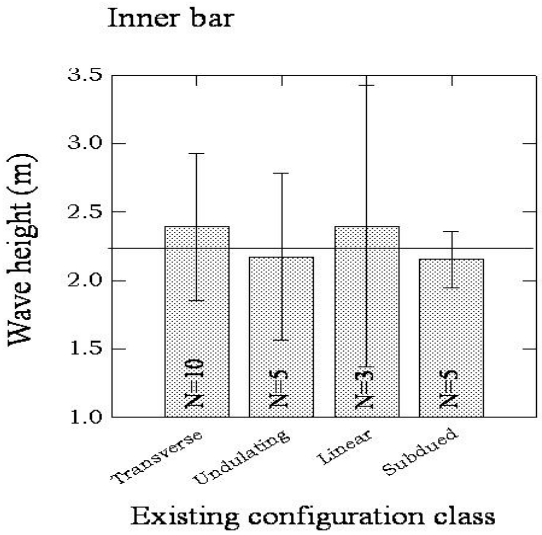

Figure 13
Mean wave height during inter-survey periods when no change in configuration class occurred for the inner bar. Vertical error bars represent one standard deviation about the mean. The number of samples (N) when no change occurred are also shown. The method of determining wave height values is detailed in the text.

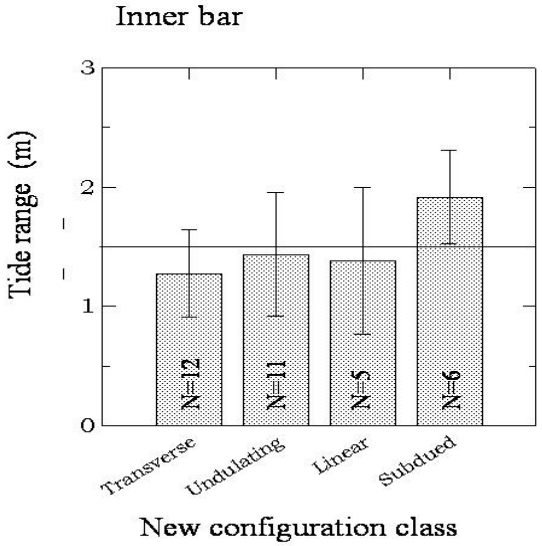

Figure 14
Mean tidal range associated with changes to each configuration class for the inner bar. Vertical error bars represent one standard deviation about the mean. The number of changes (N) to each class are also shown. The method for determining tidal range values is detailed in the text.

13

Shand, R.D., 2003. Relationships between episodes of bar switching, cross-shore bar migration and outer bar degeneration at Wanganui, New Zealand. Journal of Coastal Research, 19(1), 157-170

Shand, R.D., 2003. Relationships between episodes of bar switching, cross-shore bar migration and outer bar degeneration at Wanganui, New Zealand. *Journal of Coastal Research*, 19(1), 157-170.

Relationships between episodes of bar switching, cross-shore bar migration and outer bar degeneration at Wanganui, New Zealand

Roger D. Shand

School of Global Studies, Massey University, Palmerston North, New Zealand
r.d.shand@clear.net.nz

ABSTRACT

Bar switching and outer bar degeneration are morphological phenomena which have recently been observed on coasts in North Carolina, the Netherlands and New Zealand. Bar switching consists of longshore sand-bars becoming discontinuous and the landward bars on one side of the discontinuity realigning and joining with the seaward bars on the other side. Two types of bar switching have been identified at Wanganui (Shand et al., 2001). The predominant type is termed shoreward propagating bar switching, because switching begins in the outer surf zone and progressively affects more landward bars. The second type is termed stationary switching because all switching occurs within the mid-surf zone. This paper analyses a 6.3 year image-based data-set from Wanganui, New Zealand, to qualitatively define the nature of both cross-shore bar migration during bar switching, and outer bar degeneration prior to bar switching.

Shoreward propagating episodes of bar switching were found to be associated with enhanced seaward bar migration on one side of the discontinuity, or transition zone, while suppressed bar migration occurred on the other side. Stationary switching was also characterised by enhanced seaward bar migration on one side of the transition zone, but with either large seaward or landward bar migration on the other side. If a bar experienced a series of switching-associated enhanced or suppressed migrations during its net offshore migration (NOM) cycle, then its NOM characteristics of duration and rate could differ significantly from the longer term average cyclic values for that particular location.

Shoreward propagating episodes were characterised by a longshore variation in the state of degeneration of the seawardmost bar prior to switching. Furthermore, where the outer bar was in an advanced state of degeneration, enhanced offshore migration of the adjacent landward bar occurred. By contrast, where the outer bar remained well developed, suppressed migration of the adjacent landward bar occurred. The pre-switch morphology for stationary switching, however, was more complex as it appeared to be characterised by multiple longshore changes in the degenerative status of the outermost bar.

ADDITIONAL INDEX WORDS: Sand-bar, multi-bar coast, surf zone, nearshore, morphodynamic, net offshore bar migration, NOM.

INTRODUCTION

Bar switching is defined as a type of morphological behaviour within the surf zone in which longshore sand-bars become discontinuous and the landward bars on one side of the discontinuity realign and join with the seaward bars on the other side (Shand and Bailey, 1999). An example of bar switching at Wanganui is shown in Figure 1. The region within which the dislocation and realignment takes place is referred to as the 'transition zone'.

Wijnberg and Wolf (1994) first observed the phenomenon of bar switching on the coast of Holland. These authors provided a sequence of bathymetric images depicting an example of bar switching and they noted that small longshore differences in the position and depth of the outer bar appeared to accompany the onset of bar switching. Furthermore, using empirical eigenfunction analysis of bathymetric data, they found that cycles of net offshore bar migration were 'out-of-phase' on each side of the transition zone.

Net offshore bar migration (NOM) refers to the systematic seaward migration of coastal sand-bars across the surf zone(see Shand and Bailey, 1999, for a review). Bars form near the shoreline and disappear several years later in the outer surf zone. The process by which the form of the seawardmost bar becomes increasingly subdued and then finally disappears is referred to as outer

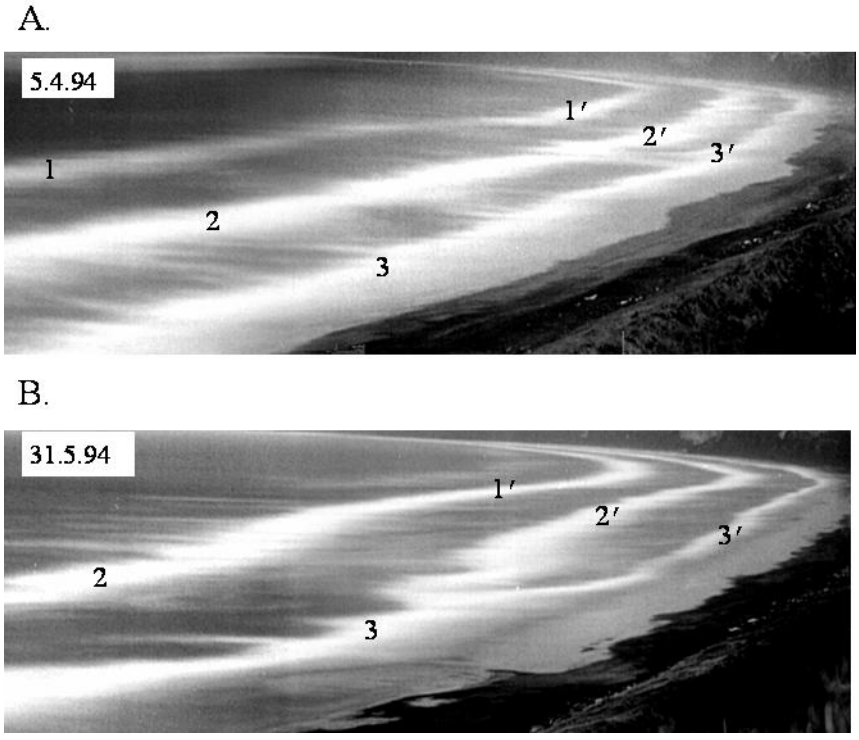

Figure 1 An example of bar switching at Wanganui, New Zealand. The high intensity bands in these 'time-exposure' images signal bar-crests. In the foreground these bars have been marked 1 to 3 and in the distance as 1' to 3'. In Figure B, bar 2 (near the observer) has realigned with bar 1', and bar 3 is realigning with bar 2'.

bar degeneration; this type of morphological behaviour will be described further in the Methods section. Since the mid 1980s, NOM has been recognised on the North Carolina coast (e.g. Birkemeier, 1984; Lippmann et al., 1993), the Dutch coasts (e.g. de Vroeg et al., 1988, Kroon and Hoekstra, 1993; Ruessink and Kroon, 1994; at Wanganui, New Zealand (Shand and Bailey, 1999), and most recently at Hasaki, Japan (Kuriyama, 2001). NOM behaviour may be either regular or irregular as depicted Figure 2. NOM has also been described as 'the offshore progression cycle' by Wijnberg (1996) and 'interannual cyclic bar behaviour' by Ruessink and Terwindt (2000).

Bar switching has been documented at sites on the west coast of the New Zealand North Island. Using rectified time-exposure video images, Donohoe (1998) identified a bar realignment at Muriwai Beach near Auckland. Further south at Wanganui, Shand and Bailey (1999) used rectified time-exposure photographic images to describe a set of inter- related realignments which is referred to as an 'episode of bar switching'. In their example, cross-shore bar migration within and adjacent to the transition zone was shown to vary markedly.

More recently, Shand et al. (2001) analysed 9 episodes of bar switching within a 6.3 yr data-set from Wanganui by studying changes in the dimensions and location of transition zones. Two types of bar switching sequence were identified: 'shoreward propagating episodes' in which bar switching began in the outer surf zone and then progressively affected the more landward bars, and 'stationary

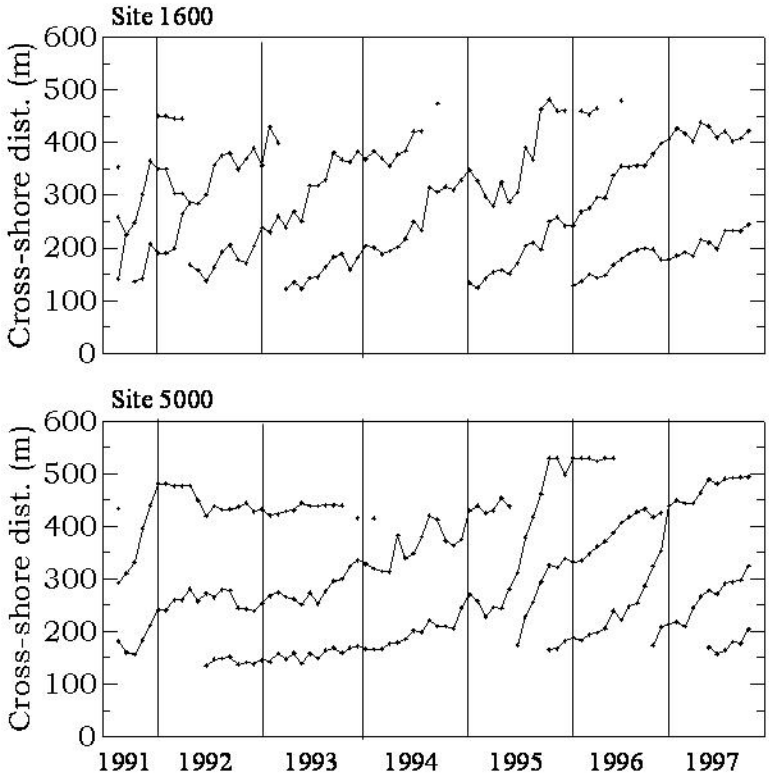

Figure 2 Examples of bar-crest time-series illustrating net offshore bar migration (NOM) at 2 sites along the Wanganui coast. The site 1600 data depicts a more regular pattern of NOM than the site 5000 data.

episodes' in which all bar switching occurred within the mid-surf zone. Significant wave heights greater than the 5% excedence level (2.6 m), occurred at some time during each episode of bar switching. However, such high energy did not always result in this type of behaviour, indicating that antecedent morphology, which will be examined in more detail in this paper, also plays an important role in bar switch morphodynamics.

Bar switching appears to occur on other multi-bar coasts. Data depicting morphological configurations consistent with bar switching have appeared in Ruessink and Kroon (1994) at Terschelling Island (the Netherlands) and in Lippmann et al. (1993) and Plant et al. (1999) at Duck, North Carolina. However, these authors did not recognise or refer to this phenomenon.

At times during the process of bar switching the morphology may have a forked or bifurcated appearance, as in Figure 1B. This type of configuration has lead some authors to refer to the transition zone as the bifurcation area (Ruessink et al., 2001), but use of the term bifurcation should be used with caution for the following reasons. Firstly, it implies that forked morphologies result from a process of bifurcation such as a section of bar splitting in the longshore direction. However, bar switching results when a bar becomes discontinuous and the ends attach to the more seaward and landward bars. Secondly, other bifurcated morphologies occur within the surf zone and these result from processes unrelated to bar switching. For example, Shand and Bailey (1999) showed a board section of longshore bar splitting (in the longshore direction) into a forked configuration with the landward portion subsequently migrating shoreward to merge with the inter-tidal beach. Such 'double bar development' has also been documented for the coast of Holland by Kroon (1991 and 1994), and Wijnberg (1995). Forked morphologies also occur in association with rip processes (e.g. see morphological data in Chappell and Eliot (1979) or Bogle et al. (2001)).

The purpose of this paper is to qualitatively define both the nature of cross-shore bar migration during bar switching and the degenerative state of the outer bar prior to the onset of bar switching, by analysis of the several episodes of bar switching evident within the aforementioned 6.3 year image-based data-set from Wanganui. The influence such bar behaviour may have upon characteristics of net offshore bar migration will also be addressed.

THE STUDY SITE

The study site covers 6 kms of coast to the northwest of the Wanganui Rivermouth (Figure 3). The Wanganui River is 305 km long and has a catchment area of 7120 km^2. Rivermouth jetties were constructed between 1884 and 1940 and the shoreline has responded by migrating seaward approximately 700 m near the entrance and 100 m at the northwestern end of the study area (Smith and Ovenden, 1998). The shoreline is now approximately stable near the rivermouth but in the western part of the study area it is prograding at rates of up to 2 m/yr. This accretion is superimposed upon a regional erosion trend of 0.2 to 0.6 m/yr (Johnston, 1985).

The nearshore and upper-shoreface bathymetry shown in Figure 3 depicts a subdued ebb-tide delta. The nearshore is characterised by fine sand (2 to 3 phi) and the cross-shore slope declines from 0.0094 near the rivermouth to 0.0082 in the northwest of the study area. The time-averaged nearshore width ranges from 425 m near the rivermouth to 625 m in the northwest of the study area.

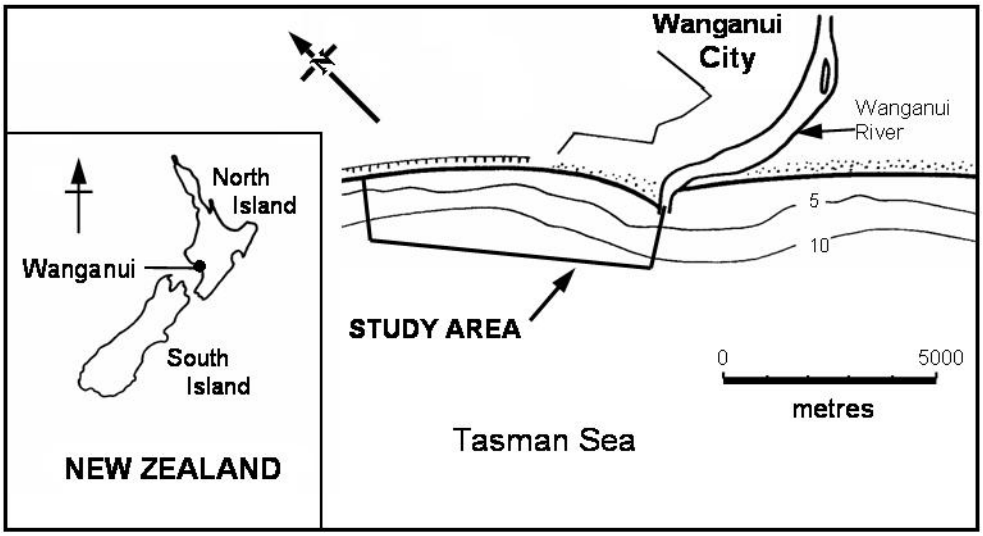

Figure 3 Location map of the Wanganui study area. Depth contours are in metres below chart datum, where chart datum is 1.8 m below MSL.

Two to three sand-bars occur closer to the rivermouth, while 2 to 4 bars occur in the northwest of the study area. Bar behaviour is characterised by net offshore bar migration. The average time interval between bar formation and bar disappearance, i.e. the life-cycle of a bar, is 2.5 yrs closer to the rivermouth and 3 yrs in the northwest of the study site. While sand-bars are typically linear, three-dimensional configurations do occur.

The process conditions affecting the study area are as follows. The mean spring tide range is 2.4 m and the mean neap tide range is 0.8 m. Deepwater significant wave height parameter values are: mean = 1.3 m; 5% excedence = 2.5 m, and 1% excedence = 3.2 m (Macky et al., 1988). Wave period ranges between 3.5 sec and 19 sec with the mean value being 10.1 sec. Sea and swell populations usually co-exist, with approximately 75% of the wave energy occurring at sea wave frequencies (Patterson, 1992). Wave observations made during the present study indicate that 34% of waves had a shore-normal approach (±1 deg), 42% approached from the northwest and 24% from the southeast.

The mean speed for wind data collected during the study period was 5.3 m/s and the 5% excedence value was 12.4 m/s. The predominant wind approach directions were west/northwest, with an average angle of ~30 to the shoreline, and south, with an average angle of ~40 deg to the shoreline from the opposite direction. Sixty percent of the time the long-term wind data had a northwesterly component, 25% of the time a southeasterly component, and during the remaining 15% of the time calm conditions prevailed.

The longshore current regime resulting from the oblique wave and wind approaches causes substantial longshore drift. Estimates reported in Patterson (1992) are 300,000 to 600,000 m^3/yr of sand toward the southeast and 60,000 to 280,000 m^3/yr toward the northwest.

METHODS

This study analyses the following 2 types of data: cross-shore bar-crest distances and outer surf zone sea-surface intensity patterns which are represented by profile shape and depth parameters. Each of these data types was derived from planimetric images in which the intensity variations depict the submarine morphology. The acquisition of these images will now be outlined, and then the derivation of the 3 types of data will be described.

Image data-base

The morphological data used in this study comprise 6.3 yrs of photographs sampled between August 1991 and November 1997. Field sampling was carried out at approximately fortnightly intervals with closer sampling (1-5 days) at times of rapid morphological change. These sampling rates enabled morphological change to be confidently tracked within a sequence of images.

The camera site was located midway along the study area, ~130 m landward of the foredune toe, and on top of a 42 m (above MSL) cliff. A panorama of 8 photographs was required to give full coverage of the study area. The 4 central photographs were taken with a 55 mm focal length lens and the end shots taken with a 135 mm telephoto lens. However, during the first (experimental) year of sampling 35 mm and 55 mm lenses were used and this resulted in a significant reduction in spatial resolution toward the ends of the study area.

Each photograph was exposed for 4 mins to minimise tidal change during the 45 to 60 mins required to sample a panorama and to provide a relatively stable representation of the breaking wave pattern. Such images are referred to as time-exposures. They provide an analogue for surf zone morphology because elevated topography such as sand-bars are characterised by locations of higher intensity resulting from wave breaking which is depth-dependent (Lippmann and Holman, 1989). The images shown in Figure 1 are examples of time-exposure photographs.

The field sampling was carried out during lower tide levels and higher wave conditions to maximise the likelihood of waves breaking on all bar-crests. Furthermore, by limiting sampling (photography) to these conditions, the influences of wave height modulation and tide level on break-point location were minimised.

Digital image processing was used to rectify each photograph to ground co-ordinates and then to merge this output with adjacent images. This combined output was subsequently transformed to straighten the coastline, thereby facilitating viewing and analysis. These particular procedures have been described by Bailey and Shand (1993, 1996).

Bar-crest location data

Time-series of cross-shore bar-crest location data were derived from time-stack images. A time-stack is constructed by stacking spatially corresponding cross-shore segments (i.e. strips) of image cut from successive time-exposes. This technique has been described in Bailey and Shand (1996, 1997), and is now a frequently used technique for analysing image-based cross-shore bar migration (e.g. Plant et al., 1999, Shand et al., 1999). Intensities within the segment are longshore averaged and the width of the segment may be varied to minimise noise associated with longshore non-uniform topography.

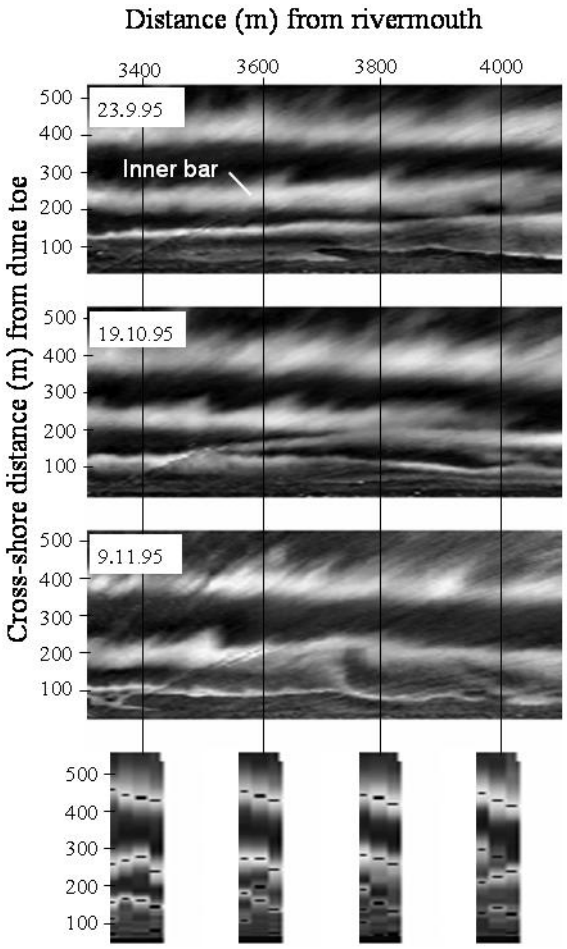

Figure 4 A series of 3 rectified time-exposure images depicting surf zone morphology along 800 metres of coast at the Wanganui study site. Four time-stacks corresponding to the marked cross-shore transects appear along the base. The black rectangles on the time-stacks locate bar-crests and illustrate their cross-shore migrations during the survey period.

Within the surf zone, a bar-crest is assumed to correspond with an intensity peak. The intensity value used to represent the bar-crest is identified by fitting a parabola to the intensity values in that area and then determining the parabola maximum. Examples of 4 time-stacks constructed from a series of time-exposure images are shown in Figure 4. The small black rectangles in the time-stacks denote the parabola maxima used to represent bar-crests.

While intensity maxima approximate sand-bar locations, environmental conditions such as sea-level and incident wave height, together with bar-crest depth and bar form, influence the break-point location (Plant and Holman, 1998). Location errors associated with these factors can be in the order of 30-40 m (van Enckevort and Ruessink, 2001). Empirical and theoretically-based corrections have been developed by van Enckevort and Ruessink (2001) which reduce wave and sea-level induced errors from 9.5 m (standard deviation) to 5.6 m and 6.2 m respectively. In addition, Kingston et al. (2000) has reduced errors to less than 10 m by using an artificial neural

network approach. However, these methods all require knowledge of the profile bathymetry, together with local wave and sea-level parameter values. Photogrammetric errors also affect accuracy unless corrections such as those outlined in Sallenger et al. (1997) are carried out.

The resources required to adjust intensity maxima location to the corresponding bathymetrically defined bar-crest location were not available for the present study so the following approach, described in detail by Shand (2000), was used. Firstly, the influence of process variables upon intensity maxima location was determined empirically and incorporated into the cross-shore distance resolution. The magnitude of such errors was found to lower if (longshore) intensity averaging was carried out over wider (longshore) segments during the time-stacking process described earlier. An explanation for this error reduction may involve longhore variation in the bathymetry (3D morphology) for the following reason. Model studies by van Enckevort and Ruessink (2001) have shown that different profile shapes influence wave breaking processes. The differing profile shapes associated with 3D-morphology would therefore cause longshore variation in the cross-shore location of intensity maxima and the magnitude of this variation would reduce if longshore intensity averaging was carried out. In the present study, 400 m wide segments were used; this resulted in maximum environmentally-associated errors being ~15 m for the inner surf zone and ~20 m for the outer surf zone. These values also include estimated photogrammetric errors.

Secondly, an empirically-based adjustment relating intensity to bathymetry has been developed by Bailey and Shand (1997). However, this adjustment was not applied to data used in the present study as the relative change in bar-crest location provided by the environmentally and photogrammetrically corrected intensity data, was satisfactory.

As switching-associated cross-shore bar migration was studied both within the transition zone and to both sides (in the longshore direction) of the transition zone, a technique to spatially identify transition zone boundaries was required. Such a technique is detailed in Shand et al. (2001). Briefly, the shoreward limit is set at the centre of the trough landward of the landwardmost bar undergoing realignment. The offshore boundary is located at the centre of the trough seaward of the outermost bar undergoing realignment. The transition zone boundaries in the longshore direction are where the bar morphology has been unaffected by the realignment process. The accuracy of such visually located cross-shore and longshore transition zone boundaries is estimated at ±10 m and ±50 m respectively.

The cross-shore resolution of the bar-crest data, and the errors in locating transition zone boundaries, are not sufficient to affect significantly the results and conclusions described later in this study.

Identifying Outer Bar Morphology

To determine the degenerative state of the seawardmost bar, a classification routine was applied to intensity patterns on rectified images. The relationship between the intensity classes and the corresponding topography was determined by matching the image-based intensity patterns of 46 samples with bar-crest depth and shape parameters derived from nearly contemporaneously

sampled sea-bed profiles. This section will firstly describe the classification scheme and then determine the relationship between intensity patterns and the degenerative state of the outer bar.

Classification of image intensity patterns was based on a set of 3 independent characteristics which involved the following binary decisions: pattern existence (non-existence); longshore continuity (discontinuity) of the intensity maxima representing the seaward-most bar-crest; and longshore continuity (discontinuity) of the intensity minima representing the adjacent (landward) trough. The 46 rectified time-exposure images were assigned to the 5 mutually exclusive categories. The image samples are considered to be independent because they are from sites spatially separated by 3 km and temporally separated by 3 months. The categorisation resulted in the following 4 non-empty classes: class A (n = 23) which has longshore continuous outer intensity maximum and longshore continuous landward intensity minimum; class B (n = 6) which has longshore continuous outer intensity maximum and longshore discontinuous landward intensity minimum; class C (n = 10) which has longshore discontinuous outer intensity maximum and longshore discontinuous landward intensity minimum; and class D (n = 7) which has no discernable intensity pattern. Examples of intensity patterns for these 4 categories are depicted in Figure 5.

Sea-bed profiles were sampled as close to the photographic sampling as sea-conditions allowed. Nonetheless, several days could separate the 2 types of survey. This time lag introduced an unresolved error into the subsequent data comparison. However this error was likely to be relatively small compared to the 3 monthly change in morphology.

As noted above, sea-bed morphology in the vicinity of the seawardmost bar was defined using 2 parameters: depth of the outer bar-crest below MSL, and elevation between this bar-crest and the adjacent landward trough. These parameters were selected because the depth of the outer bar increases, and its form becomes increasingly subdued, during the degeneration process.

The cross-shore location of the outer bar-crest and the landward trough were determined by fitting a curve to the surveyed profile, calculating the residuals and then identifying the cross-shore locations corresponding to local maximum (bar-crest location) and minimum (trough location) residual values. An advantage of this method is that it enables crest/trough locations to be determined when the bar-depth is greater than the trough depth, a situation that occurs during advanced bar degeneration. The method is described in greater detail in, for example, Holman and Bowen (1982), and Ruessink and Kroon (1994). Outer bar-crest and adjacent landward trough locations, together with the outer bar morphological parameter values, have been marked on the examples in Figure 5.

The profile parameter values and corresponding intensity classification values for each of the 46 samples are plotted in Figure 6. Class A values are separated from class B values by the bar-crest depth parameter; this intensity pattern is therefore depth-dependent rather than shape-dependent. By comparison, classes B, C and D are separated on the basis of shape, with class separation occurring in approximately 80% - 90% of the cases. These results show that the intensity classes represent increasing levels of seaward bar degeneration, with class A corresponding to a well developed and relatively shallow outer bar and class D corresponding to a deeper and almost formless feature.

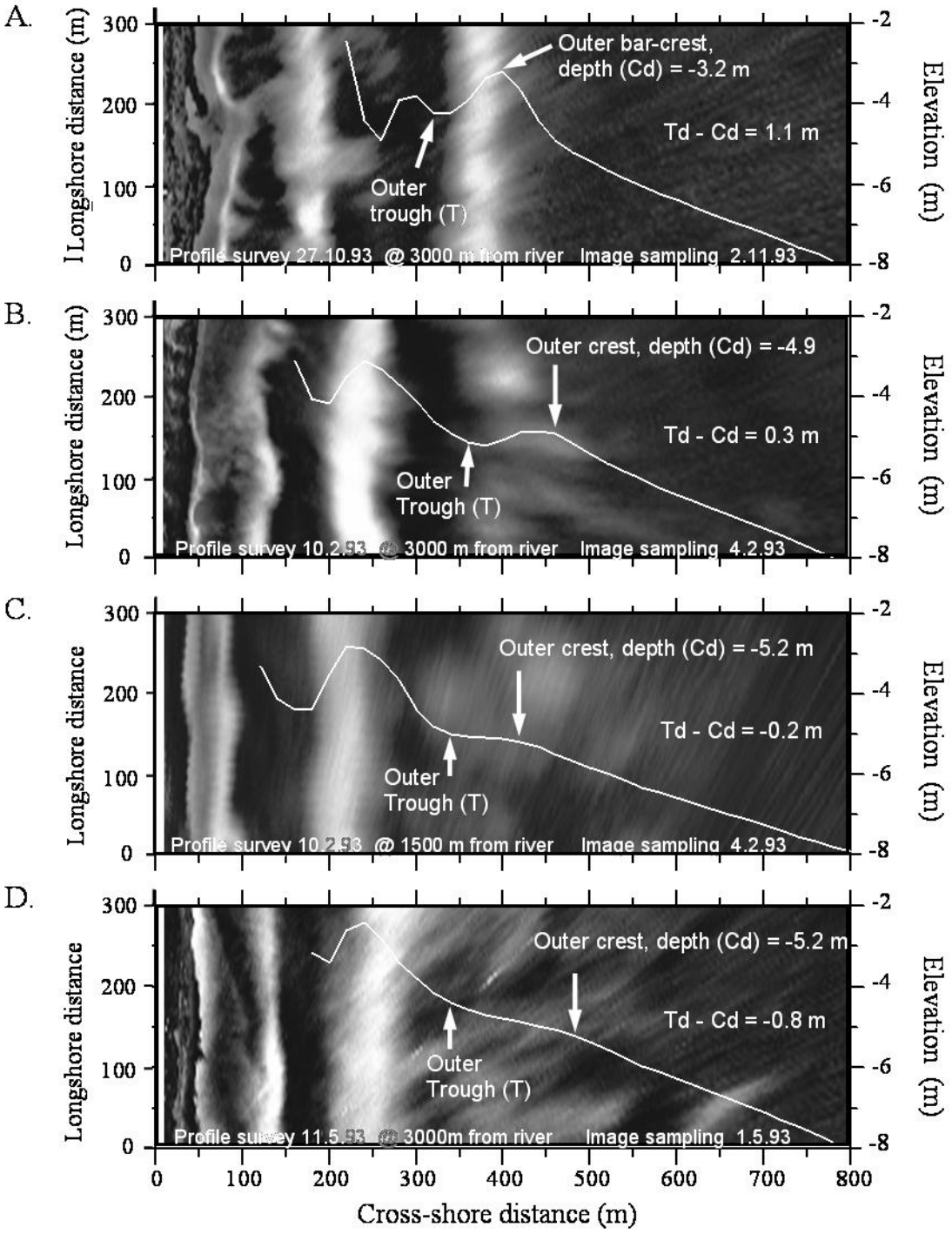

Figure 5 Cross-shore profiles depicting an increasing level of degeneration of the seawardmost bar. The degeneration is represented by increasing values for the outer bar-crest elevation, and decreasing values for the difference between the outer trough elevation and the outer bar-crest elevation. The location of these 2 morphological features was determined using the 'maximum residual' method described in the text. The surface intensity pattern associated with each profile is also shown. These patterns approximate the four classes defined in the text, with Figure A illustrating class A, Figure B illustrating class B, Figure C illustrating class C and Figure D illustrating class D.

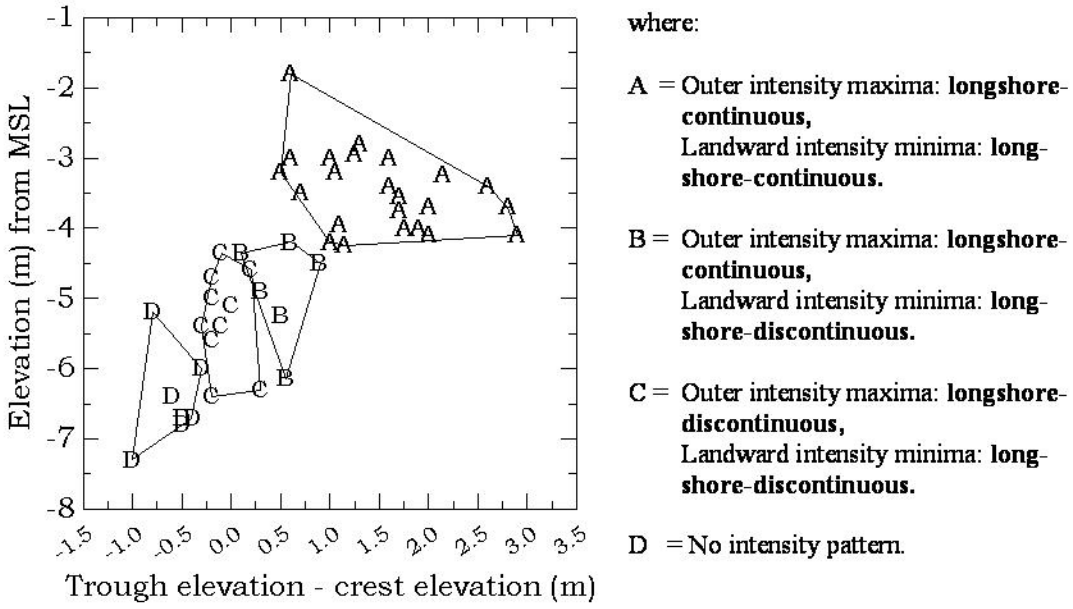

Figure 6 Intensity pattern categories (A,B,C,D) plotted in terms of the two bar degeneration parameters: bar-crest elevation (with respect to MSL), and elevation difference between the outer trough and outer bar-crest.

The occurrence of overlapping parameter values for the different intensity classes probably arises from the error sources noted earlier, i.e. environmental noise associated with the image data, and non-synchronous photography and echo-sounding. The overall strength of the grouping, however, supports the validity of using intensity patterns to infer differing levels of outer bar degeneration. During the present investigation, the classification scheme was applied to ~1000 m longshore sections of pre-switch image data, and in some cases dual classes had to be assigned. However, this did not affect the conclusions.

RESULTS

This section will first consider the time/space distribution of switching during the study period. Cross-shore bar migration associated with switching is then analysed both within, and in the vicinity of, the transition zones. Next, associations between bar switching and NOM characteristics are considered, and finally, the degenerative state of the seawardmost bar prior to the onset of bar switching is described.

Switching Distribution

The time/space distribution for the 9 episodes of bar switching which occurred during the study period are depicted in Figure 7. Each horizontal band denotes transition zone within which the bar realignment occurred.

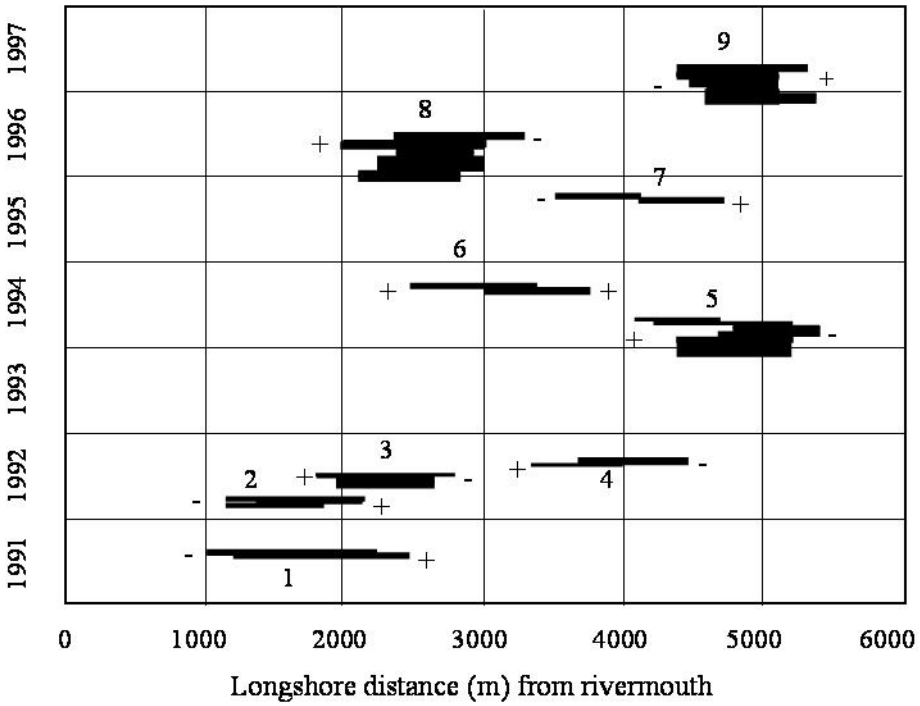

Figure 7 Longshore distribution of transition zones defining the chronologically numbered episodes of bar switching which occurred during the study period. The + symbol denotes enhanced seaward bar migration, whereby bars on the indicated side of the transition zone undergo rapid seaward migration during the episode. The - symbols refers to suppressed bar migration, whereby bars on the indicated side of the transition zone remain in approximately the same cross-shore location.

Cross-shore Bar Migration

Identification of bar migration patterns both within, and adjacent (in the longshore direction) to transition zones, was based on the analysis of time-stack data from episodes 2 to 9. Episode 1 was not included because the initial surveys comprised echo-sounded data with low (longshore) resolution. Rectified time-exposure images bracketing each episode of bar switching were used as input for the time-stacks. For each episode, one time-stack was located within the transition zone and one on each side of the transition zone. The resulting time-stacks are shown in Figure 8. Lines depicting the landward and seaward boundaries of the zone of systematic offshore bar migration are also shown on the time-stacks. These boundaries were determined from the position of local maxima on time-averaged intensity profiles as described in Shand et al, (1999). Only those cross-shore bar migrations which occurred predominantly within the zone of systematic offshore migration were included in the analysis for the following reasons:

- data points located shoreward of the landward boundary, and seaward of the offshore boundary, usually relate to bars undergoing generation and degeneration respectively (Shand et al., 1999);

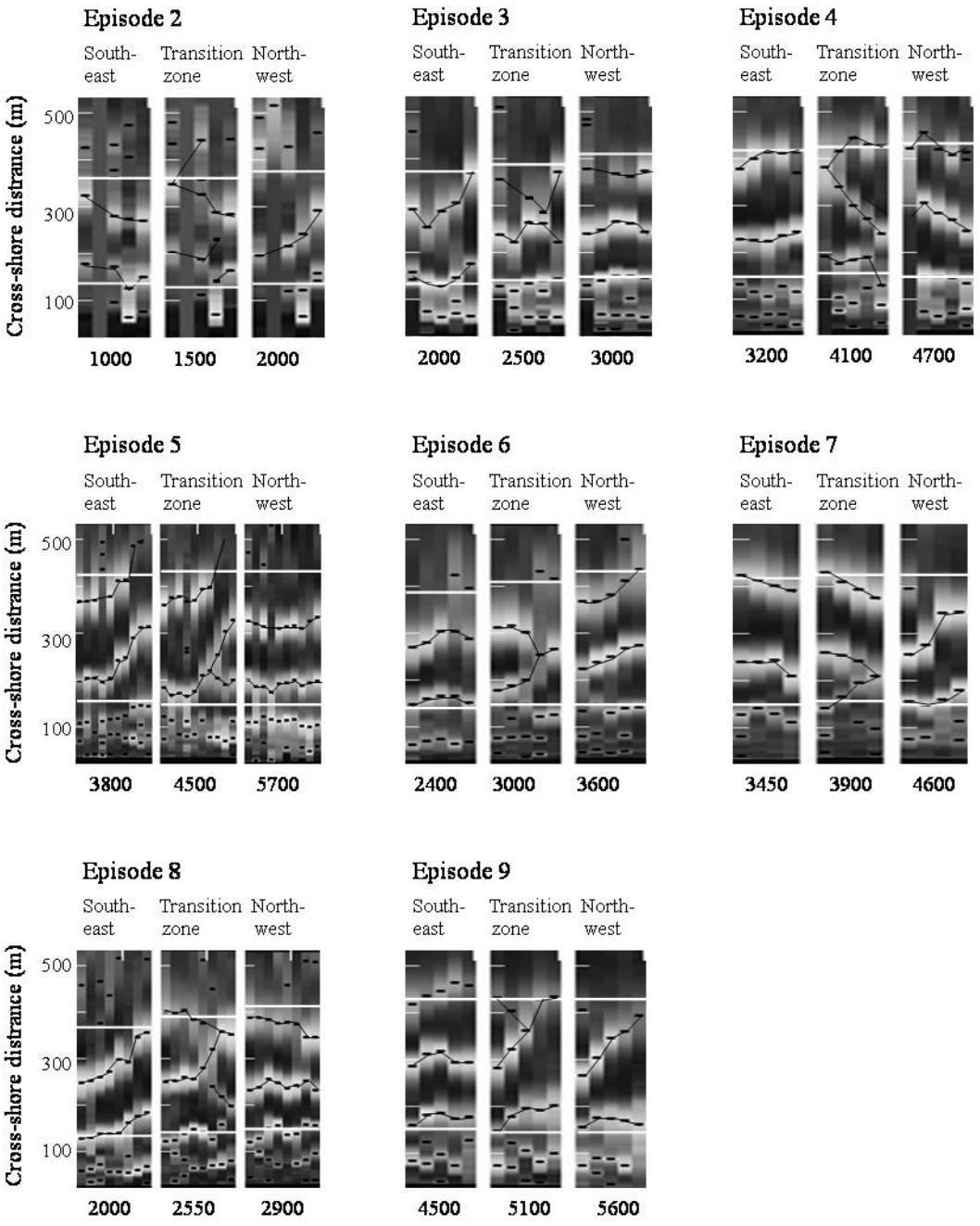

Figure 8 Time-stacks depicting cross-shore bar migration for bar switching episodes 2-9. Bar migrations within the transition zone and also at locations to the southeast (river) side and northwest side of the transition zone for each episode are depicted. Horizontal lines mark the cross-shore boundaries of the zone of systematic offshore bar migration which is defined in the text. Only bar tracks which lie mainly within this zone are shown.

- the locational accuracy of these data-points is less reliable than those within the encompassed zone where systematic offshore bar migration predominates; and

- the shoreward and seaward intensity maxima may represent artifacts associated with image processing, or environmental phenomena, rather than bar-crests.

Cross-shore bar migration within transition zones are characterised by both temporally continuous and temporally discontinuous tracks (Figure 8). The continuous migration tracks may span the entire survey period or split or merge during this time. By contrast, the discontinuous tracks may appear, disappear, or occur in isolation.

Cross-shore bar migrations immediately adjacent to transition zones, i.e. labeled southeast and northwest in Figure 8, show only continuous tracks occurring within the zone of systematic offshore migration.

To better recognise differences in bar migration to each side of the transition zone, bar migrations were analysed in terms of their magnitude and direction (Figure 9). Migration distance was obtained from the distances between the ends of a linear regression model fitted to each bar-crest time-series in Figure 8, i.e. to each series of black rectangles on the time-stacks. Shaded regions in Figure 9 represent stationary episodes of switching, while unshaded regions represent shoreward propagating episodes.

The results in Figure 9 show that for the 6 episodes of shoreward propagating switching, bar(s) on one side of the transition zone underwent large (enhanced) seaward migrations of between 93 and 143 m. Bars on the opposite side of the transition zone underwent minimal, and often landward-directed, migrations, i.e. suppressed migration. Such enhanced and suppressed migrations associated with bar switching, were previously referred to as positive and negative switching respectively by Shand and Bailey (1999).

The 2 stationary episodes of switching (4 and 6) were also characterized by enhanced seaward bar migration on one side of the transition zone (61 m and 78 m respectively); however, bar migration on the opposite side was not suppressed. In the case of episode 4, substantial landward migration (82 m) occurred, and in the case of episode 6, seaward migration of 40 m occurred.

For each episode, the type of switch-associated bar migration, i.e. enhanced seaward migration or suppressed migration, which occurred alongshore from each transition zone, has been depicted in Figure 7 by + and – notation respectively. For completeness, the large landward bar migration in episode 4 has been marked as negative, and positive notation is shown on both sides of the transition zone for episode 6.

There is no spatial consistency in the longshore orientation of the + and - coding in Figure 7, shows no consistency in their longshore orientation. For example, episodes 5 and 9 occurred at approximately the same longshore location, but for episode 5 the enhanced seaward bar migration occurred on the river side of the transition zone, while episode 9 had suppressed bar migration on

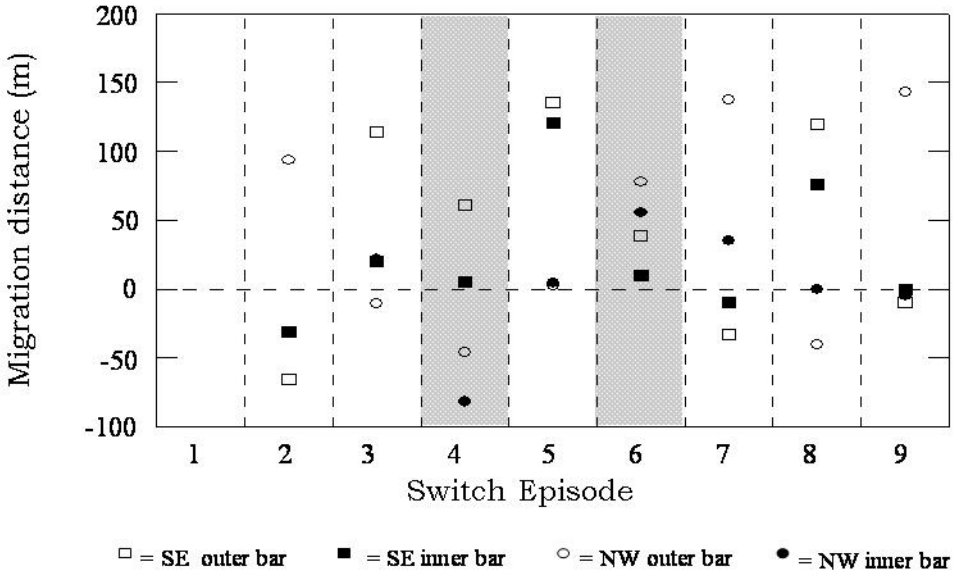

Figure 9 Cross-shore bar migration distances on each side of the transition zone for switching episodes 2-9. Distances are based on linear models fitted to the bar migration tracks depicted in Figure 8. Positive migration distances refer to seaward directed movement. The shaded regions represent stationary episodes of switching, while the unshaded regions represent shoreward propagating episodes.

the river side. This lack of consistency in longshore orientation of transition zones will minimise the likelihood of systematic longshore changes in longer-term NOM characteristics.

The enhanced and suppressed cross-shore bar migration associated with switching (Figure 8 and 9) explains the irregular migration tracks shown in Figure 2 (site 5000, 1995-96). The effect such irregularities may have on NOM characteristics is now considered.

Characteristics of NOM

To qualitatively assess relationships between bar switching and NOM characteristics, 2 contemporaneously sampled sand-bars were analysed. These bars were located approximately 3000 and 5000 m from the river-mouth and will henceforth be referred to as B3000 and B5000. They were selected because they entered their cycles of NOM at approximately the same time in 1995, and then experienced different types of bar migration (enhanced seaward migration, suppressed migration, and the within transition zone behaviours) associated with episodes 7-9 (see Figure 10).

Cycles of NOM can be characterised using parameters such as duration or (average) rate of offshore migration (Shand and Bailey, 1999). These parameters are illustrated in Figure 10. Data collection ceased before either bar had crossed the seaward boundary of the zone of systematic offshore bar migration, i.e. they had not completed their individual cycles of NOM. In the case of B3000, the track was extrapolated to the seaward boundary in the shortest time on the basis of longer-term bar migration records. The duration value is therefore a minimum, while the average

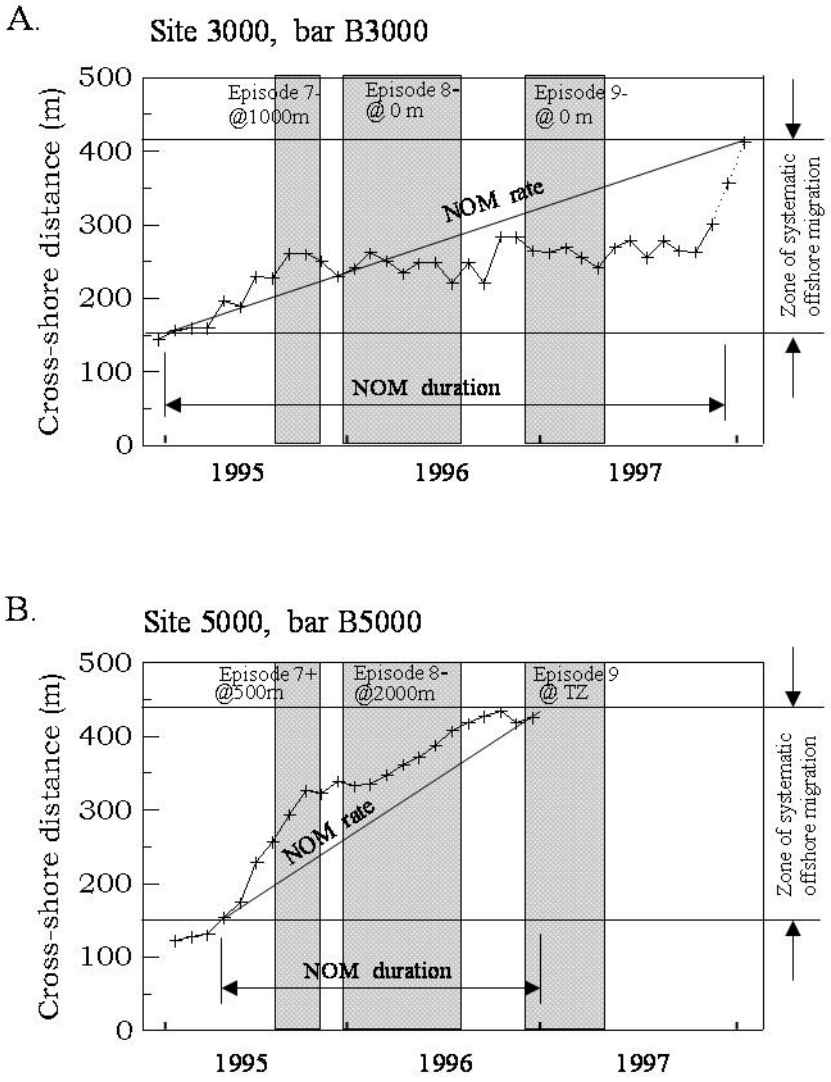

Figure 10 Time-series depicting the cross-shore location of selected bars at sites 3000 m (Figure A) and 5000 m (Figure B) alongshore from the Wanganui Rivermouth. These 2 bars are referred to as B3000 and B5000 respectively. The shaded regions mark the time intervals in which switch episodes 7, 8 and 9 occurred. The + and – notation following each episode identifies the type of switch-associated cross-shore bar migration, i.e. enhanced or suppressed migration. For example, "Episode 7+" means that the bar in question underwent enhanced seaward migration associated with episode 7. The stated distance, e.g. "@1000m", relates to the longhore distance that the bar in question was from the transition zone boundary. The horizontal lines locate the boundaries of the zone of systematic offshore bar migration (see text). The diagonal lines define the average offshore migration rate of each NOM cycle. The NOM durations are also depicted. The method used to extrapolate between the final bar-crest location and the seaward boundary of the zone of systematic offshore migration (see dashed line), is described in the text. The NOM parameter values for B3000 and B5000 are given in Table 1.

Table 1. Parameter values and descriptive statistics for all cycles of NOM which occurred during the 6.3 yr study period at sites 3000 m and 5000 m. NOM parameter values for bars B3000 and B5000 (see Figure 10) have been included in the final column.

Longshore site	NOM parameter	Parameter value (excluding B3000 & B5000)	Mean	Standard deviation	Parameter values for B3000 & B5000
3000	Duration (yr)	2.8, 1.5, 1.0	1.8	0.93	3.0
3000	Rate (m/yr)	95, 169, 240	168	72.5	88
5000	Duration (yr)	4.3, 2.5, 1.4, 2.4	2.7	1.21	>1.6
5000	Rate (m/yr)	67, 113, 205	128	70.2	<178

rate is a maximum. In the case of B5000, the track terminated, i.e. the bar disappeared, within 20 m of the seaward boundary so the parameter value calculations were based upon the final data point. The NOM durations and the average NOM rates for B3000 and B5000, and also for the other bars which completed cycles of NOM at these sites during the 6.3 yr study period, are given in Table 1.

B3000 was in an area of suppressed migration for each of the 3 episodes; during episode 7 it was located 1000 m from the transition zone, while during episodes 8 and 9 it was located adjacent to the transition zone. During its NOM cycle, B3000 had a duration value of 3 yr and an average NOM rate of 88 m/yr (see Table 1). These values were greater than the duration values for the other bars at this site (1 to 2.8 yr) and less than the other rate values (95 - 240 m/yr).

The results for B3000 suggest that for a significant change in NOM cycle characteristics to occur, a series of similarly orientated episodes of switching are required; in this case suppressed migration associated with the 3 episodes affected the bar migration pattern.

B5000 lay within the region of enhanced seaward bar migration during episode 7, within the region of suppressed migration for episode 8 and within the transition zone for episode 9. During episode 7, the bar was located 500 m from the transition zone and enhanced seaward migration is evident in Figure 10. During episode 8, B5000 was 2000 m from the transition zone and its migration rate of 138 m/yr is similar to this site's background rate of 128 m/yr (Table 1). During episode 9, B5000's migration track became discontinuous. B5000 had a NOM rate <178 m\yr which is within one standard deviation of the background mean for site 5000 (Table 1). B5000's duration value of >1.6 yr is also within one standard deviation of the longer-term mean value.

The results for B5000 suggest that bar migration associated with switching is minimal at distances in the order of 2000 m from the transition zone. However, this appears to depend upon individual switches as Shand (2000) showed that enhanced bar migration associated with switching episode 5 and suppressed migration associated with switching episode 9, could still be detected up to 3000 m from the transition zone.

Outer Bar Degeneration

To identify any relationship between bar switching and the pre-switch degenerative state of the outer bar, rectified time-exposure images sampled prior to the onset of episodes 5 to 9 were analysed. These 5 images are depicted in Figure 11. Episode 1 was excluded from the analysis for reasons explained earlier. Episodes 2 to 4 were excluded for the following reasons. While images depicting the pre-switching morphology of the seaward bar for episodes 2, 3 and 4 were available, as noted earlier, during this time period only 35 and 55 mm focal length lenses were being used. Consequently the images lacked detail toward the ends of the study area, such detail being required to satisfactorily classify the intensity patterns. In Figure 11, the location of the initial transition zones have been marked on each image. Approximately 1000 m of coast alongshore from each transition zone boundary is depicted and the intensity pattern classification for the seawardmost bar has been marked

With the exception of episode 6, the classes depicted in Figure 11 show that a difference of at least one class unit occurred between the intensity patterns on each side of the transition zone. In the case of episode 6, the southeastern (river) classification was C/D while the northwestern side was D.

A comparison of the degenerative states in Figure 11 with the bar migration behaviours depicted in Figures 8 and 9, indicates that higher levels of seaward bar degeneration (intensity classes B,C,D) are associated with those areas which subsequently experienced rapid or enhanced seaward bar migration. By contrast, areas with well developed seaward bars (class A) are associated with suppressed bar migration. These relationships are more clearly illustrated in Table 2.

DISCUSSION

This study identified cross-shore bar migration signatures associated with the 2 types of switching previously identified at Wanganui. The 6 shoreward propagating episodes were characterised by substantial seaward bar migration on one side of the transition zone and minimal migration on the opposite side (Figure 9). While substantial seaward migrations to one side of the transition zone also characterised the 2 episodes of stationary switching, larger bar migrations also occurred on the opposite side and these could be directed either shoreward as in episode 4, or seaward as in episode 6.

The only published data sequence depicting an episode of bar switching from another coast appeared in Wijnberg and Wolf (1994). This example from Egmond, on the coast of Holland, fits the definition for stationary switching, with minimal net change in the cross-shore location of the transition zones and the bars on each side of the transition zones moving substantial distances in a seaward direction.

Table 2 Contingency table showing frequencies of intensity pattern classes and type of switching-associated cross-shore bar migration, i.e. enhanced seaward migration and suppressed migration. The intensity pattern classes are defined and illustrated in Figures 5 and 6. The dashed vertical line depicts the separation between intensity pattern and type of switching-associated bar migration.

	Intensity Pattern Class							
	A		B		C		D	
Enhanced seaward migration			2	1	1		2	
Suppressed migration	3	1						

Results from Figures 8, 9 and 11 suggest that a degenerating outer bar along one section of coast facilitates substantial offshore migration by landward bars, while a well formed outer bar along the adjacent section of coast constrains migration of landward bars. Under such a scenario, bar-crests must undergo realignment in the longshore direction, i.e. bar switching is a consequence of longshore contrast in the degeneration status of the seawardmost bar.

A mechanism by which the state of degeneration of the outermost bar could control the offshore migration potential of the landward bars was proposed by Ruessink and Kroon (1994). Briefly, a well-developed outer bar, i.e. with strong relief and relatively shallow crest depth, enables a higher proportion of incident waves to break upon it, thereby reducing the incident energy available for wave breaking within the landward bar system. Return flows which are capable of driving substantial seaward migration by the landward bars during storm conditions, would occur less frequently. By contrast, a degenerated seaward bar, i.e. with subdued relief and relatively deep crest, would cause a lower proportion of incident waves to break upon it, thereby maximising both storm-driven return flows and consequent offshore bar migration within the inner bar system.

The pre-switch level of degeneration of the seawardmost bar also shows different characteristics for each type of switching (Figure 11). In the cases of shoreward propagating episodes, the level of degeneration of the seaward bar differed on either side of the transition zone. The outermost bar during stationary episode 6, however, had similar status to each side of the transition zone. In addition, the intensity pattern for episode 6 shows that a different level of degeneration may have occurred close to the transition zone; this area is marked by the asterisk in Figure 11. While stationary episode 4 was not included in the analysis, multiple longshore differences in degeneration level also appear to have occurred. Unrectified time-exposure photographs depicting the pre-switch morphology for episode 4 are reproduced as Figure 12. While the photographs were taken with a 35 mm focal length lens and have relatively low spatial resolution, it is evident that the intensity pattern close to the transition zone differed from the patterns further alongshore.

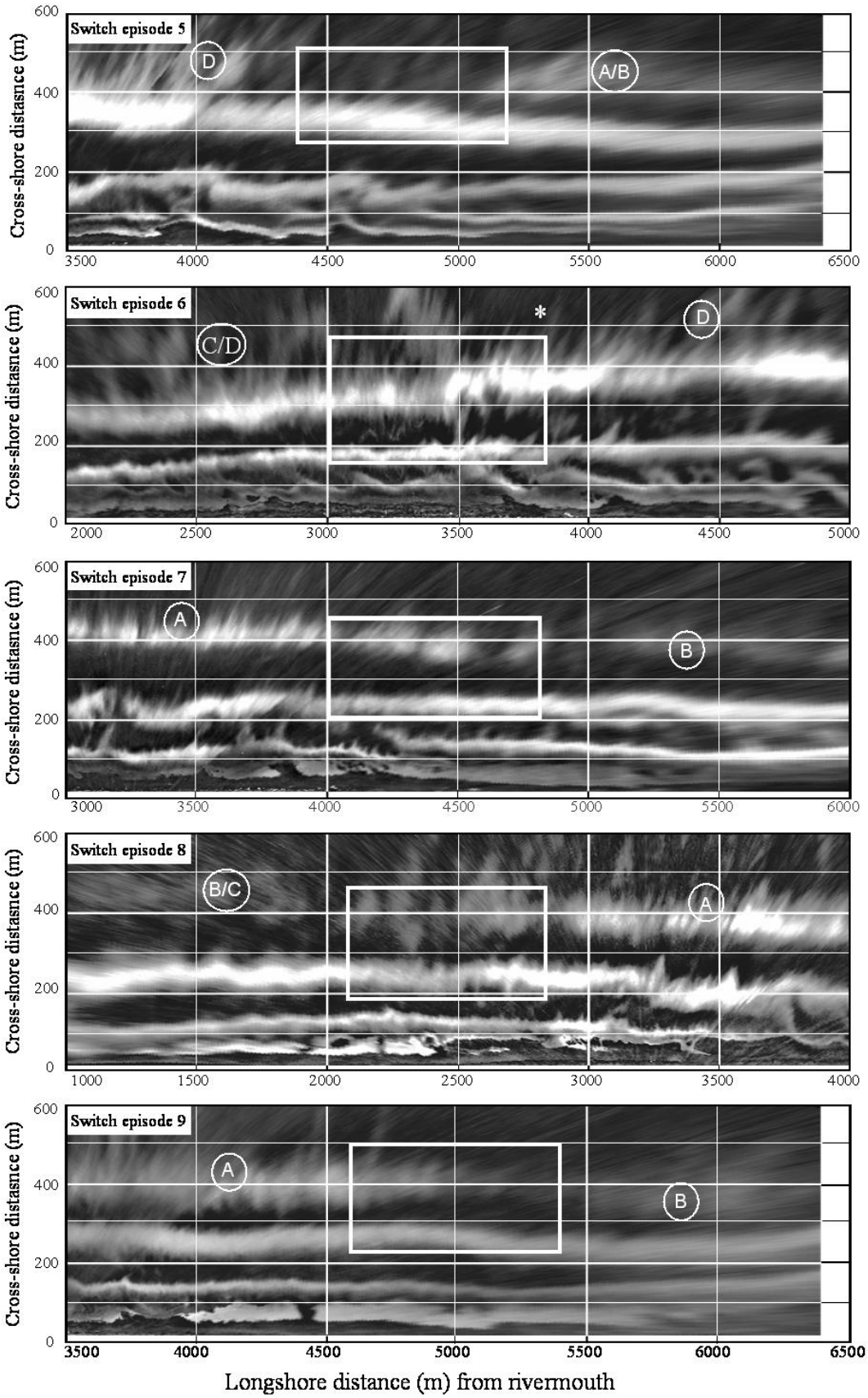
Switch episode 5
D
A/B
Switch episode 6
C/D
*
D
Switch episode 7
A
B
Switch episode 8
B/C
A
Switch episode 9
A
B
Cross-shore distasnce (m)
Longshore distance (m) from rivermouth

Figure 11 Images depicting morphology prior to the onset of bar switch episodes 5 to 9. Codes A to D refer to outer surf zone intensity pattern classifications which relate to differing levels of outer bar degeneration (see Figures 5 and 6). The rectangles denote the dimensions and location of the subsequent (initial) transition zone within which bar switching occurred. The possible significance of the intensity pattern in the vicinity of the asterisk is discussed in the text.

The pre-switch morphology was not included in Wijnberg and Wolf's (1994) example of stationary switching at Egmond. Nonetheless, the initial image of the switching sequence does suggest that multiple contrasts in degeneration status of the seawardmost bar may have occurred prior to the onset of switching.

Longshore differences in degeneration status of the seawardmost bar may result from longshore variation in the local sediment supply, as it seems plausible that such an increase (or reduction) could cause a bar to take more (or less) time to degenerate. Support for such a mechanism is suggested by results from a nourishment project at Terschelling (Hoekstra et al., 1996), which showed that seaward bar degeneration slowed down following sediment input in the vicinity of the outer bar. Variation in sediment availability may be associated with the occurrence of low amplitude migrating sand-waves or blankets. Such features have been documented on a variety of coasts, e.g. along the Nile delta (Inman et al., 1992), along the eastern USA seaboard (Trowbridge, 1995), along the Danish coast (Brunn, 1955) and along the German coast (Antia 1996). Such features have also been observed by the author in side-scan sonar images of the shoreface at Wanganui.

CONCLUSION

The phenomenon of bar switching accounts for much of the irregularity in cross-shore bar migration time-series and extreme NOM cycle characteristics evident in Wanganui data (Figure 2). Shoreward propagating bar switching was associated with enhanced seaward bar migration on one side of the transition zone and suppressed migration on the other side. Such switch-associated bar migration has been detected 2 to 3 km alongshore from the transition zone. Stationary switching was also characterised by enhanced seaward bar migration on one side of the transition zone; however, in this case, either large seaward or landward migrations occurred on the other side. If a bar experienced a series of either switch-associated enhanced seaward migrations or suppressed bar migrations, then its NOM characteristics of duration and rate could be significantly different to longer-term average values for that particular site. Furthermore, such switching could affect NOM characteristics for several hundred metres beyond the transition zone. Because bar switching is associated with significant and atypical variation in cross-shore bar migration, coastal researchers need to be mindful of this phenomenon when interpreting temporally or spatially limited morphological data-sets.

Bar switching appears to be a consequence of longshore contrast in the degeneration status of the seawardmost bar prior to the onset of bar switching. Shoreward propagating episodes were characterised by a single longshore variation in the degenerative state of the seawardmost bar. Where the outer bar had a high level of degeneration, enhanced offshore migration of the adjacent

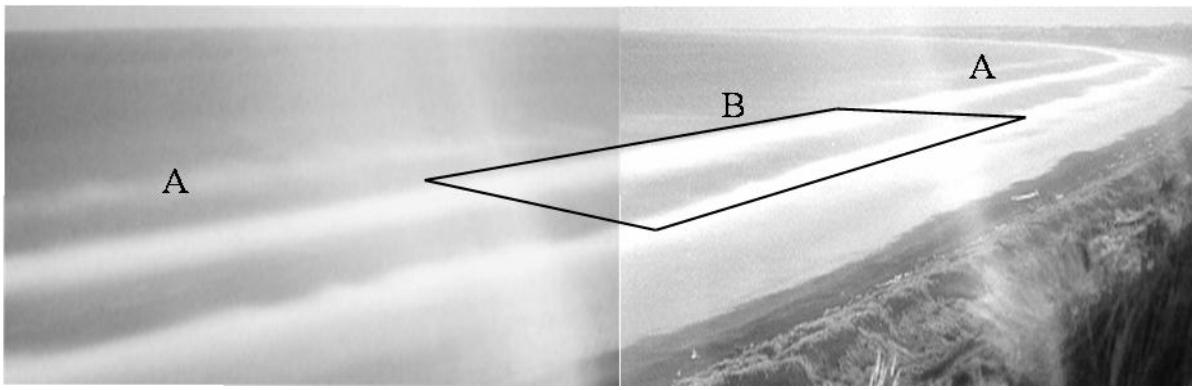

Figure 12 Time-exposure photographs depicting pre-switch morphology for episode 4. The initial transition zone for the subsequent switching has been marked on the image and the intensity pattern classes are shown for the outer bar. The photos were taken using a 35 mm lens (left) and a 55 mm lens (right) which cause merging difficulties and also reduced spatial resolution compared with later sampling. The oblique high intensity flare on each photo is due to light leaking into the camera-body ; this problem was later overcome by placing the camera-body within a light-proof bag.

---

landward bar occurred. Where the seawardmost bar was well developed, migration of the adjacent landward bar was suppressed. However, the episodes of stationary switching were more complex as the pre-switch morphology of the seawardmost bar appeared to be characterised by multiple longshore changes in its state of degeneration.

ACKNOWLEDGEMENTS

This study was supported by the Massey University Research Fund, a Vice-Chancellors Special Grant and a Research Fellowship (contract MAUX0104) from the New Zealand Foundation for Science and Technology. The author thanks Dr Mike Shepherd (Massey University, NZ), and the two JCR appointed reviewers, for their useful comments on the manuscript.

LITERATURE CITED

Antia, E. E., 1996. Shoreface-connected ridges in German and U.S. Mid-Atlantic Bights: similarities and contrasts. Journal of Coastal Research, 12(1), 141-146.

Bailey, D.G., and Shand, R.D., 1993. Determining large-scale sand-bar evolution. Proceedings of the First New Zealand Conference on Image and Vision Computing, pp. 109-116.

Bailey, D.G., and Shand, R.D., 1996. Determining large-scale sand bar behaviour. Proceedings of the IEEE International Conference on Image Processing, Lausanne, Switzerland, (2), 637-640.

Bailey, D.G., and Shand, R.D., 1997. Data fusion issues in analysing coastal morphodynamic systems. Proceedings of the first joint Australian and New Zealand conference on Digital Image and Vision Computing: Techniques and Applications, Auckland, New Zealand, pp. 107-112.4

Birkemeier, W.A., 1984. Time scales of nearshore profile change. Proceedings of the 19th International Conference on coastal Engineering, ASCE, pp. 1507-1521.

Bogle, J.A.; Bryan, K.R.; Black, K.P.; Hume, T.M, and Healy, T.R., 2001. Video observations of rip formation and evolution. Journal of Coastal Research, Special Issue 34, 117-127.

Bruun, P. 1955. Migrating sand waves or sand humps, with special reference to investigations carried out on the Danish North Sea coast. Proceedings of the 5th Conference on Coastal Engineering, ASCE, pp. 269-295.

Chappell, J., and Eliot, I.G., 1979. Surf-beach dynamics in time and space - an Australian case study, and elements of a predictive model. Marine Geology, 32, 231-250.

De Vroeg, J.H.; Smit, E.S.P., and Bakker,W.T., 1988. Coastal Genesis. Proceedings of the 21st International Conference on coastal Engineering, ASCE, pp. 2825-2839.

Donohoe, B.F.P., 1998. Spatial and temporal bar morphodynamics of Muriwai Beach. MSc thesis, Auckland University, New Zealand, 104p.

Hoekstra, P.; Houwman, K.T.; Kroon, A.; Ruessink, B.G.; Roelvink, J.A., and Spanhoff, R., 1996. Morphological development of the Terschelling shoreface nourishment in response to hydrodynamic and sediment transport processes. Proceedings of the 25th International Conference on Coastal Engineering, ASCE pp. 2897-2910.

Holland, K.T.; Holman, R.; Lippmann, T.; Stanley, J and Plant, N., 1997. Practical use of video imagery in nearshore oceanographic field studies. Journal of Ocean Engineering, 22, 81-92.

Holman, R.A., and Bowen, A.J., 1982. Bars, bumps, and holes: models for the generation of complex beach topography. Journal of Geophysical Research, 84, 457-468.

Inman, D.L.; Hany, M; Elwany, S; Khafagy, A A., and Abraham, G., 1992. Nile delta profiles and migrating sand blankets. Proceedings of the 23rd International Conference on Coastal Engineering, pp. 3273-3284.

Johnston, R.M.S., 1985. Coastal change and hazard delineation on the Rangitikei-Wanganui coast. Proceedings of the 8th Australasian Conference on Coastal and Ocean Engineering, pp. 411-420.

Kingston, K.S; Ruessink, B,G,; van Enckevort, I.M.J., and Davidson, M.A., 2000. Artificial neural network correction of remotely sensed sandbar location. Marine Geology, 169: 137-160.

Kroon, A., 1990. Three-dimensional morphological changes of nearshore bar system along the Dutch coast near Egmond aan Zee. Proceedings of the Skagen Symposium, Journal of Coastal Research, Special Issue, 9, 430-451.

Kroon, A., 1994. Sediment transport and morphodynamics of the beach and nearshore zone near Egmond, the Netherlands. PhD thesis, Utrecht University, The Netherlands, 275p.

Kroon, A., and Hoeskstra, P., 1993. Nearshore bars and large-scale coastal behaviour. In: List, J.H., (ed.), Large-Scale Coastal Behaviour '93. U.S. Geological Survey, Open-File Report 93-381, pp. 92-95.

Kuriyama, Y., and Lee J.H., 2001. Medium-term beach profile change on a bar-trough region at Hasaki, Japan, investigated with complex principal component analysis. Proceedings of Coastal Dynamics'01, ASCE, pp. 959-968.

Lippmann, T.C., and Holmam, R.A., 1989. Quantification of sand-bar morphology: a video technique based on wave dissipation. Journal of Geophysical Research, 94, 995-1011.

Lippmann, T.C. Holman, R.A. and Hathaway, K.K. 1993: Episodic, non-stationary behaviour of a double bar system at Duck, North Carolina, U.S.A., 1986-1991, Journal of Coastal Research, Special Issue, 15, 49-75.

Macky, G.H.; Cumming. R, J., and Valentine, E. M., 1988. Measurements of ocean wave climate at Wanganui and Himitangi Beach. Hydrology Centre, Department of Scientific and Industrial Research, Christchurch New Zealand.

Patterson, D.C., 1992. Wanganui Port development feasibility studies: coastal engineering aspects. A report for Ocean Terminals and the Wanganui District Council, New Zealand, 51p.

Pillans, B.J., 1983. Late Quaternary marine terrace chronology and deformation, South Taranaki, New Zealand. Geology, 11, 292-297.

Plant, N.G., and Holman, R.A., 1998. Extracting morphologic information from field data. Proceedings of the 26th International Conference on Coastal Engineering, ASCE, pp. 2773-2784.

Plant, N.G.; Holman, R.A.; Freilich, M.H., and Birkemeier, W.A., 1999. A simple model for inter-annual sand bar behaviour. Journal of Geophysical Research, 104(C7), 15755- 76.

Ruessink, B.G. and Kroon, A. 1994: The behaviour of a multiple bar system in the nearshore zone of Terschelling, the Netherlands: 1965-1993, Marine Geology, 121, 187-197.

Ruessink, B.G., and Terwindt, J.H.J, 2000. The behaviour of nearshore bars on a time scale of years: a conceptual model. Marine Geology, 163, 289-302.

Ruessink, B.G.; Holman, R.A., and Wijnberg, K.M., 2001. Interannual nearshore bar behaviour: an intersite comparison. Proceedings of Coastal Dynamics'01, ASCE, pp. 646-655.

Shand, R.D., 2000. Offshore migration of coastal sand-bars at Wanganui New Zealand. PhD thesis, Massey University, New Zealand. School of Global Studies, Miscellaneous Publication Series, 00/8, 295p.

Shand, R.D. and Bailey, D.G. 1999: A review of net offshore bar migration with photographic illustrations from Wanganui, New Zealand, Journal of Coastal Research, 15(2), 365-378.

Shand, R.D.; Bailey, D.G., and Shepherd, M.J., 1999. An inter-site comparison of net offshore bar migration characteristics and environmental conditions. Journal of Coastal Research, 15(3) 750-765.

Shand, R.D.; Bailey, D.G., and Shepherd, M.J., 2001. Longshore realignment of shore-parallel sand-bars at Wanganui, New Zealand. Marine Geology, 179, 147-161.

Smith, R.K. and Ovenden, R., 1998. Wanganui District Council Coastline Stability Investigation Between Kai Iwi and Harakeke. Report: WNG80202. National Institute of Water and Atmospheric Research Ltd, New Zealand, 32p.

Trowbridge, J.H., 1995. A mechanism for the formation and maintenance of shore-oblique sand ridges on storm-dominated shelves. Journal of Geophysical Research, 100-C8, 16071- 16086.

Van Enckevort, I.M.J., and Ruessink, B.G., 2001. Effect of hydrodynamics and bathymetry on video estimates of near shore sandbar position. Journal of Geophysical Research, 106: 16969-16980.

Wijnberg, K.M., 1995. Morphologic behaviour of a barred coast over a period of decades. PhD thesis, Utrecht University, the Netherlands, 245p.

Wijnberg, K.M., 1996. On the systematic offshore decay of breaker bars. Proceedings of the 25th International Conference on Coastal Engineering, ASCE, pp. 3600-3613.

Wijnberg, K.M. and Wolf, F.C.J. 1994: Three-dimensional behaviour of a multiple bar system. Proceedings of Coastal Dynamics '94, ASCE, pp. 59-73.

Shand, R.D.; Hesp, P.A., Bailey, D.G., and Shepherd, M.J., 2003. A conceptual beach-state model for the inner bar of a storm-dominate, low to moderate tidal range coast at Wanganui, New Zealand. Proceedings of Coastal Sediments '03.

Conceptual beach-state model for the inner bar of a storm-dominated, micro/meso tidal range coast at Wanganui, New Zealand

R.D. Shand[1]; D.G. Bailey[2]; P.A. Hesp[3], and M.J. Shepherd[1]

Abstract

Plan-view morphological configurations were identified for the inner sub-tidal bar at Wanganui, New Zealand, and configuration behaviour was related to wave height, longshore current (in terms of longshore wind components), tidal range (in terms of neap tide-spring tide variation), and antecedent morphology to derive a conceptual model for this type of coast. The Wanganui coast is characterised by fine sand, multiple sand bars, frequent storm waves, longshore current, a neap tidal range of 0.8 m and a spring tidal range of 2.4 m. Transverse configurations occur more frequently and were more persistent than the other 3 types of configuration used in the study: linear, undulating and subdued. The predominant class transitions consist of transverse configurations changing to subdued and undulating; undulating configurations changing to transverse; linear configurations changing to undulating, and subdued configurations changing to transverse. Configuration change to transverse, undulating and linear occur under lower (neap) tidal conditions, with linearity increasing with increasing wave height and strength of the longshore current. Change to subdued configurations corresponds with higher (spring) tides, lower wave height and weaker longshore current. The direction of longshore currents also influences configuration change. In particular, the formation of transverse configurations are facilitated by longshore currents aligned with the oblique rip currents which characterise the Wanganui coast. By contrast, the formation of subdued and undulating configurations appear to be facilitated by longhore currents opposing obliquely orientated rip currents. Morphological feedback enables transverse configurations to resist greater wave height and stronger longshore current than occur during their formation. While undulating and linear configurations remain coherent during higher tidal range, bar-crests broaden in the cross-shore direction with the opposite occurring during times of lower tidal range. Transverse configurations may also persist during higher tidal range; however, in this situation bar-crest broadening and channel infill can result in a class change to subdued configurations.

INTRODUCTION

Sand-bar plan-view configurations on sand-dominated coasts depend on the energy regime, sediment characteristics and physical boundary conditions. This paper is

1) Geography Programme, Massey University, Private Bag 11222, Palmerston North, New Zealand, r.d.shand@clear.net.nz
2) Institute of Information Sciences and Technology, Massey University, Private Bag 11222, Palmerston North, New Zealand.
3) Department of Geography and Anthropology, Louisiana State University, Baton Rouge, LA 70803-4105, United States of America, pahesp@lsu.edu

concerned with configurations of the landwardmost (inner) sub-tidal bar on the Wanganui coast of the New Zealand North Island This is a multi-bar coast characterised by fine sand, storm waves, micro-meso tidal range (as defined by Davies, 1980), and longshore currents. In a recent study of daily to monthly configuration change at Wanganui, Shand (submitted) found that bar behaviour within the mid surf zone was consistent with the Short and Aagaard (1993) model, a comprehensive configuration-based conceptual model for multi-bar coasts with micro tidal range. However, the Short and Aagaard model did not account for bars in the outer surf zone at Wanganui becoming subdued and disappearing, this being the final stage in the process of net offshore bar migration (see Shand and Bailey, 1999). Furthermore, inner bar behaviour at Wanganui had several characteristics which differed from the Short and Aagaard model and these differences form the basis of the present paper.

The inner bar component of the Short and Aagaard multi-bar model is the frequently referenced Wright and Short (1984) morphodynamic model for single bar beaches. The Wright and Short model describes sub-tidal bars as moving seaward and becoming linear during higher energy conditions, this configuration or state being termed 'longshore bar and trough' in their model. As wave energy subsequently decreases, the bar migrates landward and develops an undulating configuration ('rhythmic bar and beach' state). Gradually, transverse bars develop between the undulating bar and the inter-tidal beach, with attachment points being separated by rip channels ('transverse bar and rip' state). Morphological feedback is important in these recovery processes. The model is also characterised by non-linear structures tending to have both symmetry about shore-normal axes and regularity in longshore spacing. Under extended fair-weather conditions the bar system continues to migrate landward to fully merge with the inter-tidal beach and form 'ridge and runnel' or 'low tide terrace' configurations.

Differences between the Wanganui inner bar study (Shand, submitted) and the Wright and Short model are now described. Cross-shore bar migration at Wanganui did not respond to changing levels in wave energy; this is possibly a consequence of wave energy filtering by the seaward bar(s). While the bar did become linear under higher wave conditions and become strongly non-linear (transverse bars and rips) under lower waves, there was not a statistically significant difference in wave height separating the formation of undulating and linear configurations. Subdued configurations with an average cross-shore width of ~100 m occurred at Wanganui. These features are substantially wider than the most subdued morphology in the Wright and Short model, i.e. low tide terraces. This situation suggests that tidal range can be important in morphodynamic processes at Wanganui. Finally, it was found that only 8% of non-linear configurations at Wanganui were symmetrical about shore-normal axes, a result which indicates longshore currents play a significant morphodynamic role.

The purpose of the present paper is to develop a conceptual beach-state model for the inner bar at Wanganui at a time-scale of days to months, and to incorporate variation in incident wave height, tidal range (in terms of neap tide/spring tide change), longshore

currents and antecedent morphology. Configurations are determined by developing and applying a mutually exclusive classification scheme to a 2 yr set of time-exposure images.

FIELD SITE

The 500 m long field site is ~3 km from the Wanganui Rivermouth on the southwestern coast of the North Island of New Zealand (Fig 1). The nearshore is characterised by fine sand (2 to 3 phi), and has a cross-shore slope of ~0.0085 and width of ~550 m. Three sand-bars are usually present; these bars undergo net offshore migration, with the mean life-cycle of a bar being ~3 yr (Shand et al., 1999). The camera used for photographing the surf zone was located on top of a 42 m high cliff which lies 100 m to the rear of the beach.

The process conditions are summarized as follows. The mean neap tide range = 0.8 m and the mean spring tide range is 2.4 m. The mean deepwater significant wave height is 1.3 m and the 5% excedence value is 2.5 m (Macky et al., 1988). The mean wave period is 10.1 s (range 3.5 s to19 s) with sea wave conditions occurring for 75% of the time and swell waves for the remaining 25% (Patterson, 1992). Five years of daily wave observations, which encompassed the study period, show 42% of waves approach from the west, 24% from the south and 34% lie within one degree of shore-normal. Longshore current measurements made using floats released into the inner surf zone as part of a Port Development Study (Patterson 1992), found the mean current = 0.42 m/s and the 5% excedence value = 1.01 m/s. Analysis of wind data collected at nearby Wanganui Airport, shows prevailing winds approach the coast at ~35 deg from the shoreline. The 5% excedence value for the wind speed is 12.4 m/s. The longshore wind component is strongly correlated with the longshore current ($p < 0.001$).

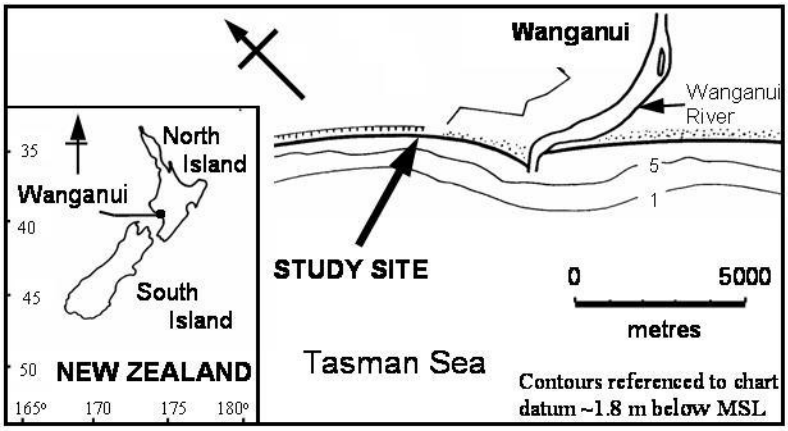

Figure 1 Location map of the Wanganui study site.

METHODS

The following methods used to derive morphological and process data for this study have been described in greater detail by Shand (submitted).

A panorama of 4 photographs captured the 500 m long study area. Each photo was exposed for 4 mins to minimise tidal change experienced during sampling and to ensure a relatively stable representation of the breaking wave pattern. Such photographs are equivalent to images produced by time-averaging video frames (Lippmann and Holman, 1989). These images provide an analogue for surf zone morphology because elevated topography such as sand-bars are characterised by locations of higher intensity due to waves breaking preferentially in shallower water (Lippmann and Holman, 1989). An example of a time-exposure panorama which encompasses the study site, is shown in the upper portion of Fig 2.

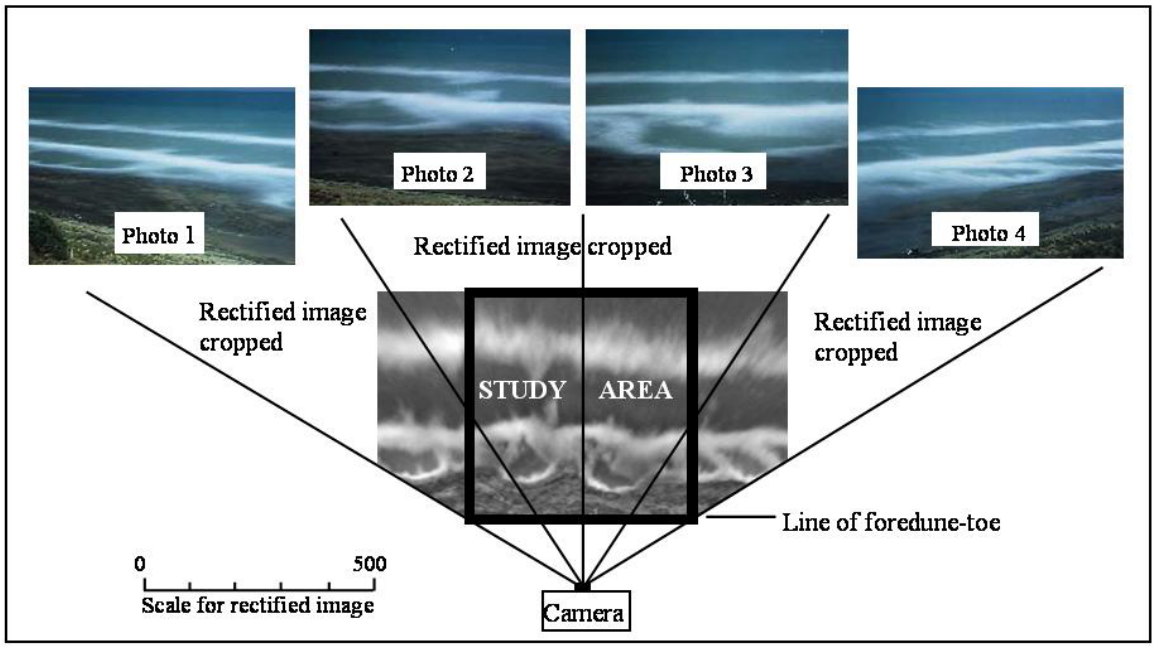

Figure 2. An example of a panorama of 4 time-exposure photographs (above), and the corresponding rectified and merged images (below). Areas of high intensity represent elevated features such as sand-bars, and the intermediate areas of low intensity represent rip channels and longshore troughs Two hundred metre wide segments of rectified image have been retained at the longshore margins of the 500 m long study site to assist in the interpretation of 3D structures.

This study utilizes a 2 yr set of photographs collected between September 1992 and August 1994. Field sampling was carried out at ~4 day intervals (standard deviation = 2 days), with more frequent sampling occurring during times of higher energy to detect faster morphological change.

Digital image processing was used firstly to rectify each photograph to ground co-ordinates, secondly to merge this rectified image with adjacent rectified images from the panorama, and thirdly to transform the image mosaic to achieve a straightened coastline. These techniques have been described in detail by Bailey and Shand (1993, 1996). An example of the final output image is shown in the lower portion of Fig 2.

Intensity maxima only approximate a bar-crest location as environmental conditions and bar morphology influence break-point location. For the present study, maximum errors (using the 95% confidence interval) are 15 m in the cross-shore direction and 12 m in the longshore direction.

Configurations were based on a mutually exclusive, shape-based, classification scheme similar to that of Lippmann and Holman (1990). Alternative procedures involve morphological assemblages (e.g. Wright and Short, 1984; Short and Aagaard 1993), complex eigenfunctions (Ruessink et al., 2000), or cross-shore deviations between the longshore bar-crest and a fitted linear model (van Enckevort and Wijnberg, 1999). However, these approaches were not considered because they require regular and relatively simple 3D morphologies, whereas non-linear configurations at Wanganui are predominantly irregular and often complex.

The following three criteria, and associated binary decisions shown within brackets, were used to categorise different intensity patterns (morphological configurations) associated with the sub-tidal inner bar at Wanganui:

- cross-shore bar profile relief (pronounced c.f. subdued);
- longshore variability (linear c.f. non-linear) of a longshore bar-crest;
- longshore variability (continuous c.f. discontinuous) of the trough, i.e. region of low intensity values located landward of a bar.

In addition, several other qualifiers are detailed in Shand (submitted) which were applied to ensure consistency when applying the classification scheme.

Four classes were defined to represent the morphologies contained within the image data-set. These morphological classes are identified using the following descriptors: subdued, linear, undulating and transverse, and an example of each is shown in Fig 3. Linear configurations are broadly equivalent to both the ‘longshore bar and trough’ in the Wright and Short model and ‘bar types F and G’ in the Lippmann and Holman (1990) classification. Undulating configurations are broadly equivalent to ‘rhythmic bar and beach’ (Wright and Short) and ‘bar type E’ (Lippmann and Holman), while transverse configurations are broadly equivalent to ‘transverse bar and rip’ (Wright and Short) and ‘bar types C and D’ (Lippmann and Holman). Subdued configurations have the appearance of either a wide area containing very low amplitude features or a wide terrace; this differs in scale and in some cases it also differs in form to Wright and Short’s ‘ridge and runnel/low tide terrace’ and Lippmann and Holman’s ‘bar type B’.

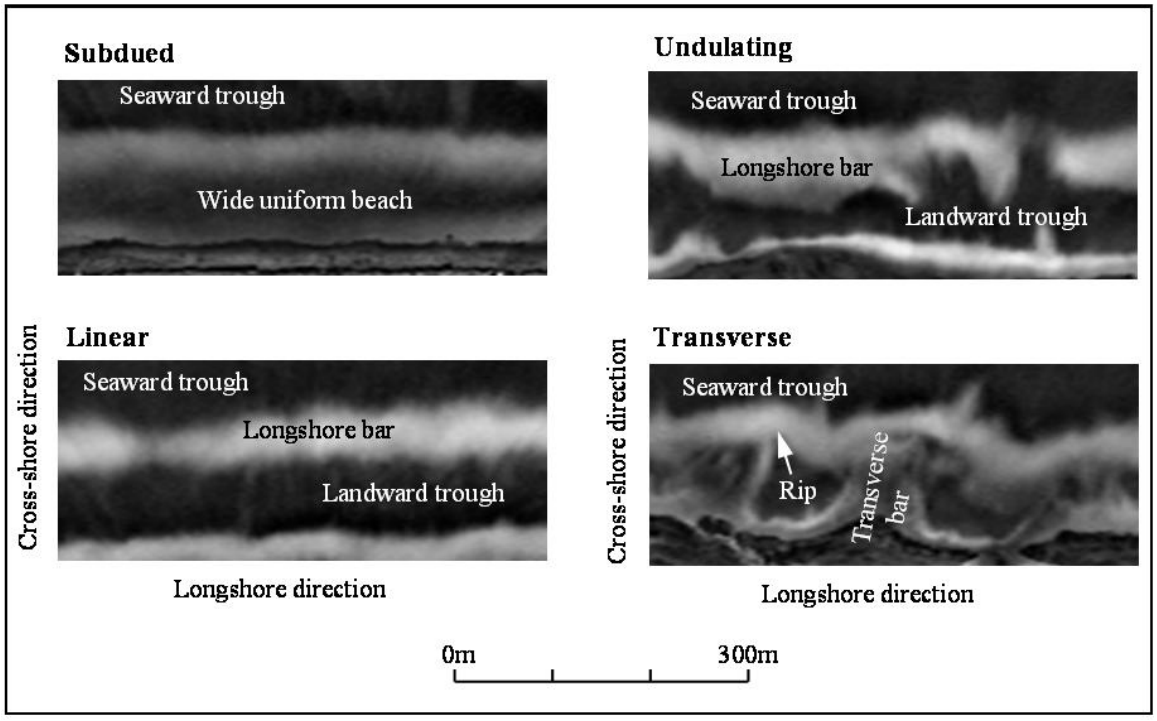

Figure 3 Examples of morphologies corresponding to the 4 configuration classes derived in the text.

Different types of configuration could occur contemporaneously at different locations within the 500 m long study site, so the modal class for each sample, i.e. the class with the greatest longshore length, was used for analysis. Furthermore, errors of up to 100 m were observed in the (longshore) length assigned to a particular class under the range of tide and wave conditions experienced during the study. So modal class status was only assigned when the length was at least 100 m greater than that of any other configuration class present within a sample. These procedures resulted in 124 inner bar samples being available for subsequent analysis.

Wave height data consisted of daily observations made at the break-point using the 'staff and horizon' method described in, for example, Patterson and Blair (1983), and Horikawa (1988). The inter-survey maximum (daily) wave height was the wave-based parameter used for analysis.

The longshore wind component has been identified as a suitable surrogate, in terms of variation, for the longshore current (Nummedal and Finley, 1978), and this approach is used in the present study. The longshore wind speed corresponding to the maximum inter-survey wave height was used in analysis, because the effectiveness of longshore current in sediment transport depends on the corresponding wave height (Komar and Inman, 1970; Hardisty, 1990). Three-hourly longshore wind measurements were averaged over the 9 hours prior to the relevant wave height measurement to

account for wind fluctuation.

Official tide data were used to determine tidal range at the time of maximum inter-survey wave height.

RESULTS and DISCUSSION

The frequencies (percentages) and residence times (persistence) for the different types of configuration are depicted in Figs 4A and B respectively. Transverse configurations occurred most frequently (55%), followed by undulating (17%), subdued (15%) and linear (13%). Transverse were also the most persistent configuration (mean = 12.6 days) followed by subdued (mean = 9.25 days), linear (mean = 5.7 days) and undulating (mean = 5.2 days).

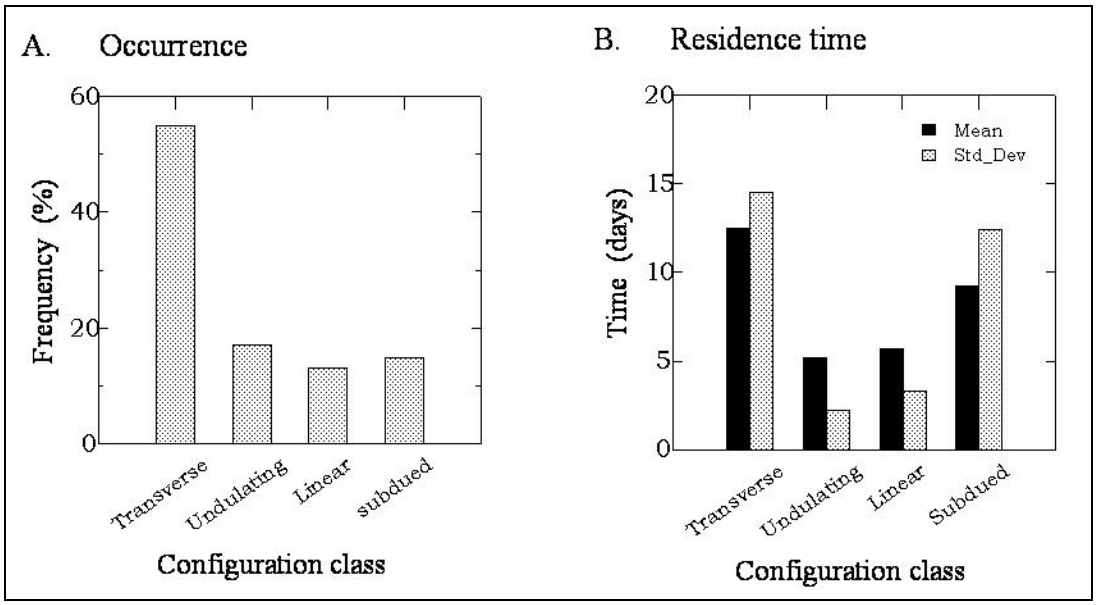

Figure 4 Frequencies (A) and, mean and standard deviation of residence times (B) for configuration classes.

Numbers and percentages of transitions between different configurations are shown in Table 1. Transverse configurations tended to change to either undulating (42%) or subdued (42%), while both undulating and subdued configurations tended to change to transverse (82% and 75% respectively). These results show configurations preferentially fluctuate between transverse and undulating, and also between transverse and subdued. A small percentage of each of these configuration changed to linear, while linear configurations changed primarily (66.6%) to undulating. There was therefore little tendency for transverse configurations to change directly to linear by omitting or 'jumping' the undulating state. Such jumps in configuration were observed by Lippmann and Holman (1990) within the inner bar at Duck, North Carolina, and rapid 'up-state' behaviour characterises the Wright and Short single bar model. The contrasting behaviour at Wanganui will be considered further later in this section.

Table 1. Transitions from configuration classes at top of table to configuration classes on left side of table.

	Transition From			
Transition To	Transverse	Undulating	Linear	Subdued
Transverse	+	9 (82%)	2 (33%)	6(75%)
Undulating	8 (42%)	+	4 (67%)	1 (12.5%)
Linear	3 (16%)	2 (18%)	+	1 (12.5%)
Subdued	8 (42%)	0 (0%)	0 (0%)	+

Wave height, tide range and wind conditions corresponding to inter-survey periods in which configuration change occurred, and also to periods in which no configuration change occurred, are depicted in Figure 5. Graphs on the left represent configuration change, while graphs on the right represent no configuration change. Two-sample t-tests were used to determine whether differences in wave height (A), tidal range (B) or longshore wind speed (C) values for different configurations within each graph were statistically significant. These test results, in terms of the 5%, 10% and 20% levels of significance, are denoted by symbols within the matrices located between each pair of graphs. The lower matrix compares environmental conditions associated with the same type of configuration in each pair of graphs. It is noted that the t-test assumption of sample normality was met in that all skewness values were non-significant. To evaluate the longshore wind direction data, either two-sample Chi-square tests, or Fisher exact probability tests were used depending on sample size and size of the expected frequencies (Siegel, 1956).

The results (Fig 5A) show similar wave heights occurred during class changes to transverse and subdued configurations, but significantly higher values occurred during class changes to undulating and linear configurations. These results have been reproduced from Shand (submitted) and, as noted earlier in the introduction, they are broadly consistent with the Wright and Short model. For undulating, linear and subdued

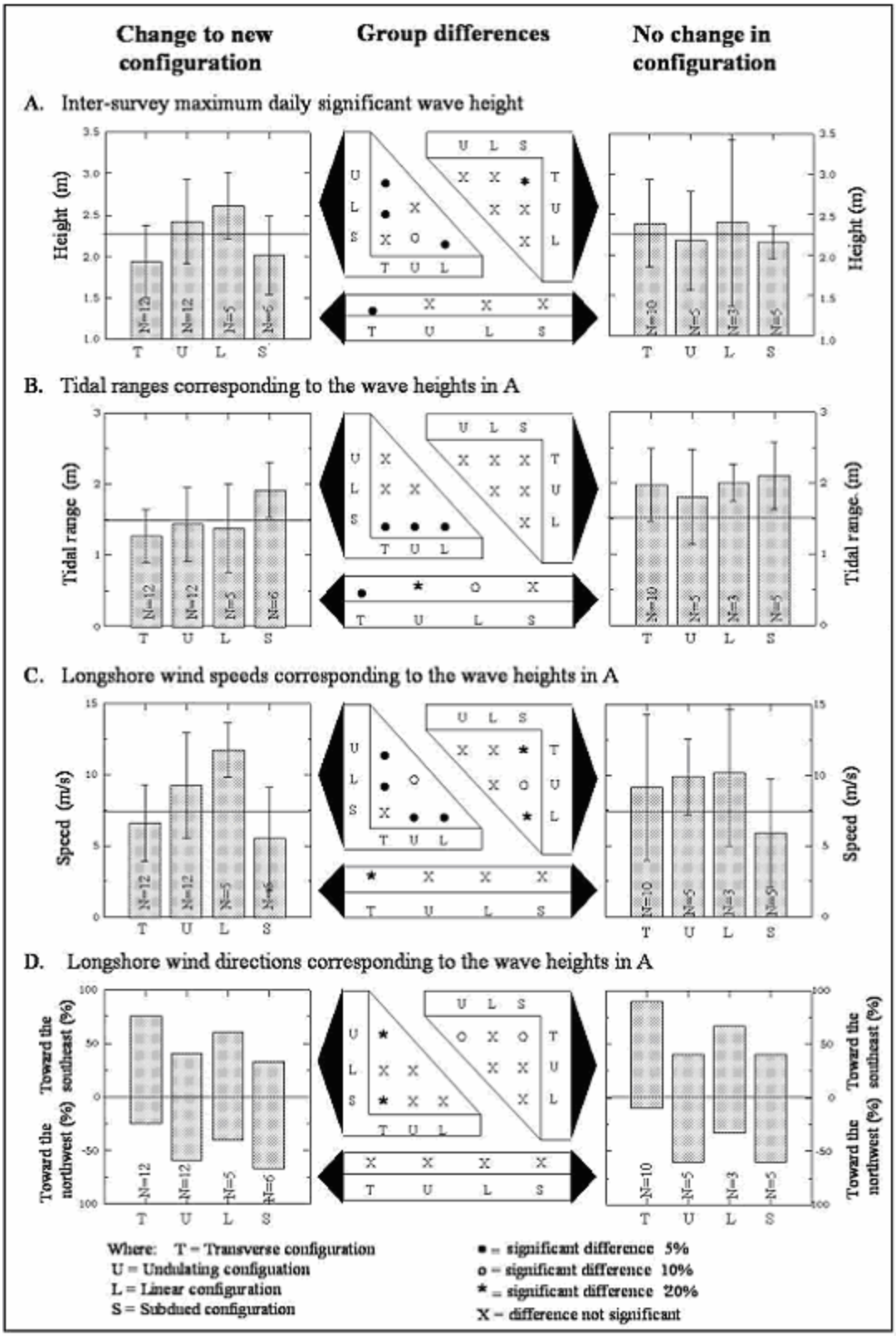
Change to new configuration
Group differences
No change in configuration
A. Inter-survey maximum daily significant wave height
Height (m)
B. Tidal ranges corresponding to the wave heights in A
Tidal range (m)
C. Longshore wind speeds corresponding to the wave heights in A
Speed (m/s)
D. Longshore wind directions corresponding to the wave heights in A
Toward the southeast (%)
Toward the northwest (%)
N=12
N=5
N=6
N=10
N=3
T U L S
Where: T = Transverse configuration
U = Undulating configuration
L = Linear configuration
S = Subdued configuration
• = significant difference 5%
o = significant difference 10%
* = significant difference 20%
X = difference not significant

Figure 5 Graphs depicting process variable values associated with inter-survey changes to new configurations are shown on the left of the figure, while graphs depicting values associated with no change in configuration are shown on the right. The vertical error bars in A-C represent one standard deviation about the mean which is represented by the bar height. The statistical significance of differences in process variable values associated with different configurations, are depicted by the symbols contained in the centrally located matrices. The upper left matrix within each set of three matrices, relates to the graph depicting changes to new configurations, the upper right matrix relates to the graph depicting no change in configuration, and the lower matrix relates to the same type of configuration in each graph. The types of statistical test used for these assessments are described within the text.

configurations, wave heights during periods when no configuration change occurred were statistically similar to wave heights during periods when change to these classes occurred. In contrast, wave heights during periods when no transverse configuration change occurred were significantly different (greater) than wave heights which occurred during the formation of such configurations. This result indicates that in some situations, strongly non-linear configurations can resist wave energy otherwise capable of increasing their linearity.

Tidal range results (Fig 5B) show the 3 pronounced configuration types tend to form under lower (neap) tide conditions, results consistent with the Wright and Short model for micro tidal beaches. However, subdued configurations form during times of higher (spring) tide. So, while both transverse and subdued morphologies form under lower wave conditions, they require contrasting tidal range. This tidal influence at Wanganui comes despite the relative tidal range (RTR), i.e. the ratio of the mean spring tide range to the modal breaking wave height which equals 1.85 at Wanganui, being below both the theoretical threshold (2.0) determined by Masselink (1993), or the field-based threshold (3.0) identified by Masselink and Short (1993). The graph on the right of Fig 5B, shows that all configuration types could survive the morphological smoothing effect other research has associated with a higher tidal range (e.g. Wright et al., 1987; Masselink , 1993). However, while linear and undulating bar-crests will not broaden to the extent of causing a change in state (Table 1), troughs and rip channels in the vicinity of transverse configurations may infill to the extent that a change to subdued configuration occurs (Table 1).

Longshore wind results (Fig 5C) are similar to the wave height results in that lower speeds occur during class change to transverse and subdued configurations, while higher speeds occur during change to undulating and linear configurations. It is noted that linear configurations occur under significantly higher longshore winds, and hence stronger longshore currents, than those which occur during the formation of undulating configurations; this difference was not statistically significant with the configuration change-associated wave data in Fig 5A. The longshore wind speed during periods in which no configuration change occurred are also similar to the wave height results, with transverse configurations being able to resist significantly higher winds (stronger

longshore current) than occurred during the formation of these configurations. The influence of strongly non-linear configurations on both the longshore and wave induced current fields, and hence on the persistence of such configurations, must reflect morphological feedback processes and free or self-organised behaviour as defined by, for example, Southgate and Beltran (1998).

Such morphological feedback may explain why strongly non-linear configurations at Wanganui tend not to change directly to linear configurations as noted earlier. In addition, the tendency for rapid and direct upstate transitions during higher wave conditions on single bar coasts and at Duck, may reflect the higher proportion of incident energy able to reach the (inner) bar due to the lack of filtering by seaward bars. Note that Duck has only a single seaward bar compared with more than one at Wanganui (Shand et al., 1999). Alternatively, the more rapid morphological change at single bar sites and at Duck, may be associated with lower tidal range and/or smaller sand-bar volumes (Shand et al., 1999).

The effects of morphological control, together with the influences of changing wave height, longshore current and tidal range, on morphological configurations at Wanganui, together with the effects of morphological control, are conceptualised in Fig 6.

The direction of longshore wind (longshore current) results in Fig 5D, show transverse configurations were more likely to occur under southeasterly directed (toward the rivermouth) winds, while undulating and subdued configurations tended to occur under northwesterly directed winds. A similar and somewhat more enhanced pattern is evident in the longshore wind directions which occurred during periods in which no configuration change occurred. The association between southeasterly directed longshore currents and the formation of transverse configurations may result from an antecedent morphological imprint with a southeasterly directed offset. It seems likely such an imprint would occur as Shand (submitted) showed that 69% of non-linear configurations at Wanganui were skewed toward the southeast and that this was directionally consistent with the long-term longshore wind pattern. Such an imprint would facilitate transverse development as the longshore current would be aligned with, and hence enhance, currents within oblique depressions or mini-rips. Further morphological control is suggested by the formation of undulating and subdued configurations, which, as noted earlier, develop exclusively from transverse configurations (Table 1). In this situation, northwesterly directed longshore currents would oppose the southeasterly skewed rip currents, thereby disrupting the underlying cellular flow and lead either to the occurrence of undulating configurations, by erosion of the transverse bar from the lower foreshore under lower tidal conditions, higher wave heights and stronger longshore currents, or to the occurrence of subdued configurations by the infill of rip channels under conditions of higher tide range, lower wave height and weaker longshore currents.

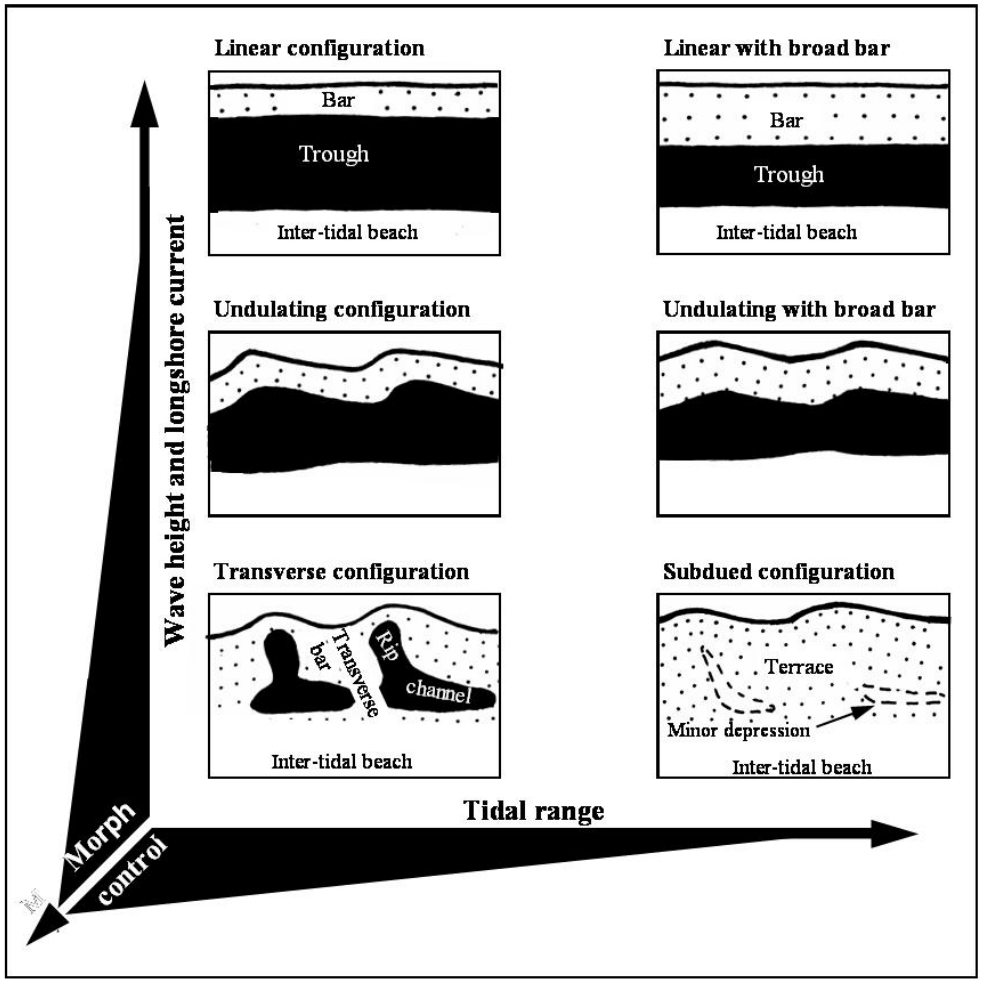

Figure 6 Schematic representation of morphological configurations and their relationship to wave height, longshore current and tidal range. The relative importance of morphological control associated with different configurations is also depicted.

CONCLUSIONS

A configuration plan-view analysis was carried out on a 2 year image-based data-set of the landward sub-tidal bar at Wanganui, New Zealand. The identified morphological behaviour was then related to wave height, longshore current (via the longshore wind component), tidal range (in terms of neap tide-spring tide variation), and antecedent morphology to derive a conceptual model for this type of coast. Transverse configurations occur more frequently and were more persistent than the other 3 types of configuration: linear, undulating and subdued. The predominant class transitions consist of transverse configurations changing to subdued and undulating; undulating configurations changing to transverse; linear configurations changing to undulating, and subdued configurations changing to transverse.

Configuration change to transverse, undulating and linear occur under lower (neap) tidal conditions, with linearity increasing with increasing wave height and strength of the longshore current. Change to subdued configurations corresponds with higher (spring) tides, lower wave height and weaker longshore current. The direction of longshore currents also influences configuration change, with the formation of transverse configurations being facilitated by longshore currents which are aligned with the oblique rip currents that characterise the Wanganui coast. By contrast, the formation of subdued and undulating configurations appear to be facilitated by longhore currents which oppose obliquely orientated rip currents. Morphological feedback enables transverse configurations to resist greater wave height and stronger longshore current than occur during their formation. While undulating and linear configurations remain coherent during higher tidal range, bar-crests broaden in the cross-shore direction with the opposite occurring during times of lower tidal range. Transverse configurations may also persist during higher tidal range; however, in this situation bar-crest broadening and channel infill can result in a class change to subdued configurations. Future quantitative morphodynamic modelling will need to incorporate interactions between 3D morphologies and obliquely orientated rip channels, tidal range (in terms of neap tide-spring tide variation) and longshore currents when considering coastal environments similar to that at Wanganui.

ACKNOWLEDGEMENTS

This study was supported by the Massey University Research Fund, a Vice-Chancellors Special Grant and a Research Fellowship (contract MAUX0104) from the New Zealand Foundation for Science and Technology.

REFERENCES

Bailey, D.G., and Shand, R.D., 1993. Determining large-scale sand bar evolution. *Proceedings of the First New Zealand Conference on Image and Vision Computing*, pp. 109-116.

Bailey, D.G., and Shand, R.D., 1996. Determining large-scale sand bar behaviour. *Proceedings of the IEEE International Conference on Image Processing*, Lausanne, Switzerland, (2), 637-640.

Davies, J.L., 1980. Geographical variation in coastal development. In: Clayton, K.M., (ed)., Geomorphology Texts 4. Longman, London. 212 p.

Hardisty, J., 1990. *Beaches: Form and Process*. Unwin Hyman, London, 319 p.

Horikawa, K. (ed.), 1988. Nearshore dynamics and coastal processes. University of Tokyo Press, 522 p.

Komar, P.D., and Inman, D.L., 1970. Longshore transport on beaches. Journal of Geophysical Research, 76, 713-721.

Lippmann, T.C., and Holmam, R.A., 1989. Quantification of sand-bar morphology: a video technique based on wave dissipation. *Journal of Geophysical Research,* 94, 995-1011.

Lippmann, T.C., and Holmam, R.A., 1990. The spatial and temporal variability of sand-bar

morphology. *Journal of Geophysical Research*, 95, 11,575-11,590.

Macky, G.H.; Cumming. R, J., and Valentine, E. M., 1988. *Measurements of ocean wave climate at Wanganui and Himitangi Beach.* Hydrology Centre, Departmemt of Scientific and Industrial Research, Christchurch New Zealand.

Masselink, G., 1993. Simulating the effects of tides on beach morphodynamics. *Journal of Coastal Research, Special Issue 15,* pp.180-197.

Masselink, G., and Short, A.D., 1993. The effect of tide range on beach morphodynamics and morphology: a conceptual beach model. *Journal of Coastal Research*, 9(3), 785-800.

Nummedal, D., and Finley, R., 1978. Wind-generated longshore currents. *Proceedings of the 16th Conference of Coastal Engineering,* pp.1428-1438.

Patterson, D.C., 1992. *Wanganui Port development feasibility studies: coastal engineering aspects.* A report for Ocean Terminals and the Wanganui District Council, New Zealand, 51p.

Patterson, D.C., and Blair, R.J., 1983. Visually determined wave parameters. *Proceedings of the Sixth Australian Conference on Coastal and Ocean Engineering,* Gold Coast, Australia, pp. 151-155.

Siegel, S. 1956: *Nonparametric Statistics for the Behavioral Sciences.* Tokyo, McGraw-Hill Kogakusha, Ltd., 303p.

Shand, R. D., (submitted). Temporal variation in morphological configuration within a multi-bar surf zone at Wanganui, New Zealand. Submitted to *Marine Geology* in October, 2002.

Shand, R.D. and Bailey, D.G., 1999: A review of net offshore bar migration with photographic illustrations from Wanganui, New Zealand, *Journal of Coastal Research*, 15(2), 365-378.

Shand, R.D.; Bailey, D.G., and Shepherd, M.J., 1999. An inter-site comparison of net offshore bar migration characteristics and environmental conditions. *Journal of Coastal Research*, 15(4) 173-202.

Short, A.D. and Aagaard, T., 1993. Single and multi-bar beach change models, *Journal of Coastal Research, Special Issue 15,* pp.141-157.

Southgate, H.N. and Beltran, L.M., 1998. Self-organisational processes in beach morphology. In Dronkers, J. and Scheffers, M.B.A.M., (eds.), *Physics of Estuaries and Coastal Seas*. A.A. Balkema, Rotterdam, pp. 409-416

Van Enckevort, I.M.J and Wijnberg, K.M., 1999 Intra-annual changes in bar plan shape in a triple bar system. *Proceeding Coastal Sediments'99*, ASCE, pp.1094-1108.

Wright, L.D., and Short, A.D., 1984. Morphodynamic variability of surf zones and beaches: a synthesis. *Marine Geology*, 56, 93-118.

Wright L D, Short A D, Boon III, Hayden B, Kimball S, and List J H, 1987: The Morphodynamic Effects of Incident Wave Groupiness and Tide Range on an Energetic Beach, *Marine Geology*, 74, 1-20.

Shand, R.D., and Shepherd, M.J., 2003. Associations between net offshore bar migration and backshore erosion. Proceedings of Coasts and Ports Australasian Conference, Auckland, New Zealand.

ASSOCIATIONS BETWEEN NET OFFSHORE BAR MIGRATION AND BACKSHORE EROSION

Roger D. Shand and Mike J. Shepherd
Geography Programme, Massey University, Private Bag 11222, Palmerston North, New Zealand.
r.d.shand@clear.net.nz, m.shepherd@massey.ac.nz

Abstract: This paper investigates the relationship between wave-induced backshore erosion and the cycle of net offshore bar migration (NOM) using a 3.4 yr morphological data-set collected at Wanganui, New Zealand. Four episodes of *laterally extensive* erosion, and 3 episodes of *localised* erosion were identified. Each type of erosion was associated with different aspects of NOM. Laterally extensive episodes coincide with higher levels of outer bar degeneration, a single subtidal bar and 2D (longshore bar/trough) or weak 3D (arrhythmic bar/trough) inner bar configurations; these configurations occur later in the inter-generation period. By contrast, isolated episodes coincide with lower levels of outer bar degeneration, double submarine bars and 3D (transverse bar/rip) inner bar configurations; these configurations occur earlier in the inter-generation period. Mechanisms explaining these associations are discussed, together with implications for coastal research and management.

Keywords: Backshore erosion, net offshore bar migration, NOM, surf zone, bar generation, bar degeneration, inner bar configurations, Wanganui, New Zealand

INTRODUCTION

Wave-induced erosion of the upper (subtidal) beach may extend into the backshore and adjacent foredune. This type of morphological behaviour has relevance for coastal management in terms of, for example, dune instability or property loss.

Net offshore bar migration (NOM) describes the systematic seaward migration of coastal sand-bars across a multi-bar surf zone. Such subtidal bars form within the inner surf zone and disappear several years later in the outer surf zone. Since the mid 1980s, NOM has been recognised on the North Carolina coast, the Dutch coasts, at Hasaki, Japan and at Wanganui, New Zealand. These oceanic coasts are characterised by moderate wave energy at predominantly sea wave frequencies.

Recently, Guillen et al. (1999) identified alternating periods of accretion and erosion affecting the foredune-toe along the coast of Holland, which correlate with the recurrence frequency of the offshore bar migration cycle. The purpose of the present paper is to identify the nature of backshore erosion at Wanganui, New Zealand, and to determine its relationship with the NOM cycle. Only erosion in which the escarpment was at least 1 m high is considered, as less severe cut was observed to recover and stabilize relatively quickly. The timing and nature of episodes of erosion will be related to a range of systematic morphological behaviours associated with the NOM cycle including degeneration of the outermost bar, number of subtidal bars in the cross-shore direction, and morphological (plan-view) configuration of the inner bar. The analysis utilises a 3.4 yr record of morphological data sampled at 2-4 weekly intervals. Before detailing the data acquisition techniques, the environmental conditions at the Wanganui study site will be described.

FIELD SITE

The field site is ~1.5 km from the Wanganui Rivermouth on the southwestern coast of the New Zealand North Island (Fig 1). The nearshore is characterised by fine sand (2 to 3 phi), has a cross-shore slope of ~0.0092 and width of ~530 m. Two subtidal sand-bars are usually

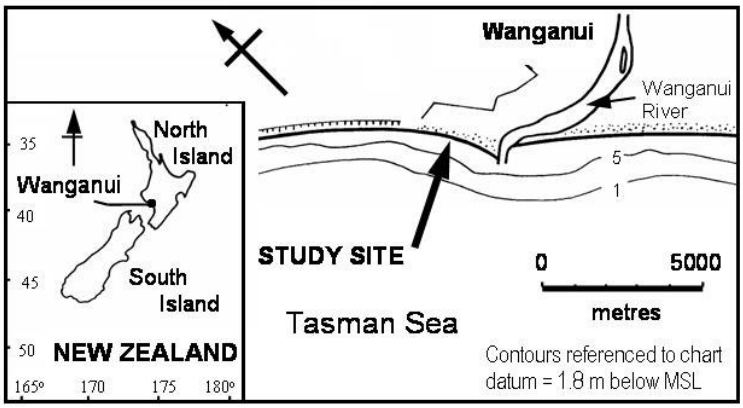

Figure 1 Location map of the Wanganui study site

present; these bars undergo net offshore migration with the mean life-cycle of a bar being ~3 yrs (Shand et al., 1999). The foreshore is characterised by medium sand (1.7 phi), has an average cross-shore slope of ~0.055 and an average width of ~85 m. About 30% of the time a small amplitude (swash) bar is present on the lower foreshore. Morphological plan-view configurations of the inner bar and lower beach are described later in the results section. The foredune is characterised by fine sand (2.2 phi), is ~5 m high, has a seaward slope of ~10^0 and the vegetation-front is encroaching seaward at ~1 m/yr. The backshore area, i.e. that area between the foreshore and the foredune, is ~10 m wide.

The mean neap tide range is 0.8 m and the mean spring tide range is 2.4 m. The mean deepwater significant wave height is 1.3 m and the 5% excedence value is 2.5 m. The mean wave period is 10.1 s (range 3.5 s to19 s) with sea wave conditions occurring for ~75% of the time and swell waves for the remaining time. Approximately forty two percent of waves approach from the west, ~24% from the south and ~34% lie within one degree of shore-normal. The prevailing WNW wind approaches the coast at ~35 deg from the shoreline, and the 5% excedence value is 12.4 m/s. The mean value for longshore currents within the inner surf zone is 0.42 m/s and the 5% excedence value is 1.01 m/s.

MORPHOLOGICAL DATA

Episodes of backshore erosion were identified on morphological maps which cover several hundred metres of coast; examples are shown in Fig 2. The maps were produced from high resolution ground surveys carried out at fortnightly intervals between August 1991 and March 1995. The fortnightly sampling detected all episodes of backshore erosion, as such erosion was only observed to occur under higher (spring) tidal range. Errors, based on 95% confidence intervals, are estimated to be 5 m in the cross-shore direction and 10 m in the longshore direction. To detect morphological variation, a 300 m long study area was used. The morphological maps were also used to determine the (average) cross-shore location for the low tide step; this location was used as a proxy for the seaward boundary of the foreshore. In addition, plan-view morphological configurations of the inner bar system were derived from the maps.

To identify cycles of NOM, the cross-shore position of sand-bars were defined by intensity maxima on a sequence of time-lapse (4 min exposure) photographs. These *time-exposure* photographs were taken at monthly intervals from on top of a 42 m high cliff located ~1600 m northwest of the study site. Examples of an instantaneous photo (1/125th sec), together with the corresponding time-exposure and rectified images, are depicted in Figs 3A-C.

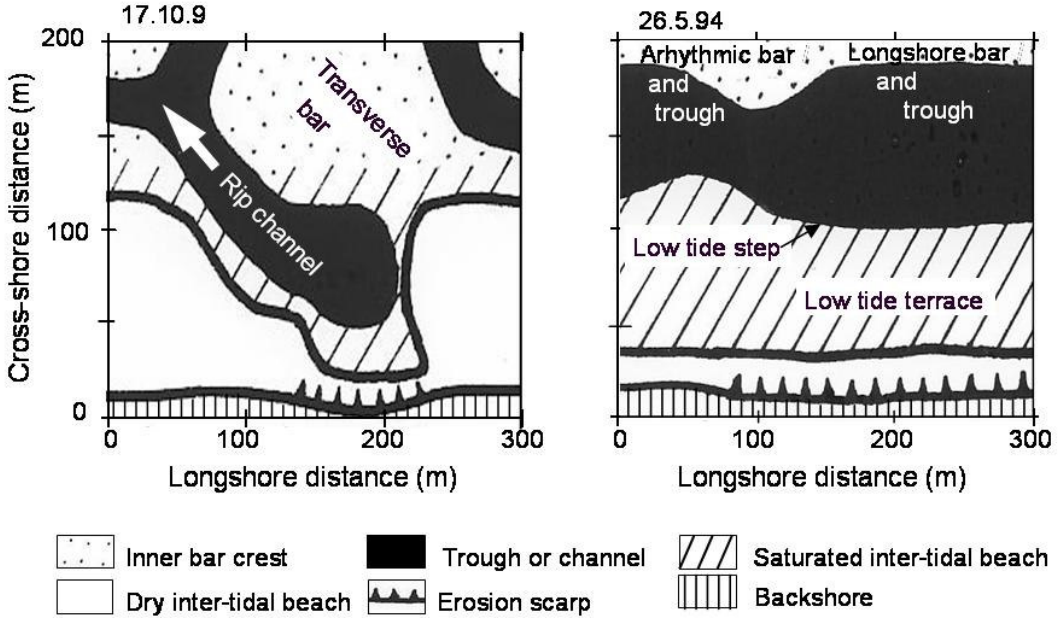

Figure 2 Examples of low tide morphological maps used to identify backshore erosion, the low tide step, and inner bar configuration.

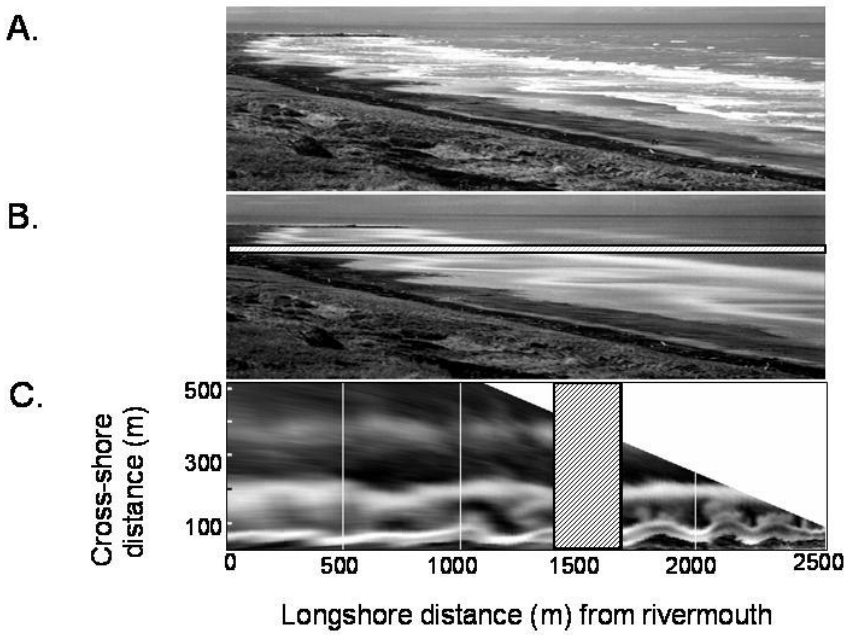

Figure 3 Examples of instantaneous (1/125th sec) photo (A), corresponding 4 min time-exposure photo (B), and rectified image with straightened coastline (C). Photo is the first in an 8 shot panorama. The 300 m wide study area is depicted by the shaded areas in B and C.

Intensity values were averaged over the 300 m long study area, and time-series of the cross-shore distances for each bar were then constructed and analysed. These techniques are described in Bailey and Shand (1996). Different levels of outer bar degeneration were determined from intensity patterns on rectified time-exposure images. Errors are estimated to be ~15 to 20 m in the cross-shore direction and ~75 m in the longshore direction. The somewhat large longshore value reflects the distance from the camera. It is acceptable for the present study, however, given the typical spatial similarity of surf zone morphology in any particular sample, together with the need to determine longer term systematic cross-shore bar migration rather than the analysis of inter-survey bar migrations.

RESULTS

Time-series for each subtidal sand-bar that existed during the study period are shown in Fig 4. While only bar 3 underwent a full NOM cycle during the 3.4 yr study, an underlying seaward migration trend still characterised the other 4 partially completed bar cycles. The merging of bars 2A and 2B early in the study is the result of bar switching, a morphological behaviour in which bars realign in the long-shore direction (see Shand et al., 2001; Shand, 2003). It is also noted that each new bar was generated after the seawardmost bar had disappeared. Bar generation was defined to occur at the time pronounced bar/trough relief first developed. The low tide step is also plotted in Fig 4, and these data show the inter-tidal beach abruptly narrows following generation of a subtidal bar, and then systematically widens until the next bar is generated. During the study period there were 4 instances of bar formation within the inner surf zone, and 4 cases of bar degeneration within the outer surf zone.

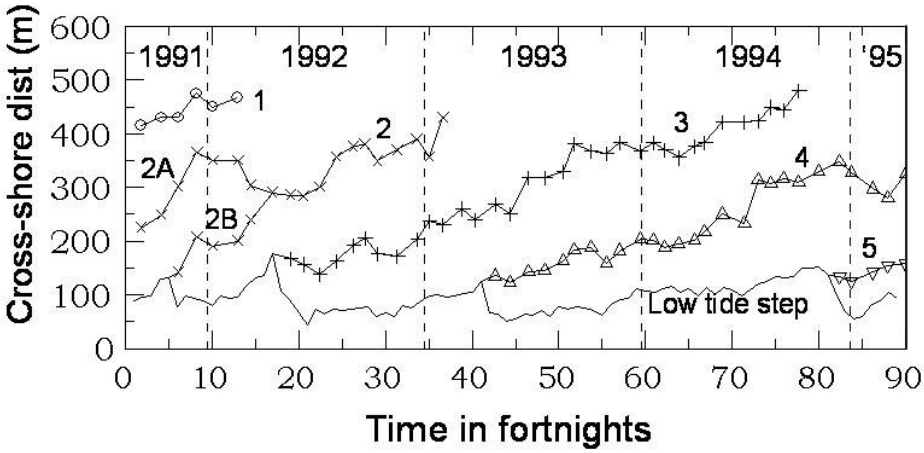

Figure 4 Cross-shore migration of subtidal bars (marked 1-5) during the study period. The low tide step between successive bar generations, is also shown.

Seven episodes of backshore erosion occurred during the study period, with scarp heights ranging up to 2 m. The timing and longshore length of each episode is depicted in Figs 5 – 7. In three instances, the eroded length extended beyond the 300 m long study area; in these cases, the total length was recorded. The longshore extent of the seven erosion episodes was bimodally distributed, with *laterally extensive* episodes having lengths of 300 to 650 m, and the more *localised* episodes having lengths between 100 and 160 m. The laterally extensive erosion also remained evident for longer with a mean value of 95 days compared with 38 days for localised episodes.

The changing degeneration status of each outer bar during its final months, are depicted in Fig 5. Outer bars were classified as being either *pronounced* or *subdued*. Pronounced bars occurred where a distinct trough was present to landward. By contrast, subdued bars lacked a distinct landward trough. This approach was used to separate relatively low and high levels of bar degeneration because it could be assessed from intensity patterns on the time-exposure images used in this study. The technique is described in Shand (2003). The results in Fig 5 show that laterally extensive episodes correspond with subdued outer bars, while localised erosion corresponds with pronounced outer bars, i.e. with higher and lower levels of outer bar degeneration respectively.

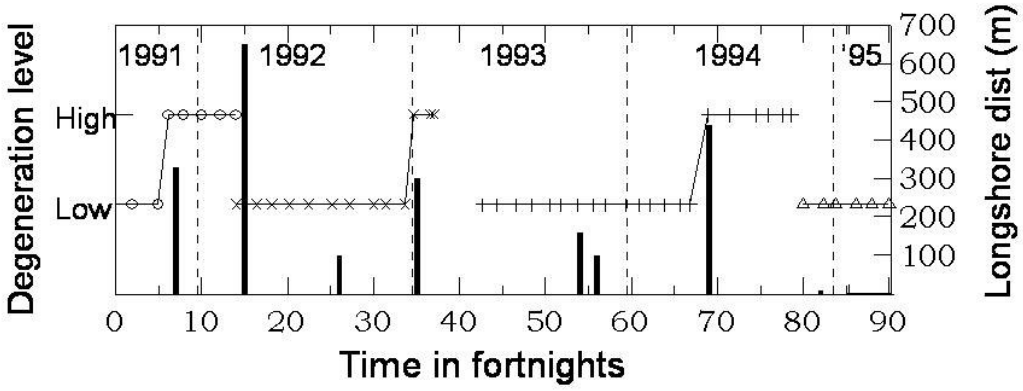

Figure 5 Relative level of outer bar degeneration, where *high* refers to a subdued profile and *low* to a pronounced profile (see text for further explanation). The overlain bar graph depicts the longshore extent of the 7 episodes of backshore erosion.

The number of bars in the cross-shore direction (bar number) are depicted in Fig 6. Only those outer bars with a low level of degeneration were included in the bar number calculation, as these bars are most likely to behave like more landward bars and, under storm conditions, significantly dissipate wave energy. The results show that two well developed subtidal bars occurred for 75% of the study period, while for the remaining 25% of the time only a single bar existed. Furthermore, double bars occurred during four separate periods, with the single bars occurring during the three intervening periods. When bar number was compared with the erosion episodes, all three cases of localised erosion corresponded with double bars, and three of the four laterally extensive episodes corresponded with single bars. While the remaining laterally extensive episode occurred with double bars, the landward bar was particularly small, having just been generated, and therefore relatively ineffective at dissipating incoming wave energy.

Morphological configurations for the innermost subtidal bar, are depicted in Fig 7. The assignment of configurations was based on the mutually exclusive classification scheme described in Shand et al. (2003). This method was developed to uniquely categorise the typically complex non-linear configurations which occur at Wanganui, into one of the following categories: linear bar and continuous trough; non-linear bar and continuous trough; non-linear bar and discontinuous trough; and subdued topography. The predominant type of morphology within each class was: *longshore bar and trough; arrhythmic bar and trough; transverse bar and rip; and wide low tide terrace* (extending to the inner bar) respectively. Examples of the first three types of morphology, together with an inter-tidal low tide terrace, are depicted in Fig 2.

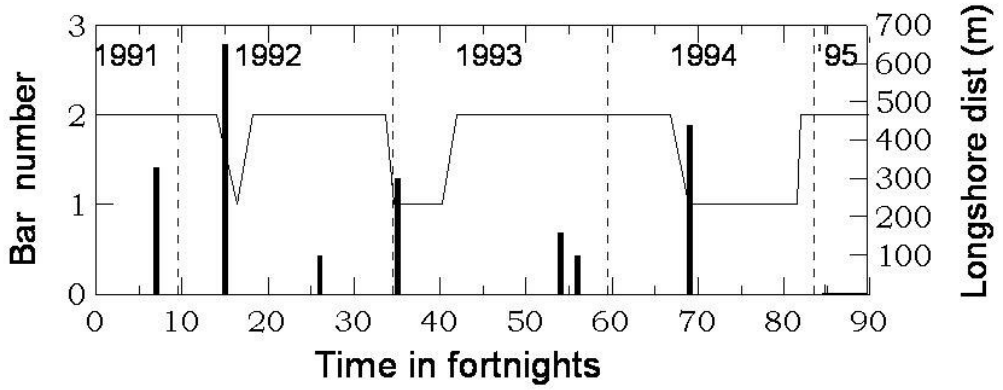

Figure 6 Number of sub-tidal bars in the cross-shore direction. Outer bars were only included where they had a *low level* of degeneration, as shown in Fig 5. The overlain bar graph depicts the longshore extent of the 7 episodes of backshore erosion.

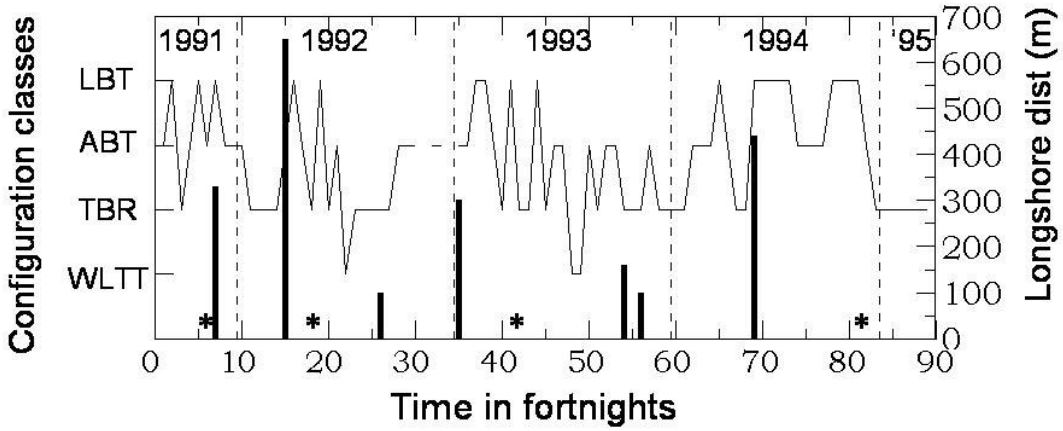

LBT=longshore bar/trough ABT=arrhythmic bar/trough TBR=transverse bar/rip WLTT=wide low tide terrace

Figure 7 Inner bar configurations represented by the predominant types of morphology in each class (see text). Vertical bars depict the longshore extent of backshore erosion episodes. Asterisks denote times of bar generation.

While the fortnightly survey interval would necessarily not detect all successive configuration changes, an underlying systematic variation is evident. In particular, the configuration time-series depicted in Fig 7, shows the predominance of transverse/rip, together with arrhythmic morphologies during the early/mid inter-generation period. Low tide terraces also occurred during this time. Later in the inter-generation period, and in conjunction with beach widening, the predominant configuration changed to longshore bar/trough, together with arrhythmic morphologies. However, it is noteworthy that these more linear morphologies often occur, albeit briefly, when a new bar is generated.

A comparison of the timing of erosion episodes with inner bar configurations indicates that the laterally extensive episodes coincide with longshore bar/trough and arrhythmic

configurations, which tend to occur later in the inter-generational period. By contrast, the localised episodes coincide with transverse bar/rip configurations, which occur earlier in the inter-generation period.

DISCUSSION

Laterally extensive episodes of backshore erosion coincide with a change in the cross-shore profile of the seawardmost bar from pronounced relief to subdued relief, and the number of subtidal bars reducing from two to one. With such morphology, a higher proportion of incident wave energy would reach the shoreline and be available for backshore erosion, as storm wave energy can be effectively dissipated when breaking occurs over an outer bar, e.g. see Keady and Coleman (1980). By contrast, at times of higher bar number and more pronounced relief, a lower portion of incident wave energy would reach the shoreline, thereby resulting in less extensive erosion. Energy conditions associated with different types of backshore and upper beach erosion are considered in a separate paper (Shand et al, in prep).

Systematic variation of configurations within the inner bar system, appears to influence the nature of backshore erosion in the following manner. Strongly 3D inner bar morphologies (transverse bar and rip) result in varying beach width in the longshore direction. This limits areas likely to undergo backshore wave attack to the rip-associated embayments, and this situation would facilitate the occurrence of episodes of localised erosion. By contrast, 2D configurations (longshore bar/trough) and weakly 3D morphologies (arrhythmic bar/trough) result in more uniform beach width, and this would facilitate the occurrence of more widespread backshore erosion. Such laterally extensive erosion appears to be consistent with *mode 2* beach cut as described by Wright (1980), while localised erosion is consistent with *mode 3* beach cut.

While both laterally extensive and localised types of backshore erosion correlate with several (contrasting) aspects of the NOM cycle, the regular erosion episodes observed along the coast of Holland (Guillen et al., 1999) are probably laterally extensive for the following reasons. Laterally extensive episodes at Wanganui occurred during each of the three inter-generation periods, while localised episodes occurred during only two inter-generation periods. In addition, laterally extensive erosion episodes had greater longshore extent and were more persistent than localised episodes.

NOM-associated backshore erosion has several implications for coastal management. Firstly, wave-induced foredune scarping is a major cause of dune instability, i.e. blowout and subsequent parabolic development (e.g. see Carter et al., 1990). Such processes have been observed at Wanganui. However, the quasi-regular nature of NOM-induced dune erosion could enable management authorities to broadly predict these events and have resources available to enable re-contouring and planting.

NOM-associated backshore erosion also has significance in identifying shoreline change, as used in, for example, the delineation of Coastal Hazard Zones. This is because commonly used coastal reference features such as the foredune-toe, the dune vegetation front, the debris line or the saturation zone boundary, are likely to systematically fluctuate in their cross-shore locations. Such variation, however, can be minimised by averaging over greater longshore reaches when calculating cross-shore distances to the shoreline indicator.

CONCLUSION

Four episodes of laterally extensive backshore erosion occurred during the 3.4 yr study period. Their longshore distances ranged between 330 and 640 m, scarp height between 1 and 2 m, and persistence between 7 and 280 days. Three episodes of localised erosion occurred, with longshore distance ranging between 100 and 160 m, scarp height between 1 and 2 m, and persistence between 7 and 42 days. Each type of erosion coincided with different aspects of the NOM cycle. Laterally extensive episodes coincided with higher levels of outer bar degeneration, a single subtidal bar, and either the 2D (longshore bar/trough) or weakly 3D (arrhythmic bar/trough) inner bar configurations which tend to occur later in the inter-generational period. With such morphology, greater amounts of storm wave energy can reach the backshore and erode a considerable longshore reach. By contrast, localised episodes coincide with lower levels of outer bar degeneration, double subtidal bars and strongly 3D (transverse bar and rip) inner bar configurations which tend to occur earlier in the inter-generational period. With this type of morphology, backshore erosion will be confined to the embayments of well-developed rip channels, thereby limiting the lateral extent of such erosion. NOM-associated backshore erosion is likely to result in quasi-regular periods of dune instablility, and also in systematic variation in the location of coastal reference features used to determine shoreline change.

ACKNOWLEDGEMENTS

This study was supported by a Research Fellowship (contract MAUX0104) from the New Zealand Foundation for Science and Technology (FRST).

REFERENCES

Bailey, D.G., and Shand, R.D., 1996. Determining large-scale sand bar behaviour. *Proceedings of the IEEE International Conference on Image Processing*, Lausanne, Switzerland, (2), 637-640.

Carter, R.W.G.; Hesp, P.A.; Nordstrom, K.F., 1990. Erosional landforms in coastal dunes. In Nordstrom, K.F.; Psuty, N.P; Carter, R.W.G (Eds.), *Coastal Dunes: Form and Process*, pp 217-250.

Guillen, J.; Stive, M.J.F. and Capobianco, M., 1999. Shoreline evolution of the Holland Coast on a decadal scale. Earth surface Processes and Landforms, 24, 517-536.

Keady, D.M., and Coleman, L.J., 1980. Incidence, breaking and reforming of waves behind submerged barriers. Pp. 249-267 in Tanner, W.F., (ed.). *Shorelines Past and Present*. Department of Geology, Florida State University.

Shand R D (2003). Relationships between episodes of bar switching, cross-shore bar migration and outer bar degeneration at Wanganui, New Zealand. *Journal of Coastal Research*, 19(1), 157-170.

Shand, R.D.; Bailey, D.G., and Shepherd, M.J., 1999. An inter-site comparison of net offshore bar migration characteristics and environmental conditions. *Journal of Coastal Research*, 15(4), 750-765.

Shand, R.D.; Bailey, D.G.; Hesp, P.A., and Shepherd, M.J. 2003. Conceptual beach-state model for the inner bar of a storm-dominate, low to moderate tidal range coast at Wanganui, New Zealand. *Proceedings of Coastal Sediments '03*.

Shand, R.D.; Hesp, P.A., and Shepherd, M.J. (in prep). Beach cut in relation to net offshore bar migration. *Proceedings of the 8th International Coastal Symposium*, Brazil, 2004.

Wright, L.D., 1980. Beach cut in relation to surf zone morphodynamics. *Proceedings of the 17th International Conference of Coastal Engineering*, pp. 978-996.

Shand, R.D., Hesp, P.A., and Shepherd, M, J., 2004. Beach cut in relation to net offshore bar migration. International Coastal Symposium 2004, Brazil.

Journal of Coastal Research	SI 39	pg - pg	ICS 2004 (Proccedings)	Brazil	ISSN 0749-0208

Beach cut in relation to net offshore bar migration

R.D. Shand†, P.A. Hesp‡, and M.J.Shepherd†

† Geography Programme, Massey University, Private Bag 11222, Palmerston North, New Zealand, r.d.shand@clear.net.nz

‡ Department of Geography and Anthropology, Louisiana State University, Baton Rouge, LA 70803- 4105, United States of America, pahesp@lsu.edu

ABSTRACT

This paper investigates the relationship between beach cut and the process of net offshore bar migration using a 3.4 yr morphological data-set collected at Wanganui, New Zealand. During the study period the following four types of beach cut occurred: four episodes of laterally-extensive erosion; three episodes of rip-embayment erosion; three episodes of overwash-channel erosion, and six episodes of berm-front erosion. Each type of erosion had distinctive physical and temporal dimensions, and characteristic morphological and energy associations. Furthermore, each type of erosion occurred systematically during a particular time within the inter-generation period of the NOM cycle. Overwash channel and berm-front erosion occurred earlier in the period, under double bars and intermediate morphologies, i.e. 2D to 3D. Rip embayment erosion occurred during the earlier/middle part of the inter-generation period, under double bars and strongly 3D morphology, while laterally extensive erosion occurred later in the period under single bars and more linear (2D) morphology. While wave energy conditions also varied systematically during inter-generation periods, morphological control nevertheless appears to be of fundamental importance.

ADITIONAL INDEX WORDS: beach erosion, inner bar, outer bar, surf zone, NOM, Wanganui, New Zealand

INTRODUCTION

Exposed sand-dominated beaches are often subject to wave-induced erosion during higher energy conditions. In the most severe cases, erosion may extend into the foredune with consequence for engineering structures, beach-front property and dune stability. While coastal research has often focused on shorter-term beach/dune/energy interactions, e.g. see Basco and Shin, 1996; Zheng and Dean 1996, longer-term controls are also important, e.g. see Psuty et al., 1988; Dolan et al., 1991.

Recently, Guillen et al. (1999) identified laterally extensive episodes of dune-toe erosion and accretion along the coast of Holland, and found that the return period of these oscillations (several years) correlate with the offshore migration return period of subtidal sand-bars. This repetitive, or cyclic, bar migration process is referred to as net offshore bar migration (NOM). It consists of a bar forming on the lower foreshore, systematically migrating seaward across the surf zone, and finally degenerating and disappearing several years later in the outer surf zone. This process has been documented for several multi-bar coasts throughout the world (see Shand and Bailey, 1999, for review).

An investigation by Shand and Shepherd (2003) into backshore erosion at Wanganui on the southwest coast of the New Zealand North Island, found that such laterally extensive erosion occurs prior to the generation of a new bar within the NOM cycle. At this time, the number of bars in the cross-shore direction is reduced, the inter-tidal beach has greater width and more uniform (or dissipative) morphology, and the inner bar has a linear, or 2-dimensional (2D), form.

This paper is an extension of the work of Shand and Shepherd (2003). In particular, it analyses all episodes of erosion, i.e. both backshore erosion and also upper beach erosion, which are evident within the same 3.4 yr record of morphological data used by Shand and Shepherd (2003). In addition, it considers the nature and role of the associated energy conditions.

FIELD SITE

The field site is ~1.5 km from the Wanganui Rivermouth on the southwestern coast of the New Zealand North Island (Fig 1). The nearshore is characterised by fine sand (2 to 3 phi), has a cross-shore slope of ~0.0092 and width of ~530 m. Two subtidal sand-bars are usually present; these bars undergo net offshore migration with the mean life-cycle of a bar being ~3 yrs (Shand et al., 1999). The foreshore is characterised by medium sand (1.7 phi), has an average cross-shore slope of ~0.055 and an average width of ~85 m. About 30% of the time a small amplitude (swash) bar is present on the lower foreshore. The foredune is characterised by fine sand (2.2 phi), is ~5 m high, has a seaward slope of ~0.176 (10 deg) and the vegetation-front is encroaching seaward at ~1 m/yr. The backshore area, i.e. that area between the foreshore and the foredune, is ~10 m wide.

The mean neap tide range is 0.8 m and the mean spring tide range is 2.4 m. The mean deepwater significant wave height is 1.3 m and the 5% excedence value is 2.5 m. The mean wave period is 10.1 s (range 3.5 s to19 s) with sea wave conditions occurring for ~75% of

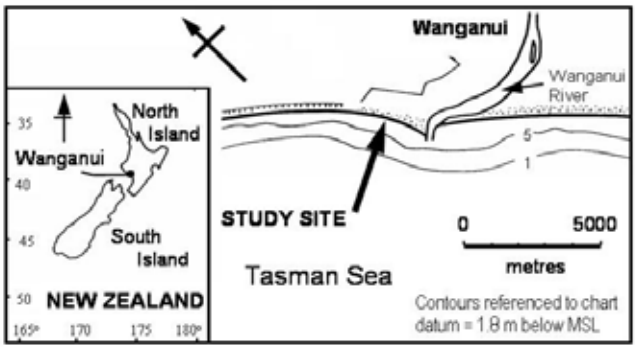

Figure 1 Location map of the Wanganui study site

the time and swell waves for the remaining time. Approximately forty two percent of waves approach from the west, ~24% from the south and ~34% lie within one degree of shore-normal. The prevailing WNW wind approaches the coast at ~35 deg from the shoreline, and the wind speed 5% excedence value is 12.4 m/s. The mean value for longshore currents within the inner surf zone is 0.42 m/s and the 5% excedence value is 1.01 m/s. Wave height, wind strength and the magnitude of longshore currents are all positively correlated, as are the direction of these process variables (Shand et al., 2001).

METHODS

Episodes of backshore erosion were identified on morphological maps which cover several hundred metres of coast; examples are shown in Fig 2. The maps were produced from high resolution ground surveys carried out at fortnightly intervals between August 1991 and March 1995. Errors, based on 95% confidence intervals, are estimated to be 5 m in the cross-shore direction and 10 m in the longshore direction. To detect morphological variation, a 300 m long study area was used. The morphological maps were also used to determine the (average) cross-shore location for the low tide step; this location was used as a proxy for the seaward boundary of the foreshore. In addition, plan-view morphological configurations of the beach and inner bar system were derived from the maps.

Cycles of NOM were identified from time-series of cross-shore bar location derived from 4 min time-exposure photographs. The photographs were taken at monthly intervals from on top of a 42 m high cliff located some 1600 m northwest of the study site. Each photo was digitised, rectified to ground co-ordinates and the coastline straightened to facilitate subsequent analysis. Intensity values were then averaged over the 300 m long study area, and intensity maxima used to represent bar-crests. These techniques are described in Bailey and Shand (1996), and Shand (2003). Errors are estimated to be ~15 to 20 m in the cross-shore direction and ~75 m in the longshore direction. The somewhat large longshore value reflects the distance from the camera. Such an error is acceptable for the present study, however, given the need to determine longer term systematic cross-shore bar migration rather than the analysis of inter-survey bar migrations.

Wave data were based on daily observations at the seawardmost break-point using the pole and horizon method described by Patterson and Blair (1983). Such measurements have been shown to provide a reliable estimate of relative wave height. In the Wanganui case, the pole and horizon data were found to approximate deepwater significant wave height.

RESULTS

Characteristics of beach cut

Sixteen episodes of beach cut occurred during the study period (Fig 3). Different types of cut were identified, and these were associated with three predominant beach morphologies. These erosion-types will now be described, together with corresponding erosion parameter values and energy associations. Note that when erosion extended beyond the 300 m long study area, the total length of cut was recorded.

Laterally extensive erosion occurred upon a featureless upper beach, relatively featureless lower beach (e.g. low tide terrace or broad ridge and mega-rippled runnel), and with 2D or weaker 3D inner bar morphology (e.g. longshore bar/trough or arrhythmic bar/trough). An example of laterally extensive erosion and such beach/inner bar morphologies is shown in Fig 2A. The erosion extended alongshore 300 to 650 m (Table 1), and in all four cases erosion reached the backshore region. Other parameter values in Table 1 show that this type of beach cut had the greatest-equal scarp height (mean = 1.5 m) and the longest persistence (mean = 13.8 wk). Laterally extensive erosion required spring tides (mean range = 2.4 m), coupled with the highest storm-wave conditions (mean = 3.1 m) of all erosion types. Laterally extensive erosion appears to be equivalent to Wright's (1980) *mode 2* beach cut.

Table 1: Descriptive statistics for erosion dimensions, persistence and energy associations with respect to different types of beach cut.

Type of cut		Length (m)	Height (m)	Duration (wks)	Tidal rng (m)	Wave ht (m)
Laterally Extensive	*Mean*	430	1.5	13.8	2.4	3.15
	Range	300 - 650	1 - 2	1 - 40	2.2 – 2.8	2.4 – 3.8
Rip Embayment	*Mean*	120	1.5	5.3	2.4	2.2
	Range	100 - 160	1 - 2	4 - 8	2.2 – 2.8	1.8 – 2.9
Overwash Channel	*Mean*	77	1.0	2.7	2.0	2.8
	Range	40 - 100	0.5 – 1.5	2 - 3	1.8 – 2.2	2.7 – 2.8
Berm-front	*Mean*	17.5	0.63	1.7	1.2	2.05
	Range	10 - 30	0.25 – 1.0	1 - 4	0.8 – 2.6	1.6 – 3.1

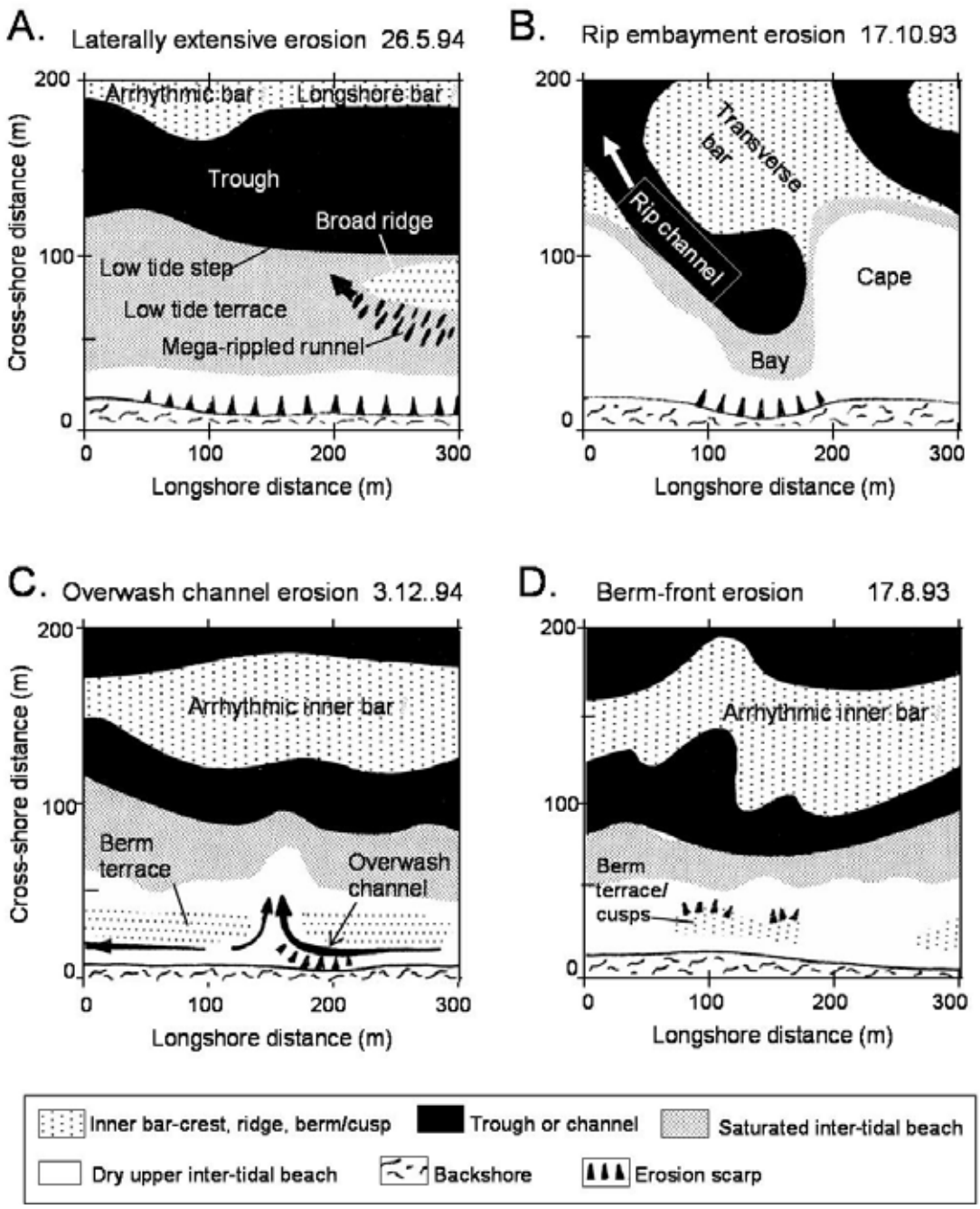

Figure 2 Examples of morphological maps used to identify erosion, low tide step and morphological configuration. A different type of erosion is depicted in each map.

Rip embayment erosion occurred with an either featureless or berm-terraced upper beach, a strongly 3-dimenional lower beach (e.g. cape and bays), and strongly 3D inner bar morphology (e.g. transverse bar/rips). An example of rip embayment erosion and such beach/inner bar morphologies is shown in Fig 2B. In this situation, and in the following types of erosion, some cusping of the berm may have occurred. In the three observed cases of rip embayment erosion, beach cut occurred at the head of a rip-associated bay (rip embayment) and extended into the backshore. Such erosion had significantly shorter (alongshore) length than laterally extensive erosion (mean = 120 m c.f. 430 m, Table 1), had equal scarp height (mean = 1.5 m), but a lower, although not

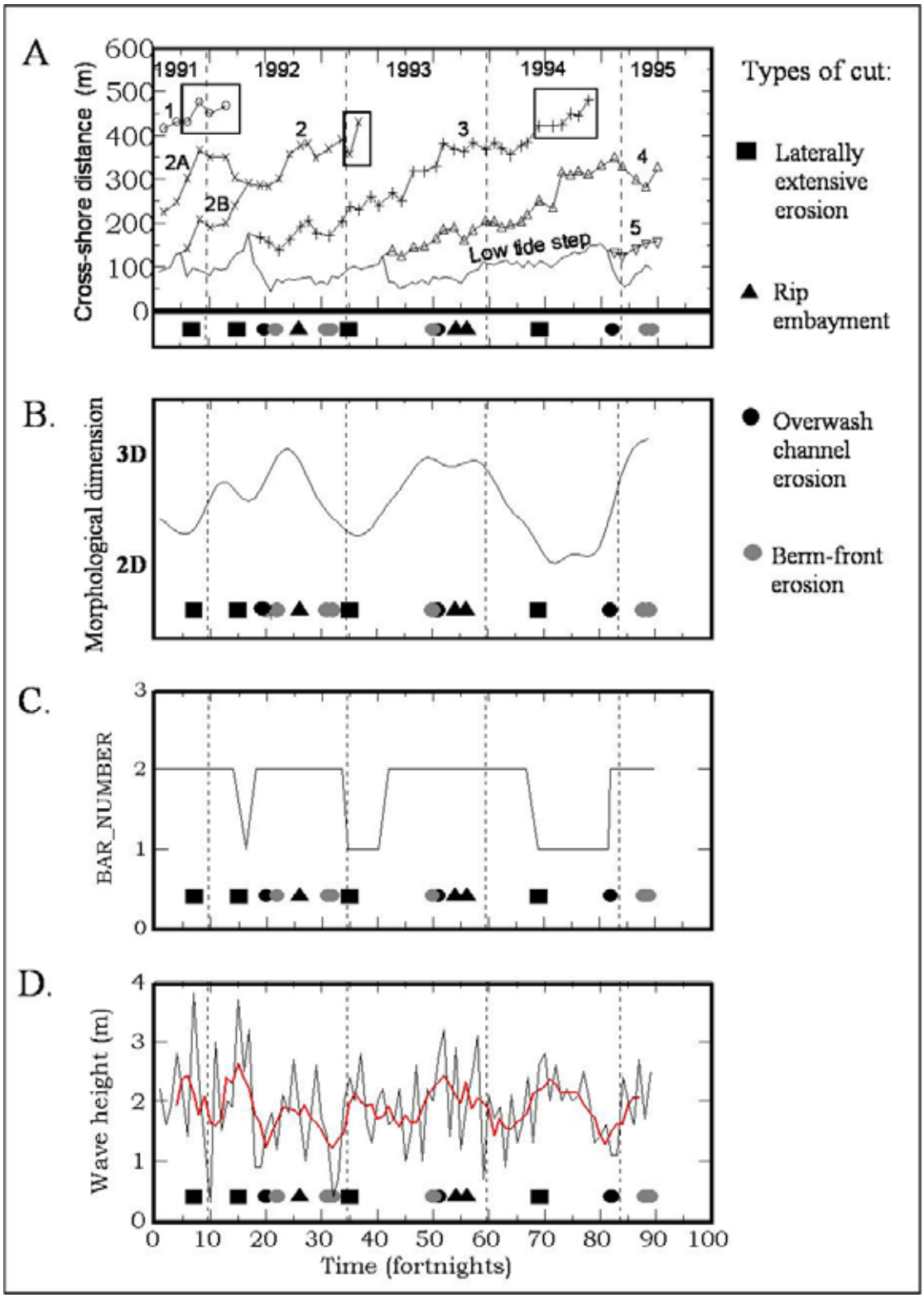

Figure 3 Comparisons of beach cut with cross-shore migration of bar-crests and the low tide step (A), relative morphological dimension (B), bar number (C) and daily wave height during the study period (D). Filtered wave height is depicted by the bolder line in D. The rectangles in A locate highly degenerated outer bar-crests; these bars were excluded when determining the bar numbers in B. All terms are described in text.

statistically different, persistence (mean = 5.3 wks c.f. 13.8 wks). Statistical significance was determined using two sample t-tests and a 20% threshold. As with laterally extensive erosion, rip embayment erosion also required spring tides (mean range = 2.4 m), but significantly lower wave height (mean = 2.2 m). Rip-embayment erosion appears to be equivalent to Wright's (1980) *mode 3* beach cut.

Both *overwash-channel erosion* and *berm-front erosion* occurred with a bermed upper beach, featureless lower beach (e.g. low tide terrace) and 3D inner bar configurations (e.g. arrhythmic bar/trough or transverse bar/rips). Examples of such erosion types, together with the associated morphologies, are provided in Fig 2C and D. In the three cases of overwash chanel erosion, scarping occurred on the landward side of the laterally orientated overwash channel, and in two of these cases, erosion extended into the backshore. In the six cases of berm-front erosion, the scarping occurred upon the terrace riser or berm-face.

Overwash channel and berm-front erosion were significantly different (less) from laterally extensive and rip embayment erosion in terms of length, height and escarpment duration. Furthermore, berm-front erosion parameters (Table 1) were significantly different (less) from overwash channel erosion, with a mean longshore distance of 17.5 m (c.f. 77 m). Berm-front erosion values were also less (but not significantly less) with respect to scarp height (mean = 0.63 m c.f. 1.0 m), and duration (mean = 1.7 c.f. 2.7 wks). Berm-front erosion occurred under conditions of significantly lower wave height (mean = 2.05 c.f. 2.8 m) and lower tidal range (mean = 1.2 m c.f. 2.0 m). A comparison of energy conditions for overwash channel and berm-front erosion with laterally extensive and rip embayment erosion, indicates that the former occur under significantly lower tidal range. It is noteworthy that overwash channel wave height (mean = 2.8 m) was significantly greater than rip embayment wave height (mean = 2.2 m). While berm-front erosion appears to be consistent with Wright's (1980) *mode 1* beach cut, overwash channel erosion was not accounted for in Wright's (1980) scheme.

NOM-associations

Time-series for each subtidal sand-bar that existed during the study period are shown in Fig 3A. While only bar number 3 underwent a full NOM cycle during the 3.4 yr study, an underlying seaward migration trend still characterised the other four partially completed bar cycles. The merging of bars 2A and 2B early in the study is the result of bar switching, a morphological behaviour in which bars realign in the longshore direction (see Shand et al., 2001; Shand, 2003). Bar generation was defined to occur at the time pronounced bar/trough relief first developed. Each new bar was generated after the seawardmost bar had disappeared. The low tide step is also plotted in Fig 3A, and these data show the inter-tidal beach abruptly narrows following generation of a subtidal bar, and then, after an approximately stationary period, the beach systematically widens until the next bar is generated. During the study period there were four instances of bar formation within the inner surf zone, and four cases of bar degeneration within the outer surf zone.

A comparison of the different episodes of beach cut with the morphology depicted in Fig 3A, shows that laterally extensive erosion tended to occur later in the inter-generation period and in conjunction with beach widening. By contrast, all other types of erosion occurred earlier in the inter-generation period with overwash and berm-front erosion tending to occur closest to the time of bar generation.

The timing of beach cut episodes was compared with the configuration dimension of the inner bar (Fig 3B). This graph of (relative) dimensionality values indicates whether configuration change is tending 2D or 3D; these data were derived by smoothing numerical values assigned to the configuration sequence provided in Shand and Shepherd (2003). The results in Fig 3B show 3D-tending configurations predominate earlier in the inter-generation period, with a change to 2D-tending configurations later in the period. It is noteworthy that 2D morphologies often occurred, albeit briefly, when a new bar was generated. A comparison of the timing of erosion episodes with inner bar configurations indicates that the laterally extensive episodes coincide with the 2D-tending configurations later in the inter-generational period. By contrast, all other types of erosion coincide with the 3D-tending configurations earlier in the inter-generation period.

Timing of beach cut episodes was next compared with the number of bars in the cross-shore direction (bar number). The method used to determine bar number has been previously detailed in Shand and Shepherd (2003). Briefly, a highly degenerated outer bar, defined as having no landward trough, was not included in the bar number count as such a bar is less likely to be effective in causing significant wave energy dissipation, while an outer bar with pronounced relief was included in the count. The level of outer bar degeneration was identified using intensity patterns on rectified time-exposure images.

The bar number results (Fig 3C) show that two well developed subtidal bars occurred for 75% of the study period, while for the remaining 25% of the time only a single bar existed. The double bars occurred during four separate periods, with the single bars occurring during the three intervening periods. A comparison of bar number with the different episodes of beach cut shows that three of the four laterally extensive episodes corresponded with the presence of single bars. Furthermore, the landward bar during the remaining (first) laterally extensive episode was particularly small, having just been generated. By comparison, all other types of beach cut corresponded with double bars. The occurrence of the greatest erosion length under the least number of longshore bars, and the least change under the greatest number, is qualitatively consistent with other studies of beach-change (e.g. Kannan et al., 2003).

To test whether systematic variation in wave conditions corresponds with the different episodes of erosion, and hence plays a fundamental role in controlling the nature and timing of erosion events, maximum inter-survey wave heights corresponding to tidal range $\geq$ 2.2 m were derived (Fig 3D). The 2.2 m threshold was chosen as all episodes of laterally extensive erosion occurred when the tidal range was greater or equal to this value. A 5-point moving average filter was applied to the raw wave data to help identify systematic change.

The results in Fig 3D show wave height during spring tides had a quasi-regular fluctuation with an average periodicity of 26.4 wks (18 to 38 wks). While a period of higher waves did occur later in the inter-generation period and coincides with each episode of laterally extensive erosion, two of the six peaks (fortnights 20 – 30 and 50 – 60) occurred earlier in the cycle. These two peaks of higher wave energy (during spring tides) were associated with the episodes of rip embayment erosion. The episodes of overwash channel erosion and berm-front erosion were associated with either periods of lower energy, or change from periods of lower energy to periods of higher energy.

The beach cut characteristics and relationships with NOM described above, together with considerations made in the following discussion, are synthesized diagrammatically in Fig 4.

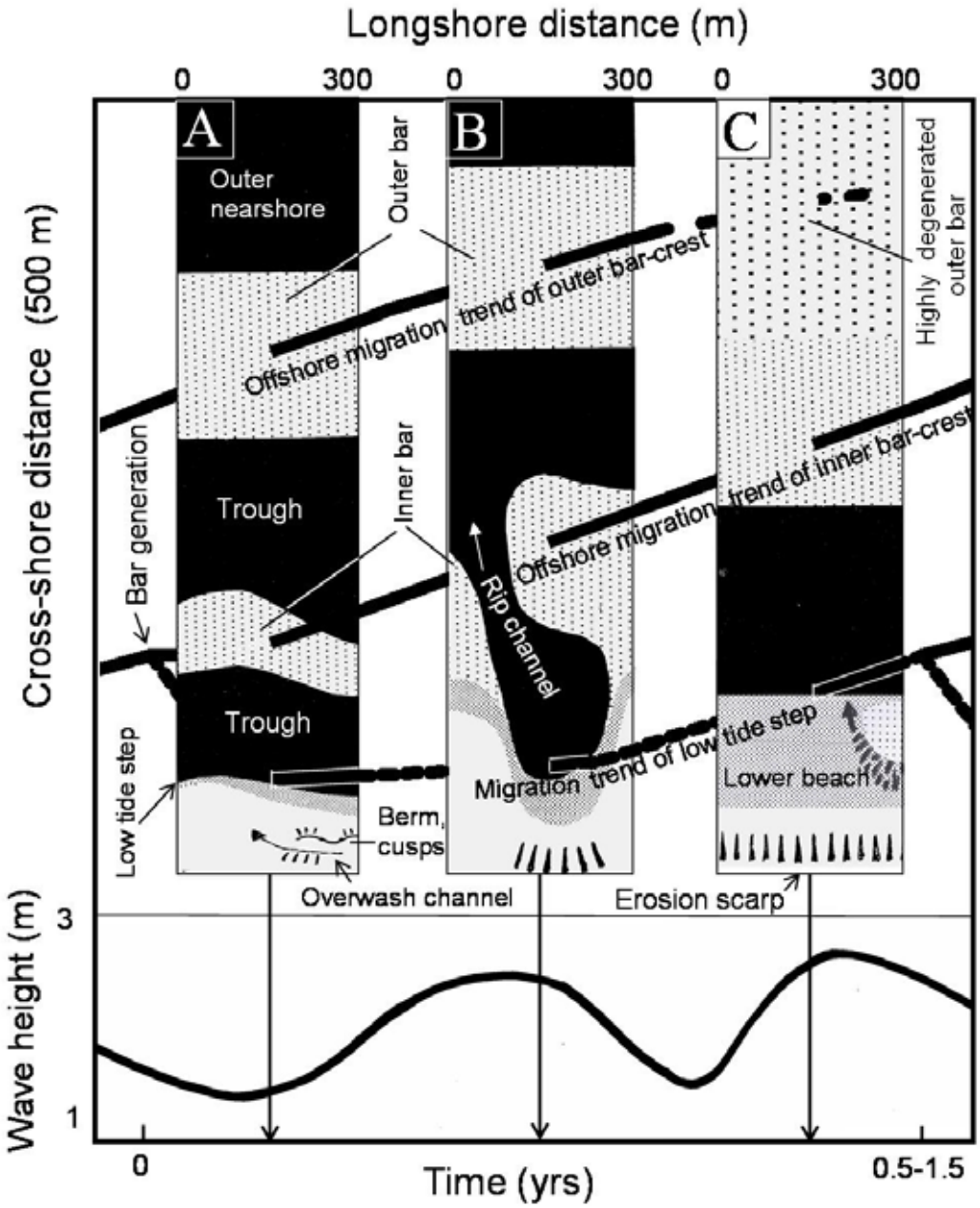

Figure 4 Conceptual model illustrating the relationships between types of beach cut and systematic variation in morphological configuration, cross-shore bar and step migration, and wave height, for the Wanganui study site. Panel A depicts overwash channel and berm-front erosion, panel B depicts rip embayment erosion and panel C depicts laterally extensive erosion.

DISCUSSION

Laterally extensive episodes of beach cut required substantially higher wave energy levels than did the other types, as such erosion not only occurred during the most energetic conditions, but coincided with a reduction in the number of subtidal bars from two to one later in the inter-generation period. With only a single bar, a higher proportion of incident wave energy would reach the shoreline and be available for erosion as up to 50% of storm-wave energy is dissipated when breaking occurs over an outer bar, e.g. see Keady and Coleman (1980). Furthermore, laterally extensive erosion tended to occur as soon as the bar number reduced, which suggests that the same storm responsible for subduing the outer bar may also linearise, and erode, the beach. It is also noted that the strong longshore currents which accompany storm wave conditions

on this coast, probably enhance backshore/dune erosion by removing sediment which accumulates at the scarp-base following wave-undercut and slumping.

The importance of local morphological control during the laterally extensive erosion process is evident in that the relatively featureless/2D morphology which accompanies this type of scarping would facilitate widespread erosion. By contrast, the two periods of higher energy when laterally extensive erosion did not occur were characterised by 3D configurations which must limit the longshore extent of erosion.

While rip embayment erosion required similar tidal range to laterally extensive erosion, it required substantially less wave energy; this is apparent by the lower values in Table 1 coupled with energy loss associated with the increased bar number. However, rip embayment erosion caused similar severity in terms of scarp height and backshore incursion as laterally extensive erosion, which indicates that the locally pronounced 3D morphology associated with rip embayment erosion must significantly enhance wave-driven hydrodynamic processes and result in particularly strong radiation stress gradients.

The occurrence of overwash/berm-front erosion shortly after bar generation corresponds with the systematic change from 2D to 3D morphology during the earlier part of the inter-generation period. During this time, ridge and runnel development is common along the lower foreshore, with the ridge migrating landward to form a berm along the upper beach during post bar generation fair-weather conditions. Berm-front erosion occurs under moderate wave height and tidal range as these conditions allow for saturation, and hence slumping, of the terrace riser while minimising runup passing beyond the crest and smearing the erosion scarp. In contrast, the higher wave energy and tidal range associated with overwash erosion reflect the need for swash to pass over the berm-crest, pond at the rear of the structure, then flow laterally along the channel with sufficient speed to erode the (landward) beach. Observation showed that overwash channel erosion tended to coincide with destruction of the berm terrace.

CONCLUSIONS

During the study period the following four types of beach cut occurred: four episodes of laterally-extensive erosion; three episodes of rip-embayment erosion; three episodes of overwash-channel erosion, and six episodes of berm-front erosion. Laterally extensive erosion had the greatest longshore extent and occurred on a relatively featureless/2D morphology during extreme storm conditions and spring tides. Rip embayment erosion had moderate longshore extent and was confined to bay areas at the head of large rips under spring tides and moderate storm events. Overwash channel erosion and berm-front erosion occurred on the landward and seaward sides respectively of an upper beach ridge (berm terrace), with berm-front erosion having the shortest longshore extent, lowest height, shortest duration, lowest wave height and lowest tidal range of any erosion type.

Each type of erosion occurred systematically during a particular time within the inter-generation period of the NOM cycle. Overwash channel and berm-front erosion occurred earlier in the period, under double bars and intermediate morphologies, i.e. 2D to 3D. Rip embayment erosion occurred during the earlier/central part of the inter-generation period, under double bars and strongly 3D morphology, while laterally extensive erosion occurred later in the period under single bars and more linear morphology. While wave energy conditions also varied systematically during each inter-generation period, morphological control still appears to be of fundamental importance in determining erosion type. For example, while both laterally extensive and rip embayment erosion occurred during periods of higher energy, morphologies associated with each type of cut were quite different.

ACKNOWLEDGEMENTS

This study was supported by a Research Fellowship (contract MAUX0104) from the New Zealand Foundation for Science and Technology (FRST).

LITERATURE CITED

BAILEY, D.G., and Shand, R.D., 1996. Determining large-scale sand bar behaviour. *Proceedings of the IEEE International Conference on Image Processing*, Lausanne, Switzerland, (2), 637-640.

BASCO, D.R., and Shin, S., 1996. Dune damage curves and their use to estimate dune maintenance costs. *Proceedings of the 25th International Conference on Coastal Engineering*, ASCE, pp. 2969-2981.

DOLAN, R.; Fenster, M.S., and Holm, S.J., 1991. Temporal analysis of shoreline recession and accretion. *Journal of Coastal Research*, 7(3), 723-744.

GUILLEN, J.; Stive, M.J.F. and Capobianco, M., 1999. Shoreline evolution of the Holland Coast on a decadal scale. *Earth surface Processes and Landforms*, 24, 517-536.

KANNAN, S., Lippman, T.C., and List, J.H., 2003. Relationship of nearshore sand bar configuration to shoreline change. *Proceedings of Coastal Sediments '03*.

KEADY, D.M., and Coleman, L.J., 1980. Incidence, breaking and reforming of waves behind submerged barriers. pp. 249-267 in Tanner, W.F., (ed.). *Shorelines Past and Present*. Department of Geology, Florida State University.

PATTERSON, D.C., and Blair, R.J., 1983. Visually determined wave parameters. *Proceedings of the Sixth Australian Conference on Coastal and Ocean Engineering*, Gold Coast, Australia, pp. 151-155.

PSUTY, N.P., Allen, J.R., Starcher, R., 1988. Spatial Analysis of dune crest mobility, Fire Island National Seashore, New York. *Journal of Coastal Research, Special Issue 3*.

SHAND, R D (2003). Relationships between episodes of bar switching, cross-shore bar migration and outer bar degeneration at Wanganui, New Zealand. *Journal of Coastal Research*, 19(1), 157-170.

SHAND, R.D.; Bailey, D.G., and Shepherd, M.J., 1999. An inter-site comparison of net offshore bar migration characteristics and environmental conditions. *Journal of Coastal Research*, 15(4), 750-765.

SHAND, R.D.; Bailey, D.G.; Hesp, P.A., and Shepherd, M.J. 2003. Conceptual beach-state model for the inner bar of a storm-dominated, low to moderate tidal range coast at Wanganui, NZ. *Proceedings of Coastal Sediments '03*.

SHAND, R.D., and Shepherd, M.J. (2003). Associations between net offshore bar migration and backshore erosion. *Proceedings of Coasts and Ports Australasian Conference 2003,* Auckland, New Zealand.

WRIGHT, L.D., 1980. Beach cut in relation to surf zone morphodynamics. *Proceedings of the 17th International Conference of Coastal Engineering*, pp. 978-996.

WRIGHT, L.D., and Short, A.D., 1984. Morphodynamic variability of surf zones and beaches: a synthesis. *Marine Geology*, 56, 93-118.

ZHENG, J., and Dean, R.D., 1996. Comparisons of erosion models for storms at Ocean City, MD. *Proceedings of the 25th International Conference on Coastal Engineering*, ASCE, pp. 3115-3128.

Shand, R.D., 2004. Rip-associated bathing hazards on beaches characterised by net offshore bar migration. School of People, Environment and Planning, Massey University, New Zealand, Occasional Paper 2004/1, 19p.

Rip-associated bathing hazards on beaches characterised by net offshore bar migration

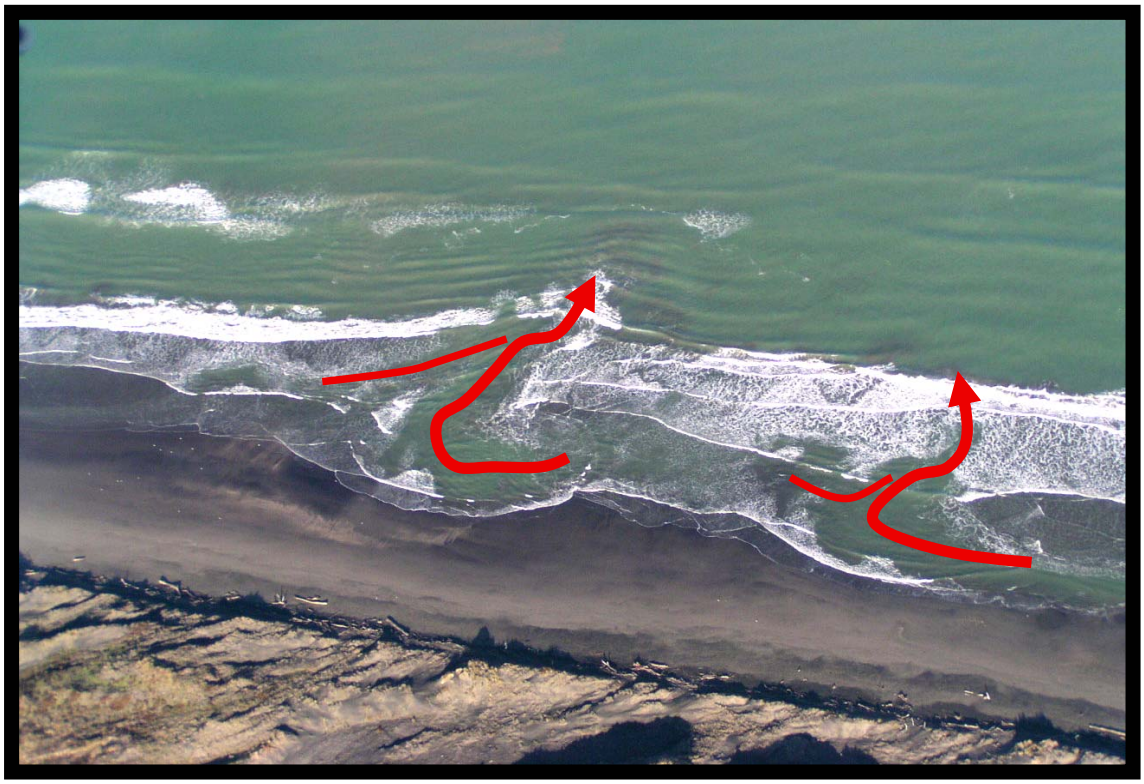

Roger D. Shand
Geography Programme
Massey University
Palmerston North

School of People Environment and Planning
Occasional Paper 2004/1

Rip-associated bathing hazards on beaches characterised by net offshore bar migration

Roger D. Shand
Geography Programme
Massey University
Palmerston North

School of People Environment and Planning
Occasional Paper 2004/1

Cover: Example of transverse inner bar configurations on the Wanganui coast. The rips, depicted by the red arrows, are asymmetric with oblique orientation, typical of those which occur along coasts characterised by strong longshore currents with alternating approach directions.

INTRODUCTION

While recreational bathing is a major pastime throughout the world, oceanic sandy beaches can be particularly hazardous. Such beaches often have sand-bars, longshore troughs and rip-channels, all of which result in varying water depth; breaking waves and bores which generate turbulence and multi-directional surf zone currents; tides which continually change water depth and current velocities; wind-driven currents, and rip currents. The level of risk to which bathers are subjected is a product of both the hazards and the characteristics of the beach-user (e.g. height and swimming ability). The risk may be mitigated, and hence bather safety increased, by surf lifeguards patrolling the beach and by public education programmes.

Rip currents pose the greatest threat to swimmers because they are the least obvious hazard (Short, 1999). Furthermore, rip currents may occur close to the shoreline, vary in strength with changing tide, wave and wind conditions, and may be fast-flowing even when waves are relatively small (0.5 to 1.0 m).

During the 1990s, coastal researchers observed a new type of morphological behaviour in which subtidal sand-bars formed near the shoreline, systematically migrated seaward across surf zone, then flattened out and disappeared within the outer surf zone. This process may take several years to complete and is referred to as net offshore bar migration or NOM. Such bar behaviour has been studied using longer-term data-sets from coastal sites in the USA (Lippmann et al., 1993), the Netherlands (Wijnberg and Terwindt ,1995; Ruessink and Kroon 1994), Japan (Kuriyama and Lee, 2001) and New Zealand (Shand et al., 1999). NOM also occurs on the southern shores of the Great Lakes during ice-free years (Howser, 2004). Recent results from the New Zealand site at Wanganui suggest that a systematic change in morphological (plan-view) configuration accompanies a bar undergoing NOM and often these configurations incorporate rip-channels (Shand et al., 2004). The present paper will focus on the relationship between NOM and those configurations which present the greatest risk to bathers.

The paper will firstly describe the Wanganui field site, its environmental conditions, and the methods used to acquire data. The process of net offshore bar migration will then be

illustrated, its salient characteristics described, and an estimate made of the extent to which it occurs on the New Zealand coast. Systematic variation in configuration during NOM will then be identified, with particular attention given to rip-dominated configurations. Finally, the results are summarized and consideration given to their application.

STUDY SITE

The Wanganui field site covers some 6 km of coast to the northwest of the Wanganui Rivermouth on the southwestern coast of the New Zealand North Island (Fig 1). The nearshore is characterised by fine sand (~0.2 mm), has a cross-shore slope of 1 in 110 and width of ~550 m. Two subtidal sand-bars are usually present; these bars undergo net offshore migration, i.e. NOM, with the mean life-cycle of a bar being ~3 yrs. The foreshore is characterised by medium sand (~0.3 mm), has an average cross-shore slope of 1 in 20 and an average width of ~85 m. About 30% of the time a small amplitude (swash) bar is present on the lower foreshore.

The mean neap tide range is 0.8 m and the mean spring tide range is 2.4 m. The mean deepwater significant wave height is 1.3 m and the 5% excedence value is 2.5 m. The mean time interval between successive waves (wave period) is 10.1 s (range 3.5 s to19 s) with sea wave conditions (periods <10 secs) occurring for ~75% of the time and swell wave conditions (periods >10 secs) for the remaining time. Approximately 42% of waves approach from the west, ~24% from the south and ~34% lie within one degree of shore-normal. The prevailing WNW wind approaches the coast at ~35 deg from the shoreline, and the 5% excedence value of the wind speeds is 12.4 m/s. The mean value for longshore currents within the inner surf zone is 0.42 m/s and the 5% excedence value is 1.01 m/s. Wave height, wind strength and the magnitude of longshore currents are all positively correlated, as are their approach directions.

DATA ACQUISITION

Inter-tidal beach characteristics were identified from morphological maps (e.g. see Fig 2). These maps were produced using ground surveys carried out at fortnightly intervals between August 1991 and March 1995. Beach (inter-tidal) width was derived from the location of the low tide step, this being used as a proxy for the seaward boundary of the foreshore. In addition, plan-view morphological configurations of the beach and inner bar system were obtained using a classification scheme.

Surf-zone morphology was identified from time-lapse photographs. The photographs were exposed for ~5 minutes and field sampled at monthly intervals from on top of a 42 m high cliff located some 3200 m northwest of the rivermouth (see asterisk Fig 1). The long-exposure results in a statistically stable intensity pattern in which higher intensity areas represent shallower depth as wave-breaking is depth-dependent (see Figs 3A and 3B). Each photo was digitised, rectified (perspective distortion removed) to ground co-ordinates and the coastline straightened to facilitate subsequent analysis. The methodology has been described in detail by Bailey and Shand (1993, 1996). The rectified image corresponding to the time-lapse image in Fig 3B, is shown in 3C.

It is noted that photo or video imaging has huge potential for increasing scientific understanding of surf zone processes, and offers real hope for morphodynamic modelling and providing real-time hydrodynamic data. For example, providing wave heights and current velocities for a grid of locations (say every 10 m^2) within a predetermined study area.

For the present exercise, a 300 m long section of coast within the Wanganui study area was used; this section was located between 1400 m to 1700 m from the rivermouth, hereafter referred to as ‘site 1550’. Cross-shore distances to the step and bar-crests were longshore-averaged over the 300 m to derive representative values for each sample.

NET OFFSHORE BAR MIGRATION

Net seaward movement of the low tide step, the inner bar and the seaward bar are all suggested in the 3 time-lapse photos (Fig 4) which span an 18 month period.

How these bar-crest locations fit within longer-term data sampled at 4 weekly intervals over 6.5 yrs can be ascertained from Fig 5. Several repetitions of NOM occurred in which bars systematically migrate seaward then disappear in the outer surf zone. It is also evident that the formation of a new bar occurs about the same time as the disappearance of the existing outer bar.

How the low tide step locations in Fig 4 fit within longer-term data sampled at 2 weekly intervals is evident in Fig 6. These data show a systematic widening and narrowing of the beach. New bars form upon a widened inter-tidal beach. The beach then narrows and remains like this for several months before widening prior to the generation of the next bar.

While NOM is repetitious, there is significant temporal and spatial variation. For example, Fig 7 shows the bar generation history for both the 1550 m site and also for a site ~5 km from the rivermouth (site 5050). While the mean generation periods are similar (1.17 yrs at site 1550 c.f. 1.13 yrs at site 5050) the ranges show substantial variation (0.25 to 1.8 yrs for site 1500 c.f. 0.3 to 3.2 yrs for site 5050). It is also evident that bar generation is non-contemporaneous between these two sites. At Wanganui, variation in NOM behaviour has been found to occur every 1-2 km in the longshore direction. Temporal variation is also evident in the rate at which the bars systematically migrate across the surf zone, with Wanganui values ranging between 75 to 320 m/yr. In addition, NOM behaviour varies on a regional basis with mean return periods at the global sites ranging between 1 yr for the Japanese Pacific coast, to 14.4 yrs for the northern coast of Holland, and NOM rates ranging between 35 m/yr for the northern coast of Holland and 164 m/yr for Wanganui.

Analysis of environmental conditions at the global NOM sites shows that such coasts are characterised by multiple sand-bars, lower cross-shore gradients, regular storm-waves and winds and micro-meso tidal range (see Tables 1 and 2). Approx 25% of the NZ oceanic coast meets these conditions and hence the potential for NOM.

CONFIGURATIONS

Because surf zone morphologies are typically complex, a classification approach was used in the present exercise. All (plan-view) configurations were assigned to one of the following four categories:

1. linear (elsewhere, e.g. Wright and Short (1984), such configuration has been referred to as a longshore bar and trough),
2. undulating (elsewhere referred to as (a)rhythmic or crescentic topography),
3. transverse (elsewhere referred to as transverse bar and rip, or simply as ripped topography) and
4. subdued (elsewhere referred to as low tide terrace; such morphology may include minor irregularities including mini-rips).

Fig 8 shows examples of each type of configuration on the series of time-lapse photos displayed earlier (Fig 4) to illustrate offshore bar and step migration.

It is noted that rips may occur in any of the 4 classes; however, they are most prevalent under transverse configurations. Rips within this class also present the greatest bathing hazard because transverse bars facilitate seaward positioning of bathers, and current strength may be relatively high even under lower energy conditions.

The images in Fig 8 suggest that undulating configurations occur following bar generation with transverse configurations predominating during the central portion of the inter-generation period, and linear configurations being characteristic prior to generation of a new bar. The associated time-series of fortnightly data (Fig 9) confirms such configuration tendencies, with the filtered 'dimensionality-based' (see below) curve more clearly illustrating the fluctuation between transverse (3D) configurations during the mid-generation period and linear (2D) configurations later in the inter-generation period.

Subdued configurations were rarely observed in these data, although they were more prevalent in another Wanganui study (Shand et al., 2003) which used higher resolution data with a closer sampling interval from a site located further (3 km) from the rivermouth. In

that study subdued configurations were found to form as a result of rip channel infill which occurred at times of higher tidal range and lower wave conditions.

Configuration 'dimension' relates to the level of morphological variation in the longshore direction. In particular, morphologies which are non-changing in the longshore direction, e.g. linear configurations, are fully definable with a single (two-dimensional or 2D) cross-shore profile because the third (longshore) dimension is constant. By contrast, descriptions of morphologies which vary in the longshore direction require several cross-shore profiles because the third dimension is not constant. The number of profiles depends on the particular morphology, with 'stronger' 3D configurations requiring a greater number of profiles than 'weaker' 3D configurations. Subdued configurations are considered to be dimensionless and as such were excluded from the filtering process referred to earlier.

On average, the duration of the transverse (ripped) configurations, hereafter referred to as the 'transverse of ripped-phase', is approximately one third of the inter-generation period.

The nature of the ripped configurations was further investigated by analysing the cross-shore rip channel length. Examples of ripped configurations and associated rip-lengths are depicted in the two time-lapse photos shown in Fig 10. These samples occurred during the same inter-generation period as the time-lapse photos used in Figs 4 and 8. These results suggest that rips increase in size during the inter-generation cycle and this is confirmed in the fortnightly time-series of rip-lengths depicted in Fig 11. The rips have been grouped to show how they relate to the inter-generation cycles, and temporal trend lines have been fitted to each group. These results confirm that rip-size, and hence bathing hazard, increases during the transverse morphology phase of the inter-generation cycle.

It is noted that during the longest inter-generation period (1993-94), the rips increased in length then decreased somewhat prior to the end of the phase. This resulted from infill within the landward part of the channel, as indicated by the seaward displacement of the step (see Fig10). Wanganui image-data (not shown) suggest that such behaviour is driven by a positive feedback processes which causes constriction within the rip channel and the eventual truncation of the landward portion of the channel.

DISCUSSION and CONCLUSIONS

Rips associated with transverse morphologies create the greatest hazard for bathers and such configurations occur systematically on NOM coasts such as that at Wanganui. In particular, they occur during the central portion of the bar generation cycle. On average this rip-phase lasts for ~5 months which is one third of the inter-generation period.

Transverse configurations evolve during the rip-phase. In particular, rip channels tend to increase in size and hence their potential as a bathing hazard also increases. However, the level of hazard for any rip channel varies according to the overall morphology, wave conditions, currents and tide.

NOM-associated rip-phases and bathing hazard affect New Zealand recreational beaches. As noted earlier, 25% of New Zealand's oceanic coast has environmental conditions conducive to NOM. In particular, these areas comprise sand-dominated surf zones of the west coast on the North and South Islands, together with exposed sandy surf zones around the base of the South Island, the east coast of the South Island, and the east coast of the North Island south of East Cape.

From a resource planning perspective, it would be useful for surf lifesavers to recognise where a bar is within the NOM cycle, or more particularly where a beach is in the bar-generation cycle. This would enable a basic prediction to be made as to how configurations are likely to (systematically) change in the foreseeable future.

To determine where sections of beach/inner-bar are within the bar generation cycle/NOM cycle, it is necessary to carry out morphological monitoring at 2 to 4 weekly intervals. Such a sampling regime is required because of the quasi-regular nature of NOM. Ideally, monitoring should consist of surf zone imaging and ground surveys for the inter-tidal beach. As changes affecting the beach are preceded by changes in the seaward bar(s), this approach provides the greatest warning time of systematic configuration changes which influence bathing hazard. Alternatively, monitoring of the inter-tidal beach width alone should enable observers to "keep in touch" with where the coast is with respect to the NOM-associated bar generation cycle and associated configuration phases. Of particular

interest is any major narrowing of the inter-tidal beach as this is likely to precede a period of hazardous rips.

ACKNOWLEDGEMENTS

This study was supported by a Research Fellowship (contract MAUX0104) from the New Zealand Foundation for Science and Technology (FRST).

REFERENCES

Bailey, D.G., and Shand, R.D., 1993. Determining large-scale sand-bar evolution. *Proceedings of the 1st New Zealand Conference on Image and Vision Computing*, pp. 109-116.

Bailey, D.G., and Shand, R.D., 1996. Determining large-scale sand-bar behaviour. *Proceedings of the IEEE International Conference on Image Processing*, Lausanne, Switzerland, (2), 637-640.

Howser, C., and Greenwood, B. Profile response of a lacustrine multiple barred nearshore over a sequence of storms. Submitted to Geomorphology, November 2003.

Kuriyama, Y., and Lee J.H., 2001. Medium-term beach profile change on a bar-trough region at Hasaki, Japan, investigated with complex principal component analysis. *Proceedings of Coastal Dynamics'01*, ASCE, pp. 959-968.

Lippmann, T.C. Holman, R.A. and Hathaway, K.K. 1993: Episodic, non-stationary behaviour of a double bar system at Duck, North Carolina, U.S.A., 1986-1991, *Journal of Coastal Research, Special Issue 15*, 49-75.

Ruessink, B.G. and Kroon, A. 1994: The behaviour of a multiple bar system in the nearshore zone of Terschelling, the Netherlands: 1965-1993, *Marine Geology*, 121, 187-197.

Shand, R.D., and Bailey, D.G., 1999. A review of net offshore bar migration with photographic illustrations from Wanganui, New Zealand, *Journal of Coastal Research*, 15(2), 365-378.

Shand, R.D., Bailey, D.G. Shepherd, M.J., 1999. An inter-site comparison of net offshore bar migration characteristics and environmental conditions. *Journal of Coastal Research, 15* (3), 750-765.

Shand, R.D.; Hesp, P.A., Bailey, D.G., and Shepherd, M.J., 2003. A conceptual beach-state model for the inner bar of a storm-dominate, low to moderate tidal range coast at Wanganui, New Zealand. *Proceedings of Coastal Sediments '03*.

Shand, R.D., Hesp, P.A., and Shepherd, M, J., 2004. Beach cut in relation to net offshore bar migration. *Journal of Coastal Research, Special Issue 39.*

Short, A.D., 1999. Beach hazards and safety. In Short, A.D. (ed.), *Handbook of Beach and Shoreface Morphodynamics*, pp. 293-303.

Wijnberg, K.M., and Terwindt, J.H.G., 1995. Extracting decadal morphological behaviour from high-resolution, long-term bathymetric surveys along the Holland coast using eigenfunction analysis. *Marine Geology,* 126, 301-330.

Wright, L.D., and Short, A.D., 1984. Morphodynamic variability of surf zones and beaches: a synthesis. *Marine Geology*, 56, 93-118.

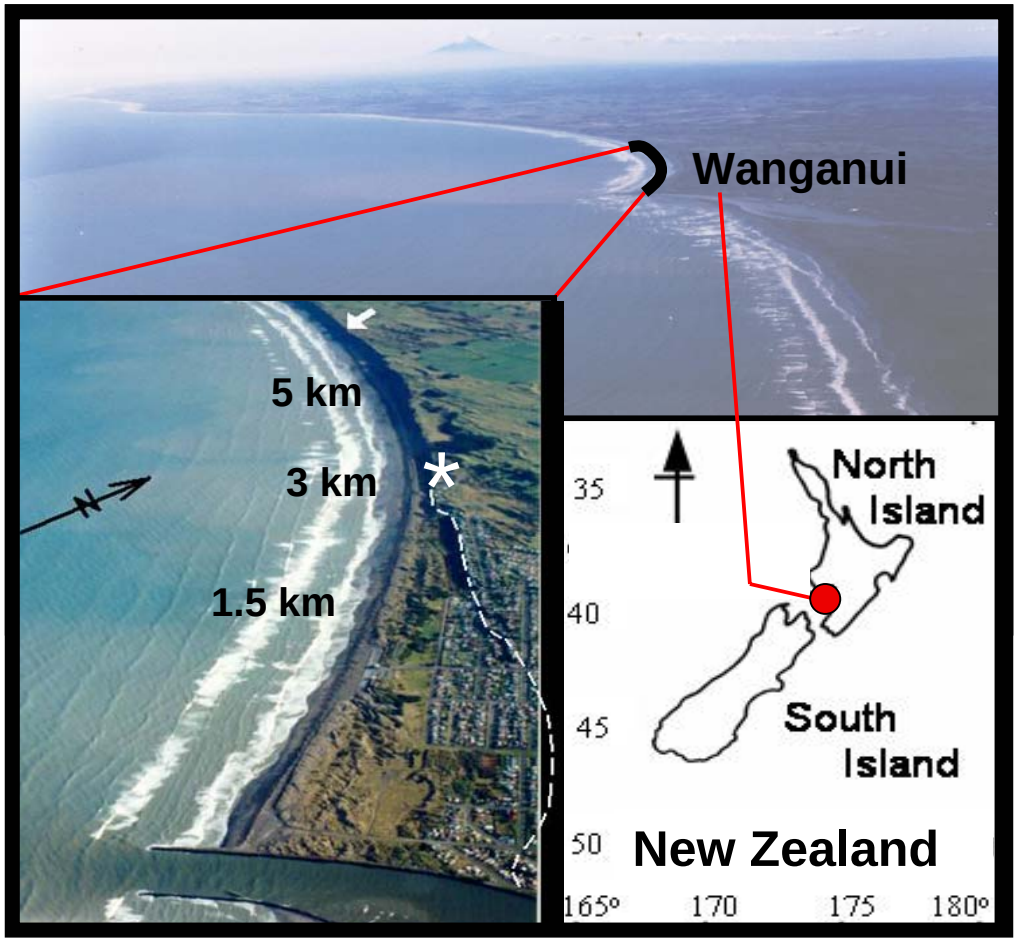

Figure 1 Location maps of the Wanganui study site. The asterisk in lower left figure marks the camera position (see text), while the dashed white line depicts the shoreline prior to construction of rivermouth jetties in the late 19th and early 20th centuries.

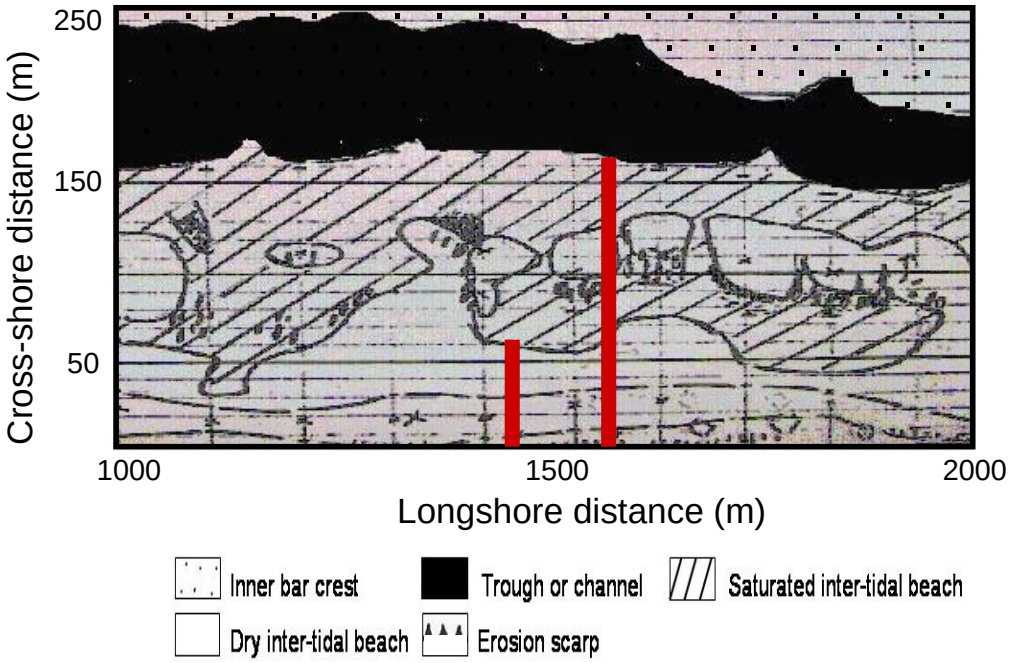

Figure 2 Example of morphological map constructed from ground surveys. The longer vertical bold line depicts inter-tidal beach width, whilst the shorter line depicts beach width at mean sea level.

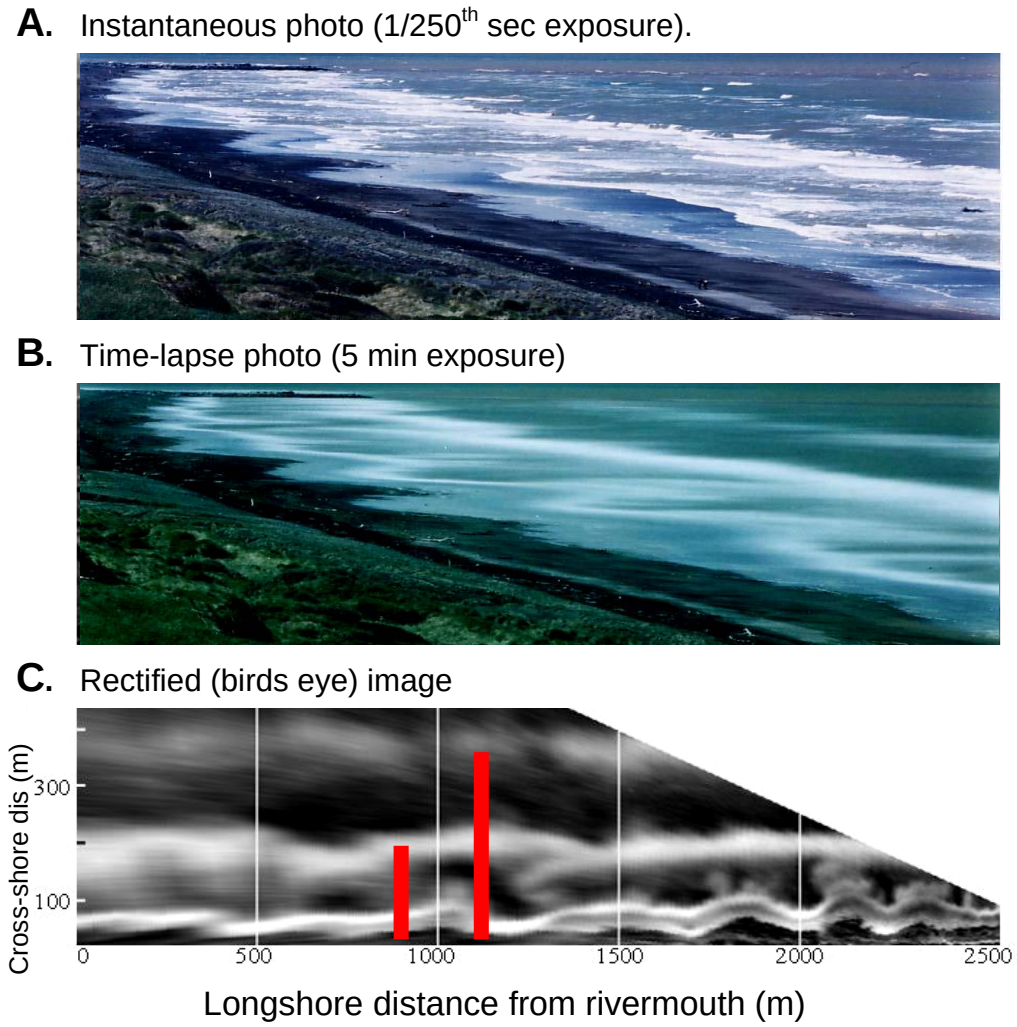

Figure 3 Instantaneous photo (A) shows the eastern portion of study area with the Wanganui River's northern jetty (North Mole) evident at top of picture. The corresponding 5 min time-lapse photo (B) more clearly depicts (relative) topographic variation, with higher intensities corresponding to shallower areas. The rectified image (C) has had the perspective distortion, associated with the oblique viewing angle, removed by digital image processing. The coastline has also been straightened in C to further facilitate analysis. The longer vertical bold line in C depicts cross-shore distance from the dune-toe to the outer bar, while the shorter line depicts distance to the inner bar-crest.

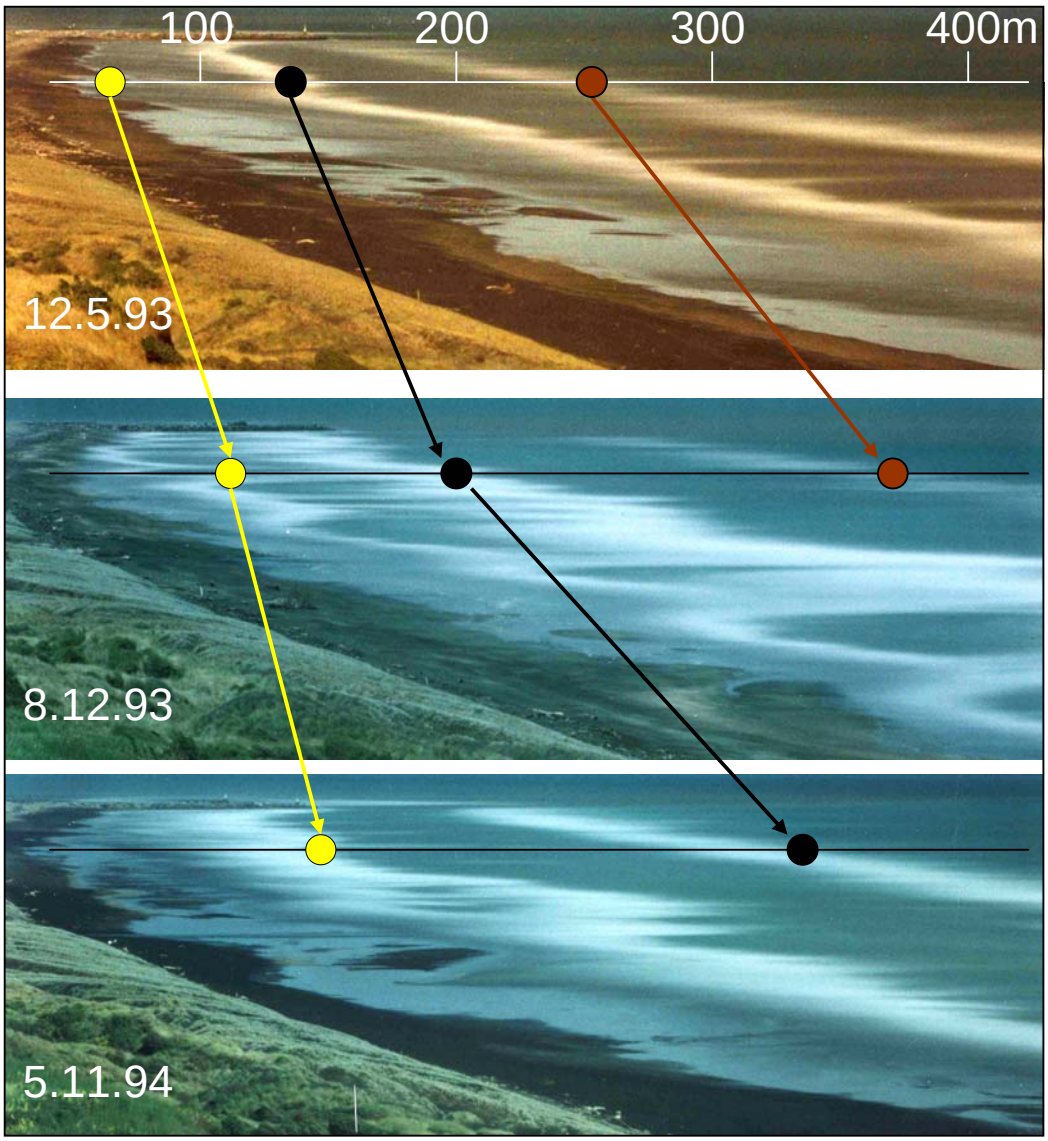

Figure 4 Time-lapse depiction of the seaward trend in bar migration and beach width at a cross-shore transect located 1550 m alongshore from the northwestern rivermouth jetty. Note how the seawardmost bar has disappeared in the final photograph.

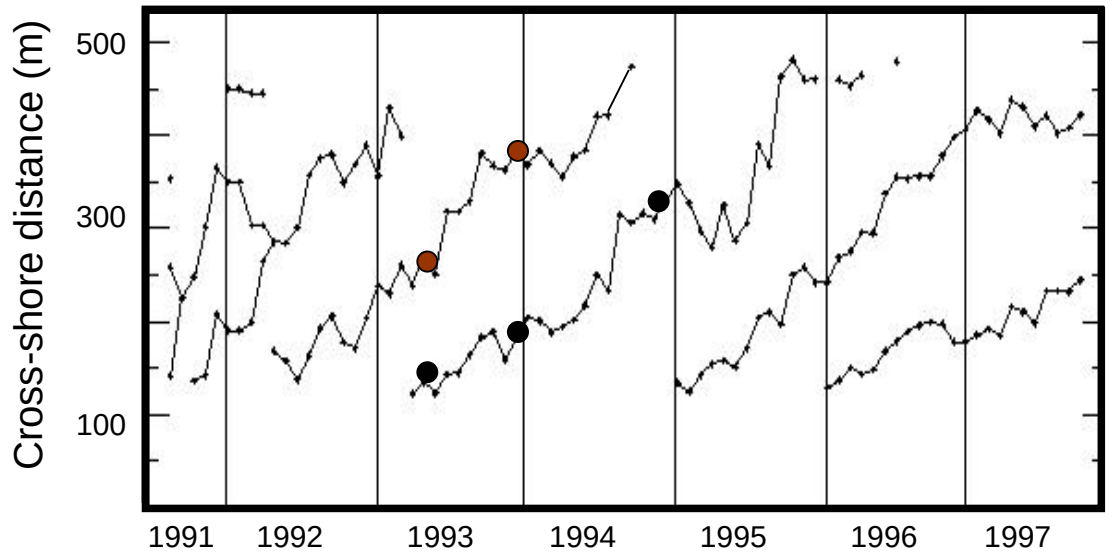

Figure 5 Time-series of sub-tidal bar-crest locations for a 300 m wide transect centered 1550 m (from the rivermouth) during the period August 1991 to November 1997. The five dots locate the bar-crests depicted in the set of three time-lapse photos shown in Figure 4.

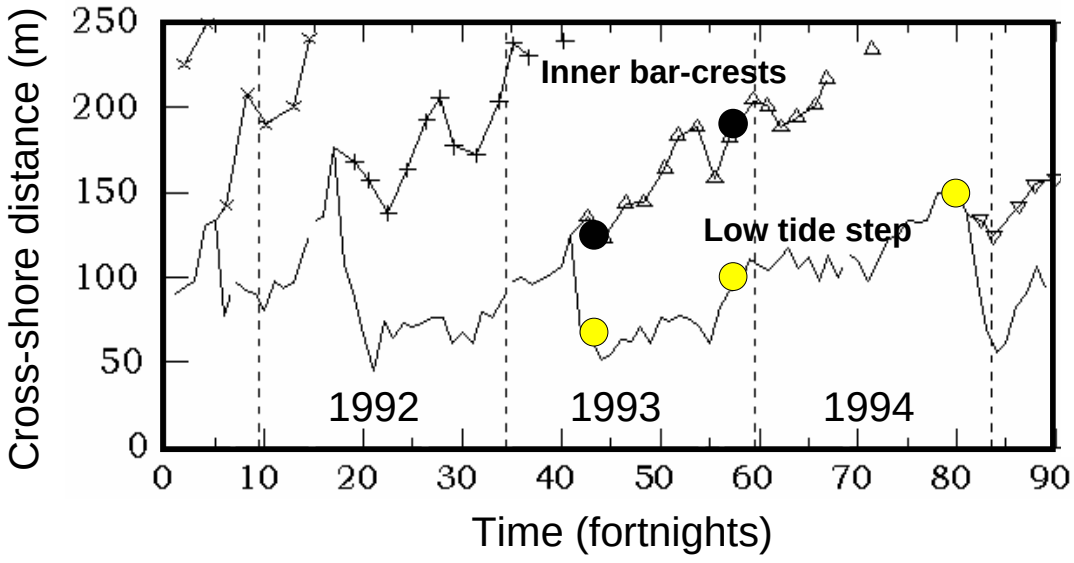

Figure 6 Time-series of low tide step and inner bar-crests for 300 m wide transect centered 1550 m during the period August 1991 to March 1995. The five dots locate the step and bar-crests as depicted in the set of time-lapse photos shown in Figure 4.

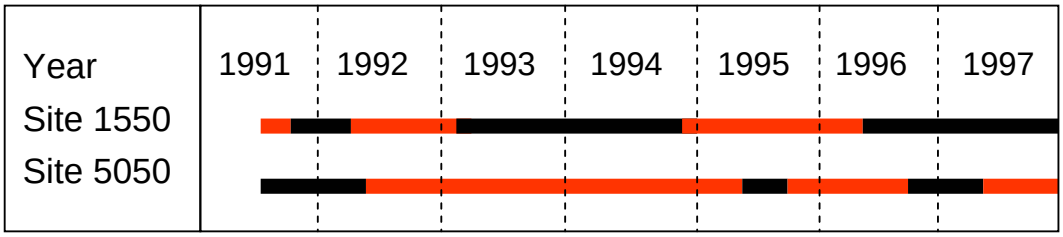

Figure 7 Bar generation periods for transects at 1550 m and 5050 m from the rivermouth.

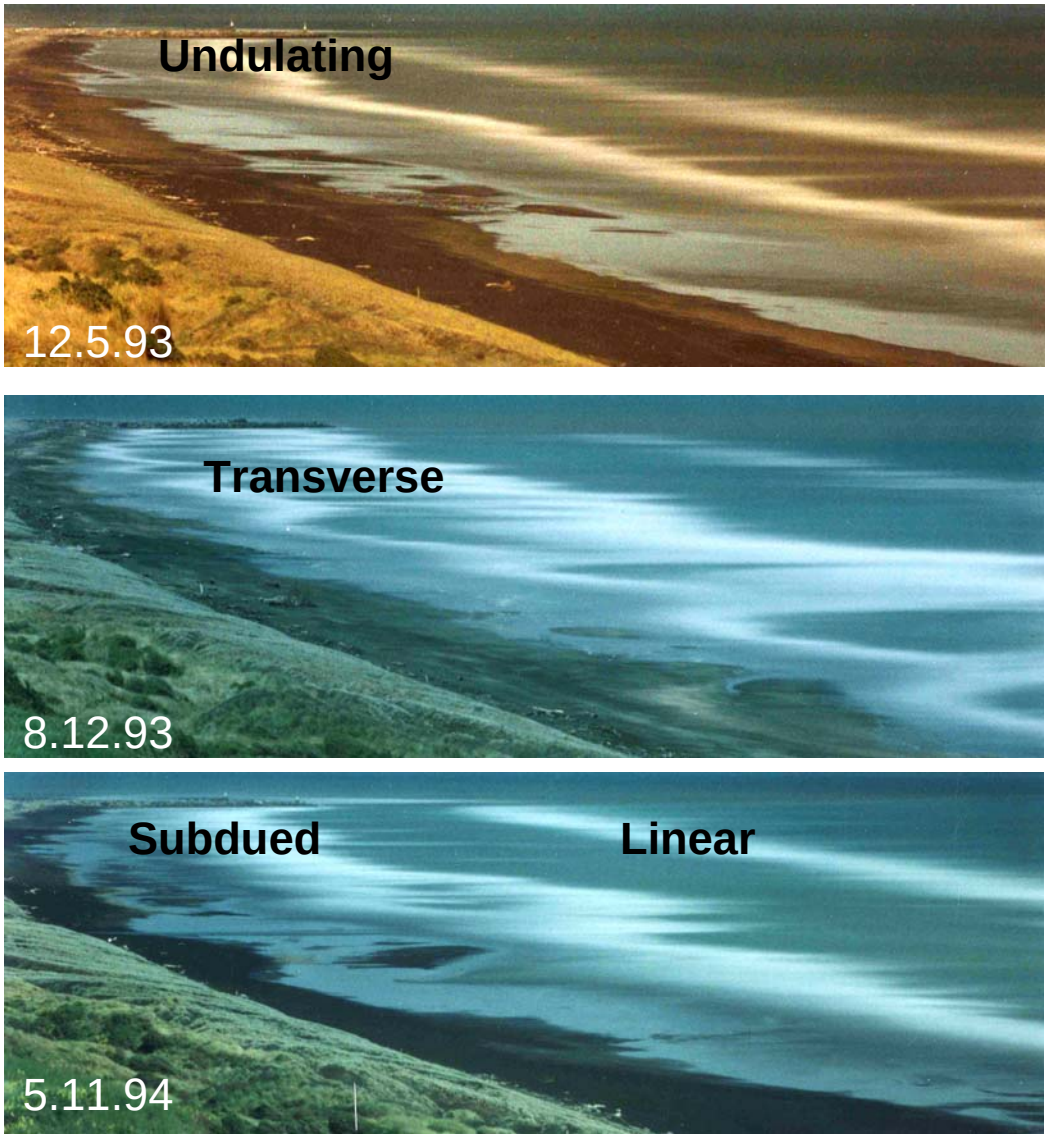

Figure 8
Examples of sections of coast exhibiting the four configuration classes used in this study. The three time-lapse photographs are the same as those used to illustrate NOM in Fig 4.

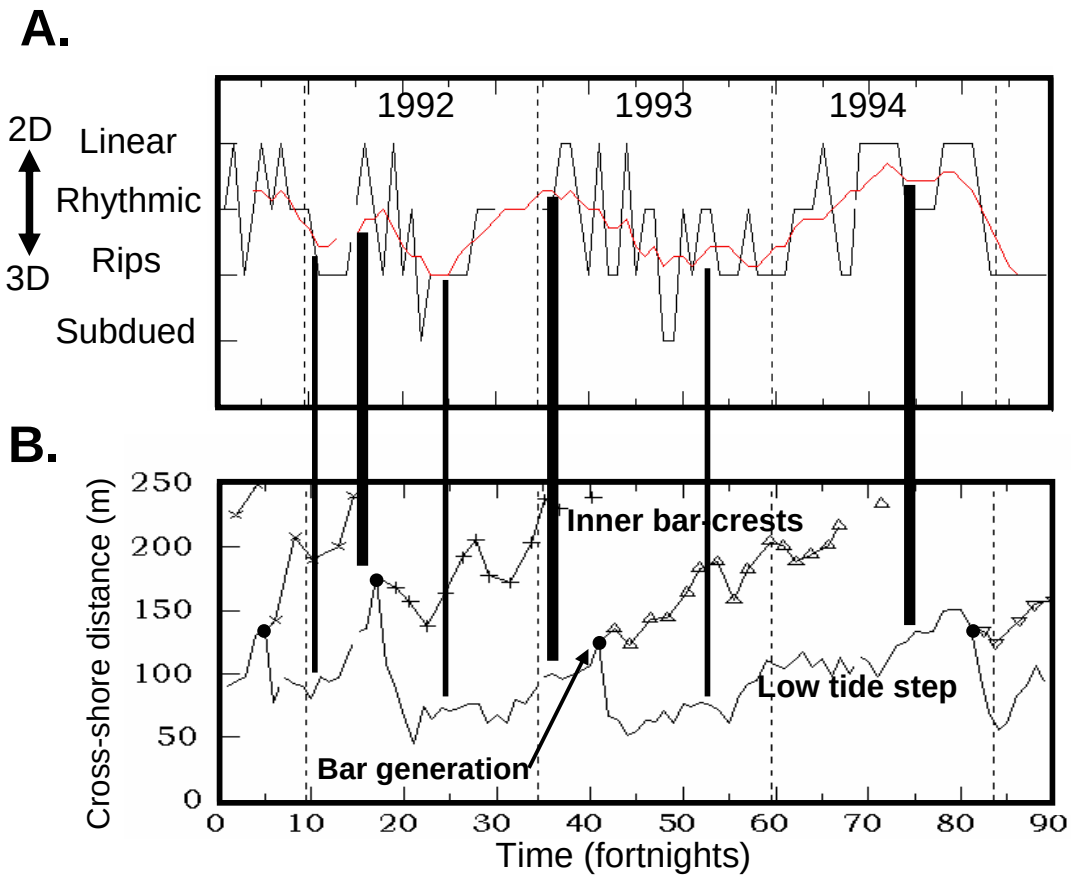

Figure 9 Time-series for configuration classes (A) and corresponding low tide step and inner bar-crest distances (B) for site 1550. The smooth line is A denotes the filtered dimensionality (see text). The vertical lines linking A and B, illustrate the nature of the correlation between configuration dimension and beach width, with the bold lines corresponding to lower dimensions and the thin lines corresponding to higher dimensions.

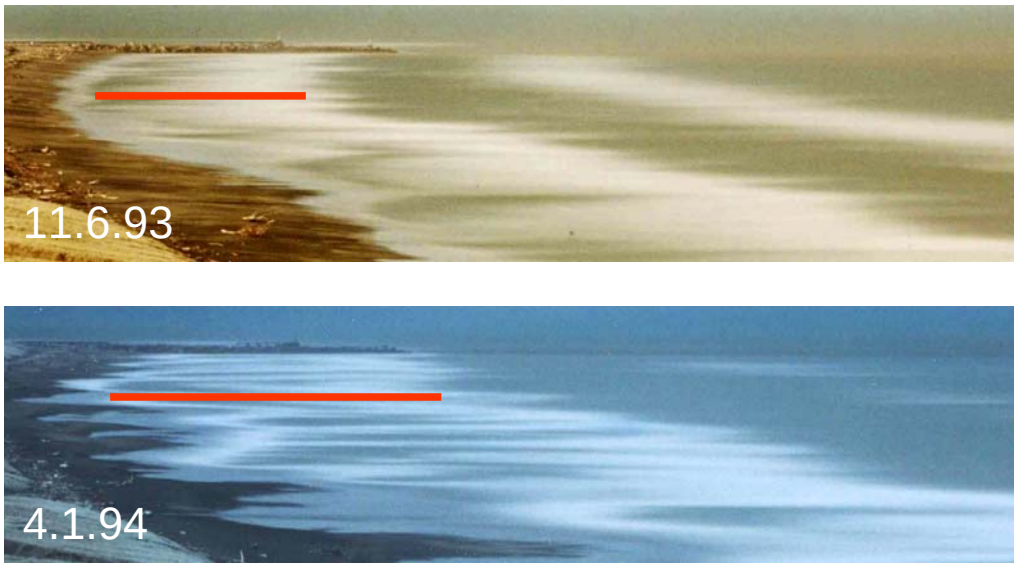

Figure 10 Examples of changing cross-shore length of rips during the ripped-phase of the same inter-generation cycle spanned by the time-lapse series in Figs 4 and 8.

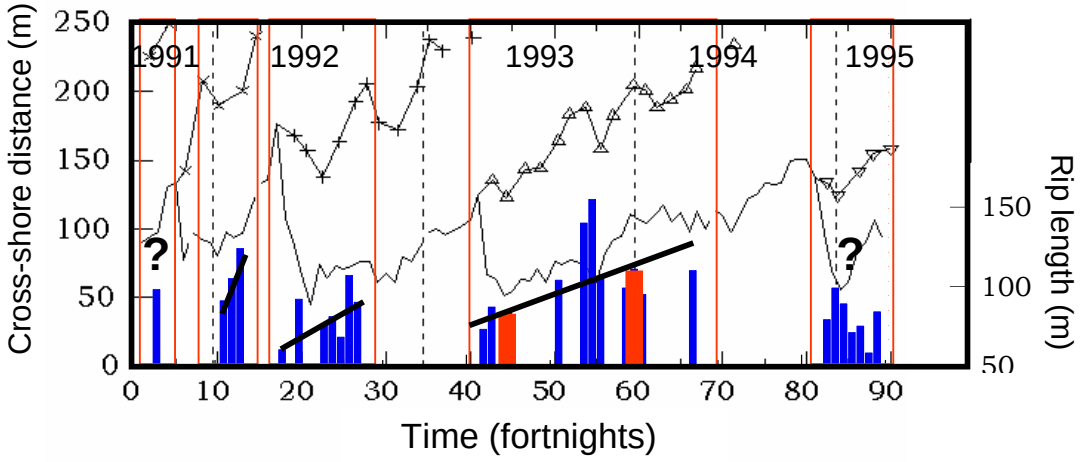

Figure 11 Time-series of rip-length for site 1550 during the period August 1992 to March 1995. The shaded areas define rip-phases and fitted linear models define the underlying change in length during each phase. There are not enough data-points in both the initial and final rip-phases to identify a trend. The two bold bars are those depicted in Fig 10.

Table 1 Physical environmental conditions on NOM coasts

Parameter	Mean	Minimum - maximum
Width (m) of sub-tidal bar zone	550	120 - 1075
Slope of nearshore	1:140 0.007	1:90 – 1:260 0.011-0.004
Bar number in cross-shore direction	2.5	2-4
Bar volume (m^3) prior to degeneration	302	10-575

Table 2 Energy condition on NOM coasts

Parameter	Mean	Minimum-maximum
H_{sig} (m) (daily average)	1.28	1.1-1.37
$H_{0.01}$(m) (extreme storm)	3.9	3.1-4.4
Wave-based seasons	2	1-4
T_{sig} (s)	7.6	6.3-11.4
Wind $speed_{0.1}$ (m/s)	13.5	12.3-14.8
Wind approach from shoreline (deg)	47	17-82
Spring tide range (m)	1.9	1.2-2.5

Hsig = mean daily significant wave height, where 'significant' refers to the mean of the upper 1/3 of values; $H_{0.001}$ = 1% exceedence wave height value; Tsig = mean daily significant wave period.

Shand, R.D., and Shepherd, M.J., 2005. Sediment budget implications associated with bar splitting within a net offshore migrating (NOM) bar system. School of People, Environment and Planning, Massey University, New Zealand, Occasional Paper 2006-2, 23p.

Sediment budget implications associated with bar splitting within a net offshore migrating (NOM) bar system

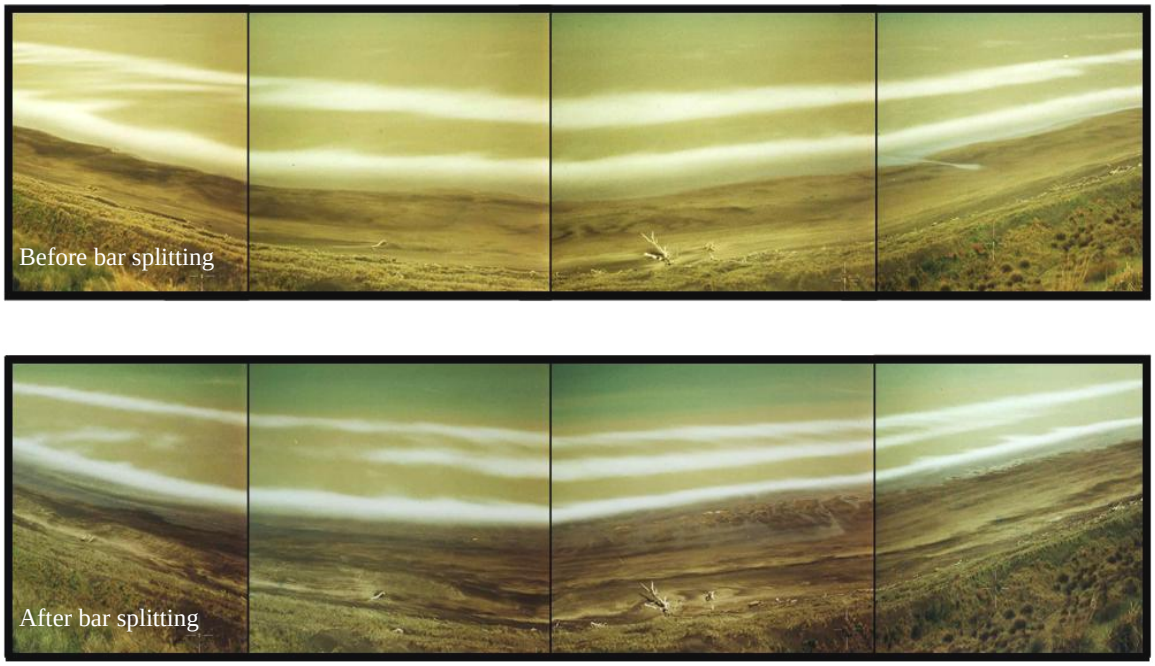

Roger D Shand and Mike J Shepherd
Geography Programme
Massey University
Palmerston North
New Zealand

School of People Environment and Planning
Occasional Paper 2005/2

Bar splitting: system attributes and sediment budget implications for a net offshore migrating bar system

Roger D Shand and Mike J Shepherd
Geography Programme
Massey University
Palmerston North
New Zealand

School of People Environment and Planning
Occasional Paper 2005/2

Front cover: example of bar splitting at the Wanganui study site using panoramas of oblique time-lapse photographs sampled on 3rd November, 2002 and 20th November, 2002. The high intensity regions represent elevated topography such as bar-crests or the low tide step.

© 2005 Roger Shand and Mike Shepherd

ABSTRACT

Net offshore bar migration or NOM, refers to the systematic seaward migration of longshore (primary) sand-bars across the surf zone. NOM appears to be the product of storm-induced seaward bar migration (sediment transport) exceeding landward bar migration (sediment transport) during intervening fairweather periods. NOM also appears to involve the cross-shore redistribution of sediment rather than the continual loss of sediment to the shoreface. While 'grain by grain' return processes appear to predominate within the outer surf zone, alternative mechanisms may exist within the inner surf zone. The aim of this paper is to assess whether sediment travelling landward within inner bifurcates formed during the process of bar splitting can offset a NOM-induced cross-shore sediment imbalance. Bar splitting has been observed on several NOM coasts and involves a longshore bar bifurcating, with the inner bifurcate detaching, moving landward, and in some cases welding to the foreshore. Analysis of several years of morphological data from Wanganui, on the west coast of the New Zealand North Island, found that the sediment gained by the foreshore from inner bifurcate welding amounted to approximately half the sediment lost from the foreshore by newly generated sand-bars which subsequently underwent NOM. In addition, during the study, several other types of 3D morphological behaviour were identified, which are able to transport sediment shoreward across the inner surf zone. Landward migrating secondary sand bodies therefore appear to be the main mechanism by which sediment returns to the inter-tidal beach. Finally, a conceptual morphodynamic model of cross-shore sediment transport mechanisms for the NOM system at Wanganui is presented.

ADDITIONAL INDEX WORDS: Sand-bar, multi-bar coast, bifurcation, surf zone, nearshore, morphodynamic.

INTRODUCTION

Net offshore bar migration (NOM) refers to the systematic seaward migration of coastal subtidal sand-bars across the surf zone; such bars form upon a widened lower foreshore and disappear several years later in the outer surf zone (Ruessink and Kroon, 1994; Shand and Bailey, 1999; Ruessink et al., 2002; Shand et al., 2004). Since the mid 1980s, NOM has been recognised on several storm-dominated, multi-barred coasts: the North Carolina coast (e.g. Birkemeier, 1984; Lippmann et al., 1993), the Dutch coasts (e.g. de Vroeg et al., 1988, Kroon and Hoekstra, 1993), at Wanganui, on the south west coast of the New Zealand North Island (Shand et al., 1999), and at Hasaki Beach on the Japanese Pacific Coast (Kuriyama, 2002). There are also several other locations where published data indicates NOM behaviour may be occurring, but longer records are required for confirmation. For example: Burley Beach, Lake Huron (Houser and Greenwood, in press); Agate Beach, Oregon (Haxel and Holman, 2004), and Muriwai Beach, near Auckland on the west coast of the New Zealand North Island (ARGUS (see Aarninkhof and Holman, 1999) data analysed by author). NOM has also been described as 'the offshore progression cycle' by Wijnberg (1996) and 'inter-annual cyclic bar behaviour' by Ruessink and Terwindt (2000). An example of NOM behaviour from the Wanganui Coast is depicted in Fig 1 using a sequence of time-lapse photographs.

Sediment dynamics associated with NOM have long puzzled researchers. Central to the issue is the widely accepted notion that bars move seaward under storm-conditions in response to undertow-dominated sediment transport. There exists a variety of field evidence to support this mechanism: sediment tracing studies (e.g. Ingle, 1966); sediment structures (e.g. Greenwood and Davidson-Arnott, 1979); and sediment transport and modelling studies (Gallager et al., 1998). If this is indeed the case, then several hundred cubic metres (per metre longshore) of sediment per bar migration cycle would be lost to the shoreface (Shand et al., 1999). However, a sediment budget analysis for the South Holland coast by Wijnberg (1995), found that the volume of sediment from the longshore sediment flux was several times smaller than the amount which would be lost seaward by NOM. Furthermore, this section of coast was accreting so coastal erosion was not providing a sediment source. Wijnberg (1995, p152) concluded that "…most of the sediment of the degenerating outer bar has to stay within the inshore area….." Sediment transport within a NOM system therefore appears to involve the cross-shore redistribution of sediment, rather than the continual lost of sediment to the shoreface and its replacement from landward or longshore sources.

Landward directed sediment transport occurs in association with sand-bars migrating onshore during lower (fair-weather) wave conditions. Under the influence of landward directed currents associated with asymmetric waves (e.g. Hoefel and Elgar, 2003), and the surface roller effect of broken waves (e.g. Svendsen, 1984), sediment is eroded from the seaward flank of a bar, transported across the bar-crest and then deposited landward of the crest. On 'equilibrium' coasts, this landward sediment transport balances storm-driven seaward transport and, in the longer-term, no net bar displacement in the cross-shore direction takes place, e.g. on single bar, micro-tidal, swell-dominated coasts (Wright and Short, 1984). However, on NOM coasts, such landward sediment transport/bar migration is insufficient to balance the storm-induced seaward transport/bar migration.

In the outer surf zone, reduced undertow and an increase in the effectiveness of asymmetric wave-induced sediment transport results in a net landward transport which can lower the seaward bar (Larsen and Kraus, 1992), thereby initiating bar degeneration. Such grain by grain transport, i.e. transport independent of a migrating morphological unit, is thought to redistribute sediment into the landward trough and onto the seaward flank of the adjacent landward bar (Wijnberg, 1995, Ruessink, 1998). Such a mechanism thus helps a bar attain its maximum volume within the mid-outer surf zone (Ruessink and Kroon, 1994).

More recently, Kuriyama (2002) interpreted cross-shore sediment transport rates coupled with an autumn typhoon season and a winter-spring depression season at Hasaki Beach, Japan, as evidence for a grain by grain return process existing across the entire surf zone. However, as at other NOM sites, this onshore sediment transport appears to be associated with the degeneration process of the outer bar which, in the Hasaki case, would be initiated annually during the lower energy summer season separating the two higher energy seasons. Other studies have shown that significant onshore sediment transport across well developed troughs within the mid-inner surf zone is unlikely (Wright et al., 1986; Houwman and Ruessink, 1996), and Ruessink (1998, p209), comments that some other mechanism is required to move sediment further landward within the inner surf zone.

The possibility of sediment return within some form of landward migrating sand body has been raised by Kuriyama and Lee (2001, p962), who interpreted the second eigenfunction from a complex principal component analysis of Hasaki Beach profile data, as the shoreward migration of an accumulation area. Shand (2000, p173) hypothesized that the return of sediment necessary to balance a NOM-associated deficit, may occur via landward migrating inner bifurcates associated with *bar splitting*.

Bar splitting involves a longshore bar developing a forked (or bifurcated) appearance with the seaward bifurcate migrating further offshore while the inner bifurcate moves into the landward trough and completely detaches from the original bar. In some instances the inner bifurcate subsequently merges with the adjacent landward bar or low tide step, causing those features to extend further seaward. An example of bar splitting from the Wanganui coast is depicted by the sequence of time-lapse photographs in Fig 2 which have been 'rectified' to correct for perspective distortion.. The mechanism(s) responsible for bar splitting remains a mystery.

The phenomenon of bar splitting has been documented at 2 sites on the west coast of the New Zealand North Island; at Wanganui (Shand and Bailey, 1999), and Muriwai (Donohoe (1998). However, the process appears to be widespread on NOM coasts with the signatures often being evident in published data; for example: on the coast of Holland (Kroon 1990, Fig 5; 1994; Wijnberg and Terwindt 1995, Figs 9-11); at Duck, North Carolina (Holman and Sallenger, 1986, Fig 4; Holman and Lippman,1987, Fig 1), at Nottawasaga Bay, Lake Huron (Bauer and Greenwood, 1990, Fig 17), at Kouchibouguac Bay, Gulf of St Lawrence (Greenwood and Davidson-Arnott, 1975, Fig 6.6), and at Hasaki Beach, Japan (Kuriyama, 2002, Fig 7).

It is noted that a variety of terms have been used to denote bar splitting and for the inner and outer bifurcates. Bar splitting was referred to as 'double bar development' by Kroon (1991), while Shand and Bailey (1999) used the term 'bar bifurcation'. However, the term bar splitting is now advocated, as a range of other surf zone processes can result in forked or bifurcated morphologies including bar switching (Shand et al., 2001) and some rip channel-based behaviour noted in Shand (2003). Greenwood and Davidson-Arnott (1975) referred to what appears to be an inner bifurcate as a 'tail', while Holman and Lippmann (1987) used the term 'winged bar'.

This paper is a first semi-quantitative attempt to shed light on whether sediment contained within landward migrating inner bifurcates can offset a NOM-associated sediment imbalance within the inner surf zone. This is achieved by analysing several years of ground survey and image-based data from the Wanganui field site. Finally, the results, together with published information from Wanganui and other NOM coasts, are synthesized into a conceptual morphodynamic model of cross-shore sediment transport for the NOM system.

STUDY SITE

The field site is ~1.5 km from the Wanganui Rivermouth on the southwestern coast of the New Zealand North Island (Fig 3). The nearshore is characterised by fine sand (2 to 3 phi), has a cross-shore slope of ~0.0092 and width of ~530 m. Two subtidal sand-bars are usually present; these bars undergo net offshore migration with the mean life-

cycle of a bar being ~3 yrs (Shand et al., 1999). The foreshore is characterised by medium sand (1.7 phi), has an average cross-shore slope of ~0.055 and an average width of ~85 m. About 30% of the time a small amplitude (swash) bar is present on the lower foreshore.

The mean neap tide range is 0.8 m and the mean spring tide range is 2.4 m. The mean deepwater significant wave height is 1.3 m and the 5% excedence value is 2.5 m. The mean wave period is 10.1 s (range 3.5 s to19 s) with sea wave conditions occurring for ~75% of the time and swell waves for the remaining time. Approximately forty two percent of waves approach from the west, ~24% from the south and ~34% lie within one degree of shore-normal. The prevailing WNW wind approaches the coast at ~35 deg from the shoreline, and the wind speed 5% excedence value is 12.4 m/s. The mean value for longshore currents within the inner surf zone is 0.42 m/s and the 5% excedence value is 1.01 m/s. Wave height, wind strength and the magnitude of longshore currents are all positively correlated, as are the direction of these process variables (Shand et al., 2001).

METHODS

To accurately determine sediment volume moving offshore (*Voff*) across the inner surf zone in association with NOM, and moving onshore (*Von*) via inner bifurcates associated with bar splitting, high spatial resolution (cross-shore= 10^0 to 10^1 m, longshore=10^1 m, and elevation=10^{-1}) data of the inter-tidal and subtidal zones are required at 1-5 day intervals. As the logistics of acquiring such data were prohibitive, the following alternative approach was developed which used available image data and morphological maps.

The seaward loss of sediment under NOM, was estimated by the cross-shore change in low tide step location associated with bar generation, while the landward gain in sediment from bar splitting was estimated by the cross-shore change in step location associated with inner bifurcate welding. It is noted that on the Wanganui coast, the low tide step corresponds with a well defined change in slope between the foreshore and the inner trough. These situations are schematically illustrated in Fig 4, and can be expressed mathematically as follows:

$$A = l*h$$

where: A ~ area of parallelogram, l = slope distance of step change,
h = perpendicular width of parallelogram.

therefore $A \propto l$

but $l \sim d$ (for low angles)

where: d = horizontal distance of step change

therefore $A \propto d$

and $A * w = V$

where: w = longshore segment width (conventionally taken as 1m), and V = volume moving offshore (*Voff*) or onshore (*Von).*

It was necessary to use two different types of data for the study as bar splitting and bar generation occur in different locations, the former within the surf zone and the latter upon the lower foreshore. Time-lapse images were used for the surf zone data, while ground survey maps provided inter-tidal data. The two highest resolution data sets available were used for this paper and are detailed below. However, as these data were originally collected for different research purposes, they spanned different, albeit overlapping, time periods, and the locations were separated by ~1 km. Nonetheless, these differences should not affect the comparison between bar generation and bifurcate welding, as while NOM cycles at the two sites were at times out-of-phase, overall bar behaviour was similar (Shand, 2000).

The generation of inter-tidal sand-bars, which subsequently underwent NOM, were identified from a set of morphological maps produced from ground surveys carried out at fortnightly intervals between August 1991 and March 1995. These maps cover an area 300 m longshore by 200 m cross-shore, thereby encompassing the inter-tidal beach and part of the inner bar system. Morphological features such as the saturation boundary and low tide step were defined by direct cross-shore measurement either using a tape measure or theodolite. Location errors on the maps, based on 95% confidence intervals, are estimated to be 5 m in the cross-shore direction and 10 m in the longshore direction. The fortnightly sampling interval could, theoretically, result in a systematic error, and this is discussed later in the paper. Examples of maps depicting the formation of a new inter-tidal sand-bar are shown in Figs 5A and 5B, with the step locations prior to, and following, bar generation being depicted in 5C. The pre and post-generation step locations are shown in Fig 5C, and the longshore-averaged value of the change in step distance (55 m) represents sediment lost from the beach in association with this bar generation.

Episodes of bar splitting were identified from a 2 yr set of rectified time-lapse photographs (4 min exposures) collected between September 1991 and August 1994, and sampled at 2-5 day intervals (e.g. Fig 2). Note that time-lapse photographs are equivalent to ‘time-exposure’ images derived from video data that have been reported elsewhere (e.g. Aarninkhof and Holman, 1999; Bogle et al., 2000; and Morris et al., 2001). Intensity differences on time-lapse photos portray the submarine morphology, with higher intensity areas (associated with relatively intense wave breaking) representing elevated features such as bar-crests or the low tide step, and darker areas signifying deeper water such as troughs and rip channels. The camera was located on top of a 42 m high cliff and located ~130 m landward of the foredune-toe. A panorama of 4 photographs centered about the camera covered ~500 m of shoreline. Each photo was digitised, rectified to ground co-ordinates and the coastline straightened to facilitate subsequent analysis. Rectified images were clipped beyond 520 m for computer storage purposes. These techniques are described in Bailey and Shand (1996), Shand (2003), and Shand et al. (2003).

Location errors (95% confidence interval) on the rectified images for this particular site are 0 m, increasing to 12 m at the lateral extremes. In the cross-shore direction the maximum error was 15 m within the inner/mid surf zone where bar splitting occurs. While the cross-shore value (15 m) is greater than that specified above (10^0 to 10^1 m), the averaging procedure used in calculating the change in step location parameter value reduces the magnitude to acceptable levels. Eamples of images depicting an

inner bifurcate welding to the foreshore are shown in Figs 6A to 6C. The pre and post-weld step locations (Fig 6D) were detected using maximum intensity values, and the longshore-averaged change in step distance (21 m) represents sediment gained by the beach from this bifurcate weld.

RESULTS

Four instances of bar generation occurred during the study period (Fig 7). The mean inter-generation period was 351 days (140 – 574 days). The mean step retreat associated with the four bar generations was 55.5 m (Table 1), and ranged between 44 and 74 m. The average bar generation retreat per inter-generation cycle will be compared with the average step advance from inner bifurcate welding per inter-generation cycle.

Eight episodes of bar splitting ocurred during the study (Fig 8A). Time-series graphs for each episode are depicted in Fig 9. These 8 graphs also describe the behaviour of the inner bifurcates in terms of the following: longshore coherence or incoherence of the crest; disappearance within, or transversing across, the landward trough; and fully welding to the landward bar/step during a single inter-survey period, or incrementally welding during several such periods. Only one inner bifurcate (episode 4) failed to weld. The bifurcate in episodes 3 and 5 welded to the inner bar, while the bifurcate in episodes 1, 2, 6, 7 and 8 welded to the low tide step. It is also noted that epsiodes 3 to 5 resulted from the splitting of a bar located seaward of the inner bar, and that the inner bifurcates were longshore-incoherent during much of their existence.

The 5 inner bifurcates which welded to the step did not equally affect the 500 m long study area (Fig10). Averaging the step-advances over the length of the study area resulted in 2.12 welds per metre alongshore. The assumption of longshore dispersion of localised sediment inputs is considered valid as the Wanganui coast, and indeed most NOM coasts (Shand et al., 1999), are characterised by moderate to strong longshore currents. Furthermore, the predominant longshore current direction at Wanganui is from NW to SE, i.e. right to left in Fig 10, thereby assisting with the dispersal of inner bifurcate sediment which, during the sampling period, happened to occur more often on the NW side of the study area, i.e. on the right side of graph.

When bar behaviour at the bar splitting site is compared with longer-term bar behaviour for this location (Fig 8B), it is evident that ~1.75 inter-generation periods occurred. The approximate number of welds per inter-generation period is therefore:

$$2.12/1.75 = 1.21 \text{ welds/cycle}$$

The mean step advance associated with the 5 epsiodes of welding to the inter-tidal beach = 22.8 m (Table 1) and ranged between 18 and 28 m. A similar value (23.1 m) is derived if the 2 bifurcates which welded to the inner bar are included within the calculation. The mean step advance per inter-generation cycle is therefore:

$$22.8*1.21 = 27.6 \text{ m/cycle}$$

A comparison of this value with the mean step retreat associated with the four bar generations, i.e. 27.6 m c.f. 55.5 m, indicates that approximately 50% (49.7%) of sediment volume lost from the inter-tidal beach during bar generation is later replaced via the process of bar splitting.

DISCUSSION

There are several limitations in the data-sets used in this study. Firstly, the 2 yr image data used to identify and analyse bar splitting contained less that 2 generation cycles and therefore may not be a true behavioural representation. The effect this may have on results is uncertain. However, the fact that bar splitting affected each landward bar during the study period, and that splitting occurs systematically within the NOM system, namely later in the inter-generation period when weak 3D morphologies predominate (Shand and Bailey, 1999; Shand et al., 2004; Shand et al., in prep), suggests that bar behaviour was probably normal during the study period.

Secondly, the 14 day sampling intervals of the bar generation data may have resulted in a systematic error in step retreat for the following reasons. Bar generation on the Wanganui coast has been observed to occur upon a wide foreshore, under neap tidal range and under storm conditions, i.e. higher waves and stronger longshore currents (Shand and Bailey, 1999; Shand et al., 2004). Bar generation would therefore tend to occur approximately one week prior to sampling which only took place during times of spring tide. However, the eastward progression of high and low pressure sytems which characterise NZ weather (Tomlinson, 1976), results in periods of fairweather following storms, conditions observed at Wanganui to be conducive to the formation of a swash bar on the lower foreshore when coupled with the typically 2D or weakly 3D new bar system (Shand et al., 2004). The subsequent landward migration of swash bars during the neap tide to spring tide change is well documented (e.g. Sonu,1972; Kroon, 1994), and the low tide step also moves landward. The position of the low tide step at sampling time would therefore over-estimate the effect of bar generation. By comparison, the higher sampling rate of the image data, used for the bar splitting exercise, avoided any systematic error in step location. The 50% sediment return to the inter-tidal beach associated with bifurcate welding therefore probably under estimates the actual value, possibly by several percent.

During the present study, other morphological behaviours associated with stronger 3D topographies were identified which are capable of transfering sediment landward. For example, transverse bars, as defined by Wright and Short (1984), or Konichi and Holman (2000), may detach from the inner bar and the ‘free arm’ realign in the direction of the longshore current. The arm then either dissipates within the trough, or migrates landward to weld with the step in the same manner as the inner bifurcate from bar splitting. There is evidence of such a ‘detached transverse bar’ process within the ellipses marked on the left hand side of the images in Figs 2B and 2C, and the resulting seaward extension of the step is evident when the distances in Figs 2C and 2D are compared.

The occurrence of 3D morphologies therefore appears to play a key role in the development of landward-migrating secondary sand bodies. At Wanganui, 3D configurations occur earlier in the NOM cycle when the bar is still within the inner

surf zone (Shand, 2002). During this time, incident energy is dissipated (filtered) on a well-developed seaward bar (Shand et al., 2004), thereby facilitating 3D pattern development via self-organisational behaviour.

Integration of the findings from this paper with those in the other referenced work, enabled the formulation of a conceptual morphodynamic model (Fig 11) of cross-shore sediment transport mechanisms for the NOM system at Wanganui. While the model is primarily based on research from Wanganui, results from the other NOM sites have been incorporated. Of additional interest is the depiction in Fig 11B of the inner bar moving seaward while ripped (stronger-3D) states predominate (see Shand, 2004). During this period which may last several months, sediment appears to move offshore via the continually reforming and/or longshore migrating rip channels, or at times when the configuration has temporarily changed to a more 2D state and undertow-dominated flow conditions occur.

CONCLUSIONS

This study used ground survey and image-based data-sets from Wanganui, New Zealand, to show that shoreward sediment transport within landward migrating inner bifurcates (associated with bar splitting), account for at least 50% of inter-tidal beach sediment which is lost seaward in association with bar generation. While bar splitting occurs upon weak to moderate 3D topographies, other types of behaviour associated with stronger 3D antecedent morphologies were identified during the study which are capable of transfering further sediment landward within migrating sand-bodies. Sediment return within landward migrating sand bodies therefore appears to be the main mechanism which restores any NOM-induced sediment deficit on the inter-tidal beach. Some sediment will also be added to the beach from longshore transport, and the possibility still exists that a portion of sediment returns via grain by grain processes within the inner surf zone.

ACKNOWLEDGEMENTS

This study was supported by the Massey University Research Fund and a Research Fellowship (contract MAUX0104) from the New Zealand Foundation for Science and Technology (FRST). The authors wish to thank Dr Giovanni Coco of the National Institute of Water and Atmospheric Research (NIWA) of New Zealand for reviewing the manuscript. Drs Rob Holman and Karin Bryan are thanked for granting access to image data from their ARGUS site at Muriwai Beach.

REFERENCES

Aarninkhof, S., and Holman, R.A., 1999. Monitoring the nearshore with video. Backscatter, 10, 8-11.

Bauer, B.O., and Greenwood, B., 1990. Modification of a linear bar-trough system by a standing edge wave. Marine Geology, 92, 177-204.

Bailey, D.G., and Shand, R.D., 1996. Determining large-scale sand bar behaviour. Proceedings of the IEEE International Conference on Image Processing, Lausanne, Switzerland, (2), 637-640.

Birkemeier, W.A., 1984. Time scales of nearshore profile change. Proceedings of the 19th International Conference on coastal Engineering, ASCE, pp. 1507-1521.

Bogle, J.A.; Bryan, K.R.; Black, K.P.; Hume, T.M.; and Healy, T.R., 2000, Video observations of rip formation and evolution. Journal of Coastal Research Special Issue 34, 117-127.

De Vroeg, J.H.; Smit, E.S.P., and Bakker,W.T., 1988. Coastal Genesis. Proceedings of the 21st International Conference on coastal Engineering, ASCE, pp. 2825-2839.

Donohoe, B.F.P., 1998. Spatial and temporal bar morphodynamics of Muriwai Beach. MSc thesis, Auckland University, New Zealand, 104p.

Gallagher, E.L.; Elgar, S.; and Guza, R.T., 1998. Observations of sand bar evolution on a natural beach. Journal of Geophysical Research, 103, 3203-3215.

Greenwood, B., and Davidson-Arnott, G.D., 1975. Marine bars and nearshore sedimentary processes, Kouchibouguac Bay, New Brunswick. In: Hails, J., and Carr, A., (eds.), Nearshore Sediment Dynamics and Sedimentation. John Wiley and Sons, New York, pp. 123-150.

Greenwood, B., and Davidson-Arnott,R., 1979. Sedimentation and equilibrium in wave formed bars: a review and case study. Canadian Journal of Earth Science, 16, 312-332.

Haxel, J.H., and Holman, R.A., 2004. The sediment response of a dissipative beach to variations in wave climate . Marine Geology, 206, 73-99.

Hoefel, F., and Elgar, S., 2003. Wave-induced sediment transport and sandbar migration. Science, 299, 1885-1887.

Holman, R.A., and Lippmann, T.C., 1987. Remote sensing of nearshore bar systems - making morphology visible. Proceeding of Coastal Sediments'87, ASCE, pp. 927-944.

Holman, R.A., and Sallenger, A.H., 1986. High energy nearshore processes. EoS Trans. AGU 67, 1369-1371.

Houser, C., and Greenwood, B. 2004. Profile response of a lacustrine multiple barred nearshore over a sequence of storm events. Geomorphology, in press.

Houwman, K.T and Ruessink, B.G., 1996. Cross-shore sediment transport mechanisms in the surfzone on a time scale of months to years. Proceedings of the 25th International Conference on Coastal Engineering, ASCE, pp. 4793-4806.

Konicki, K.M., and Holman, R.A., 2000. The statistics and kinematics of transverse sand bars on an open coast, Marine Geology, 169, 69-101.

Kroon, A., 1991. Three-dimensional morphological changes of a nearshore bar system along the Dutch coast near Egmond aan Zee. Proceedings of the Skagen Symposium, Journal of Coastal Research, Special Issue, 9, 430-451.

Kroon, A., 1994. Sediment transport and morphodynamics of the beach and nearshore zone near Egmond, The Netherlands. PhD thesis, Utrecht University, the Netherlands, 275p.

Kroon, A., and Hoeskstra, P., 1993. Nearshore bars and large-scale coastal behaviour. In: List, J.H., (ed.), Large-Scale Coastal Behaviour '93. U.S. Geological Survey, Open-File Report 93-381, pp. 92-95.

Kuriyama, Y., 2002. Medium-term bar behaviour and associated sediment transport at Hasaki, Japan. Journal of Geophysical Research, 107.

Kuriyama, Y., and Lee J.H., 2001. Medium-term beach profile change on a bar-trough region at Hasaki, Japan, investigated with complex principal component analysis. In Proceedings Coastal Dynamics '01, ASCE, pp. 959-968.

Larsen, M., and Kraus, N.C., 1992. Analysis of cross-shore movement of natural longshore bars and material placed to create longshore bars. Technical Report CERC DRP-29-5, 115p.

Lippmann, T.C.; Holmam, R.A., and Hathaway, K.K., 1993. Episodic, nonstationary behaviour of a double bar system at Duck, North Carolina, U.S.A., 1986-1991. Journal of Coastal Research, Special Issue, 15, 49-75.

Morris, B.D; Davidson, M.A., and Huntley, D.A., 2001. Measurements of the response of a coastal inlet using video monitoring techniques. Marine Geology, 175, 251-272.

Ruessink, B.G., 1998. Infragravity waves in a dissipative multiple bar system. PhD thesis, Utrecht University, the Netherlands, 245p.

Ruessink, B.G., and Kroon, A., 1994. The behaviour of a multiple bar system in the nearshore zone of Terschelling, the Netherlands: 1965-1993. Marine Geology, 121, 187-197.

Ruessink, B.G., and Terwindt, J.H.J, 2000. The behaviour of nearshore bars on a time scale of years: a conceptual model. Marine Geology, 163, 289-302.

Shand, R.D., 2000. Offshore migration of coastal sand-bars at Wanganui, New Zealand. PhD thesis, School of Global Studies, Massey University, New Zealand, Miscellaneous Publication Series, 00/8, 295p.

Shand, R.D., 2002. Temporal variation in morphological configuration within a multi-bar surf zone at Wanganui, New Zealand. Occasional Paper 2002/4, School of People Environment and Planning, Massey University, New Zealand, 42p.

Shand, R.D., 2003. Relationships between episodes of bar switching, cross-shore bar migration and outer bar degeneration at Wanganui, New Zealand. Journal of Coastal Research, 19(1), 157-170.

Shand, R.D., 2004. Rip-associated bathing hazards on beaches characterised by net offshore bar migration. Occasional Paper 2004/1, School of People Environment and Planning, Massey University, New Zealand, 19p.

Shand, R.D., and Bailey, D.G., 1999. A Review of Net Offshore Bar Migration with Photographic Illustrations from Wanganui, New Zealand, Journal of Coastal Research, 15(2), 365-378.

Shand, R.D.; Bailey, D.G., and Shepherd, M.J., 1999. An inter-site comparison of net offshore bar migration characteristics and environmental conditions. Journal of Coastal

Research, 15(4) 750-765.

Shand, R.D., Bailey, D.G., and Shepherd, M.J., 2001. Longshore realignment of nearshore parallel sand-bars at Wanganui, New Zealand. Marine Geology 179, 147-161

Shand, R.D.; Hesp, P.A., Bailey, D.G., and Shepherd, M.J., 2003. A conceptual beach-state model for the inner bar of a storm-dominate, low to moderate tidal range coast at Wanganui, New Zealand. Proceedings of Coastal Sediments '03.

Shand, R.D.; Hesp, P.A., and Shepherd, M, J., 2004. Beach cut in relation to net offshore bar migration. Journal of Coastal Research, Special Issue 3, in press.

Shand et al., in prep. Characteristics of bar switching on a multi-barred coast.

Sonu, C.J., 1972. Field observation of nearshore circulation and meandering currents. Journal of Geophysical Research, 77(18), 3232-3247.

Svendsen, I. A. 1984. Mass flux and undertow in a surf zone. Coastal Engineering, 8, 347-365.

Tomlinson, A.I., 1976. Climate. In Woods, I. (ed.) New Zealand Atlas, Government Printer, New Zealand, pp. 82-89.

Wijnberg, K.M., 1995. Morphologic behaviour of a barred coast over a period of decades. PhD thesis, Utrecht University, the Netherlands, 245p.

Wijnberg, K.M., 1996. On the systematic offshore decay of breaker bars. Proceedings of the 25th International Conference on Coastal Engineering, ASCE, pp. 3600-3613.

Wijnberg, K.M., and Terwindt, J.H.G., 1995. Extracting decadal morphological behaviour from high-resolution, long-term bathymetric surveys along the Holland coast using eigenfunction analysis. Marine Geology, 126, 301-330.

Wright, L.D., and Short, A.D., 1984. Morphodynamic variability of surf zones and beaches: a synthesis. Marine Geology, 56, 93-118.

Wright, L.D.; Nielsen, P,; Shi, N.C., and List, J.H., 1986. Morphodynamics of a bar-trough surf zone. Marine Geology, 70, 251-285.

Table 1 Change in cross-shore location of low tide step associated with bar generation and for episodes where inner bifurcate welding affected the low tide step. Event numbers as depicted in Fig 8.

Event type	Event number and step location change (m)								Mean
	1	2	3	4	5	6	7	8	
Generations	55	44	74	49	-	-	-	-	55.5
Step welds	20	27	-	-	-	21	18	28	22.8

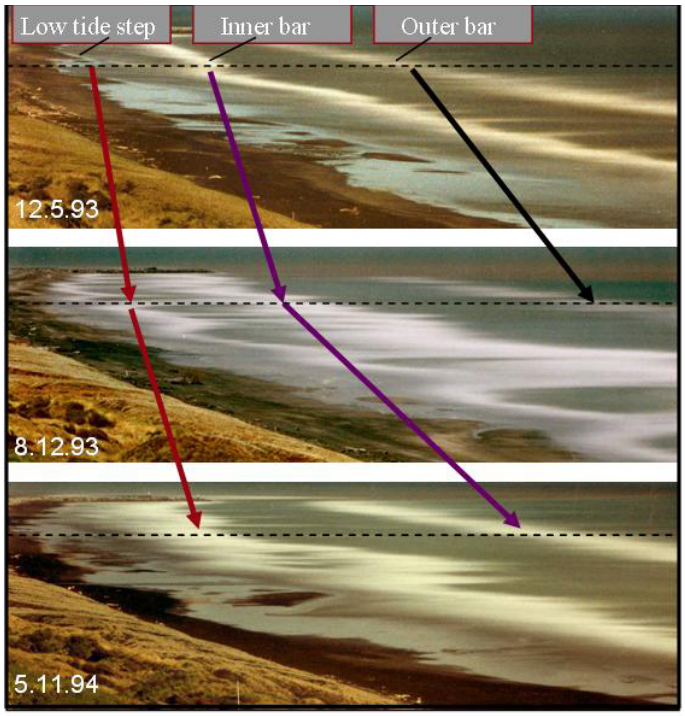

Figure 1 An example of net offshore bar migration along the marked transect (dashed line) using a sequence of 4 minute time-lapse photographs from Wanganui, New Zealand. The high intensity areas result from breaking waves and locate topographic highs such as bar-crests and the low tide step (marked). The outer bar disappeared prior to the last sampling. The inter-sample migration records confirm the arrowed trends, and these data are presented later in Fig 7.

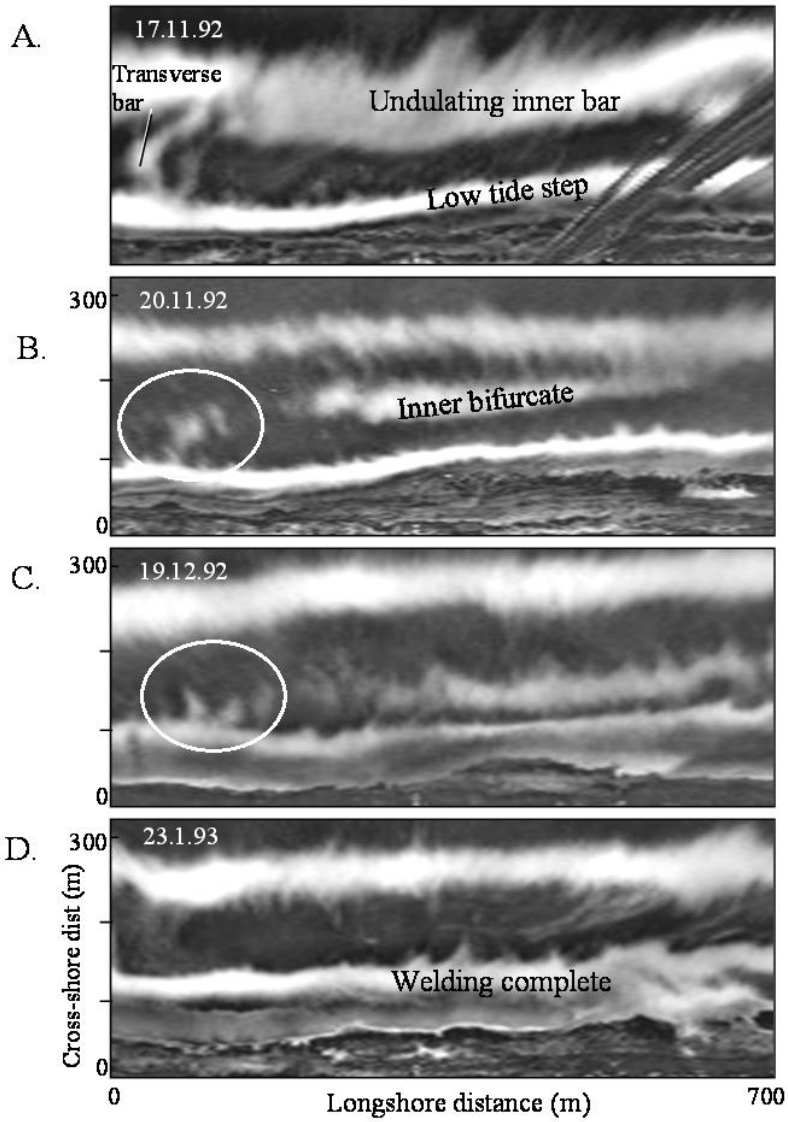

Figure 2
An example of bar splitting using a sequence of 'rectified' (see text) time-lapse photographs from Wanganui, New Zealand.. The form of the inner bar prior to splitting is depicted in A, with B illustrating the recently bifurcated morphology. The inner bifurcate has progressed landward in C, and has welded to the inter-tidal beach in D. This episode of bar splitting was the second observed during the study period. The ellipses in B and C depict a detached transverse bar migrating toward, and welding to, the step (see text).

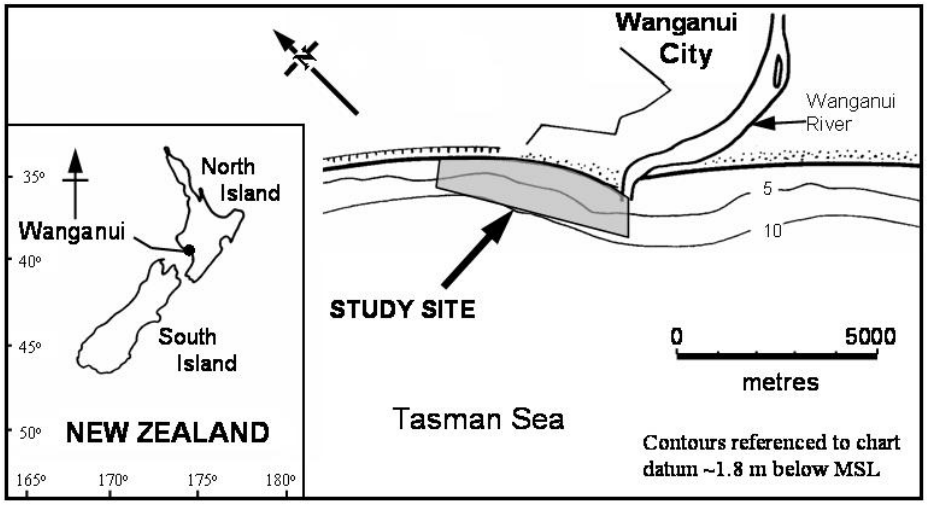

Figure 3 Location map of the Wanganui study site.

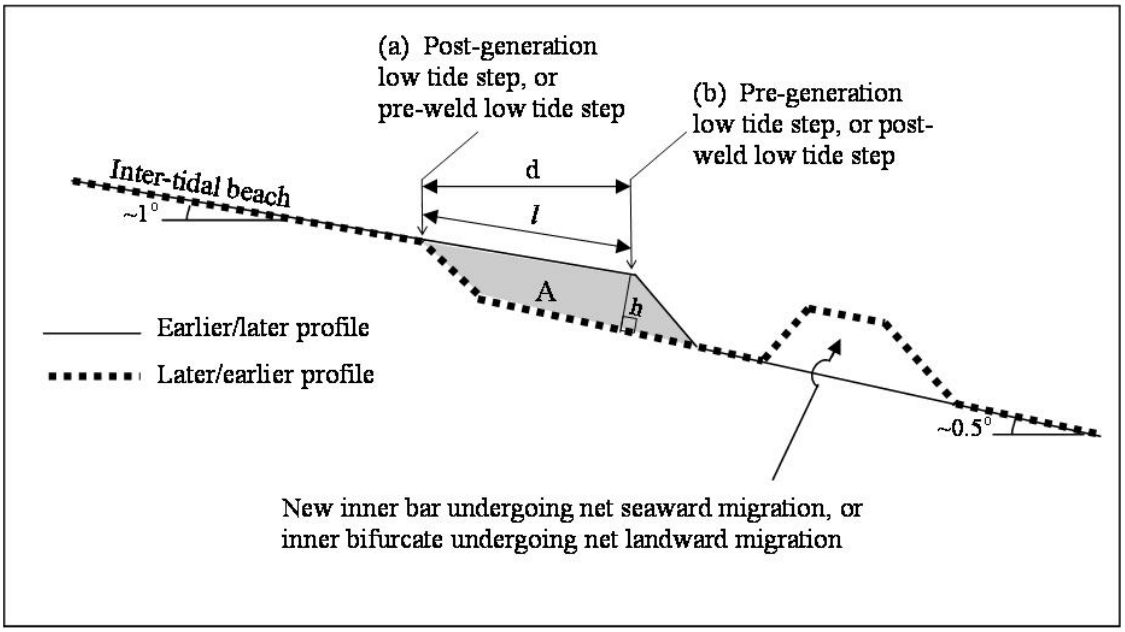

Figure 4 Schematic diagram depicting cross-shore locations of the low tide step (a) before inner bifurcate welding, or following bar generation, and (b) before bar generation, or after bifurcate welding. Components are also depicted which are used in the text to relate the distance between the step locations to the volume of displaced sediment.

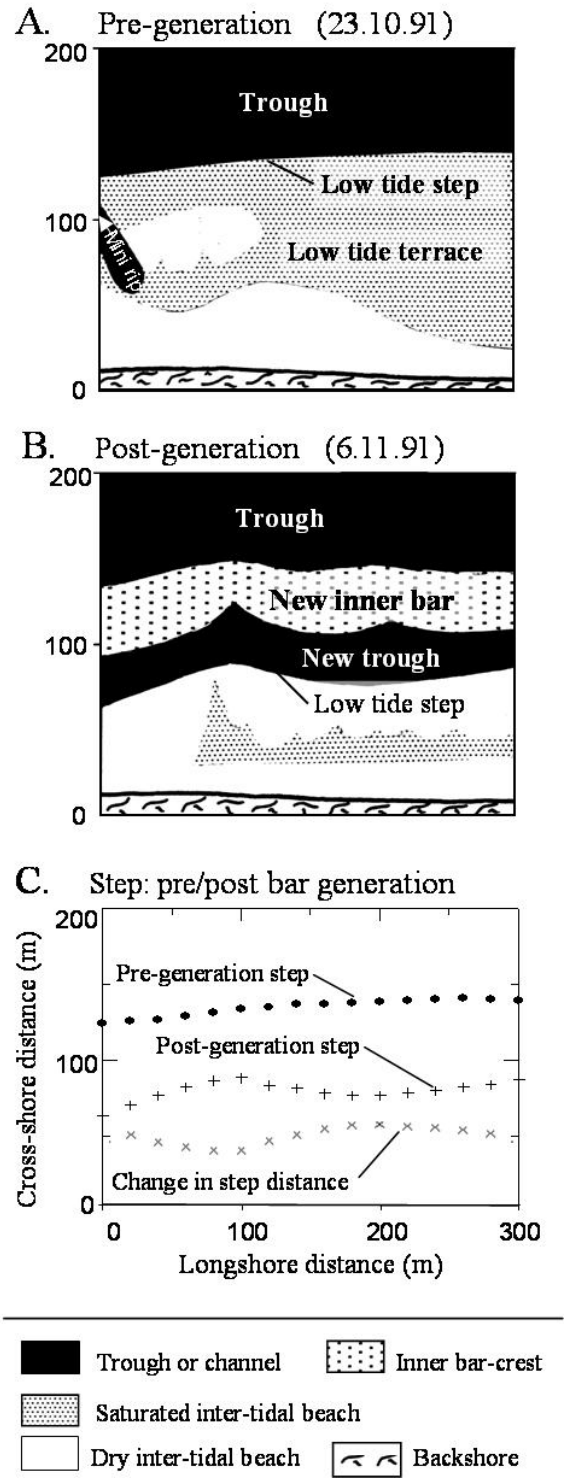

Figure 5 Morphological maps depicting a relatively featureless inter-tidal beach (A) upon which a new subtidal bar forms (B). This bar generation is the first of 4 occurrences during the study period. Comparison of the pre/post generation cross-shore positions of the low tide step are depicted in C.

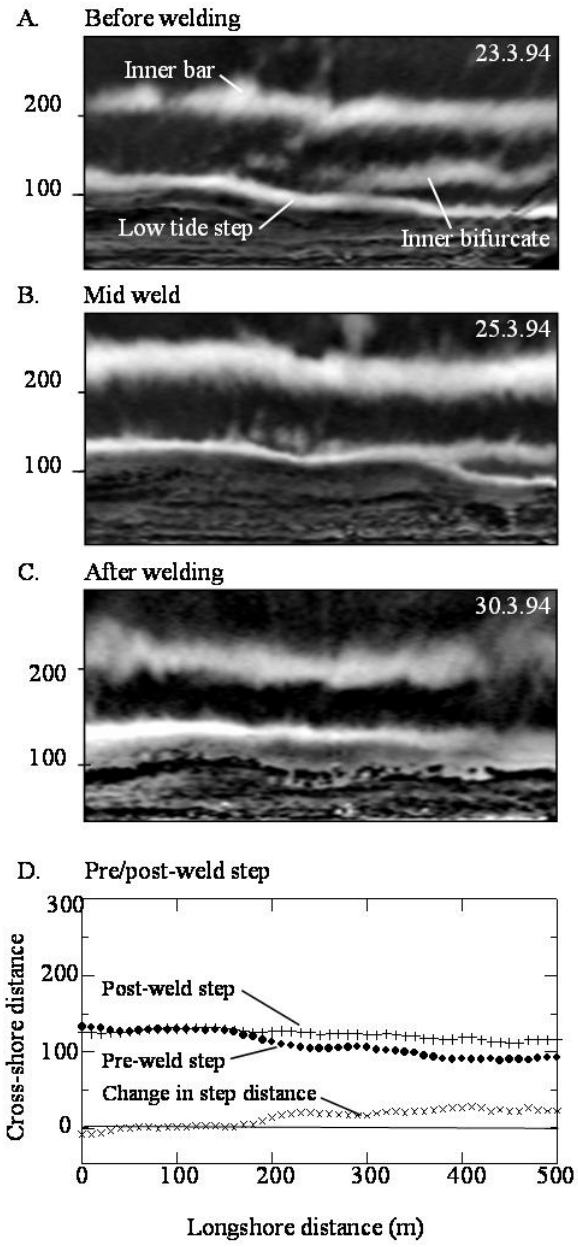

Figure 6
Sequence of rectified images depicting an inner bifurcate (A) incrementally welding to the inter-tidal beach (B and C). This episode of bar splitting was the 6th observed during the study period. A comparison of the pre/post weld cross-shore positions of the low tide step are depicted in D.

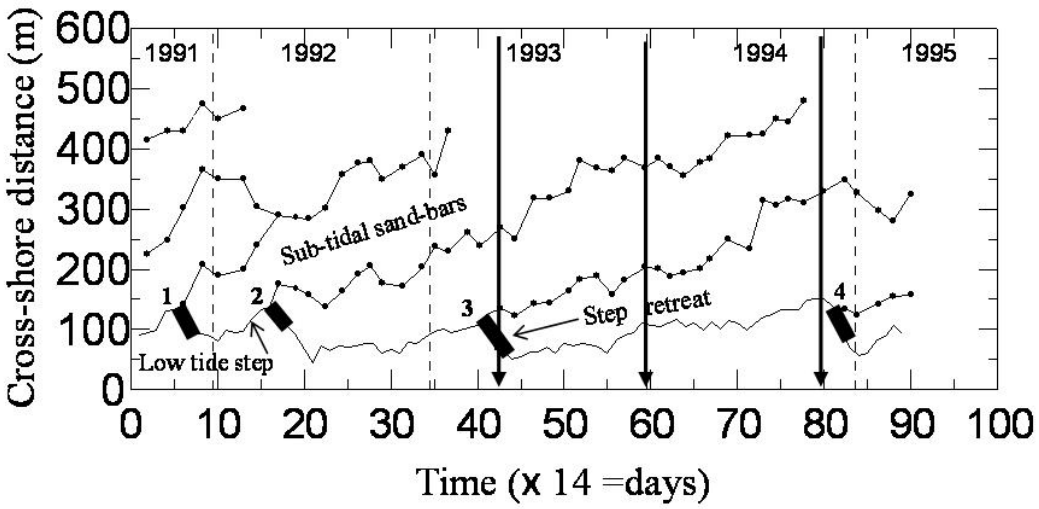

Figure 7 Bar-crest location and low tide step location time-series for cross-shore transect ~1500 m from the Wanganui Rivermouth. Four episodes of bar generation and step retreat are depicted by bold line segments. The vertical arrows mark times of sampling for the 3 images used to illustrate NOM behaviour in Fig 1.

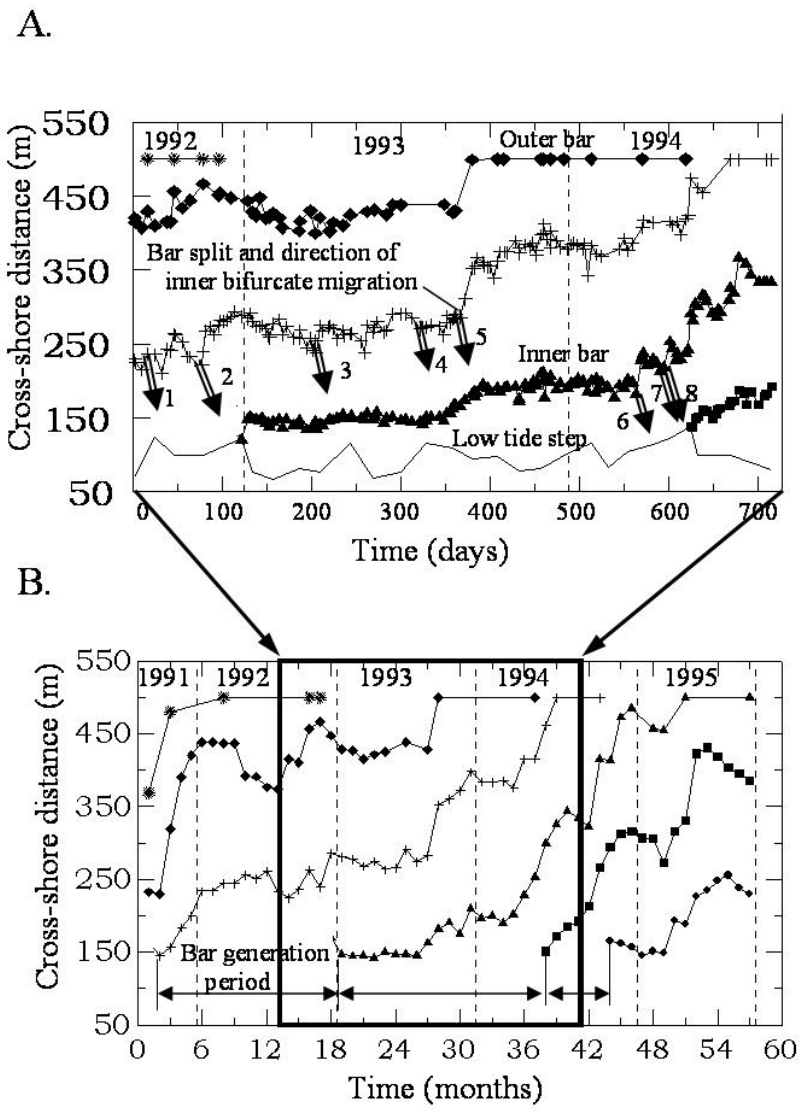

Figure 8 Time-series of bar-crest location and low tide step location for the transect located ~3000 m from the Wanganui Rivermouth. Data used in the present study are depicted in A, and the 8 episodes of bar switching are marked. A temporally extended time-series (B) is included to illustrate how the shorter-term bar and step location data, along with bar generation periods, fit within the longer-term pattern of NOM. Note outer bar migrates beyond 520 m as explained in text.

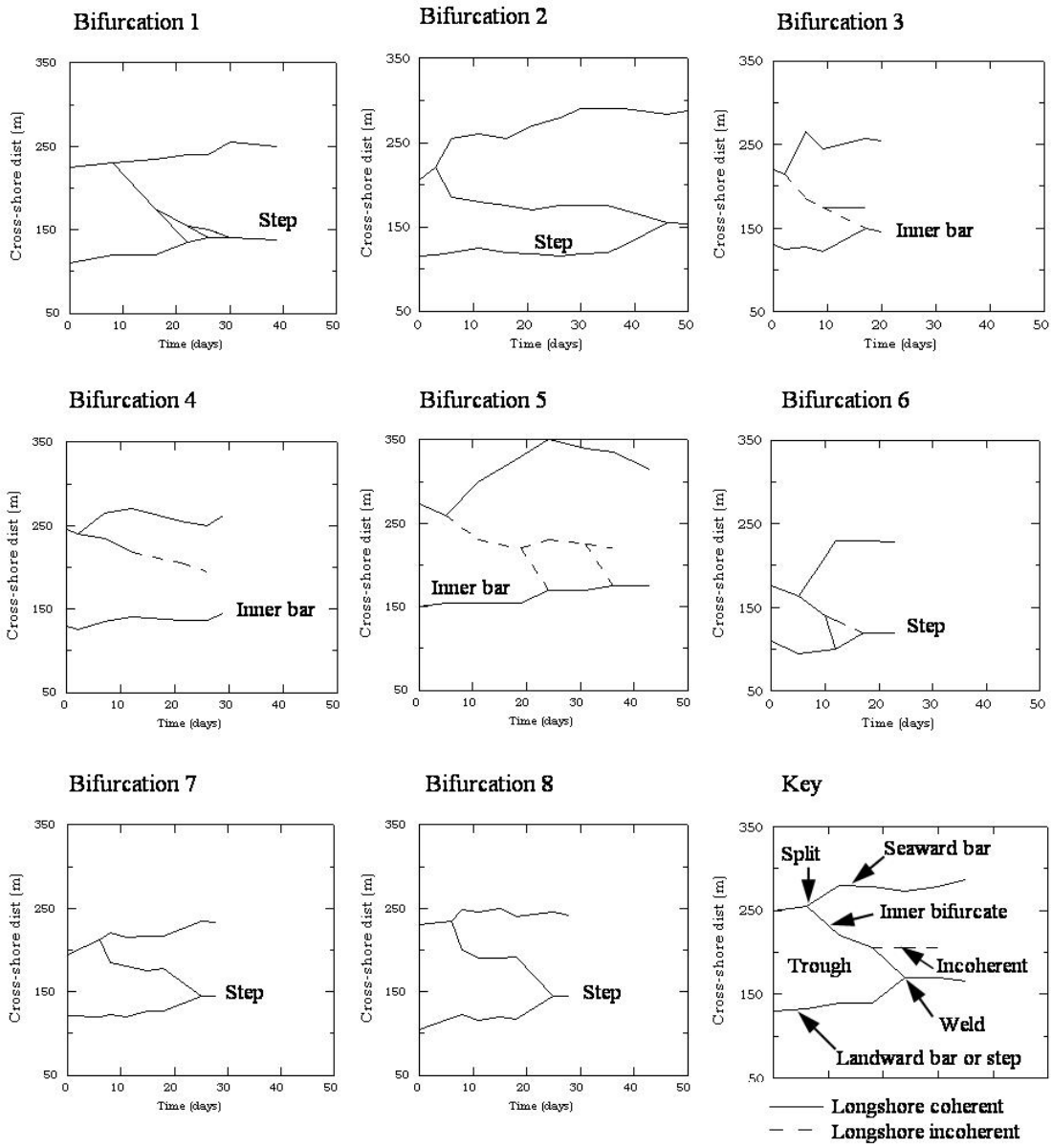

Figure 9 Bar-crest location time-series for the 8 bifurcations (bar splits) which occurred during the 2 yr study period. Each graph also depicts the behaviour of the inner bifurcate in terms of the following: longshore coherence/incoherence of crest; disappearance within, or traversing across, the landward trough; fully welding to the landward bar/step during a single inter-survey period, or incrementally welding during several such periods. The timing of these episodes of bar splitting are marked in Fig 8.

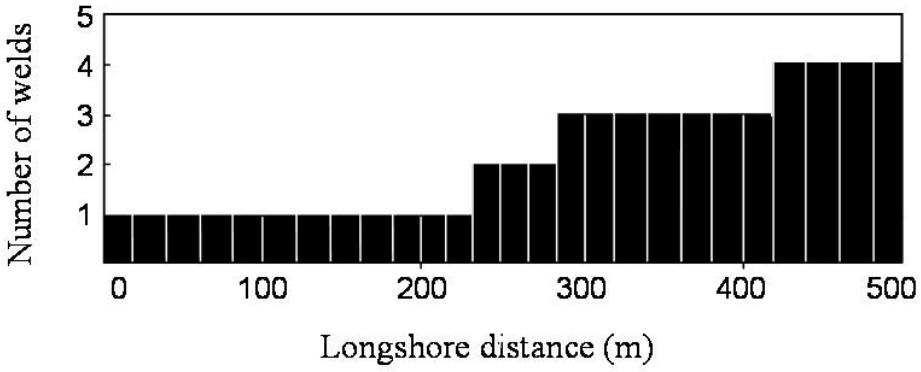

Figure 10 Histogram depicting inner bifurcate welds along study site.

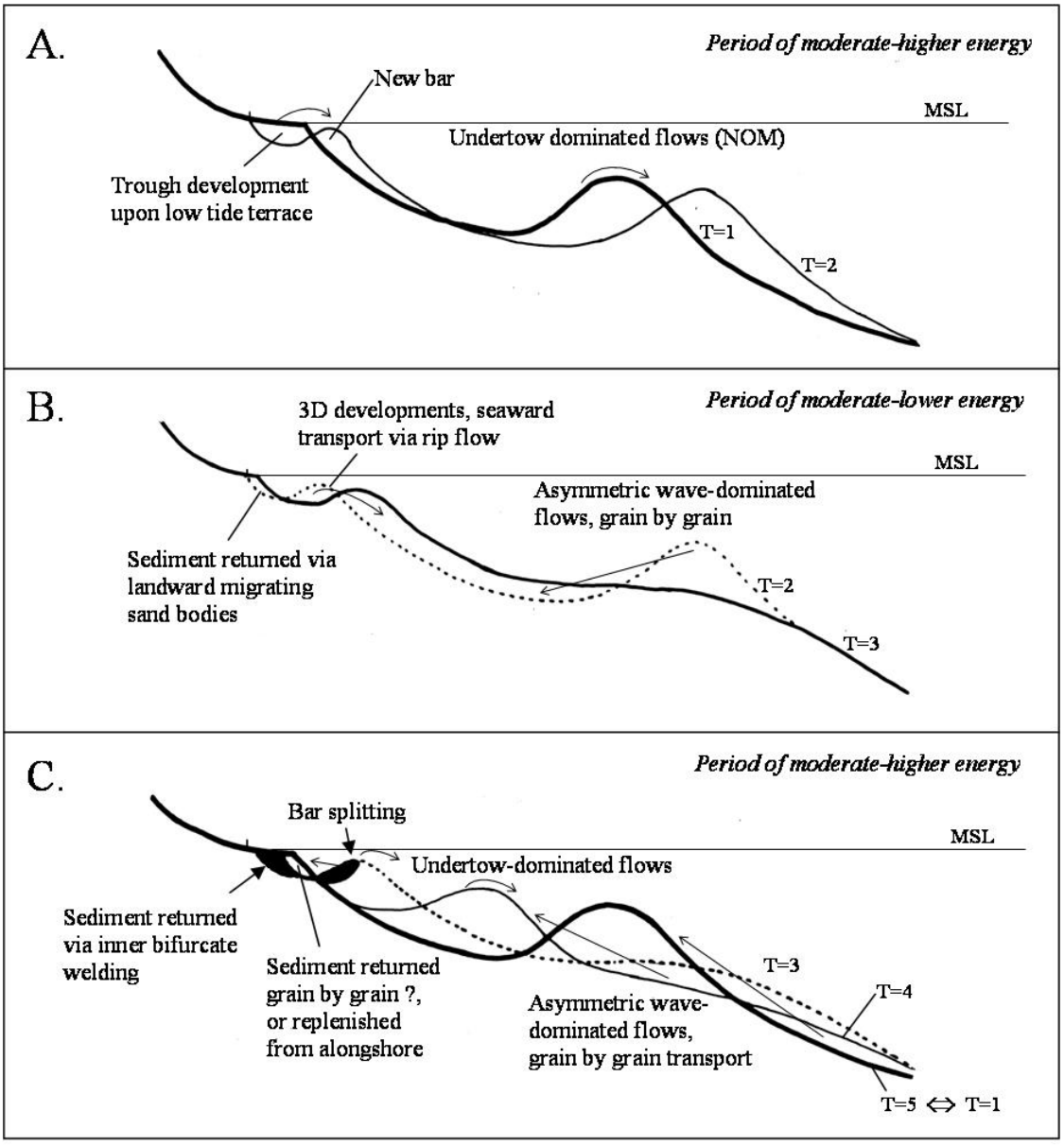

Figure 11 A conceptual model of sediment transport mechanisms for the NOM system at Wanganui. At time T=1, the profile contains a single sub-tidal sand-bar. At T=2, an additional bar has formed. The sequence terminates at T=5 at which time the new bar has reached the cross-shore location of the bar at T=1. The 'return period' of the system is thus defined by T=5. The processes depicted in the diagrams are either described, or referenced, within the text.

Shand, R.D., 2007. Bar splitting: system attributes and sediment budget implications for a net offshore migrating bar system. Journal of Coastal Research, Special Issue 50.

Journal of Coastal Research	SI 50	pg - pg	ICS2007 (Proceedings)	Australia	ISSN

Bar Splitting: Systems Attributes and Sediment Budget Implications for a Net Offshore Migrating Bar System

R.D. Shand † ‡

†Geography Programme,
Massey University,
Palmerston North,
New Zealand.
r.shand@massey.ac.nz

‡ Coastal Systems (NZ) Ltd.,
70 Karaka Street, Wanganui,
New Zealand.
rshand@coastalsystems.co.nz
www.coastalsystems.co.nz

ABSTRACT

SHAND, R.D., 2007. Bar splitting: system attributes and sediment budget implications for a net offshore migrating bar system. Journal of Coastal Research, SI 50 (Proceedings of the 9th International Coastal Symposium), pg – pg. Gold Coast, Australia, ISBN

Net offshore bar migration or NOM, refers to the systematic seaward migration of longshore (primary) sand-bars across the surf zone. NOM appears to be the product of storm-induced seaward bar migration (sediment transport) exceeding landward bar migration (sediment transport) during intervening fairweather periods. NOM also appears to involve the cross-shore redistribution of sediment rather than the continual loss of sediment to the shoreface. While 'grain by grain' return processes appear to predominate within the outer surf zone, alternative return mechanisms may exist within the inner surf zone. The aim of this paper is to assess whether sediment traveling landward within inner bifurcates formed during the process of bar splitting can offset a NOM-induced cross-shore sediment imbalance. Bar splitting has been observed on several NOM coasts and involves a longshore bar bifurcating, with the inner bifurcate detaching, moving landward, and in some cases welding to the foreshore. Analysis of several years of morphological data from Wanganui, on the west coast of New Zealand's North Island, found that the sediment gained by the foreshore from inner bifurcate welding amounted to approximately half the sediment lost from the foreshore by newly generated sand-bars which subsequently underwent NOM. In addition, during the study, several other types of 3D morphological behaviour were identified which are also capable transporting sediment shoreward across the inner surf zone as a coherent sand body. Landward migrating secondary bars therefore appear to play a significant role in returning sediment to the inter-tidal beach. Finally, a conceptual morphodynamic model of the NOM system at Wanganui is presented which incorporates 3D morphological behaviour in contrast with existing models which are entirely 2D.

ADDITIONAL INDEX WORDS: *Sand-bar, multi-bar coast, bifurcation, surf zone, nearshore, morphodynamic*

INTRODUCTION

Net offshore bar migration (NOM) refers to the systematic seaward migration of coastal subtidal sand-bars across the surf zone; such bars form upon a widened lower foreshore and disappear several years later in the outer surf zone (Ruessink and Kroon, 1994; Shand and Bailey, 1999; Ruessink et al., 2002; Shand et al., 2004). Since the mid 1980s, NOM has been recognised on several storm-dominated, multi-barred coasts: the North Carolina coast (e.g. Birkemeier, 1984; Lippmann et al., 1993), the Dutch coasts (e.g. de Vroeg et al., 1988, Kroon and Hoekstra, 1993), at Wanganui, on the south west coast of the New Zealand North Island (Shand et al., 1999), and at Hasaki Beach on the Japanese Pacific Coast (Kuriyama, 2002). There are also several other locations where published data indicates NOM behaviour may be occurring, but longer records are required for confirmation. For example: Burley Beach, Lake Huron (Houser and Greenwood, 2004); Agate Beach, Oregon (Haxel and Holman, 2004), and Muriwai Beach, near Auckland on the west coast of the New Zealand North Island (ARGUS data analysed by author). NOM has also been described as 'the offshore progression cycle' by Wijnberg (1996) and 'inter-annual cyclic bar behaviour' by Ruessink and Terwindt (2000). An example of NOM behaviour from the Wanganui Coast is depicted in Fig 1 using a sequence of time-lapse photographs.

Sediment dynamics associated with NOM have long puzzled researchers. Central to the issue is the widely accepted notion that bars move seaward under storm-conditions in response to sediment transport driven by bed return flow (undertow). There exists a variety of field evidence to support this mechanism: sediment tracing studies (e.g. Ingle, 1966); sediment structures (e.g. Greenwood and Davidson-Arnott, 1979); and sediment transport and modelling studies (Gallager et al., 1998). If this is indeed the case, then several hundred cubic metres (per metre longshore) of sediment per bar migration cycle would be lost to the shoreface (Shand et al., 1999). However, a sediment budget

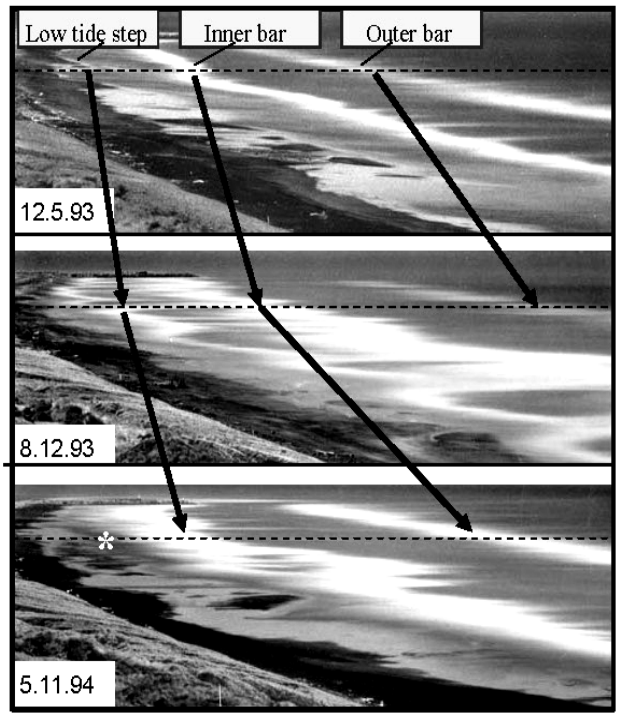

Figure 1. An example of net offshore bar migration along the marked transect (dashed line) using a sequence of 4 minute time-lapse photographs from Wanganui, New Zealand. The high intensity areas result from breaking waves and locate topographic highs such as bar-crests and the low tide step (marked). The inter-sample migration record, presented later in Fig 7, confirms the temporal trends depicted by the arrows. Note from Fig 7 it can be seen that the outer bar disappeared prior to the last sampling (5.11.94), and a new trough is about to develop on the lower foreshore (in the vicinity of the askerisk) therby defining a new low tide step and inner bar.

analysis for the South Holland coast by Wijnberg (1995), found that the volume of sediment from the longshore sediment flux was several times smaller than the amount which would be lost seaward by NOM. Furthermore, this section of coast was accreting so coastal erosion was not providing a sediment source. Wijnberg (1995, p152) concluded that "…most of the sediment of the degenerating outer bar has to stay within the inshore area..." Sediment transport within a NOM system therefore appears to involve the cross-shore redistribution of sediment, rather than the continual lost of sediment to the shoreface and its replacement from landward or longshore sources.

Landward directed sediment transport occurs in association with sand-bars migrating onshore during lower (fair-weather) wave conditions. Under the influence of landward directed currents associated with asymmetric waves (e.g. Hoefel and Elgar, 2003), and the surface roller effect of broken waves (e.g. Svendsen, 1984), sediment is eroded from the seaward flank of a bar, transported across the bar-crest and then deposited landward of the crest. On 'equilibrium' coasts, this landward sediment transport balances storm-driven seaward transport and, in the longer-term, no net bar displacement in the cross-shore direction takes place, e.g. on single bar, micro-tidal, swell-dominated coasts (Wright and Short, 1984). However, on NOM coasts, such landward sediment transport/bar migration must be insufficient to counteract the storm-induced seaward transport/bar migration.

In the outer surf zone, reduced undertow and an increase in the effectiveness of asymmetric wave-induced sediment transport results in a net landward transport which can lower the seaward bar (Larsen and Kraus, 1992), thereby initiating bar degeneration. Such grain by grain transport, i.e. transport independent of a migrating morphological unit, is thought to redistribute sediment into the landward trough and onto the seaward flank of the adjacent landward bar (Wijnberg, 1995, Ruessink, 1998). Such a mechanism thus helps a bar attain its maximum volume within the mid-outer surf zone (Ruessink and Kroon, 1994).

More recently, Kuriyama (2002) interpreted cross-shore sediment transport rates coupled with an autumn typhoon season and a winter-spring depression season at Hasaki Beach, Japan, as evidence for a grain by grain return process existing across the entire surf zone. However, as at other NOM sites, this onshore sediment transport appears to be associated with the degeneration process of the outer bar which, in the Hasaki case, would be initiated annually during the lower energy summer season separating the two higher energy seasons.

Other studies have shown that significant onshore sediment transport across well developed troughs within the mid-inner surf zone is unlikely (Wright et al., 1986; Houwman and Ruessink, 1996), and Ruessink (1998, p209), comments that some other mechanism is required to move sediment further landward within the inner surf zone.

The possibility of sediment return within some form of landward migrating sand body has been raised by Kuriyama and Lee (2001, p962), who interpreted the second eigenfunction from a complex principal component analysis of Hasaki Beach profile data, as the shoreward migration of an accumulation area. Shand (2000, p173) hypothesized that the return of sediment necessary to balance a NOM-associated deficit, may occur via landward migrating inner bifurcates associated with *bar splitting*.

Bar splitting involves a longshore bar developing a forked (or bifurcated) appearance with the seaward bifurcate migrating further offshore while the inner bifurcate moves into the landward trough and completely detaches from the original bar. In some instances the inner bifurcate subsequently merges with either the adjacent landward bar or the low tide step, causing those features to extend further seaward. The low tide step refers to the step-like feature separating the seaward margin of foreshore from the longshore trough. An example of bar splitting from the Wanganui coast is depicted by the sequence of time-lapse photographs in Fig 2 which have been 'rectified' to correct for perspective distortion.. The mechanism(s) responsible for bar splitting remains a mystery.

The phenomenon of bar splitting has been documented at 2 sites on the west coast of the New Zealand North Island; at Wanganui (Shand and Bailey, 1999), and Muriwai (Donohoe (1998). However, the process appears to be widespread on NOM coasts with the signatures often being evident in published data; for example: on the coast of Holland (Kroon 1990, Fig 5; 1994; Wijnberg and Terwindt 1995, Figs 9-11); at Duck, North Carolina (Holman and Sallenger, 1986, Fig 4; Holman and Lippman,1987, Fig 1), at Nottawasaga Bay, Lake Huron (Bauer and Greenwood,

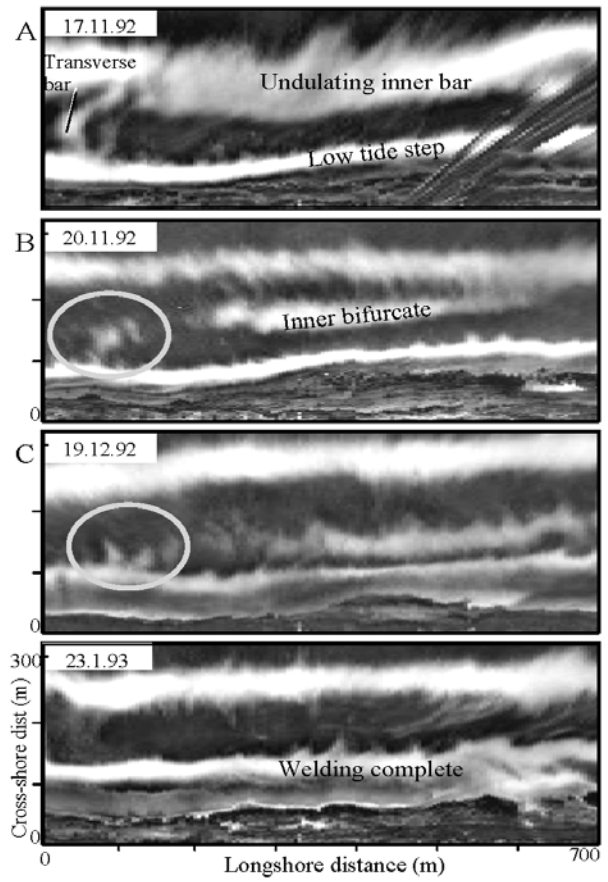

Figure 2 An example of bar splitting using a sequence of 'rectified' (see text) time-lapse photographs from Wanganui, New Zealand.. The form of the inner bar prior to splitting is depicted in A, with B illustrating the recently bifurcated morphology. The inner bifurcate has progressed landward in C, and welded to the inter-tidal beach in D. This episode of bar splitting was the second observed during the study period (Figs 8 and 9). Also depicted is a transverse bar in A detaching from the inner bar and migrating landward (within ellipses in B and C). It has welded to the beach in D. The significance of such behaviour is discussed in text.

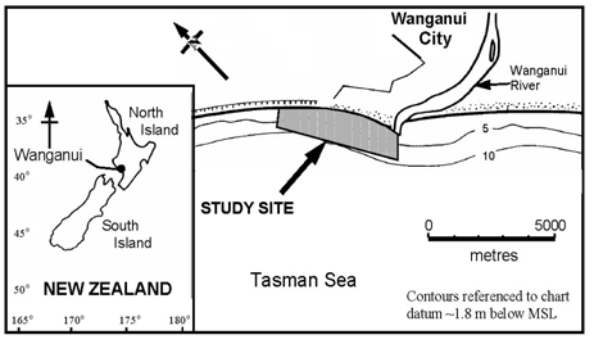

Figure 3. Location map of the Wanganui study site.

1990, Fig 17), at Kouchibouguac Bay, Gulf of St Lawrence (Greenwood and Davidson-Arnott, 1975, Fig 6.6), and at Hasaki Beach, Japan (Kuriyama, 2002, Fig 7).

It is noted that a variety of terms have been used to denote bar splitting and for the inner and outer bifurcates. Bar splitting was referred to as 'double bar development' by Kroon (1991), while Shand and Bailey (1999) used the term 'bar bifurcation'. However, the term bar splitting is now advocated, as a range of other surf zone processes can result in forked or bifurcated morphologies including bar switching (Shand et al., 2001) and some rip channel-based behaviour noted in Shand (2003). Greenwood and Davidson-Arnott (1975) referred to what appears to be an inner bifurcate as a 'tail', while Holman and Lippmann (1987) used the term 'winged bar'.

This paper is a first semi-quantitative attempt to shed light on whether sediment contained within landward migrating inner bifurcates can offset a NOM-associated sediment imbalance within the inner surf zone. This is achieved by analysing several years of ground survey and image-based data from the Wanganui field site. Finally, the results, together with published information from Wanganui and other NOM coasts, are synthesized into a conceptual morphodynamic model of cross-shore sediment transport for the NOM system.

STUDY SITE

The field site is ~1.5 km from the Wanganui Rivermouth on the southwestern coast of the New Zealand North Island (Fig 3). The nearshore is characterised by fine sand (2 to 3 phi), has a cross-shore slope of ~0.0092 and width of ~530 m. Two subtidal sand-bars are usually present; these bars undergo net offshore migration with the mean life-cycle of a bar being ~3 yrs (Shand et al., 1999). The foreshore is characterised by medium sand (1.7 phi), has an average cross-shore slope of ~0.055 and an average width of ~85 m. About 30% of the time a small amplitude (swash) bar is present on the lower foreshore.

The mean neap tide range is 0.8 m and the mean spring tide range is 2.4 m. The mean deepwater significant wave height is 1.3 m and the 5% excedence value is 2.5 m. The mean wave period is 10.1 s (range 3.5 s to19 s) with sea wave conditions occurring for ~75% of the time and swell waves for the remaining time. Approximately forty two percent of waves approach from the west, ~24% from the south and ~34% lie within one degree of shore-normal. The prevailing WNW wind approaches the coast at ~35 deg from the shoreline, and the wind speed 5% excedence value is 12.4 m/s. The mean value for longshore currents within the inner surf zone is 0.42 m/s and the 5% excedence value is 1.01 m/s. Wave height, wind strength and the magnitude of longshore currents are all positively correlated, as are the direction of these process variables (Shand et al., 2001).

METHODS

To accurately determine sediment volume moving offshore across the inner surf zone in association with NOM, and moving onshore via inner bifurcates associated with bar splitting, high spatial resolution (cross-shore= 10^0 to 10^1 m, longshore=10^1 m, and elevation=10^{-1}) data of the inter-tidal and subtidal zones are required at 1-5 day intervals. As the logistics of acquiring such data were prohibitive, the following alternative approach was developed which used available image data and morphological maps.

The seaward loss of sediment under NOM was estimated by the cross-shore change in location of the low tide step associated with bar generation, whilst the landward gain in sediment from bar splitting was estimated by the cross-shore change in location of the step associated with inner bifurcate welding. The cross-shore locational change of the low tide step is thus used to represent sediment volume change. This concept is illustrated in Fig 4 and the mathematical justification provided in Shand and Shepherd (2005). The general morphological dimensions are given in Fig 4. On the Wanganui coast, the low tide step corresponds with a well defined change in slope between the foreshore and the inner trough. Finally it is noted that surveys indicate similar cross-shore location and elevation of the low tide step when associated with both pre-bar generation and post-bar welding.

It was necessary to use two different types of data for the study as bar splitting and bar generation occur in different locations, the former within the surf zone and the latter upon the lower inter-tidal beach. Time-lapse images were used for the surf zone data, while ground survey maps provided inter-tidal data. The two highest resolution data sets available were used for this paper and are detailed below. However, as these data were originally collected for different research purposes, they spanned different, albeit overlapping, time periods, and the locations were separated by ~1 km. Nonetheless, these differences should not affect the comparison between bar generation and bifurcate welding, as while NOM cycles at the two sites were at times out-of-phase, overall bar behaviour was similar (Shand, 2000).

The generation of inter-tidal sand-bars, which subsequently underwent NOM, were identified from a set of morphological maps produced from ground surveys carried out at fortnightly intervals between August 1991 and March 1995. These maps cover an area 300 m longshore by 200 m cross-shore, thereby encompassing the inter-tidal beach and part of the inner bar system. Morphological features such as the saturation boundary and low tide step were defined by direct cross-shore measurement either using a tape measure or theodolite. Location errors on the maps, based on 95% confidence intervals, are estimated to be 5 m in the cross-shore direction and 10 m in the longshore direction. The fortnightly sampling interval could, theoretically, result in a systematic error, and this is discussed later in the paper.

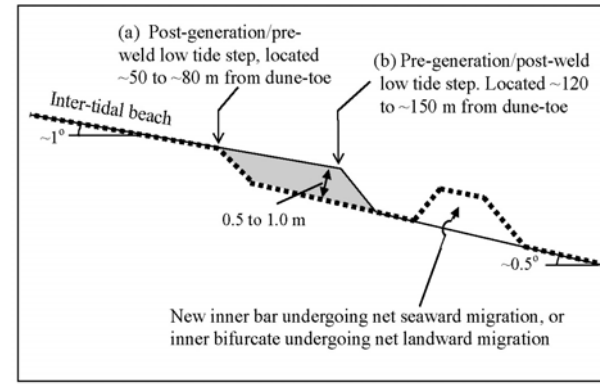

Figure 4. Schematic diagram depicting cross-shore locations of the low tide step either following bar generation or before inner bifurcate welding (a), and either prior to bar generation or following bifurcate welding (b). The shaded area depicts material either lost from the beach via bar generation or gained by birurcate welding. Dimensional approximations are also shown.

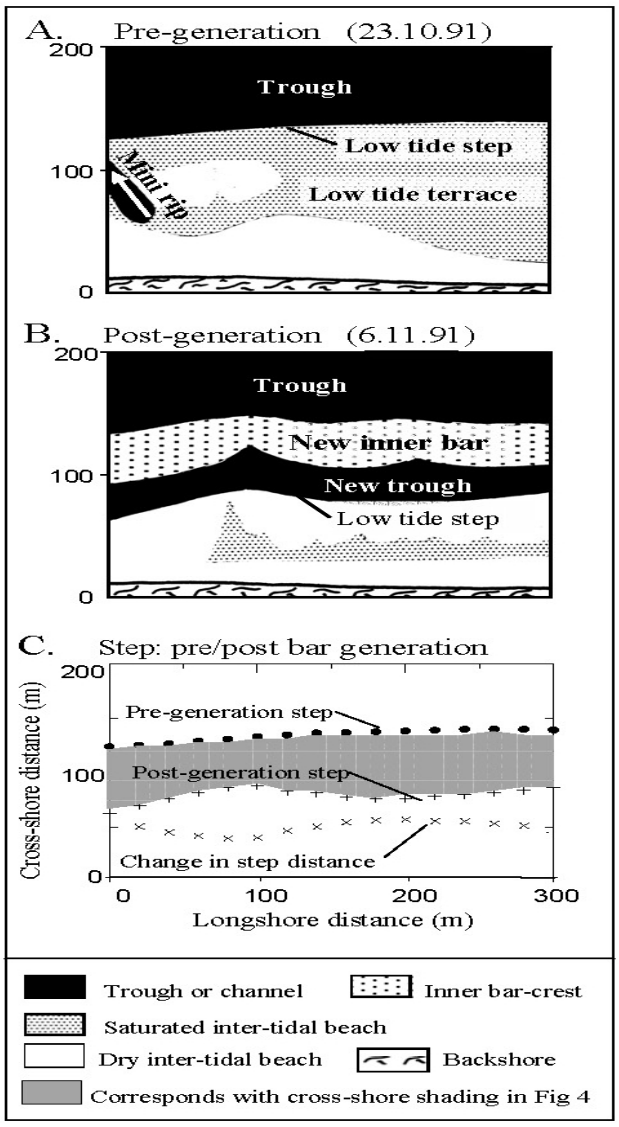

Figure 5. Morphological maps depicting a relatively featureless inter-tidal beach (A) upon which a new bar forms (B). This generation is the first of 4 occurrences during the study period (see Fig 7). Comparison between the pre/post generation cross-shore positions of the low tide step is depicted in C.

Examples of maps depicting the formation of a new inter-tidal sand-bar are shown in Figs 5A and 5B, with the step locations prior to, and following, bar generation being depicted in 5C. The pre and post-generation step locations are shown in Fig 5C, and the longshore-averaged value of the change in step distance (55 m) represents sediment lost from the beach in association with this bar generation.

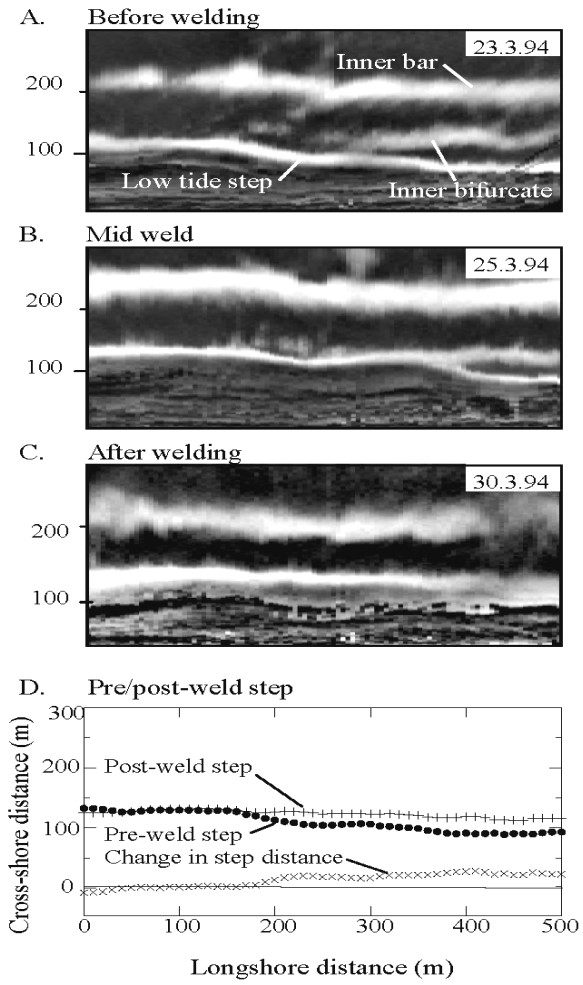

Figure 6. Sequence of rectified images depicting an inner bifurcate (A) incrementally welding to the inter-tidal beach (B and C). This episode of bar splitting was the 6th observed during the study period. A comparison of the pre/post weld cross-shore positions of the low tide step is depicted in D.

Episodes of bar splitting were identified from a 2 yr set of rectified time-lapse photographs (4 min exposures) collected between September 1991 and August 1994, and sampled at 2-5 day intervals (e.g. Fig 2). Note that time-lapse photographs are equivalent to 'time-exposure' images derived from video data that have been reported elsewhere (e.g. Aarninkhof and Holman, 1999; Bogle et al., 2000; and Morris et al., 2001). Intensity differences on time-lapse photos portray the submarine morphology, with higher intensity areas (associated with relatively intense wave breaking) representing elevated features such as bar-crests or the low tide step, and darker areas signifying deeper water such as troughs and rip channels. The camera was located on top of a 42 m high cliff and located ~130 m landward of the foredune-toe. A panorama of 4 photographs centered about the camera covered ~500 m of shoreline. Each photo was digitized, rectified to ground co-ordinates and the coastline straightened to facilitate subsequent analysis. Rectified images were clipped beyond 520 m for computer storage purposes. These techniques are described in Bailey and Shand (1996), Shand (2003), and Shand et al. (2003).

Location errors (95% confidence interval) on the rectified images for this particular site are 0 m, increasing to 12 m at the lateral extremes. In the cross-shore direction the maximum error was 15 m within the inner/mid surf zone where bar splitting occurs. While the cross-shore value (15 m) is greater than that specified above (10^0 to 10^1 m), the averaging procedure used in calculating the change in step location parameter value reduces the magnitude to acceptable levels. Eamples of images depicting an inner bifurcate welding to the foreshore are shown in Figs 6A to 6C. The pre and post-weld step locations (Fig 6D) were detected using maximum intensity values, and the longshore-averaged change in step distance (21 m) represents sediment gained by the beach from this bifurcate weld.

RESULTS

Four instances of bar generation occurred during the study period (Fig 7). The mean inter-generation period was 351 days (140 – 574 days). The mean step retreat associated with the four bar generations was 55.5 m (Table 1), and ranged between 44 and 74 m. The average bar generation retreat per inter-generation cycle will be compared with the average step advance from inner bifurcate welding per inter-generation cycle.

Table 1: Change in cross-shore location of low tide step associated with bar generation and for episodes where inner bifurcate welding affected the low tide step. Event numbers as depicted in Fig 8.

Event type	Event number and step location change (m)								Mean
	1	2	3	4	5	6	7	8	
Generations	55	44	74	49	-	-	-	-	55.5
Step welds	20	27	-	-	-	21	18	28	22.8

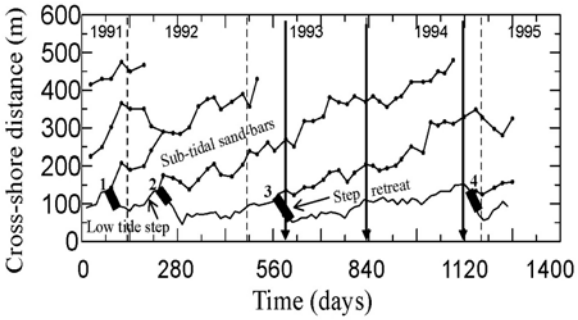

Figure 7. Time-series of bar-crest location and low tide step location at a cross-shore transect ~1500 m alongshore from the Wanganui Rivermouth. The 4 episodes of bar generation are numbered and the associated step retreats are depicted by bold line segments. The vertical arrows mark times of sampling for the 3 images used to illustrate NOM behaviour in Fig 1.

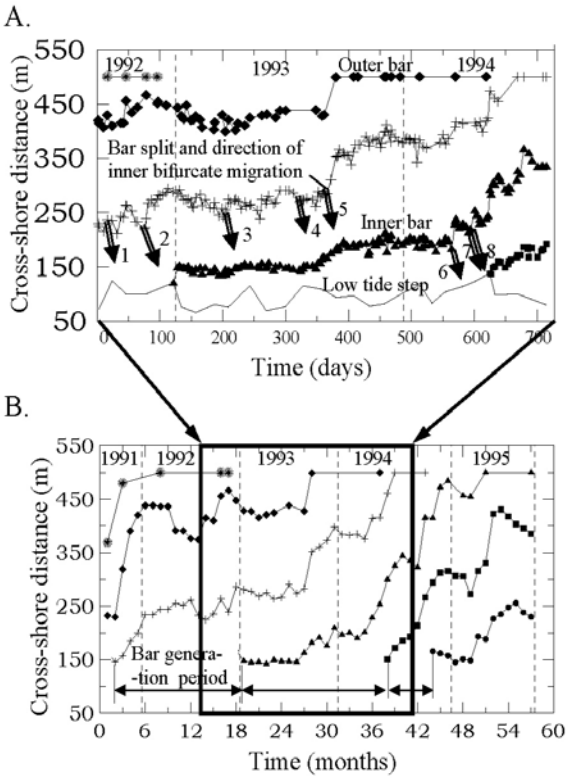

Figure 8. Time-series of bar-crest location and low tide step location for the transect located ~3000 m from the Wanganui Rivermouth. Data used in the present study are depicted in A, and the 8 episodes of bar switching are marked. A temporally extended time-series (B) is included to illustrate how the shorter-term bar and step location data, along with bar generation periods, fit within the longer-term pattern of NOM. Note outer bar migrates beyond 520 m as explained in the text.

Eight episodes of bar splitting ocurred during the study (Fig 8A). Time-series graphs for each episode are depicted in Fig 9. These 8 graphs also describe the behaviour of the inner bifurcates in terms of the following: longshore coherence or incoherence of the crest; disappearance within, or transversing across, the landward trough; and fully welding to the landward bar/step during a single inter-survey period, or incrementally welding during several such periods. Only one inner bifurcate (episode 4) failed to weld. The bifurcate in episodes 3 and 5 welded to the inner bar, while the bifurcate in episodes 1, 2, 6, 7 and 8 welded to the low tide step. It is also noted that epsiodes 3 to 5 resulted from the splitting of a bar located seaward of the inner bar, and that the inner bifurcates were longshore-incoherent during much of their existence.

The 5 inner bifurcates which welded to the step did not equally affect the 500 m long study area (Fig10). Averaging the step-advances over the length of the study area resulted in 2.12 welds per metre alongshore. The assumption of longshore dispersion of localised sediment inputs is considered valid as the Wanganui coast, and indeed most NOM coasts (Shand et al., 1999), are characterised by moderate to strong longshore currents.

Furthermore, the predominant longshore current direction at Wanganui is from NW to SE, i.e. right to left in Fig 10, thereby assisting with the dispersal of inner bifurcate sediment which, during the sampling period, happened to occur more often on the NW side of the study area, i.e. on the right side of graph.

When bar behaviour at the bar splitting site is compared with longer-term bar behaviour for this location (Fig 8B), it is evident that ~1.75 inter-generation periods occurred. The approximate number of welds per inter-generation period is therefore:

$$2.12/1.75 = 1.21 \text{ welds/cycle}$$

The mean step advance associated with the 5 epsiodes of welding to the inter-tidal beach = 22.8 m (Table 1) and ranged between 18 and 28 m. A similar value (23.1 m) is derived if the 2 bifurcates which welded to the inner bar are included within the calculation. The mean step advance per inter-generation cycle is therefore:

$$22.8*1.21 = 27.6 \text{ m/cycle}$$

Comparing of this value with the mean step retreat associated with the four bar generations, i.e. 27.6 m c.f. 55.5 m, suggests that approximately half (49.7%) the sediment volume lost from the inter-tidal beach during bar generation is later replaced via the process of bar splitting.

DISCUSSION

There are several limitations in the data-sets used in this study. Firstly, the 2 yr image data used to identify and analyse bar splitting contained less that 2 generation cycles and therefore may not be fully representativeof bar behaviour. However, the fact that bar splitting affected each landward bar during the study period, and that splitting occurs systematically within the NOM system, namely later in the inter-generation period when weak 3D morphologies predominate (Shand and Bailey, 1999; Shand et al., 2004), suggests that bar behaviour was probably normal during the study period.

Secondly, the 14 day sampling intervals of the bar generation data may have resulted in a systematic error in step retreat for the following reasons. Bar generation on the Wanganui coast has been observed to occur upon a wide foreshore, under neap tidal range and under storm conditions, i.e. higher waves and stronger longshore currents (Shand and Bailey, 1999; Shand et al., 2004). Bar generation would therefore tend to occur approximately one week prior to sampling which only took place during times of spring tide. However, the eastward progression of high and low pressure sytems which characterise NZ weather (Tomlinson, 1976), results in periods of fairweather following storms, conditions observed at Wanganui to be conducive to the formation of a swash bar on the lower foreshore when coupled with the typically 2D or weakly 3D new bar system (Shand et al., 2004). The subsequent landward migration of swash bars during the neap tide to spring tide change is well documented (e.g. Sonu,1972; Kroon, 1994), and the low tide step also moves landward. The position of the low tide step at sampling time would therefore over-estimate the effect of bar generation. By comparison, the higher sampling rate of the image data, used for the bar splitting exercise, avoided any systematic error in step location. The 50% sediment return to the inter-tidal beach associated with bifurcate welding therefore probably under estimates the actual value, possibly by several percent.

During the present study, other secondary morphological behaviours associated with stronger 3D topographies were identified which are capable of transfering sediment landward. For example, transverse bars, as defined by Konichi and Holman (2000), and formed, for example, when horn areas associated with (a)rhythmic morphology welds onto the beach (Wright and Short, 1984; van Enckevort et al., 2004), may detach from the inner bar and the 'free arm' realign in the direction of the longshore current. The arm then either dissipates within the trough, or migrates landward to weld with the step in the same manner as the inner bifurcate from bar splitting. There is evidence of such a 'detached transverse bar' process within the ellipses marked on the left hand side of the images in Figs 2B and 2C, and the resulting seaward extension of the step is indicated when the distances in Figs 2C and 2D are compared.

The occurrence of 3D morphologies therefore appears to play a key role in the development of landward-migrating secondary sand bodies. At Wanganui, 3D configurations occur earlier in the NOM cycle when the bar is still within the inner surf zone (Shand,

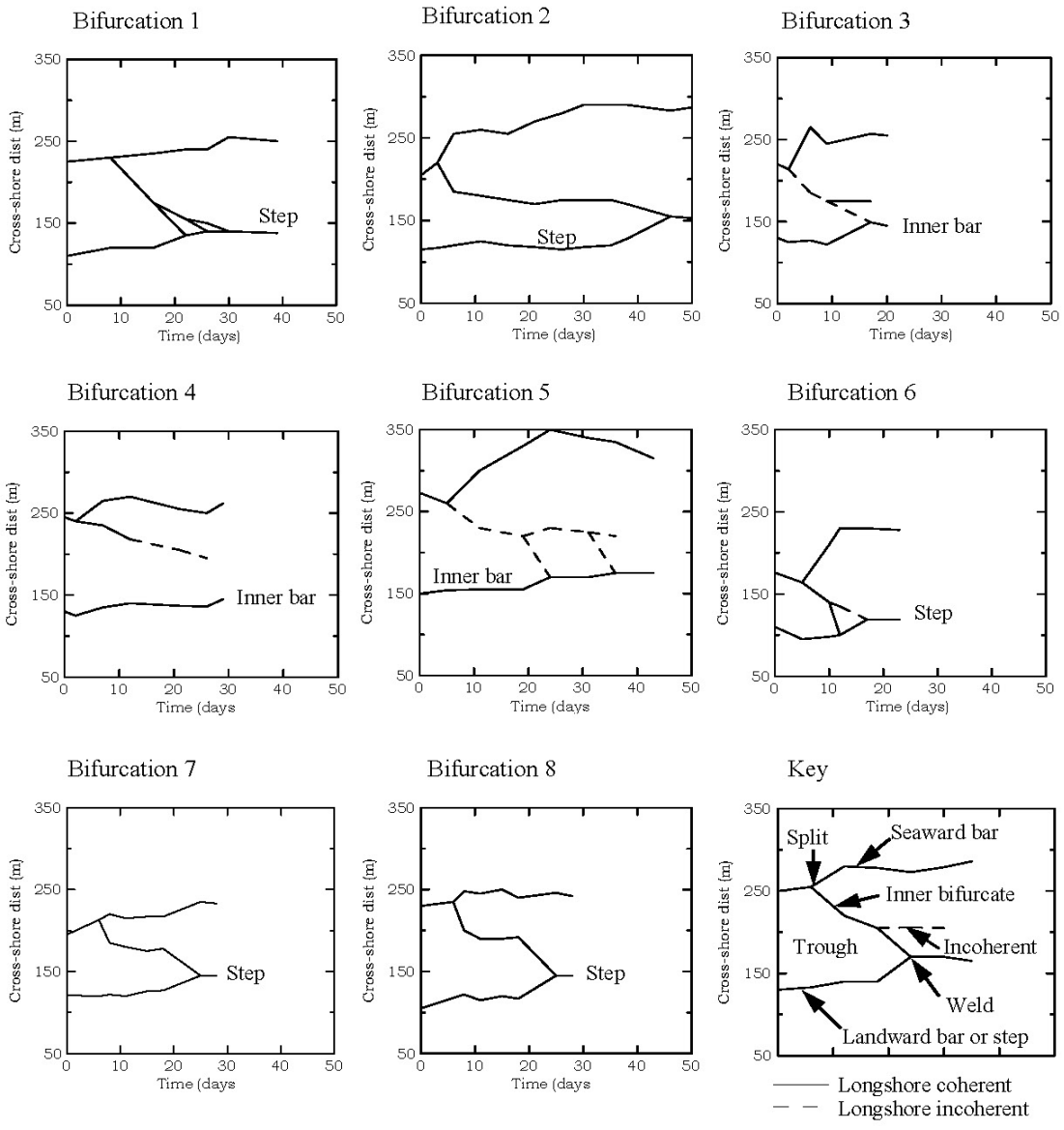

Figure 9. Bar-crest location time-series for the 8 bifurcations (bar splits) which occurred during the 2 yr study period. Each graph also depicts the behaviour of the inner bifurcate in terms of the following: longshore coherence/incoherence of crest; disappearance within, or traversing across, the landward trough; fully welding to the landward bar/step during a single inter-survey period, or incrementally welding during several such periods. The timing of these episodes of bar splitting have been marked on Fig 8.

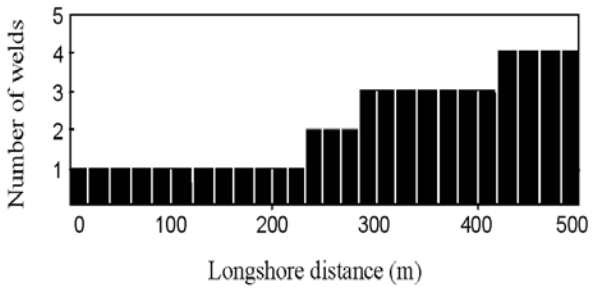

Figure 10. Histogram depicting inner bifurcates which welded onto the step along study area.

2002). During this time, incident energy is dissipated (filtered) on a well-developed seaward bar (Shand et al., 2004), thereby facilitating 3D pattern development via self-organisational behaviour.

Integration of the findings from this paper with those in the other referenced work, enabled the formulation of a conceptual morphodynamic model of cross-shore sediment transport mechanisms for the NOM system at Wanganui (Fig 11). The model is primarily based on research from Wanganui with results from other sites have also been incorporated. The model is expected to have application at other NOM coasts. Of additional interest is the depiction in Fig 11B of the inner bar moving seaward while ripped (stronger-3D) states predominate (see Shand, 2004). During this period which may last several months, sediment appears to move offshore via the continually reforming and/or longshore migrating rip channels.

The inclusion of 3D configurations within the conceptual morphodynamic model presented in Fig 11, contrasts with previous models for NOM systems (Ruessink and Kroon, 1994; Wijnberg, 1995; Ruessink and Terwindt, 2000; Kuriyama, 2002)

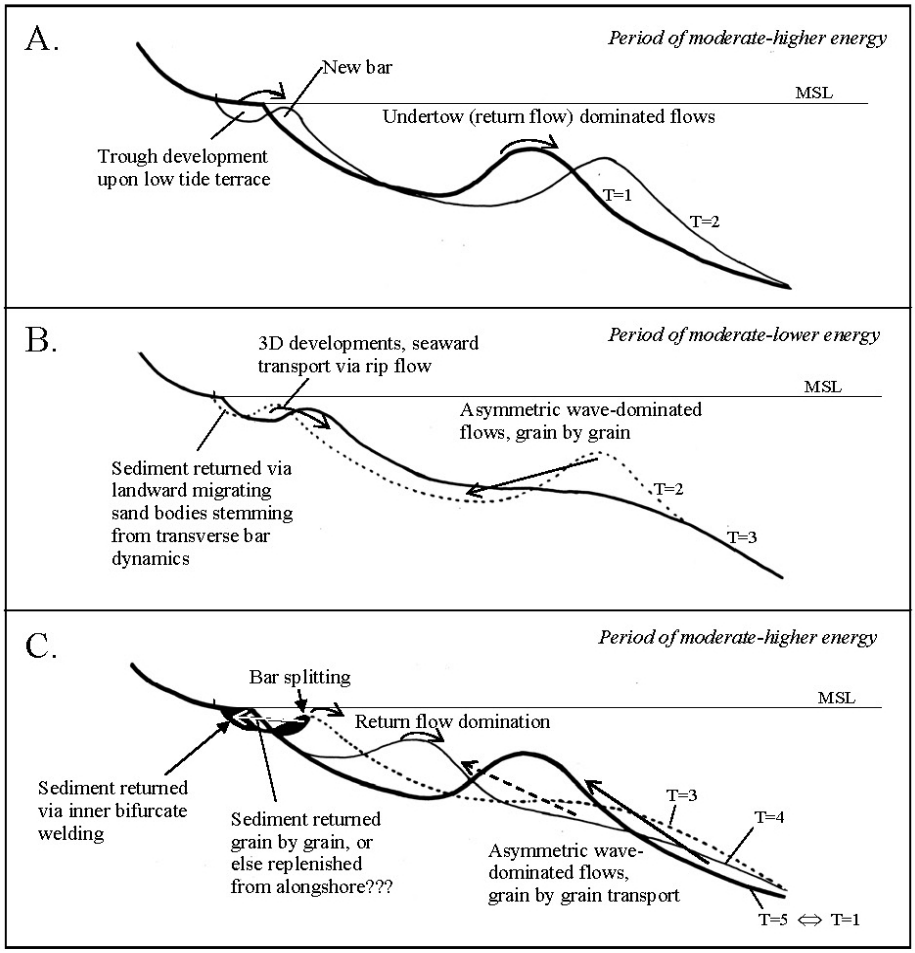

Figure 11. A conceptual model of sediment transport mechanisms for the NOM system at Wanganui. At time T=1, the profile contains a single sub-tidal sand-bar. At T=2, an additional bar has formed. The sequence terminates at T=5 at which time the new bar has reached the cross-shore location of the bar at T=1. The 'return period' of the system is thus defined by T=5. The processes depicted in the diagrams are either described, or referenced, within the text.

which are entirely 2D. The systematic occurrence of several types of 3D behaviour, enables a significant portion of sediment within the inner-mid surf zone to move shoreward and thus help counter any sediment imbalance associated with the underlying process of NOM. In addition, the systematic occurrence of rip-channels, provide an additional mechanism to undertow (return-flow) driven seaward sediment transport within the inner surf zone. Finally, it is noted that existing inter-annual process-based modeling (e.g. Roelvink et al., 1995; Aarninkhof, 1998?) will need to incorporate 3D non-linear dynamical behaviour if the NOM system is to be numerically replicated.

CONCLUSIONS

This study used ground survey and image-based data-sets from Wanganui, New Zealand, to show that shoreward sediment transport within landward migrating inner bifurcates (associated with bar splitting), account for at least half of the inter-tidal beach sediment which is lost seaward in association with bar generation. While bar splitting occurs upon weak to moderate 3D topographies, other types of behaviour associated with stronger 3D antecedent morphologies were identified during the study which are capable of transfering further sediment landward within migrating sand-bodies. Landward migrating secondary bars therefore appear to play a significant role in returning sediment to the inter-tidal beach. Some sediment will also be added to the beach from longshore transport, and the possibility still exists that a portion of sediment returns via grain by grain processes within the inner surf zone. A conceptual morphodynamic model of the NOM system is presented in which 3D behaviour is an essential component, in contrast to existing models which are entirely 2D.

.

ACKNOWLEDGEMENTS

This study was supported by the Massey University Research Fund and a Research Fellowship (contract MAUX0104) from the New Zealand Foundation for Science and Technology (FRST). The author wishes to thank Dr Giovanni Coco of the National Institute of Water and Atmospheric Research (NIWA) of New Zealand, Dr Gerben Ruessink (Utrecht University), Dr Andy Short (University of Sydney) and the two ICS2007 reviewers for comments on the manuscript. Drs Rob Holman (Oregon State University) and Karin Bryan (University of Waikato) are also thanked for allowing access to image data from their ARGUS site at Muriwai Beach, NZ.

REFERENCES

ARNINKHOF, S., and HOLMAN, R.A., 1999. Monitoring the nearshore with video. Backscatter, 10, 8-11.

BAUER, B.O., and GREENWOOD, B., 1990. Modification of a linear bar-trough system by a standing edge wave. Marine Geology, 92, 177-204.

BAILEY, D.G., and SHAND, R.D., 1996. Determining large-scale sand bar behaviour. *Proceedings of the IEEE International Conference on Image Processing*, Lausanne, Switzerland, (2), 637-640.

BIRKEMEIER, W.A., 1984. Time scales of nearshore profile change. *Proceedings of the 19th International Conference on coastal Engineering*, ASCE, pp. 1507-1521.

BOGLE, J.A.; BRYAN, K.R.; BLACK, K.P.; HUME, T.M.; and HEALY, T.R., 2000, Video observations of rip formation and evolution. *Journal of Coastal Research Special Issue 34*, 117-127.

DE VROEG, J.H.; SMIT, E.S.P., and BAKKER,W.T., 1988. Coastal Genesis. *Proceedings of the 21st International Conference on coastal Engineering*, ASCE, pp. 2825-2839.

DONOHOE, B.F.P., 1998. *Spatial and temporal bar morphodynamics of Muriwai Beach*. MSc thesis, Auckland University, New Zealand, 104p.

GALLAGHER, E.L.; ELGAR, S.; and GUZA, R.T., 1998. Observations of sand bar evolution on a natural beach. *Journal of Geophysical Research*, 103, 3203-3215.

GREENWOOD, B., and DAVIDSON-ARNOTT, G.D., 1975. Marine bars and nearshore sedimentary processes, Kouchibouguac Bay, New Brunswick. In: Hails, J., and Carr, A., (eds.), *Nearshore Sediment Dynamics and Sedimentation.* John Wiley and Sons, New York, pp. 123-150.

GREENWOOD, B., and DAVIDSON-ARNOTT, R., 1979. Sedimentation and equilibrium in wave formed bars: a review and case study. *Canadian Journal of Earth Science*, 16, 312-332.

HAXEL, J.H., and HOLMAN, R.A., 2004. The sediment response of a dissipative beach to variations in wave climate. *Marine Geology*, 206, 73-99.

HOEFEL, F., and ELGAR, S., 2003. Wave-induced sediment transport and sandbar migration. *Science*, 299, 1885-1887.

HOLMAN, R.A., and LIPPMANN, T.C., 1987. Remote sensing of nearshore bar systems - making morphology visible. *Proceeding of Coastal Sediments'87*, ASCE, pp. 927-944.

HOLMAN, R.A., and SALLENGER, A.H., 1986. High energy nearshore processes. *EoS Trans. AGU* 67, 1369-1371.

HOUSER, C., and GREENWOOD, B. 2004. Profile response of a lacustrine multiple barred nearshore over a sequence of storm events. *Geomorphology*, 69, 118-137.

HOUWMAN, K.T and RUESSINK, B.G., 1996. Cross-shore sediment transport mechanisms in the surfzone on a time scale of months to years. *Proceedings of the 25th International Conference on Coastal Engineering*, ASCE, pp. 4793-4806.

KONICKI, K.M., and HOLMAN, R.A., 2000. The statistics and kinematics of transverse sand bars on an open coast, *Marine Geology*, 169, 69-101.

KROON, A., 1991. Three-dimensional morphological changes of a nearshore bar system along the Dutch coast near Egmond aan Zee. Proceedings of the Skagen Symposium, *Journal of Coastal Research, Special Issue, 9*, 430-451.

KROON, A., 1994. *Sediment transport and morphodynamics of the beach and nearshore zone near Egmond, The Netherlands*. PhD thesis, Utrecht University, the Netherlands, 275p.

KROON, A., and HOESKSTRA, P., 1993. Nearshore bars and large-scale coastal behaviour. In: List, J.H., (ed.), *Large-Scale Coastal Behaviour '93*. U.S. Geological Survey, Open-File Report 93-381, pp. 92-95.

KURIYAMA, Y., 2002. Medium-term bar behaviour and associated sediment transport at Hasaki, Japan. *Journal of Geophysical Research*, 107.

KURIYAMA, Y., and LEE J.H., 2001. Medium-term beach profile change on a bar-trough region at Hasaki, Japan, investigated with complex principal component analysis. In *Proceedings Coastal Dynamics '01*, ASCE, pp. 959-968.

LARSEN, M., and KRAUS, N.C., 1992. *Analysis of cross-shore movement of natural longshore bars and material placed to create longshore bars*. Technical Report CERC DRP-29-5, 115p.

LIPPMANN, T.C.; HOLMAN, R.A., and HATHWAY, K.K., 1993. Episodic, nonstationary behaviour of a double bar system at Duck, North Carolina, U.S.A., 1986-1991. *Journal of Coastal Research, Special Issue, 15*, 49-75.

MORRIS, B.D; DAVIDSON, M.A., and HUNTLEY, D.A., 2001. Measurements of the response of a coastal inlet using video monitoring techniques. *Marine Geology*, 175, 251-272.

ROELVINK, J.A.; MEIJER, J.G.P.; HOUWMAN, K.; BAKKER, R., AND SPANHOFF, R., 1995. Field validation and application of a coastal profile model. *Proceedings of Coastal Dynamics'95*, ASCE, pp. 818-828

RUESSINK, B.G., 1998. *Infragravity waves in a dissipative multiple bar system.* PhD thesis, Utrecht University, the Netherlands, 245p.

RUESSINK, B.G., and KROON, A., 1994. The behaviour of a multiple bar system in the nearshore zone of Terschelling, the Netherlands: 1965-1993. *Marine Geology*, 121, 187-197.

RUESSINK, B.G., and TERWINDT, J.H.J, 2000. The behaviour of nearshore bars on a time scale of years: a conceptual model. *Marine Geology*, 163, 289-302.

SHAND, R.D., 2000. Offshore *migration of coastal sand-bars at Wanganui, New Zealand*. PhD thesis, School of Global Studies, Massey University, New Zealand, Miscellaneous Publication Series, 00/8, 295p.

SHAND, R.D., 2002. *Temporal variation in morphological configuration within a multi-bar surf zone at Wanganui, New Zealand*. Occasional Paper 2002/4, School of People Environment and Planning, Massey University, New Zealand, 42p.

SHAND, R.D., 2003. Relationships between episodes of bar switching, cross-shore bar migration and outer bar degeneration at Wanganui, New Zealand. *Journal of Coastal Research*, 19(1), 157-170.

SHAND, R.D., 2004. *Rip-associated bathing hazards on beaches characterised by net offshore bar migration.* Occasional Paper 2004/1, School of People Environment and Planning, Massey University, New Zealand, 19p.

SHAND, R.D., and BAILEY, D.G., 1999. A Review of Net Offshore Bar Migration with Photographic Illustrations from Wanganui, New Zealand, *Journal of Coastal Research*, 15(2), 365-378.

SHAND, R.D and SHEPHERD, M,J., 2005. *Sediment budget implications associated within a net offshore migrating (NOM) bar system.* Occasional Paper 2005/2, School of People Environment and Planning, Massey University, New Zealand, 23p.

SHAND, R.D.; BAILEY, D.G., and SHEPHERD, M.J., 1999. An inter-site comparison of net offshore bar migration characteristics and environmental conditions. *Journal of Coastal Research*, 15(4) 750-765.

SHAND, R.D., BAILEY, D.G., and SHEPHERD, M.J., 2001. Longshore realignment of nearshore parallel sand-bars at Wanganui, New Zealand. *Marine Geology* 179, 147-161

SHAND, R.D.; HESP, P.A., BAILEY, D.G., and SHEPHERD, M.J., 2003. A conceptual beach-state model for the inner bar of a storm-dominate, low to moderate tidal range coast at Wanganui, New Zealand. *Proceedings of Coastal Sediments '03.*

SHAND, R.D.; HESP, P.A., and SHEPHERD, M, J., 2004. Beach cut in relation to net offshore bar migration. *Journal of Coastal Research, Special Issue 3*, in press.

SONU, C.J., 1972. Field observation of nearshore circulation and meandering currents. *Journal of Geophysical Research*, 77(18), 3232-3247.

SVENDSEN, I. A. 1984. Mass flux and undertow in a surf zone. *Coastal Engineering*, 8, 347-365.

TOMLINSON, A.I., 1976. Climate. In Woods, I. (ed.) *New Zealand Atlas*, Government Printer, New Zealand, pp. 82-89.

VAN ENCKEVORT, I.M.J.; RUESSINK, B.G.; COCO, G.; SUZUKI, K .; TURNER, I.L.; PLANT, N.G., and HOLMAN, R.A., 2004. Observations of nearshore crescentic sandbars. *Journal of Geophysical Research* , 109, 1029-1046.

WIJNBERG, K.M., 1995. *Morphologic behaviour of a barred coast over a period of decades*. PhD thesis, Utrecht University, the Netherlands, 245p.

WIJNBERG, K.M., 1996. On the systematic offshore decay of breaker bars. *Proceedings of the 25th International Conference on Coastal Engineering*, ASCE, pp. 3600-3613.

WIJNBERG, K.M., and TERWINDT, J.H.G., 1995. Extracting decadal morphological behaviour from high-resolution, long-term bathymetric surveys along the Holland coast using eigenfunction analysis. *Marine Geology*, 126, 301-330.

WRIGHT, L.D., and SHORT, A.D., 1984. Morphodynamic variability of surf zones and beaches: a synthesis. *Marine Geology*, 56, 93-118.Wright, L.D.; Nielsen, P,; Shi, N.C., and List, J.H., 1986. Morphodynamics of a bar-trough surf zone. *Marine Geology*, 70, 251-285.

Shand. T.D.; Bailey, D.J., and Shand, R.D., 2012. Automated detection of breaking wave height using an optical technique. Journal of Coastal Research, 28(3), 671-682.

Journal of Coastal Research	28	3	671–682	West Palm Beach, Florida	May 2012

Automated Detection of Breaking Wave Height Using an Optical Technique

Thomas D. Shand[†], Donald G. Bailey[‡], and Roger D. Shand[§]

[†]Water Research Laboratory
School of Civil and Environmental Engineering
University of New South Wales
110 King Street
Manly, NSW 2095, Australia
t.shand@wrl.unsw.edu.au

[‡]School of Engineering and Advanced Technology
Massey University
New Zealand
d.g.bailey@massey.ac.nz

[§]Coastal Systems Ltd. and Geography Program
Massey University
Palmerston North, New Zealand
rshand@coastalsystems.co.nz

www.cerf-jcr.org

www.JCRonline.org

ABSTRACT

SHAND, T.D.; BAILEY, D.G., and SHAND, R.D., 2012. Automated detection of breaking wave height using an optical technique. *Journal of Coastal Research,* 28(3), 671–682. West Palm Beach (Florida), ISSN 0749-0208.

Obtaining accurate information of nearshore wave characteristics including the position and height of individual breaking waves is essential to understanding the drivers of coastal processes, for engineering design and hazard prediction. Demand for such information in real time for recreational planning and hazard assessment is also high. Remote optical techniques would offer considerable economic and spatial coverage advantages over conventional *in situ* instrumentation. However, optical methods for obtaining wave height information have been slow to develop and those available remain computationally expensive and require "favourable" environmental conditions. This paper presents a relatively simple yet robust approach to detecting and quantifying breaking wave position and height across a wide surf zone using a twin video camera configuration coupled with an image time-stack analysis approach. A numerical algorithm, HbSTACK, is developed and successfully tested under the environmental conditions experienced during field trials. Errors and uncertainties may arise in both the photogrammetric transformation from pixels to real-world coordinates and in the detection of wave crest and trough positions. These errors have been assessed using both field verification of the transformation model and manually detected crest and trough locations by experienced practitioners. Errors in output wave heights were thus estimated to be less than 7%.

ADDITIONAL INDEX WORDS: *Wave height, Wave breaking, Surf zone, Optical detection.*

INTRODUCTION

Obtaining accurate information of nearshore wave characteristics is essential to understanding the drivers of coastal processes for engineering design, hazard prediction, and recreational planning. Fundamental characteristics include the position and height of individual breaking waves and their distribution across the surf zone. However, acquisition of these parameters in the field presents a significant challenge due to the variability and hostility of the coastal environment. A variety of methods have previously been used to extract wave height information including *in situ* instrumentation such as wave buoys, pressure transducers or manometers (*i.e.,* Grace, 1978), wave staffs, and capacitance and resistance probes (Whittenbury, Huber, and Newell, 1959) and shore-based remote techniques such as visual estimation or measurement (Balisllie and Carter, 1984; Patterson and Blair, 1983), high-frequency (HF) radar (Heron and Prytz, 2002; Wyatt, 1988), and single and stereo camera imagery (*e.g.,* Bechle and Wu, 2011; de Vries *et al.*, 2010; Hilmer, 2005; Mitchell, 1983; Sasaki, Horikawa, and Hotta, 1976).

The placement of instrumentation directly within the surf zone can provide general hydrodynamic data such as surface elevation and flow velocity. Limitations associated with such *in situ* placement include deployment and maintenance costs, risks to personal safety and instruments, and reductions in measurement accuracy and reliability due to aerated flow (Grace, 1978). Additionally, the spatially discrete nature of such data may result in critical break points being missed entirely.

To overcome such limitations, a range of remote techniques have been developed. The most basic involves a shore-based observer estimating wave height (Kelly, 1965) or aligning the horizon with the breaking wave crest and a graduated staff (Balsillie and Carter, 1984; Patterson and Blair, 1983). However, although these methods are cost efficient and easily done, they all involve user subjectivity to a greater or lesser extent.

The use of photo and video imagery to extract breaking wave and surf zone properties has the potential advantages of providing more affordable data than *in situ* instrumentation and at a range of spatial and temporal scales. Digital rectification using photogrammetric colinearity equations allows the removal of perspective distortion and the application of image scaling. Wave properties such as direction and velocity (Holland, 2001; Stockdon and Holman, 2000) and swash-zone processes (Bailey and Shand, 1994; Holland *et al*, 1997; Holman and Guza, 1984) may then be quantified. However, techniques for determining wave height within the surf zone are more complex and have been slower to develop.

DOI: 10.2112/JCOASTRES-D-11-00105.1 received 19 June 2011; accepted in revision 8 August 2011.
Published Pre-print online 17 November 2011.
© Coastal Education & Research Foundation 2012

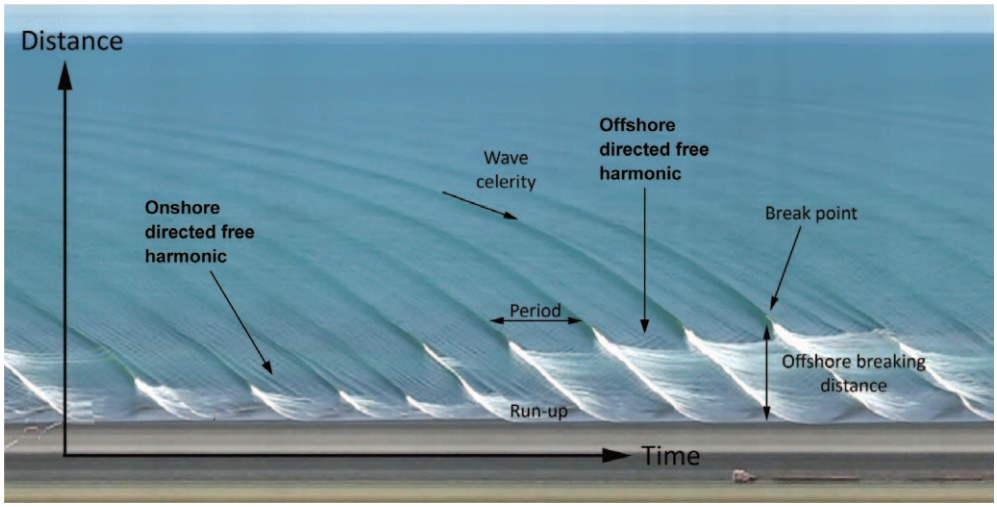

Figure 1. Example of a time-stack image comprising a horizontal stack of vertical slices (a single pixel wide) extracted from a sequence of video frames in which the camera was elevated 43.7 m above MSL. The image thus has a space (nonequidistant) dimension on the *Y*-axis and a time dimension on the *X*-axis. Features such as wave celerity, period, break point, surf zone processes, and run-up are evident and have been marked.

Stereo photogrammetry to examine sea surface and wave characteristics has been used by several researchers, including manual approaches by Cox and Munk (1954), Mitchell (1983), Sasaki, Horikawa, and Hotta (1976), and Schooley (1956), and later automated digital analysis by Benetazzo (2006), de Vries *et al*. (2010), and Wanek and Wu (2005). Although this approach has been shown to be relatively successful under ideal environmental conditions, a major limitation is the requirement for surface textures which facilitates correlation of stereo pairs. Computation times in the processing of imagery also remain problematic, although recent work by Bechle and Wu (2011) claim improved computational time by tracking selected points of interest only. However, although the above approaches provide a measure of water-level elevation, they do not, without additional processing, yield specific breaking wave height.

An alternative, two-dimensional (2D) photogrammetric approach that has the potential to provide wave height information uses time-stack analysis. Time stacking involves the extraction of a single line of pixels from sequential images and chronological placement to provide a record of change over time that can then be analysed to define spatially and temporally varying processes. Figure 1 provides an example of a (nonrectified) time-stack image showing waves approaching the shore, shoaling, and slowing before break point; the generation of free harmonics following breaking directed in both onshore and offshore directions; and wave energy dissipation within the surf zone and swash zone processes. Time stacking has successfully been used to obtain incident wave celerity, period, break point, and run-up (Aagaard and Holm, 1989; Bailey and Shand, 1994).

Although the possibility of deriving breaking wave height (H_b) from time-stack imagery was described and illustrated during the 1990s (Shand and Bailey, 1995), the technique was not developed further until Hilmer (2005) derived breaking wave height on a reef edge using a time stack from a single, low-level camera. The image was "rectified" to a vertical plane (rather than the previously used time-stack approaches noted above where rectification was to a horizontal plane). An example from Hilmer's paper is shown in Figure 2 where a vertical intensity gradient was applied to the time stack

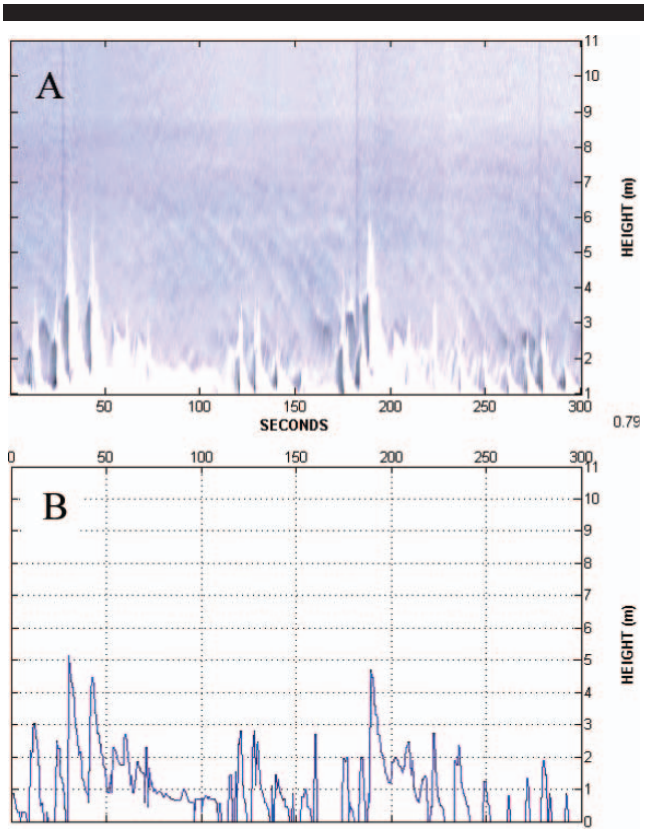

Figure 2. Estimation of breaking wave height at the edge of Togcha Bay reef, Guam (source: Hilmer, 2005).

(Figure 2A) to enable detection of the white-water boundary (Figure 2B). Local boundary maxima were then used to define individual break points, and breaking wave heights were estimated on the basis of elevation above an assumed datum. The measurements were found to have a "clear visual correlation" with corresponding measurements obtained from a wave buoy located beyond the surf zone, *i.e.,* they were in qualitative agreement with the buoy data. The simplicity of such an approach is appealing. However, Hilmer's method has several limitations preventing more general application. These limitations include an assumption of wave breaking at a discrete cross-shore distance to provide vertical scale. Although this assumption has some validity in the reef situation where it was developed as break point location is close to constant, it clearly does not apply in most field situations, with irregular waves of differing heights breaking across a wide surf zone. In addition, Hilmer used a fixed lower datum rather than the variable trough position, and maximum splash-up elevation rather than crest elevation to defined wave height.

Lane *et al.* (2010) recently described a general H_b processing approach for the single-camera time stack. However, their paper is largely devoid of specific technical detail. Their approach appears to use a variable lower datum; however, there is no definition of the trough or how to locate its position. Furthermore, their lack of definition in the offshore breaking position due to a low camera angle severely limits the accuracy in converting pixels (defining wave height) to real-world units, especially in a wide surf zone.

This present paper develops a robust approach to detecting and quantifying breaking wave position and height across a wide surf zone by using a twin camera configuration coupled with an automated image processing routine to abstract H_b from time stacks. The paper begins by discussing and defining wave breaking and breaking wave height. A new methodology for obtaining break point and breaking wave height across a wide surf zone is then outlined. Results of applying the algorithm to field data collected under different environmental conditions are next presented and compared with manually derived wave heights. Finally, accuracy and limitations of the technique are discussed.

THEORETICAL CONSIDERATIONS

Defining Break Point

Fundamental to developing a method for deriving breaking wave height from a time-stack image is a workable and acceptable definition of individual wave break points. Several definitions of the wave break point have been suggested within the literature (Singamsetti and Wind, 1980), and although a universal definition has yet to eventuate, Smith and Kraus (1991) considered a practical definition to be the point at which the "front face of the wave becomes vertical". Once this form is attained the wave either spills progressively down the wave face (Duncan, 2001), or plunges forward, impacting the water surface at some location on the lower wave face or in the preceding trough (Peregrine, 1983).

Breaking wave height is similarly ill defined, with wave buoys or probes providing a vertical distance between trough and crest at a single spatial location (but separated temporally), whereas observers from the shoreline generally estimate height on the basis of the crest-to-trough distance at the moment of breaking (coincident temporally, but separated spatially). As shown in Figure 3, the breaking process is spatially extensive, with the trough minimum often far ahead of the wave crest at break point. Then as the lip moves outward and down to impact the surface, the wave form moves similarly forward and landward and finally the maximum splash-up location occurs still farther landward (see Peregrine, 1983 for more complete description). The definitions of the various breaking terms are shown within Figure 3 in profile (wave tank), frontal (field) perspective, and also within a time stack derived from field imagery.

Although the maximum splash-up elevation was used to define the upper limit of wave height by Hilmer (2005), this elevation can be substantially higher than the breaking wave height in intensely plunging waves (Ting and Kirby, 1995) and, as shown within Figure 3, also occurs further landward than the initial break point.

In the present study, the breaking wave height is assumed to correspond to the apparent vertical distance between the crest and the trough at break point. Break point is defined as the point where white water first becomes apparent. This occurs in a spilling wave when the turbulence first starts to descend down the wave face and in a plunging wave immediately after the crest becomes vertical, in agreement with Smith and Kraus (1991). Trough detection in the case of plunging waves is relatively straightforward as the breaking wave directly intersects the landward unbroken water surface at the minimum surface elevation, consistent with the general definition. However, in the case of spilling waves, the white water takes longer to reach minimal elevation, and the trough location is more difficult to detect. The algorithm (HbSTACK) was modified to accommodate the spilling waves contained in the field data, and additional detail on detecting the trough for verification purposes is provided in the method evaluation section.

Image Transformation

The present study has utilised two time-synchronised, high-definition digital video cameras with one positioned at a low level (referred hereafter as lower camera) and one at high level (referred hereafter as upper camera) on an adjacent cliff top (Figure 4). Imagery from the upper camera was first used to define the offshore location of a wave-breaking event. The same feature was then identified in the imagery from the lower camera with the offshore breaking location used to derive an appropriate transformation relationship for converting wave height in pixels to real-world units. This process is described in detail below.

To derive wave height across a wide surf zone, the cross-shore location of the break point must first be determined. Whereas imagery obtained from a camera orientated vertically above the surf zone exhibits a linear pixel-to-real-world distance relationship, an obliquely orientated camera is subject to perspective distortion. This distortion increases with camera angle from vertical. Image rectification allows an oblique image plane to be transformed onto another 2D plane (Holland *et al.*, 1997).

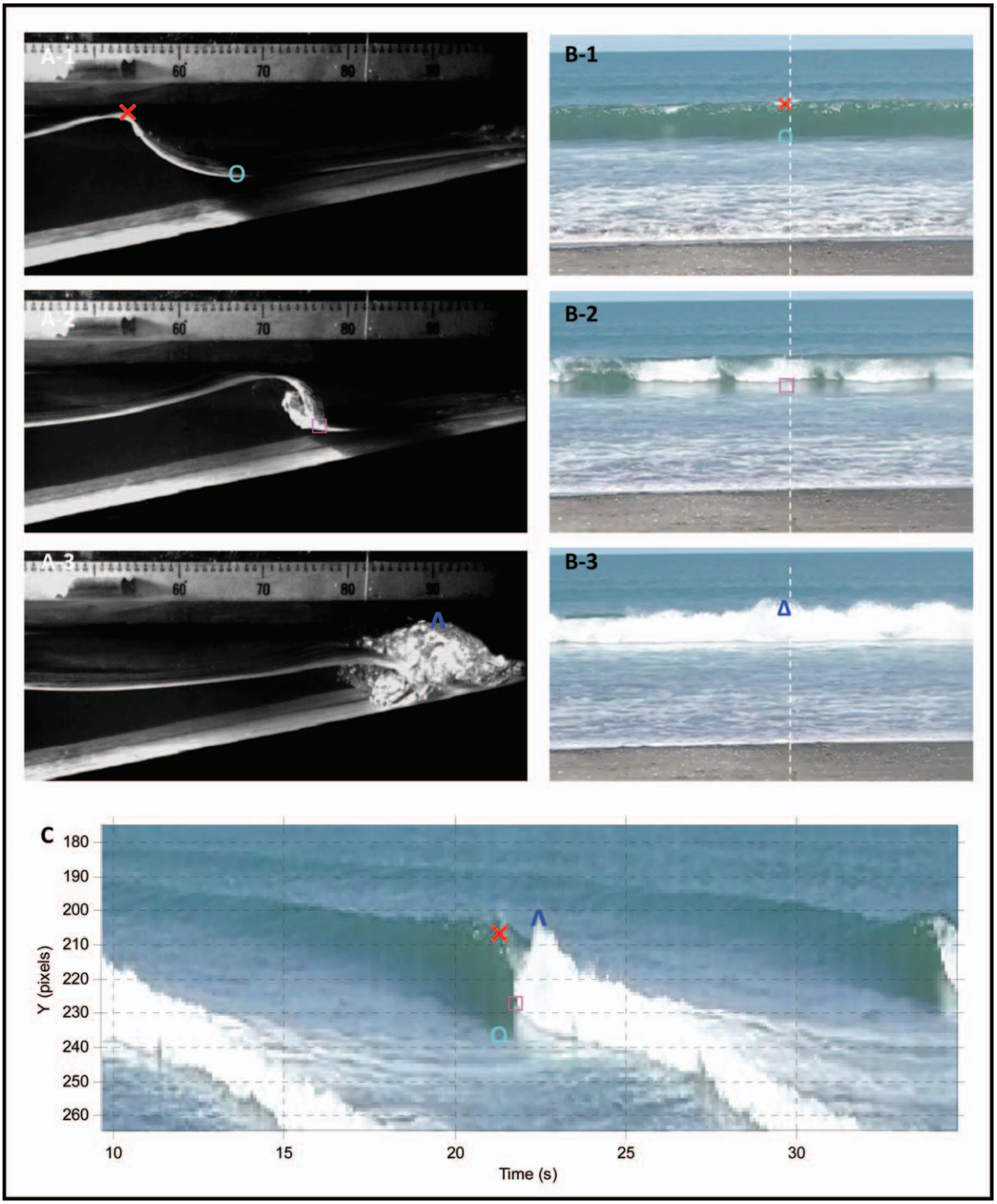

Figure 3. Defining breaking parameters including wave crest (×) and trough position (O) at break point, jet impact point (□), maximum extent of splash-up (Δ) from a side perspective (A; source: Shand, 2009) and frontal perspective (B), with the same features identified in a time-stack image (C). (Color for this figure is only available in the online version of this paper.)

First, we define real-world coordinates as (X,Y,Z) where X is in the offshore direction, Y is the longshore direction, and Z is the height above still-water level (see Figure 4). Also let the image coordinates from the upper camera be (x_u, y_u) and those from the lower camera be (x_l, y_l). A perspective transformation (Equation 1) enables the view from the upper camera to be projected onto the sea surface ($Z = 0$), associating each pixel with a location in world coordinates (Bailey and Shand, 1996).

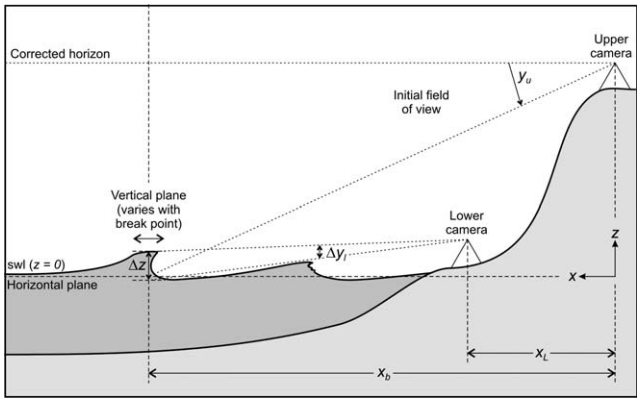

Figure 4. Schematic diagram of camera locations and coordinate system.

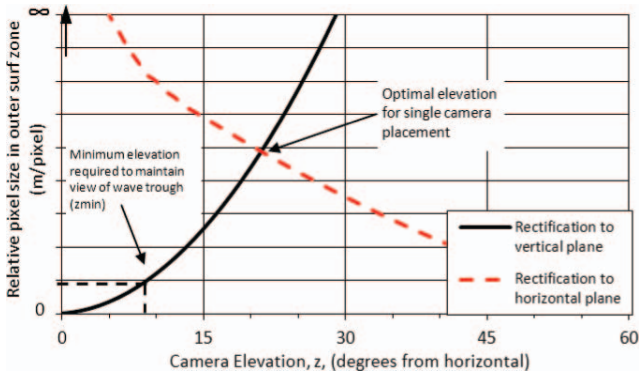

Figure 5. Qualitative errors associated with camera placement in transforming data from pixel to real-world coordinates.

$$X = \frac{a_0 x_u + a_1 y_u + a_2}{a_6 x_u + a_7 y_u + a_8}, Y = \frac{a_3 x_u + a_4 y_u + a_5}{a_6 x_u + a_7 y_u + a_8}. \quad (1)$$

The nine unknowns can be solved with information on the camera position and orientation relative to ground control points (GCPs) and perspective vanishing line (the line of points in the image where points on the object plane at infinite distance would appear) (Bailey and Shand, 1996). If the earth were flat the vanishing line occurs at the horizon; however, because of the curvature of the earth, the vanishing line occurs above the observed horizon at an angle defined by Equation (2) where Z_u is the height of the upper camera above still-water level and R is the radius of the earth. Although this angle is relatively small, the error becomes large if not corrected.

$$\theta = \sqrt{\frac{2Z_u}{R}} \quad (2)$$

Full image rectification would be required if multiple cross-shore profiles are to be assessed. However, as the present study builds a time stack along a single shore-normal profile directly offshore from the upper camera, the perspective transformation equations are simplified to a one-dimensional model as Equation (3):

$$X = \frac{a'_0 y_u + a'_1}{a'_2 y_u + a'_3} \quad (3)$$

where y_u corresponds to the vertical position within the image along the selected cross-shore profile, and X is the offshore distance of the corresponding point on the sea surface. The denominator of Equation (3) corresponds to the vanishing point (the intersection with the vanishing line in the image with the one-dimensional profile). Therefore by setting the vertical origin within the upper image at the vanishing point, $a'_3 = 0$, this reduces Equation (3) to Equation (4):

$$X = \frac{a'_1}{a'_2}\frac{1}{y_u} + \frac{a'_0}{a'_2} \quad (4)$$

The two unknown coefficients are determined by calibration through fitting to a series of GCPs as detailed in the next section.

Once a breaking event is identified in the time-stack image from the upper camera (refer field-data section) its off-shore location, X_b, is determined using the above relation. The same breaking event is then identified in the lower camera. The height of the breaking event (from the wave crest to the trough; refer field-data section for detail) in pixels can be measured from the lower time-stack image for the lower camera as Δy_l. Since the distance between the lower camera and the break point is known, the wave height can then be calculated directly by scaling the pixel height of the breaking event according to Equation (5):

$$H_b = k\Delta y_l (X_b - X_l) \quad (5)$$

where X_l is the offshore position of the lower camera, and k is a constant scale factor, determined by calibration (described within the Field Data Collection section). Note that Equation (5) assumes that the lower camera is looking horizontally. If this is not the case, an additional transformation would be required to correct for the perspective distortion introduced by the camera tilt.

Accuracy of the transformation models is maximised by reducing the perspective distortion of imagery. Whereas a single camera, positioned at an appropriate elevation could, theoretically, be transformed to both horizontal and vertical planes (using a multidimensional calibration), the stretching of pixels during high-angle rectification rapidly decreases spatial resolution and measurement accuracy. This is qualitatively shown within Figure 5 with cameras positioned at lower levels giving greater error in defining horizontal (offshore) distance and cameras at higher levels giving greater error in defining vertical distance (wave height). Practically, this is analogous to observers at low elevations (*i.e.,* near water level) having difficulty judging offshore distance and observers at high elevation (*i.e.,* atop a cliff) having difficulty accurately judging wave height.

It is for this reason that the present study utilised two time-synchronised cameras with one positioned at a low level and one at high level on an adjacent cliff top (Figure 4). This two-camera arrangement reduces transformation errors and enables more detailed interrogation of the particular region of interest. Perspective distortion associated with rectification of the lower camera image to a vertical plane is eliminated by ensuring that the line of sight of the lower camera is parallel to

Figure 6. Coastal Systems Field Research Site, Castlecliff Beach, New Zealand with approximate camera location indicated (map source: Department of Survey and Land Information, 1996).

the sea surface. In practise, small angle error would introduce negligible perspective distortion over the scales of interest. To maximise the accuracy, a narrow angle of view is desired (the camera is zoomed), requiring the camera to be placed close to the still-water level. The minimum lower camera elevation, Z_{lmin}, was found necessary to minimise obstruction of the wave trough by the preceding wave. A first-order estimate of Z_{lmin} is given by Equation 6:

$$Z_{\mathrm{lmin}} > \frac{H_{\mathrm{max}} X_{\mathrm{max}}}{L} \tag{6}$$

where H_{max} is the largest breaking wave height, X_{max} is the maximum breaking distance offshore from the lower camera, and L is the approximate wavelength at break point. Higher

Table 1. *Summary of environmental conditions during the field data collection.*

Date	20 January 2010	21 January 2010	22 January 2010
Time	1030–1200	0930–1030	1230–1330
Tide	0 to 0.5 m MSL (mid-tide incoming)	−0.5 to 0 m MSL (low to mid-tide incoming)	0 to 0.5 m MSL (mid-tide incoming)
Light conditions	Sun mid-height behind to overhead, clear; high contrast	Sun mid-height behind, clear; high contrast	Overhead sun, overcast; low contrast
Wind	W: <5 km/h	W: <5 km/h	W: 15–20 km/h
Visual sea state	~1 m, 10–12-s swell; breaking by weak plunge offshore of upper beach	~1.5 m, 8–10-s swell; larger waves breaking by plunging on outer bar, deshoaling and breaking on low tide step, smaller waves breaking on low tide step only	~1.5 m, 8-s swell with small sea overlying; breaking irregularly by spilling to weak plunging across wide surf zone
Camera configuration	Upper and lower camera	Upper and lower camera	Lower camera only

relative camera placement is required for steeper (spilling type) waves breaking a long distance offshore with lower camera placement possible for lower steepness (plunging) waves that typically break nearer the shoreline and dissipate their energy more rapidly.

FIELD DATA COLLECTION

Field data collection was undertaken on 20, 21, and 22 January 2010 at the Coastal Systems Field Research Site on Castlecliff Beach, situated on the west coast of the New Zealand North Island (Figure 6). The nearshore is characterised by fine sand ($D_{50} \approx 0.16$–0.2 mm) and has a cross-shore slope of 0.009 with two subtidal sandbars usually present (Shand, 2007). The mean spring tide range is 2.4 m with a mean deepwater significant wave height of 1.3 m and 10.1-second period. Sea wave conditions occur for approximately 75% of the time and swell waves for 25% of the time. Observed site conditions during the three days of field investigation are presented within Table 1.

Waves typically break over a 200- to 500-m-wide surf zone, making a fixed break point assumption invalid and necessitating the variable height transformation method described earlier. The upper camera was placed on the cliff-top camera platform, 43.7 m above mean sea level (MSL) and the lower camera on the foredune some 4.1 m above MSL (Figure 6). Cameras and GCPs were georeferenced to the local coordinate system and elevation datum. The upper camera transformation model was calibrated using a series of temporary GCPs extending from onshore to outside the surf zone. The lower camera transformation model was calibrated using a graduated staff placed at the temporary GCPs. Pixel resolution in the images from the upper camera, after rectification to the horizontal plane, ranged from 0.9 m to 2.75 m per pixel from the inner to outer surf zone. For the lower camera, pixel resolution in the vertical plane varied from 0.015 m to 0.04 m per pixel across the surf zone.

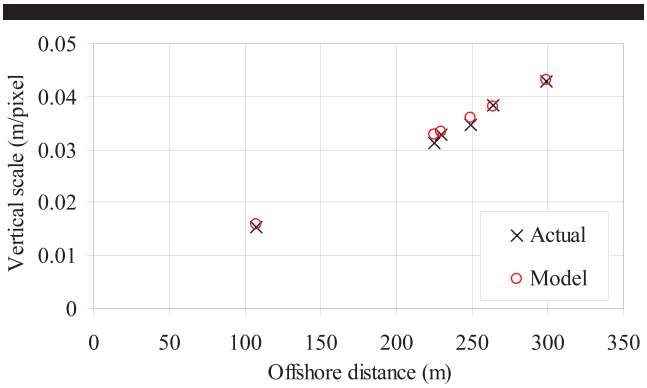

Figure 7. Verification of the derived model coefficients relating pixel location to vertical scale (Equation 4 and 5).

The coefficients derived for the transformation model (Equations 4 and 5) by site survey were verified by tracking a graduated staff from onshore to outside the surf zone. The vertical scale predicted by the transformation model is compared with that of the staff with errors ranging between 1 and 4% (Figure 7).

AUTOMATED ALGORITHM

A numerical algorithm, HbSTACK, was developed using the MatLab (R2010a; MathWorks, 2010) software platform. This algorithm extracts time-stack images from video records, detects the breaking edge of wave faces in the time-stack images, and translates the derived pixel values into real-world distance and elevation values using the earlier-described transformation models.

HbSTACK initially extracts a single pixel line from each video frame and stacks the pixel columns sequentially, thereby creating a time stack. The user controls the frequency of frame capture, selects the pixel lines for extraction, and any time offset between upper and lower video records to align the time-stacks temporally. The resultant red–green–blue time-stack images have dimensions of space in the y-axis and time in the x-axis. The algorithm then processes these time-stack images to identify breaking edges by first applying a temporal edge detection (by differencing in along the x-axis of the time-stack image), smoothing the results with a Gaussian filter, averaging the results along the y-axis, and applying a threshold to detect significant edges shown by red shading on Figure 8.

The above subroutine was first applied to the upper camera time stack to detect individual break points. The breaking event is not a single point in upper camera time stack, but rather extends over several pixels, between the crest and the trough. The still-water level ($Z = 0$) at break point was assumed to occur at one-third of the position between the detected crest and trough. The need for, and effect of, this assumption is

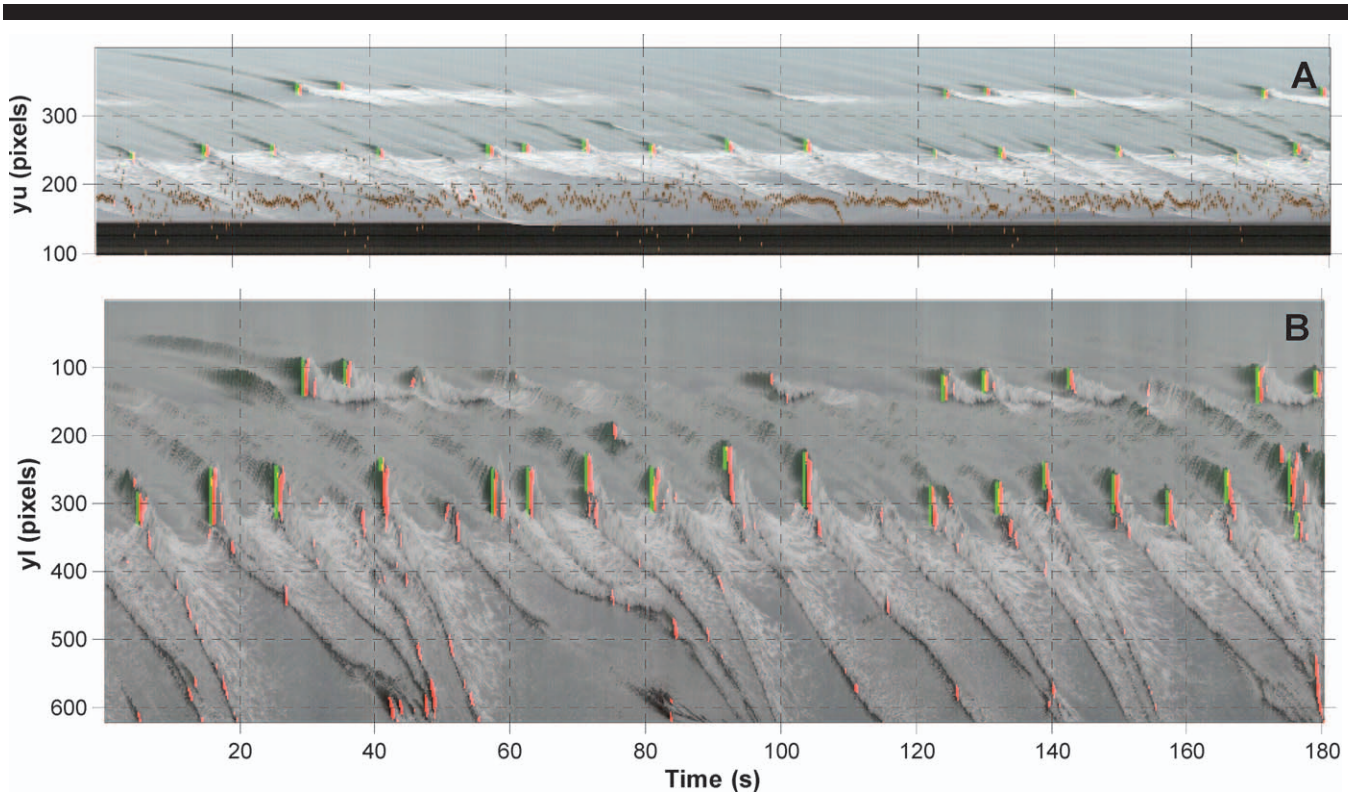

Figure 8. Examples of edge detection (red) used to extract break point from the upper camera (A) and the vertical extent of the breaking edge defined by green strips used to extract wave height from the lower camera (B) for a time-stack image sampled from the 21 January 2010 data set. (Color for this figure is only available in the online version of this paper.)

further discussed in the environmental variation section. Once breaking locations were defined in time and space, the corresponding offshore distances were computed using the transformation equation (Equation 4). A region of interest was established in the lower stack image around each break point defined by the upper stack image. This region of interest is based on a time threshold in the *x*-axis and a position within the surf zone in the *y*-axis and was necessary within a wide surf zone as waves may break at two different cross-shore locations simultaneously. This also ensures that only breaking events detected in both the upper and lower cameras are considered.

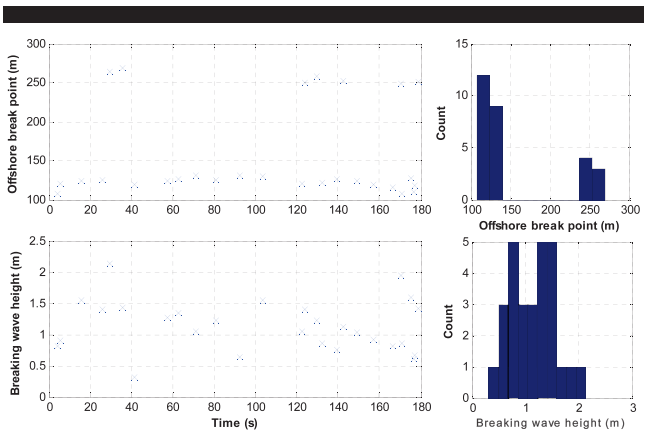

Figure 9. Offshore distance (A) and wave height (B) computed using HbSTACK for the data set shown in Figure 8.

The corresponding breaking wave heights were then obtained by defining the vertical extent of the breaking edge within the region of interest in the lower camera image. These heights are depicted by the green bars in Figure 8. This example figure shows that some edges detected in the lower camera (red shading) were not identified as significant edges in the upper camera and were therefore not defined as breaking events. The sensitivity of this detection may be adjusted using the Gaussian and threshold filters described earlier. Finally, the breaking wave height calculated in metres was determined on the basis of the offshore breaking distance using Equation 5. Data recorded (example shown in Figure 9) included individual breaking wave position, time, and height; these then enabled the period and statistical quantities including mean, significant, and 10% exceedance values to be derived (example shown in Table 2).

For this example, several waves are detected breaking on an outer bar, with a larger number breaking on the inner beach. Breaking wave height varies between 0.8 and 2.2 m, with a mean height of 1.4 m. This time-stack image shows waves breaking on the outer bar to deshoal in deep water after breaking before breaking again on the beach. Additionally,

Table 2. *Statistical quantities of breaking waves detected by the HbSTACK and manual detection methods for an example data set.*

	Manual Assessment 1	Manual Assessment 2	Manual Assessment 3	Manual Mean	Numerical Algorithm	% Difference
N	30	30	30	30	27	−10.0
H_{max}	2.11	2.11	2.15	2.12	2.19	3.1
H_{min}	0.83	0.83	0.95	0.87	0.77	−11.5
H_{mean}	1.35	1.42	1.38	1.38	1.38	−0.2
H_{sig}	1.74	1.81	1.72	1.76	1.74	−0.9
σ	0.33	0.34	0.31	0.33	0.36	10.2

some small, gently spilling events on the outer bar are omitted by the algorithm. Detection of these events may be improved by reducing the size of the threshold filter to define significant events, although increased noise is detected.

Mean wave period obtained by dividing the number of breaking incidents (N) by the sample time (t_{sample}) may be underestimated if individual waves break more than once. Results are likely to be more accurate on uniform sloping beaches where each wave breaks only once as they propagate toward the shoreline compared with barred beaches where breaking, deshoaling, and rebreaking often occur. Such multiple breaking events may be filtered on the basis of break location before averaging.

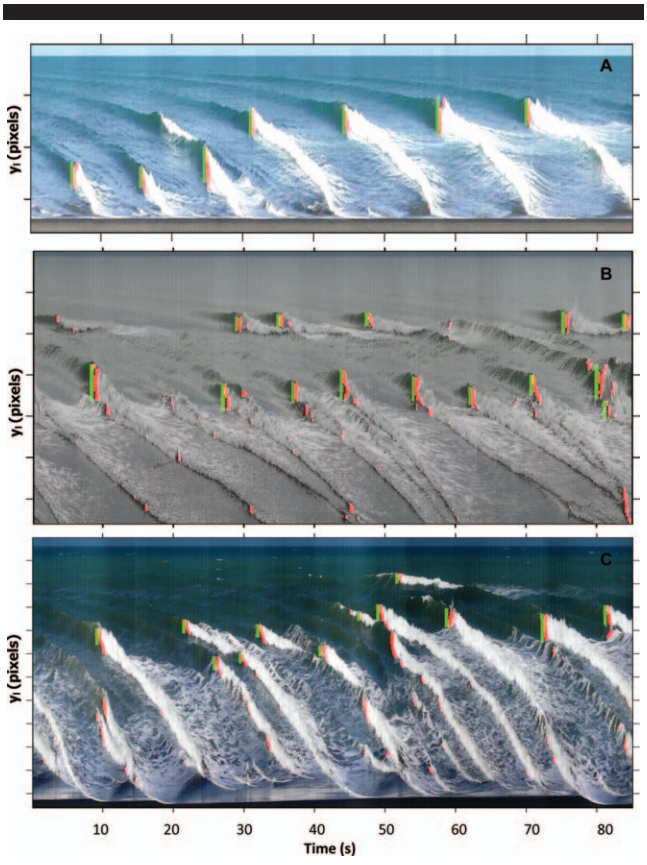

Figure 10. Examples of wave height detection during differing environmental conditions on 20 (A), 21 (B), and 22 (C) January 2010. (Color for this figure is only available in the online version of this paper.)

METHOD EVALUATION

Manual Comparison

Although verification of accuracies associated with transforming pixel data to real-world units is relatively straightforward (refer Field Data Collection section), verifying the derived wave height at break point is more difficult. First, instrumentation such as upward-looking acoustic Doppler velocimeters, wave buoys, and capacitance wave probes provide water-level information, but are placed at spatially discrete locations and the probability of wave breaking at an instrument site within a wide surf zone is low. Second, as discussed previously, the precise definition of breaking wave height is subject to interpretation.

The wave heights determined by HbSTACK were therefore compared with wave-by-wave examination of the raw video by three experienced coastal practitioners. Break point was defined as the location when the wave crest first becomes vertical and evident to a frontal observer by the wave crest or lip first beginning to propagate down the wave face. Breaking wave height was defined as the elevation difference between the crest and associated trough, as assessed by the practitioners on the basis of their knowledge of breaking wave processes and associated tonal variation on the water surface. Digitising the practitioner selections was carried out using the JavaScript video analysis and modelling tool Tracker (V1.7.4; Brown, 2007). The transformation equations (Equations 4 and 5) were used to convert the digitised pixel locations to offshore distance and elevation. These results thus offer a quantified visual assessment of breaking wave height.

Results of the manual assessments are compared with the algorithm results for the data set collected on 21 January 2010 in Table 2. There is close agreement in results, with the numerical algorithm underestimating mean and significant wave heights by less than 1% compared with the manual assessment, although the algorithm detects slightly fewer events (9%) and exhibits a greater range in wave heights (11%).

Environmental Variation

As with all visual observation and image-based techniques, wave characteristics and surface and light conditions affect the capabilities and accuracies of the methods. Examples of detected wave height under different environmental conditions on 20, 21, and 22 January 2010 are shown in Figure 10, with the resultant wave statistics presented in Table 3. Failure of the upper camera on 22 January prevented transformation of extracted wave characteristics from pixel to real-world units. Height statistics on 20 and 21 January were similar, although

Table 3. *Wave statistics from the three example data sets.*

Data	20 January 2010	21 January 2010—Set A	21 January 2010—Set B	22 January 2010[1]
Time (s)	300	180	300	300
N	20	27	38	36
T_{mean} (s)	14.8	6.7	7.9	8.3
H_{max} (m)	2.19	2.19	2.25	-
H_{min} (m)	0.27	0.21	0.25	-
H_{mean} (m)	1.07	1.08	1.13	-
H_{sig} (m)	1.55	1.52	1.68	-
σ (m)	0.49	0.46	0.53	-

[1] Top camera failed, preventing image transformation to real-world measurement.

the lower tide on 21 January induced multiple breaking for some waves, thereby reducing the observed mean period.

Although the sea states on 20 and 21 January were relatively smooth with predominantly plunging waves, 22 January was wind-affected, with predominantly spilling waves occurring. With plunging waves, the prebreaking face is near vertical and the projecting white water reaches the base (trough) almost instantaneously. This results in a sharp and high angle contrast change in the associated time-stack image. By contrast, faces of spilling waves have lower slope and the troughs are less well defined, particularly under low contrast conditions. As a result, the white water takes longer to reach the trough and the associated contrast change detected by HbSTACK has a lower angle and is less well delineated.

A time limit for defining that part of the white-water edge that contributes to the breaking height is therefore implemented within the routine. This limit defines the maximum time after breaking is first initiated that may be used to define the wave trough and therefore height. This time limit is intended to allow the white water to progress down the wave face to the trough but to restrict subsequent landward propagation of white water from being incorporated into the wave height calculation. An example is shown within Figure 11, where the detected edge is shown in red shading (see the online journal for the color version of the figure). The breaking edge is seen to propagate rapidly down the wave face before slowing (evidenced by the decreased angle, *i.e.,* more horizontal-tending track) as it continues to propagate onshore. The derived breaking height (green bars [see the online journal for the color version of the figure]) is shown without a time limit (11B), with a 3-second limit (11C), and with a 1-second time limit (11D). Without any time limit, the wave height is overestimated as the white-water interface is tracked after it reaches the trough. Incorporation of such a time constraint appears to provide reasonable results under spilling and low-contrast conditions where even manual definition of wave height is challenging. Automatic assignment of a time limit within HbSTACK for different wave conditions will be the subject of future investigation.

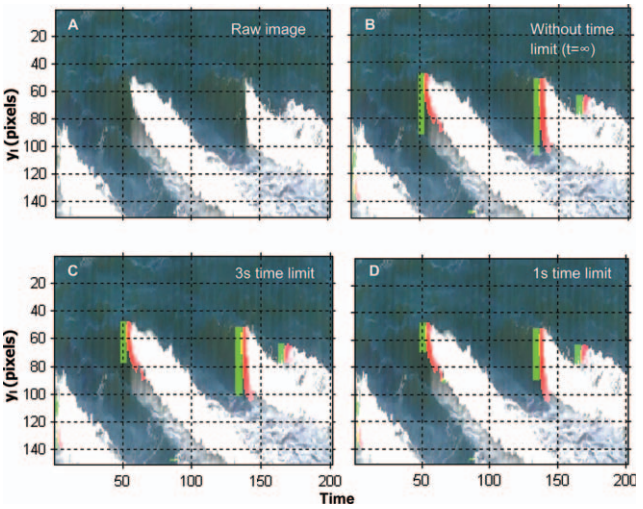

Figure 11. Example of low-contrast spilling wave (A) with the edge detected without a time limit (B), with a 3-s time limit (C), and with a 1-s time limit (D). (Color for this figure is only available in the online version of this paper.)

Errors and Uncertainty

Errors are introduced within the photogrammetric processes as a result of lens distortion, camera movement, or where the image is incorrectly transformed to real-world coordinates; this may occur through errors in estimating the correct plane and introduced in the feature identification process when breaking wave parameters such as break point and wave crest and trough positions are incorrectly identified.

The simple geometric transformation model based on a single-line field calibration was verified by field survey and found to be in agreement with measurement to within 5% across the surf zone. This error incorporates the photogrammetric errors described above. Readers are referred to Holland et al. (1997) for more complete descriptions of such errors and methods of error reduction. Regardless of environmental conditions, this error remains constant for any particular camera because it is a function of lens characteristics and geometry.

A critical assumption involved defining the cross-shore location of break point in the upper camera image. If the wave crest is selected, then the apparent break point is registered further seaward on a true horizontal plane and, similarly, if the

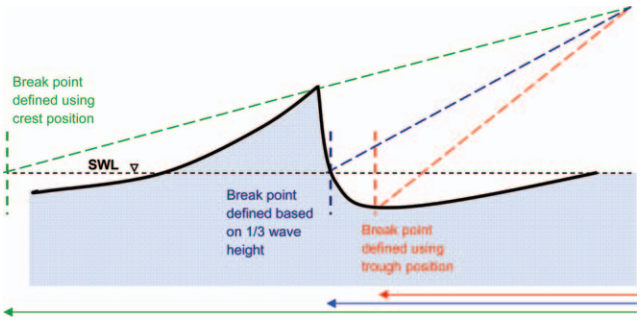

Figure 12. Variation in true location of the apparent break point dependent on definition used.

Table 4. *Variation in wave statistics using different definitions for break point for an example data set.*

Break point defined by:	Trough	⅓ of H	½ of H	Crest
N	27	27	27	27
T_{mean} (s)	6.7	6.7	6.7	6.7
H_{max} (m)	2.06	2.19	2.22	2.43
H_{min} (m)	0.75	0.77	0.76	0.78
H_{mean} (m)	1.30	1.38	1.40	1.52
H_{sig} (m)	1.63	1.74	1.77	1.94
σ (m)	0.33	0.36	0.37	0.42

trough is selected, the apparent break point is registered further landward (Figure 12). This is overcome by making an empirically based assumption that the still water level (Z=0) occurs roughly one-third of the vertical distance from trough to crest. This assumption, although not strictly valid across all wave types, is commonly observed in laboratory (Flick, Guza, and Inman, 1981) and higher-order, nonlinear wave theory (*i.e.,* Le Méhauté, Divoky, and Lin, 1968) where vertical asymmetry develops in a propagating waveform before breaking with a narrower, high crest and wider low trough. Results presented in Table 4 show the effect of alternative definitions of break point on the derived breaking wave height. In particular, note that the difference in the derived significant or mean wave height assuming $Z = 0$ occurs at one-half wave and one-third of the trough-to-crest distance is less that 2%, thus making this parameter relatively insensitive.

For waves breaking within the inner surf zone, there may also be an error resulting from setup above still-water level ($Z = 0$). This will cause the position of the event determined from the upper camera to be slightly seaward of its true position. The subsequent scaling of the wave height from the lower camera will result in a slight overestimation of wave height. However, since water-level variation due to setup effects is generally small within the mid- to outer surf zone (Nielsen, 1988), errors associated with setup in all but the smallest waves will be negligible. If wave statistics in the inner surf zone are of specific interest, allowance for setup in the $Z = 0$ plane may be incorporated using an empirical expression (*i.e.,* Nielsen, 1988).

Verification of the feature identification is less straightforward. However, assumptions on the definitions of break point and breaking wave height were consistent with those in the literature, and manually derived values from experienced practitioners compared well with the numerical algorithm (HbSTACK) output. Confidence in the practitioner values is obtained from the low variation between individuals (Table 2). The resultant H_b values may thus be described as an automated quantification of visual breaking wave height.

The combined effect of multiple errors can be determined using the properties of variance addition, with independent terms being combined using Equation 7 (*e.g.,* see Larsen and Marx, 1986):

$$CE = \sqrt{(E_1^2 + \ldots\ldots\ldots + En^2)} \quad (7)$$

where CE = combined error, E_1 = first error term, and En = nth error term. As the error sources in the present exercise are independent, the combined uncertainty is ~7%. However, this level of accuracy may decrease under lesser light conditions, wave breaking conditions, and camera arrangements than those experienced during our fieldwork.

CONCLUSION

Optical methods for determining surf zone properties offer a viable and practical alternative to conventional *in situ* instrumentation. However, although existing three-dimensional (3D) photogrammetric techniques are capable of extracting surface elevation, they do not provide specific wave-breaking characteristics of position and height. Additionally, they are reliant on favourable environmental conditions and computational "expense" remains prohibitive in terms of developing real-time systems.

The 2D photogrammetric methodology presented in this paper utilises dual cameras, with the upper camera images being used to determine the breaking distance offshore and, on the basis of this distance, the lower camera's corresponding images being used to derive the breaking wave height. This methodology is suitable for use in a wide surf zone with large variations in breaking height and position. Errors arise with both the photogrammetric transformation from pixels to real-world distance and in the definition of the wave crest and trough used to determine height. The transformation algorithm derived during the field study showed errors of less than 5%.

The numerical algorithm, HbSTACK, was tested using imagery obtained over 3 days at the Coastal Systems Field Research Site at Castlecliff Beach, New Zealand. Wave height was assessed manually by three experienced practitioners with difference in mean and significant height between the practitioners and the numerical algorithm of less than 5%. The combined accuracy of the numerical algorithm, including both the photogrammetric transformation error and the feature detection error, was less than 7%. Although this accuracy was achieved under relatively favourable conditions, accuracy under lower light or low-contrast conditions and spilling waves is expected to be less. More precise verification of the algorithm using spatially-discrete, *in situ* instrumentation will be difficult because of the nondiscrete nature of wave breaking and inaccuracy of conventional instrumentation within the aerated breaking surf zone. The resultant H_b values may thus be described as an automated quantification of visual breaking wave height.

The automated optical method presented in this paper successfully quantifies breaking wave height across a wide surf zone along a single, shore-normal transect centrally located within the camera view. Further field data and analysis is required to develop an automatic variable selection procedure capable of accommodating the wide range of atmospheric and marine conditions typically experienced in the coastal environment. The method's relative simplicity shows promise for real-time application.

LITERATURE CITED

Aagaard, T. and Holm, J., 1989. Digitization of wave run-up using video records. *Journal of Coastal Research,* 5(3), 547–551.

Bailey, D.G. and Shand, R.D., 1994. Determining wave run-up using automated video analysis. *Proceedings of the Second New Zealand Conference on Image and Vision Computing*, pp. 2.11.1–2.11.8.

Bailey, D.G. and Shand, R.D., 1996. Determining large-scale sandbar behaviour. *IEEE International Conference on Image Processing*, Volume 2, pp. 637–640.

Balisllie, J.H. and Carter, R.W.G., 1984. The visual estimation of shore-breaking wave heights. *Coastal Engineering,* 8, 367–385.

Bechle, A.J. and Wu, C.H., 2011. Virtual wave gauges based upon stereo imaging for measuring surface wave characteristics. *Coastal Engineering*, 58, 305–316.

Benetazzo, A., 2006. Measurements of short water waves using stereo-matched image sequences. *Coastal Engineering,* 53(12), 1013–1032.

Brown, D. 2007. *Tracker V 1.7.4*. Cabrillo College, CA.

Cox, C. and Munk, W., 1954. Measurements of the roughness of the sea surface from photographs of the sun's glitter. *Journal of the Optical Society of America,* 44(11), 838–850 .

de Vries, S.; Hill, D.F.; de Schipper, M. A., and Stive, M.J.F., 2010. Remote sensing of surf zone waves using stereo imaging. *Coastal Engineering*, 58, 239–250.

Department of Survey and Land Information. 1996. New Zealand 1 : 3,000,000 Topomap. InfoMap 267.

Duncan, J.H., 2001. Spilling breakers. *Annual Review of Fluid Mechanics* 33, 519–547.

Flick, R.E.; Guza, R.T., and Inman, D.L., 1981. Elevation and velocity measurements of laboratory shoaling waves. *Journal of Geophysical Research* 86(C5), 4149–4160.

Grace, R.A., 1978. Surface wave heights from pressure records. *Coastal Engineering* 2, 55–67.

Heron, M.L. and Prytz, A., 2002. Wave height and wind direction from the HF coastal ocean surface radar. *Canadian Journal of Remote Sensing*, 28, 385–393.

Hilmer, T., 2005. Measuring Breaking Wave Heights Using Video. Manoa, Hawai'i: University of Hawai'i, undergraduate thesis, 21p.

Holland, T.K., 2001. Application of the linear dispersion relation with respect to depth inversion and remotely sensed imagery. *IEEE Transactions on Geoscience and Remote Sensing*, 39(9), 2060–2072.

Holland, T.K.; Holman, R.A.; Lippman, T.C.; Stanley, J., and Plant, N., 1997. Practical use of video imagery in nearshore oceanographic field studies. *IEEE Journal of Oceanic Engineering*, 22(1), 81–92.

Holman, R.A. and Guza, R.T., 1984. Measuring run-up on a natural beach. *Coastal Engineering*, 8, 129–140.

Kelly, J.M., 1965. *Surf and Sea*. New York: A.S. Barnes and Co. Inc.

Lane, C.; Gal, Y.; Browne, M.; Short, A.; Strauss, D.R.; Tomlinson, R.B.; Jackson, K.; Tan, C., and Blumenstein, M., 2010. A new system for break zone location and the measurement of breaking wave heights and periods. *Proceedings of IEEE International Geoscience and Remote Sensing Symposium* (Hawaii), pp. 2234–2236.

Larsen, R.J. and Marx, M.L., 1986. *An Introduction to Mathematical Statistics and Its Applications*. London: Prentice-Hall International Editions, 630p.

Le Méhauté, B.; Divoky, D., and Lin, A., 1968. Shallow water waves: a comparison of theories and experiments. *Proceedings of 11th Conference of Costal Engineering*, Vol. 1.

Mathworks. 2010. Matlab®, Version R2010A. Natick, Massachusetts: The MathWorks Inc.

Mitchell, H.L., 1983. Wave heights in the surf zone. *Photogrammetric Record,* 11(62), 183–193.

Nielsen, P., 1988. Wave setup: a field study. *Journal of Geophysical Research*, 93(C12), 15643–15652.

Patterson, D.C. and Blair, R.J., 1983. Visually determined wave parameters. *Proceedings of the 6th Australian Conference on Coastal and Ocean Engineering*, pp. 151–155.

Peregrine, D.H., 1983. Breaking waves on beaches. *Annual Review of Fluid Mechanics,* 15, 149–178.

Sasaki, T.; Horikawa, K., and Hotta, S., 1976. Nearshore currents on a gently sloping beach. *15th Conference on Coastal Engineering* (Honolulu, Hawaii).

Schooley, A.H., 1956. A simple optical method for measuring the statistical distribution of water surface slopes. *Journal of the Optical Society of America*, 44(1), 37–40.

Shand, R.D., 2007. Bar splitting: system attributes and sediment budget implications for a net offshore migrating bar system. *Journal of Coastal Research*, Special Issue 50, International Coastal Symposium 2007, Brisbane, April 2007.

Shand, R.D. and Bailey, D.G., 1995. Videographic Acquisition of Surf Zone Data: Present Techniques and Future Possibilities. Massey University, New Zealand: Geography Department. Miscellaneous Publication Series, 33p.

Shand, T.D., 2009. The Effect of Wave Grouping on Shoaling and Breaking Processes. Sydney, Australia: University of New South Wales, doctoral thesis, 355p.

Singamsetti, S.R. and Wind, H.G., 1980. *Characteristics of Breaking and Shoaling Periodic Waves Normally Incident onto Plane Beaches of Constant Slope*. Delft, the Netherlands: Delft Hydraulics Laboratory.

Smith, E.R. and Kraus, N.C., 1991. Laboratory study of wave-breaking over bars and artificial reefs. *Journal of Waterway, Port, Coastal and Ocean Engineering,* 177, 307–325.

Stockdon, H.F. and Holman, R.A., 2000. Estimation of wave phase speed and nearshore bathymetry from video imagery. *Journal of Geophysical Research*, 105(C9), 22015–22033.

Ting, F.C.K. and Kirby, J.T., 1995. Dynamics of surf-zone turbulence in a strong plunging breaker. *Coastal Engineering,* 24(3–4), 177–204.

Wanek, J.M. and Wu, C.H., 2006. Automated trinocular stereo imaging system for three-dimensional surface wave measurements. *Ocean Engineering,* 33(5–6), 723–747.

Whittenbury, C.G.; Huber, E.A., and Newell, G.S., 1959 Instrument for measuring water waves. *The Review of Scientific Instruments,* 30(8), 674–676.

Wyatt, L.R., 1988. Significant wave height measurement with H.F. radar. *International Journal of Remote Sensing*, 9, 1987–1095.